Association between Long-Term Ultrafine Particulate Matter Exposure and Premature Death

REPORT TO THE

California Air Resources Board Research Division

Project # 14-314

Prepared by:

Dr. Michael J. Kleeman[1]
Dr. Anikender Kumar[1]
Dr. Jian Xue[1]
Dr. Xin Yu[1]
Dr. Melissa Venecek[1]
Melissa Traverso[1]
Abhishek Dhiman[1]
Wei Xue[1]
Yiting Li[1]

Dr. Bart Ostro[2]
Dr. Peggy Reynolds[3]

[1]Department of Civil and Environmental Engineering
[2]Air Quality Research Center
University of California, Davis
One Shields Avenue, Davis, CA, 95616

[3]Department of Epidemiology and Biostatistics
University of California, San Francisco

April 29, 2019

DISCLAIMER

The statements and conclusions in this report are those of the contractor and not necessarily those of the California Air Resources Board. The mention of commercial products, their source, or their use in connection with material reported herein is not to be construed as actual or implied endorsement of such products.

Portions of this project were supported by the Bay Area Air Quality Management District under project #2013.218 and the Coordinating Research Council under project #A-96. None of the project sponsors nor any person acting on their behalf: (1) makes any warranty, express or implied, with respect to the use of any information, apparatus, method, or process disclosed in this report, or (2) assumes any liabilities with respect to use, or damages resulting from the use or inability to use, any information, apparatus, method, or process disclosed in this report.

ACKNOWLEDGEMENTS

This project was funded under the CARB's Dr. William F. Friedman Health Research Program. During Dr. Friedman's tenure on the Board, he played a major role in guiding CARB's health research program. His commitment to the citizens of California was evident through his personal and professional interest in the Board's health research, especially in studies related to children's health. The Board is sincerely grateful for all of Dr. Friedman's personal and professional contributions to the State of California.

The authors thank Lori Miyasato at the California Air Resources Board for her help with project management.

The authors thank the Scientific Advisory Committee for helpful feedback. Members include Arden Pope, Michael Jerrett, Mary Ross, Jason Sacks, Peter Adams, and Andrea Polidori.

The authors thank Debbie Goldberg at UCSF for providing analytic support for the CTS data analyses.

The authors thank Mohammad H. Sowlat and Constantinos Sioutas at the University of Southern California for help with ambient particle sampling in Los Angeles. The authors thank Anabelle Lolinco and Alam Hasson at the California State University – Fresno for help with ambient particle sampling in Fresno.

The authors thank Saffet Tanrikulu, Steven Randall, Robert Boynton, Robert Graul, and David Beyer at the Bay Area Air Quality Management District for help with ambient particle sampling in East Oakland and San Pablo.

The authors thank Philip Stevens's group of the University of Indiana for providing the HO_2 and OH radical concentrations measured during the CalNex 2010 field campaign.

TABLE OF CONTENTS

LIST OF TABLES

LIST OF FIGURES

LIST OF ACRONYMS

AB32 – Assembly Bill 32 or Global Warming Solutions Act
AIHL – Air and Industrial Hygiene Laboratory
ACS – American Cancer Society
AQS – Air Quality System
BAAQMD – Bay Area Air Quality Management District
BAK – Bakersfield
BMI – Body Mass Index
CAAP – Clean Air Action Plan
CAAQS – California Ambient Air Quality Standards
CalNex–California Nexus
CARB – California Air Resources Board
CBSA - core-based statistical area
CCAQS – Central California Air Quality Standards
CHS – Children's Health Study
CI – Confidence Interval
CO – Carbon Monoxide
CMAQ – Community Multiscale Air Quality model
CMB – Chemical Mass Balance
CPC – Condensation Particle Counter
CRP - C-reactive protein
CRPAQS – California Regional PM10/PM$_{2.5}$ Air Quality Study
CSN – Chemical Speciation Network
CTM – Chemical Transport Model
CTMP – Clean Truck Management Plan
CTS – California Teachers Study
CV - Cardio Vascular
DGI – Dekati Gravimetric Impactor
DLPI – Dekati Low Pressure Impactor
DPF – Diesel Particle Filter
DRUM – Davis Rotating-drum Universal-size-cut Monitor
EAA – Electrical Aerosol Analyzer
EC – Elemental Carbon
ELPI – Electrical Low Pressure Impactor
EO – East Oakland
EMFAC – Emissions Factor
EPA - Environmental Protection Agency
EPC – Environmental Particle Counter
FAA – Federal Aviation Administration
FDDA – four dimensional data assimilation
FR – Fresno
FRM – Federal Reference Method
GC-MS – Gas Chromatography – Mass Spectrometry
GDI – Gas Direct Injection

GFED – Global Fire Emissions Database
GFS – global forecast system
GHG – Green House Gas
GVWR – Gross-Vehicle Weight Rating
HDV – heavy duty vehicle
HFO – Heavy Fuel Oil
HI – Harvard Impactor
HR – Hazard Ratio
ICD - International Classification of Diseases
ICP-MS - Inductively Coupled Plasma Mass Spectrometry
IHD – Ischemic Heart Disease
IMAGE - Integrated Model for the Assessment of the Global Environment
IMPROVE - Interagency Monitoring of Protected Visual Environments
IMO - International Maritime Organization
IQR – Inter Quartile Range
LA – Los Angeles
LAX - Los Angeles International Airport
LB - Long Beach
LDV – light duty vehicle
LUR – Land Use Regression
MAQIP - Marine Air Quality Improvement Program
MATES-IV - Multiple Air Toxics Exposure Study (Fourth Edition)
MB – Mean Bias
MCIP - meteorology-chemistry interface processor
MDV – Medium Duty Vehicle
MEGAN –Model of Emission of Gases and Aerosols from Nature
MFB – Mean Fractional Bias
MFE – Mean Fractional Error
MOUDI – Micro Orifice Uniform Deposit Impactor
MOZART - model for ozone and related chemical tracers
N_7 – number concentration of particles with diameter greater than 7 nm
N_{10} – number concentration of particles with diameter greater than 10 nm
N_X – number concentration of particles with diameter greater than X nm
NAAQS – National Ambient Air Quality Standards
NARR - North American Regional Reanalysis
NCEP - National Centers for Environmental Prediction
NEI – National Emissions Inventory
NIOSH - National Institute for Occupational Safety & Health
NMAM - NIOSH Manual of Analytical Methods
NO_x – oxides of nitrogen
NSS-SO_4 – Non-sea salt sulfate
OA – Organic Aerosol
OC – Organic Carbon
OGV – Ocean-going Vessel
OP – Pyrolized Organic Carbon

PAH - Polycyclic Aromatic Hydrocarbon
PCIS - Personal Cascade Impactor Sampler
PFI – Port Fuel Injection
PIXE - Proton Induced X-Ray Emissions
PM – particulate matter
$PM_{0.1}$ – mass of particulate matter with diameter less than 0.1 μm
$PM_{0.25}$ – mass of particulate matter with diameter less than 0.25 μm
$PM_{2.5}$ – mass of particulate matter with diameter less than 2.5 μm
PM_{10} – mass of particulate matter with diameter less than 10.0 μm
PMF – Positive Matrix Factorization
POA – primary organic aerosol
POLA – Port of Los Angeles
POLB – Port of Long Beach
ppb – parts per billion
ppm – parts per million
PyC – Pyrolized Carbon
RCTM – regional chemical transport model
RH – relative humidity
RMSE – root Mean Square Error
RV – Riverside
RWC – Residential Wood Combustion
SAPRC – State Air Pollution Research Center
SAPRC11 – gas-phase chemical reaction mechanism created by William Carter in 2011
SAPRC16 – gas-phase chemical reaction mechanism created by William Carter in 2016
SCAQMD – South Coast Air Quality Management District
SFBA – San Francisco Bay Area
SIP – State Implementation Plan
SJV – San Joaquin Valley
SJVUAPCD – San Joaquin Valley Unified Air Pollution Control District
SMAQMD - Sacramento Metropolitan Air Quality Management District
SMOKE – Sparse Matrix Operator Kernel Emissions
SMPS - Scanning Mobility Particle Sizer
SOA – secondary organic aerosol
SOAa – secondary organic aerosol from anthropogenic sources
SOAb – secondary organic aerosol from biogenic sources
SoCAB – South Coast Air Basin
SOM – Statistical Oxidation Model
SOx – Sulfur Oxides
SP – San Pablo
T96 – Trajectory Study of 1996
THC – Total Hydrocarbons
TN – Ternary Nucleation
TOR – Total Optical Reflectance
UCD/CIT – University of California Davis/California Institute of Technology
UCPC – Ultrafine Condensation Particle Counter

UFP – Ultrafine Particle
ULSD – Ultra-Low Sulfur Diesel
USC – University of Southern California
VMT – Vehicle Miles Traveled
VOCs – volatile organic compounds
WRF – Weather Research & Forecast
XRF – X-Ray Fluorescence

ABSTRACT

Ultrafine particles (UFPs) have diameters ≤ 100 nm allowing them to penetrate into regions of the human body that are not accessible to larger particles. Numerous laboratory studies over the past two decades have found that UFPs are toxic but the epidemiological evidence over this same time period is inconsistent. Past epidemiological studies have typically focused on particle number concentration measured at central site monitors, but this approach cannot adequately represent the sharp spatial gradients in UFP exposure. New techniques are needed to better represent the spatial gradients for UFP number and mass concentrations to fully explore UFP public health impacts.

The objective of the current project is to estimate exposure to UFP number and UFP mass using new approaches that capture variations in space and time over the past two decades. A regional chemical transport model was created to predict UFP concentrations across California by combining criteria pollutant emissions inventories with measured particle size and composition profiles that extend into the UFP size range. Model calculations include all of the atmospheric processes that influence UFP concentrations including emissions, transport, deposition, coagulation, condensational growth, and nucleation. UFP concentration fields generated for California between the years 2000 – 2016 are in reasonable agreement with the available measured UFP number concentrations and measured UFP mass concentrations. UFP source apportionment information contained in the predicted UFP exposure fields is also in good agreement with measured UFP source apportionment calculated using the Chemical Mass Balance (CMB) model at Los Angeles, East Oakland, and San Pablo over a 12 month period in 2015 - 2016. Looking across all of California, UFP concentrations were highest in large cities with dense populations. Major UFP sources included on-road vehicles, wood burning, food cooking, airports, and natural gas combustion. UFP concentrations associated with on-road vehicles and biomass combustion declined between the years 2000 – 2016 due to the effects of targeted emissions control programs.

Final UFP exposure fields were combined with the health data from the California Teachers Study (CTS) cohort (+90,000 participants) to analyze health effects using a Cox proportional hazard model. The risk estimate on all-cause mortality per 10 $\mu g/m^3$ of $PM_{2.5}$ calculated using the CTS cohort agrees with corresponding published estimates from the ACS and Medicare cohorts. Specifically, the hazard ratio (HR) associated with a 10 $\mu g/m^3$ of $PM_{2.5}$ were 1.07 (95% CI = 0.99, 1.06), 1.09 (0.99, 1.22) and 1.20 (1.02, 1.45) for all-cause, cardiovascular and ischemic heart disease mortality, respectively. Extending the analysis to the UFP size range, multiple UFP metrics were associated with all-cause mortality at the 95% confidence level including mass, EC, OC, metals, and on-road diesel. UFP metrics associated with CV mortality at the 95% confidence level included Cu, EC, and SOA. UFP metrics associated with IHD mortality at the 95% confidence level included Cu, Fe, EC, metals, SOA, gasoline, off-road diesel, food cooking, and natural gas. The sum of primary $PM_{0.1}$ from all fossil fuel combustion activities is associated with all-cause, CV, and IHD mortality at the 95% confidence level. There is a suggestion from our results that UFP may correlate with the mortality outcomes as well or better than $PM_{2.5}$. However, given the high correlations between the $PM_{2.5}$ and UFP mass and species and the likely differential in measurement error, it is difficult to reach a firm conclusion on this issue. Two pollutant models of UFP individual species plus mass provide additional support for the effects of individual species.

Future studies are needed to analyze the UFP exposure fields using additional cohorts to create further weight of evidence for the health effects of UFPs in epidemiological studies.

EXECUTIVE SUMMARY

Background: Ultrafine particles (UFPs; $Dp \leq 0.1$ μm) have toxic properties, possibly because they can transport metals, oxidized organic compounds, and other toxic substances adsorbed onto their high surface area to regions of the body that cannot be reached by larger particles [1]. The 1998 US National Research Council blueprint for particulate matter (PM) research identified UFPs as a research priority [2]. Fifteen years later, the 2013 HEI Perspective on the Health Effects of Ultrafine Particles [3] confirmed the robust evidence for the toxicity of ultrafine particles but noted that epidemiological studies were inconclusive and in the case of long-term exposures, non-existent [4]. The lack of consistent epidemiologic results was also a factor in the 2009 US-EPA Integrated Science Assessment which concluded that the evidence was suggestive but not yet sufficiently developed to infer a causal relationship between UFPs and human health [5]. Most previous UFP epidemiological studies, which have focused on short-term (i.e. daily or multi-day) exposures, have relied on a single central site monitors for exposure assessments. This approach is challenging for UFPs due to the choice of different UFP metrics (number vs. surface area vs. mass) that each have uniquely sharp spatial gradients. More recent studies have addressed this complexity by using source-oriented Regional Chemical Transport Model (RCTM) calculations to fill in the gaps between measured UFP concentrations [6]. Epidemiological studies using this approach have identified robust associations between UFP and increased hazard ratios for death by ischemic heart disease [7] and robust associations between UFP and birth outcomes [8]. The purpose of this project is to extend these techniques to create long-term UFP exposure fields for California and to assess the health effects associated with long-term exposure to UFPs.

Methods: The standard criteria pollutant emissions inventories for California were combined with measured profiles for the size and composition of particles emitted from major combustion sources to create UFP emissions inventories. RCTM calculations were updated to incorporate the latest science describing the atmospheric processes that influence UFP concentrations including emissions, transport, deposition, coagulation, condensational growth, and nucleation. UFP concentration fields were generated for California between the years 2000 – 2016 with hourly time resolution and 4km spatial resolution. Predicted UFP concentrations were compared to measurements conducted over a 12 month period at Los Angeles, East Oakland, and San Pablo plus a 6 month period at Fresno. Predicted UFP concentrations were also compared to the historical record of UFP measurements made shorter term field studies carried out prior to the year 2015. Final UFP exposure fields were combined with the health data from the California Teachers Study (CTS) cohort (+90,000 participants) to analyze potential UFP health effects using a Cox proportional hazard model.

Results: Predicted UFP concentration fields meet the performance goals for PM modeling applications (mean fractional error (MFE) ≤ ±0.5 and mean fractional bias (MFB) ≤ 0.75) for both $PM_{0.1}$ mass and N_7 number concentration. A consistent negative MFE for predicted UFP EC concentrations suggests that wind speeds may be over-predicted during stagnation events, but the spatial pattern of the UFP exposure fields should not be biased by this offset in absolute concentrations when averaging over long time periods. Predicted source contributions to $PM_{0.1}$ mass are in good agreement with source contributions calculated using the Chemical Mass Balance (CMB) model at Los Angeles, East Oakland, and San Pablo. Looking across all of California, UFP concentrations were highest in large cities with dense populations. Major sources of UFPs included on-road vehicles, biomass combustion, food cooking, airports, and natural gas combustion. UFP concentrations associated with on-road vehicles and biomass combustion declined between the years 2000 – 2016 due to the effects of targeted emissions control programs. The risk estimate on all-cause mortality per 10 μg/m^3 of $PM_{2.5}$ calculated using the CTS cohort compares favorably with corresponding estimates developed using central site monitor exposures combined with the ACS cohort and the Medicare cohort. Specifically, the HR associated with a 10 μg/m^3 of $PM_{2.5}$ were 1.07 (95% CI = 0.99, 1.06), 1.09 (0.99, 1.22) and 1.20 (1.02, 1.45) for all-cause, cardiovascular and ischemic heart disease mortality, respectively. Extending the analysis to the UFP size range, UFP mass and multiple subcomponents of UFP mass were associated with all-cause mortality at the 95% confidence level including EC, OC, metals, and on-road diesel sources. UFP mass subcomponents associated with CV mortality at the 95% confidence level included Cu, EC, and SOA. UFP mass subcomponents associated with IHD mortality at the 95% confidence level included Cu, Fe, EC, metals, SOA, gasoline, off-road diesel, food cooking, and natural gas combustion. The most consistent association across all the health endpoints is the sum of primary $PM_{0.1}$ mass from all fossil fuel combustion activities which is associated with all-cause, CV, and IHD mortality at the 95% confidence level. These health associations of UFP mass and selected species persist in two pollutant models combined with their corresponding $PM_{2.5}$ metrics. This suggests that UFP may correlate with the mortality outcomes as well or better than $PM_{2.5}$. However, given the high correlations between the $PM_{2.5}$ and UFP mass and species and the likely differential in measurement error, it is difficult to reach a firm conclusion on this issue. Two pollutants models of UFP individual species plus mass provide additional support for the effects of individual species.

Conclusions: The UFP exposure fields predicted for the years 2000 – 2016 in the current project are lower than measured values due to over-predicted wind speed during stagnation events, but the spatial pattern of predicted UFP concentration still adds to the knowledge derived from sparse measurements at central site monitors. The predicted UFP exposure fields also contain new information about chemical components and source contributions that would be impossible to extract from the limited historical measurement database. Epidemiological cohorts that span a geographical region greater than 100 times the spatial resolution of the exposure fields (4 km x 100 =400 km) can take advantage of the newly resolved information present in the predicted UFP exposure fields. Preliminary results from the CTS cohort suggest that UFPs derived from fossil fuel combustion are associated with all-cause, CV, and IHD mortality at the 95% confidence level.

Future Work: Future epidemiological studies should be carried out using additional large cohorts combined with exposure estimates from regional chemical transport models to investigate the health effects of UFPs. These studies should focus on data sets where contrasts between UFP, NO_2, and $PM_{2.5}$ can be utilized. Further studies should be carried out to identify a chemical signature for natural gas combustion particles that can be included in CMB calculations to more definitely quantify natural gas source contributions to ambient UFP concentrations. The sources that contribute to increased UFP EC concentrations during winter between the years 2000 – 2016 should be identified and properly represented in the UFP emissions inventories. The sources of UFP Cu should be identified and the accuracy of the exposure fields should be confirmed. The spatial distribution of mobile source emissions predicted using different techniques should be reconciled. The $PM_{0.1}$ exposure fields developed in this study should be updated to reflect new findings on secondary organic aerosol (SOA) formation when they become available so that the health effects of the UFP SOA can also be updated.

1 INTRODUCTION

1.1 Motivation

Numerous studies have identified associations between the mass of particles with aerodynamic diameter < 2.5 µm ($PM_{2.5}$) and premature mortality (see for example [9]) but far less is known about the public health threat associated with smaller particle size fractions within the $PM_{2.5}$ range. One size range of great interest is ultrafine particles (Dp < 0.1 µm) due to the ability of these particles to translocate to different regions of the body [10, 11] and their apparent toxicity in multiple studies [1, 12-14]. The 1998 US National Research Council blueprint for a research program on PM identified ultrafine particles (UFPs) as a research priority [2]. Extensive studies have been conducted for atmospheric UFP concentrations, composition, and source contributions over the past 20 years (see for example [15-25]) with the potential to now apply these findings in a health effects study.

There are multiple potential mechanisms for health effects associated with UFPs: (a) high surface area-to-volume ratio inherent in UFPs can provide numerous sites for heterogeneous reactions [26], (b) the large number of UFPs may overwhelm the alveolar macrophages that clear foreign objects from the respiratory system [27], and (c) UFPs may translocate out of the alveolar region of the respiratory tract into the bloodstream or from the olfactory mucosa to the brain. Each of these independent hypotheses merits further study.

Epidemiological evidence linking UFPs to health outcomes will be required in order to fully evaluate the potential public health impacts from UFP exposure. Despite the robust toxicology results for UFPs, the majority of the epidemiological studies carried out to date have not been able to identify strong independent health effects alluded to in experimental studies [28-30]. It is likely that the exposure assessment used for UFP surface area and number has been inadequate in previous epidemiological studies, resulting in inconclusive results. Establishing a more accurate exposure assessment and evaluating the true epidemiological evidence is of paramount importance for regulators charged with protecting public health from the adverse effects of air pollution.

Realistic exposure assessments for UFPs are challenging to construct because these particles exhibit more dynamic behavior and sharper spatial gradients than traditional air pollutants such as ozone and $PM_{2.5}$ mass [31]. UFPs can be directly emitted by sources [23, 24, 32] or they can form spontaneously from gas-phase precursors over broad geographical regions [33, 34] or in the plumes downwind of roadways [35]. Once in the atmosphere, UFPs can grow to larger particle size fractions Dp > 0.1 µm or they can fully evaporate as the concentrations become more dilute downwind of the source [36]. All of these effects combine to create UFP exposure fields that vary sharply in space and time. Standard monitoring networks based on central site measurements that work well for exposure assessment of relatively stable pollutants like ozone and $PM_{2.5}$ mass cannot adequately capture the details of population exposure to UFPs that are needed for robust epidemiological studies. This problem is apparent in several of the early studies for health effects of UFPs (see for example [37, 38]). New approaches for exposure assessment are needed to support future epidemiological studies of UFPs.

Regional models may be the most practical near-term method to calculate UFP exposure for large populations given the challenges associated with measurement networks. Hu et al. showed that regional chemical transport models can accurately predict UFP concentrations at multiple sites across California [39-41]. Ostro et al. used these UFP exposure fields to identify significant associations between UFP concentrations and mortality [7]. Wu et al. used the ultrafine exposure fields to identify significant associations between UFP concentrations and birth outcomes [8, 42]. These studies suggest that a combination of model predictions, measurements, and epidemiology can be used to study the public health effects of UFPs. These methods will be extended in the current project to further investigate the public health impacts of UFPs in California.

1.2 Research Objectives

The overall objective of this report is to determine if any feature of ultrafine particles (number, mass, chemical components, or sources) is positively associated with premature death in California. Regional chemical transport models will be used to predict exposure fields across California for different chemical components and sources that contribute to ultrafine particle concentrations. Measurements will be made at multiple locations to evaluate the accuracy of these predicted UFP exposure fields. Preliminary epidemiological studies will then be conducted to calculate hazard ratios associated with UFPs. Where possible, the health effects of UFPs will be tested relative to other pollutants such as $PM_{2.5}$.

The specific project objectives are to:

Objective 1. Measure the UFP concentrations in three (3) major CA population centers and perform source apportionment using the Positive Matrix Factorization (PMF) model and the Chemical Mass Balance (CMB) model.

Objective 2. Predict UFP concentrations across CA using a Reactive Chemical Transport Model (RCTM). UFP predictions will be made from the period 2000-2016 using spatial resolution varying from 1km to 4km. RCTM model predictions will be compared to the measurements made in Objective 1.

Objective 3. Evaluate the associations between UFPs and premature mortality using standard epidemiological methods applied to the California Teachers Study (CTS) cohort of +90,000 women.

1.3 Hypotheses

The hypotheses that were tested in this report are:

Hypothesis 1. A year of UFP measurements analyzed with Positive Matrix Factorization (3-day averages) and Chemical Mass Balance (monthly averages) can identify unique sources of UFPs in the Bay Area of San Francisco, Fresno, and Los Angeles that are consistent with emissions and meteorological patterns in those regions.

Hypothesis 2. Regional chemical transport models using standard emissions inventories combined with UFP source profiles can predict UFP concentrations and source distributions in major CA population centers including the Bay Area, San Joaquin Valley, and Los Angeles for episodes in the years 2000-2016.

Hypothesis 3. UFP number (total and/or from different sources) is positively associated with premature death in California.

Hypothesis 4. UFP mass (total and/or from different sources) is positively associated with premature death in California.

Hypothesis 5. UFP surface area (total and/or from different sources) is positively associated with premature death in California.

Hypothesis 6. Regions can be identified with sufficiently independent behavior for UFPs vs. other pollutants ($PM_{2.5}$, O3, NO, NO2, etc.) to identify associations with premature death without confounding effects.

1.4 Report Structure

This report is comprised of thirteen chapters, including introduction (Ch. 1) and conclusions (Ch13).

Chapter 2 describes a review and analysis of measured ultrafine particle concentrations in California between the years 1996 and 2016. Overall trends are discussed along with the likely factors that contribute to those trends.

Chapter 3 describes results from a year of intensive ultrafine particle composition measurements carried out at four sites in California (San Pablo, East Oakland, Fresno, and Los Angeles). Day-of-week cycles are identified for several of the ultrafine particle components and the implications for the weekly variation of ultrafine particle sources are discussed.

Chapter 4 performs a statistical analysis on the year of ultrafine particle measurements using the Positive Matrix Factorization (PMF) approach. The resolved factor profiles are linked back to sources where possible and comparisons are made between source contributions as a function of season and location.

Chapter 5 performs a second statistical analysis on the year of ultrafine particle measurements using the Chemical Mass Balance (CMB) approach. Identified source contributions are summarized as a function of season and location.

Chapter 6 tests a new photochemical mechanism in regional grid model calculations to determine if this mechanism would improve predictions of gas-phase oxidants that influence particulate nitrate and particulate secondary organic aerosol formation.

Chapter 7 introduces a nucleation algorithm into the UCD/CIT air quality model and tests the ability of the model to predict ambient concentrations of particles with diameter greater than 10 nm (N_{10}) across California in the year 2012. Source contributions to N_{10} are predicted for different locations throughout the state.

Chapter 8 compares predictions of $PM_{0.1}$ made by the UCD/CIT model to concentrations measured during the comprehensive year of sampling conducted in 2015-2016 as summarized in Chapters 3-5. $PM_{0.1}$ source contributions predicted by the UCD/CIT model are compared to measured source contributions calculated using the Chemical Mass Balance (CMB) model as discussed in Chapter 5. Final UCD/CIT predictions are resolved by chemical species, source contributions, and total concentrations.

Chapter 9 summarizes predictions made by the UCD/CIT model for long-term trends in regional ultrafine particle concentrations in California. Predictions are resolved by chemical species, source contributions, and total concentrations. Comparisons are made to the historical measurements summarized in Chapter 2.

Chapter 10 summarizes predictions of regional patterns in ultrafine particle concentrations in California using regional grid model calculations applied with 1km spatial resolution. Predictions are resolved by chemical species, source contributions, and total concentrations. Comparisons are made to the measurements that overlap with the simulation periods.

Chapter 11 extends the methods for ultrafine particle predictions developed for California across the entire continental United States focusing on the peak photochemical episode occurring in 39 major cities in the year 2010. Predictions are resolved by chemical species, source contributions, and total concentrations. Note that Chapter 11 is outside the scope of the current project and is carried out as a demonstration study to examine how the results in California compare to the results in the rest of the US. The peak summer photochemical period was chosen partly based on scientific interest (summer PM concentrations are highest in much of the US) and partly out of convenience (the meteorological fields and emissions had already been created for a separate project).

Chapter 12 performs a preliminary epidemiological analysis using the exposure fields developed in Chapters 7-10 combined with the California Teachers Study (CTS) cohort. Hazard ratios are resolved for multiple health endpoints using different models constructed from features of the ultrafine and fine particle exposure fields.

Chapter 13 draws conclusions from each of the segments of the entire project and makes recommendations for future work.

1.5 Background

Atmospheric UFPs account for a minor amount of total suspended particle mass, but a much more significant amount of particle surface area and the majority of the particle number. Fig 1-1 illustrates a typical particle size distribution for ambient aerosols measured in Fresno, CA, as an example [25]. Individual size distributions in Fig 1-1 show the (a) mass (dM), (b) surface area (dS), and (c) number (dN) distribution of the same particle population. Different modes of the distribution (mass, surface area, number) are dominated by different particle size ranges (Dp) which influences their potential health effects.

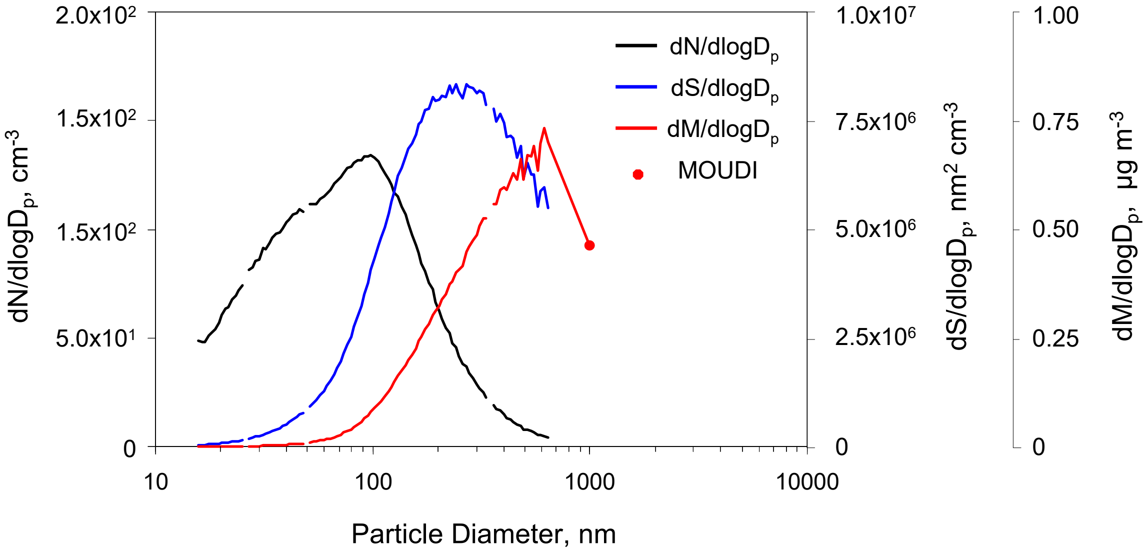

Figure 1-1: Ten day average PM size distribution: number ($dN/dlogD_p$), surface area ($dS/dlogD_p$), and mass ($dM/dlogD_p$) at Fresno, California, during the summer of 2006. The red circle represents the extension of SMPS mass measurement using MOUDI samples captured during the same sampling period. Ultrafine particles have diameter (Dp) < 100nm.

The majority of atmospheric UFPs are formed by chemical reactions (including combustion processes) with very little contribution from mechanical abrasion processes (sea salt, dust, tire wear, etc). UFPs in urban areas therefore mostly originate from dominant combustion sources such as motor vehicles, biomass combustion, food cooking, etc. Measurements have determined carbonaceous organic compounds and elemental carbon make up the majority of the UFP mass with smaller contributions from inorganic ions and metals [15, 16, 43]. UFPs have much larger ratios of surface area to volume compared to larger particles. The Kelvin effect generally enhances the vapor pressure of compounds above the surface of ultrafine particles, making ultrafine particle populations unstable and prone to spontaneous growth at the expense of reduced number concentrations over timescales of hours to days. UFPs are removed from the atmosphere by (i) condensational growth to larger sizes, (ii) coagulation with larger particles, (iii) dry deposition, and (iv) wet deposition. In general, these processes act more quickly on ultrafine particles than on particles in other size fractions, once again making the atmospheric lifetime of UFPs shorter.

A number of recent studies have characterized “quasi-ultrafine particles” defined to be those with diameter less than approximately 250 nm (see for example [44-49]). Quasi-ultrafine particles contain more of the primary particulate matter emissions from motor vehicles, biomass combustion, and food cooking than traditional ultrafine particles. The model predictions generated in the current study can be processed to predict quasi-ultrafine particle concentrations, but this task was beyond the scope of the current report.

2 REVIEW AND ANALYSIS OF MEASURED LONG TERM TRENDS IN AMBIENT ULTRAFINE PARTICLE CONCENTRATIONS IN CALIFORNIA

Preamble: Chapter 2 describes a review and analysis of measured ultrafine particle concentrations in California between the years 1996 and 2016. Overall trends are discussed along with the likely factors that contribute to those trends. This analysis identifies issues that will be addressed in the following chapters.

2.1 Introduction

Ultrafine particles (UFPs) and nanoparticles make up the smallest size fraction of airborne particles. By definition, UFPs are particles with an aerodynamic diameter ≤ 100 nanometers while the term nanoparticles is generally used to describe particles with diameters less than a few 10's of nanometers [15, 16, 18, 50, 51]. $PM_{0.1}$ is defined as the PM mass in the ultrafine particle size fraction while N_7 is the number concentration of particles with diameter greater than 7nm (dominated by particles with $7nm < Dp < 100nm$). UFPs make a small contribution to total particle mass due to their small size but UFPs make significant contributions to particle surface area (well correlated with $PM_{0.1}$) and UFPs dominate contributions to total particle number concentrations [43, 50-52]. Both $PM_{0.1}$ and N_7 are commonly used metrics that are considered in health effects studies.

This analysis reviews UFP measurements carried out in California over the past two decades to examine long-term trends in UFP concentrations. The assessment seeks to determine whether the trends in $PM_{0.1}$ and N_7 match long-term trends in fine particle mass ($PM_{2.5}$). $PM_{2.5}$ is used as a comparison point for the analysis because $PM_{2.5}$ concentrations have been continuously monitored in California and across the U.S. over the past several decades. Factors such as atmospheric mixing will have similar impacts on all particle sizes, and so a comparison of $PM_{2.5}$ and UFPs trends identifies changes associated with emissions and changing chemical regimes. In the sections below, the emissions control programs that have influenced ambient PM concentrations are reviewed, trends in UFPs over multiple decades are plotted, and conclusions are drawn about the correlation in long-term UFPs vs. $PM_{2.5}$ trends.

2.2 Factors Affecting Ultrafine Particle Emissions

Ambient UFPs originate from multiple sources that vary spatially and temporally, but most UFPs are the products of either combustion or secondary chemistry [18, 40, 43, 50, 53]. Combustion processes that are most important for UFP formation include biomass burning, on-road fossil fuel combustion, as well meat cooking and residential heating [18, 19, 40, 54-56]. In addition to direct emissions, UFP can also nucleate from low-volatility reaction products formed by photochemical atmospheric reactions [51, 57, 58]. Direct emissions tend to produce more localized UFP concentrations while nucleation events create more regionally dispersed concentrations over an urban or rural area [51]. Nucleation processes were not analyzed in the current report and so these effects are beyond the scope of the current analysis.

Numerous programs and regulations have been implemented over the past several decades to reduce atmospheric $PM_{2.5}$ concentrations. Examples of programs include, but are not limited to, advancements in motor vehicle technology, clean truck programs, residential wood burning advisories, and low-sulfur fuel for ships. The sections below examine these programs and their likely effects on UFP concentrations.

2.2.1 Motor Vehicle Technology

Motor vehicles are a significant source of UFPs in urban areas where heavy-duty vehicles (HDVs) (predominantly diesel) and on-road light-duty vehicles (LDVs) (predominantly gasoline) emit large numbers of particles to the atmosphere. Beginning in 1980, motor vehicle emissions have continuously evolved, often encouraged by regulations [59]. In 1987, the U.S. EPA and CARB began implementing emissions standards for heavy-duty engine manufacturers. Standards have progressively tightened, culminating in the 2007 engine standards and the requirements for Diesel Particle Filters (DPFs). These changes have strongly reduced emissions from heavy duty diesel engines [59]. The new standards also required heavy-duty diesel engines to use ultra-low sulfur diesel (ULSD) fuel (i.e., < 15 ppm sulfur) which decreased secondary PM formation. The widespread adoption of DPFs in the U.S and California has reduced UFP emissions from diesel engines by approximately 98% below original levels [18, 59-61]. Looking forward, CARB established the California Statewide Truck and Bus Rule in December 2008 requiring all heavy duty trucks and buses to retrofit their engines to reduce PM emissions by 85% before 2020 [62].

Tailpipe emissions from LDVs and medium duty vehicles (MDVs) powered by gasoline are a significant source of UFPs in urban areas. Beginning in 1980, more stringent regulations began developing for PM, Carbon Monoxide (CO) and total hydrocarbons (THC) motivating improved engine design and after treatment technology. In addition, the Global Warming Solutions Act of 2006 (AB 32) initiated a wide range of programs to reduce Greenhouse gas emissions (GHGs) including increases in automotive efficiency. Advancements in engine efficiency have led to improvements in Port Fuel Injection (PFI) engines and more recently the increased adoption of Gas Direct Injection (GDI) engines in LDVs and MDVs [63]. PFI gasoline engines improved continuously from 1980 to early 2000s. The more recently adopted GDI engines have increased fuel economy, but higher PM emissions rates compared to the best PFI engines [63]. Thus, trends in ambient UFP may reflect the increased use of GDI engines with higher PM emissions.

2.2.2 Clean Truck Programs

The Ports of Oakland, Long Beach (POLB) and Los Angeles (POLA) have implemented cleaner drayage truck fleets over the past decade as part of CARB's Drayage Truck Regulation to reduce emissions containing toxic soot (PM) and smog forming nitrogen oxides (NO_x) [64]. Drayage fleet emissions depend on the distribution of vehicle age, emission control devices and site conditions. The State regulation applies to all on-road class 7 and class 8 diesel-fueled vehicles with a Gross Vehicle Weight Rating (GVWR) >26,000 pounds regardless of origin or visiting frequency [64]. Drayage trucks operate near ports and rail yards arriving at the terminals via freeway interchanges to unload and load transport cargo. The emissions from these trucks have been shown to contribute to adverse health effects in nearby communities [64].

In 2006 the governing boards of POLA and POLB approved the San Pedro Bay Ports Clean Air Action Plan (CAAP). A central element to this plan is the Clean Truck Program that banned all pre-1989 trucks from the port in 2008. In addition, the program banned 1989-1993 trucks as well as retrofitted trucks with model years 1994-2003 in 2010 and by 2012 it banned all trucks that did not meet the 2007 Federal Clean Truck Emission Standards [65]. The Clean Truck program reduced Port truck emissions by roughly 70% in the first year and over 80% in 2012 when the program became fully implemented [65].

The Port of Oakland partnered with the Bay Area Air Quality Management District (BAAQMD) and West Oakland Environmental Indicators Project to develop the Maritime Air Quality Improvement Program (MAQIP). As part of a broad effort to reduce Port emissions, the Port of Oakland committed to an 85% reduction in sea-port related diesel health risk by 2020 based on a 2005 baseline [66]. A key element to achieving this commitment is the Port of Oakland's Comprehensive Management Truck Plan (CTMP) that requires all drayage trucks to use after-treatment devices for emissions control. The Port of Oakland's Seaport 2015 Emission Inventory reported a 98% reduction in truck DPM compared to the 2005 inventory displayed in Figure 2-1 below [66].

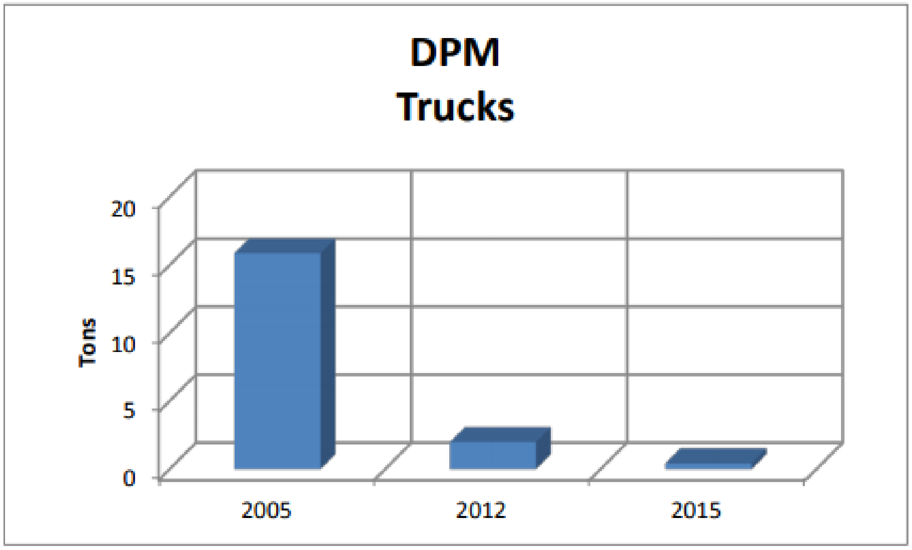

Figure 2-1: Port of Oakland Drayage Truck DPM Emission Inventory for 2005, 2012 and 2015 [66].

2.2.3 *Residential Wood Burning Advisories*

Smoke from Residential Wood Combustion (RWC) for home heating continues to be the leading source of winter PM pollution in northern California. Ambient PM concentrations from RWC peak during winter stagnation events associated with low wind speeds and inhibited vertical mixing. Stagnation events are often caused by a high-pressure (warm) air mass that subsides over a colder air mass below (cooled by clear-sky radiation at night). The resulting stagnation events trap source emissions near the surface that would otherwise be diluted under normal atmospheric conditions.

The major pollutants contained in wood smoke include PM, CO, NO_x as well as VOCs and other toxic air pollutants (TACs) such as benzene, formaldehyde and benzo-a-pyrene, a polycyclic aromatic hydrocarbon (PAH) [67]. The health effects associated with residential wood smoke include burning of eyes as well as respiratory inflammation that can induce coughing, decrease lung function, and increase cases of acute and chronic bronchitis [67]. Epidemiological evidence has shown long-term exposure leading to certain types of cancers and birth defects [67, 68].

Wood burning is regulated by local air quality management districts across California through use of no-burn advisories and the implementation of updated building codes for housing developments that reduce or restrict various types of residential wood burning devices. Burn day advisories are typically issued based on the local Air Quality Index (AQI) in each control district. Higher AQIs indicate increasing health risks associated with air pollution. No-burning advisories generally range from burning discouraged (moderately unhealthy AQI) to a complete prohibition on burning (extremely unhealthy AQI).

The San Joaquin Valley Unified Air Pollution Control District implemented Rule 4901 to create more stringent controls on residential wood burning beginning in 2003. This rule applies to areas that are below 3,000 feet elevation with natural gas heating capabilities. An Environmental Health Evaluation submitted in 2008 showed the seasonal impact the rule made in reducing $PM_{2.5}$ concentrations in Fresno [69]. A diurnal profile of $PM_{2.5}$ concentrations during pre and post-rule violation days is displayed in Figure 2-2 below. On average, the diurnal concentration profile of the post-rule violation days is 12% lower than the pre-rule violation days, and 26% lower during the evening hours when wood burning is most likely to occur.

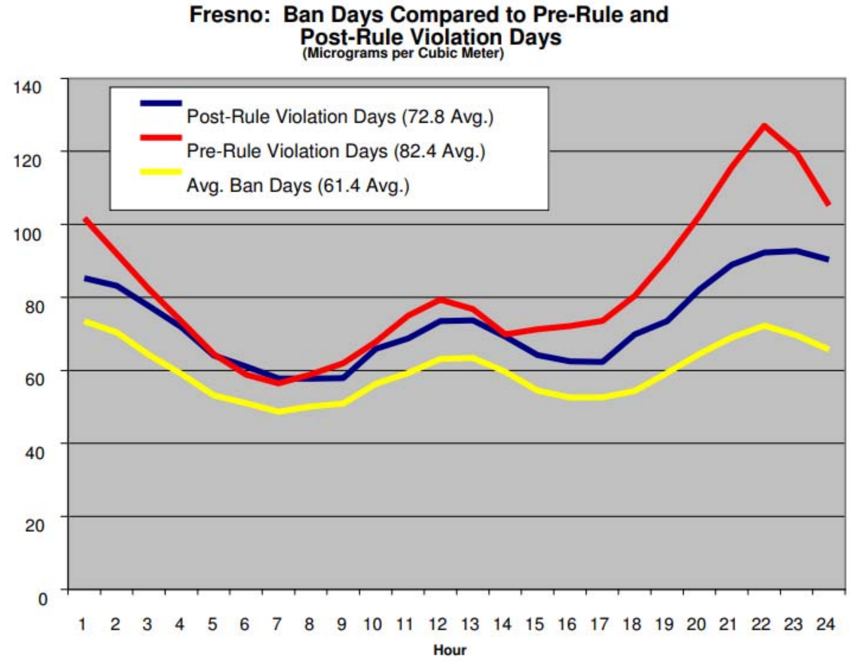

Figure 2-2: Average diurnal profile of $PM_{2.5}$ in Fresno, CA during violation days before and after the Rule 4901 [69].

The Bay area Air Quality Management District (BAAQMD) adopted a wood burning device rule in 2008. These rules included no burn day advisories, use of cleaner burning devices, proper labeling of fire wood sold in the Bay Area, bans on burning of toxic substances and limitations on excessive burning. In 2015, BAAQMD reduced the number of exemptions to the original wood burning rule adopted in 2008. These included bans on wood burning devices in new building developments as well as updated requirements on the registration of burning devices.

The Sacramento Metropolitan Air Quality Management District (SMAQMD) also enacted a curtailment program for wood burning. SMAQMD partnered with a local Low-Income Weatherization Program from 2008 to 2011 to fund installments of less polluting wood devices and gas stoves in low-income areas [68].

The adoption of wood burning restrictions and regulations in California has coincided with a major reduction in ambient PM concentrations since 2003 [69]. It is difficult to directly attribute these reductions to wood burning rules without detailed measurements before and after the rule adoption, but the available evidence does suggest that wood burning rules have been effective at reducing $PM_{2.5}$ concentrations [25, 69].

2.2.4 Low Sulfur Fuel for Ships

Ocean-Going Vessels (OGVs) typically use Heavy Fuel Oil (HFO) which has a high sulfur content leading to high PM and SO_X emissions [70, 71]. In 2009, CARB adopted the regulation "Fuel Sulfur and Other Operational Requirements for OGVs within California Waters and 24 Nautical Miles of the California Baseline" which requires OGVs visiting California seaports to use cleaner marine distillate fuels to reduce PM, nitrogen oxides and sulfur oxide emissions [71, 72]. Distillate fuel has a lower sulfur content than HFO. Following the 2009 regulation on OGVs, a study from 2009 to 2011 was conducted to assess the air quality impact of the switch to distillate fuels [71]. The study measured changes in non-sea-salt sulfate ($NSS\text{-}SO_4$), Sulfur Dioxide (SO_2) and $PM_{2.5}$ as well as vanadium (V) (frequently used as a specific marker for HFO combustion). The results showed a substantial reduction in vanadium followed by a $3.1 \pm 0.6\%$ or 0.28 ± 0.05 μg m^{-3} reduction in $PM_{2.5}$ suggesting that the increased controls on the sulfur content of OGVs has contributed to a decline in ambient PM concentrations since 2009 [71]. In addition, according to the International Maritime Organization (IMO), ships in emission controlled areas were required to use fuel oil with a Sulfur content of $\leq 0.10\%$ m/m (mass by mass) as of January 1st, 2015 which decreased from a previous $\leq 1\%$ m/m requirement prior to the end of December, 2014 [73].

2.2.5 Airports

In 1998 the South Coast Air Quality Management District (SCAQMD) conducted several studies near the Los Angeles International Airport (LAX) as a response to community concerns regarding exposure to airport related pollutants [74]. The SCAQMD analyzed PM_{10} but could not identify any specific markers related to airport operations at the time. In the spring of 2003, a study was conducted by the University of Southern California (USC) to analyze potential impacts on downwind mixed-use communities from airport operations at LAX. This study focused on airports as a potential source of UFPs which had not been previously evaluated [74]. A number of studies under controlled conditions have been performed to measure emissions from jet engines both on the ground and in flight [75-77]. The combustion process of jet engines uses large quantities of fuel during takeoff and landing. UFPs, VOCs, CO, carbon, NO_x and sulfuric acid are all pollutants released during jet engine combustion [74-77]. In addition, ground operations on the terminal roadways that can contribute to airport related pollution include aircraft taxiing as well as airport vehicles running on either diesel, compressed natural gas or gasoline. The results of the 2003 USC study found low pollutant levels at an upwind coastal site of LAX dominated by particles 90 nm in diameter where N_7 ranged between 580 and 3800 particles cm^{-3} and higher UFP counts 500 meters downwind of LAX dominated by particles 10 to 15 nm in diameter with average counts of 50,000 cm^{-3}. The study also noted peaks in UFPs during landings and takeoff suggesting that there is an association between airport operations and elevated UFP levels downwind. More recent studies carried out by researchers at USC confirm the importance of airports as an emissions source of UFPs [74, 78, 79]. Although the health effects associated with communities nearby airports still remains unclear, this study emphasized that there is a need to further investigate the potential health risks associated with air pollutants from airport operations and evaluate potential aircraft emission standards.

The Vision 100 program enacted by the EPA in 2003 is intended to encourage voluntary emission reduction projects from airport ground operations funded by the Federal Aviation Administration (FAA) [80]. In addition, in 2016 as part of the International Civil Aviation Program (ICAO), the U.S. agreed to contribute to reducing carbon emissions from commercial aircraft as part of an effort to decrease the impact of climate change. Airplane manufacturers are in the process of constructing more fuel efficient aircraft which are expected to meet the ICAO emissions standards [80, 81]. Even though these standards target the reduction of GHG emissions, there is also potential for PM reductions. In the future, health effects associated with aviation emissions will also depend on changes in background concentrations and in non-aviation emissions and population growth [81].

2.2.6 *Economic Activity*

Criteria air pollutant emissions are proportional to generation activities which are reflected by economic indicators such as gross domestic product (GDP). During the financial crisis between the years 2007 - 2009, economic output decreased significantly suggesting that upstream activities were also suppressed. Figure 2-3 shows that vehicle miles traveled (VMT) declined significantly between 2007 to 2009 during the financial crisis [82].

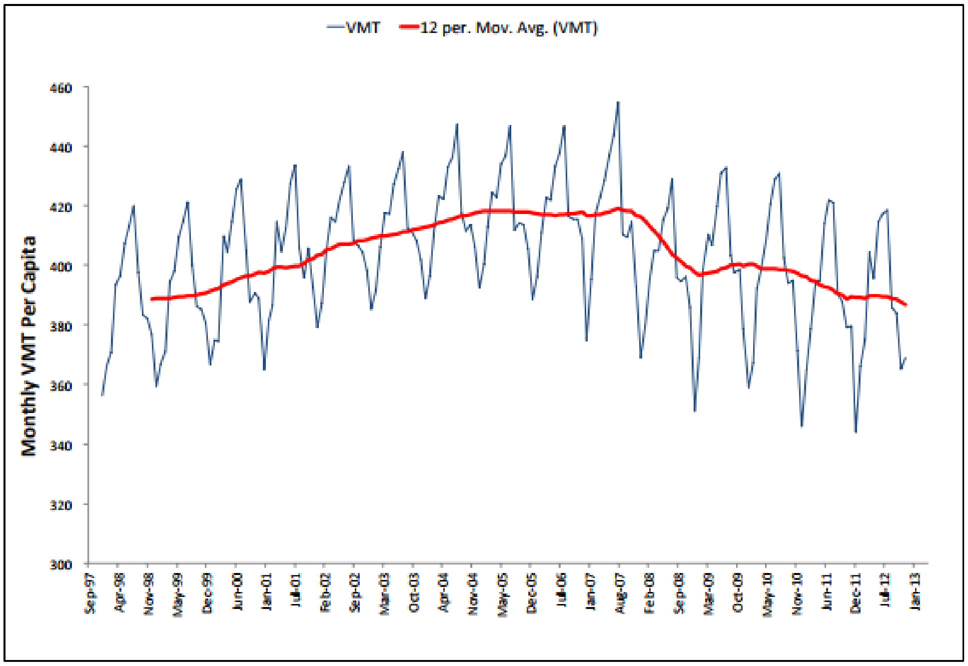

Figure 2-3: Caltrans VMT trends from 1997 to 2013 [82].

Figure 2-4 illustrates that increases in the unemployment rate are associated with decreases in vehicle usage which decreases VMT [82]. This data was obtained from the Bureau of Labor Statistics and the Federal Highway Administration (FHWA). The report's statistical analysis shows that the correlation slope between VMT and unemployment from 1990 to 2011 is strongly negative (-0.85) at the 0.01 significance level. Thus, when the employment rate declined during the recession, there were fewer passenger vehicles commuting to work. In addition, commercial heavy-duty vehicles (HDVs) are typically the largest polluters on state highways, emitting more grams per unit energy relative to emissions from passenger vehicles, and during the recession there were likely fewer commercial vehicles in route compared to periods when the economy was thriving [82, 83]. The decline in VMT from both passenger and commercial vehicles may have played a role in the decline in PM 2007 to 2009 [62, 82-84].

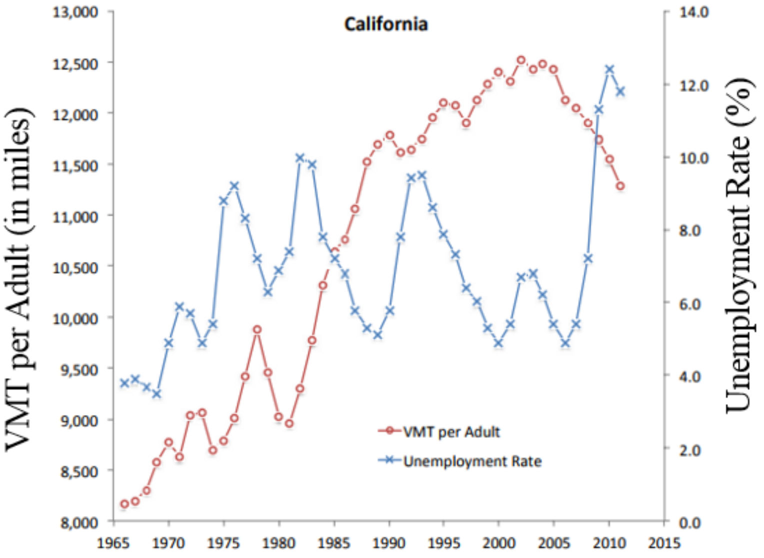

Source: Bureau of Labor Statistics and FHWA

Figure 2-4: VMT per adult (red) and unemployment rate (blue) from 1965 to 2011 according to the Bureau of Labor Statistics and the Federal Highway Administration (FHWA) [82].

2.3 Review and Analysis Methodology

This review and analysis includes a total of eight different studies from 1996 to 2016 in various locations throughout California including the Sacramento Valley, San Francisco Bay Area, San Joaquin Valley and the South Coast Air Basins. Table 2-1 below summarizes details of each study reviewed in this report including the name of the study, location, month(s), years and feature analyzed as well as instrumentation specs and the citation of the study. Section 2.3.1 describes the methods used for studies where PM$_{0.1}$ and PM$_{2.5}$ Elemental Carbon (EC) and Organic Carbon (OC) data were sampled. Section 2.3.2 describes the methods used for the studies where N$_7$ was collected and analyzed.

Table 2-1. A summary of studies included in the analysis with their respective location, time period, instrumentation size fractions, and citation.

Study	Location	Month(s)	Year(s)	Feature	Instrument	Cut Points	Citation
Trajectory Study	Fullerton, Long Beach & Riverside	9-10	1996	Mass	MOI MSP Corp., model 110	0.56 µm ≤ D_p≤ 1.8 µm	[85]

Study	Location	Month(s)	Year(s)	Feature	Instrument	Cut Points	Citation
Detection of Alkaline Atmospheric Particles	Bakersfield	1	1999				[15]
CRPAQS	Bakersfield, Davis, Modesto & Sacramento	12 (2000), 1-2 (2001)	2000 & 2001		MOUDI (MSP Corp., model 110)		[86-88]
CHS	12 communities in Southern CA.	1-12	2001	N_7	CPC (TSI Model 3022A)	$D_p \geq 7$ nm	[57]
SAHERC	Fresno, Coalinga	8-9, 2	2006-2010	Mass	MOUDI (MSP Corp., model 110)	0.56 µm ≤ $D_p \leq$ 1.8 µm	[25]
	Sacramento	10-12 (2009), 1-11 (2010)	2009-2010				[19]
MATES-IV	10 fixed sites in Southern CA.	7-9	2012	N_7	(CPC Model 651; Teledyne API, San Diego, CA)	$D_p \geq 7$ nm	[56]
Post MATES-IV	Anaheim, Central LA, Fontana & Rubidoux	1-12	2013-2015	N_7			
California Four Cities UFP Study	Fresno, East Oakland, San Pablo & USC	8-12 (2015), 1-7 (2016)	2015-2016	Mass	MOUDI (MSP Corp., model 110)	0.56 µm ≤ $D_p \leq$ 1.8 µm	Currently in process of publication

2.3.1 Ultrafine Particle Mass ($PM_{0.1}$)

Ultrafine Particle Mass was collected in most of the studies considered in this report using Micro-Orifice Uniform Deposit Impactors (MOUDIs). There are many other types of impactors and samplers designed to collect time resolved and size-segregated PM including but not limited to the Harvard Impactor (HI), Personal Cascade Impactor Sampler (PCIS), Electrical Low Pressure Impactor (ELPI), Davis Rotating-drum Universal-size-cut Monitor (DRUM), Rotating Drum Impactor (RDI), Dekati Low Pressure Impactor (DLPI) and Dekati Gravimetric Impactor (DGI) [89-91]. The HI is typically utilized for PM_{10} and $PM_{2.5}$ sampling and the PCIS has been used in quasi-ultrafine particle studies (aerodynamic diameter ≤ 0.25 µm). A PCIS does not measure true $PM_{0.1}$ mass and therefore is not included in this analysis [49, 89]. Furthermore, ultrafine particle mass measurements made in California using the DRUM, RDI, ELPI, DLPI samplers have not been widely reported in the scientific literature. The current study therefore focuses on MOUDI samples to characterize long-term trends in California.

Particles reported here were collected on MOUDI stage 10 which includes particles in the size range 0.056 to 0.1 µm in diameter. This size range accounts for the majority of the ultrafine particle mass in a typical ambient particle size distribution. Some of the particles with diameter between 0.056 to 0.1 µm can bounce off MOUDI stage 10 and be collected by the after filter. Larger particles bouncing off upper impaction stages may also knock UFPs off stage 10. Anti-bounce coatings may be used to reduce particle bounce, but these coatings can contaminate subsequent trace chemical analysis. Many of the studies reviewed in the current report used an AIHL-design cyclone to remove larger particles from the sample stream, and relied on the inherent stickiness of smaller particles to minimize bounce.

Some of the studies considered in this report summed the mass collected on MOUDI stages 5-10 including the after-filter (AF) which corresponds to particles with diameters from ~0.005-1.8 μm in diameter. These MOUDI masses were summed to calculate the fine particle mass ($PM_{1.8}$) for trends analysis when available. When MOUDI stages 5-9 were not available, nearby filter measurements of $PM_{2.5}$ were used to represent fine particle trends. For example, the San Joaquin Aerosol Health Effects Research Center Studies in Section 3.1.4 (b) and 3.1.4 (c) as well as the California Four Cities UFP Study in Section 3.1.5 all utilize the US EPA National $PM_{2.5}$ Chemical Speciation Network (CSN) data for trends comparison to $PM_{0.1}$ because only UFPs (stage 10) was measured with the MOUDIs. Methods used for the EPA data are described in Section 3.1.4 (b).

Concentrations summarized for studies spanning 1 year or longer were evaluated by seasons in the current report. Months June-August represented Summer (S), September-November represented Fall (F), December-February represented Winter (W) while March through May represented Spring (Sp).

2.3.1.1 Trajectory Study 1996

The Trajectory Study (T96) was conducted in early fall of 1996 by researchers at the California Institute of Technology. The study objective was to determine how particles and gases in the same air mass change during transit over Los Angeles [85]. The motivation behind this study was to understand the chemical and physical processes involved in particle evolution to enhance the efficacy of air quality models as tools in the design of air pollution control strategies [85, 92].

Ambient air samples were collected over the course of a 2 week period from September 21st - October 2nd, 1996 [85]. Instruments were located at three urban sites in Los Angeles, CA: Long Beach, Fullerton, and Riverside. Measurements were taken at each urban site over a 4 hour period, 11-15 PST, on each day of two 2-day periods of intensive sampling with the exception of Riverside. The first period was September 23rd-24th for Fullerton and Long Beach and September 21st-26th for Riverside. The second period was October 1st-2nd at all sites. These sampling days were chosen to account for the travel time of air parcels during periods of onshore flow.

The T96 Study utilized a pair of cascade impactors at each site, one MOUDI (MSP Corp., model 110) loaded with Teflon substrates and one non-rotating Micro-Orifice Impactor (MOI MSP Corp., model 110) loaded with aluminum substrates in order to measure size-segregated mass and chemical composition of fine particles [85, 92]. Both impactors utilized a Teflon-coated cyclone separator to remove coarse particles ($D_p \geq 1.8$ μm). A total and fine particle filter sampler was also used to collect particles on Teflon and quartz fiber filters for consistency checks. In addition, an electrical aerosol analyzer (EAA, TSI model 3030) was used at all three sampling locations. Laser optical particle counters (OPCs, Particle Measuring Systems model ASASP-X) were used at Long Beach and Riverside. Further, impactor and filter-based measurements were taken at Santa Catalina Island to measure background concentrations.

Samples collected on aluminum substrates and quartz fiber filters were analyzed for EC and OC which accounted for the majority of the ultrafine particle mass in the analysis. The 10-stage non-rotating cascade impactor (MOI) loaded with Aluminum substrates is seen in Figure 2-5 below [92, 93]. Prior to chemical analysis, potential organic contaminants were eliminated from the aluminum substrates by baking for 40 to 50 hours at 550 °C and removed from the quartz filter substrates by baking for 10 hours at 550 °C [92]. Teflon substrates collected in the second MOUDI were cut in half to support the full range of chemical analyses. The first half of each Teflon impactor substrate underwent ion chromatography (Dionex Corp, model 2020i) for anions and the second half underwent neutron activation analysis to detect trace elements [92-94]. These components did not make significant contributions to ultrafine particle mass and will not be discussed further in this report.

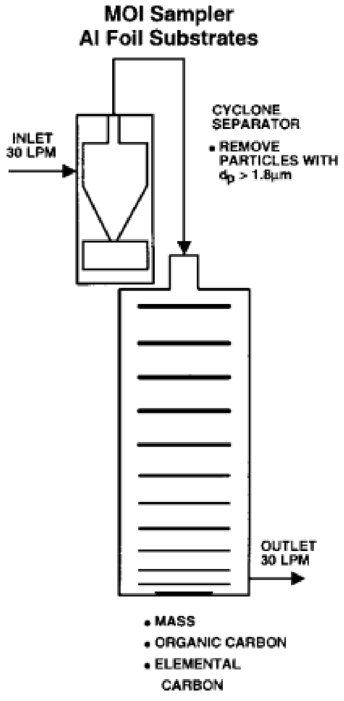

Figure 2-5: MOI MSP Corp., Model 110 [92]. The cut point diameters of the stages 5-10 measured in μm are 1.8, 1.0, 0.56, 0.32, 0.18, 0.1, and 0.056 respectively.

A thermal-optical carbon method was used to analyze the EC and OC collected on the aluminum substrates. The original method was designed for quartz fiber filters but modifications were made in order to perform the analysis on impactor substrates [60, 85, 95]. Mass concentrations were derived by pre-weighing and post-weighing foil and Teflon impaction substrates and Teflon AFs using a Mettler model M-55-A microbalance.

Fine and total suspended particle samplers were used as important checks on the overall quantity of fine PM in the atmosphere. Particle filter samples in comparison to the summation of the impactor stages show agreement within ±10% for EC and ±25% for OC on average [85]. The impactor samples showed higher EC and lower OC compared to the filter samples [85].

The T96 Study ultimately showed that the particle characteristics change significantly during transport from Long Beach to Riverside. The number of large particles that contain sodium decreases during transport away from the coast and the accumulation of complex particles containing ammonium, nitrate and carbonaceous material increases. The current re-analysis of the T96 Study represent fine PM mass using mass summed from Stages 5 through 10 averaged over the 4 days at Fullerton and Long Beach and averaged over 8 days at Riverside.

2.3.1.2 Bakersfield 1999

The Bakersfield 1999 study was designed to make the first measurements of UFPs in the San Joaquin Valley (SJV) to improve our understanding of potential health effects associated with the prominent build-up of pollutants in the region [15]. These results were compared with previous measurements made in Los Angeles to better understand how different sources and formation processes influenced UFP concentrations in Bakersfield.

The Bakersfield 1999 study was conducted over a 7 day period from January 14th – January 23rd, 1999. Samples were collected daily between the hours of 10-18 PST on the roof of the CARB office located at 5558 California Avenue, Bakersfield, CA [15]. The sample collection methods in this study were nearly identical to the T96 Study. Samples of airborne PM were collected using a filter-based sampler and two MOUDIs to allow for consistency checks as well as a broader range of chemical analyses. The filter-based sampler and MOUDIs were equipped with an Air and Industrial Hygiene Laboratory (AIHL) cyclone separator to remove coarse particles. The first MOUDI (MSP Corp., model 110) was loaded with 47-mm aluminum substrates and a 37-mm quartz AF (Pallflex 2500 QAO) that were analyzed for total carbon, OC and EC [15]. The second MOUDI used 47-mm Teflon substrates (Teflo, R2PJ047) and a 37-mm Teflon AF (Zeflour, P5PJ037). Potential containments on the aluminum substrates and the quartz AF were removed by baking for 48 hours at 550 °C. All samples were stored in sterile Petri dishes at -20 °C until chemical analysis. Teflon substrates were cut in half and the first half was analyzed for water soluble ions while the second half was analyzed for trace elements using proton induced X-ray emissions (PIXE) and X-ray fluorescence (XRF). The EC/OC analysis in this study was identical to the method used in the T96 Study. The aluminum and Teflon substrates were weighed multiple times using a CAHN-33 microbalance.

The comparison of the mass of $PM_{2.0}$ collected on filter-based sampler with the mass of $PM_{1.8}$ collected using the MOUDI showed a correlation coefficient (R^2) of 0.93 [15]. Further, the comparison of OC from the filter-based sampler and the OC from MOUDI equipped with foil substrates showed an R^2 of 0.945 [15]. The study noted that these correlations are typical of chemical species measured in airborne particles. Minor differences in MOUDI vs. filter sampler performance during the Bakersfield 1999 Study and the T96 study may be caused by the configuration of the filter sampler used for the performance evaluation, differences in meteorological conditions during sample collection, and differences in the analysis methods for the split of EC and OC from impactor substrates.

The results of the Bakersfield study noted that the fine-particle mass concentrations decreased from 92 µg m^{-3} on January 14, 1999 to 3 µg m^{-3} on January 21st, 1999 as the stagnation episode dissipated. The chemical analysis also showed that the UFPs were primarily composed of OC on both the heavily and less heavily polluted days. Data representative of $PM_{2.5}$ for Bakersfield 1999 in this review and analysis was averaged and summed using the same methods as the T96 Study.

2.3.1.3 *California Regional PM10/$PM_{2.5}$ Air Quality Study (CRPAQS)*

The California Regional PM_{10}/$PM_{2.5}$ Air Quality Study (CRPAQS) was a multi-agency collaboration carried out as part of the Central California Air Quality Studies (CCAQS). The study was conducted to better understand causes of excessive PM in Central California (primarily the San Joaquin Valley) and develop methods to improve air quality in this region [86-88]. In the U.S, the SJV is the largest nonattainment zone for PM_{10} and $PM_{2.5}$ and multiple studies have noted that the variability in topography, meteorology and terrain in the SJV play a major role in the distribution and build-up of PM across the region [25, 69, 86, 88].

Samples included in this study were collected during separate winter time intensive operating periods (IOPs) from December 16, 2000- February 3, 2001 at Sacramento, Modesto, Bakersfield and Davis, CA [16, 54]. IOP dates were selected based on air quality forecasts.

Table 2-2. IOP dates during CRPAQS [86-88].

IOP1	12/15/2000 – 12/18/2000
IOP2	12/26/2000 – 12/28/2000
IOP3	1/4/2001– 1/7/2001
IOP4	1/31/2001 – 2/3/2001

Sample collection methods were identical to those used during the Bakersfield 1999 study. Two MOUDIs and a filter-based sampler (RAAS2.5-400, Andersen Instrument) were equipped with AIHL cyclone separators and collected samples during the day (10-18 PST) and night (20-8 PST) at all sites with the exception of Davis which was operated during hours 0-22 PST [43, 86]. A scanning mobility particle sizer (SMPS, TSI Model 3936 L25) was used at the Modesto site during IOP3. At each site, one of the MOUDIs was loaded with 47-mm aluminum substrate and 37-mm quartz AF substrate (Pallflex 2500 QAO) while the other was loaded with 47 mm Teflon substrates

(Teflon R2PJ047) and a 37 mm Teflon AF (Zeflour, P5PJ037). The filter-based sampler collecting $PM_{1.8}$ contained 6 sample legs where the first leg had a Teflon filter (R2PJ047, Pall Corp.) followed by two glass fiber filters (Type A/E, Pall Corp.) and the fifth leg contained an unheated quart fiber filter (QAO 47, Pall Corp.). Each aluminum substrate and quartz AF was baked prior to analysis to remove preexisting carbon. All samples were stored in sterile Petri dishes at -18 ºC until chemical analysis [16]. The aluminum and Teflon substrates were weighed before and after sampling using a CAHN-33 microbalance to determine gravimetric mass concentrations. Total particle mass from the MOUDIs was also calculated by summing all of the measured chemical components.

Teflon filters were extracted with 75% acetone (FisherOptima grade) and 25% 1N HNO_3 (Fisher Trace Metal Gradediluted with MilliQ ultra-pure water) and evaporated under 99.9995% pure nitrogen prior to being analyzed by Inductively Coupled Plasma Mass Spectrometry (ICP-MS, Agilent 7500i).

A Thermal Optical Transmittance method (TOT) based on the National Institute for Occupational Safety and Health (NIOSH) 5040 method was used to determine EC and OC concentrations [16, 96]. In the NIOSH 5040 method, the OC is developed in an atmosphere of Helium during a stepwise increase in temperature to 870 ºC. The initial temperature ramp in the CRPAQS study, however, was modified from the original NIOSH 5040 method and instead increased to only 800ºC to prevent the substrates from melting. During the second stage of the chemical analysis, the temperature is decreased and an Oxygen-He mix is added as the temperature ramps back up to 900 º C. An example of a typical thermogram displaying a commonly used temperature ramp and analysis time is displayed in Figure 2-6 below.

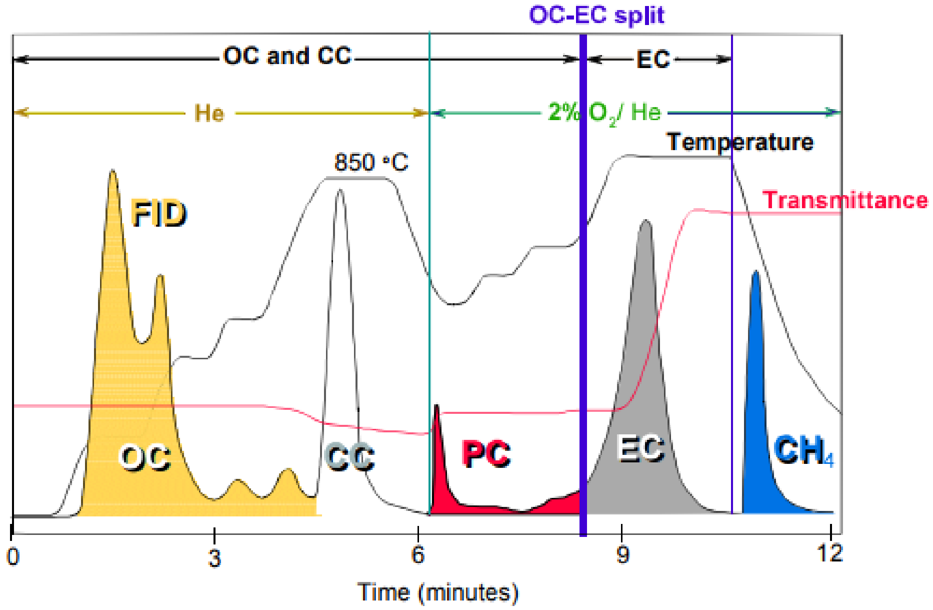

Figure 2-6: Example Thermogram for EC/CO analysis. Figure from the NIOSH Manual of Analytical Methods (NMAM) [96].

The “blackness” of the sample is evaluated during both phases of the EC/OC analysis using laser transmittance in order to correct for the pyrolized EC generated during the analysis [96, 97]. Sample blackness generally increases during the first phase of the analysis as carbon pyrolyzes to EC. Sample blackness begins to decrease following the introduction of oxygen into the oven during phase 2 of the analysis. Pyrolyzed EC is said to be completely removed when the value of the filter transmittance reaches the starting value. The opaqueness of the foil substrates loaded in MOUDIs does not allow for the determination of the EC/OC split. Thus, the fraction of OC developed on the quartz filters in the O_2-He atmosphere was used in order to correct the ratio of EC/OC measurements on MOUDI foil substrates. The adsorption artifact of gaseous OC on quartz filters was removed by subtracting the amount of carbon adsorbed on downstream quartz filters from the upstream measurements. No backup quartz filters were used in Sacramento and Davis so the corrections of the carbon concentrations were done by subtracting the average of the gas-phase adsorbed fraction from the other locations (approximately 15%). Impactor substrates have negligible adsorption because they have smaller surface areas.

For a consistency check, the MOUDI filter samples and filter-based samples were compared and the carbon agreement was reported to have improved as concentrations increase to above 1 µg m^{-3}, however, a correlation coefficient was not reported for EC and OC [16]. The reported minimum detection limits for 8 hour, 12 hour and 22 hour samples for EC and OC were 0.11 µg m^{-3}, 0.07 µg m^{-3} and 0.04 µg m^{-3} respectively and the average uncertainty for the EC and OC measurements was 8.7%.

The results from CRPAQS showed that $PM_{0.1}$ did not follow the same trends as $PM_{1.8}$ and that UFPs followed a very different diurnal pattern where nighttime concentrations were 50% higher than daytime concentrations [16].

In the current review and analysis, each EC and OC sample concentration (µg m^{-3}) reported in the CRPAQS study was multiplied by the number of hours over which that sample was taken, summed with other samples collected on the same day and then divided by the number of hours sampled over that day in order to determine a daily average for $PM_{0.1}$ (Stage 10) and $PM_{1.8}$ (Summation of Stages 5-10). The data representative of EC and OC $PM_{0.1}$ and $PM_{1.8}$ was calculated by taking the average of all daily averages over all IOP sampling days per location. This resulted in one averaged $PM_{0.1}$ and $PM_{1.8}$ value for each location during the CRPAQS study.

2.3.1.4 San Joaquin Aerosol Health Effects Research Center (SAHERC) Studies

Three separate SAHERC studies were carried out in the Central Valley by researchers at the University of California, Davis (UCD). The studies carried out in Fresno (urban) and Westside or Coalinga, CA (rural) between 2006 and 2008 used the same methodology to collect $PM_{0.1}$ and $PM_{2.5}$ during summer and winter seasons. The SAHERC measurements made in Sacramento in 2009-2010 used a different protocol to measure $PM_{0.1}$ over an entire annual cycle. The corresponding $PM_{2.5}$ measurements were obtained from the US EPA National $PM_{2.5}$ Chemical Speciation Network (CSN). The sections below describe the sampling schedules and methodologies in greater detail.

2.3.1.4(a). Fresno 2006-2007 and Westside 2007-2008

The objective of the SAHERC Fresno and Westside studies was to better understand the link between exposure to different sources of ultrafine particles and human health effects [25]. Both a size-resolved source apportionment analysis and exposure assessment were conducted at Fresno and Westside in central California's heavily polluted SJV during the winter and summer months. Ambient PM samples at Fresno were collected during the summer of 2006 and winter of 2007 and at Westside during the summer of 2007 and winter of 2008. OC and EC concentrations used in this analysis were weekly averages from samples collected between the hours of 9-15 PST in a 2-week pattern [25]. Table 2-3 below lists the actual dates the samples were collected.

Table 2-3. Sampling dates for Fresno and Westside

Location	Season	Week 1 Dates	Week 2 Dates
Fresno	Summer	9/4/2006 – 9/9/2006	9/12/2006 – 9/16/2006
	Winter	2/13/2007 – 2/17/2007	2/20/2007 – 2/24/2007
Westside	Summer	8/14/2007 – 8/20/2007	8/21/2007 – 8/25/2007
	Winter	2/6/2008 – 2/11//2008	2/12/2008 – 2/17/2008

The study used a molecular marker chemical mass balance (MM-CMB) method for source apportionment and a Multiple Path Particle Dosimetry Model (MPPD v 2.0) for respiratory deposition calculations [25]. Six MOUDIs (MSP Corp., Model 110) were operated in this study to collect samples in different size fractions below 1.8 μm in order to analyze the size distribution of OC, EC, trace organic compounds and metals. Three MOUDIs were operated with Teflon (R2PJ047, Pall Corp.) substrates to perform gravimetric and metals analyses and the other three MOUDIs used aluminum substrates and quartz fiber filter substrates for EC/OC analysis and organics speciation analysis. Foil and quartz filters were analyzed for molecular markers used in source apportionment by the Wisconsin State Laboratory of Hygiene. A filter-based method (similar to the one employed during CRPAQS) was used in this study to act as a check on the quality of the MOUDI samples. All other methods carried out pre and post chemical analysis are identical to the CRPAQS study [25, 87]. Refer to the Section 3.1.3 for details.

The results from SAHERC studies in Fresno and Westside showed total $PM_{1.8}$ ranged from 9.5 $\mu g\ m^{-3}$ in the summer of 2007 at Westside to 17.4 $\mu g\ m^{-3}$ in the winter of 2007 at Fresno and $PM_{1.8}$ OC from 1.6 $\mu g\ m^{-3}$ to 4 $\mu g\ m^{-3}$. The trends analyzed in this study show the success of emissions control programs designed to control wood burning within the SJV and the effects of stagnation events on $PM_{0.1}$ OC. Data from this study was provided as individual weekly averages for each stage 5-10 including a MOUDI averaged sum of stages 5-10. The two weeks were averaged together to determine EC and OC values for the winter and summer events at Fresno and Westside.

2.3.1.4(b). Fresno Summer 2009 and Winter 2010

The overall objective of the Fresno 2009-2010 study was to combine measurements and model analysis for UFPs to estimate $PM_{0.1}$ exposure fields in the SJV. The study was carried out in Fresno, CA. Measurements were made in the Summer of 2009 and Winter of 2010 using methods identical to those described in Section 3.1.3. The specific study dates are listed in Table 2-4 below. Six MOUDIs (MOUDI model 110, MSP Corp.) were used to collect ambient $PM_{1.8}$ in six size fractions. Three MOUDIs were operated with aluminum substrates and quartz fiber filter substrates for EC/OC as well as detailed organics speciation analysis and the other three MOUDIs used Teflon substrates (R2PJ047, Pall Corp.) for metals analyses using ICP-MS. Bulk $PM_{1.8}$ samples were collected using Teflon and quartz filters with co-located Reference Ambient Air Samplers (RAAS, RAAS2.5e400, Andersen) operating alongside MOUDI samplers for consistency checks. Aluminum and quartz filter media were pre-baked at 550 ° C for 48 hours to remove background carbon before analysis. The same thermo-optical method (NIOSH 5040) outlined in Section 3.1.3 was used to determine OC and EC concentrations on foil and quartz substrates.

Table 2-4. Sampling Dates for Fresno.

Location	Season	Sample Dates
Fresno	Winter	2/7/2009 – 2/11/2009
	Summer	7/10/2009 – 7/19/2009
	Winter	1/11/2010 – 1/15//2010
		1/18/2010 – 1/22/2010

Foil and quartz filters were composited based on PM size and analyzed by the Wisconsin State Laboratory of Hygiene. Samples were extracted with organic solvents (dichloromethane and methanol), evaporated under nitrogen, and analyzed with Gas Chromatography and Mass Spectrometry (GC-MS). Isotopically labeled molecular standards were added to sample extracts and served as internal standards for quantification. All Teflon and aluminum foil sample composite concentrations were field blank subtracted and all quartz sample composites were QBQ-backup subtracted. Data representative of $PM_{0.1}$ EC and OC were each averaged per season.

The $PM_{2.5}$ EC and OC data used for comparison to $PM_{0.1}$ measurements was obtained from the U.S. EPA CSN [98]. The $PM_{2.5}$ EC and OC data was collected with a URG-3000N sampler and analyzed using the Interagency Monitoring of Protected Visual Environments (IMPROVE) $PM_{2.5}$ EC/OC protocol [99]. The IMPROVE EC/OC protocol is an alternative to the NIOSH protocol described in Section 3.1.3 that generally predicts twice as much EC in locations with high concentrations of wood smoke aerosol. The Fresno data for 2009 and 2010 was a 1-in-6 day filter sampling on Pall quartz filters analyzed with reflectance and transmittance lasers using an Atmosylic Model 2001 IMPROVE carbon analyzer [100].

The results of this study showed $PM_{0.1}$ total mass ranged from 0.35 $\mu g\ m^{-3}$ during the 2010 winter sampling event to 0.70$\mu g\ m^{-3}$ during the 2009 summer event. $PM_{0.1}$ OC ranged from 0.074 $\mu g\ m^{-3}$ during the 2007 winter sampling event to 0.364 $\mu g\ m^{-3}$ during the 2009 summer sampling event.

2.3.1.4(c). Sacramento 2009-2010

The objective of the Sacramento 2009-2010 study was to analyze a full year of UFP measurements in a major California city. The study summarized 24 hour average $PM_{0.1}$ concentrations, chemical composition, and source contributions in Sacramento, CA. Daily samples were collected between 12 to 12 PST from October 26th, 2009- November 3rd, 2010 [19]. The study period overlapped a time when Heavy Duty Diesel Vehicle (HDDV) emissions were changing dramatically due to the adoption of Diesel Particle Filters (DPFs). UFP measurements were compared between pre and post April 1, 2010 when the Comprehensive Truck Management Plan (CTMP) came into full effect at the Port of Oakland leading to altered emissions along goods movement corridors [19, 61, 66]. $PM_{0.1}$ samples were collected on the roof of the CARB facility at 1309 T St. Sacramento, CA using methods identical to those employed in the CRPAQS and SAHERC studies. Two MOUDIs were operated at all times during the study, one loaded with foil substrates (Foil 0100-96-0573A-X; MSP Corp., Shoreview, MN, USA), and the other loaded with Teflon substrates (Teflo R2PJ047; Pall Corp., Port Washington, NY, USA). Both MOUDIs were equipped with upstream AIHL cyclone separators. Stage 10 substrates were changed after each 24 hour sampling period whereas stages 5-9 were changed weekly [19]. The samples on Teflon substrates were analyzed with ICP-MS for trace metals while the samples on foil substrates were analyzed for carbon using the NIOSH protocol summarized in previous studies described above [19, 25] . For quality control and consistency checks, ten percent of samples were analyzed twice [19].

The $PM_{2.5}$ data used to compare against the $PM_{0.1}$ measurements made in Sacramento 2009 and 2010 was obtained from the U.S. EPA CSN. Methods and instrumentation are described in Section 3.1.4 (b) above. It is important to note that the $PM_{2.5}$ data available for these years at this site was provided as unadjusted fractions which means that this data was not adjusted for sampling artifacts in the CSN [100].

The major conclusions from the Sacramento 2009-2010 study are that UFP concentrations declined after the adoption of emission controls on April 1, 2010. Older diesel engines accounted for 27% of $PM_{0.1}$ mass prior to full implementation of the CTMP but only 2% after full adoption. The $PM_{0.1}$ EC from on-road diesel decreased from 0.012 $\mu g\ m^{-3}$ to 0.00064 $\mu g\ m^{-3}$ and the $PM_{0.1}$ OC decreased from 0.027 $\mu g\ m^{-3}$ to 0.00095 $\mu g\ m^{-3}$ [19]. This study provided evidence that the CTMP at the Port of Oakland reduced UFP concentrations from on-road diesel engines by 97% which was estimated to be about 0.011 $\mu g\ m^{-3}$ less EC and 0.026 $\mu g\ m^{-3}$ less OC in Sacramento, CA [19].

2.3.1.5(c). California Four Cities UFP Study

$PM_{0.1}$ samples were collected at four sampling sites across California from August 2015 to July 2016. Two measurement sites were located in the San Francisco Bay Area (SFBA) with the highest population density in California. The first SFBA site was in the downtown area of San Pablo while the second was in East Oakland. The third sampling site was on the USC campus in Los Angeles, the second largest city in the United States. The fourth site was located at the California State University, Fresno, which is the largest city in California's polluted San Joaquin Valley. Each sampling period was a 3 day average with successful operation during 70-90% of the annual cycle. Fresno samples were collected over a truncated time period for 6 months from January-April and June-July of 2016.

The methods used in the California Four Cites UFP Study were nearly identical to the studies in Sections 3.1.4 (b) and 3.1.4 (c) as well as previous studies outlined in Sections 3.1.1-3.1.4 (a). Two MOUDIs were operated at each site, one with Teflon substrates and the other with aluminum substrates. The NIOSH 5040 method with temperature modifications was used for EC/OC analysis (described in Section 3.1.3 and displayed in Figure 2-6). The fraction of the foil substrate that was not analyzed for EC/OC was analyzed for molecular markers at the Molecular & Environmental Toxicology Center at the University of Wisconsin using solvent extraction and gas chromatography-mass spectrometry (GC-MS).

The $PM_{0.1}$ OC and EC fractions for the four sites were analyzed for each season during the study using the method described in Section 3.1.4 (c). The data representative of $PM_{2.5}$ OC and EC in this report was obtained from the U.S. EPA $PM_{2.5}$ CSN described in Section 3.1.4 (b). Measurement sites at San Pablo and East Oakland were not available and therefore the $PM_{2.5}$ data included here only accounts for USC and Fresno. The CSN site located at 1630 N. Main St. in Central Los Angeles was used as a comparison point for USC $PM_{0.1}$ samples, and the CSN site located at 3727 N. First St. was used as a comparison point for Fresno $PM_{0.1}$ samples. The measurements used as a comparison to $PM_{0.1}$ for this particular study were adjusted EC and OC concentrations.

The main conclusions from this study were that the UFP mass shows seasonal concentration patterns with higher concentrations in winter, due to meteorological conditions as well as increased emissions for heating purposes. In addition, the CMB results show cooking, biomass burning and mobile sources as the dominate sources for $PM_{0.1}$. Biomass burning only appears during the winter season and more importantly in Fresno. Mobile sources were more important at highly urbanized areas where port transportation takes place such as downtown Los Angeles and Oakland, CA.

2.3.2 Ultrafine Particle Number (N_X)

Particle number concentrations are described using the diameter of the smallest detectable particle. The typical reported parameter N_7 refers to the countable number of particles with diameter larger than 7 nm (the cutoff diameter). Particles in the UFP size range dominate the total particle number concentration (N_7) under typically atmospheric conditions [50, 51, 91]. Thus, N_7 is another useful metric to consider when analyzing long-term UFP trends. Here we analyze N_7 measured in various Southern California communities in 2001 and 2012-2015. The studies included are the Children's Health Study (CHS) and the Multiple Air Toxics Exposure Studies (MATES-IV and Post MATES-IV). Details of each study are described in Sections 2.3.2.1-2.3.2.3 below.

All N_7 studies utilized condensation particle counters (CPCs), however, the CHS study used butanol based CPCs while the MATES studies used water based CPCs. The lower detection limit for both types of CPCs were reported to be ≥ 7 nm in particle diameter.

The CHS study was carried out in 12 communities listed in Table 2-5. The locations included in this report that aligned closest with the MATES locations were Long Beach, UC Riverside (UCR) and Upland. The MATES-IV study included N_7 sampling in 10 communities listed in Table 2-6 below. The locations that aligned well with CHS were Fontana, Rubidoux and Long Beach and the locations that were identical to the Post MATES-IV sites were Anaheim, Central Los Angeles (LA), Long Beach and Rubidoux.

Table 2-5. CHS study site locations [57].

CHS Sites	UTM* Easting Coordinates (km)	UTM Northing Coordinates (km)	UTM Zone
Alpine	522.950	3632.500	10
Atascadero	711.500	3929.900	11
Glendora	421.530	3778.250	
Lake Arrowhead	480.580	3787.730	
Lake Elsinore	468.560	3725.940	
Lancaster	396.730	3839.060	
Lompoc	731.500	3843.700	10
Long Beach *	389.850	3743.020	11
Mira Loma	451.610	3762.080	
San Dimas	423.090	3774.740	
Santa Maria	734.300	3870.100	10
UC Riverside (UCR) *	469.030	3757.760	11
Upland *	437.570	3773.090	

* UTM = Universal Transverse Mercator
* Long Beach, UCR and Upland were locations reviewed in this report.

Table 2-6. MATES-IV, Post MATES-IV and U.S. $PM_{2.5}$ CSN site locations.

MATES-IV Sites	UTM Easting Coordinates (km)	UTM Northing Coordinates (km)	UTM Zone	Post MATES-IV Sites	U.S. $PM_{2.5}$ CSN Sites
Anaheim *	412.969	3743.783	11	✓	✓
Burbank	378.629	3782.436		NA	
Central LA *	386.722	3770.215		✓	✓
Compton	388.465	3751.8		NA	
Inland Valley San * Bernardino/Fontana	454.629	3773.308		✓	✓
Huntington Park	387.679	3748.832		NA	
Long Beach *	389.979	3743.249		✓	✓
Pico Rivera	401.354	3763.961		NA	
Rubidoux *	461.663	3762.297		✓	✓
West Long Beach	387.09	3740.795		NA	

✓ = Same location
NA = Location was not sampled during this study
*Anaheim, Central LA, Long Beach and Rubidoux were locations reviewed in this report.

The Upland location in the CHS study was the closest in proximity to the Fontana site from the MATES-IV and Post MATES-IV sampling, at a distance of 10.6 miles and mapped in Figure 2-7 below. The CHS Long Beach site measured at only 0.2 miles from the MATES sampling site mapped in Figure 2-8.

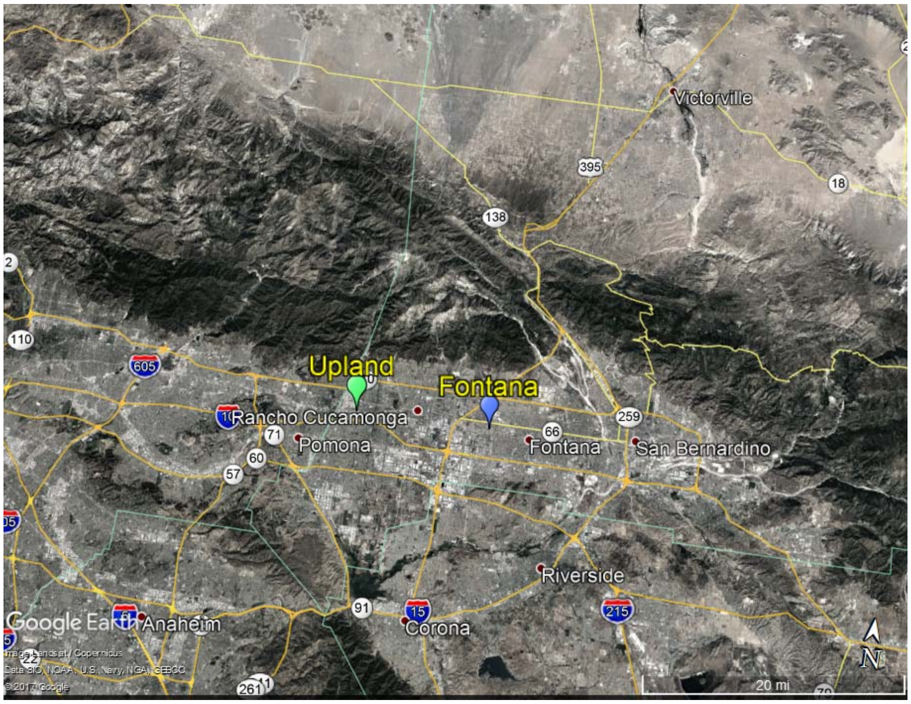

Figure 2-7: CHS Upland monitoring site in proximity to MATES-IV and Post MATES-IV Fontana site [56, 57].

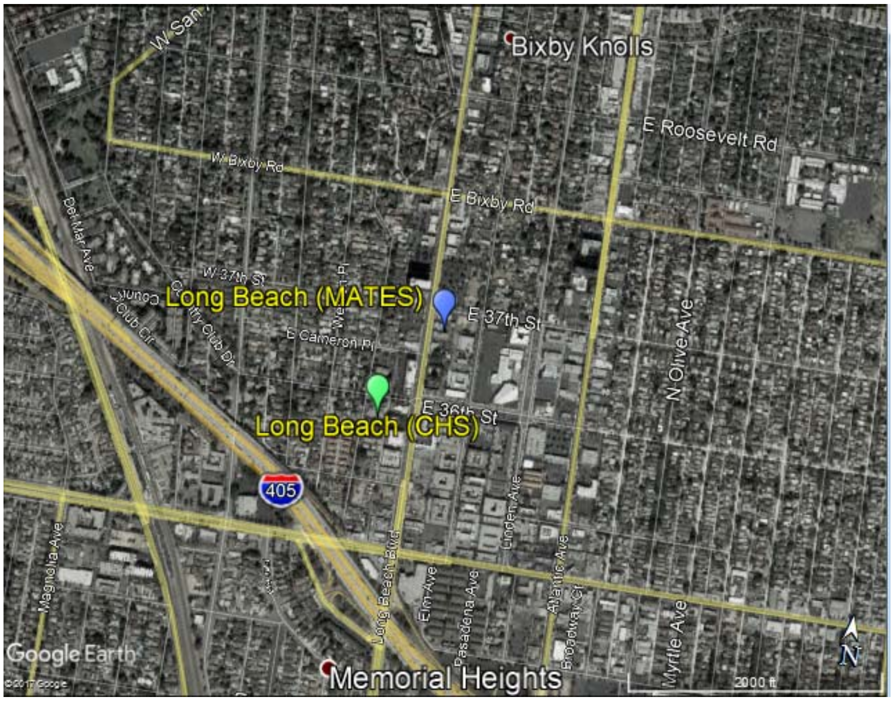

Figure 2-8: CHS (green) and MATES (blue) sampling site locations in Long Beach, CA [56, 57].

$PM_{2.5}$ measurements used for comparison to N_7 trends were measured using a Graseby Andersen Sequential Reference Ambient Air Sampler (RAAS, RAAS2.5e300, Andersen) configured for a continuous 24 hour sample period at a flow rate of 16.67 liters min^{-1} [100]. The samples were analyzed gravimetrically with a lower detection limit of 2 $\mu g\ m^{-3}$ [98, 100]. $PM_{2.5}$ measurements were collected every 1-in-3 or 1-in-6 days. For the data represented in this review and analysis analysis, yearly averages were determined at each site from all data points from January through December within each year 2000-2015.

2.3.2.1 Children's Health Study (CHS)

The USC Children's Health Study (CHS) is one of the largest and longest exposure studies on the respiratory health of children in the world [101]. Results have shown improvements in the lungs of children over the past two decades coinciding with improved air quality due to air quality regulations [57, 101]. The data represented in this report is from a study done from 1994-2001. During this period, CARB took responsibility for field operations and data collection. The objective of the study was to understand the potential chronic health effects from air pollutants in 12 communities of Southern California through measurement and analysis of ozone, NO_2, PM_{10}, $PM_{2.5}$, CO, EC, OC and N_7 [57, 101].

The N_7 data used in this analysis was sampled using a Condensation Particle Counter (CPC, TSI Model 3022A) installed at all of the stations and set at a flow rate of 1.51 min^{-1} [51, 57]. The TSI Model 3022A is butanol based and detects airborne particles with diameter ≥ 7 nm. This older model works reliably in environments with N_7 as high as 10^7 particles cm^{-3} [102]. The monthly average distribution of CHS CPC concentrations collected in 2001 are represented as box plots as described in Section 3.2.

The CHS conducted a comparison of PM_{10} and N_7 in an attempt to identify a seasonal or diurnal similarity in trends. The results concluded a very weak comparison and this was reported to be expected because UFP counts are dominated by small particles while PM_{10} make up the largest size fraction of particles [103]. The results from the CHS indicated that the season and geographical location both play a critical role in N_7 and size distribution of particles within Southern California communities. N_7 showed a strong diurnal and seasonal pattern as a result of the mixture of formation mechanisms, meteorological conditions, time of day and year as well as the direct effects of sources [103].

2.3.2.2 Multiple Air Toxics Exposure Study (MATES)

The Multiple Air Toxics Exposure Study (MATES) was conducted in the South Coast Air Basin by the South Coast Air Quality Management District (SCAQMD). The MATES-IV study included an updated emissions inventory of toxic air contaminants, a monitoring program as well as a modeling project to determine exposure risk [56]. The motivation behind the study was to understand the carcinogenic risk of exposure to air pollutants. The locations in this analysis are listed in Table 2-6 and samples were taken 1-in-6 days July through September of 2012 as is listed in Table 2-1 [56]. MATES-II and MATES-III were carried out prior to MATES-IV enabling a comparison of pollutant concentrations over time, but N_7 measurements were not available for MATES-II and MATES-III and are not included in the current analysis.

N_7 data was collected continuously during MATES-IV at a one minute time resolution using water-based condensation particle counters (CPC Model 651; Teledyne API, San Diego, CA) [56]. The lower particle detection limit of this instrument is 7 nm and the particular model used was designed for routine ambient air quality monitoring [56]. CPCs were calibrated at regular intervals, consistency checks were performed using a co-located reference instrument (i.e., “Gold Standard” CPC) yielding high correlation coefficients, and the final data from the CPCs was evaluated for anomalies [104].

The results of MATES-IV showed that the cancer risk on average in the South Coast Air Basin was 65% lower than the estimated risk from the 2004-2006 time period and that diesel exhaust was the major driver of air toxics risk. In addition, the concentrations measured during MATES-IV were lower compared to the MATES-III study from 2004-2006. Diesel PM reduced by 70% compared to MATES-III. This shows that control strategies have helped in the reduction of exposure to pollutants. N_7 data revealed that UFPs are higher in western areas of the basin which is likely due to high population and subsequently higher traffic density. Further, just as in the CHS, measurements indicated high variability in UFP concentrations both spatially and temporally. This can be explained by a mixture of factors including distance to the source, source type, wind speed and direction, temperature and traffic volumes which all play a role in UFP dispersion, composition and concentrations.

2.3.2.3 Post MATES-IV Study

The Post MATES-IV study included N_7 data for all months 2013-2015 at 4 sampling sites in Southern California: Anaheim, Central LA, Fontana and Rubidoux. The methods utilized for N_7 were identical to MATES-IV described in Section 2.3.2.2. The data collected Post MATES-IV has not yet been reported in a final draft as part of MATES-V by the SCAQMD.

2.4 Results

2.4.1 Fine and Ultrafine Particle Mass ($PM_{2.5}$ and $PM_{0.1}$)

The seasonal distributions of UFP concentrations in each study can be seen in the box plots of OC in Figure 2-9 and EC in Figure 2-10 below. Both figures display trends in the fine particle size range of OC and EC alongside UFPs during the same seasons and years as the studies outlined in Section 3.1.

On average, the $PM_{0.1}$ OC from the T96 Study carried out in 1996 has declined by a factor of 15.7 to the values measured in the California Four Cities Study carried out in 2015-2016 (from 1.62 µg m^{-3} to 0.103 µg m^{-3}). The $PM_{0.1}$ EC concentrations have declined by a factor of 6.5 over the same time period (from 0.331 µg m^{-3} to 0.051 µg m^{-3}). The $PM_{2.5}$ OC concentrations have declined by a factor of 9 between 1996 and 2015-2016 (from 25.11 µg m^{-3} to 2.75 µg m^{-3}) while the $PM_{2.5}$ EC concentrations have declined by a factor of 8 (from 5.43 µg m^{-3} to 0.685 µg m^{-3}).

Data availability for Fresno and Westside from the SAHERC studies were bi-weekly averages and therefore box plots of data distributions were not created for years 2006-2010. The EC concentrations in Westside Winter 2008 (W-08) are higher than Sacramento Fall 2009 (F-09), however, this is a minor perturbation.

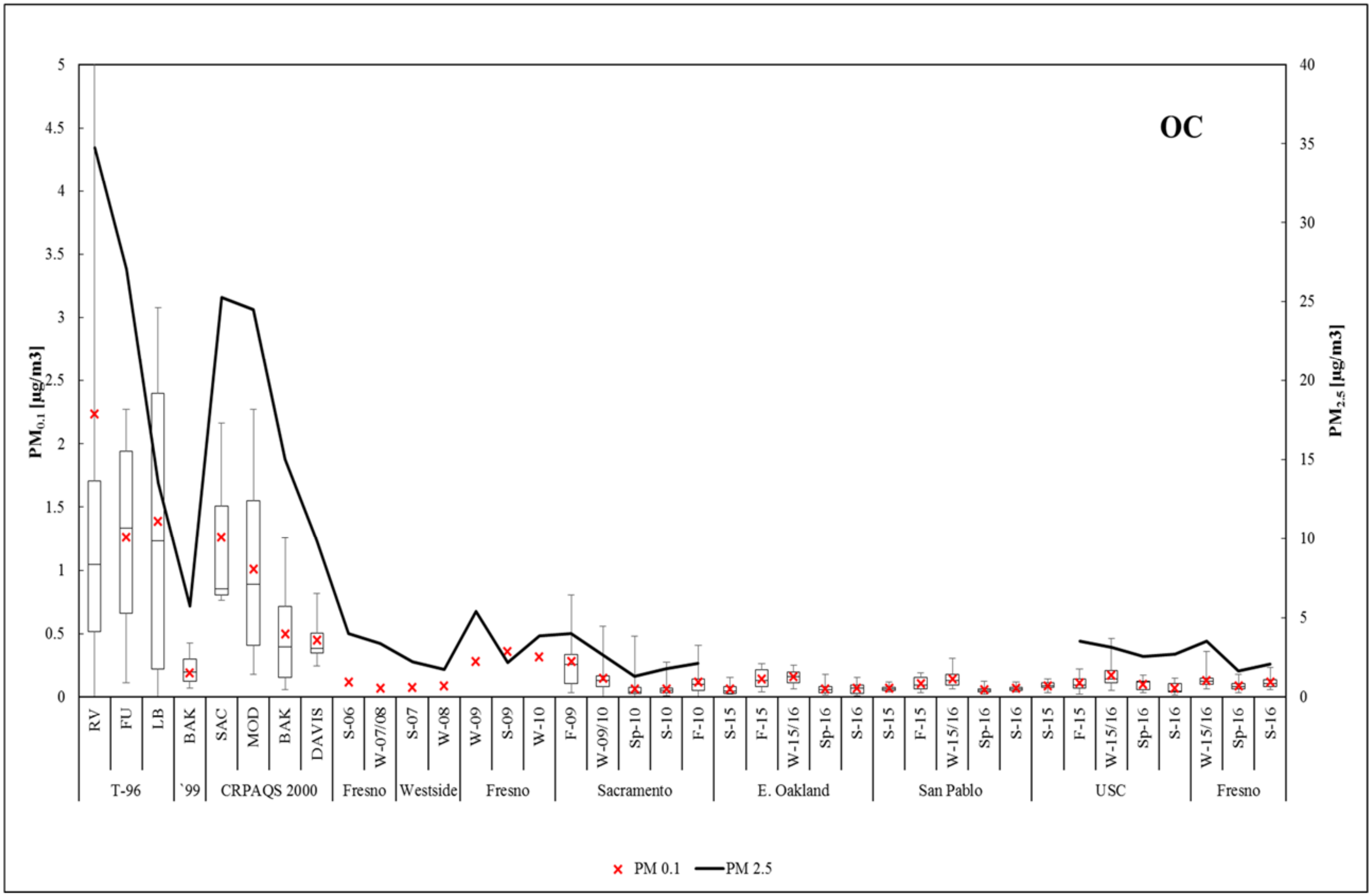

Figure 2-9: Average OC concentrations from PM$_{0.1}$ and PM$_{2.5}$ measured from 1996 to 2016 in multiple studies at various locations throughout California. PM$_{0.1}$ concentrations use left axis while PM$_{2.5}$ concentrations use right axis.

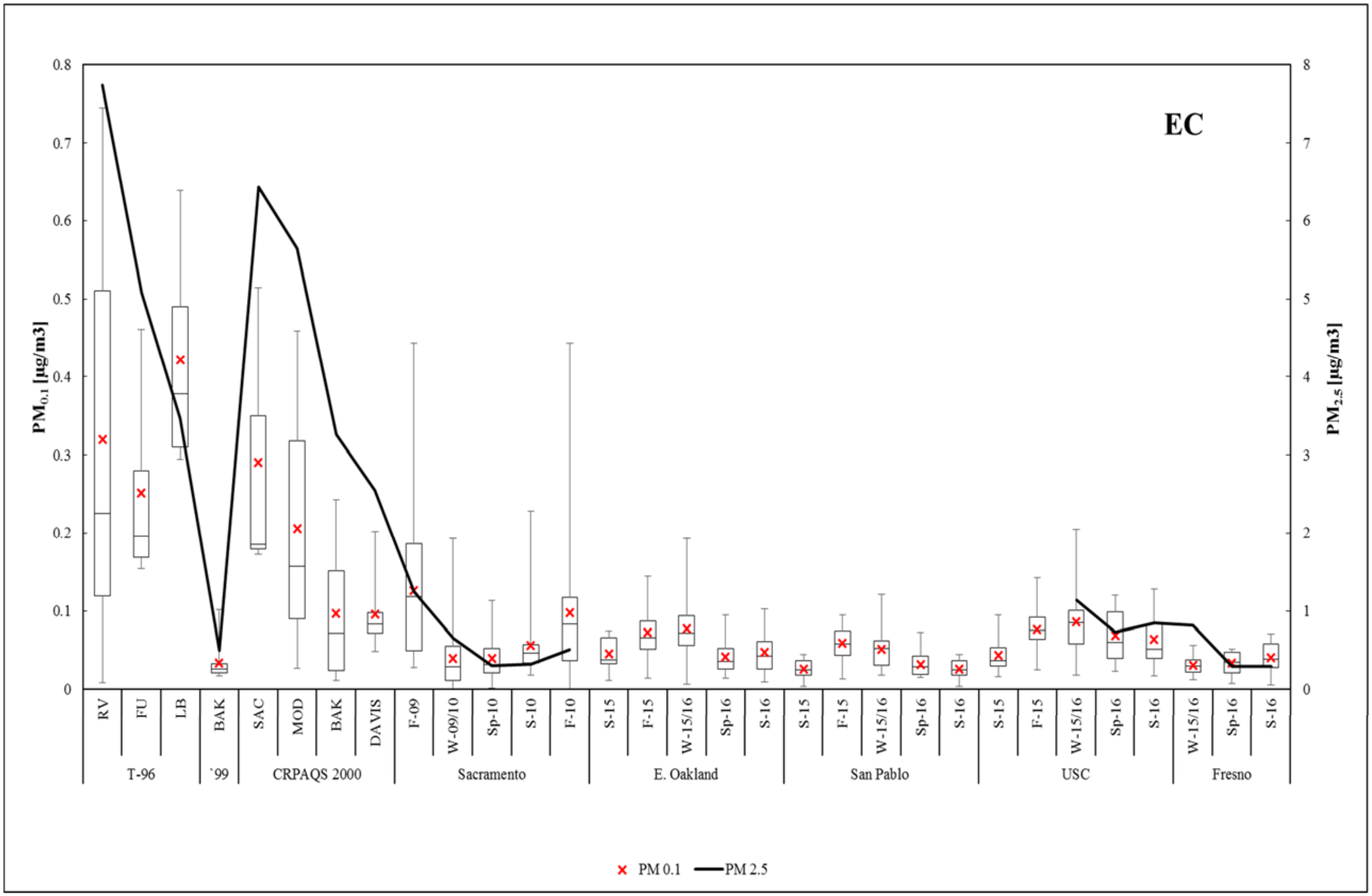

Figure 2-10: Average EC concentrations from PM$_{0.1}$ and PM$_{2.5}$ measured from 1996 to 2016 in multiple studies at various locations throughout California. PM$_{0.1}$ concentrations use the left axis while PM$_{2.5}$ concentrations use the right axis.

In analyzing long-term trends, it was noted that the EC fraction of $PM_{0.1}$ has increased over time (Figure 2-11) while the EC fraction of $PM_{2.5}$ has not changed over time (Figure 2-12). A hypothesis test was conducted to understand whether there is a significant linear relationship between the ratio of EC/OC (dependent variable Y) and the 38 measurement periods spaced uniformly in time over two decades (independent variable *X*) represented in equation 1 below. The test focuses on the slope of the regression line (β1 in equation 1). The null hypothesis (H_0) and hypothesis (H_1) are stated in equation 2. The null hypothesis (H_0) states the slope (β1) between Y and X will be equal to zero while the alternative hypothesis (H_1) states that the slope will be non-zero. A two-tailed t-test with 95% certainty was used to carry out the hypothesis testing [105].

$$Y = \beta_0 + \beta_1 X \tag{1}$$

$$\begin{aligned} H_0&: \beta_1 = 0 \\ H_1&: \beta_1 \neq 0 \end{aligned} \tag{2}$$

The standard error (SE) of the slope was calculated using equation 3 where n is the number of observations, yi is the value of EC/OC for observation i, ŷi is the estimated value of EC/OC for observation i using equation 1, xi is the independent variable at observation i, and $\overline{x}$ is the mean of the independent variable.

$$SE = \mathrm{sqrt}\,[\,\Sigma(\mathrm{yi} - \hat{\mathrm{y}}\mathrm{i})^2 \,/\, (\mathrm{n} - 2)\,] \,/\, \mathrm{sqrt}\,[\,\Sigma(\mathrm{xi} - \bar{x})^2\,] \tag{3}$$

The degrees of freedom (dof) was calculated using equation 4 where n is the number of observations. The test statistic was calculated using equation 5 to determine the t-score. A t-distribution curve was analyzed to determine the p-value of 0.0268, which is less than the significance level of 0.05. Thus, the measurements suggest that the EC fraction of $PM_{0.1}$ increased over the 38 measurements from 1996 to 2016 with more than 95% certainty. A similar test conducted for the EC fraction of $PM_{2.5}$ in Figure 2-12 generated a p-value of 0.71 which is much greater than 0.05. Thus, there is no measured evidence to suggest that the EC fraction of $PM_{2.5}$ has increased over the period 1996 to 2016 based on the measurements analyzed in the current study.

$$Dof = n - 2 \tag{4}$$

$$t = \frac{\beta_1}{SE} \tag{5}$$

The OC fraction of PM can either be directly emitted (POA) or formed in the atmosphere (SOA). The EC fraction of PM is always directly emitted [18, 87, 106]. Combustion sources dominate emissions of both OC and EC. The ratio of EC to OC is an indicator of the relative contributions from various combustion sources and the relative importance of SOA formation vs. primary emissions. The OC/EC ratio is sometimes used to generate an estimate of the SOA / POA ratio. The increase in the EC fraction of $PM_{0.1}$ illustrated in Figure 2-12 suggests that either the mixture of primary sources has changed such that the EC emissions have increased, or the SOA formation in the $PM_{0.1}$ size fraction has decreased over the period 1996-2016.

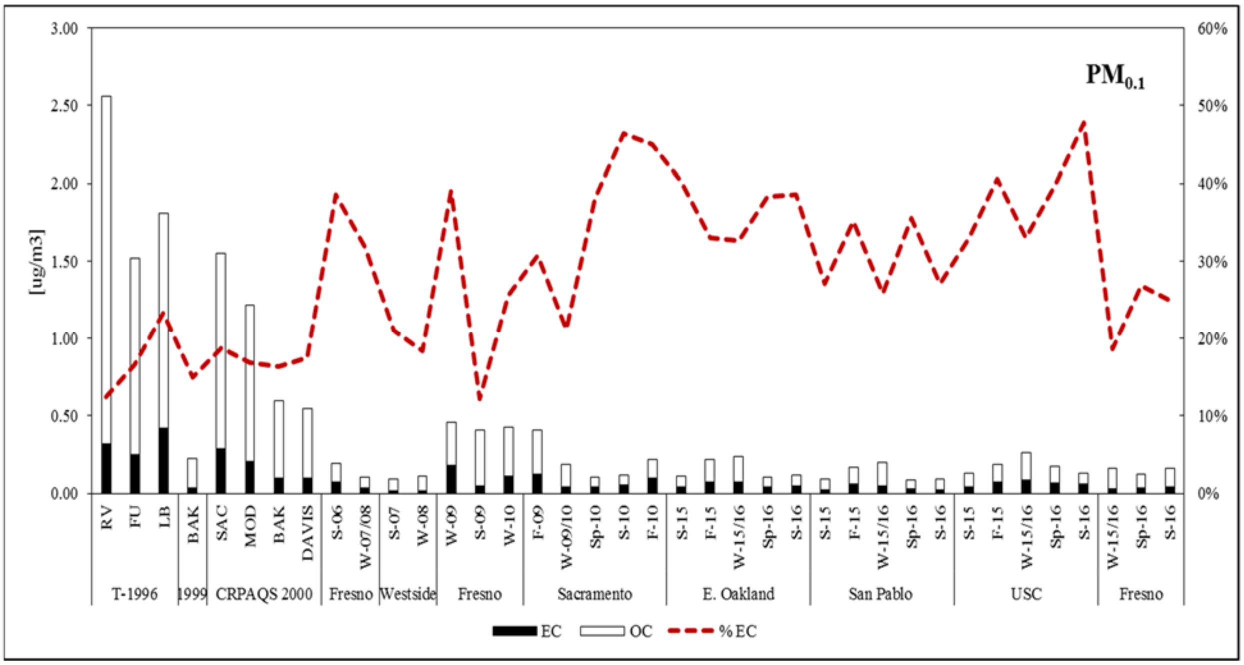

Figure 2-11: EC/OC concentrations from PM0.1 on the primary axis and the percent contribution of EC on the secondary axis measured from 1996 to 2016.

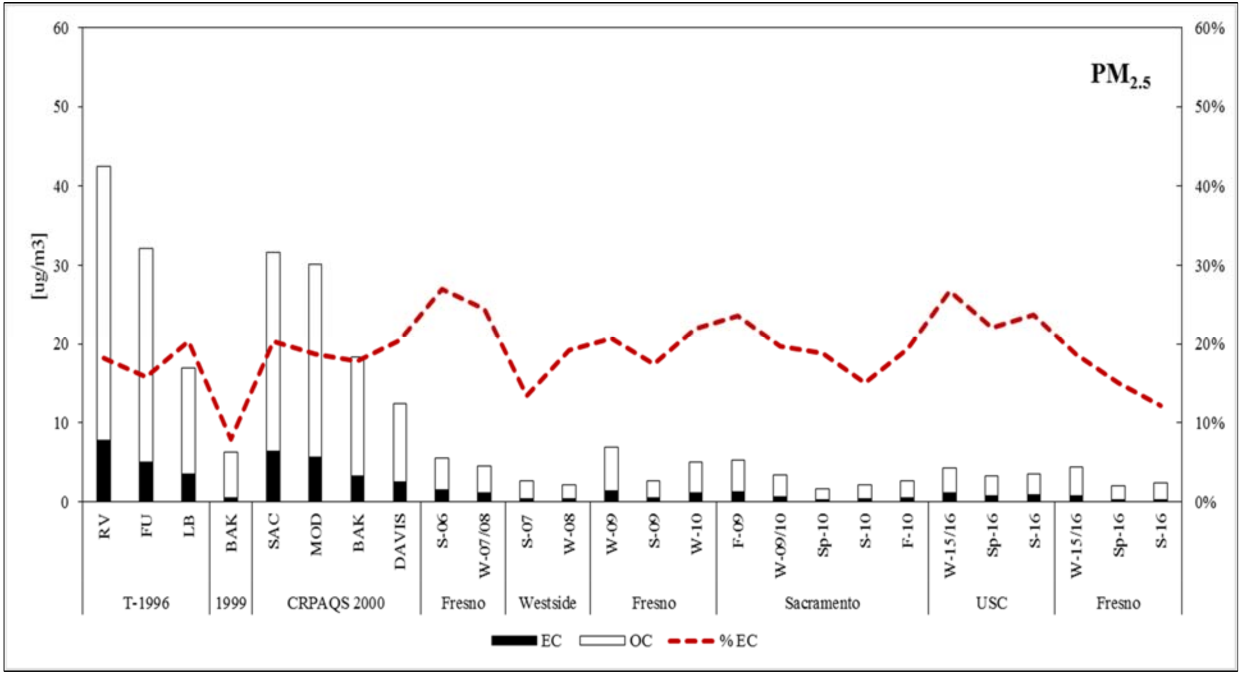

Figure 2-12: EC/OC concentrations from PM2.5 on the primary axis and the percent contribution of EC on the secondary axis measured from 1996 to 2016.

2.4.2 Particle Number

The Southern California cities analyzed for long-term trends in N_7 were Fontana, Long Beach, Rubidoux, Anaheim and Central Los Angeles. Box plots of annual N_7 distributions are displayed for each city in Figures 2-13 through 2-17. The primary vertical axes displays N_7 measured in thousands of particles cm^{-3} while the secondary vertical axes shows $PM_{2.5}$ measured in $\mu g\ m^{-3}$. The average N_7 decreased by 37% (from 24, 949 particles cm^{-3} to 15,661 particles cm^{-3}) in Fontana, 43% in Long Beach (from 21,931 particles cm^{-3} to 12,490 particles cm^{-3}) and 56% in Rubidoux (from 30, 666 particles cm^{-3} to 13, 456 particles cm^{-3}) in 2015 compared to 2001. Central LA and Anaheim were not studied in 2001 and N_7 appears to increase in Central LA and remain relatively constant in Anaheim between 2012 and 2015. Although MATES-II and MATES-III studies carried out from 2004-2006 are missing in this analysis, the MATES-IV final report did indicate substantial decreases in diesel PM and carcinogenic risk from 2004 to 2012.

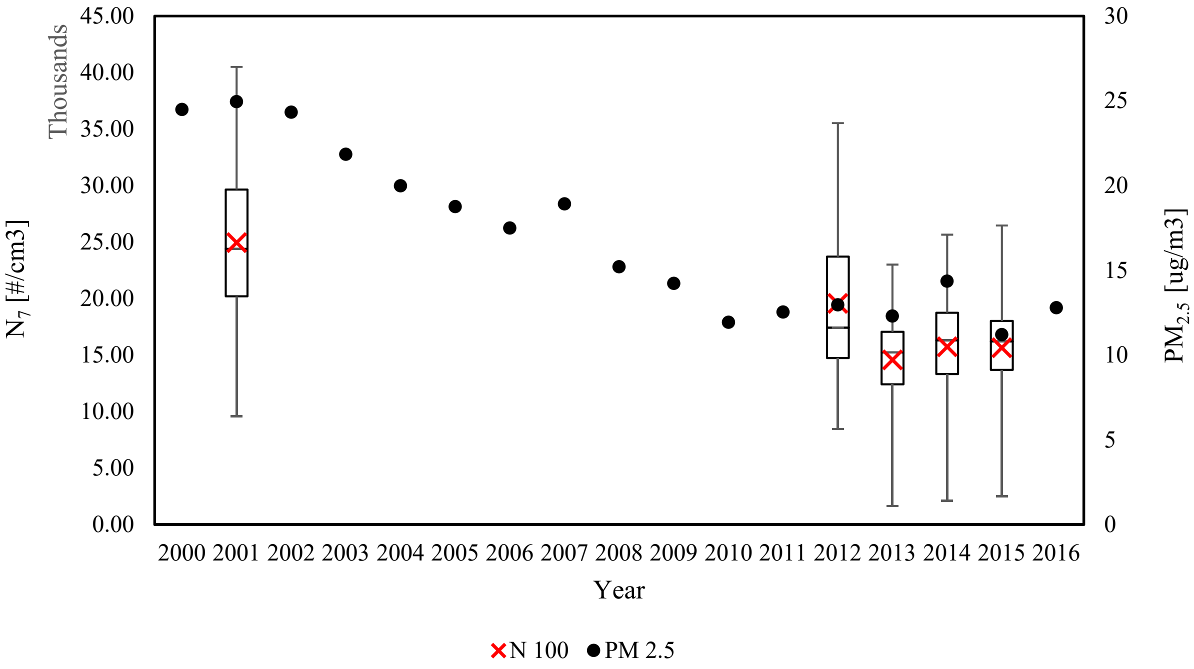

Figure 2-13: N_7 distributions from CHS and MATES-IV as well as Post MATES-IV measured alongside $PM_{2.5}$ trends in Fontana, CA.

Statistical analysis shows that there is strong positive correlation between N_7 and $PM_{2.5}$ at the three sites (Fontana, Rubidoux and Long Beach) where data from 2001 as well as 2012-2015 was available. The correlation coefficients (R^2) among annual averages of N_7 and $PM_{2.5}$ for Fontana and Rubidoux are 0.79 and 0.92 respectively and the strongest correlation is found at the Long Beach site with an R^2 of 0.96. Together these three cities have a R^2 of 0.48. It is important to note that the CHS sites in 2001 did not align well with the Anaheim and Central LA sites from MATES-

IV (Figures 2-16 through 2-17) therefore a correlation coefficient between N_7 and $PM_{2.5}$ from 2001-2015 could not be determined.

Long term trends in N_7 are difficult to determine due to the lack of measurements between 2001 and 2012, however, Figures 2-13 through 2-17 show that N_7 concentrations are positively correlated with declining $PM_{2.5}$ concentrations between 2000 and 2016. $PM_{2.5}$ concentrations at the five measurement sites decreased by a factor of 2.3 over this time period (25.82 µg m^{-3} to 11.2 µg m^{-3}), while N_7 concentrations decreased by a factor of 1.7 (25,849 particles cm^{-3} to 15,278 particles cm^{-3}).

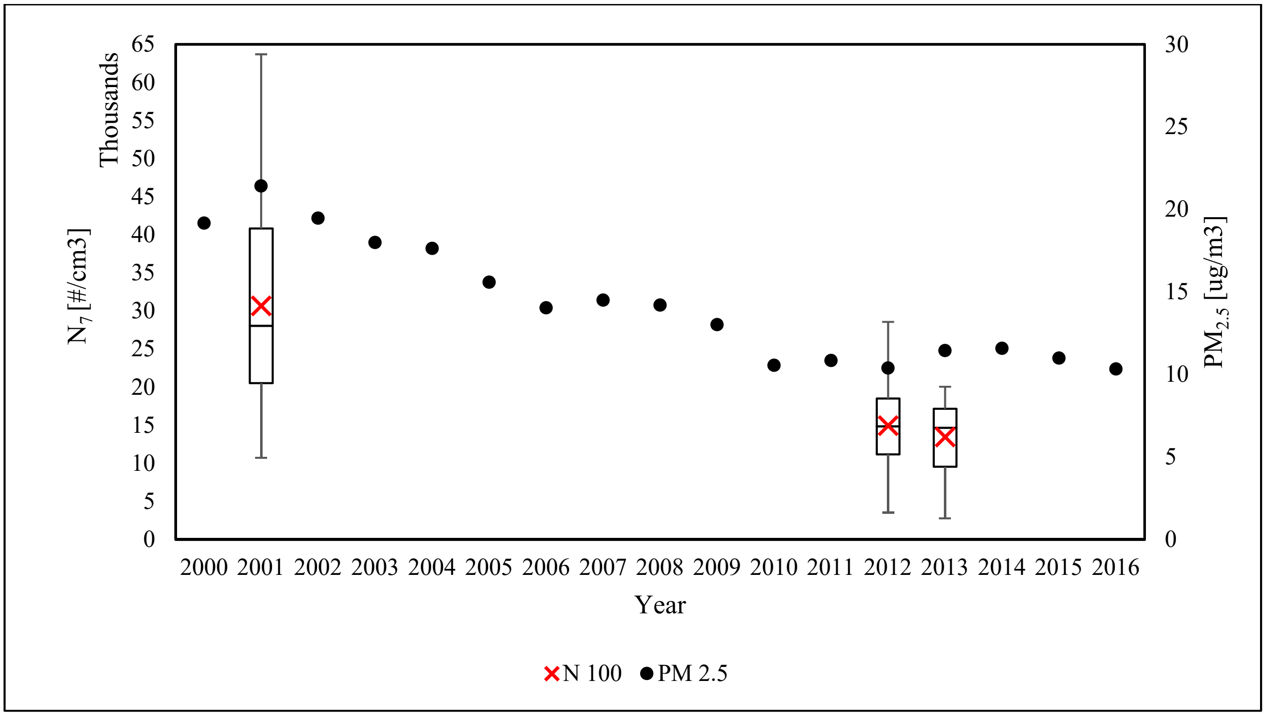

Figure 2-14: N_7 distributions from CHS and MATES-IV as well as Post MATES-IV measured alongside $PM_{2.5}$ trends in Long Beach, CA.

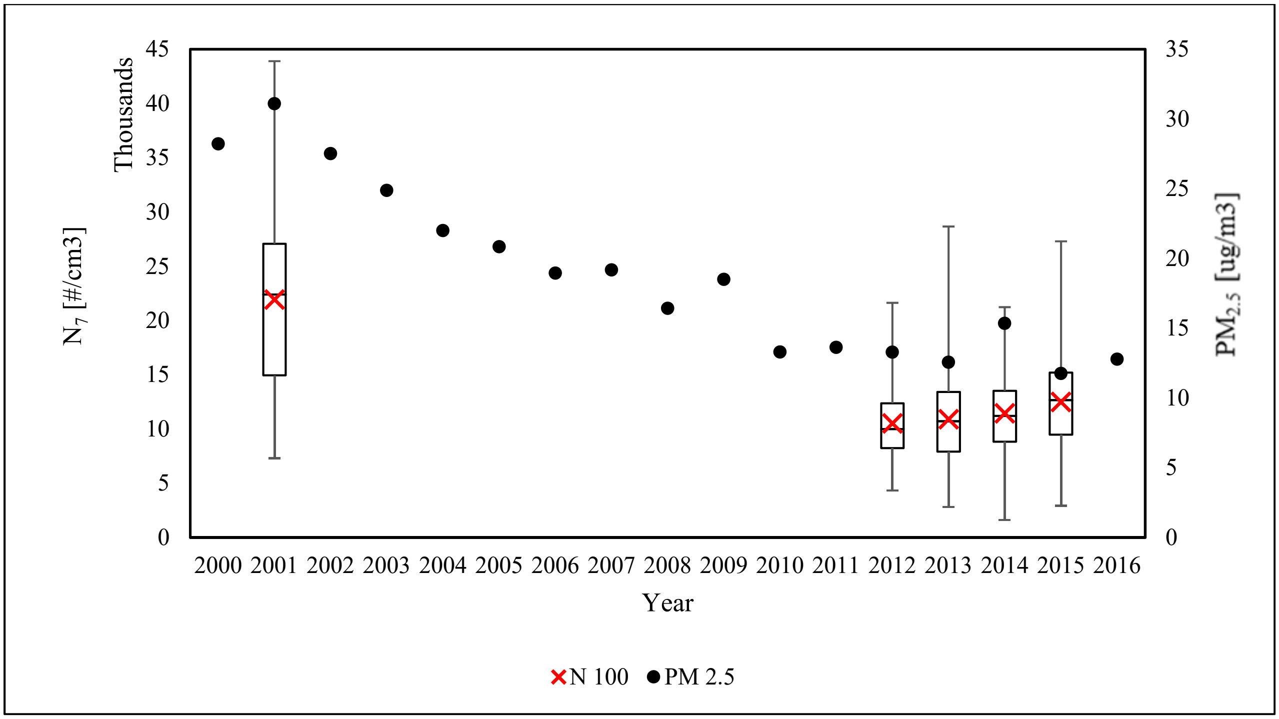

Figure 2-15: N_7 distributions from CHS and MATES-IV as well as Post MATES-IV measured alongside $PM_{2.5}$ trends in Rubidoux, CA.

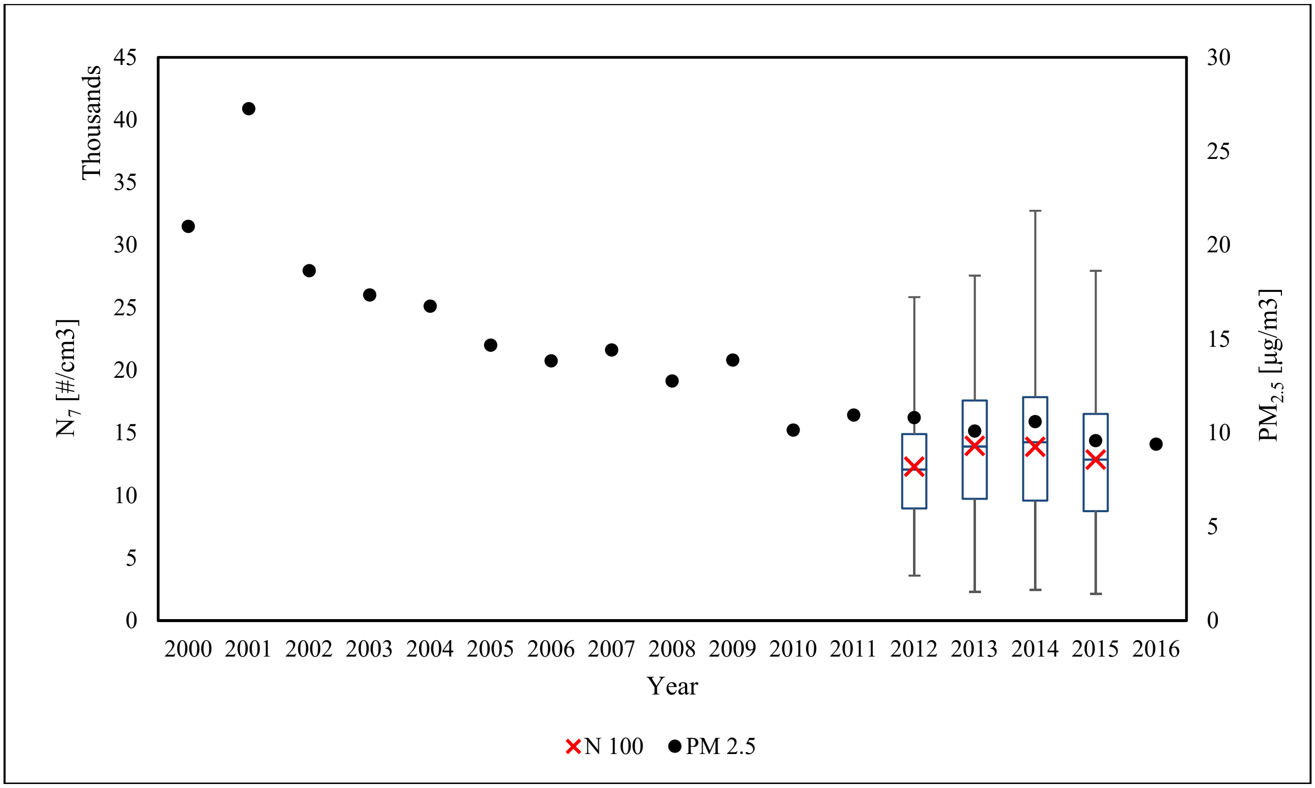

Figure 2-16: N_7 distributions from CHS and MATES-IV as well as Post MATES-IV measured alongside $PM_{2.5}$ trends in Anaheim, CA.

In analyzing the long-term trends collected from these eight different studies, $PM_{0.1}$ measurements of both OC and EC across California from 1996 to 2016 have declined at a rate very similar to $PM_{2.5}$. Long-term trends in N_7 are positively correlated with $PM_{2.5}$ and therefore decreasing over time, however, N_7 decreases by a smaller factor than $PM_{2.5}$ (1.7 vs. 2.3). Unlike a conclusion made in the CHS study which did not identify short-term trends between N_7 and PM_{10}, the long-term behavior of N_7 demonstrates that there are instances when ultrafine N_7 does follow the same trend as ambient particle mass [15, 103].

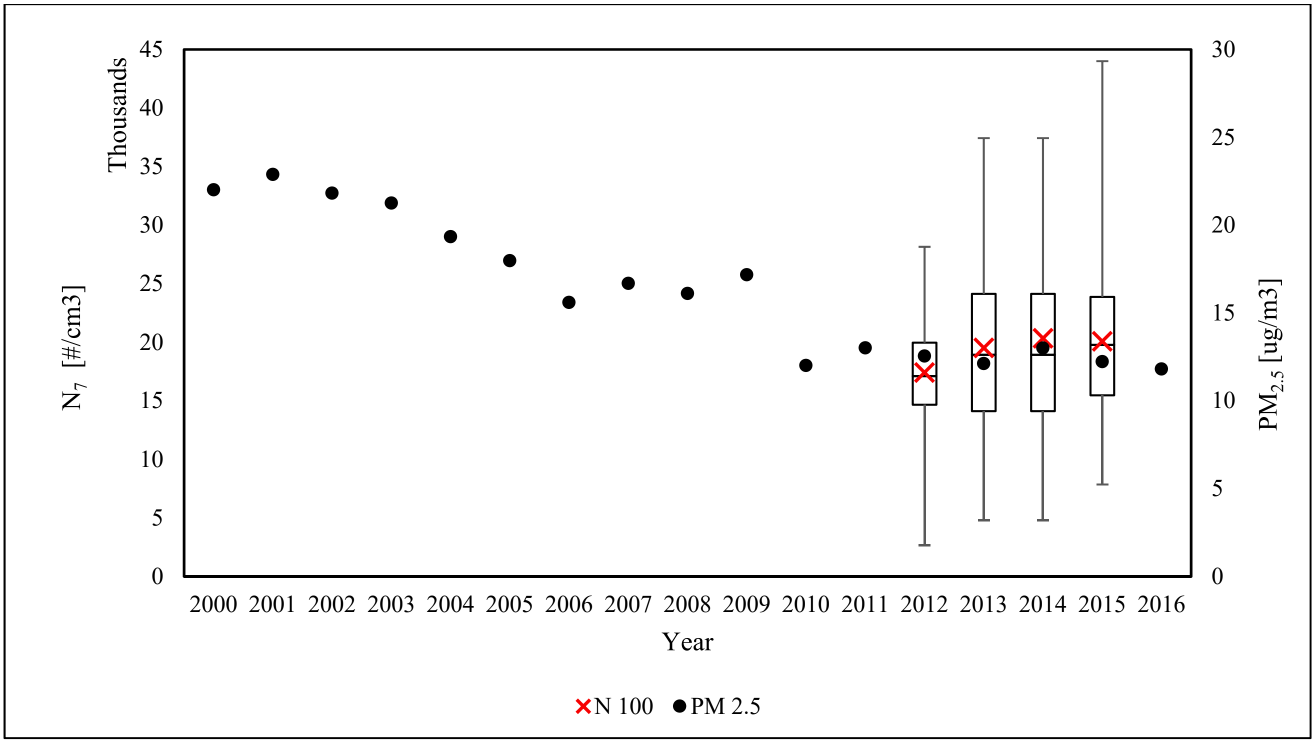

Figure 2-17: N_7 distributions from CHS and MATES IV as well as Post-MATES IV measured alongside $PM_{2.5}$ trends in Central Los Angeles, CA.

2.5 Discussion

The current report analyzes the long-term trends of UFPs in California from a collection of different studies. Care should be taken when interpreting and comparing the results across studies as there were varying sampling time periods, methods and geographical locations with different sources, formation mechanisms, and microclimates. There is potential for inconsistent findings in concentrations and size distributions which can complicate comparison results.

Over the past several decades, there have been a number of methods used to measure ambient concentrations and chemical composition of UFPs and each offers different techniques to analyze particles [15, 16, 18, 25, 50, 107]. In addition, particle number counters have varying degrees of collection efficiency which can also limit a long-term trend analysis since different models may count particles in different size ranges.

2.5.1 Particle Mass

The methodology used for particle mass measurements is very similar in all the studies but there are a few differences worth noting. For studies outlined in Section 3.1.4 (b) and 3.1.4 (c), the $PM_{2.5}$ mass was obtained from the EPA AQS Data Mart. $PM_{2.5}$ samples for these studies were collected with a URG-3000N sampler which agrees well with the IMPROVE fine particle methodology.

UFPs were collected using MOUDIs and EC/OC concentrations were measured following the NIOSH protocol for chemical analysis.

Early UFP sample measurements (1996-2001) targeted air pollution episodes, while the later measurements (2006-2008) did not. The schedule for the Fresno and Westside samples from 2006-2008 were based on animals in a co-located toxicity study, not based on actual pollutant concentrations. Further, sampling time periods varied from a ~weeks to a ~months prior to 2009 and samples thereafter were continuously collected as discussed in Table 2-1.

2.5.2 Particle Number

The CPCs used in this analysis had the same lower detection limit of 7 nm, however, the CHS CPCs were butanol based and the MATES CPCs were water based. In addition, two locations in the CHS study did not match the locations for the MATES studies, Upland being the farthest (~10.6 miles) from the closest MATES study site in Fontana. The N_7 data was difficult to obtain for years prior to 2001 and between 2001 and 2012. Lastly, N_7 typically has high variability throughout the day and this variability is lost when looking at annual distributions over time.

2.6 Conclusions

$PM_{0.1}$ trends follow a very similar pattern to the declining trends of $PM_{2.5}$ from 1996-2016. This pattern is likely the result of the emission control programs outlined in Section 2.2. Between 1996 and 2016, ambient concentrations of $PM_{0.1}$ decreased by a factor of approximately 15.7. The majority of $PM_{0.1}$ decline was measured between 2000-2006 corresponding to the implementation of wood burning controls and the adoption of new engine standards for diesel vehicles.

The behavior of N_7 in three of the five Southern California cities analyzed in this report shows that long-term trends in N_7 are positively correlated with $PM_{2.5}$. The ratio of ultrafine EC/OC increases over time due to changing source contributions. This trend has possible implications for public health given that UFP EC is associated with increased mortality. Identifying trends in the ratio of EC/OC may also be beneficial in understanding long-term trends in primary versus secondary formation.

The strong decline in $PM_{0.1}$ concentrations over the last 20 years and the weaker decline in N_7 concentrations over the same time period presents an opportunity for epidemiology studies to probe the differential associations between human health vs. $PM_{0.1}$ and human health vs. N_7. Future studies should take advantage of these different rates of decreasing concentrations.

National Ambient Air Quality Standards (NAAQS) and California Ambient Air Quality Standards (CAAQS) currently exist for airborne PM_{10} and $PM_{2.5}$ but decades of research has suggested that UFPs also pose serious health concerns [15, 16, 50, 51, 107]. Further investigation on the sources of UFPs and the mechanisms which govern their behavior need to be conducted to evaluate if UFPs pose a separate public health threat from $PM_{2.5}$.

3 DAY-OF-WEEK PATTERNS FOR ULTRAFINE PARTICULATE MATTER COMPONENTS AT FOUR SITES IN CALIFORNIA

Preamble: Chapter 3 describes results from a year of intensive ultrafine particle composition measurements carried out at four sites in California (San Pablo, East Oakland, Fresno, and Los Angeles). Day-of-week cycles are identified for several of the ultrafine particle components and the implications for the weekly variation of ultrafine particle sources are discussed. The analysis of UFP measurements will build confidence in later comparisons to modeled exposures.

3.1 Introduction

Airborne particulate matter (PM) is hazardous to human health. Many studies have found that exposure to elevated $PM_{2.5}$ is associated with respiratory and cardiovascular morbidity and mortality (see for example [108, 109]). Ultrafine particles (UFPs) (particles with aerodynamic diameter less than 100 nm) are a sub-fraction of $PM_{2.5}$ that accounts for the majority of total suspended particle number concentration [110, 111] and a significant portion of $PM_{2.5}$ surface area. Toxicological studies suggest that inhaled UFPs deposit deep into the lung where they may penetrate cellular membranes and translocate to other compartments in human body in ways that larger particles do not [10, 112]. Given the potential toxicity of UFPs, exposure assessments are needed to characterize the spatial and temporal trends of UFP concentrations, chemical composition, and source contributions.

UFPs have been measured during multiple short-term studies in California over the past 20 years as summarized in Chapter 2 and Table 3-1. Early work carried out in Southern California in 1995-1997 determined that $PM_{0.1}$ concentrations were composed of organic compounds (50%), elemental carbon (8.7%), metal oxides (14%), and small portions of nitrate (6.8%), sulfate (8.2%), and ammonium ion (3.7%) [113]. Later UFP studies in Southern California starting in 2002 characterized the organic and inorganic components in quasi-ultrafine particles ($PM_{0.25}$) focusing on source and receptor locations over timescales ranging from weeks to months [44, 114-117]. UFP studies began in California's Central Valley in 2000 with short term studies conducted every few years to measure concentrations and perform source apportionment calculations [25, 43]. Kuwayama et al [19] collected daily UFP mass samples for a full year in Sacramento, CA, but only monthly trends of particle components were reported with no analysis of trends at higher time frequency.

Table 3-1. Summary of previous UFP studies in California that measured ultrafine particles.

Location	Date Range and # of sampling days	Particle Size Range	Reference
Pasadena, CA	One month, January/February, 1996	0.017 – 0.250 µm	[118]
Long Beach, Fullerton, and Riverside, CA	Two weeks, September/October, 1996	0.017 – 0.250 µm	[119]

Location	Date Range and # of sampling days	Particle Size Range	Reference
Modesto and Bakersfield, CA	15 days, December 2000 – January 2001	0.056 – 0.1 µm	[43]
Ten sites in urban LA and remote location, CA	Weekly samples, April 2008 – March 2009	<0.25 µm	[45]
Sacramento, CA	Daily sampling, October 2009 – November 2010	0.056 – 0.1 µm	[19]
Central LA and Anaheim, CA	Five-day sampling, July 2012 – February 2013	<0.18 µm	[114]

An important gap in the studies summarized in Table 3-1 is the absence of any analysis for day-of-week trends in UFP concentrations. The importance of day-of-week cycles in ambient pollutants has long been recognized for ozone (O3) concentrations in Los Angeles which are higher on weekends than weekdays [120, 121]. A series of studies followed up on the O3 finding to analyze the weekly trends of carbon dioxide, $PM_{2.5}$ and its components (OC, EC, NO_x, NH_4^+, NO_3^-, SO_4^{2-}) to determine the association between day-of-week cycles and the activity of gasoline / diesel vehicles [122-124]. The net results of this work show that day-of-week patterns provide insight on the important sources, chemical pathways, and atmospheric processes that influence pollutant concentrations. Day-of-week cycles also provide an opportunity to better understand the public health impacts of pollutants. Multiple epidemiological studies find that hospital admissions exhibit weekly patterns. For example, acute admissions to hospitals peak on Monday [125], and emergency room visits for asthmatic children are better correlated with a week cycle than daily cycle [126]. These patterns are likely influenced by a range of socioeconomic factors, but the possible effects of weekly trends in air pollutant concentrations also merits consideration.

The purpose of the current study is to analyze day-of-week patterns in UFP concentrations at four locations across California's most heavily polluted air basins. Measurements of UFP chemical composition were made for a period of one year so that trends could be analyzed in all seasons. Day-of-week patterns are identified for individual chemical species within UFP size fraction at each measurement site. Statistical analysis is conducted to examine similarities between weekly trends for different elements at the same site, and for similarities between the same elements at different sites. Likely combination of sources, chemical reactions, and atmospheric processes that yield the observed day-of-week patterns are discussed.

3.2 Methods

Ultrafine particulate matter samples were collected at four locations in the current study: (i) San Pablo and (ii) East Oakland in the San Francisco Bay Area, (iii) the USC campus in Los Angeles, and (iv) the CSUF campus in Fresno. These locations span the diverse sub-regions of California that experience heavy air pollution. The San Francisco Bay Area has one of the highest population densities in California, and the San Pablo site (SP) and East Oakland (EO) sites are separated by a distance of 30 km within this region. A comparison between these locations enables an evaluation of the sharp spatial gradients for UFP driven by the influence of local sources. Both SP and EO are surrounded by vehicular, industrial, commercial and residential sources. The SP location is within 5 km of a major chemical refinery while the EO location is within 5km of the Oakland International Airport and within 15 km of the Port of Oakland. The greater Los Angeles (LA) region is one of the largest population and economic hubs in the United States. The USC campus in Los Angeles is near major freeways and downwind of important sources including Los Angeles International Airport and the trucking routes connecting the Port of Los Angeles and the Port of Long Beach to the interstate freeway system. Fresno (FR) is the largest city in the heavily polluted San Joaquin Valley, which has some of the worst air quality in the state because of the topography that encourages long stagnation events. The Fresno sampling location is bounded by commercial/residential neighborhoods on 3 sides and agricultural fields on the remaining side. The FR sampling location was within 3 km of a moderately busy state highway (99) that is a major route for the movement of agricultural goods.

Sample collection at SP, EO and LA started August 2015 and ended July 2015 (duration of twelve months). Due to scheduling difficulties, sampling at FR was conducted during Jan, Feb, Apr, Jun, Jul of 2016 (five months of sampling). Each sampling site was equipped with two Micro-Orifice Uniform Deposit Impactor (MOUDIs) that were operated in parallel to obtain samples averaged over 3-days. UFP samples in the diameter range 56 – 100 nm were collected on the last stage of each MOUDI accounting for ~80% of the UFP mass [16]. The first MOUDI was loaded with pre-baked aluminum substrates (Foil 0100-96-0573A-X; MSP Corp., Shoreview, MN, USA) for subsequent analysis of elemental carbon and organic carbon. The second MOUDI used Teflon membrane filters (Teflo R2PJ047; Pall Corp., Port Washington, NY, USA) that were later extracted and analyzed for the concentration of elements.

A 1.5 cm^2 portion of each foil substrate was analyzed with Sunset Laboratory EC/OC analyzer following the National Institute for Occupational Safety and Health (NIOSH) temperature protocol [127] modified to avoid melting the aluminum in the sample by reducing the final temperature below 800°C [16]. Teflon samples were extracted by sonicating them in a mixture of nitric acid and acetone followed by evaporation under nitrogen [128]. Samples were then analyzed using Inductively Coupled Plasma Mass Spectrometry (Agilent ICP-MS 7900) for a series of elements (Li, S, K, Mn, Fe, Ga, As, Se, Br, Rb, Sn, Sb, Ba, and Pb, etc). Instrument minimum detection limits [129] and method minimum detection limits were calculated. Precision of the OC/EC and elemental analysis was assessed by re-analysis of 10% of total samples (shown in Supporting Information). Table 3-2 summarizes the components quantified in the current analysis, along with potential sources and health effects of those components.

Table 3-2. Ultrafine particulate matter components measured in the current study, potential sources for these components, and potential health effects.

Component	Sources	Health effects
OC	Fossil fuel, biomass burning, agricultural	Cardiovascular, respiratory, heart rate variability [130, 131]

Component	Sources	Health effects
Py C	Biomass burning	Respiratory[132]
EC	Fossil fuel, biomass burning	Cardiovascular, respiratory, heart rate variability [130, 131]
Li	Glazed ceramic production [133]	Respiratory [134]
Mg	Fossil fuels	No measurable pulmonary toxicity [135]
S	Fossil fuels	Cardiovascular [131]
K	Biomass burning, meat cooking	Respiratory [130, 131]
V	Fossil fuels, smelting	Cardiovascular, respiratory [131, 136-138]
As	Fossil fuels, automotive, smelting	Vasospasticity, cell function, heart rate variability, cancer, chronic arsenic poisoning [139, 140]
Se	Fossil fuels, steel production, glazed ceramic production[133]	Selenium poisoning[140]
Br	Marine aerosol, biomass burning, pesticides[141]	Cell function, heart rate variability[130]
Rb	Biomass burning	Respiratory[130]
Mo	Steel production [133]	Respiratory [142]
Sn	Fossil fuels, steel production [133, 143]	Respiratory [144]
Sb	Fossil fuels, crustal dust, smelting[143, 145, 146]	Cell function, heart rate variability, respiratory[145]
Pb	Fossil fuels, smelting, glazed ceramic production[133, 143]	Metabolic disorder and neuropsychological problems [143]

Daily concentrations of ultrafine particulate matter components were created at each sampling location by applying the 3-day average measurements to each individual day of the week over the full year analysis period. The 3-day collection pattern does not repeat on a weekly basis and so trends for individual days of the week emerge from analyzing multiple weeks of samples. Measurements falling on holidays were not used in the analysis to avoid biasing the non-holiday weekly profiles. It should be noted that the use of 3-day averages partially smooths day-of-week trends.

3.3 Results

3.3.1 Annual Mean Concentration and Weekly Trends

Table 3-3 shows the annual mean concentrations of UFP species at SP, EO, LA, and FR. Organic carbon (OC), elemental carbon (EC) and pyrolized carbon (PyC) make up the majority of the UFP mass. $PM_{0.1}$ OC is emitted from most combustion sources including vehicles, industrial sources, biomass burning, and meat cooking [147] . $PM_{0.1}$ EC is emitted from diesel vehicles and sources of incomplete combustion [147]. Trace elements (lithium, magnesium, sulfur, potassium, vanadium, arsenic, selenium, bromine, rubidium, molybdenum, tin, antimony and lead) are analyzed here because they were measured above detection limits and previous studies have shown that they can be measured in the UFP size fraction with reasonable accuracy and precision [128]. Sulfur is the most abundant trace ultrafine element measured in the current study, with annual mean concentration ranging from 2.75 ng/m^3 to 16.34 ng/m^3. Possible sources of S in California include diesel trucks, commercial marine vessels, and oil refineries. Potassium (0.94 – 2.41 ng/m^3) and magnesium (0.14 – 0.29 ng/m^3) are the second and third most abundant elements measured. Potassium has been used as a tracer for residential wood burning [148, 149]; it could also be present in other forms of biomass burning, such as wildfire, campfire, and meat cooking. Comparing the four sites in the current study, Los Angeles (LA) had the highest OC and EC concentrations. FR had the highest annual mean sulfur concentration, which is probably because only data from Jan to May was available for FR, or because there is local source that emits sulfur. FR also had the highest magnesium, potassium, arsenic, bromine, rubidium and tin concentrations.

Table 3-3. Annual mean concentrations of ultrafine particle components at San Pablo (SP), East Oakland (EO), Los Angeles (LA) and Fresno (FR) in ng/m^3.

	SP	EO	LA	FR
OC	97.7	129.4	142.2	125.0
Py C	35.0	49.9	47.8	50.0
EC	37.8	37.5	55.9	30.6
Li	0.0004	0.0008	0.0014	0.0010
Mg	0.1730	0.1417	0.152	0.286
S	7.37	7.88	3.00	17.3
K	0.941	1.1861	1.06	2.41
V	0.0080	0.0067	0.0132	0.0019
As	0.0125	0.0170	0.0205	0.0267
Se	0.0272	0.0207	0.0458	0.0165
Br	0.0804	0.0883	0.173	0.1980
Rb	0.0015	0.0020	0.0018	0.0035
Mo	0.0087	0.0147	0.0196	0.0024
Sn	0.0360	0.0691	0.122	0.107
Sb	0.0169	0.0393	0.0949	0.0182
Pb	0.0592	0.0967	0.0514	0.0630

The day-of-week trends for ultrafine species based on a full year of measurements are shown in Figures 3-1 through 3-4 for the four sites considered in the current analysis. All day-of-week profiles are normalized to the annual mean concentrations shown in the title of each sub-panel. Student t-tests were performed on the highest and lowest day-of-week for each subpanel displayed in Figures 3-1 through 3-4. Asterisks (*) denote significant difference ($p<0.05$) between the highest and lowest day of the week, while plus signs (+) denote strong ($0.05< p < 0.1$) difference. Among all the species, OC, EC and pyrolized carbon (PyC) display similar patterns for highly urbanized locations SP, EO and LA. The weekly trends of OC and PyC are relatively flat with slightly higher values in the middle of the week or on the 5th day of the week, while EC values start to rise on Monday, peak on Wednesday and then decline through the weekend. The observation of the higher EC concentrations on weekdays vs. weekends is consistent with greater activity level of diesel vehicles on weekdays as found in previous studies (see for example, [122, 124],). It is interesting to note that these day-of-week EC trends are still apparent despite the widespread adoption of diesel particle filters (DPFs) in California which remove 99% of EC emissions from diesel vehicles [19]. The EC difference between the highest and lowest days of the week are statistically significant at SP (*p*=0.0001), EO (*p*=0.0028), and LA (*p*=0.0083). OC, PyC and EC day-of-week trends at FR are not statistically significant, which could be reflect a different source mixture around this sampling location vs. the other more heavily urbanized locations.

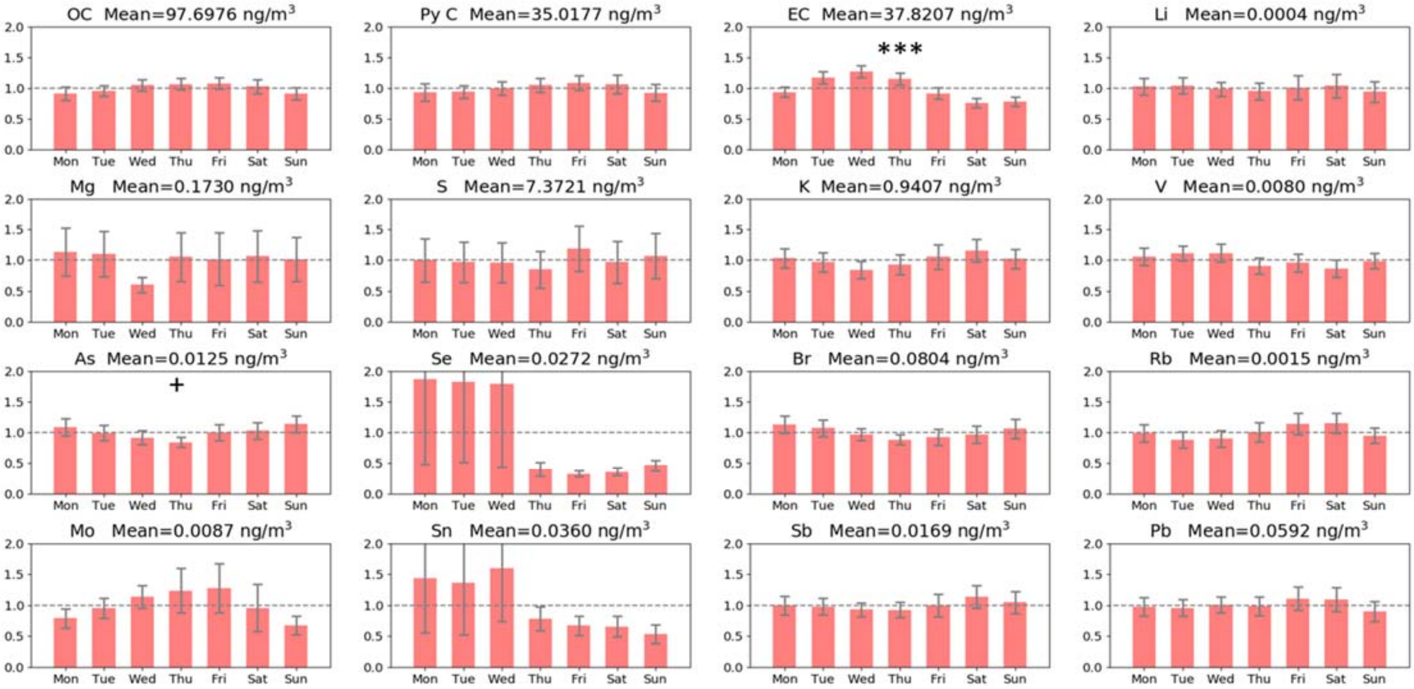

Figure 3-1. Annually averaged weekly profiles normalized to annual mean concentrations for ultrafine components at San Pablo. Error bars represent 1 standard deviation of the mean concentrations. * denotes $p<0.05$, ** $p<0.01$, *** $p<0.001$. + denotes $0.05<p<0.1$.

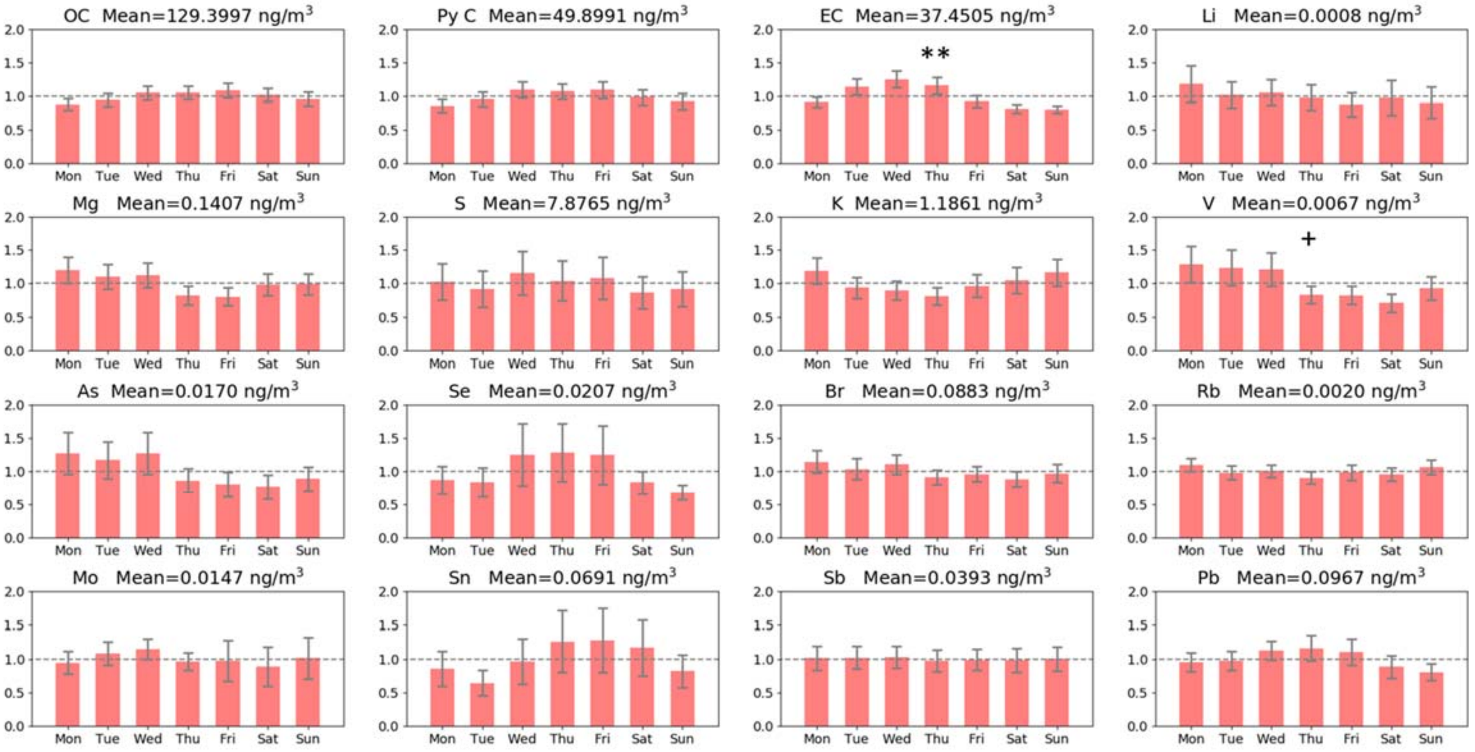

Figure 3-2. Annually averaged weekly profiles normalized to annual mean concentrations for ultrafine components at East Oakland. Error bars represent 1 standard deviation of the mean concentrations. * denotes $p<0.05$, ** $p<0.01$, *** $p<0.001$. + denotes $0.05<p<0.1$.

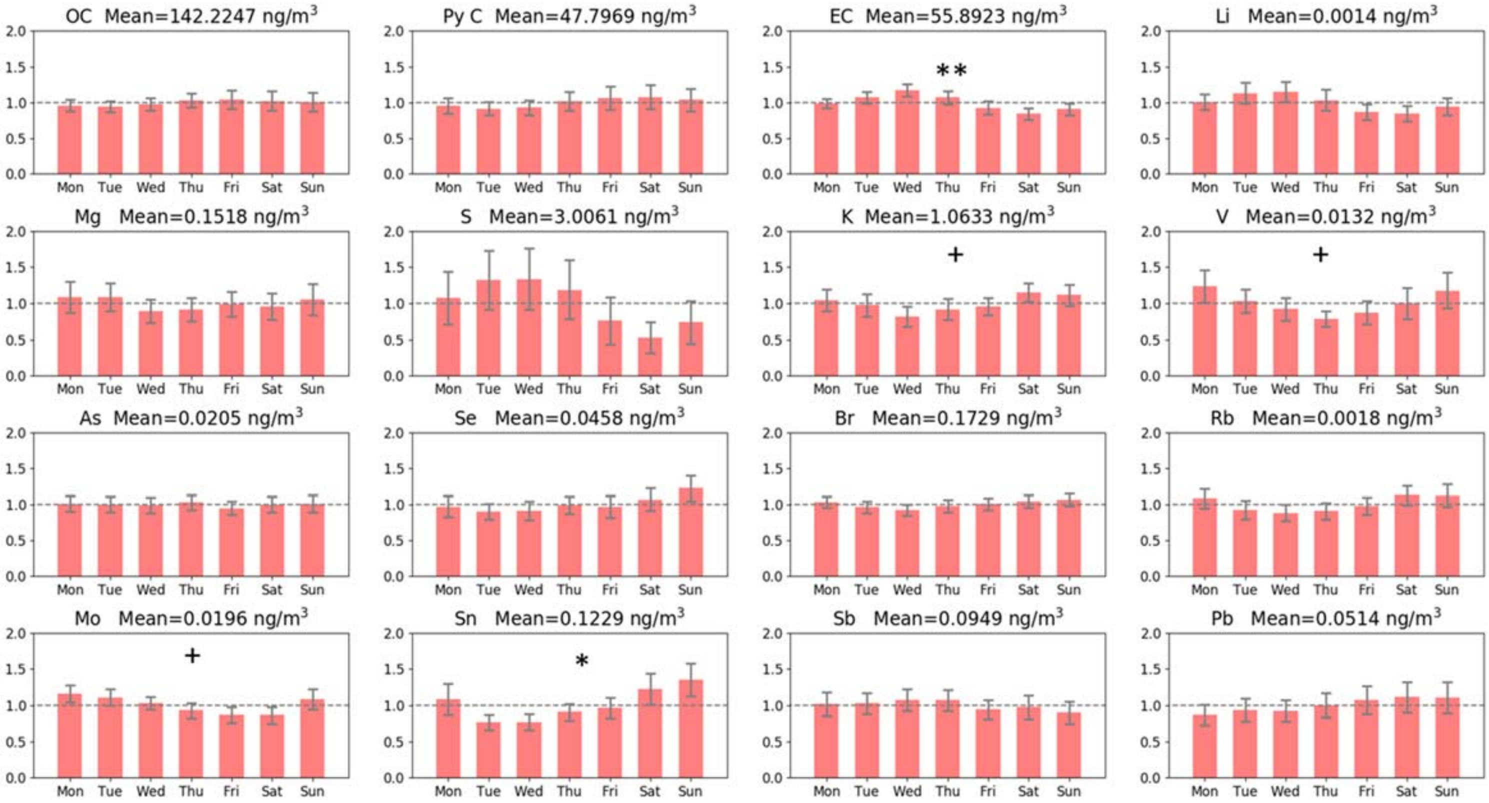

Figure 3-3. Annually averaged weekly profiles normalized to annual mean concentrations for ultrafine components at Los Angeles. Error bars represent 1 standard deviation of the mean concentrations. * denotes $p<0.05$, ** $p<0.01$, *** $p<0.001$. + denotes $0.05<p<0.1$.

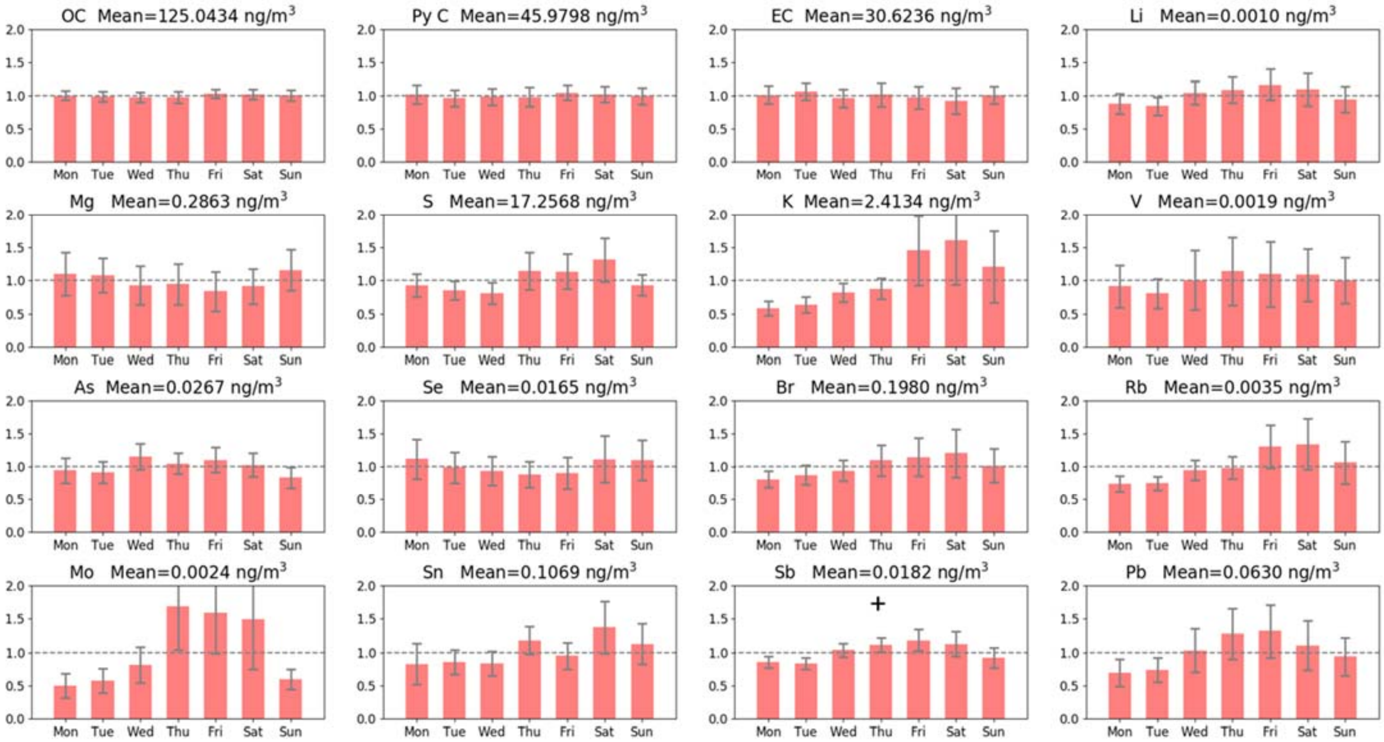

Figure 3-4. Annually averaged weekly profiles normalized to annual mean concentrations for ultrafine components at Fresno. Error bars represent 1 standard deviation of the mean concentrations. * denotes $p<0.05$, ** $p<0.01$, *** $p<0.001$. + denotes $0.05<p<0.1$.

Concentrations of Mg, K, and Rb follow similar day-of-week trends at all four sampling sites, with higher concentrations on Friday, Saturday and Sunday. These trends are visually apparent, but they are not statistically significant due to high variability from week to week. This pattern may result from a subset of sources that emit Mg, K, and Rb having a strong day-of-week activity pattern. $PM_{0.1}$ K and Rb are correlated [43], and both elements have been found in woodsmoke [148]. K and Rb can therefore be treated as tracers for UFP biomass burning sources, such as residential woodsmoke, wildfires, and campfires. The measured day-of-week trends suggest greater activity from these sources on weekends.

3.3.2 Correlation Analysis

The similarity in two day-of-week profiles ("A" and "B") was quantified using a dotproduct (eq 1).

$$\text{dotproduct} = \frac{\sum_{i=1}^{7} C_i^{(A)} \cdot C_i^{(B)}}{\sqrt{\sum_{i=1}^{7}(C_i^{(A)})^2} \cdot \sqrt{\sum_{i=1}^{7}(C_i^{(B)})^2}} \qquad \text{E1}$$

where $C_i^{(A)}$ denotes the concentration of the ith day of the week of trend A, and $C_i^{(B)}$ denotes the concentration of the ith day of the week of trend B. Dotproduct values of 1.0 indicate perfect agreement between two day-of-week profiles, while dotproduct values of 0.0 indicate no agreement. Comparisons can be made where "A" and "B" represent different elements at the same site, or where "A" and "B" represent the same element at different sites.

3.3.2.1 Correlation between Different Elements at the Same Site

Tables 3-4 through 3-7 display the correlation between weekly trends for different elements at the same site. Values greater than 0.9 are marked in bold to represent strong similarity in day-of-week trends. The weekly trends for various species at each site can be grouped based on the dotproducts in combination with the plots in Figures 3-1 through 3-4.

In Table 3-4 (site SP) UFP species OC, PyC, Mo, and Pb are assigned to be Group I(M-F) because these species all follow the pattern with concentration increasing from Monday, peaking on Friday and then declining through weekend. Trends for OC, PyC and Pb are very flat while Mo has much more obvious difference between highest and lowest day of the week. UFP species K, As, Br, Rb and Sb are assigned to Group II(S-M). Each of these UFP elements has minimum concentrations during the middle of the week and higher concentrations on the weekend or immediately following the weekend. Timing is slightly different for subsets of Group II(S-M) species since K, Rb and Sb (Group IIa) peak on Saturday while As and Br (Group IIb) peak on Sunday / Monday. Group III(M-W) (V, Sn, and Se) features higher concentrations from Monday to Wednesday and decreasing concentration thereafter. Sn and Se are abnormally high on Mondays to Wednesday which could be driven by unusual events. Several refinery flares occurred in the San Francisco Bay Area during June 2016 that may have released ultrafine metals to the atmosphere.

Table 3-4. Dot products between ultrafine constituents at the same site. Dot product is calculated based on one (1) year of measurements at San Pablo (SP).

SP	OC	Py C	EC	Li	Mg	S	K	V	As	Se	Br	Rb	Mo	Sn	Sb	Pb
OC	1															
Py C	**0.969**	1														
EC	0.747	0.583	1													
Li	0.627	0.634	0.629	1												
Mg	0.647	0.669	0.610	0.830	1											
S	0.649	0.665	0.512	0.738	0.789	1										
K	0.636	0.721	0.408	0.837	**0.926**	0.835	1									
V	0.529	0.391	0.865	0.742	0.674	0.707	0.536	1								
As	0.454	0.479	0.453	0.764	0.868	0.885	0.898	0.727	1							
Se	0.367	0.228	0.801	0.730	0.562	0.498	0.413	**0.938**	0.596	1						
Br	0.325	0.286	0.579	0.785	0.820	0.735	0.748	0.856	**0.921**	0.823	1					
Rb	0.792	0.899	0.364	0.715	0.795	0.774	**0.910**	0.348	0.695	0.203	0.467	1				
Mo	**0.979**	**0.926**	0.831	0.684	0.713	0.692	0.641	0.639	0.501	0.488	0.425	0.756	1			
Sn	0.536	0.396	0.882	0.753	0.595	0.537	0.456	**0.939**	0.583	**0.978**	0.772	0.318	0.636	1		
Sb	0.497	0.602	0.240	0.751	0.793	0.737	**0.949**	0.425	0.868	0.316	0.692	0.825	0.459	0.339	1	
Pb	**0.911**	**0.948**	0.600	0.822	0.755	0.786	0.832	0.542	0.645	0.422	0.494	**0.930**	0.893	0.552	0.726	1

In Table 3-5 (site EO), OC, PyC, S, Se, Sn and Pb are assigned to Group I(M-F) because of the higher concentrations in the middle of the week. Consistent with site SP, Group II(S-M) at EO also demonstrates higher concentrations on weekends, but the elements in this group are different at EO and SP. Group II(S-M) elements at EO include K and Rb, while Group III(M-W) elements (concentrations higher Monday to Wednesday) include Li, Mg, V, As, and Br. It should be noted that SP and EO are separated by a distance of approximately 30 km and so they can be used to investigate the spatial gradients in UFP concentrations. Although SP and EO both have three day-of-week trends (Groups I(M-F), II(S-M), and III(M-W)), the species contained in each group varies between sites. This finding is consistent with past measurements indicating that UFPs are dominated by fresh emissions and therefore more influenced by emissions sources around the measurement site as opposed to $PM_{2.5}$ concentrations that are strongly influenced by secondary concentrations.

Table 3-5. Dot products between ultrafine constituents at the same site. Dot product is calculated based on one (1) year of measurements at East Oakland (EO).

EO	OC	Py C	EC	Li	Mg	S	K	V	As	Se	Br	Rb	Mo	Sn	Sb	Pb
OC	1															
Py C	**0.988**	1														
EC	0.743	0.826	1													
Li	0.495	0.524	0.712	1												
Mg	0.505	0.519	0.672	**0.930**	1											
S	0.823	0.870	0.845	0.710	0.651	1										
K	0.532	0.467	0.341	0.730	0.823	0.534	1									
V	0.521	0.573	0.792	**0.908**	**0.944**	0.761	0.714	1								
As	0.484	0.547	0.801	**0.923**	**0.939**	0.764	0.654	**0.989**	1							
Se	**0.915**	**0.952**	0.855	0.602	0.501	**0.940**	0.407	0.607	0.600	1						
Br	0.528	0.574	0.743	**0.914**	**0.934**	0.810	0.747	**0.982**	**0.980**	0.630	1					
Rb	0.559	0.536	0.508	0.805	0.897	0.689	**0.956**	0.857	0.814	0.512	0.893	1				
Mo	0.724	0.781	0.892	0.680	0.793	0.818	0.555	0.874	0.857	0.728	0.838	0.723	1			
Sn	**0.941**	**0.905**	0.614	0.532	0.451	0.781	0.577	0.438	0.404	0.889	0.477	0.550	0.530	1		
Sb	0.565	0.609	0.775	0.818	**0.937**	0.743	0.705	**0.963**	**0.954**	0.578	**0.946**	0.854	**0.934**	0.417	1	
Pb	0.892	**0.937**	**0.907**	0.682	0.586	**0.938**	0.450	0.698	0.686	**0.988**	0.701	0.561	0.781	0.857	0.653	1

Tables 3-4 and 3-5 identify OC, PyC and Pb as species in Group I(M-F) for both SP and EO. UFP day-of-week profiles for Pb were somewhat correlated with Group I species at both of these locations. Pb was phased-out of motor-vehicle gasoline over 40 years ago, but Pb is still present in paved road dust and Pb is still used in general-aviation gasoline for piston-engine aircraft. Pb is also emitted from metal recycling facilities and from waste incinerators. K and Rb belong to Group II(S-M) at both SP and EO, reflecting the higher incidence of biomass burning activities such as fireplaces (winter) or campfires (summer) on weekends. The higher concentration at the beginning of the week is likely associated with lingering $PM_{0.1}$ from Sunday. V present in Group III(M-W) for both SP and EO is associated with shipping activities during weekdays, because both SP and EO are adjacent to the Port of Oakland.

Table 3-6 summarizes correlations between day-of-week profiles for different UFP elements at LA. Group I(M-F) consists of OC, PyC and Pb, with relatively flat weekly trends and a slight increase starting Friday. Group II(S-M) exhibits lower concentration in the middle of the week and contains Mg, V, Mo, K, Br, Rb, Sn and Se. Among these Group II(S-M) species, only K and Rb have similar values on Saturday and Sunday, with other species having Saturday concentrations lower than Sunday concentrations. Group III(M-F) at LA includes EC, Li and S which peak on Wednesday and then decrease throughout the week.

Table 3-6. Dot products between ultrafine constituents at the same site. Dot product is calculated based on one (1) year of measurements at Los Angeles (LA).

LA	OC	Py C	EC	Li	Mg	S	K	V	As	Se	Br	Rb	Mo	Sn	Sb	Pb
OC	1															
Py C	**0.962**	1														
EC	0.543	0.392	1													
Li	0.435	0.315	**0.978**	1												
Mg	0.499	0.572	0.575	0.641	1											
S	0.525	0.398	**0.987**	**0.984**	0.672	1										
K	0.755	0.863	0.449	0.474	0.844	0.510	1									
V	0.519	0.604	0.579	0.648	**0.930**	0.647	0.884	1								
As	0.687	0.670	0.786	0.810	0.775	0.826	0.825	0.825	1							
Se	0.757	0.835	0.326	0.334	0.645	0.346	0.871	0.750	0.731	1						
Br	0.803	0.891	0.457	0.459	0.842	0.513	**0.981**	0.880	0.817	**0.904**	1					
Rb	0.697	0.831	0.334	0.360	0.791	0.390	**0.972**	0.889	0.749	0.888	**0.970**	1				
Mo	0.368	0.362	0.781	0.857	0.879	0.840	0.670	**0.904**	0.838	0.542	0.674	0.630	1			
Sn	0.767	0.875	0.324	0.330	0.721	0.362	**0.946**	0.829	0.749	**0.961**	**0.968**	**0.976**	0.576	1		
Sb	0.615	0.500	**0.946**	**0.914**	0.575	**0.947**	0.553	0.598	0.844	0.347	0.539	0.441	0.725	0.406	1	
Pb	**0.936**	**0.963**	0.467	0.417	0.610	0.467	0.866	0.634	0.702	0.866	0.874	0.806	0.433	0.858	0.516	1

Table 3-7 shows that OC and PyC comprise Group I(M-F) at FR, with very flat day-of-week profiles. Mg and Se are placed in Group II(S-M) with lower concentrations in the middle of the week. Li, S, K, Br, Rb, Mo, Sn, Sb and Pb are grouped because their day-of-week profiles is low at the beginning of the week and then peaks on Thursday, Friday or Saturday. This profile is assigned as Group IV since it was not observed at the other sites.

Table 3-7. Dot products between ultrafine constituents at the same site. Dot product is calculated based on one (1) year of measurements at Fresno (FR).

FR	OC	Py C	EC	Li	Mg	S	K	V	As	Se	Br	Rb	Mo	Sn	Sb	Pb
OC	1															
Py C	**0.954**	1														
EC	0.557	0.550	1													
Li	0.776	0.849	0.511	1												
Mg	0.571	0.552	0.895	0.398	1											
S	0.833	0.836	0.486	0.882	0.435	1										
K	0.897	0.858	0.429	0.893	0.447	**0.900**	1									
V	0.774	0.852	0.609	**0.972**	0.547	**0.897**	0.874	1								
As	0.643	0.776	0.582	**0.917**	0.435	0.728	0.711	0.878	1							
Se	0.763	0.742	0.644	0.501	0.855	0.635	0.660	0.610	0.480	1						
Br	0.826	0.825	0.541	**0.956**	0.476	**0.946**	**0.958**	**0.952**	0.808	0.601	1					
Rb	0.877	0.867	0.431	**0.939**	0.413	**0.911**	**0.992**	**0.912**	0.776	0.612	**0.974**	1				
Mo	0.701	0.751	0.467	**0.948**	0.289	**0.929**	0.832	**0.923**	0.831	0.387	**0.940**	0.881	1			
Sn	0.687	0.655	0.437	0.771	0.496	**0.913**	0.864	0.835	0.568	0.660	**0.902**	0.852	0.809	1		
Sb	0.764	0.832	0.478	**0.997**	0.354	0.898	0.893	**0.962**	**0.907**	0.473	**0.960**	**0.940**	**0.965**	0.784	1	
Pb	0.734	0.793	0.556	**0.986**	0.407	0.868	0.864	**0.969**	0.883	0.441	**0.954**	**0.912**	**0.960**	0.775	**0.984**	1

3.3.2.2 Correlation between Different Sites for the Same Element

Table 3-8 examines the similarity between day-of-week profiles for the same UFP elements at different sites. Dotproduct values greater than 0.90 are interpreted as strong agreement and are marked in bold. The only UFP species that have strong agreement between sites are OC, EC, PyC, K, V and Rb. As discussed previously, OC and PyC are in Group I(M-F) for all sites, showing relatively consistent weekly trend with slightly higher concentration on Friday for SP, EO and LA. This trend reflects the combined effect from vehicular emission, food cooking, and industrial activities. K and Rb are in Group II for SP, EO and LA, with concentrations lowest in the middle of the week. This trend reflects higher biomass burning activity on weekends. The dotproducts for Rb day-of-week profiles between SP, EO and LA are not as large as those for K, probably due to the slightly different trend between Saturday and Sunday. Weekend concentrations are still higher than weekday concentrations for both K and Rb. The proximity of site SP and EO leads to dotproducts as high as 0.996 for these two sites for PyC, 0.98 for V, 0.971 for OC and 0.911 for EC.

Table 3-8. Dot products between four sites for same elements. Dot product is calculated based on annual mean concentrations of each day of a week.

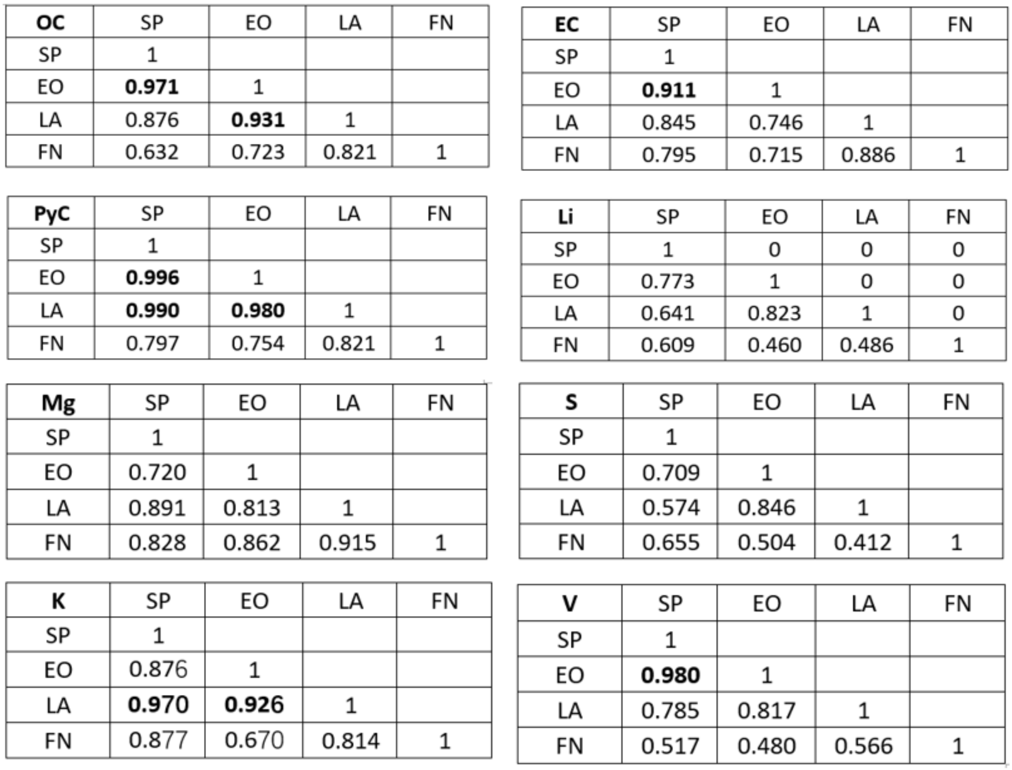

OC	SP	EO	LA	FN
SP	1			
EO	**0.971**	1		
LA	0.876	**0.931**	1	
FN	0.632	0.723	0.821	1

EC	SP	EO	LA	FN
SP	1			
EO	**0.911**	1		
LA	0.845	0.746	1	
FN	0.795	0.715	0.886	1

PyC	SP	EO	LA	FN
SP	1			
EO	**0.996**	1		
LA	**0.990**	**0.980**	1	
FN	0.797	0.754	0.821	1

Li	SP	EO	LA	FN
SP	1	0	0	0
EO	0.773	1	0	0
LA	0.641	0.823	1	0
FN	0.609	0.460	0.486	1

Mg	SP	EO	LA	FN
SP	1			
EO	0.720	1		
LA	0.891	0.813	1	
FN	0.828	0.862	0.915	1

S	SP	EO	LA	FN
SP	1			
EO	0.709	1		
LA	0.574	0.846	1	
FN	0.655	0.504	0.412	1

K	SP	EO	LA	FN
SP	1			
EO	0.876	1		
LA	**0.970**	**0.926**	1	
FN	0.877	0.670	0.814	1

V	SP	EO	LA	FN
SP	1			
EO	**0.980**	1		
LA	0.785	0.817	1	
FN	0.517	0.480	0.566	1

As	SP	EO	LA	FN
SP	1			
EO	0.648	1		
LA	0.782	0.737	1	
FN	0.554	0.645	0.655	1

Se	SP	EO	LA	FN
SP	1			
EO	0.512	1		
LA	0.185	0.340	1	
FN	0.591	0.328	0.803	1

Br	SP	EO	LA	FN
SP	1			
EO	0.875	1		
LA	0.806	0.584	1	
FN	0.435	0.359	0.791	1

Rb	SP	EO	LA	FN
SP	1			
EO	0.562	1		
LA	0.772	0.829	1	
FN	**0.936**	0.544	0.733	1

Mo	SP	EO	LA	FN
SP	1			
EO	0.718	1		
LA	0.443	0.800	1	
FN	0.893	0.406	0.187	1

Sn	SP	EO	LA	FN
SP	1			
EO	0.458	1		
LA	0.296	0.667	1	
FN	0.169	0.789	0.812	1

Sb	SP	EO	LA	FN
SP	1			
EO	0.458	1		
LA	0.420	0.770	1	
FN	0.646	0.391	0.674	1

Pb	SP	EO	LA	FN
SP	1			
EO	0.809	1		
LA	0.790	0.601	1	
FN	0.879	0.851	0.868	1

e

Groups II(S-M), III(M-W), and IV identified in Tables 3-4 through 3-7 often contained different UFP species indicating that the same UFP species have different day-of-week patterns at different sites. This is reflected by the lack of strong correlations between these species at different locations in Table 3-8. For example, at SP the species As and Br are in Group II(S-M) together with K and Rb, while at EO they belong to Group III(M-W) with higher concentrations from Monday to Wednesday. Similarly, UFP Se is present in Group III(M-W) at SP, in Group I(M-F) at EO, and Group II(S-M) at LA. These day-of-week patterns reflect the emission pattern of nearby sources that will be investigated in the following Chapter 4.

3.3.3 Day of Week Profiles in Different Seasons

In the previous sections, measured 3-day average concentrations at each site were used to build up the day-of-week profiles. This approach increases the power of the analysis mapping 3-day averages to specific days of the week, but seasonal variations may also contribute to variation that maks important differences. Paired t tests were carried out based on the original 3-day average data to study day-of-week variation while normalizing for seasonal variability. Samples spanning Friday to Sunday or Saturday to Monday were treated as weekend samples, and samples that are right before or after the weekend samples were regarded as paired weekday samples. Paired samples are likely to experience similar meteorological conditions which reduces the uncertainty in the paired comparison.

Table 3-9 summarizes the statistically-significant results from the paired t-test analysis across the entire 12 month measurement period. Statistically significant differences in paired weekend – weekday samples were identified for UFP EC, K and Rb. As discussed previously, K and Rb are markers for biomass combustion. Surveys of consumer behavior indicate that Friday, Saturday and Sunday night are the most frequent residential wood burning periods [150]. Therefore, weekend – weekday pairs including Friday in weekday samples were excluded in the later analysis for K and Rb. Pairs including Monday in weekday samples were also excluded from paired t test since Monday may have lingering effect carried from weekend. The number of pairs tested for K and Rb are about half the number of pairs tested for EC due to this data exclusion criteria. There is significant difference between weekday and weekend for Rb at SP, for K and Rb at EO, and for Rb at LA. The weekday/weekend difference is statistically significant for EC at SP, EO and LA. There are no statistically significant differences observed at FR since the number of available pairs is too limited.

Table 3-9. *p* values for paired t-test of weekend vs weekday K, Rb and EC values. * denotes $p<0.05$, ** $p<0.01$, *** $p<0.001$.

Site	Number of pairs	K	Rb	Number of pairs	EC
SP	25	0.185	0.027*	43	7.509E-06***
EO	22	0.004**	0.022*	42	0.006**
LA	15	0.107	0.018*	29	0.019*
FR	4	0.306	0.270	8	0.080

The box plots of seasonal EC, K and Rb values on weekdays and weekends at EO are displayed in Figures 3-5 through 3-7, where statistical significance is denoted with an asterisk. In Figure 3-5, EC is significantly higher on weekdays than weekends in winter, and this trend is also visible for fall. The weekday concentrations are only slightly higher than weekend concentrations in spring and summer. This pattern could be explained by the annual cycle in mixing depth that amplifies the effects of changing emissions rates when mixing depth is low (fall and winter) with less amplification when mixing depth is higher (spring and summer). Another possible explanation is the effect of cold-start emissions from gasoline vehicles in the colder fall and winter seasons leading to higher UFP EC emissions. Gasoline vehicle activity on weekends occurs later in the day when temperatures have increased.

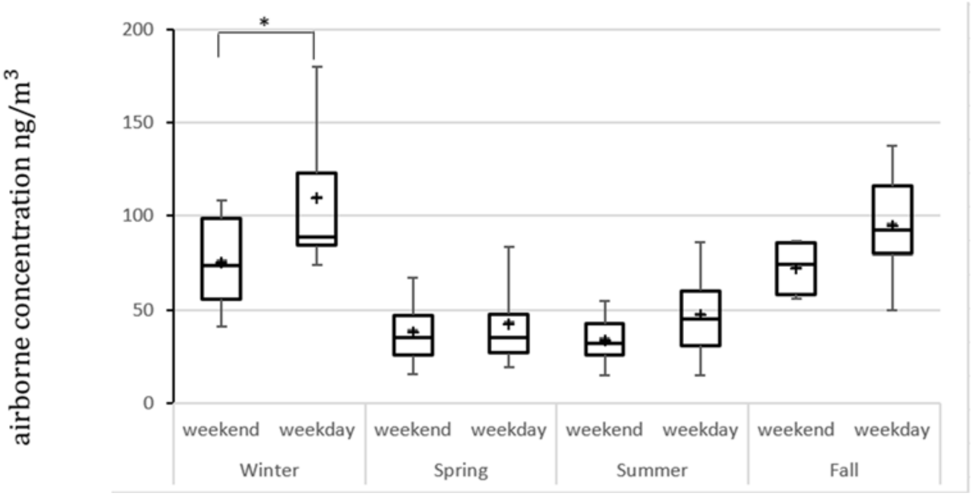

Figure 3-5. Weekend vs weekday concentrations for ultrafine EC at East Oakland in four seasons. * denotes $p < 0.05$. + represents the mean values. Boxes represent 25th and 75th percentile and whiskers represent 5th and 95th percentile.

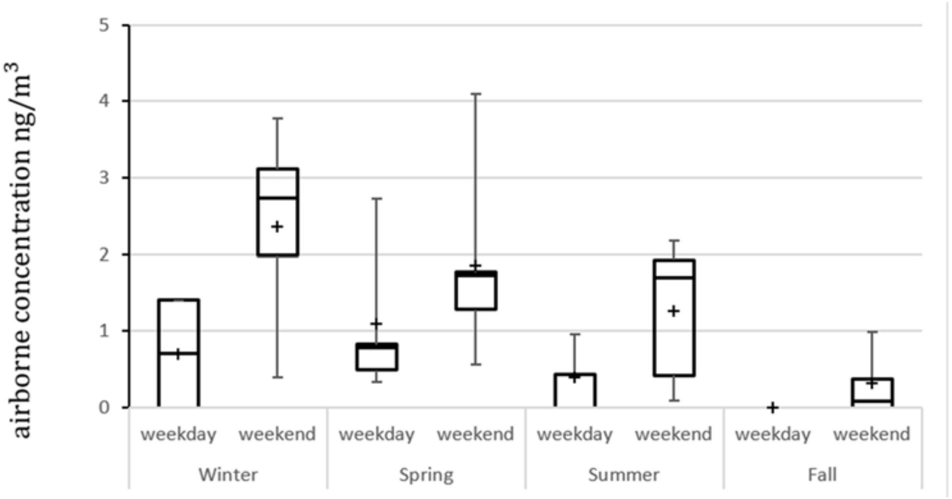

Figure 3-6. Weekend vs weekday concentrations for ultrafine K at East Oakland in four seasons. * denotes $p < 0.05$. + represents the mean values. Boxes represent 25th and 75th percentile and whiskers represent 5th and 95th percentile.

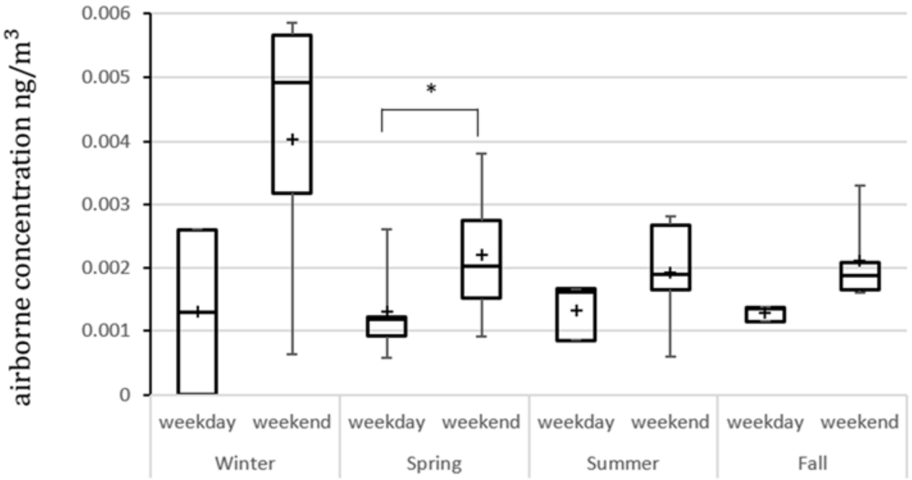

Figure 3-7. Weekend vs weekday concentrations for ultrafine Rb at East Oakland in four seasons. * denotes $p < 0.05$. + represents the mean values. Boxes represent 25th and 75th percentile and whiskers represent 5th and 95th percentile.

3.4 Discussion

The presence of a day-of-week trend for $PM_{0.1}$ EC and the absence of a day-of-week effect for $PM_{0.1}$ OC suggests that diesel engine emissions do not dominate $PM_{0.1}$ OC in the current study. Volatility measurements indicate that approximately 50-70% of the OC emitted by modern diesel engines may evaporate in the atmosphere [151] which suggests that particle evaporation does not completely mask the diesel $PM_{0.1}$ OC trend.

The presence of a minor day-of-week trend for $PM_{0.1}$ K and the absence of a trend for $PM_{0.1}$ OC also suggests that wood combustion does not strongly dominate $PM_{0.1}$ concentrations. By process of elimination, the overall results of the current study suggest that common combustion sources that are known to emit large amounts of $PM_{0.1}$ OC must be responsible for the observed concentrations, or secondary organic aerosol (SOA) formation must strongly contribute to the $PM_{0.1}$ OC. These questions will be investigated using a variety of techniques in the remaining Chapters of the current report.

3.5 Conclusions

A comprehensive analysis of the day-of-week trends for sixteen components of ultrafine particulate matter was carried out over an annual cycle at four sites in California. This analysis reveals location-specific patterns along with important general trends. A comparison between different elements at the same location identified ultrafine components with highest concentrations on weekdays (Group I(M-F)), weekends (Group II(S-M)), or during the early week (Group III(M-W)). Across the most heavily urban sites, Group III(M-W) always contains EC (diesel engines). Across all sites, Group II(S-M) always contains K and Rb (biomass combustion). Ultrafine OC, PyC, and 11 other trace components did not display strong day-of-week concentration patterns, suggesting that multiple sources contribute to these ultrafine components.

A paired t-test constructed using measurements on weekends compared to measurements immediately preceding or immediately following the weekend confirms that ambient ultrafine particle concentrations associated with diesel engines (EC) are highest on weekdays while ambient ultrafine particle concentrations associated with biomass combustion (K and Rb) are highest on weekends in California. These weekly cycles in ultrafine particulate matter source contributions may have implications for public health.

A detailed trend analysis for the same element at different locations shows that the two closest sampling locations (SP and EO) have the great number of ultrafine particle components with identical weekly trends, but even at these locations only four out of 16 components displayed the exact same day-of-week profiles. Less similarity was observed in measured day-of-week profiles for ultrafine particle elements at other sites. This suggests that the details of ultrafine particle concentrations at each sampling site reflect the mixture of sources immediately adjacent to that site. By extension, individual neighborhoods across California will each experience unique day-of-week concentration profiles for ultrafine particle components that reflect the surrounding sources.

4 POSITIVE MATRIX FACTORIZATION OF ULTRAFINE PARTICLE MASS ($PM_{0.1}$) AT THREE SITES IN CALIFORNIA

Preamble: Chapter 4 performs a statistical analysis on the year of ultrafine particle measurements using the Positive Matrix Factorization (PMF) approach. The resolved factor profiles are linked back to sources where possible and comparisons are made between source contributions as a function of season and location. The analysis in Chapter 4 is the first of three independent methods that estimate source contributions to UFP in the current report.

4.1 Introduction

Receptor-based source apportionment studies for environmental pollutants typically use chemical mass balance (CMB) models or factor analysis techniques to quantify source contributions to ambient concentrations. Both approaches assume that the ratio of chemicals emitted by a source are conserved during transport and dilution in the environment so that the ambient concentration pattern can be described as a linear combination of source contributions. The CMB approach measures the "source profiles" in advance of the ambient concentrations and can be applied to one or more ambient measurements. The factor analysis approach derives the "factor profile" from a long series of ambient measurements (typically > 60) but then must rely on expert opinion to assign source names to each factor.

CMB and factor analysis each have advantages and disadvantages that complement one another. CMB source identification is unambiguous but the method requires that all sources are a-priori using expensive analysis techniques in order to yield accurate results for complex environmental samples. Factor analysis requires a long time series of environmental measurements with (potentially) less expensive analytical techniques, but the resulting factors may represent blended source contributions.

Ultrafine particulate matter (UFP; $Dp < 0.1$ μm) is an emerging environmental pollutant of concern. UFP is toxic in laboratory tests [152-154] and recent epidemiological studies have found associations between UFP (characterized by the mass of particles with diameter < 0.1 μm; $PM_{0.1}$) and increases mortality [7] and adverse birth outcomes [8, 42]. Both CMB and factor analysis have been used to calculated source contributions to $PM_{0.1}$ in California at multiple sites during a 4-week intensive study or at a single site during a full annual cycle [18, 155]. A broader set of long-term measurements at multiple sites would provide additional information about the sources that contribute to $PM_{0.1}$ concentrations that may affect public health in California.

The purpose of this Chapter is to describe factor analysis results from a year of $PM_{0.1}$ samples collected at two sites in Northern California and one site in Southern California. The details of the factor analysis solution are reviewed, major sources of UFP are identified, the locations of sources relative to measurement sites are discussed, and the seasonal patterns of source contributions to UFP concentrations are analyzed. The results provide new information about source contributions to UFP concentrations in California.

4.2 Methods

4.2.1 Sample Collection and Analysis

$PM_{0.1}$ samples were collected continuously over 3 day intervals from August 2015 to July 2016 at San Pablo (SP), East Oakland (EO), and Los Angeles (LA) yielding approximately 120 samples at each location. The SP location is 3 km to the northwest of San Francisco Bay and is within 5 km of a major chemical refinery. The EO location is 5 km northeast of the Oakland International Airport and 15 km east of the Port of Oakland. Both the SP and EO measurements sites are surrounded by vehicular, industrial, commercial and residential sources. The sampling site at LA was located at the University of Southern California campus which is surrounded by major highways and downwind of the Los Angeles International Airport and the Port of Los Angeles. $PM_{0.1}$ samples at Fresno were also collected over six months from late December 2016 to July 2016 with a gap of one month leaving only five months of data or approximately 50 samples that were insufficient for PMF analysis. Results for Fresno are will not be discussed further in the current Chapter, but they are discussed in Chapter 5 using CMB analysis.

$PM_{0.1}$ samples at all sites were collected using Micro Orifice Uniform Deposit Impactors (MOUDIs) on Teflon and aluminum foil impaction substrates. Thirty-four elements were solvent extracted off Teflon substrates and analyzed by ICP-MS following the methods described by Herner et al. [128]. Organic carbon (OC) and elemental carbon (EC) concentrations were measured on samples collected with aluminum foil substrates using thermal optical method methods as described by Herner et al. [16]. OC and EC were separated into OC 1,2,3,4, and EC 1,2,3,4,5,6 at different temperature ranges under helium only, or 98% helium and 2% oxygen conditions. Figure 2-6 illustrates a generic thermogram for OC and EC analysis.

Samples periods with missing analytes were excluded from the PMF analysis.

4.2.2 Positive Matrix Factorization (PMF) Analysis

EPA PMF 5.0 is a factor analysis model that quantifies source-factor contributions within a multicomponent time series. PMF solves the chemical balance equation between measured species concentrations $X_{i,j}$ and derived source-factor chemical profiles $f_{k,j}$ assuming some a-priori number of important sources P to predict the amount of mass $g_{i,k}$ contributed by each source-factor to concentrations in each individual sample , as shown in Eq. (1).

$$x_{ij} = \sum_{k=1}^{p} g_{ik} f_{kj} + e_{ij} \tag{Eq.1}$$

$X_{i,j}$ is the concentration of species j in sample i, and e_{ij} is the residual for each sample/species. The factor-source contributions $g_{i,k}$ and profiles $f_{k,j}$ are calculated by minimizing the objective function Q (Eq. 2), where μ_{ij} represents the uncertainty associated with species j in sample i.

$$Q = \sum_{i=1}^{n} \sum_{j=1}^{m} \left[\frac{x_{ij} - \sum_{k=1}^{p} g_{ik} f_{kj}}{u_{ij}} \right]^2$$

(Eq.2)

PMF differs from traditional factor analysis techniques by requiring that all factor contributions are positive but it does not require that all factor profiles be orthogonal. The uncertainty for each reconstructed species concentration in the PMF analysis is calculated based on the measurement method detection limit (MDL) and error fraction when the concentration is greater than the MDL (Eq. 3); if the concentration is less than the MDL, the uncertainty was calculated as a fixed fraction of the MDL (Eq. 4).

$$Unc = \sqrt{(Error\ Fraction \times concentration)^2 + (0.5 \times MDL)^2}$$

(Eq. 3)

$$Unc = \frac{5}{6} \times MDL$$

(Eq. 4)

The signal to noise ratio (S/N) is calculated to quantify the input data quality, with automatic downweighting of species with low S/N. In the current study, species with $S/N > 1$ were categorized to Strong species while species with $0.5 < S/N < 1$ were categorized to Weak species. The uncertainty for Weak species was increased by a factor of 3 to reduce their influence on the model fit. Species with $S/N < 0.5$ were categorized to Bad and removed from the analysis [156].

A range of PMF solutions based on three to seven important sources (P) were examined in the current study. The optimal solution was determined considering the Q values, the results of model fit, and interpretability of the resulting factor profiles and time series [157]. Bootstrap and Displacement runs were performed to evaluate the stability of the solution. Rotation with different FPEAK strengths were run to find the optimal solution.

4.2.3 CPF Plots

Conditional Probability Function (CPF) plots were constructed by coupling hourly wind data with factor concentration throughout the sampling period using (Eq. 5)

$$\mathrm{CPF} = \frac{m_{\Delta\theta}}{n_{\Delta\theta}}$$

(Eq. 5)

where $m_{\Delta\theta}$ stands for the number of wind readings in direction θ with factor concentration exceeding a specified threshold and $n_{\Delta\theta}$ is the total number of wind readings in the same direction θ. Multiple target thresholds were tested and the upper 20th percentile was found to best resolve the directionality for factors in the current study. Wind speeds lower than 2 m sec^{-1} were excluded from the analysis. All wind data used in the analysis was “vectorized”.

4.3 Results and Discussion

4.3.1 Diagnostics

Table 4-1 summarizes the settings of the PMF base runs and results from error estimation including Displacement and Bootstrap. OC fractions, Pyrolised carbon, EC fraction, K, V, Br, Rb, Sn and Sb were categorized to Strong for all three sites because of their high S/N ratio and good fit by PMF. The species listed as Weak either had low S/N ratio or couldn't be simulated well ($R^2<0.7$) by PMF. This includes the most volatile OC fraction (OC1) which is prone to sampling bias due to partitioning between the gas and condensed phases. The Weak species also include EC1 consistently had $R^2<0.8$ in the PMF solution. The uncertainties for Weak species were thus enlarged in the PMF calculations but their existence in the species profile for factors could aid the identification of souces.

Q_{true} is the goodness-of-fit parameter calculated including all points input to the model, while Q_{robust} measures the goodness-of-fit calculated excluding points not fit by the model, which are defined as samples for which the uncertainty-scaled residual is greater than 4. The difference between these two parameters reflects the impact of data points with high scaled residuals. The small difference between Q_{true} and Q_{robust} for all three sites shows that most of the data points were predicted well by the model. Different numbers of factors were explored for all three sties, and the final solution was determined by assesing Q values, regression analysis for PM0.1 total mass and the Strong species, and interpretability of the resolved sources. The seven-factor solution was selected for all three locations since they achieved the best model fit for important species and they resolved factor profiles that were consistent with current knowledge about UFP source composition and weekly/sesonal activity patterns.

Correlation coefficient R^2 measures how well the predicted values match with the observed values. The R^2 values for the total $PM_{0.1}$ mass at SP, EO and LA are 0.96, 0.94 and 0.94, indicating that the resolved sources can effectively reproduce the measured values. Displacement (DISP) evaluates the stability of the PMF solution by adjusting each value in the factor profile and computing the new Q-value. The Q-values didn't increase or only had a minimal increase after the Displacement and no factors swapped after the DISP recomputation, indicating that the PMF solutions are robust. Bootstrap (BS) can be used to estimate whether a small set of observations affects the PMF solution by randomly sampling blocks of observations until the BS data set is the same size as the originial data set. A hundred BS data sets were processed with PMF and the factors resolved by each BS run would be mapped with base factors with which the BS factor contribution has the highest and greater than $R>0.8$ correlation. The mapping of BS runs for all three sites are all larger than 96% which indicates that the PMF solution is not overly influenced by a small portion of data points.

Table 4-1 Summary of PMF parameters and error estimation results at San Pablo, East Oakland, and Los Angeles

Diagnostic	San Pablo	East Oakland	Los Angeles
Strong species	OC2-4, PyC, EC2-3, K, V, Br, Rb, Sn, and Sb	OC2-3, PyC, EC2-3, K, V, Br, Rb, Sn, and Sb	OC2-3, PyC, EC2-3, K, V, Br, Rb, Sn and Sb
Weak species	OC1, EC1, EC4, Li,Na, Mg, Ca, Cr, Mn, Co, Zn, Ga, As, Se, Sr, Mo, Ag, Cd, Tl, Pb, and U	OC1, OC4, EC1, EC4, Li, Na, Mg, Ca, Cr, Mn, Zn, Ga, As, Se, Sr, Mo, Ag, and Pb	OC1, OC4, EC1, EC4, Li, Na, Mg, Ca, Mn, Co, Zn, Ga, As, Se, Sr, Mo, Ag, Cd, and Pb
Number of factors	7	7	7
Q_{robust}	2178	2012	2438
Q_{true}	2238	2106	2512
Slope for total PM0.1 mass	0.94	0.94	1.02
R^2 for total PM0.1 mass	0.96	0.94	0.96
DISP drop of Q	0	0	-0.098
DISP swapping	0	0	0
BS mapping, for Min Corr R=0.8	100% for 4 factors, and 96%, 99%	100% for 5 factors, and 98% for the other 2 factors	100% for all factors

4.3.2 Source Identification

Seven consistent $PM_{0.1}$ factors were resolved for SP, EO, and LA: Factor1-Gasoline+Motor Oil+Meat Cooking, Factor 2- Diesel+Motor Oil, Factor 3-Wood Burning, Factor 4-Shipping, Factor 5-Sea Spray, Factor 6-Sb (very low contribution at San Pablo), and Factor 7-Sn. Factor source names were chosen based on the chemical composition of each factor (Figures 4-1 through 4-3), the contribution that each factor makes to total $PM_{0.1}$ mass (Figures 4-4 through 4-6), the direction of each factor relative to the sampling site (Figures 4-7 through 4-9), and the time series of the factor concentrations (Figures 4-10 through 4-12).

Factors 1 and 2 contain the majority of the measured $PM_{0.1}$ OC and EC mass meaning they dominate total $PM_{0.1}$ mass. Factor 1 contains almost no EC3 while Factor 2 contains the majority of the EC3. Total EC is composed primarily of EC3, and so Factor 2 dominates total EC concentrations. Day-of-week analysis discussed in Chapter 3 indicates that total $PM_{0.1}$ EC concentrations peak in the middle of the week due to the increased activity of diesel engines during this time. Based on this evidence, Factor 2 is assigned the name diesel engines + motor oil.

Factor 3 was recognized to be Wood Burning because it contains more than half of the K and Rb which are known tracers for biomass combustion PM2.5 [43, 158], and because it contains significant amounts of OC1-4 and EC1-2. Pyrolyzed carbon formed during the analysis of wood smoke is expected to be measured as EC1-2. Factor 3 has peak concentrations during the winter season consistent with the pattern of residential wood combustion in California. This time pattern causes the wood burning factor to be unambiguously separated from all other PMF factors in the range of possible solutions.

Factor 4 contains over 80% of the V measured in $PM_{0.1}$ samples. Vanadium is often present in particles emitted from heavy fuel oil (HFO) combustion emission [133]. The source of Factor 4 is located in the direction of the San Francisco Bay and the Port of Oakland for the San Pablo and East Oakland locations. Based on this evidence, Factor 4 is assigned the name "shipping and other heavy fuel oil combustion".

Factor 5 is also from the direction of the ocean and contains high concentrations of Mg and Br, thus identifying it as Sea Spray. Factor 6 contains over 70% of Sb and Factor 7 contains over 70% of Sn. These two factors could be attributed to local industrial sources although it is curious that they are present at all three sampling locations. The exact source identify of these factors is not critical given that they contribute only a minor amount of total $PM_{0.1}$ mass.

Factor 1 is the largest contributor to PM0.1 mass at the two Northern California sites and the second largest contributor to PM0.1 mass at the Los Angeles site. Factor 1 is mainly composed of OC1-4 and EC1-2. It is expected that Factor 1 should correspond to the major sources of PM0.1 OC not already associated with the factors discussed above. Previous CMB studies carried out in Northern California [18] identified wood burning, food cooking, gasoline engine exhaust, and diesel engine exhaust as major sources of $PM_{0.1}$ OC. By process of elimination, Factor 1 in the current study was named to be a blend of gasoline, motor oil and meat cooking. PMF was not capable of individually resolving PM0.1 contributions from these three sources because they lack unique chemical tracers in the current study. Molecular markers capable of separating gasoline, motor oil, and meat cooking were measured in monthly composite samples (see Chapter 5) but not in 3-day average samples due to prohibitive costs.

PMF solutions using five and six factors were also considered in the analysis, but these solutions were not able to resolve the diesel factor which is a source of primary interest. Likewise, increasing the number of factors to eight caused a minor factor to be split from the Sn or Sb factor, further complicating the identification of sources. Overall, the seven factor PMF solution has better performance than other possible PMF solutions.

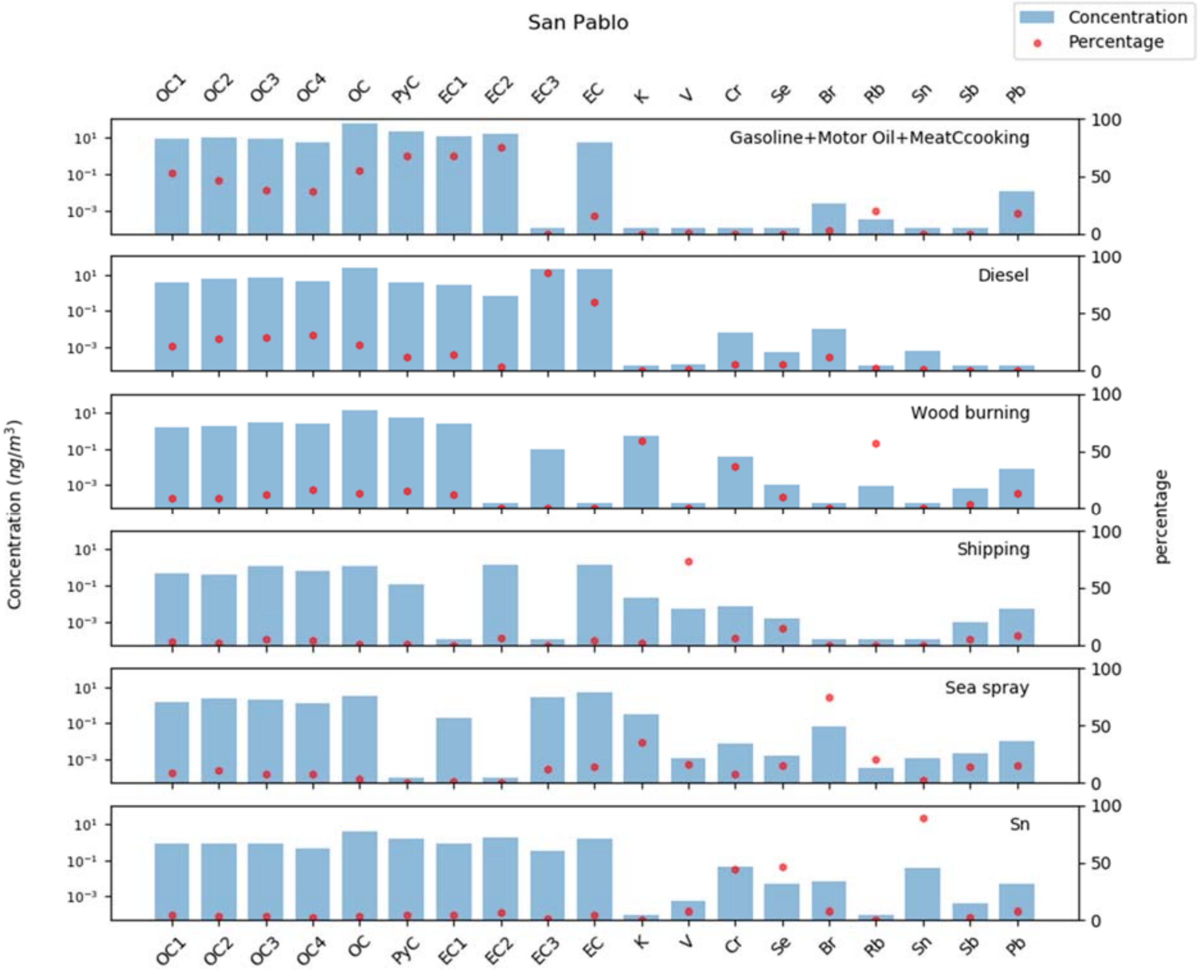

Figure 4-1: PMF species profile at San Pablo. Blue bar (left axis) represents concentration of species in each factor and red dots (right axis) represents the percentage of speices mass in each factor. Note that OC1, EC1, Cr, and Pb are weak species with higher uncertainty in the concentration profile.

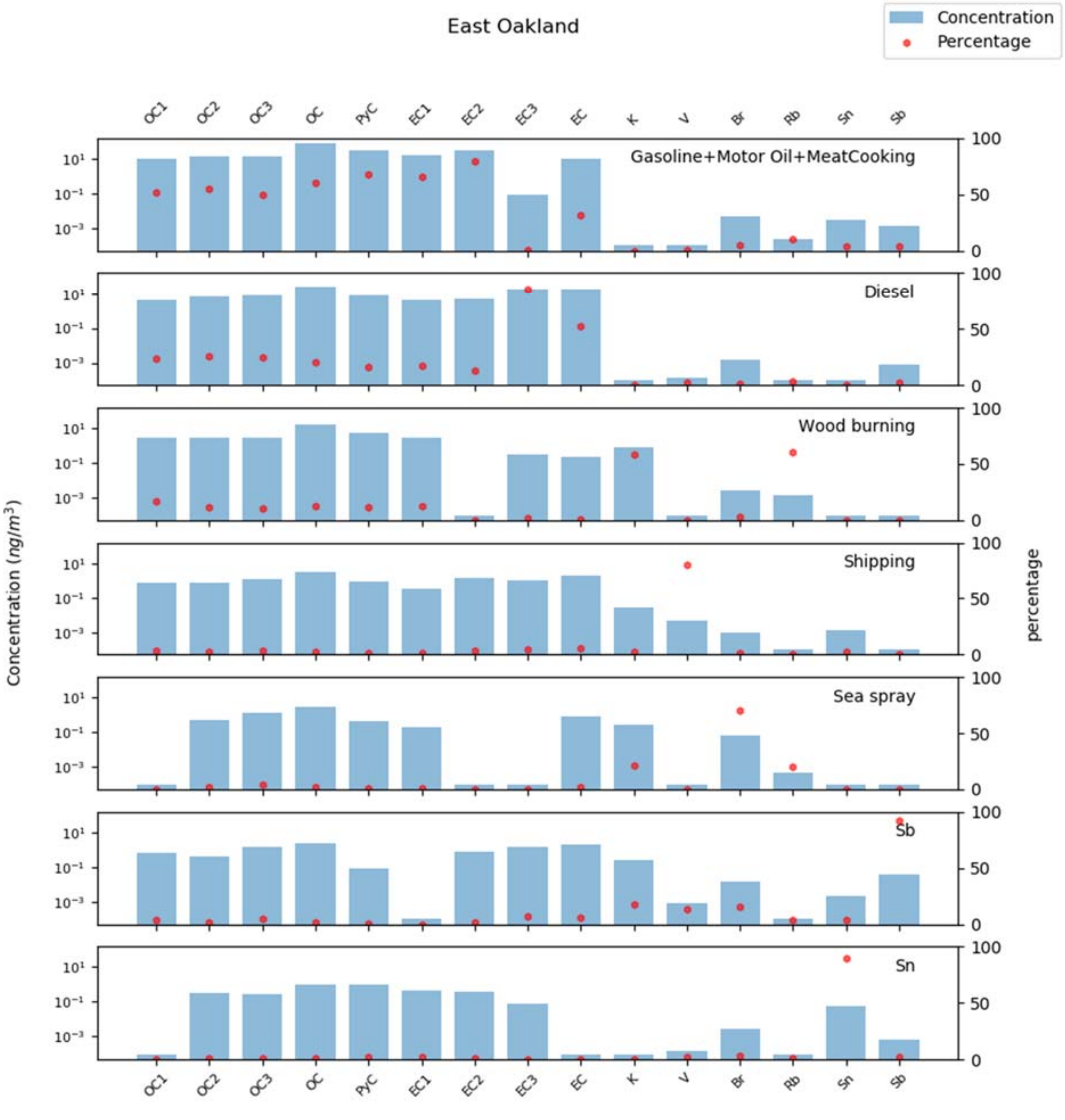

Figure 4-2: PMF species profile at East Oakland. Blue bar (left axis) represents concentration of species in each factor and red dots (right axis) represents the percentage of speices mass in each factor. Note that OC1 and EC1 are weak species with higher uncertainty in the concentration profile.

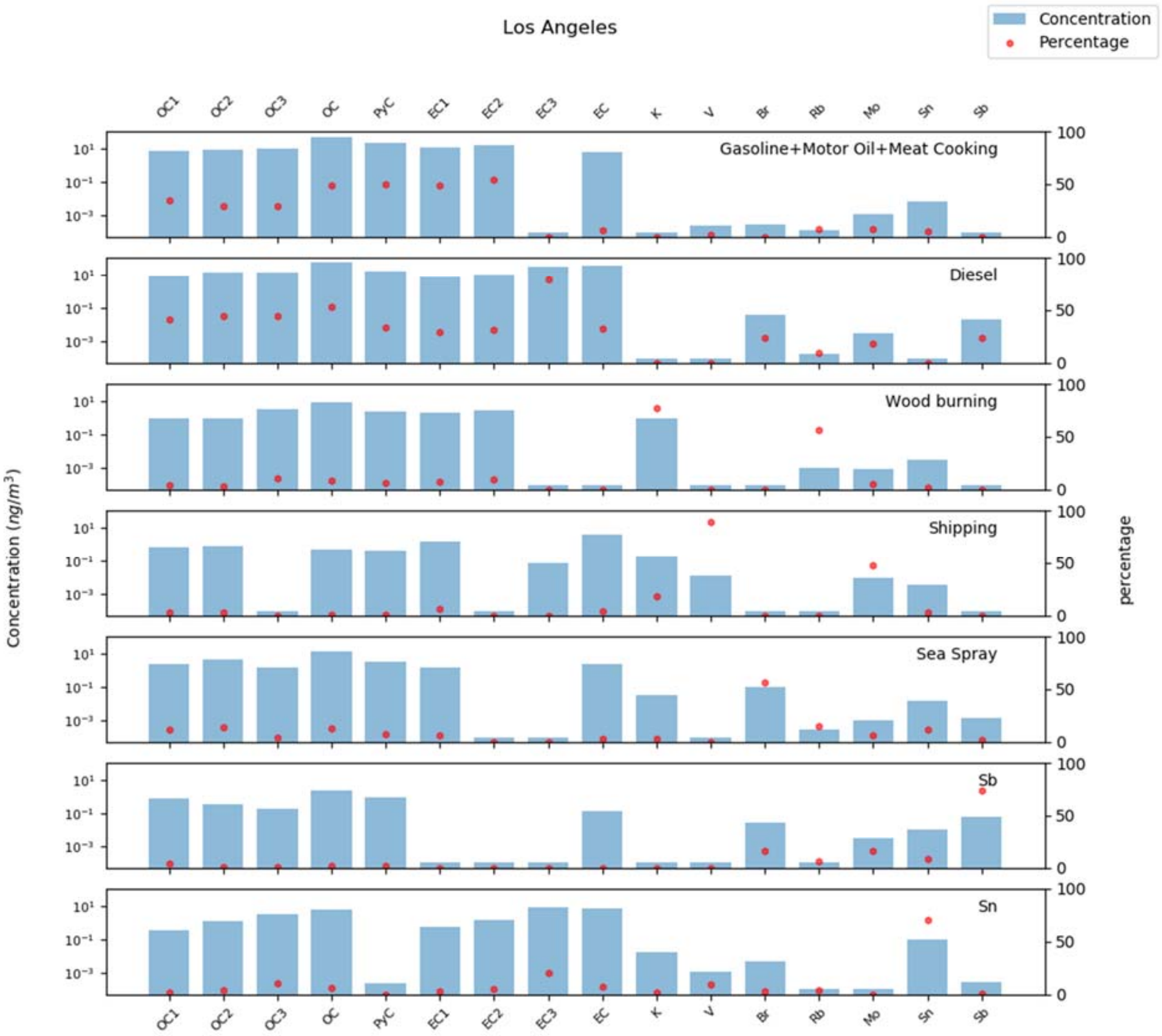

Figure 4-3: PMF species profile at Los Angeles. Blue bar (left axis) represents concentration of species in each factor and red dots (right axis) represents the percentage of speices mass in each factor. Note that OC1, EC1, and Mo are weak species with higher uncertainty in the concentration profile.

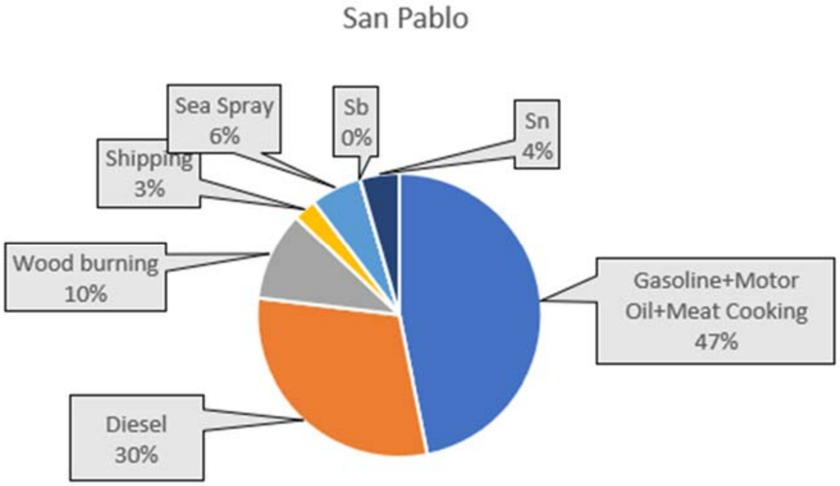

Figure 4-4: Factor contribution to PM0.1 mass at San Pablo.

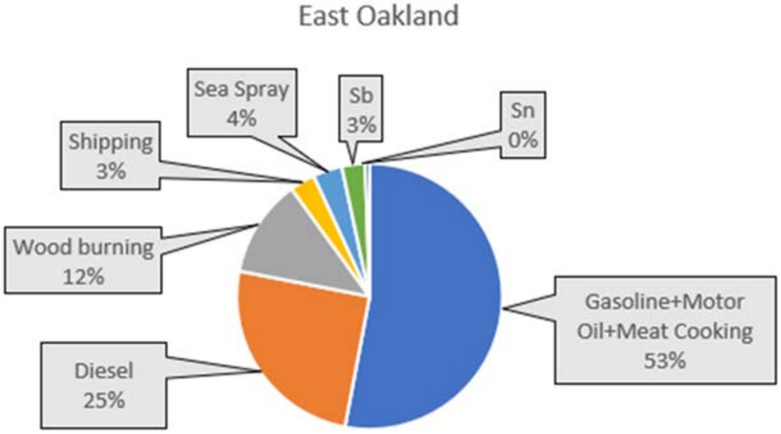

Figure 4-5: Factor contribution to PM0.1 mass at East Oakland.

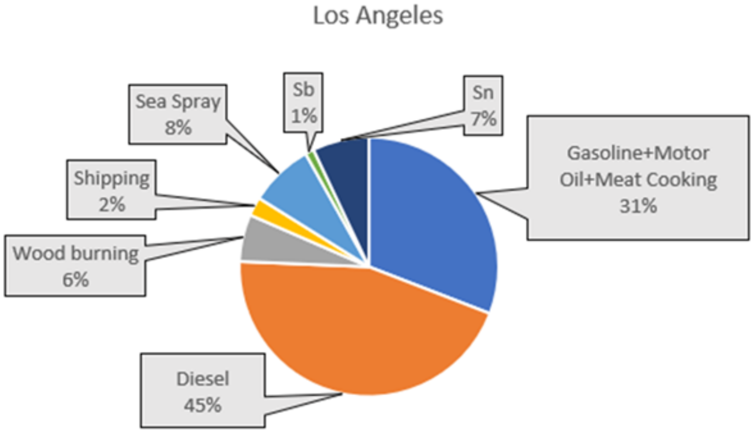

Factor 4-6: Factor contribution to PM0.1 mass at Los Angeles.

4.3.3 Source Location Conditional Probability Function (CPF)

Source Conditional Probability Function (CPF) plots show the most probable direction of sources relative to the measurement sites. As described in the previous section, “Shipping and other heavy fuel oil combustion” and “Sea Spray” at SP and EO are located in the direction of the ocean, which corroborates their source identification. The Wood Burning and Gasoline+Motor Oil+Meat Cooking sources at SP and EO are from the northeast, east and southeast, which is consistent with the location of commercial and residential areas. The CPF plot for diesel engines + motor oil at SP shows slightly more contribution from the east than the west, because although the sampling site is surrounded by major highways and road both in the east and the west, the I80 highway has higher traffice volume. Site EO has I880 to the west and I580 to the east, explaining why the CPF doesn’t show clear directionality. The CPF plots at LA have no directionality because the wind speed at the sampling location is very low which makes it difficult to conduct the analysis.

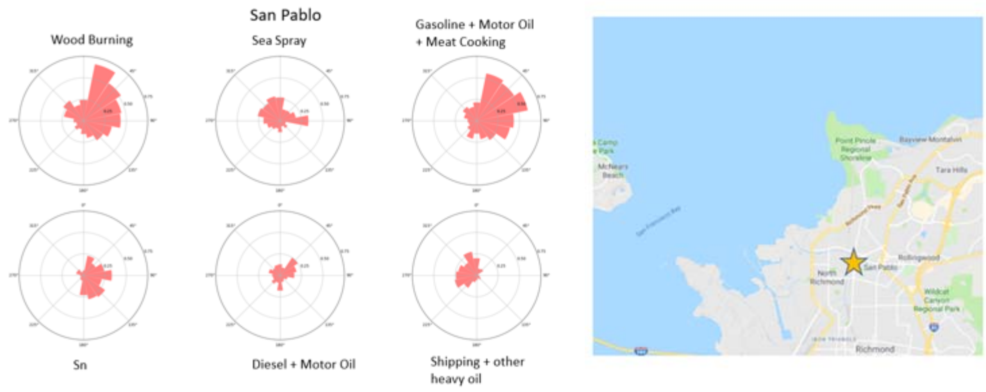

Figure 4-7: CPF plots and map of sampling location for San Pablo.

Figure 4-8: CPF plots and map of sampling location for East Oakland.

Figure 4-9: CPF plots and map of sampling location for Los Angeles.

4.3.4 Time Series

Figures 4-10 through 4-12 show the time series of source factor contributions to PM$_{0.1}$ concentrations over the annual sampling period with 3-day resolution. Monthly averaged source-factor contributions were plotted alongside the results from CMB (Chapter 5) in Figure 4-13 through 4-15. The source Gasoline+Motor Oil+Meat Cooking generally increases in fall/winter season at all three sites, most likely due to reduced atmospheric mixing in the colder season. Wood burning PM$_{0.1}$ concentrations also increased during winter due to increased source activity and reduced atmospheric mixing. Wood burning PM0.1 peaks during the Thanksgiving holiday in late November due to the effects of increased residential wood combustion. Diesel engine + motor oil contributions to PM0.1 are relatively constant thoughout the annual cycle at all three sites. The Sea Spray contributions are higher in warm season at SP and EO, coinciding with greater wind speed in warm season. This effect is not observed at Los Angeles, possibly because the sampling site is located farther from the coast giving the ultrafine particles time to coagulate with larger particles. The "Shipping ad other heavy fuel oil combustion", Sb and Sn sources have no clear seasonal trend. Sn exhibits a pattern consistent with a point source with plumes intermittently washing over the sampling site.

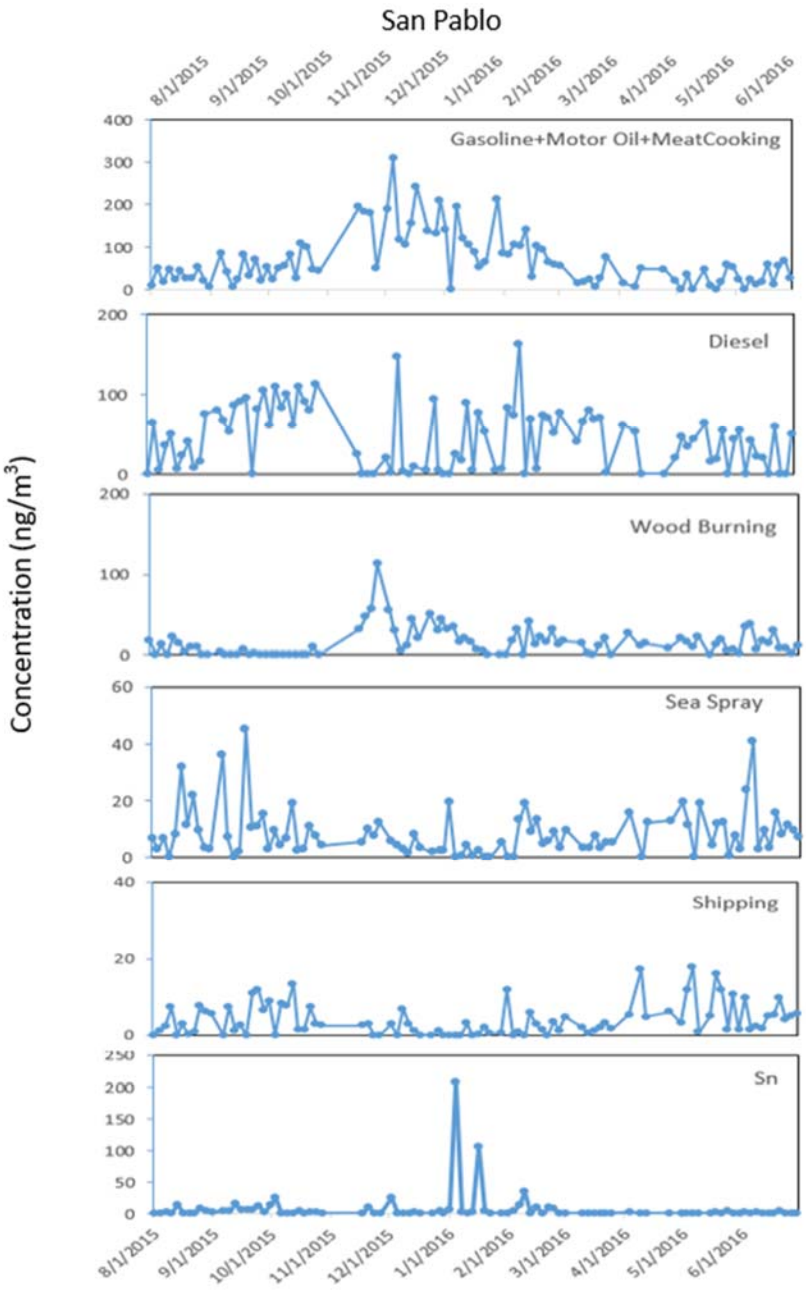

Figure 4-10. Time series of resolved factors at San Pablo.

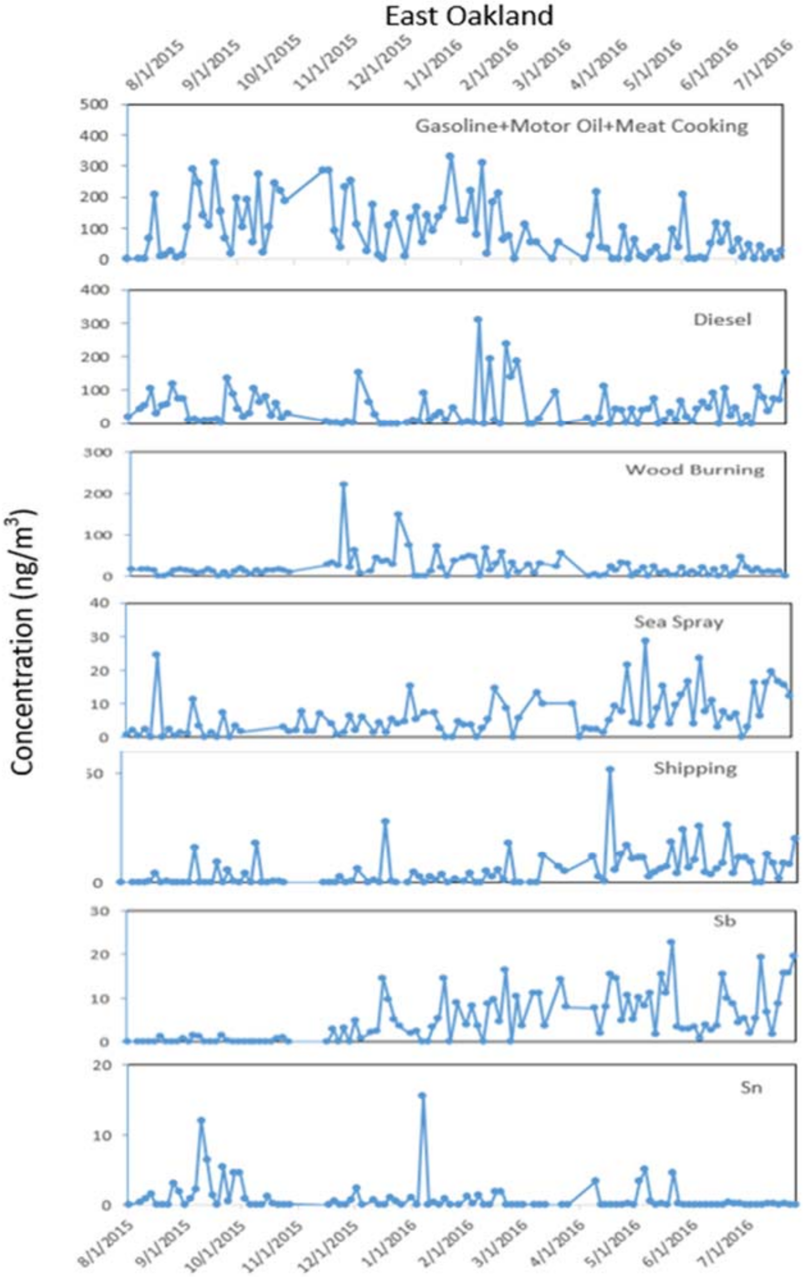

Figure 4-11. Time series of resolved factors at East Oakland.

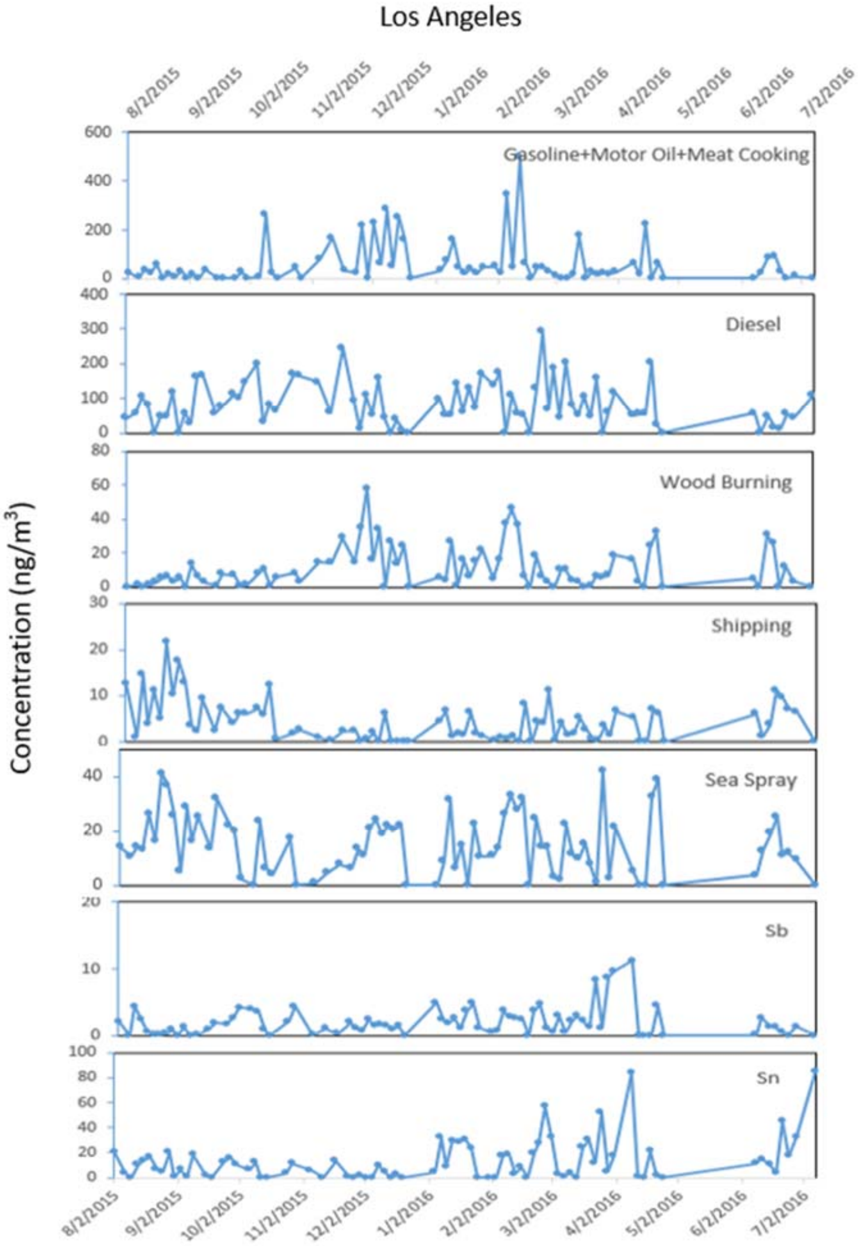

Figure 4-12. Time series of resolved factors at LA.

4.3.5 Comparison with CMB Results

Figures 4-13 through 4-15 compare monthly $PM_{0.1}$ concentrations from Wood burning, Diesel Engines + Motor Oil, and Gasoline+Motor Oil+Meat Cooking predicted by the PMF calculations in the current Chapter and the CMB calculations summarized in Chapter 5. PMF and CMB source predictions generally follow similar seasonal trends at all three sites, which confirms that both PMF and CMB can correctly resolve $PM_{0.1}$ sources. The PMF-Wood burning is higher than the CMB-Wood burning, especially in warmer seasons. This may be due to the chemical reaction of the Levoglucosan tracer used in CMB analysis. The K and Rb tracers used in PMF are non-reactive. This difference may be especially important for predicting the contribution to $PM_{0.1}$ mass from wildfires during the late summer and early fall when oxidant concentrations are high. Despite the differences in PMF vs. CMB predictions to wood burning in summer, both models predict that the highest $PM_{0.1}$ concentrations associated with wood burning occur during the late fall and winter seasons associated with residential wood combustion.

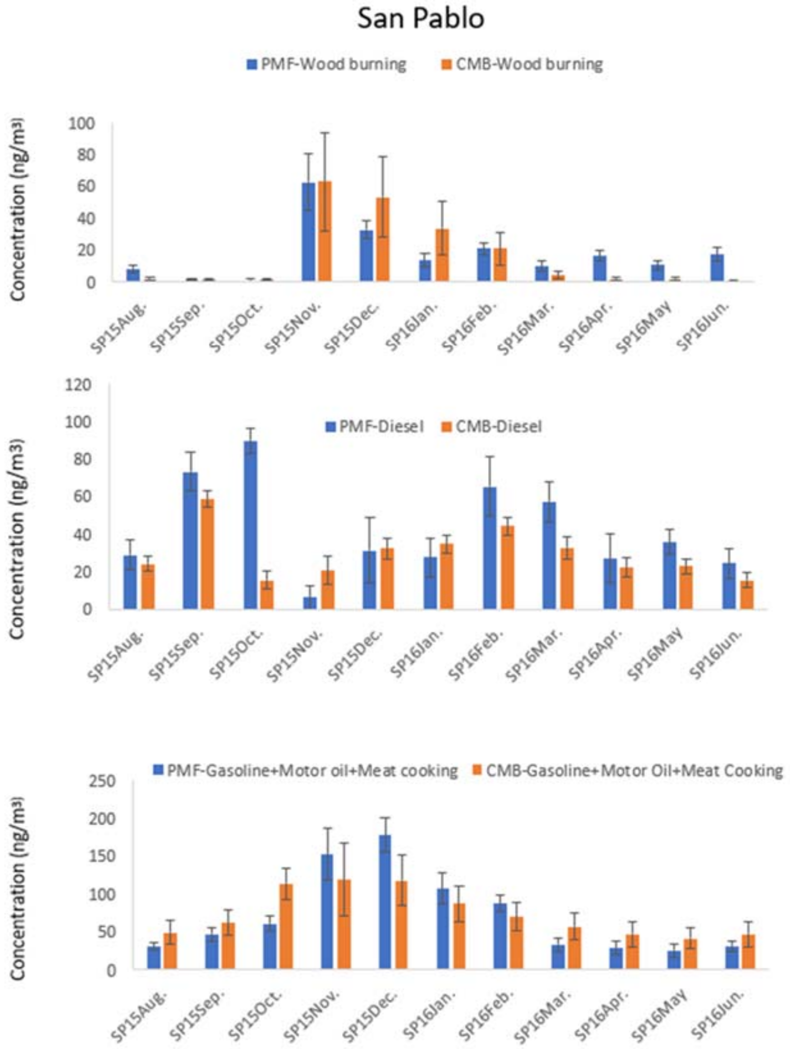

Figure 4-13. Comparison of monthly source contributions to PM0.1 predicted by PMF and CMB for San Pablo.

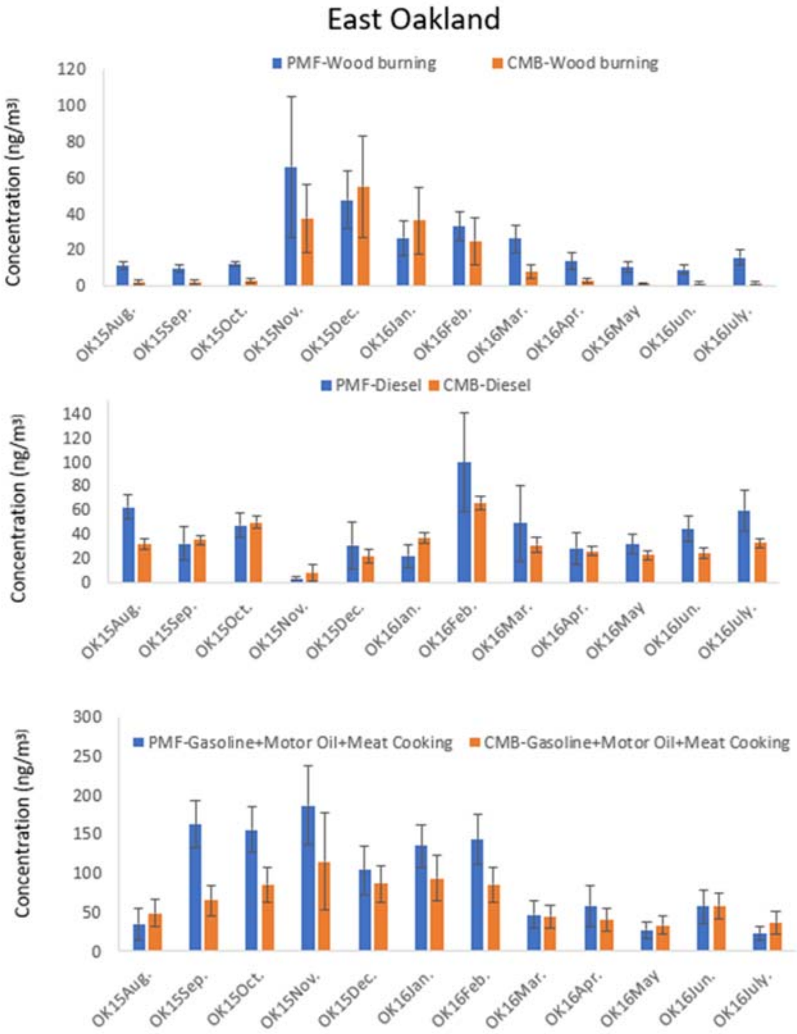

Figure 4-14. Comparison of monthly source contributions to PM0.1 predicted by PMF and CMB for East Oakland.

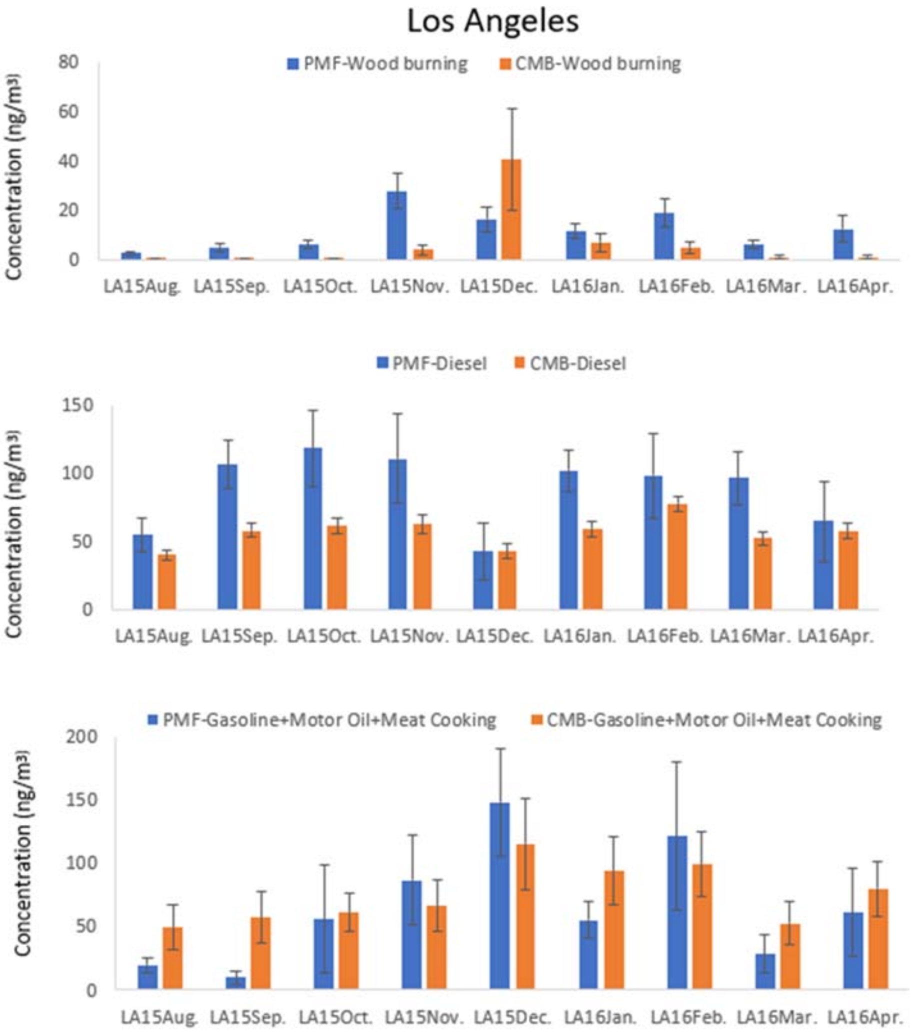

Figure 4-15. Comparison of monthly source contributions to PM0.1 predicted by PMF and CMB for Los Angeles.

4.4 Discussion

The inability to separately resolve source contributions to $PM_{0.1}$ from gasoline engines + motor oil + food cooking at a reasonable cost identifies a major limitation in the PMF analysis for long-term UFP trends. Molecular marker analysis for cholesterol, hopanes+steranes, and heavy PAHs would improve the ability to resolve gasoline engines, motor oil, and food cooking but the cost for this analysis would exceed \$550/sample * 120 samples * 4 sites = \$264,000 in the current project. These molecular markers are measured in monthly composite samples and analyzed with CMB analysis in Chapter 5 of the current report. This provides monthly source contributions from gasoline engines, motor oil, and food cooking, but does not identify possible day-of-week trends or high concentration spikes associated with special events.

The diesel engine + motor oil factor resolved in the current PMF analysis confirms that UFPs from diesel engines have a distinct weekly profile with highest concentrations in the early part of each week. This time profile may be useful in future health effects studies.

Perhaps the greatest strength of the PMF analysis presented in the current Chapter is the ability to identify new sources of $PM_{0.1}$ currently identified with the tracer elements Sb and Sn. The exact source name associated with these factors is an important topic for further research.

4.5 Conclusions

Three-day average samples of $PM_{0.1}$ collected over a full year at Los Angeles, East Oakland, and San Pablo were analyzed using Positive Matrix Factorization to identify source-factor contributions at each location. Seven $PM_{0.1}$ source-factors were identified: Factor1-Gasoline+Motor Oil+Meat Cooking, Factor 2- Diesel + Motor Oil, Factor 3-Wood Burning, Factor 4-Shipping and other heavy fuel oil combustion, Factor 5-Sea Spray, Factor 6-Sb and Factor 7-Sn. The majority of the $PM_{0.1}$ OC and $PM_{0.1}$ total mass was associated with the blended source Factor 1- Gasoline+Motor Oil+Food Cooking. The majority of the $PM_{0.1}$ EC as associated with source Factor 2 – Diesel Engines + Motor Oil. Source Factor 3 – Wood Burning contributions to $PM_{0.1}$ were highest in the winter season when residential wood combustion was active. The monthly-averaged $PM_{0.1}$ source apportionment results calculated by PMF in the current study are consistent with the $PM_{0.1}$ source apportionment results calculated using CMB in Chapter 5. PMF was able to split Diesel +Motor Oil from Gasoline+Motor Oil+Meat Cooking $PM_{0.1}$ based on the species EC3, but PMF failed to further resolve the major sources of $PM_{0.1}$ OC due to the lack of unique tracers. PMF further resolved "Shipping and other heavy fuel oil combustion" and Sea Spray sources based on inorganic tracers. The two factors Sn and Sb may be indicative of local industrial sources, but further research will be required to confirm this hypothesis.

5 SEASONAL AND ANNUAL SOURCE APPORTIONMENT OF CARBONACEOUS ULTRAFINE PARTICULATE MATTER ($PM_{0.1}$) IN POLLUTED CALIFORNIA CITIES

Preamble: Chapter 5 performs a statistical analysis on the year of ultrafine particle measurements using the Chemical Mass Balance (CMB) approach. Identified source contributions are summarized as a function of season and location. The analysis in Chapter 5 is the second of three independent methods that estimate source contributions to UFP in the current report.

5.1 Introduction

Ultrafine particles (with aerodynamic diameter ≤ 0.1 μm) have toxic properties, possibly because of their high surface area that can adsorb toxic substances, which may then be translocated to different regions of the body [1, 11, 12, 14]. The 1998 US National Research Council blueprint for particulate matter (PM) research identified ultrafine particles as a research priority [2]. Fifteen years later, the 2013 HEI Perspective on the Health Effects of Ultrafine Particles [3] confirmed the robust evidence for the toxicity of ultrafine particles but noted that epidemiological studies were inconclusive due to inconsistencies and limitations in the findings from both short- and long-term studies [4]. The lack of consistent epidemiologic results was also a factor in the 2009 US-EPA Integrated Science Assessment which concluded that the evidence was suggestive but not yet sufficiently developed to infer a causal relationship between ultrafine particles and human health [5].

A major limitation inherent in many epidemiological studies for ultrafine particles is simply lack of consistent long-term measurements necessary to support an accurate exposure assessment for all the features of interest. Ultrafine particle concentrations are typically quantified using number concentration (N_X; number of particles with diameter ≥ X nm) or mass ($PM_{0.1}$; mass of particles with diameter ≤ 0.1 μm). Total particle number concentration (N_X) is continuously measured at multiple locations in major California cities[159, 160] but measurements for $PM_{0.1}$ and ultrafine particle source contributions have been limited to shorter time periods (< 1 year) at a smaller number of sites. [15, 16, 18-24, 114, 161, 162] Recent epidemiological studies have found multiple adverse health outcomes associated with $PM_{0.1}$. [42, 163, 164] Longer-term (≥ 1 year) $PM_{0.1}$ measurements spanning a broader range of cities would help to fully test the relevant hypotheses about the potential health effects of ultrafine particles.

Here we describe a network of $PM_{0.1}$ measurements and source apportionment calculations carried out in four polluted California cities: Los Angeles (twelve months), East Oakland in the San Francisco Bay Area (SFBA) (twelve months), San Pablo in the SFBA (twelve months), and Fresno in the San Joaquin Valley (SJV) (six months). We focus on $PM_{0.1}$ organic carbon (OC) and elemental carbon (EC) concentrations at all locations since these two components are expected to comprise +90% of the total $PM_{0.1}$ mass.[16] Source contributions to $PM_{0.1}$ OC and EC are calculated using molecular markers. Semi-volatile $PM_{0.1}$ source profiles are developed to account for partial evaporation of OC and molecular markers after dilution in the atmosphere. A method to account for photochemical reaction is developed to account for the observed seasonal variation.

The effects of these modifications on calculated $PM_{0.1}$ source contributions are evaluated and trends in $PM_{0.1}$ concentrations and source contributions are discussed as a function of season and location. To the best of our knowledge, this is the first demonstration of an annual $PM_{0.1}$ sampling network with source apportionment in the world. The resulting dataset describing $PM_{0.1}$ concentrations and source contributions will be a useful resource for testing $PM_{0.1}$ exposure models that can support future epidemiological studies.

5.2 Sampling and Analysis

5.2.1 Sampling sites and periods

The $PM_{0.1}$ sampling network was deployed across four polluted cities spanning the wide range of air quality issues experienced in California. Los Angeles is the largest city in California and the second largest city in the United States. The Los Angeles (LA) site was located, on the campus of the University of Southern California (USC), approximately 3 km to the south of downtown Los Angeles. The LA site was 1 km from a major, heavily congested, interstate freeway (i.e., I-110) and approximately 13 km from the Los Angeles International Airport (LAX). Fresno is the largest city in California's heavily polluted San Joaquin Valley (SJV). The Fresno (FR) site was located on the campus of California State University, Fresno, which is within 3 km of a moderately busy highway (i.e., State Highway 99). The FR site was bounded by commercial/residential neighborhoods on 3 sides and agricultural fields on the remaining side. The San Francisco Bay Area has the highest population density in California. The San Pablo (SP) and East Oakland (EO) monitoring sites were approximately 30 km apart in the Bay Area. Both SP and EO were influenced by traffic, commercial, and residential sources, but their proximity to industrial sources differed. Most notably, the SP location is within 5 km of a major chemical refinery, while the EO location is within 5km of the Oakland International Airport and within 15 km of the Port of Oakland. All the sampling locations are shown in Figure 5-1 below.

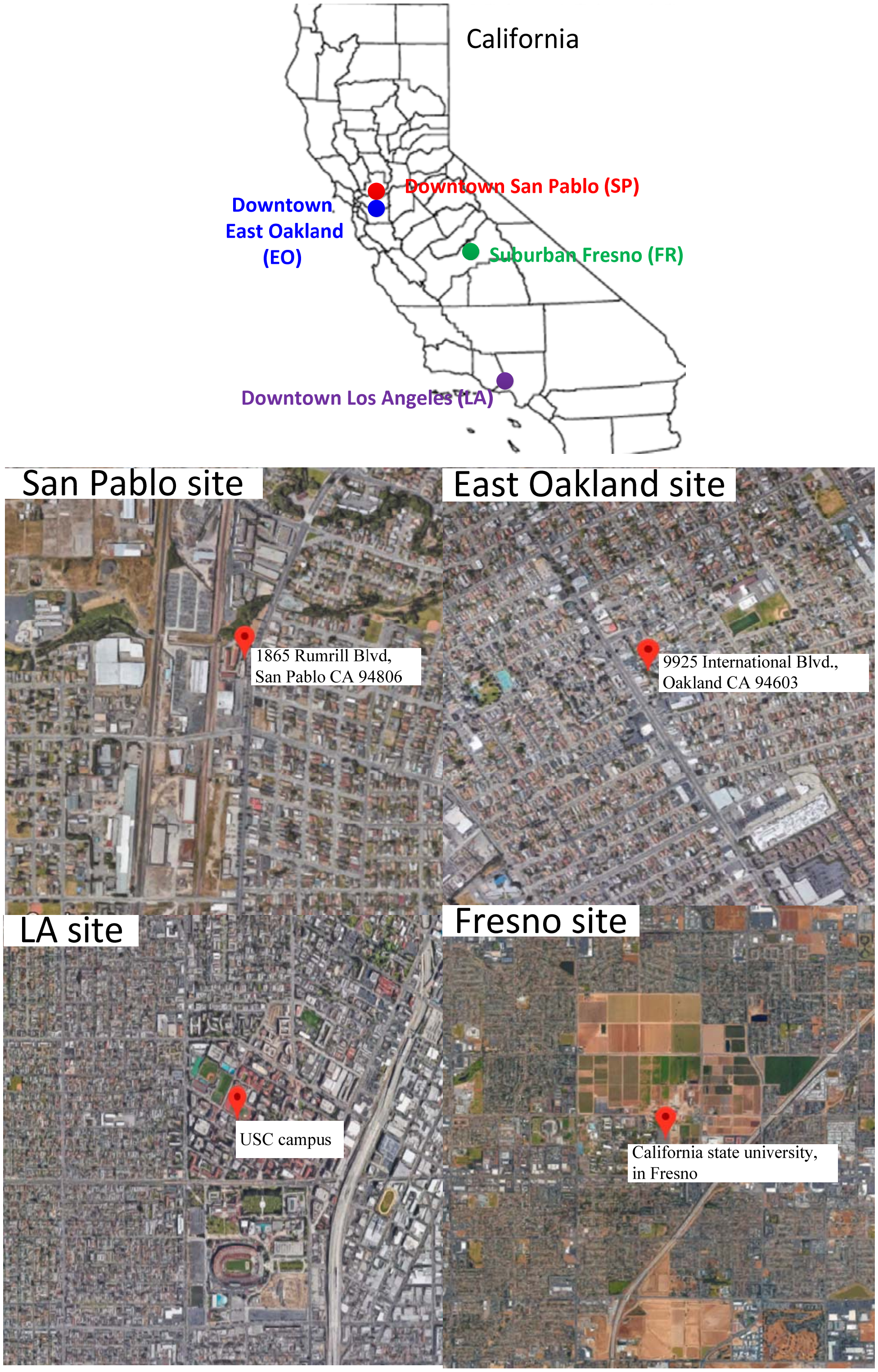

Figure 5-1: Aerial view of the sampling sites showing degree of urbanization. (map source: Google map)

The sampling period covered one year from August 2015 to July 2016 at the SP, EO and LA sites, and 6 months (January-April, June-July 2016) at the FR site. Each sample collection event lasted for 70-71 hours to collect sufficient $PM_{0.1}$ mass for chemical analysis. Quality control / quality assurance checks were performed at the conclusion of each sample collection event prior to the collection of the subsequent sample. Overall, 102, 110, 95 and 42 valid samples were collected at SP, EO, LA and FR sites, respectively, covering 70-90% of the total sampling periods.

5.2.2 Sampling Methods

The detailed $PM_{0.1}$ measurement methods used in this study have been described previously[16, 21] and so only a brief summary is presented here. Two Micro-Orifice Uniform Deposit Impactors (MOUDIs) were operated in parallel to collect $PM_{0.1}$ samples that could be tested for both carbonaceous speciation and elemental analysis. The first MOUDI was equipped with pre-baked aluminum substrates (Foil 0100-96-0573A-X; MSP Corp., Shoreview, MN, USA) and quartz fiber after-filters (Tissuquartz filters; Pall Corp., Port Washington, NY, USA) that were analyzed for elemental carbon (EC), organic compounds (OC), and organic molecular markers, such as cholesterol, levoglucosan, alkanes, etc. The second MOUDI was equipped with Teflon membrane substrates (Teflo R2PJ047; Pall Corp., Port Washington, NY, USA) that were analyzed for trace elements. Measurements from the aluminum MOUDI substrates are used for the analysis in the current paper.

Each MOUDI was operated at the flow rate recommended by the manufacturer (30 L min^{-1}) with an AIHL-design cyclone placed upstream to remove particles with diameter larger than 1.8 μm due to their tendency to bounce off uncoated impaction stages.[165] Ultrafine particles ($Dp<0.1$ μm) were captured on MOUDI stage 10 ($0.056<Dp<0.1$ μm) and on the MOUDI after-filters ($Dp<0.056$ μm). A preliminary analysis of monthly-averaged particle OC size distributions indicated that the after-filters suffered from positive OC sampling artifacts associated with adsorption of gaseous vapor (see Figure S5-3 and associated text) which is consistent with previous studies documenting adsorption onto quartz fiber filters.[166, 167] Similar analysis of monthly-averaged EC size distributions did not indicate evidence of significant bounce artifacts. Therefore, $PM_{0.1}$ concentrations were approximated by particles collected on stage 10 substrates which accounts for >80% of the $PM_{0.1}$ mass in typical central California conditions[16] and which is consistent with measured particle size distributions in other urban areas.[168]

A 1.5 cm^2 portion of each foil substrate was analyzed for EC and OC using a thermal optical method[169] following the National Institute for Occupational Safety and Health (NOISH) temperature protocol.[170] The remainder of each foil substrates was then composited by site and month for the analysis of organic molecular markers using solvent extraction followed by analysis using gas chromatography-mass spectrometry (GC-MS) [171, 172] at the Molecular & Environmental Toxicology Center at the University of Wisconsin, Madison.

5.2.3 Chemical Mass Balance (CMB) Analysis

The Chemical Mass Balance (CMB) receptor model uses linear combinations of known source composition profiles to reconstruct the measured composition of ambient samples.[171, 173-175] In this study, $PM_{0.1}$ source composition profiles are mainly based on a series of molecular markers that are dominated by specific individual sources with atmospheric lifetimes sufficiently long to make them useful in urban/regional source apportionment studies (1-2 days). These molecular markers include cholesterol (meat cooking); levoglucosan (biomass combustion); 17α(H)-21β(H)-30-Norhopane, 17α(H)-21β(H)-Hopane and αββ20R-C29-ethylcholestane (motor oil); and benzo[ghi]perylene and coronene (dominated by gasoline fuel with minor contributions from biomass combustion).[25] Each of these molecular markers is used to predict source contributions to $PM_{0.1}$ EC, with residual EC concentrations assigned to diesel fuel combustion products (which do not have a unique molecular marker. In theory, using residual EC as a marker for diesel exhaust could under-predict contributions from other potentially important sources active in some regions. In practice, the sources included in the current analysis are thought to explain the majority of the $PM_{0.1}$ EC in California. The only possible major source of $PM_{0.1}$ that has not been characterized for EC content in the literature is natural gas combustion, but recent measurements in our group have found that natural gas combustion particles have a small EC/OC ratio. The individual molecular markers are similarly used to predict source contributions to $PM_{0.1}$ OC with the exception that EC associated with diesel fuel combustion is used as a tracer for OC associated with this same source. Residual $PM_{0.1}$ OC in the calculation is interpreted as a missing source and/or formation of secondary organic aerosol. Further standard details of $PM_{0.1}$ source-apportionment methods have been described in previous studies [18, 25] and the conventional $PM_{0.1}$ source-profiles used in the current work are summarized in Table S5-1.

5.2.4 Correction for the volatility of POA and source markers

Previous CMB applications generally assume that the tracer/OC ratio measured during source tests can be directly used during the analysis of ambient measurements.[171, 173, 176] This constant ratio will only be maintained if the tracer and the OC have similar partitioning behavior between the gas and particle phase. Recent emission tests show that primary organic aerosol (POA) emitted from multiple combustion sources behaves like a series of semi-volatile compounds,[151, 177, 178] subject to the re-partitioning between the gas and particle phase when the sampling temperature or organic aerosol concentrations change. Additional studies have demonstrated that molecular markers are also semi-volatile,[179-181] although perhaps with different properties than the POA. Assuming equilibrium conditions hold between the gas- and particle-phases, the fraction of a semi-volatile organic compound that partitions to the particle phase (X_p) can be described as

$$X_p = \sum_1^n f_x \left(1 + \frac{C_x^*(T)}{C_{OA}}\right)^{-1} \quad \text{(eq.1)}$$

where n is the number of volatility bins characterized by a specified saturation concentration $C_x^*(T)$ (inverse of the partitioning coefficient Kp) for a given temperature T, f_x is the mass fraction of material falling into the volatility bin x, and C_{OA} is the concentration of total organic aerosol across all $C_x^*(T)$ volatility bins. The source profile composed of a (molecular marker)/P_{OA} ratio can be calculated as:

$$source\_profile = X_p^{molecular\ marker} / X_P^{POA} \quad \text{(eq.2)}$$

Ambient conditions differ from source test conditions because atmospheric dilution reduces C_{OA} below the levels typically used for source tests. Corrected source profiles can be calculated using equations (1-2) along with atmospherically-relevant C_{OA} concentrations. If particle composition is not a strong function of particle size, then these corrected profiles will apply across all size bins at equilibrium.

Individual molecular markers fall into a single C^* bin while bulk POA spans a range of bins. POA volatility distributions in the current study were based on previous measurements of POA evaporation with pre-defined C^* bins over a wide range of C_{OA} as summarized in Tables S5-2 and S3.[19, 151, 178] The net effect of these volatility distributions under ambient conditions were predicted using equations 1-2 above with measured ambient C_{OA} and T at (or near) the $PM_{0.1}$ monitoring sites.

5.2.5 Correction for the oxidation of the molecular markers

Particle-phase molecular markers used in CMB analysis are traditionally considered to be inert in the atmosphere but recent chamber studies have shown that they can be oxidized by OH radical, leading to underestimation of the contributions from corresponding sources. The estimated half-life of the molecular markers can vary from a few hours to >1000 hours, depending on ambient oxidant levels and the type of absorbing particulate matter.[182-184] In a recent ambient study[185], Skiles et al. observed exceptionally strong seasonal variation of $PM_{2.5}$ cholesterol in the SJV, which was most likely due to the effects of oxidation reactions between the source and receptor. Similarly, the seasonal variation of $PM_{0.1}$ molecular markers observed in the current study was much stronger than the seasonal variation for $PM_{0.1}$ EC (Fig. S5-2), suggesting that oxidation of molecular markers occurred under atmospheric conditions.

In the current study, the warm-season concentrations of the molecular markers associated with vehicle exhaust, motor oil, and cooking sources were scaled to the concentration of $PM_{0.1}$ EC measured at the same site to correct for the effects of oxidation reactions using equations (3-4).

$$C'_{i,ws} = max(C_{i,ws}, C_{EC,ws}\, S^*) \quad \text{(eq.3)}$$

$$S^* = C_{i,cs} / \, C_{EC,cs} \quad \text{(eq.4)}$$

where $C_{i,ws}$ and $C'_{i,ws}$ are the measured and modified concentration of the molecular marker *i* in the warm season (*ws*), $C_{EC,ws}$ is the co-measured $PM_{0.1}$ EC in the warm season, and S^* is the ratio of (tracer *i*)/($PM_{0.1}$ EC) measured during the cold season (*cs*) defined as November to February. Note that equations (3-4) assume that seasonal changes to PBL height equally affect C_{EC} and C_i. The original and corrected seasonal patterns of molecular markers are presented in Figures S5-3 and S5-4, respectively.

The oxidation corrections described by equations (3-4) assume that the emissions from vehicle exhaust, motor oil and cooking sources were relatively constant over the year and the true seasonal variation of the molecular marker concentrations associated with these sources was mainly controlled by the seasonal change of the atmospheric mixing conditions driven by wind speed and mixing height. Oxidation corrections were not applied to biomass combustion because these emissions were not constant throughout the year. Measured concentrations of levoglucosan (biomass combustion tracer) were essentially negligible at all sites during the summer season reflecting a combination of reduced source emissions and increased tracer reaction rates. Oxidation corrections were also not applied to the measurements at FR because summer construction activities at this site emitted additional EC. The source apportionment results from Fresno without oxidation corrections therefore represent a lower-bound estimate of primary source contributions to $PM_{0.1}$ concentrations.

5.3 Results

5.3.1 Volatility of Bulk POA and Molecular Markers

Figures 5-1(a) and (b) present the calculated mass fraction (X_p) of POA and selected molecular markers that remain in the particle-phase at 20 ºC after continued dilution beyond the emissions test conditions resulting in decreasing C_{OA} concentrations. Figure 5-1(a) clearly demonstrates that the volatility distribution measurements from previous experiments generate semi-volatile POA distributions from all sources except gasoline fuel combustion. Motor oil emitted from both gasoline and diesel engines is semi-volatile,[178] but Kuwayama et al.[177] found that the tailpipe exhaust from gasoline-powered vehicles was best explained using two volatility distributions: one from semi-volatile unburned lubricating oil, and one from essentially non-volatile gasoline fuel combustion. Figure 5-1(a) shows that reducing C_{OA} from typical emission source test conditions (e.g. 100-1000 $\mu g\ m^{-3}$ C_{OA}) to typical ambient sampling condition (e.g. 5 $\mu g\ m^{-3}$ C_{OA}), causes 30-49% of the POA to evaporate depending on the source. The corresponding source markers, however, were generally less semi-volatile than the bulk POA (Figure 5-1(b)). Benzo[ghi]perylene, EC and cholesterol, the selected markers for sources of gasoline exhaust, diesel exhaust and meat cooking, were constant over a variety of sampling conditions, while levoglucosan, the marker for wood burning, has 15% loss when reducing C_{OA} from 1000 to 5 $\mu g\ m^{-3}$. The exception is 17α(H)-21β(H)-30-Norhopane which is more semi-volatile than bulk POA from motor oil emission.

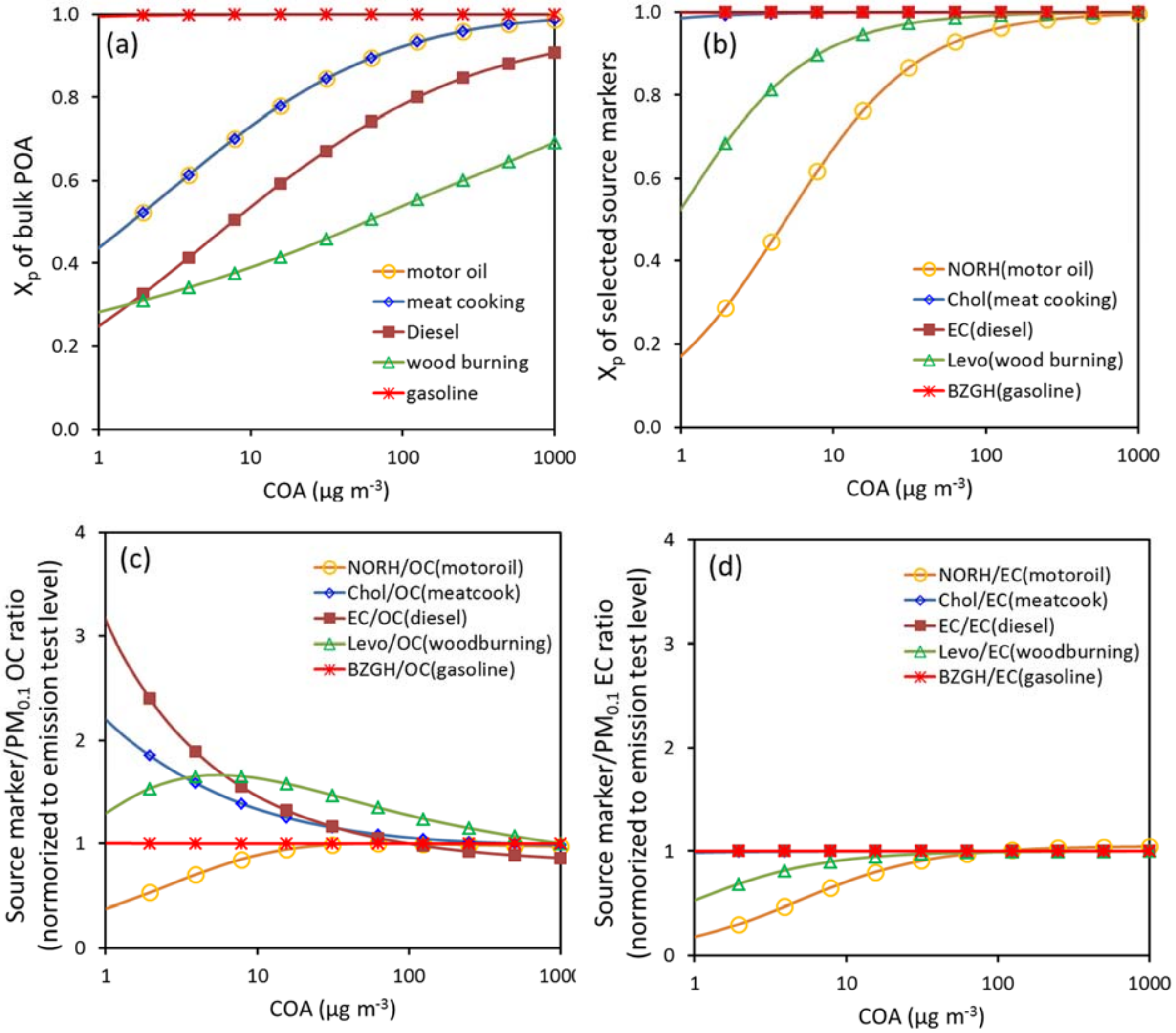

Figure 5-1: (a) Mass fraction (X_p) of primary organic aerosols (POA) that remain in the particle phase after continued dilution beyond the emissions test conditions. The calculation was performed at 20°C. Volatility distributions for the POA were reported in previous studies of May et al.[151, 178] and Kuwayama et al. [177]. The volatility distribution for motor oil POA was used to represent the volatility distributions for meat cooking POA, for which source such values were not reported. (b) X_p calculated for selected molecular markers. The parameters used for calculation were given in Table S5-1 in SI.NORH, Chol, EC, Levo and BZGH represent 17α(H)-21β(H)-30-Norhopane, Cholesterol, element carbon, Levoglucosan and Benzo[ghi]perylene, respectively. (c) The ratio of selected source tracers to $PM_{0.1}$ OC at various C_{OA} concentrations. (d) The ratio of selected source tracers to $PM_{0.1}$ EC at various C_{OA} concentrations.

Figure 1(c) and (d) illustrate the ratio of selected source tracers to $PM_{0.1}$ OC and $PM_{0.1}$ EC at various ambient C_{OA} concentrations relative to the emissions source test conditions. Ratios > 1 indicate the source marker is less semi-volatile than the bulk POA at the indicated C_{OA} concentrations. A ratio < 1 indicates the source marker is more semi-volatile than the bulk POA.

5.3.2 Concentration of $PM_{0.1}$ EC and OC

Figure 5-2 illustrates $PM_{0.1}$ EC and OC concentrations measured at the four sampling sites. The annual averaged $PM_{0.1}$ OC concentration varied from 104 to 137 ng m^{-3}, notably lower than the concentrations of 175 ng m^{-3} measured in central Sacramento in 2009-2010.[19] The annual averaged $PM_{0.1}$ EC concentration in the current study varied from 30 to 53 ng m^{-3}, which was lower than or comparable to the concentrations measured previously in Sacramento (62 ng m^{-3}).[19] $PM_{0.1}$ EC concentrations were proportional to urbanization levels surrounding each sampling site, in the order of LA>EO>SP>FR. $PM_{0.1}$ EC concentrations in downtown LA were higher than those measured at other sites ($p<0.05$), suggesting that $PM_{0.1}$ EC concentrations are proportional to the traffic density. $PM_{0.1}$ OC concentrations did not follow these trends; measured $PM_{0.1}$ OC concentrations were higher in Fresno than in San Pablo. This finding suggests that traffic sources do not dominate $PM_{0.1}$ OC concentrations at all sites.

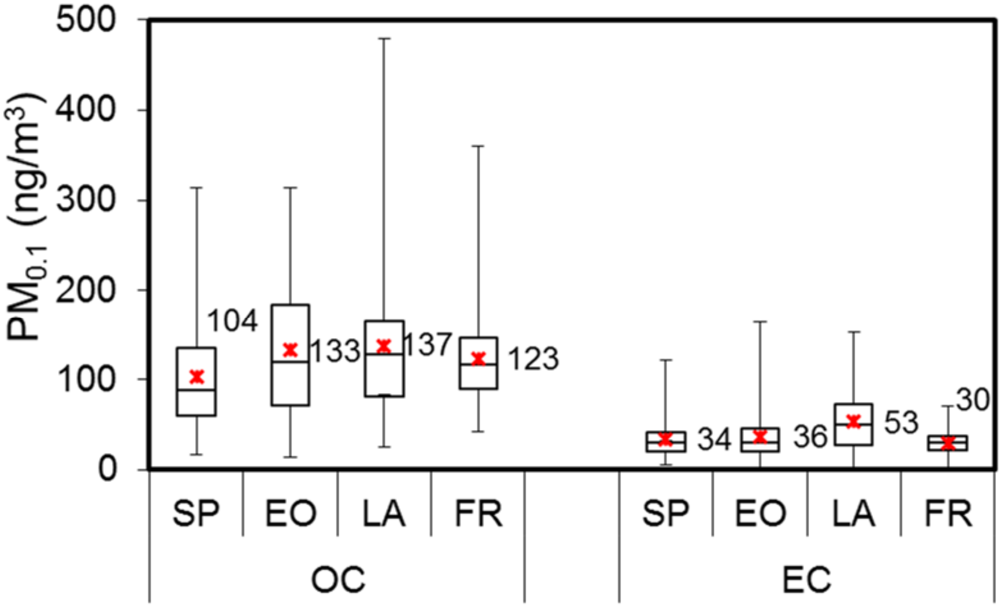

Figure 5-2: Yearly averaged $PM_{0.1}$ OC and EC concentration measured at four sites across California. The box represents the first quartile, median and the third quartile. The whiskers represent the max / min values. The red markers and the values represent the averages.

5.3.3 Annual averaged source apportionment of $PM_{0.1}$ OC and EC

Annual average source contributions to $PM_{0.1}$ OC predicted using modified source profiles are illustrated in Figure 5-3 and detailed in Table 5-1. Results generated with the conventional source profiles are shown in Figure S5-8. The uncertainties listed in Table 5-1 reflect the sum of uncertainty in source profiles and ambient measurements calculated using the method described by Kleeman et al.[18]. The "unresolved" OC category was calculated as the residual difference between the measured $PM_{0.1}$ OC and the apportioned $PM_{0.1}$ OC from the five specified sources.

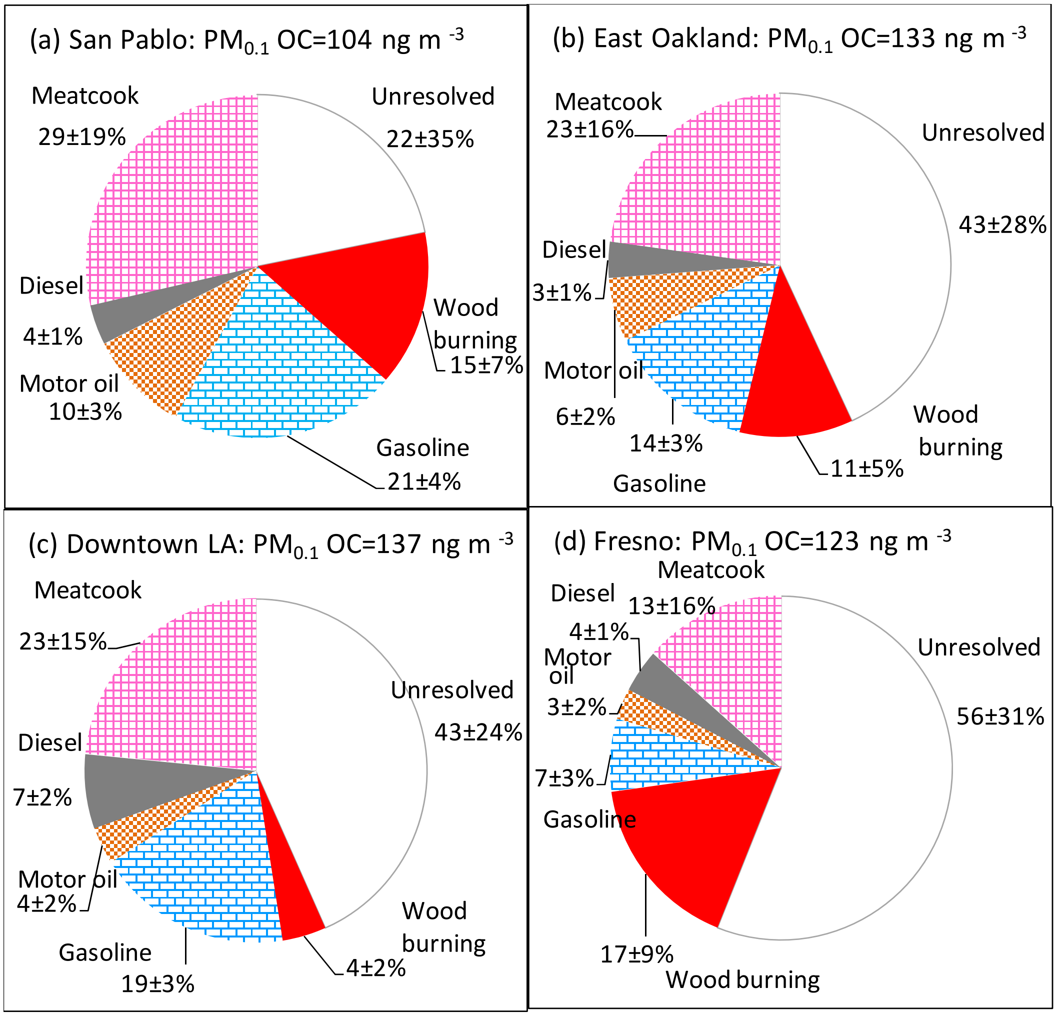

Figure 5-3: Annual averaged source contribution to $PM_{0.1}$ OC predicted by CMB model using modified source profile. Uncertainty with the unresolved $PM_{0.1}$ OC is derived from the model predicted uncertainty for all other sources.

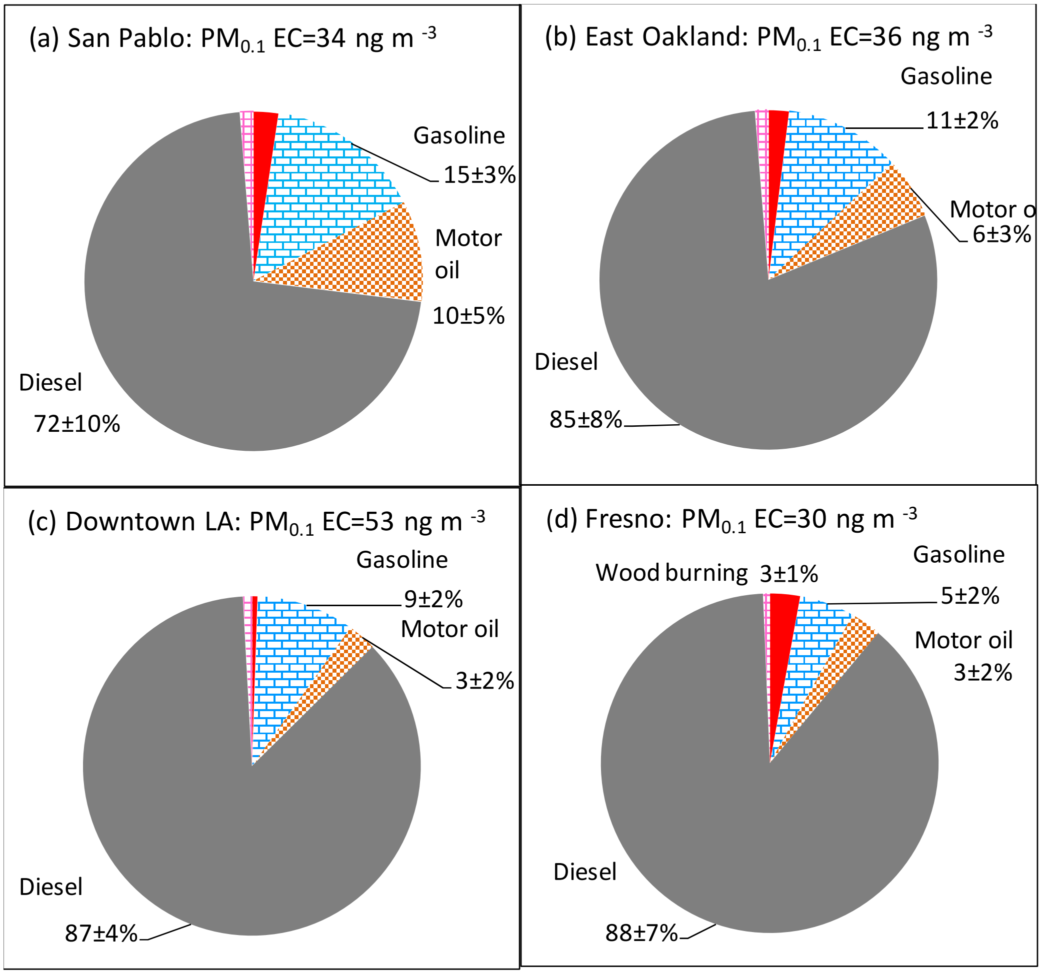

Figure 5-4: Annual averaged source contribution to $PM_{0.1}$ EC predicted by CMB model using modified source profile

Table 5-1. Annual averaged $PM_{0.1}$ EC/OC measured at four sampling sites and CMB predicted source contributions (ng m^{-3})

Site	mass	Wood burning	Gasoline	Motor oil	Diesel*	Meat cooking	Unknown*
$PM_{0.1}$ OC (ng m^{-3})							
SP	96±57	16±8	19±4	10±3	6±2	27±20	23±22
EO	110±68	15±8	15±3	8±3	9±2	28±21	37±23
LA	120±74	7±3	20±4	6±2	14±3	26±19	57±21
FR	119±57	20±10	8±4	4±3	6±2	16±18	58±47
$PM_{0.1}$ EC (ng m^{-3})							$PM_{2.5}$ (µg m^{-3})
SP	42±23	1±0	27±8	4±2	8±21	0±0	8.62±3.98
EO	59±34	1±0	20±8	3±2	34±14	0±0	6.03±4.09
LA	73±36	0±0	33±7	2±1	38±28	0±0	11.73±5.52
FR	34±15	1±1	6±9	1±1	26±9	0±0	11.30±8.17

*: The overall uncertainty estimated for $PM_{0.1}$ OC and EC was used to represent the uncertainties associated with unknown OC and EC contributed by diesels.

Figure 5-3 shows meat cooking accounted for 13-29% of $PM_{0.1}$ OC, acting as the single largest source of $PM_{0.1}$ OC in California cities. This finding is consistent with previous $PM_{0.1}$ source apportionment results during shorter intensive monitoring periods [25]. Elevated cholesterol concentrations have been measured at rural locations in the middle of the U.S.[176], leading to the conclusion that cholesterol sources other than food cooking (cigarette smoke, industry, aquatic or soil organisms) can be important in some locations.[186-189] The majority of the sampling sites analyzed in the current study were located in major cities near commercial and residential cooking sources. It is likely that the cholesterol measured in the current study was released primarily from cooking activities. Fresno was more rural than the other sampling locations, but measured cholesterol concentrations at this location also generally followed the activity pattern of nearby restaurants which was directly related to the number of students on the CSU Fresno campus. The uncertainty associated with meat cooking source contributions to $PM_{0.1}$ OC was significant (15-19%) at all sampling locations, primarily due to variability in the fat content of meat during source profile measurements. Future emissions tests should better quantify the relationship between fat content, cholesterol, and POA emissions. Future emissions tests should also measure the volatility of meat cooking POA under different ambient OA concentrations.

Wood burning was the single largest CMB-resolved source in Fresno, accounting for 17%-of the total $PM_{0.1}$ OC, and the third largest source of $PM_{0.1}$ OC resolved by the CMB model at the San Francisco Bay Area sites (SP and EO), accounting for 11-15% of the $PM_{0.1}$ OC. Residential wood combustion is a major fuel for winter home heating in Northern California[174, 190, 191] with up to one third of the $PM_{2.5}$ mass associated with wood combustion in the San Joaquin Valley.[37] Much smaller wood burning contributions to $PM_{0.1}$ OC (4%) were measured in downtown LA, mainly because homes in this region are primarily heated by natural gas or electricity.

Aggregate vehicle exhaust (diesel fuel combustion products, gasoline fuel combustion products, and motor oil) accounted for approximately 30% of the $PM_{0.1}$ OC mass at the heavily urbanized locations (LA, EO, SP) and approximately 14% of the $PM_{0.1}$ OC mass at the moderately urban Fresno site, reflecting the traffic density surrounding each location. All sampling locations were more than 300 m away from major freeways, which mitigated the signature of the vehicle traffic source.[35] $PM_{0.1}$ OC contributions from gasoline combustion products were 2-5 times larger than contributions from diesel combustion products at these sampling locations, but this ratio reflects the proximity of the sampling sites to goods movement corridors. Motor oil contributions to $PM_{0.1}$ OC (3-10%) may have been emitted by either gasoline or diesel sources.

A significant fraction of the $PM_{0.1}$ OC (23-52%) came from unresolved sources across the four measurements sites, with the largest unresolved fraction observed in LA (44%) and FR (56%). This unresolved $PM_{0.1}$ OC may be associated with a combination of primary sources that were not included in the analysis and secondary organic aerosol (SOA). For example, a recent study by Yu et al. used emissions inventories, measured emissions profiles, and a regional chemical transport model to predict that natural gas combustion accounts for up to 23% of the observed $PM_{0.1}$ mass concentration in San Francisco Bay Area.[192] Unique tracers for natural gas combustion particles have not been previously reported, making it difficult to quantify primary natural gas contributions to ambient ultrafine particle concentrations in the current study. Freshly emitted natural-gas combustion particles have a log-normal size distribution with a mean diameter of approximately 20 nm that increases to approximately 60 nm due to SOA condensation after 3-h of aging in a photochemical smog chamber with a realistic surrogate for an urban atmosphere[193] (see Figure S5-2). These coated natural gas particles would be measured as an unresolved source in the current study since they fall into the collected diameter range (56 -100 nm). New particle formation (nucleation) could also provide seed particles for SOA condensation that could contribute to unresolved $PM_{0.1}$ mass. Secondary organic aerosol condensation onto nucleation mode particles (D_p<30 nm)[168, 194] is known to be an important growth mechanism[195, 196], but these modified nucleation mode particles account for less than 10% of the $PM_{0.1}$ mass in a typical large urban area[168]. A weak positive correlation (R^2=0.44) was found between the monthly average particle number concentration at central Los Angeles and the amount of "unresolved" $PM_{0.1}$ mass at nearby USC site in the current study. This suggests that the conditions that encourage new particle formation generally have a positive influence on the "unknown" fraction, but other more dominant factors must be involved as well. Annual averaged source contributions to $PM_{0.1}$ EC predicted using modified CMB source profiles are illustrated in Figure 5-4 with detailed values listed in Table 5-1. Similar results using the conventional source profiles are shown in Figure S5-9. Diesel exhaust accounted for 72-88% of the $PM_{0.1}$ EC at the four sampling sites. As expected, diesel fuel combustion made larger contributions to $PM_{0.1}$ EC at sites closer to goods movement corridors (LA and EO) than at urban locations further from goods movement corridors (SP). The Fresno site did not follow this trend, with 88% of the $PM_{0.1}$ EC associated with diesel engines. As discussed previously, this diesel source contribution is the residual $PM_{0.1}$ EC not associated with other resolved sources that have unique tracers. The sampling site in Fresno was heavily influenced by construction activities, which prevented the collection of a full twelve months of data at this site. Off-road diesel construction equipment likely contributed strongly to the $PM_{0.1}$ EC measured at Fresno, especially during the summer. Gasoline exhaust (5-15%), motor oil (3-10%), wood burning (1-3%), and meat cooking (0-1%) made relatively small contributions to $PM_{0.1}$ EC at all sites.

5.3.4 Monthly source contribution to $PM_{0.1}$ OC and EC

Figures 5-5 and 5-6 illustrate predicted monthly source contributions to $PM_{0.1}$ OC and EC, respectively, using the modified CMB source profiles. Individual source contributions are shown in Figures S5-7 through S5-12 (OC) and Figures S5-13 through S5-17 (EC). Monthly results generated with the conventional source profile are presented in Figures S5-18 and S5-19.

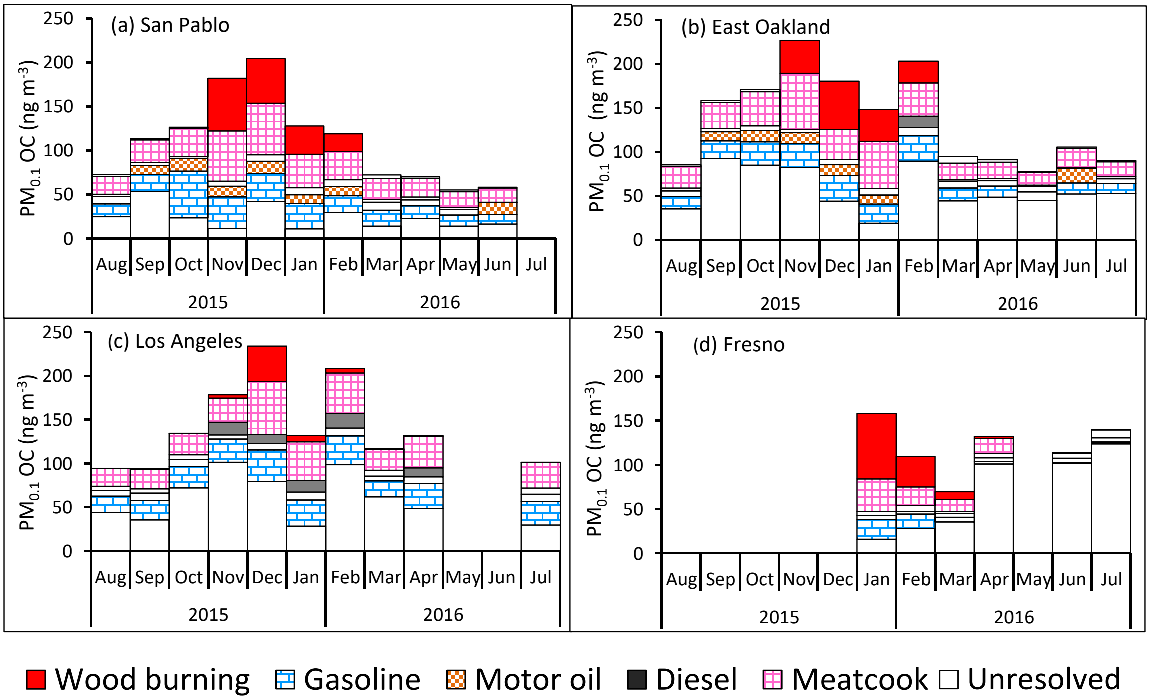

Figure 5-5: Model predicted monthly source contribution to $PM_{0.1}$ OC

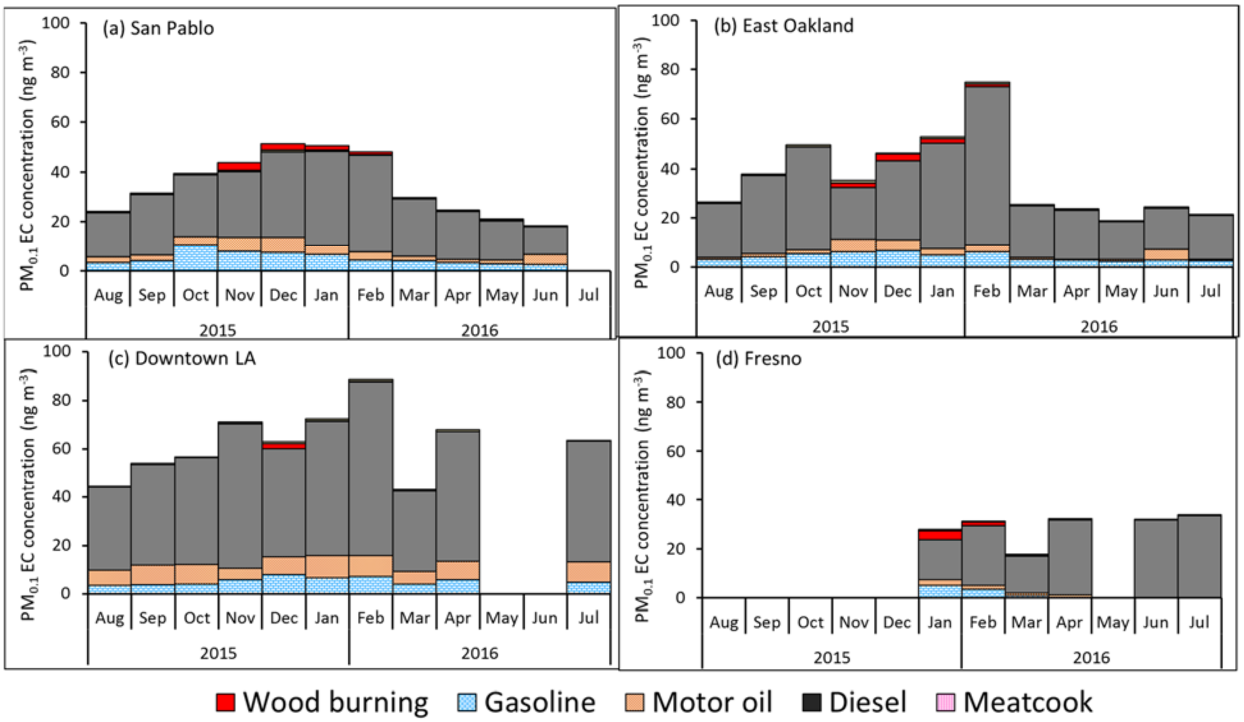

Figure 5-6: Model predicted monthly source contribution to $PM_{0.1}$ EC using modified source profile

Figure 5-5 shows that monthly-averaged $PM_{0.1}$ OC ranged from 55 ng m^{-3} in May, 2016 at the San Pablo site to 233 ng m^{-3} in December, 2015 at the LA downtown site. Similar seasonal patterns were observed at all sampling sites, with concentrations peaking in late fall and winter, when heating sources became more active and atmospheric mixing height was low. Wood burning contributions from home heating peaked in the cold season (up to 47%) but became negligible during other times of the year, indicating that fireplaces and woodstoves play a larger role than wildfires in determining long-term wood smoke ultrafine particle concentrations during the sampling period. Wood burning was only important in December at the LA site most likely due to the use of fireplaces during the holiday season at the end of the calendar year. In contrast, wood burning was the single largest source of resolved $PM_{0.1}$ OC at the Fresno site in winter (32-47%), because biomass serves as a significant heating source in this region.

$PM_{0.1}$ OC concentrations associated with sources other than wood burning exhibited less significant seasonal patterns after correction for the oxidation of molecular markers, reflecting relatively consistent emissions throughout the year. The exceptionally higher contribution from motor oil at two Bay Area sites (SP and OA) in June 2016 (Figure S5-15) coincided with a documented refinery upset that likely released hopanes and steranes directly into the atmosphere.[197, 198]

Unresolved $PM_{0.1}$ OC concentrations do not have a clear seasonal pattern across the sites after molecular marker volatility and oxidation are accounted for (Fig 5-5 and Fig S5-8). Unresolved $PM_{0.1}$ concentrations are generally less than 50 ng m^{-3} at San Pablo and generally less than 100 ng m^{-3} at East Oakland and Los Angeles. Minimum concentrations occur in Jan, but near-maximum concentrations occur in Feb at two of these three sites. The six months of data at Fresno show increasing unresolved concentrations between Jan-Jul with peak concentrations above 100 ng m^{-3}, but diesel $PM_{0.1}$ EC concentrations also peaked during the summer (Figure 5-6d and Figure S5-18), suggesting a primary source may partially be responsible for both OC and EC trends. Construction activities were performed near the Fresno site during the summer, raising the possibility that off-road diesel engines are responsible for the observed seasonal trends. SOA formation could also contribute to the unresolved $PM_{0.1}$ OC, but SOA formation typically follows a seasonal pattern determined by changes to precursor concentrations and oxidant levels. Seasonal SOA patterns have been measured in megacities such as Tokyo where the ratio of secondary organic aerosol to total organic aerosol increased in summer[199], at regional background sites in the Pearl River Delta of China where anthropogenic SOA increased in autumn and winter[200], and in a roadside environment in the United States where biogenic SOA increased in summer[201]. Overall, the lack of a seasonal pattern in the unresolved $PM_{0.1}$ OC concentrations at the three major urban sites in the current study is consistent with a primary source (or sources) that emits UFPs in all seasons. Natural gas combustion is one potential source that fits this pattern. Unfortunately, molecular markers in the ultrafine size range for natural gas combustion are not available and so this source cannot be included explicitly in the current study.

Figure 5-6 shows that $PM_{0.1}$ EC ranged from 28 ng m^{-3} in March 2016 at the FR site to 74 ng m^{-3} in February 2016 at the OA site. Diesel exhaust was the single dominant contributor in all seasons, consistent with results reported by previous studies.[18, 25] $PM_{0.1}$ EC generally followed a seasonal pattern with higher concentrations in the colder winter months in San Pablo, East Oakland, and LA. The seasonal change in boundary layer mixing height and wind speed at these sites explain the majority of this seasonal variation. $PM_{0.1}$ EC at Fresno did not decrease between winter and summer, likely because of diesel construction emissions at this location.

5.4 Discussion

Molecular markers such as PAHs have been used in source-receptor models for over 35 years under the assumption that these species were conserved (non-volatile and non-reactive) in the atmosphere.[202] The current study shows that volatility and reactivity must both be accounted for to properly represent the seasonal variation of $PM_{0.1}$ source contributions under the conditions experienced in California between 2015-16. The consequences of not accounting for these factors are illustrated in Figure 5-7 that compares source contributions to $PM_{0.1}$ OC and EC using the modified source profiles and the traditional source profiles. Figure 5-7 shows that the relative ranking of annual-average source contributions is not drastically altered by failing to consider volatility and reactivity of the molecular markers and POA. The biggest change associated with the modified source profiles is an increase in the unresolved $PM_{0.1}$ OC by a factor of almost two and a decrease in meat cooking and wood burning contributions. This adjustment reflects the fact that the molecular markers (except the tracers for motor oil) were generally less volatile than the bulk POA from the same source. The adjusted ratio of (molecular marker)/POA is therefore larger under ambient conditions than source test conditions, which decreases the amount of POA attributed to each ambient source. Corrections to account for tracer oxidation also modify the source apportionment results by increasing the amount of POA attributed to each source. Both the modified and conventional source profiles identify meat cooking, wood burning, gasoline combustion, diesel fuel combustion, and motor oil as major sources of $PM_{0.1}$ OC. Molecular markers for sources that contribute strongly to $PM_{0.1}$ EC (benzo[ghi]perylene and coronene) were generally less volatile than molecular markers for other sources. The differences between the modified and traditional $PM_{0.1}$ EC source apportionment results are therefore minor, with both methods identifying diesel fuel combustion as the dominant source of $PM_{0.1}$ EC. For both $PM_{0.1}$ OC and EC, the choice of modified or traditional source profiles does not greatly impact the interpretation of annual average source apportionment results.

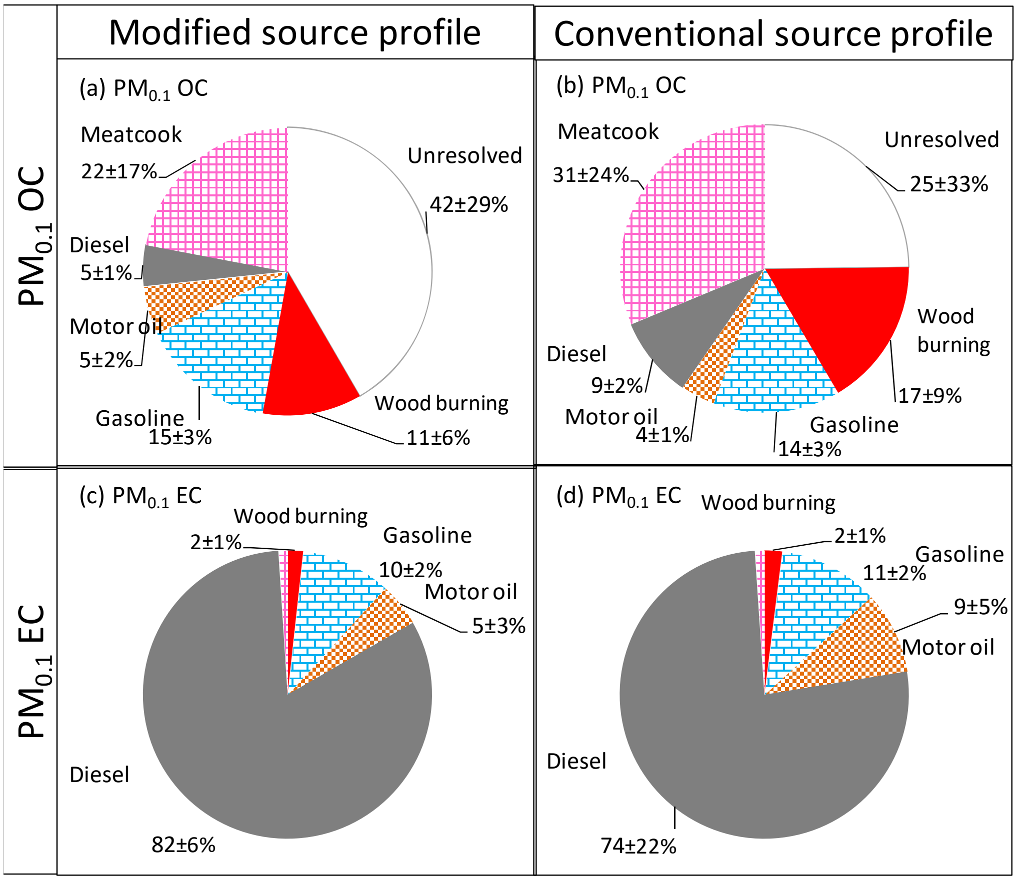

Figure 5-7: Averaged source contribution to $PM_{0.1}$ OC and EC in four California cities using modified source profile ((a) and (c)) and original source profile ((b) and (d)).

5.5 Appendix

Table S5-1 summarizes the source profiles used for the CMB analysis. Table S5-2 lists the parameters used to calculate the volatility of individual source tracers. Table S5-3 shows the volatility distribution for the POA emitted from wood burning, diesel engines, gasoline engines, motor oil, and food cooking.

Table S5-1. Conventional source profiles used for simplified CMB analysis

tracers	Wood	Gasoline	Motor oil	Diesel	Meat cooking
ECTC	3.36E-02	2.36E-01	7.50E-01	2.56E+00	1.00E-02
ECTU#	6.72E-03	4.81E-02	1.50E-01	5.12E-01	2.00E-03
BZGH*	0.00E+00	1.10E-03	0.00E+00	0.00E+00	0.00E+00
BZGU	0.00E+00	1.30E-04	0.00E+00	0.00E+00	0.00E+00
CORO	0.00E+00	8.00E-04	0.00E+00	0.00E+00	0.00E+00
CORU	0.00E+00	9.60E-05	0.00E+00	0.00E+00	0.00E+00
NORH	0.00E+00	0.00E+00	6.00E-04	0.00E+00	0.00E+00
NORU	0.00E+00	0.00E+00	2.70E-04	0.00E+00	0.00E+00
HOPA	0.00E+00	0.00E+00	6.00E-04	0.00E+00	0.00E+00
HOPU	0.00E+00	0.00E+00	2.70E-04	0.00E+00	0.00E+00
SITO	0.00E+00	0.00E+00	3.00E-04	0.00E+00	0.00E+00
SITU	0.00E+00	0.00E+00	1.30E-04	0.00E+00	0.00E+00
LEVO	1.50E-01	0.00E+00	0.00E+00	0.00E+00	0.00E+00
LEVU	7.50E-02	0.00E+00	0.00E+00	0.00E+00	0.00E+00
CHOL	0.00E+00	0.00E+00	0.00E+00	0.00E+00	1.50E-03
CHOU	0.00E+00	0.00E+00	0.00E+00	0.00E+00	7.50E-04

#: ECTU: uncertainty of EC. *:BZGH: Benzo[ghi]perylene; CORO: Coronene; NORH: 17α(H)-21β(H)-30-Norhopane; HOPA: 17α(H)-21β(H)-Hopane; SITO: α β β -20R-C29-Sitostane.

Table S5-2. Parameters used to calculate volatility of individual source tracers in this study

Organic tracers	Formula	MW (g mol^{-1})	Vapor P at 298K (atm)	ΔH(kJ mol^{-1})
EC	C	12	0	0
Benzo[ghi]perylene	$C_{22}H_{12}$	276	1.32E-13	96.1
Coronene	$C_{24}H_{12}$	300	2.91E-10	142
17α(H)-21β(H)-30-	$C_{29}H_{50}$	399	5.15E-10	82
17α(H)-21β(H)-Hopane	$C_{30}H_{52}$	413	5.15E-10	82
αββ20R-C29-ethylcholestane	$C_{29}H_{52}$	401	5.15E-10	82

Levoglucosan	$C_6H_{10}O_5$	162	2.38E-10	84
Cholesterol	$C_{27}H_{46}O$	387	2.38E-10	136

Table S5-3. Volatility distribution (f_i) for POA emissions for each emission sources

C* at 298K (μg m^{-3})	ΔH$^{\#}$ (kJ	f_i				
		Wood	Diesel[151]	Gasoline[178]	Lubricate	Meat
0.01	93	0.2	0	0.14	0.04	0.04
0.1	89	0	0.03	0.13	0.15	0.15
1	85	0.1	0.25	0.15	0.31	0.31
10	81	0.1	0.37	0.26	0.36	0.36
100	77	0.2	0.23	0.15	0.13	0.13
1000	73	0.1	0.06	0.03	0.01	0.01
10000	69	0.3	0.03	0.02	0	0
100000	65	0	0.01	0.01	0	0
1000000	61	0	0.01	0.11	0	0

#: from best fit for the wood burning emission[151]; *: Data were not available for emission from the meat cooking source. Therefore, we use the volatility distribution measured for lubricate oil emission instead.

New Particle Formation and SOA Contributions to $PM_{56\text{-}100}$ Measurements

Figure S5-1 illustrates typical particles size distributions in an urban area and shows the collection range for $PM_{56\text{-}100}$ used in the current study. Here we use the measurements by Cheung et al.[168] in the urban area in Queensland, Australia, along with some reasonable assumptions. For example, particle number concentrations in the nucleation and Aiken modes measured by Cheung and coworkers were $5.6*10^3$ and $3.7*10^3$ cm^{-3}. Typical values of the geometric mean diameter (D_g) and geometric standard deviation (σ_g) for the nucleation mode and Aiken mode particles measured by Cheung and coworkers were D_g=18 nm / σ_g = 1.5 and D_g=50 nm / σ_g = 2.5, respectively.

Particles were assumed to have unit density of 1 g cm^{-3}. Using these parameters, Figure S5-1 showed that particles over 56 nm account for ~80% of the UFP mass. The nucleation mode particles (<30 nm) accounted for +60% of the UFPs number but only ~10% of the UFPs mass.

Recent studies have observed new particle formation followed by growth through the condensation of secondary aerosols[195, 196]. Some of the freshly nucleated particles can grow larger than 50 nm but their overall contribution to $PM_{0.1}$ mass remains relatively small (<20%) as indicated in Figure S5-1.

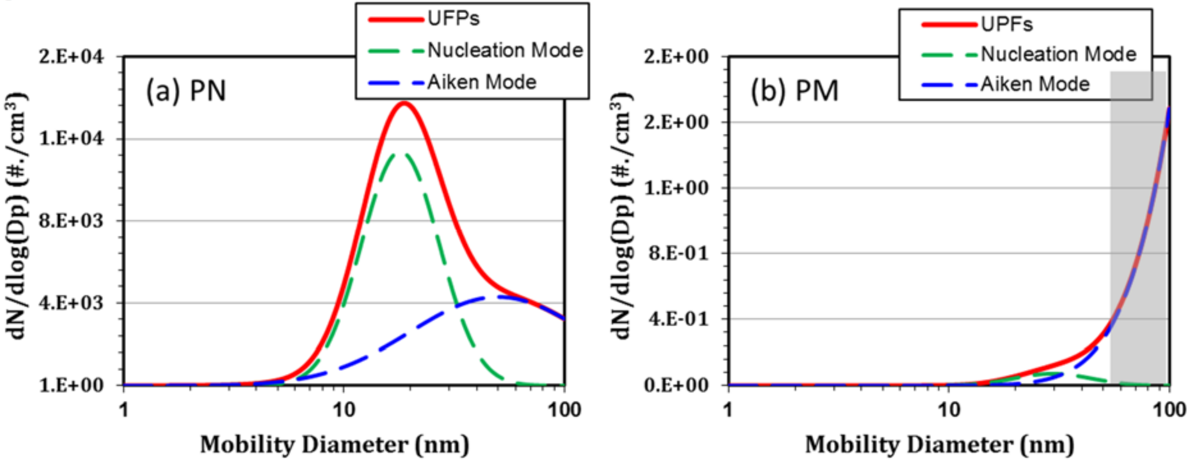

Figure S5-1: Typical particle number (PN) and particle mass (PM) distribution in an urban area[168]. Particle number concentrations in the nucleation mode and the Aiken mode were $5.6*10^3$ cm^{-3} and $3.7*10^3$ cm^{-3}, respectively. The GMD/σ_g for the nucleation mode and Aiken mode particles were GMD=18 nm / σ_g=1.5 and GMD=50 nm / σ_g=2.5, respectively. Particles were assumed to have the unit density of 1 g cm^{-3}. MOUDI stage 10 collects particles in the gray shaded area in the right panel.

Natural Gas Combustion and SOA Contributions to PM_{56-100} Measurements

Figure S5-2 illustrates the measured particle size distribution from the combustion of methane after 0 to 3 h of aging in a photochemical reaction chamber with a representative amount of urban surrogate VOC[193]. Fresh methane combustion particles have a diameter of 20 nm that increases over time due to the condensation of SOA. Methane combustion particles may grow slower in the real atmosphere because accumulation mode particles provide competing surface area for SOA condensation. Thus, natural gas combustion particles in the ambient atmosphere may have diameters between 20 – 60 nm, meaning they could have been collected by either the MOUDI after-filter (Dp<56nm) or MOUDI stage 10 (56nm < Dp < 100nm) in the current study depending on the atmospheric conditions.

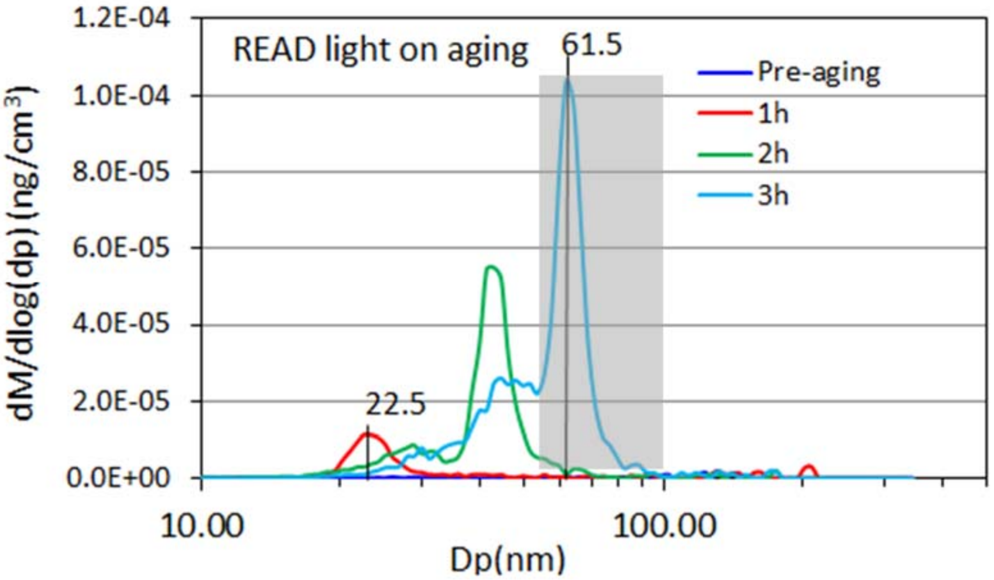

Figure S5-2: Growth of methane combustion particles due to condensation of SOA under atmospherically-relevant conditions. Background dilution air did not contain particles and so atmospheric growth rates may be slower due to competition with other particle surface area. MOUDI stage 10 collects particles in the gray shaded area in the right panel.

Contamination of After-Filters by Adsorption of Organic Vapors Sampling artifacts on quartz after-filters have been consistently observed by numerous researchers over several decades[166, 167]. Within our own group, Herner et al.[16] observed that the MOUDI after-filter mass was dominated by organic carbon that was not consistent with co-located Scanning Mobility Particle Size measurements. In the current study, the monthly averaged full particle size distributions (0-10 µm) were plotted for three sampling sites in August, 2015 (Figure S5-3). The EC size distributions are unimodal, peaking at diameter between 0.18-0.32 or 0.32-0.56 µm. This suggests that sampling artifacts related to particle bounce are minimal. The apparent OC size distributions are bimodal at all sites due to a large amount of OC mass on the after-filter, which exceeds the mass collected on MOUDI stage 10 (56<dp<100 nm). A portion of this after-filter OC may be associated with primary natural gas combustion particles that have not grown larger than 56 nm through the condensation of secondary organic aerosol (see previous section), but some additional portion of this after-filer OC is almost certainly associated with gas-phase adsorption of organic vapors. Fitz et al.[167] suggest that up to 90% of the OC on the after-filter may due to adsorption of organic vapors. This makes it difficult to interpret the after-filter data, and these measurements will not be discussed further in the current study.

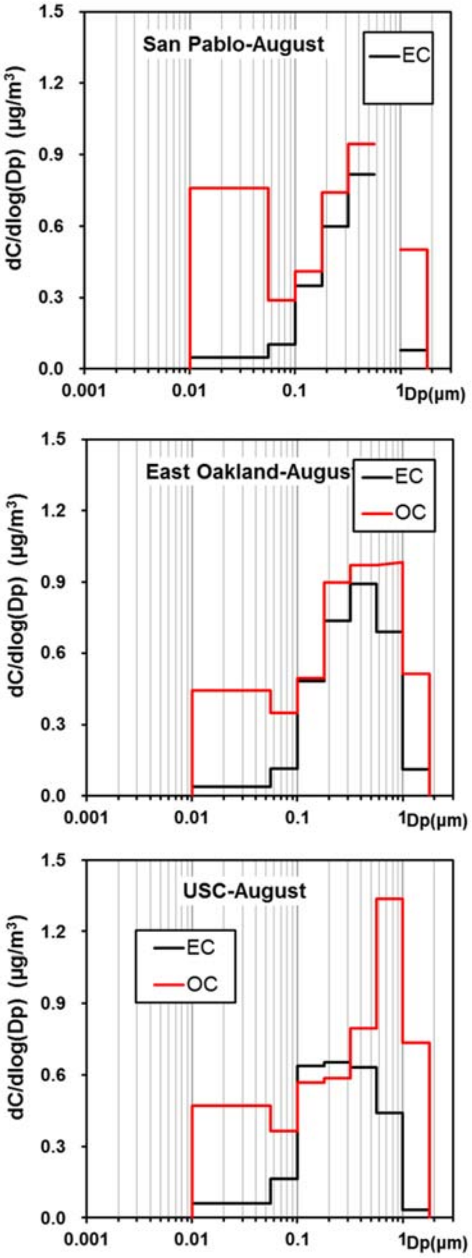

Figure S5-3: Size distribution of the aerosols collected at three sampling sites in August, 2015. The smallest size bin corresponds to the MOUDI after-filter data that suffers from adsorption artifacts for organic vapors.

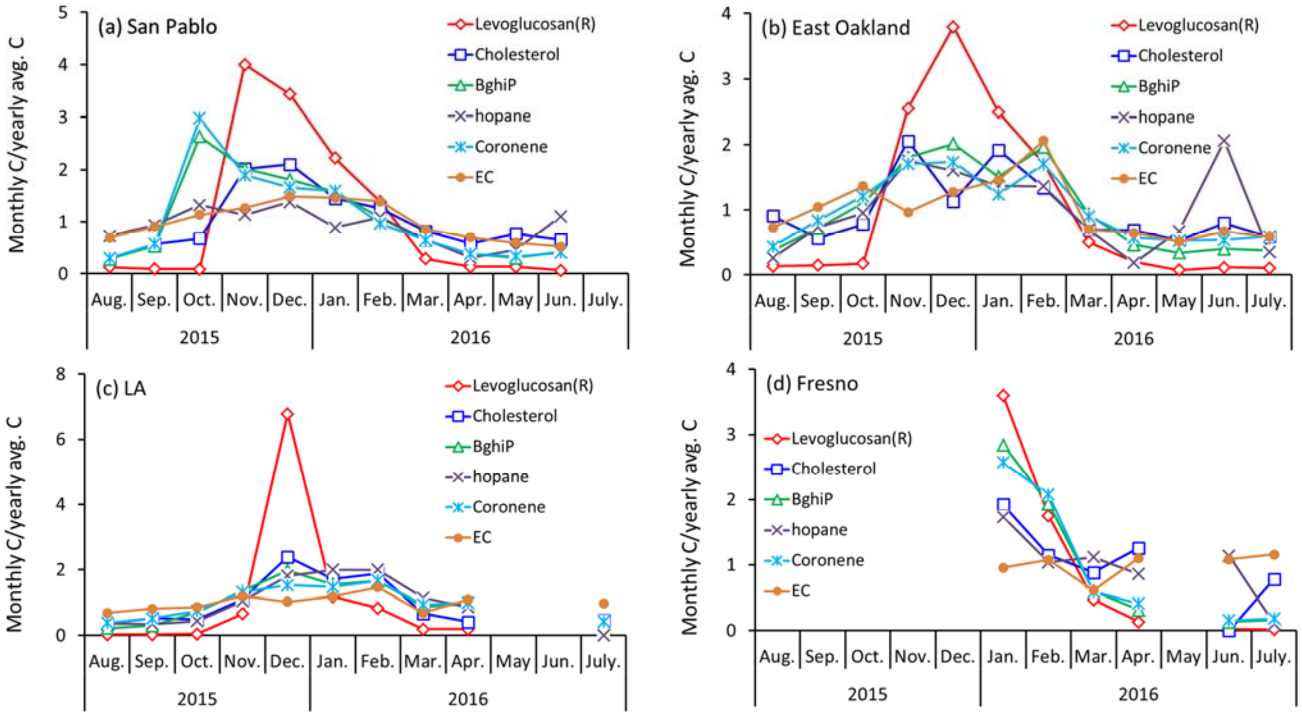

Figure S5-4: The ratio of monthly concentration of source tracers to their averaged concentration over the measured period. This figure demonstrates the seasonal variation of the source tracers.

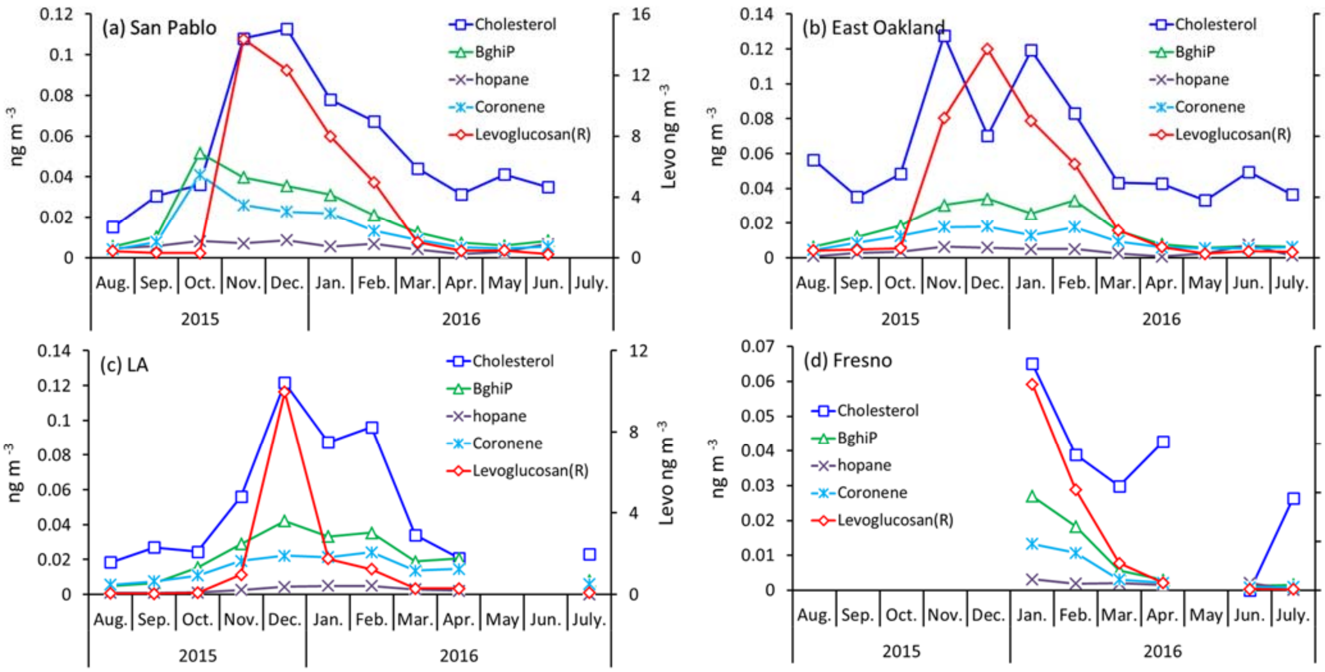

Figure S5-5: The seasonal patterns of molecular markers without correction

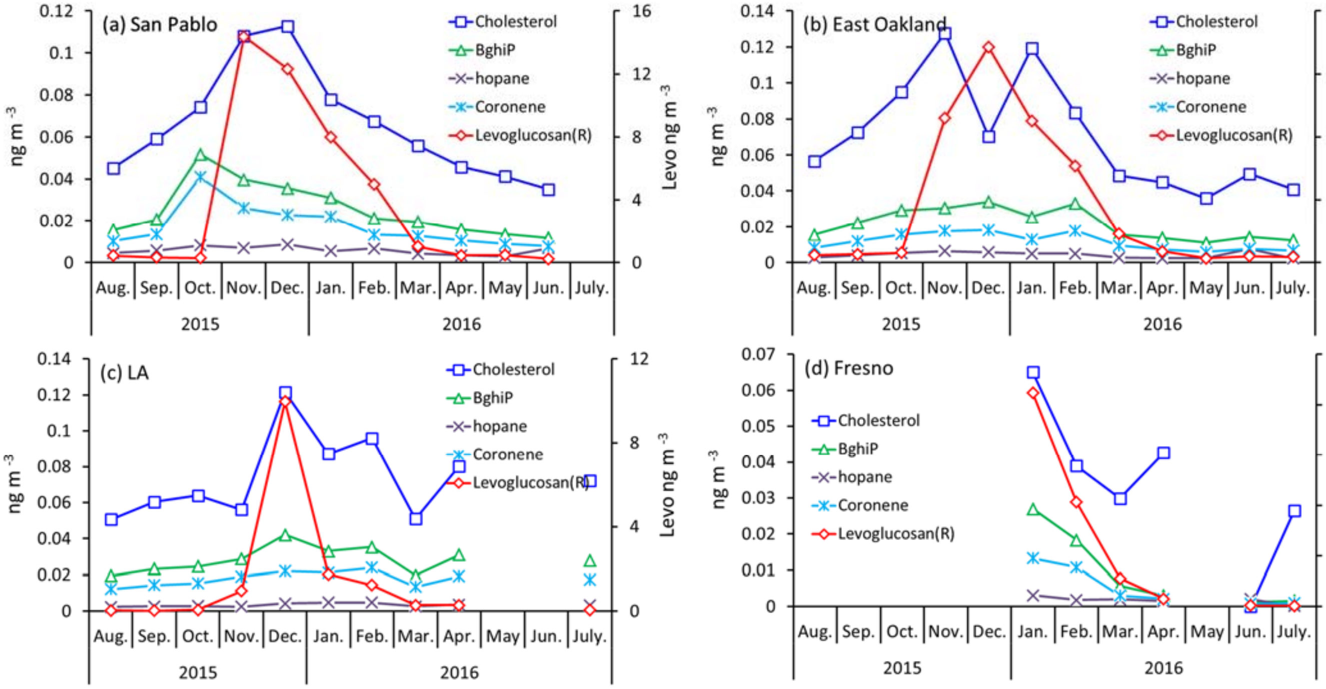

Figure S5-6: The seasonal patterns of molecular markers with correction

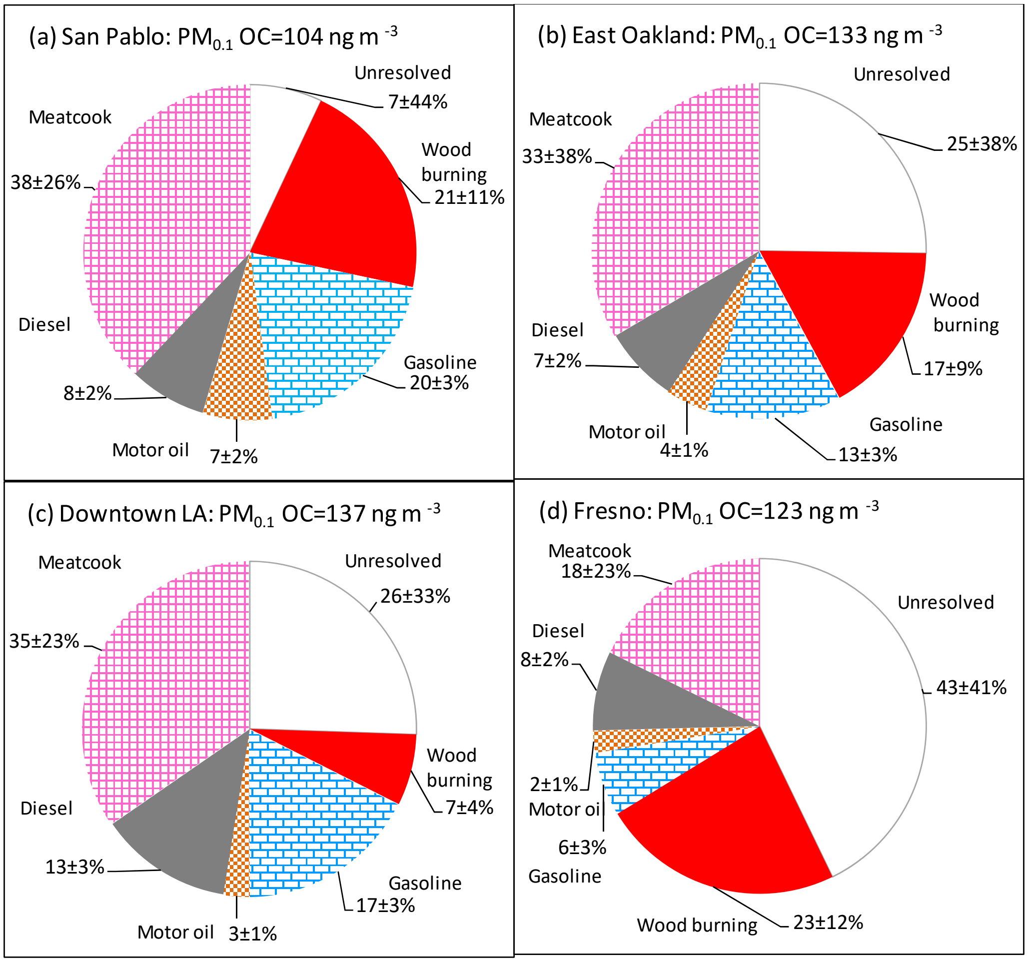

Figure S5-7: Annual averaged source contribution to $PM_{0.1}$ OC predicted by CMB model using conventional source profile. Uncertainty with the unresolved $PM_{0.1}$ OC is derived from the model predicted uncertainty for all other sources.

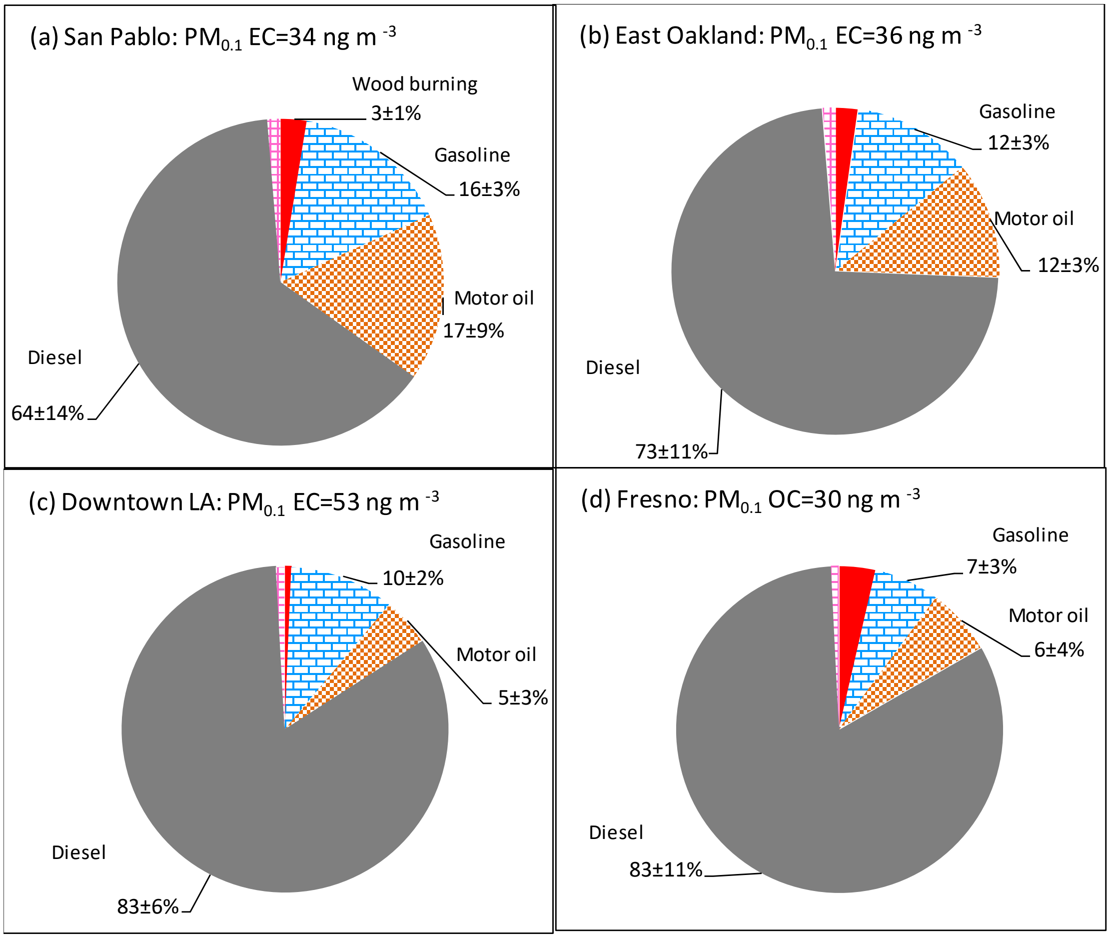

Figure S5-8: Annual averaged source contribution to $PM_{0.1}$ EC predicted by CMB model using conventional source profile.

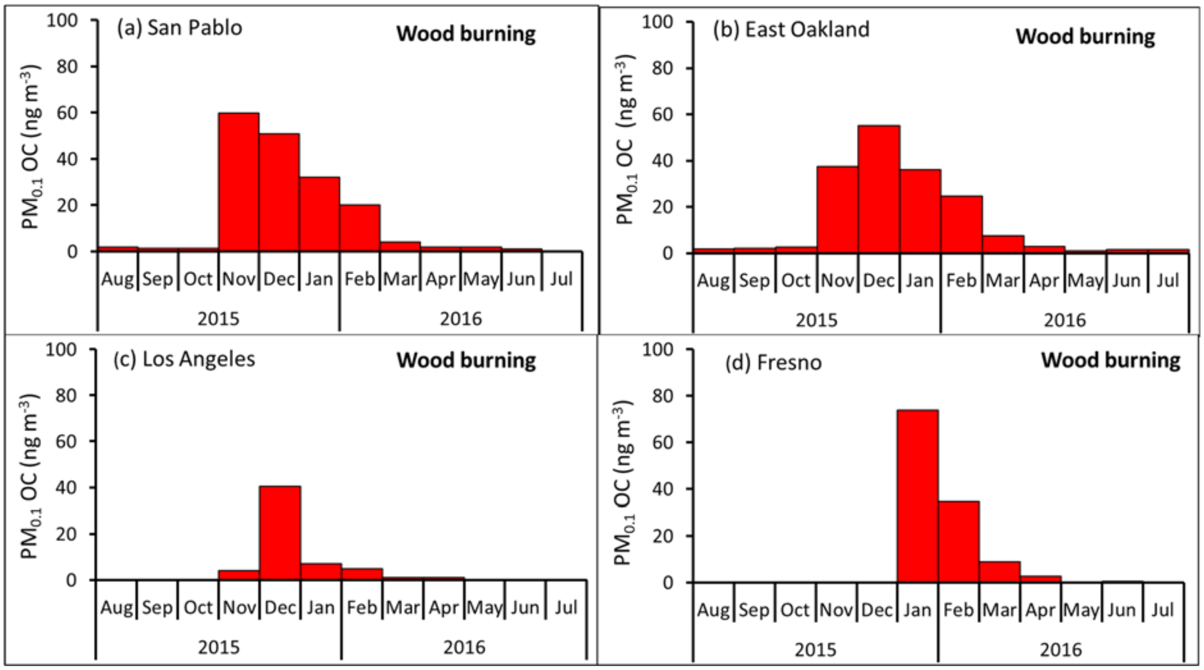

Figure S5-9: Model predicted monthly $PM_{0.1}$ OC contributed by wood burning using semi-volatile source profile.

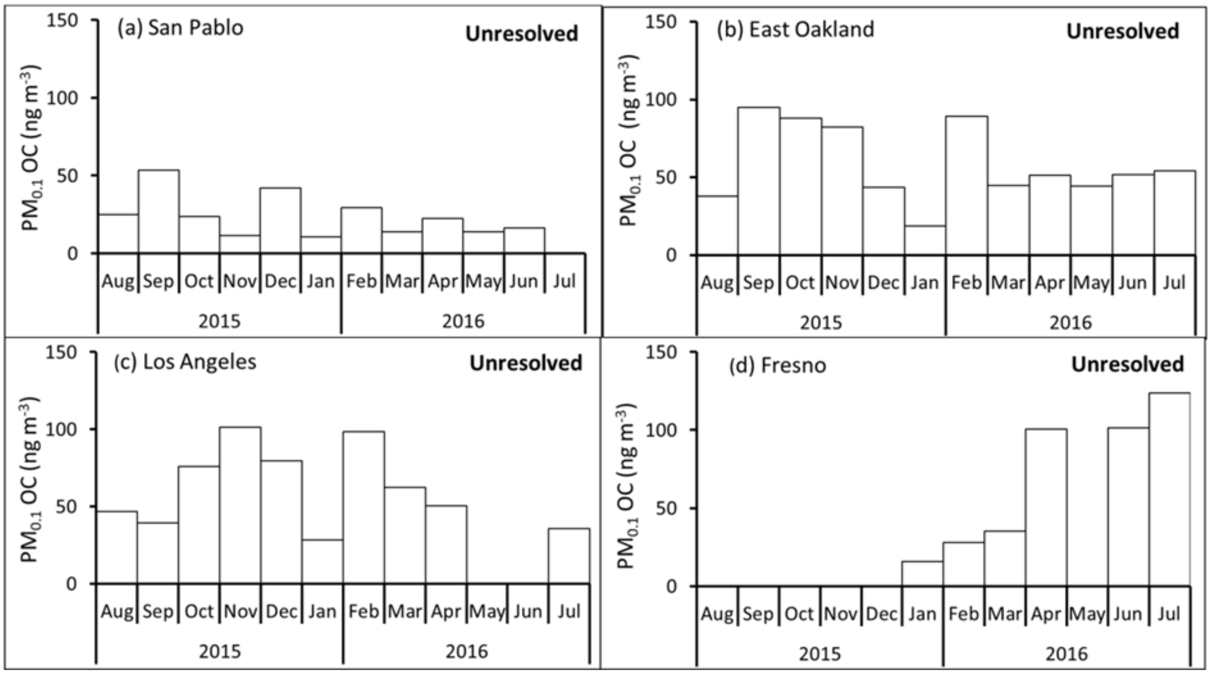

Figure S5-10: Model predicted monthly $PM_{0.1}$ OC contributed by unresolved OC fractions using semi-volatile source profile.

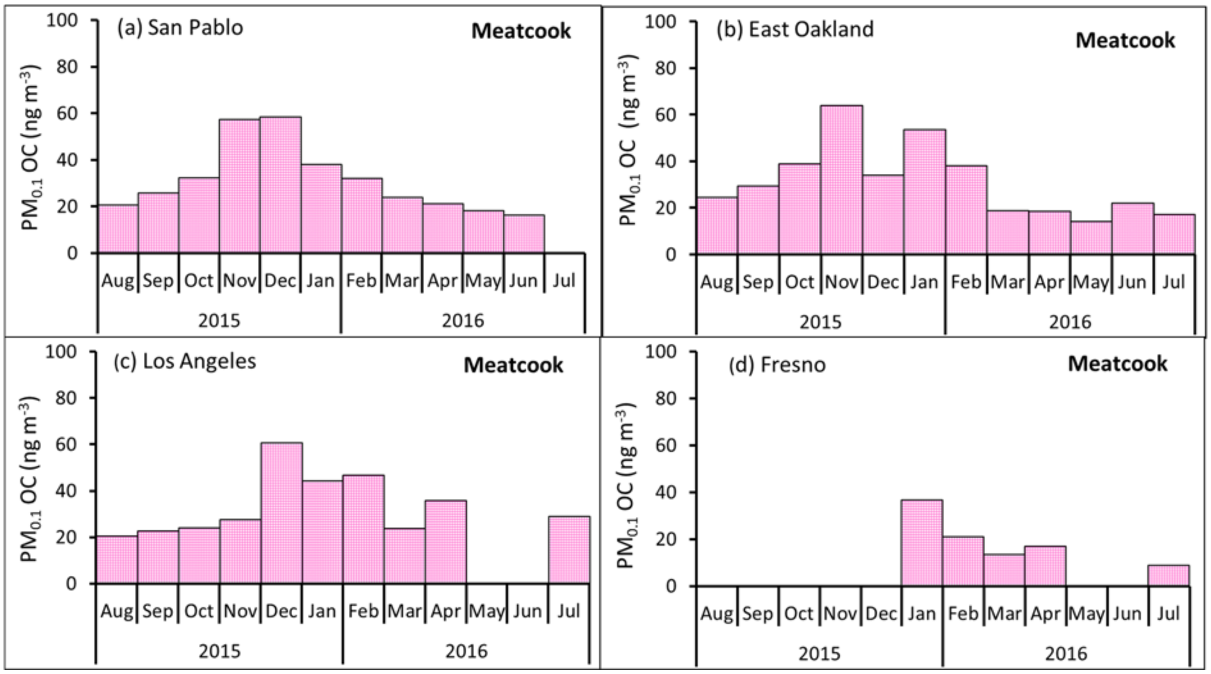

Figure S5-11: Model predicted monthly $PM_{0.1}$ OC contributed by meat cooking using semi-volatile source profile.

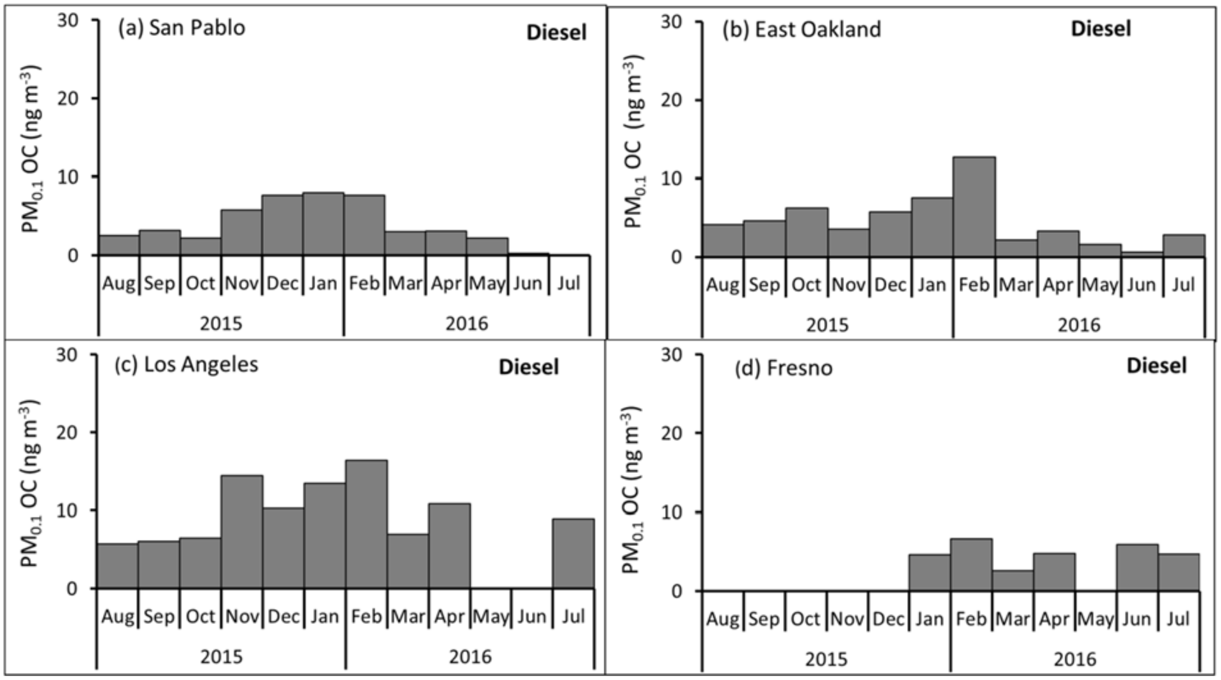

Figure S5-12: Model predicted monthly $PM_{0.1}$ OC contributed by diesel engines using semi-volatile source profile.

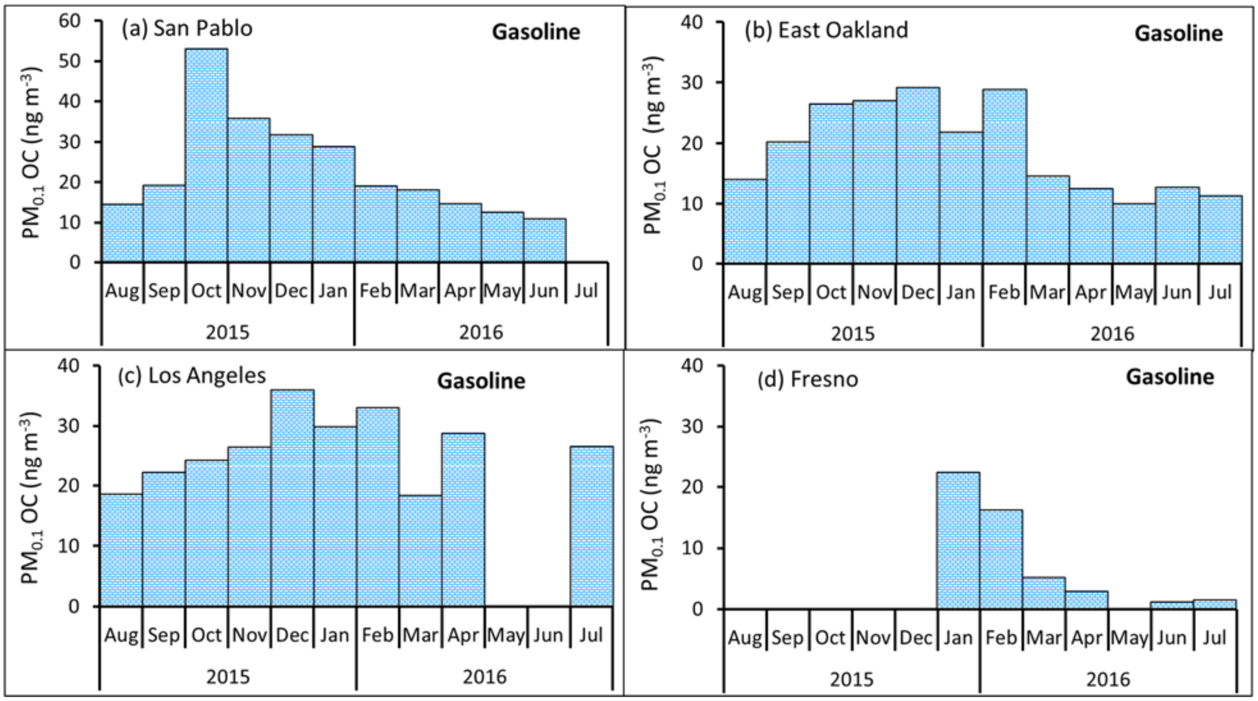

Figure S5-13: Model predicted monthly $PM_{0.1}$ OC contributed by gasoline engines using semi-volatile source profile.

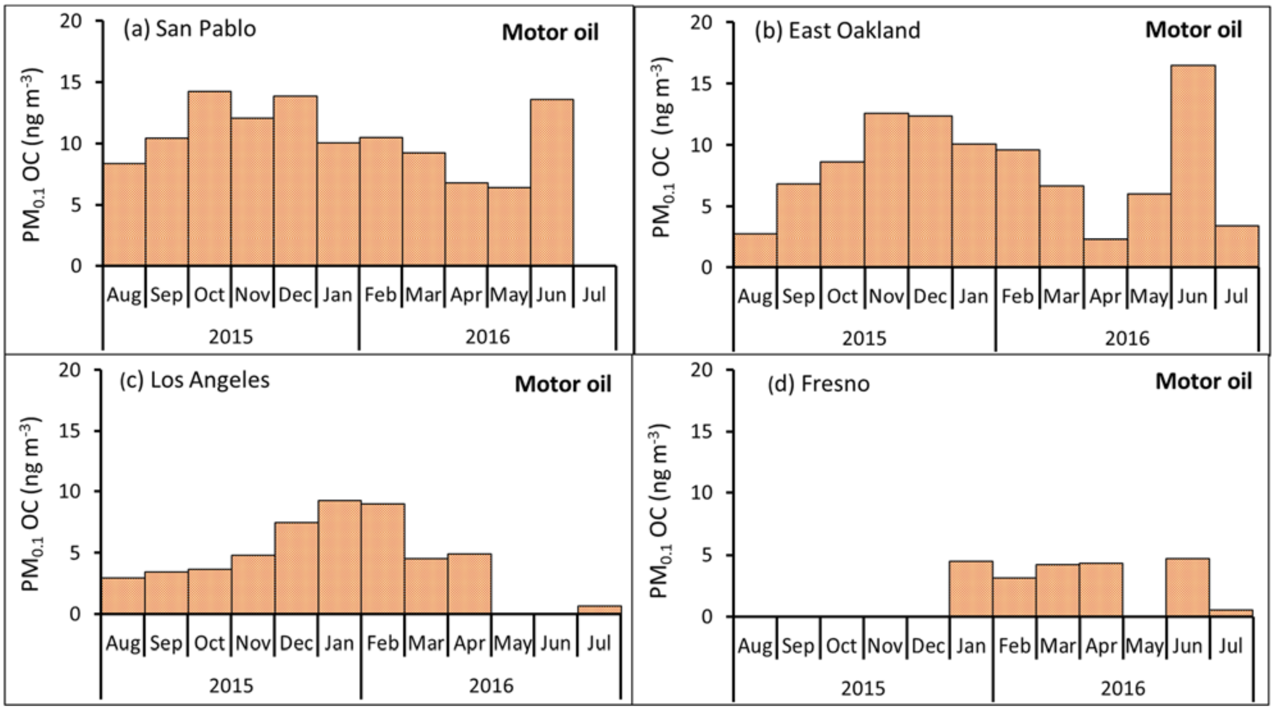

Figure S5-14: Model predicted monthly $PM_{0.1}$ OC contributed by motor oil using semi-volatile source profile.

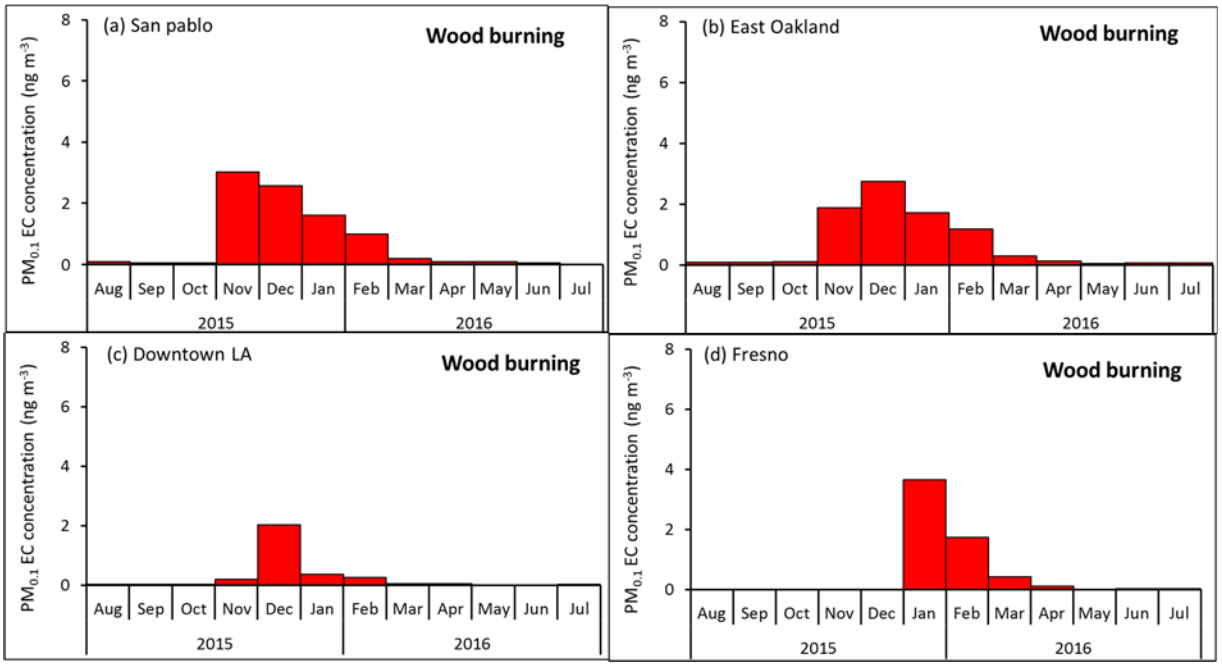

Figure S5-15: Model predicted monthly PM$_{0.1}$ EC contributed by wood burning using semi-volatile source profile.

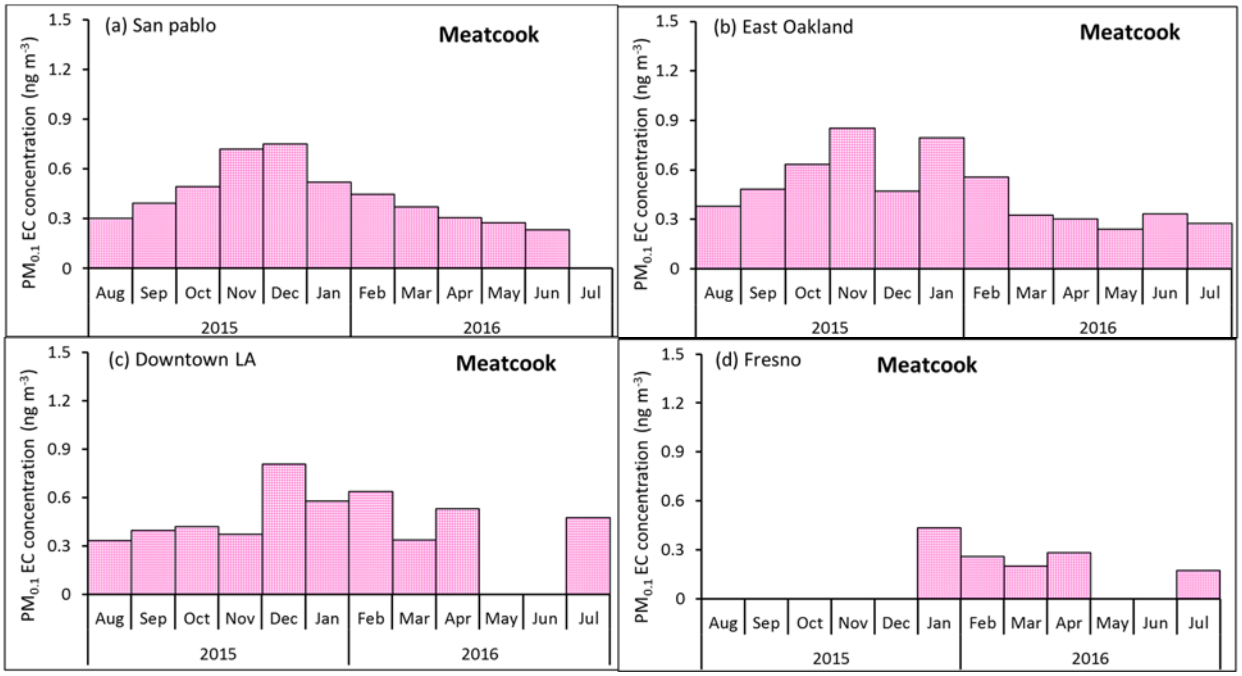

Figure S5-16: Model predicted monthly PM$_{0.1}$ EC contributed by meat cooking using semi-volatile source profile.

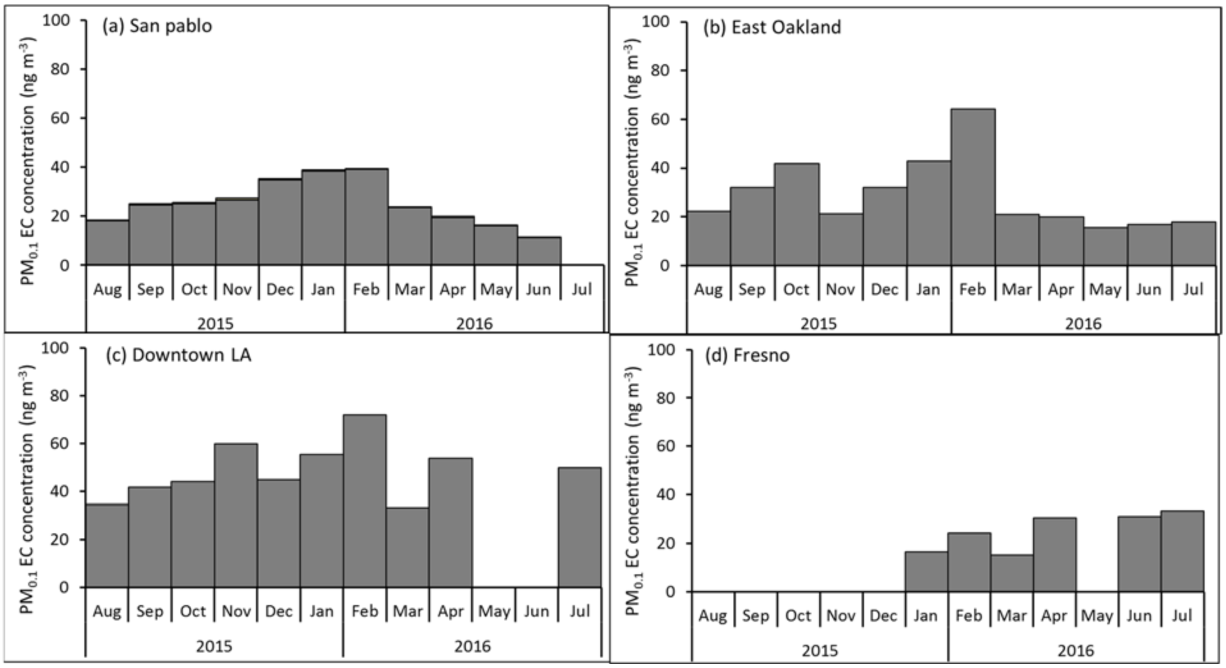

Figure S5-17: Model predicted monthly $PM_{0.1}$ EC contributed by diesel engines using semi-volatile source profile.

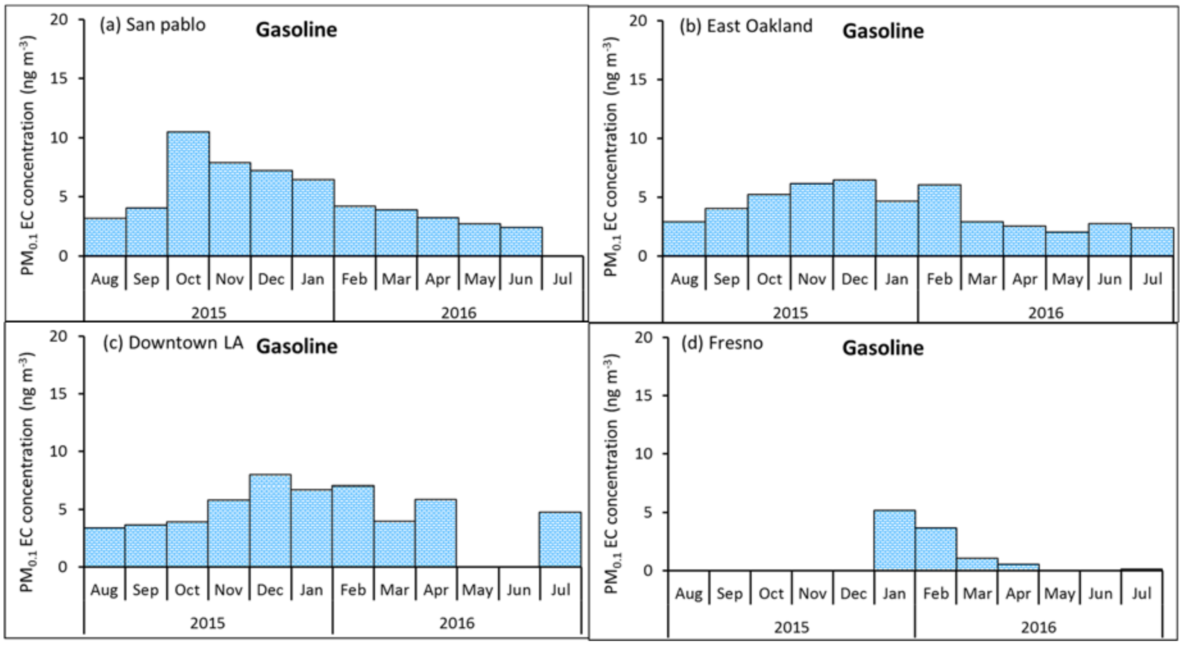

Figure S5-18: Model predicted monthly $PM_{0.1}$ EC contributed by gasoline engines using semi-volatile source

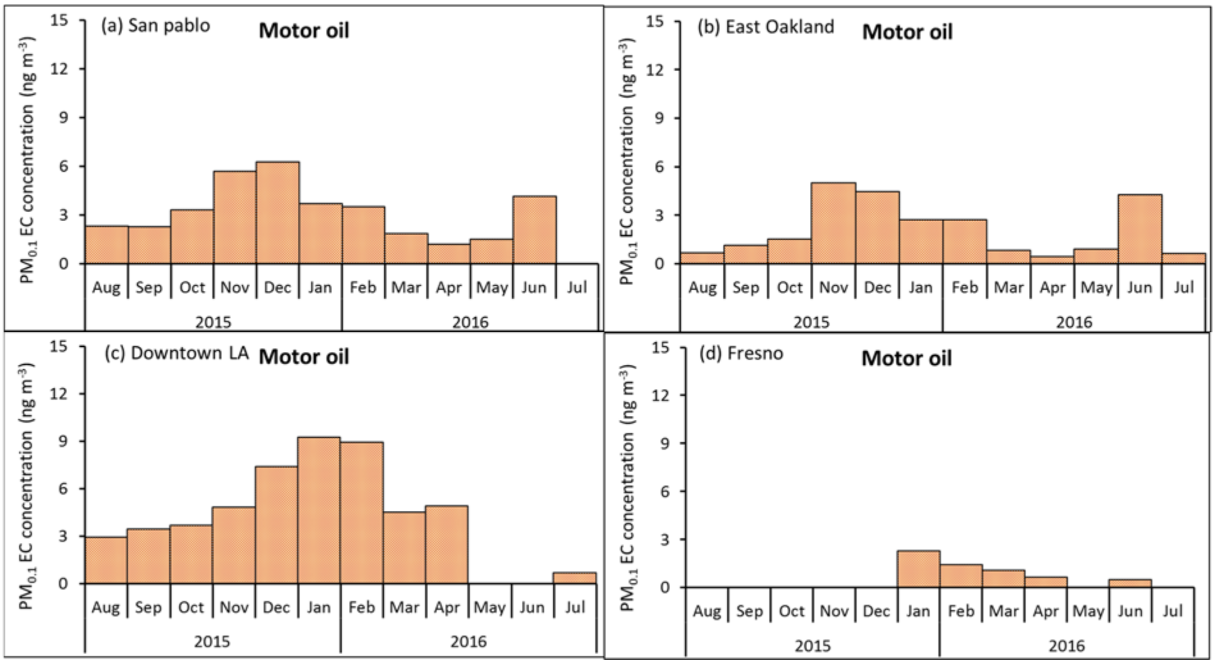

Figure S5-19: Model predicted monthly $PM_{0.1}$ OC contributed by motor oil using semi-volatile source profile.

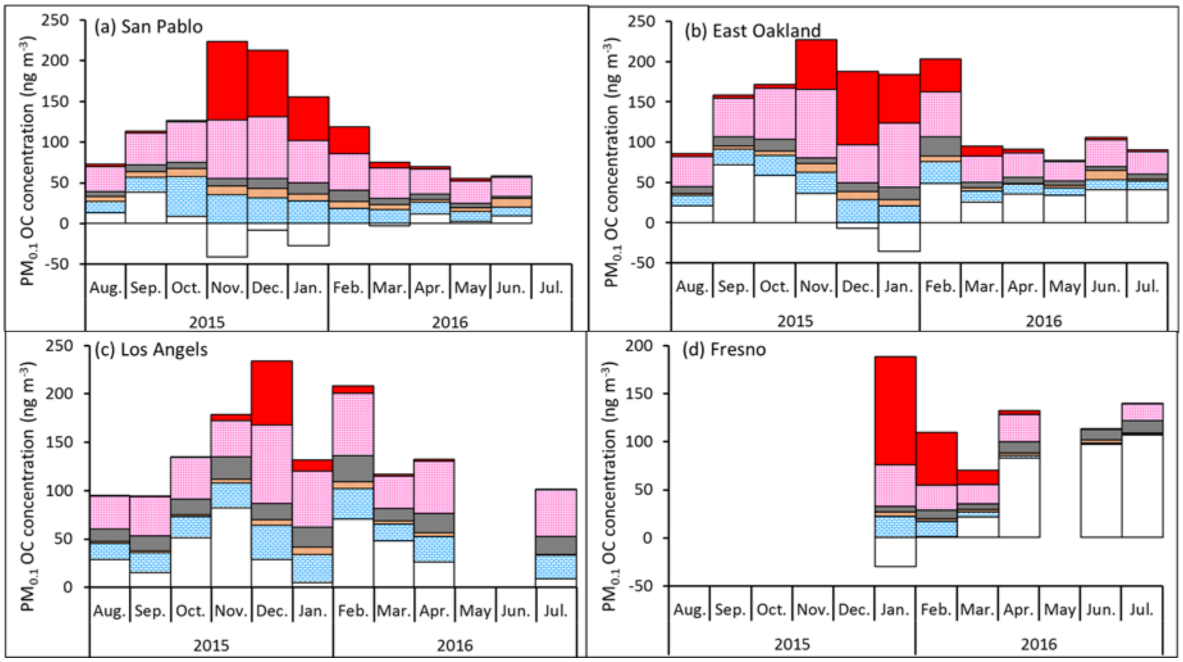

Figure S5-20: Model predicted monthly source contribution to $PM_{0.1}$ OC using conventional source profile.

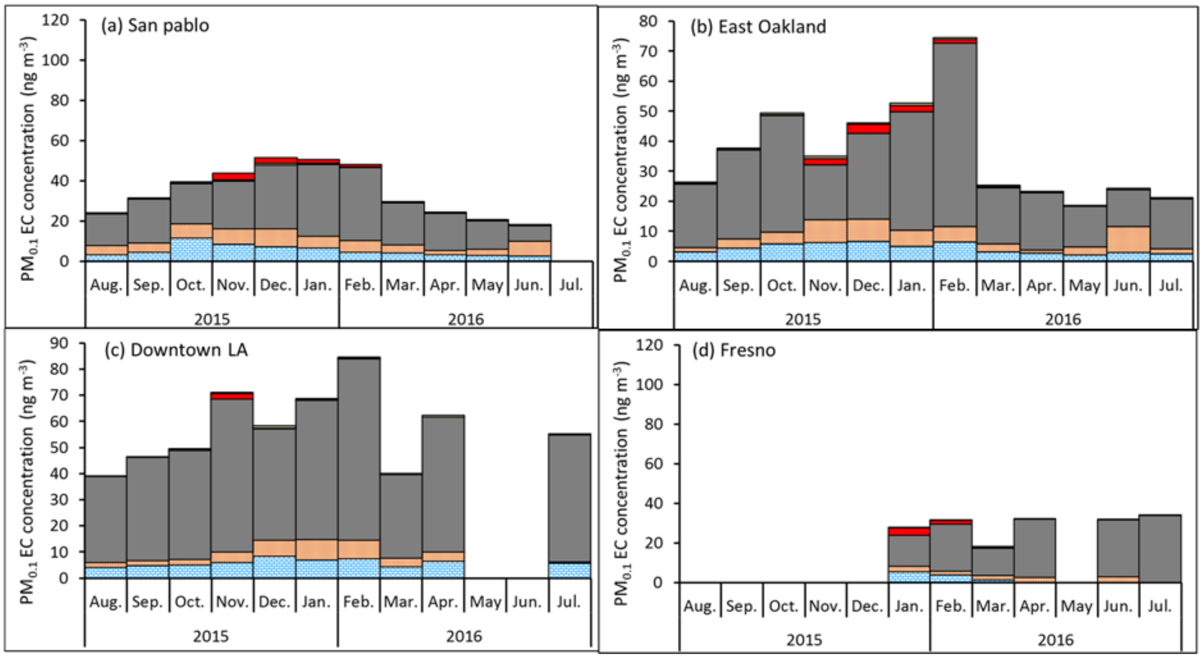

Figure S5-21: Model predicted monthly source contribution to PM$_{0.1}$ EC using conventional source profile

6 ANALYSIS OF SAPRC16 CHEMICAL MECHANISM FOR AMBIENT SIMULATIONS

Preamble: Chapter 6 tests a new photochemical mechanism in regional grid model calculations to determine if this mechanism would improve predictions of gas-phase oxidants that influence particulate nitrate and particulate secondary organic aerosol (SOA) formation. Previous studies identified SOA in the UFP size range as highly toxic, but the mechanisms used to predict that SOA were known to be incomplete. The current study attempts to adopt the latest science to improve predictions if possible.

6.1 Introduction

Human health is greatly influenced by atmospheric pollutants such as ground level ozone (O_3) that can degrade lung function and cause cardiovascular disease [203]. As of December 31, 2017, 168 counties and 107 million people (based on 2010 population census) throughout the United States were in non-attainment areas of the national ambient air quality standard (NAAQS) for ground level 8-hour ozone (75 ppb) [204]. These regions must develop State Implementation Plans (SIPs) that demonstrate future attainment with the ozone NAAQS in the presence of current and future sources and meteorology. Chemical transport models (CTMs) and their chemical kinetic reaction mechanisms play a critical role in the development of these pollutant abatement strategies [205]. CTMs describe the physical and chemical mechanisms that impact air pollutant emission, reaction, transport and deposition. The chemical mechanism is the core of the CTM representing chemical reactions by which emitted pollutants form secondary pollutants [206].

Ozone is a secondary pollutant that is produced in the lower atmosphere by non-linear photochemical reactions between volatile organic compounds (VOCs) and oxides of nitrogen (NOx). These reactions have the common attribute that they initiate and then propagate peroxy-radicals (HO_2 and higher-order RO_2). Control strategies for ozone are complex since the optimal target levels of NOx and VOCs change based on location, emissions and variable meteorology [207]. The chemical mechanism utilized in a CTM represents all atmospheric constituents (reactions, rate constants, etc.) that influence formation of photochemical pollutants, including O_3, secondary organic aerosols, peroxides and organic nitrates [208].

California State Implementation Plans (SIPs) developed over the past decades have generally used the SAPRC chemical mechanism in CTMs to determine ozone concentrations under current and future emissions levels. Other examples of chemical mechanisms utilized in CTMs are Carbon Bond 4 [209], RADM-2 [210], RACM [211], MCM [212] and Carbon Bond 05 [213]. Each of these mechanisms includes reactions that form and propagate peroxy-radicals, but they differ in their choice of how much detail they include and how they describe the precursor VOC chemistry. Attempts to predict ambient concentrations of peroxy-radicals in different field campaigns using various chemical mechanisms have produced mixed results [214]. Some studies observe model under-prediction of radical concentration which could be due to missing or underestimated sources of radicals or an over estimation of a radical sink [215] [216, 217] [218, 219]. Other studies have found that models over predict radical concentrations [220] [221] [222]. In addition, some studies have found variation between over and under prediction of OH and HO_2 [223] [224]. Incorrect assumptions of radical concentration in CTMs could cause biased ozone concentrations, which in turn may affect emission reduction strategies developed in a SIP. It is for this reason that chemical mechanisms are continually updated to incorporate the most recent science and understanding of the HOx radical chain chemistry and the formation of secondary pollutants.

The evolution of the SAPRC chemical mechanisms over the past 30 years reflects our expanding knowledge about atmospheric gas-phase chemistry [225-230]. In the most recent stage of this continual evolution, the SAPRC11 mechanism is being revised (i) to incorporate the latest rate constants used in the base mechanism, (ii) to include a new speciation lumping scheme, (iii) to better develop predictions of secondary organic aerosol (SOA) precursors, and (iv) to update methods used to estimate reactions of individual organic compounds. The updated mechanism is designed to represent more compounds explicitly and to include a larger number of lumped organic species to improve SOA modeling. Although this update process is still underway, an interim version, designated SAPRC16, has been made available for evaluation purposes [231].

The SAPRC16 condensed mechanism lumps explicit species using a computer mechanism generation system that estimates individual reactions of organic compounds and the radicals they form. Similar approaches have been used for SAPRC99, SAPRC07, and SAPRC11 [226, 228, 231, 232]. SAPRC16 incorporates updates to the mechanism generation system as of October, 2016 (Carter, 2016). Future updates will use the same base mechanism and lumping approach as SAPRC16 but will incorporate different predictions for reaction products from higher molecular weight organic compounds, which may affect predicted SOA concentrations. SAPRC16 successfully predicts ozone formation in a wide range of environmental chamber experiments [231, 233, 234].

In this study, SAPRC16 has been implemented into the UCD-CIT air quality model and evaluated for its predictions of ambient ozone (O_3) and peroxy-radical formation against the previous version of the chemical mechanism, SAPRC11. Both mechanisms are used to predict ambient concentrations that are compared to measured values in cities across the United States. In addition, a box model was used to simplify and evaluate the changes in the reactions and rate constants between the SAPRC11 and SAPRC16 mechanisms to better understand the impacts of the updated lumping scheme and reactions. These comparisons will provide useful information to help guide the continued development of the SAPRC mechanism, and to evaluate if SAPRC16 could potentially improve predicted concentrations of secondary organic aerosol (SOA) in the UFP size range that have been identified as highly toxic in prior epidemiological studies [7].

6.2 Methods

6.2.1 Model Scenarios

Ozone, NOx and HOx concentrations were predicted in the summer of 2010 using the UCD/CIT CTM with SAPRC11 and SAPRC16 chemical mechanisms over seven urban locations within the continental United States. The areas of interest and dates simulated are displayed in Table 6-1.

With the exception of the Pasadena location, the episodes selected correspond with summer time air pollution events lasting 3-4 days during which measured 1-hr maximum ozone concentrations exceeded 70 ppb. The Pasadena/CalNex simulation period did not meet this criteria, however this episode was included in the analysis in order to take advantage of the measurements of ambient HOx radical concentrations during this time period.

Table 6-1. Locations of interest and dates simulated for evaluation of SAPRC11 and SAPRC16 chemical mechanisms.

City/Area	**Dates Simulated**
North East (NYC and Philadelphia), US	Aug. 29 – Sep. 01, 2010
San Joaquin Valley, CA	Aug. 24 – Aug. 27, 2010
South Coast Air Basin, CA	Sep. 23 – Sep. 26, 2010
Baltimore, MD	Aug. 8 – Aug. 11, 2010
Houston, TX	Oct. 4 – Oct. 8, 2010
Atlanta, GA	Mar. 30 – Apr. 2, 2010
Pasadena, CA	May 15 – Jun. 15, 2010

The UCD/CIT chemical transport model predicts the evolution of gas and particle phase pollutants in the atmosphere in the presence of emissions, transport, deposition, chemical reaction and phase change [235] as represented by equation (1)

$$\frac{\partial C_i}{\partial t} + \nabla \cdot uC_i = \nabla K \nabla C_i + E_i - S_i + R_i^{gas}(C) + R_i^{part}(C) + R_i^{phase}(C) \tag{1}$$

where C_i is the concentration of gas or particle phase species i at a particular location as a function of time t, u is the wind vector, K is the turbulent eddy diffusivity, E_i is the emissions rate, S_i is the loss rate, R_i^{gas} is the change in concentration due to gas-phase reactions, R_i^{part} is the change in concentration due to particle-phase reactions and R_i^{phase} is the change in concentration due to phase change [235]. A total of 50 particle-phase chemical species are included in each of 15 discrete particle sizes that range from 0.01-10 µm particle diameter [235]. The UCD/CIT model is selected for this study as a matter of convenience since SAPRC16 and SAPRC11 are not officially supported to run in the Community Multiscale Air Quality (CMAQ) model.

In addition to the full 3D airshed predictions, a box model supporting both SAPRC11 and SAPRC16 chemical mechanisms was used to simplify ambient conditions and focus on the changes between the two mechanisms. Ozone isopleths were generated for six VOC species that have the same lumping representation in both SAPRC11 and SAPRC16: formaldehyde, acetaldehyde, ethene, isoprene, ethane and alkanes that have a kOH between 1.7 and 3.4 x 10^{-12} cm^3 $molec^{-1}$ s^{-1}. These species were selected in order to observe how the mechanisms respond with identical inputs within various functional groups and chain length. Each VOC concentration was initialized at 20 ppb but then scaled by ratios spanning from 0.1 to 1.2. NOx concentrations were initialized to 80 ppb but then scaled with ratios spanning from 0.1 to 1.2. Each box model simulation ran over a 12-hour cycle (720 min) and the maximum ozone from the final (12th) hour was selected for Figures 6-1 and 6-2.

6.2.2 Model Inputs

Meteorology parameters for the episodes listed in Table 6-1 were developed using the Weather Research and Forecasting model (WRFv3.6) and WRF preprocessing system (WPSv3.6). All simulations were generated within 3 nested domains with horizontal resolutions of 36km, 12km, and 4km, respectively. Each domain had 31 telescoping vertical levels up to a top height of 12km. Four-dimensional data assimilation (FDDA) or "FDDA-nudging" was used in order to yield meteorology results that better correlated to the observed data [236].

Anthropogenic emissions for all simulations were developed using the Sparse Matrix Operator Kernel Emissions (SMOKEv3.7) modeling system with the 2011 US EPA national emissions inventory (NEI). Biogenic emission rates were developed using the Model of Emissions of Gases and Aerosols from Nature (MEGANv2.1) and wildfire emissions were developed using the global fire emissions database (GFED) [237]. Source speciation profiles for SAPRC16 lumping approach were generated by Carter's updated speciation database [238]. Source apportionment profiles were designed by assigning a specific source classification code within each of SMOKE's four source sectors (area, mobile, non-road and point) to each of the following six tracked source groups: biomass, diesel, gasoline, food cooking, natural gas and all other emissions.

6.2.3 Supporting Measurements

Ambient hourly ozone measurements were obtained from the EPA Query AirData (https://aqs.epa.gov/api). Ambient HOx concentrations were obtained from the CalNex 2010 field campaign as analyzed by Griffith et al (2016). The CalNex field study was conducted in 2010 to address and understand issues in atmospheric pollution and climate change [239]. Included in that study were the measurements of radical OH and HO_2 concentration at the ground site located on the campus of the California Institute of Technology (Caltech) in Pasadena, CA. The site was located approximately 18 km northeast of downtown Los Angeles (34.1408 °N, 118.1223°W). HO_2 and OH measurements were made from May 15 to Jun 15, 2010. OH was measured by fluorescent assay by gas expansion while HO2 [214] was measured as OH after conversion using NO [240]. OH measurements were averaged for 15 min around the reported Mid_UTC time and reported in molecules cm^{-3} while HO_2 measurements were irregularly spaced in time and measured for 20 seconds around the reported Mid_UTC time in molecules cm^{-3}. Measurements were converted to ppm for comparison to model simulations.

6.3 Results

6.3.1 Box Model Analysis

Hourly ozone concentrations were predicted using a box-model with the SAPRC11 and SAPRC16 chemical mechanisms. The box model was used to simplify ambient conditions and focus on the changes inherent in the two mechanisms. Figure 6-1 illustrates ozone isopleths generated from the box model simulation when an individual VOC species and NOx are present initially with no subsequent emissions. A transect line with equal scaling factors for NOx and VOC is shown on each isopleth as a reference. VOCs with similar treatment in SAPRC11 and SAPRC16 were selected to directly compare results generated with identical inputs. The VOC species span different functional groups: formaldehyde, acetaldehyde, ethene, isoprene, ethane and alkanes that have kOH between 1.7 and 3.4 x 10^{-12} cm^3 $molec^{-1}$ s^{-1} The isopleths show ozone formation from SAPRC16 is quenched at lower NOx concentrations in comparison to SAPRC11 for formaldehyde, acetaldehyde, ethane, ethene and alkanes that have kOH between 1.7 and 3.4 x 10^{-12} cm^3 $molec^{-1}$ s^{-1}. Isoprene is more reactive in SAPRC16 and yields a higher O_3 concentration at all VOC/NOx ratios in comparison to SAPRC11. At low NOx conditions, SAPRC16 predicts higher O_3 concentrations in all the box model simulations with individual VOC species.

Figure 6-2 illustrates the ozone concentrations along the "equal scaling" transect from the isopleths in Figure 6-1. Initial concentrations of VOC and NOx along this transect were scaled by the same factor (ranging from 0.2 to 1.2) yielding the indicated final O_3 concentrations. Figure 6-3 shows the final summed peroxy-radical concentrations along this same transect. SAPRC11 includes eight (8) peroxy-radicals: HO2, MEO2, RO2C, MECO3, RCO3, HCOCO3, BZCO3 and MACO3 while SAPRC16 includes 160 peroxy-radicals (see supporting information for a complete lists) with HO_2 dominating total peroxy-radical totals in both mechanisms. Figure 6-2 shows that O_3 concentrations peak at lower NOx concentrations for SAPRC16 in comparison to SAPRC11 for formaldehyde, acetaldehyde, ethane, ethene and alkanes that have kOH between 1.7 and 3.4 x 10^{-12} cm^3 $molec^{-1}$ s^{-1}. The SAPRC16 peroxy-radical concentrations also peak at lower NOx concentrations in comparison to the SAPRC11 peroxy-radical concentrations (Figure 6-3), which explains the O_3 trends as a function of NOx (Fig 6-2). Peroxy-radicals (RO_2) react with NO to increase O_3 production via the pathway

$$RO2 + NO = NO2 + PRODUCTS \tag{1}$$

$$NO2 + hv = NO + O \tag{2}$$

$$O + O2 = O3 \tag{3}$$

but excess NO_2 also scavenges OH

$$OH + NO2 = HNO3 \tag{4}$$

which terminates radical initiation and propagation reactions when NOx is high.

The rate constants for the parent VOC reactions with OH, O_3, or UV that initiate the peroxy-radical formation mechanism are identical in SAPRC16 and SAPRC11. The dominant peroxy-radical is HO_2 in both SAPRC16 and SAPRC11 (see panel captions in Fig 6-3) and the reaction rates of HO_2+NO are identical in the two mechanisms. SAPRC16 has a more detailed representation of organic peroxy radical species, but the total rates of their reactions with NO and HO_2 in the box model calculations are similar. However, SAPRC16 differs from SAPRC11 and most other current mechanisms in that it includes H-shift isomerizations of some peroxy radicals, which can compete and in some cases dominate over their reactions with NO and HO_2 . However, the isomerization reactions ultimately form HO2 and/or other peroxy radicals, though they will reduce the total amount of peroxy radicals that react with NO to promote ozone formation.

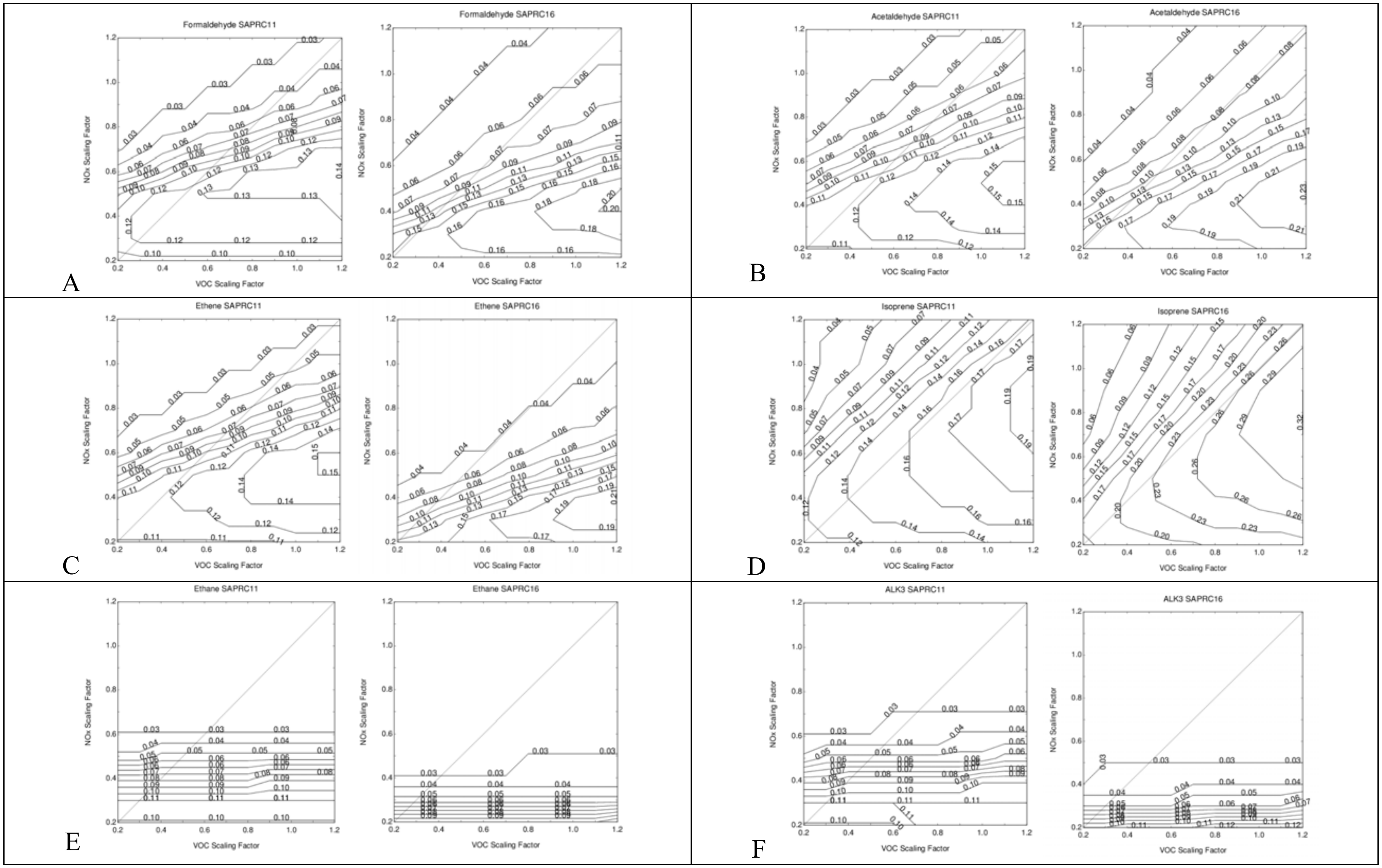

Figure 6-1: SAPRC11 and SAPRC16 O_3 isopleths generated by a box model with a single VOC species of interest and NOx initial conditions. Each panel (A-E) illustrates a different species and compares the two mechanisms scaled O_3 concentrations (ppm). SAPRC11 left figure, SAPRC16 right figure. The species of interest are: panel A – formaldehyde, B – acetaldehyde, C – ethene, D – isoprene, E – ethane, F – ALK3 lumped species. Grey line denotes 45° transect line.

a) Formaldehyde

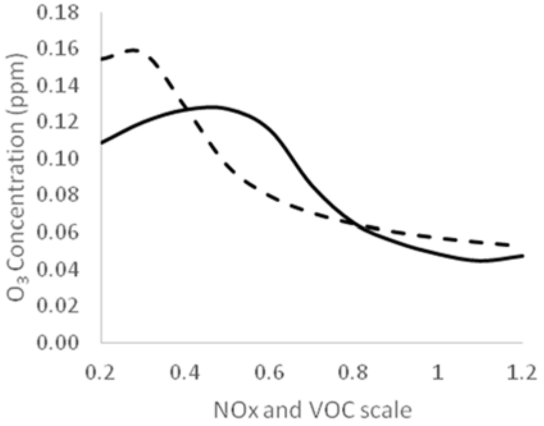

b) Acetaldehyde

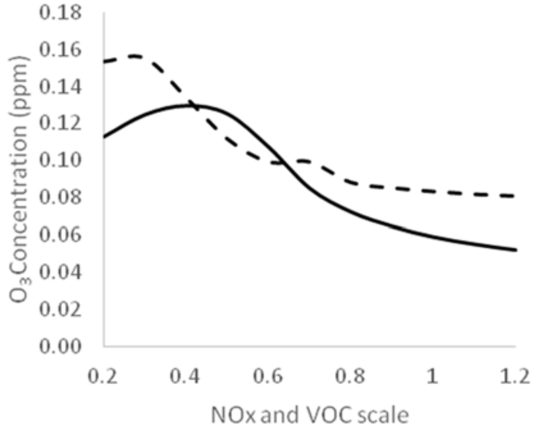

c) Ethene

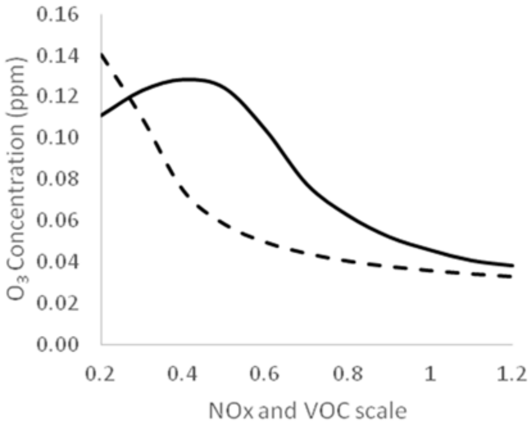

d) Isoprene

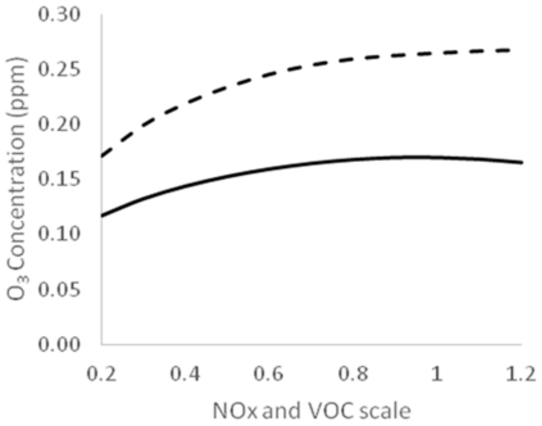

e) Ethane

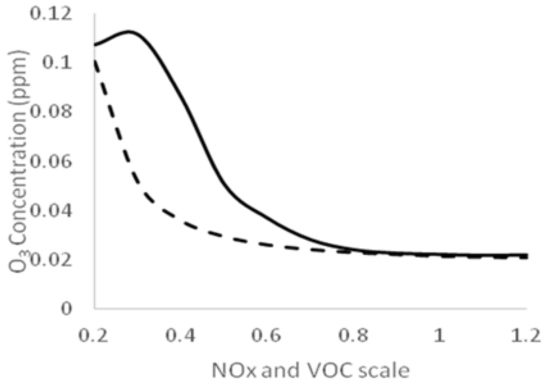

f) ALK3 Lumped Species

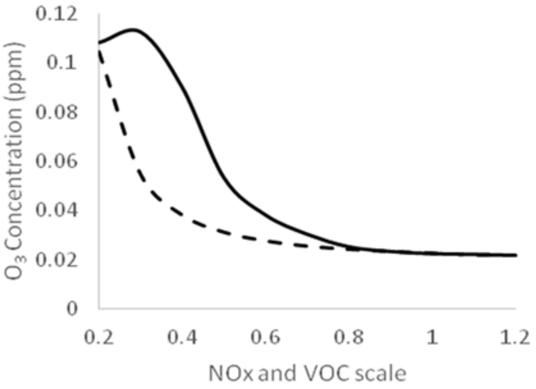

Figure 6-2: SAPRC11 and SAPRC16 O$_3$ concentrations (ppm) along the “equal scaling” transect of the isopleths from Figure 6-1. Each panel (a-e) illustrates a different parent VOC. SAPRC11 = bold line, SAPRC16 = dashed line.

a) Formaldehyde
(S11 HO_2: 100%, S16 HO_2: 100%)

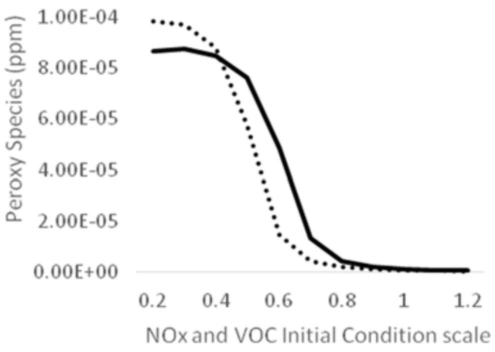

b) Acetaldehyde
(S11 HO_2: 96%, S16 HO_2: 96%)

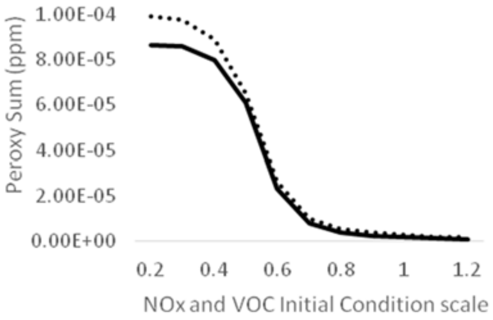

c) Ethene
(S11 HO_2:97%, S16 HO_2:87%)

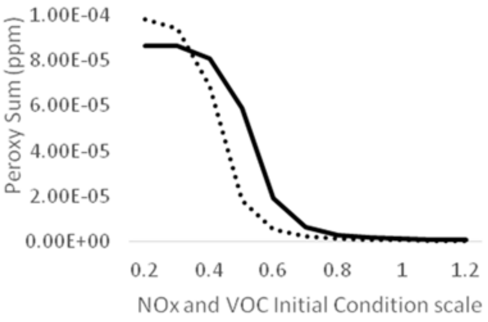

d) Isoprene
(S11 HO_2: 90%; S16 HO_2: 91%)

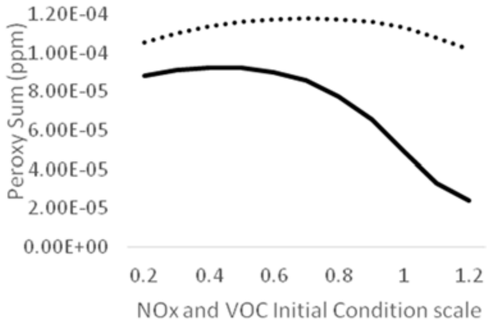

e) Ethane
(S11 HO_2: 98%, S16 HO_2: 97%)

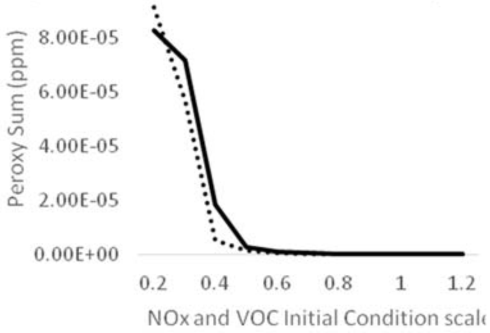

f) ALK3 Lumped Species
(S11 HO_2: 95%, S16 HO_2: 91%)

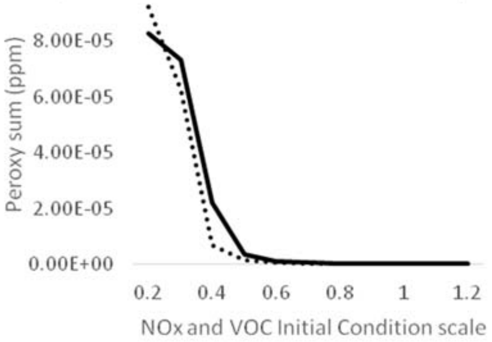

Figure 6-3: SAPRC11 and SAPRC16 sum of Peroxy Species concentrations (ppm) along the "equal scaling" transect of the isopleths from Figure 6-1. Each panel (a-e) illustrates a different parent VOC. SAPRC11 = bold line, SAPRC16 = dashed line

6.3.2 UCD-CIT Model Analysis

The UCD-CIT CTM predicted O_3 concentration using both the SAPRC11 and SAPRC16 chemical mechanisms. Predicted 1-hour O_3 concentrations were compared to measured 1-hour O_3 values for each of the seven locations and dates reported in Table 6-1. Figure 6-4 illustrates performance statistics for SAPRC11 and SAPRC16 vs measured 1-hour concentrations for each city. The western US locations (CA), which include the San Joaquin Valley and South Coast Air Basins, show a lower mean fractional error and root mean square error for SAPRC11 in comparison to SAPRC16. The model performance for SAPRC11 and SAPRC16 lack a consistent pattern for the eastern and south eastern US cities. In general, SAPRC11 predicts O_3 concentrations with slightly less bias and error (based on MFE) than SAPRC16 in four out of the six analyzed urban areas.

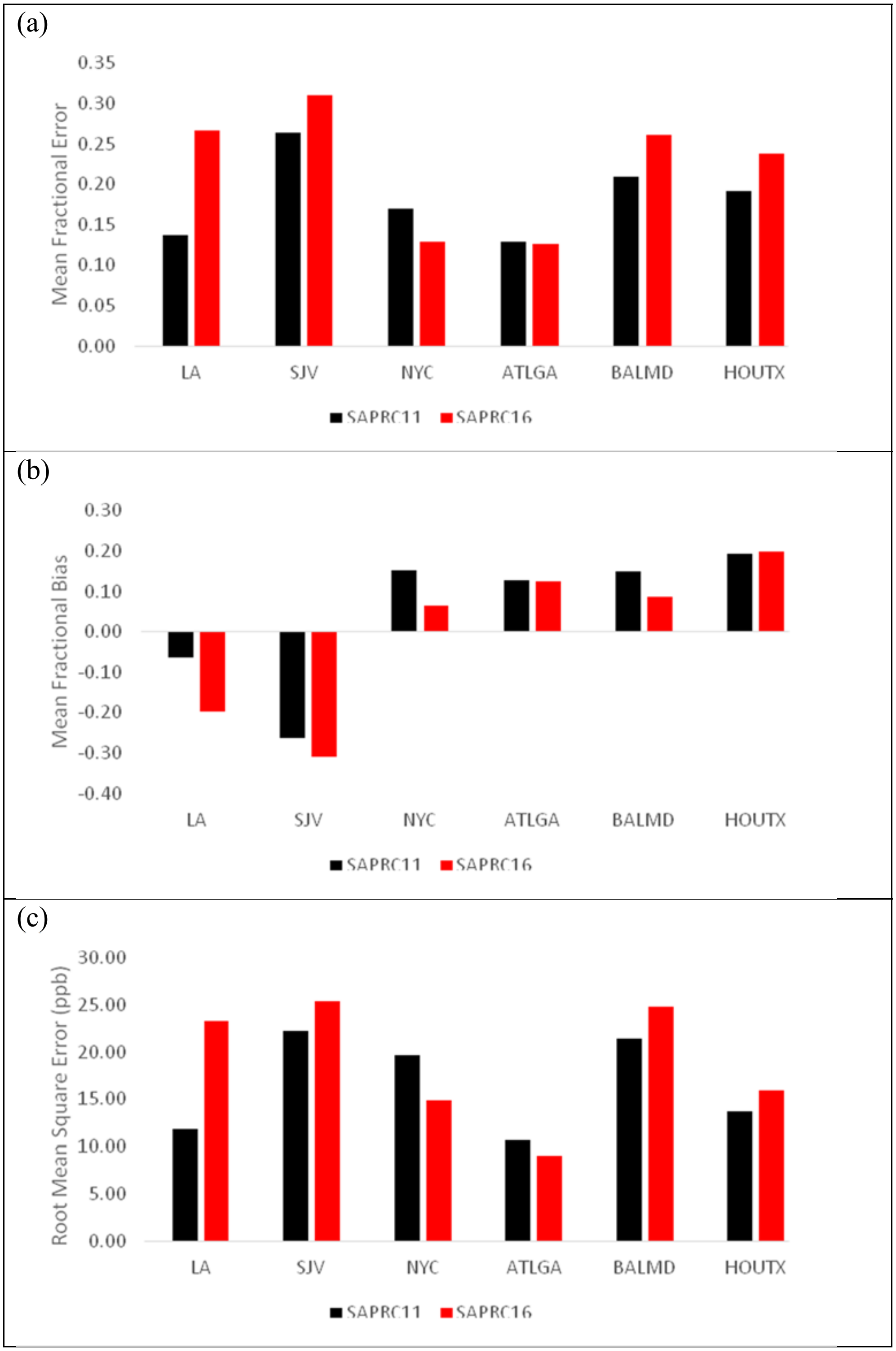

Figure 6-4: Performance Statistics for SAPRC11 and SAPRC16 vs measured 1-hour O_3 (ppb) concentrations. Panel A = mean fractional error, Panel B = mean fractional bias (MFB), Panel C = root mean square error (ppb).

Four sites in the South Coast Air Basin (SoCAB) were selected for further comparison between the two mechanisms. Tables 6-2 illustrates the name, latitude, longitude and description of each site in SoCAB.

Table 6-2. SoCAB Ambient O_3 Measurement Sites

Site	Name	Latitude	Longitude	Description
A	North Main St. /DT LA	34.06	-118.23	Urban/DT source region
B	Long Beach	33.80	-118.22	North of Port of Long Beach
C	West Anaheim	33.83	-117.94	Urban source region
D	La Habra	33.92	-117.95	Suburban source region

Figure 6-5 displays a time series of hourly ozone predicted using the SAPRC11 and SAPRC16 chemical mechanisms vs the measured 1-hour O_3 concentration at each site. Some locations had missing hourly measured O_3 data (typically between hours 0300-0400 when photochemical production of O_3 does not occur) and therefore are represented with a break in the time series. Figure 6-6 illustrates a time series of hourly NO, NO_2 and HO_2 concentrations predicted using SAPRC11 and SAPRC16 for SoCAB site A. The analysis time period at each site was chosen such that the latter times in the simulation were ozone non-attainment days (exceeded the 8-hour ozone NAAQS) in 2010. Higher concentrations of NO and NO_2 were predicted on Sep. 25-26, coinciding with O_3 non-attainment days. O_3 concentrations predicted by SAPRC16 diverge from concentrations predicted by SAPRC11 on Sep. 25-26 when NOx concentrations were higher. This result is consistent with the isopleths generated by the box model in which SAPRC16 predicted lower O_3 concentrations as NOx concentrations increased. Predicted concentrations of HO_2 vary between the two mechanisms as a result of the changes in the species lumping representation that impacts the VOC/NOx reaction pathways. Predicted SAPRC16 HO_2 concentrations are much lower than SAPRC11 HO_2 concentrations on the ozone non-attainment days. These trends are consistent with the results shown in Fig 6-2 and 6-3 where the summed peroxy-radical concentrations are lower in SAPRC16 than SAPRC11 when O_3 concentrations are lower in SAPRC16. HO_2 radical predictions will be discussed further in section 3.3.

South Coast Air Basin A

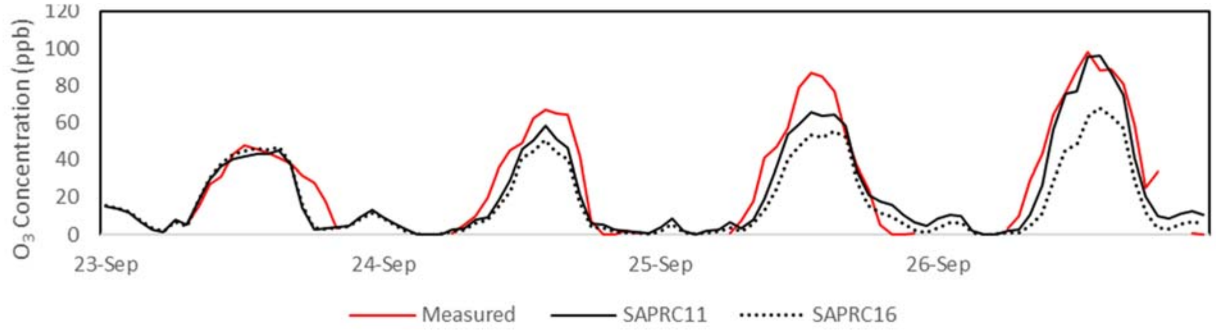

South Coast Air Basin B

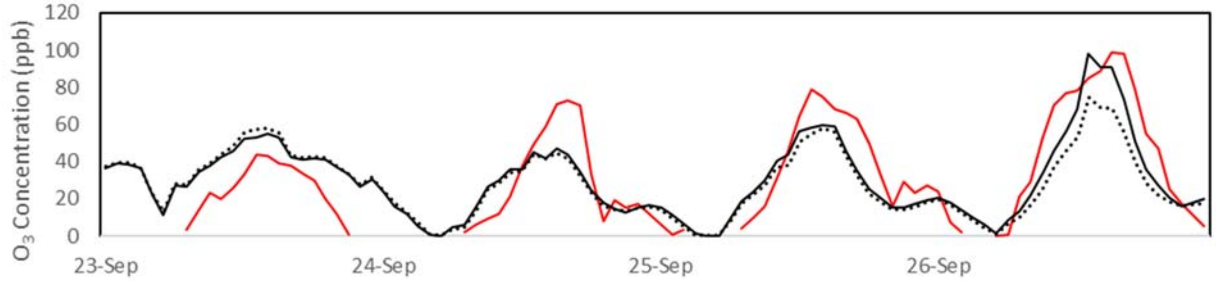

South Coast Air Basin C

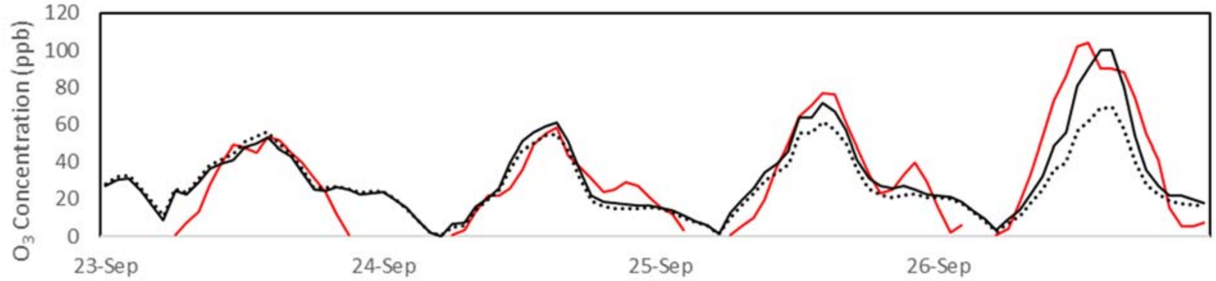

South Coast Air Basin D

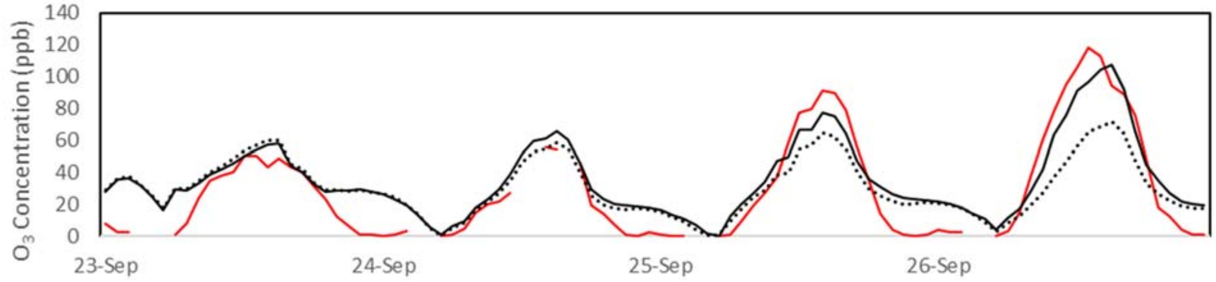

Figure 6-5:SAPRC11 vs SAPRC16 time series plots for O$_3$ (ppb) at four sites (a-b) in the South Coast Air Basin (Los Angeles Region). SAPRC11 = bold black line, SAPRC16 = dashed black line. Measured 1-hour O$_3$ concentration illustrated with red line. Locations are illustrated in Figure 6-7.

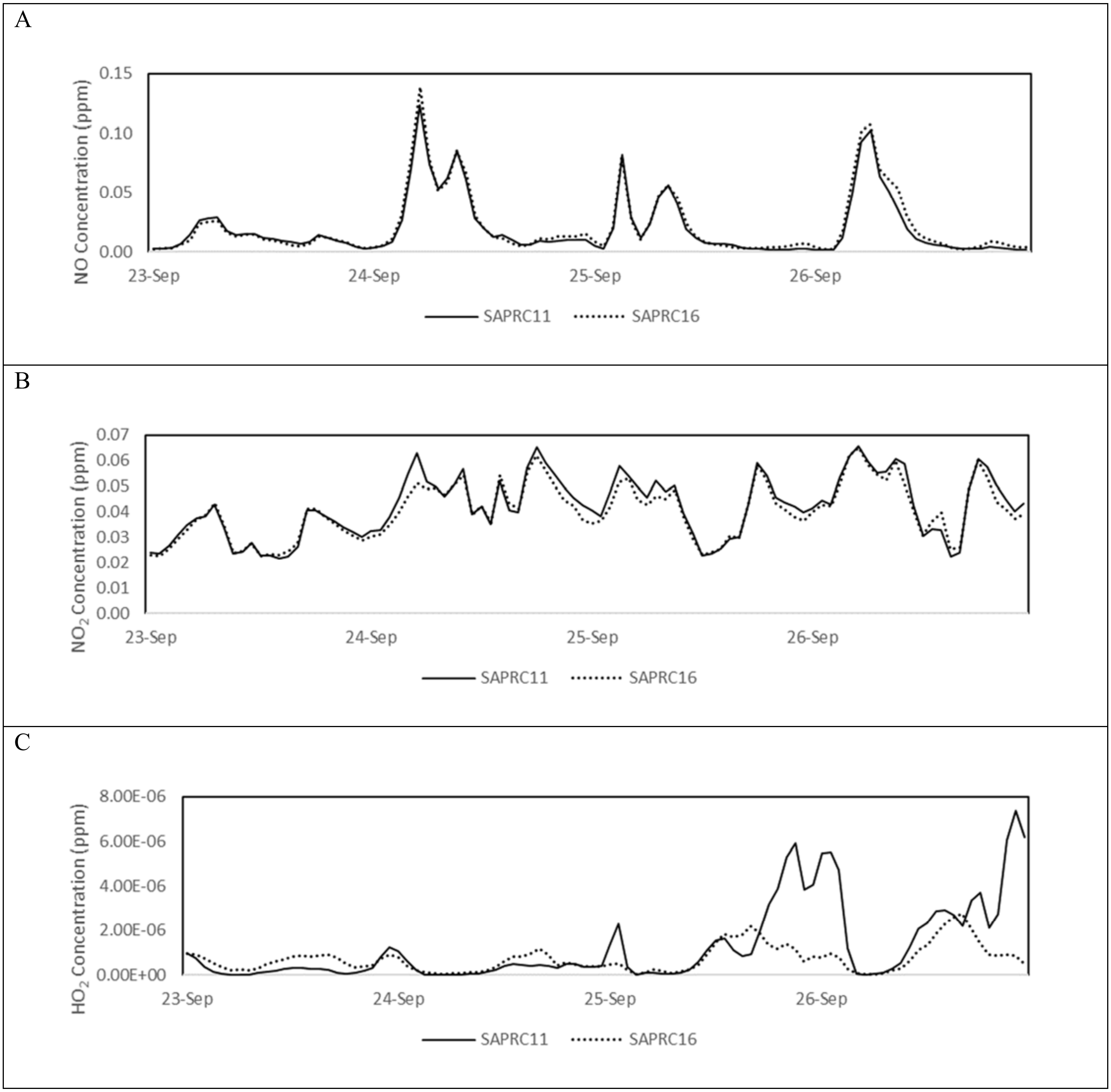

Figure 6-6: SAPRC11 vs SAPRC16 time series plots for a) NO, b) NO_2 and c) HO_2 at South Coast Air Basin, CA site A. SAPRC11 = black line and SAPRC16 = dashed black line. Locations are illustrated in Figure 6-7.

Figure 6-7 compares regional O_3 concentrations predicted with SAPRC11 (Fig 6-7a), SAPRC16 (Fig 6-7b), and the difference SAPRC11-SAPRC16 (Fig 6-7c) over the four sites in the SoCAB. SAPRC16 predicts maximum ozone concentrations that are as much as 57.1% lower than SAPRC11 predictions, specifically over urban regions where NOx concentrations are higher.

(a) SAPRC11 SoCAB Ozone Concentration Sep 26, 2010 @ 1500

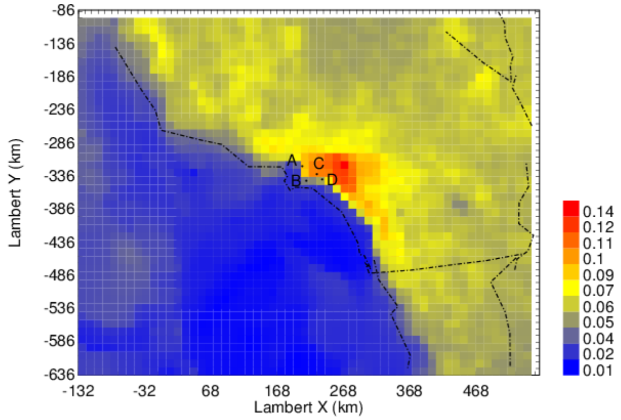

(b) SAPRC16 SoCAB Ozone Concentration Sep 26, 2010 @1500

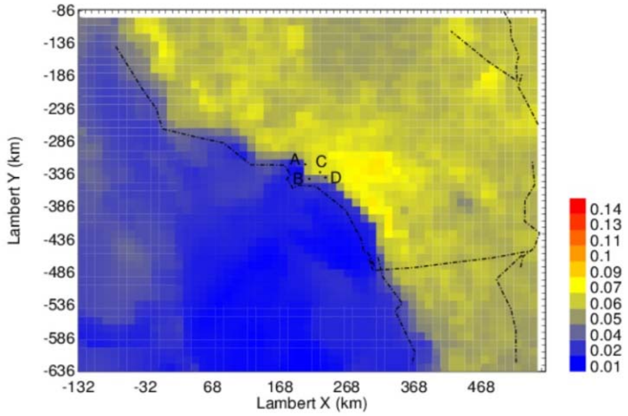

(c) SAPRC11-SAPRC16 Ozone Concentration Sep 26, 2010 @1500

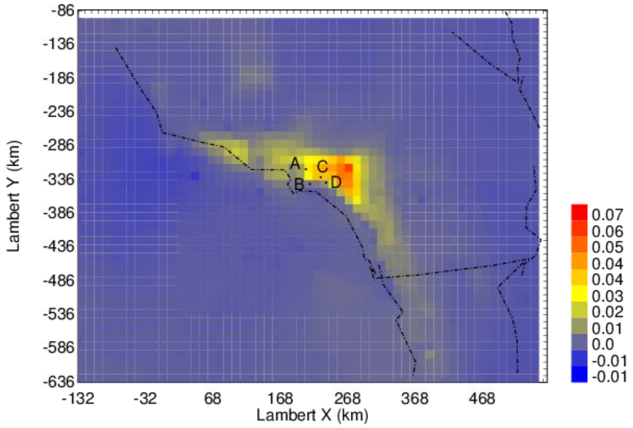

Figure 6-7: Comparison of regional ozone concentrations predicted by (a) SAPRC11 and (b) SAPRC16 on an O_3 non-attainment day in the South Coast Air Basin (SoCAB), CA.

Four additional sites in the north-eastern part of the US (New York City and Philadelphia) were selected for further comparison between SAPRC16 and SAPRC11: two sites in New York City and two sites in Philadelphia. Table 6-3 illustrates the latitude, longitude and description of each site.

Table 6-3. East Coast Ambient O_3 Measurement Sites

Site	Name	Lat	Lon	Description
A	Queens College/ Queens	40.736	-73.821	Urban source region
B	Fordham University/ Bronx	40.867	-73.878	Urban source region
C	PHIPA 1: Castro Avenue	40.01	-75.098	Suburban source region
D	PHIPA 2: Chester County/New Garden Airport	39.834	-75.768	Suburban/rural source region

Figure 6-8 displays a time series of predicted hourly ozone using the SAPRC11 and SAPRC16 chemical mechanisms vs 1-hour observed O_3 concentration over the simulation period at each site. Figure 6-9 illustrates a time series of hourly NO, NO_2 and HO_2 concentrations predicted using SAPRC11 and SAPRC16 for Queens, NY. The analysis period was chosen such that the latter times in the simulation were ozone non-attainment days for each site in 2010. Similar trends in ozone predictions were observed in Queens, NY and the four California sites analyzed previously. SAPRC16 predicts 13.6% less ozone than SAPRC11 on Sep. 1, 2010 which was an O_3 non-attainment day in the northeastern US.

Figure 6-10 compares regional O_3 concentrations predicted with SAPRC11 (Fig 6-10a), SAPRC16 (Fig 6-10b), and the difference SAPRC11-SAPRC16 (Fig 6-10c) over the four sites in the North Eastern United States. SAPRC16 predicted 20% lower maximum ozone compared to SAPRC11, specifically over urban regions where NOx concentrations are highest. The differences between SAPRC16 and SAPRC11 across these locations may result from other transport processes and major sources in the model calculations that have a larger impact on east coast simulations.

A– Queens (NYC)

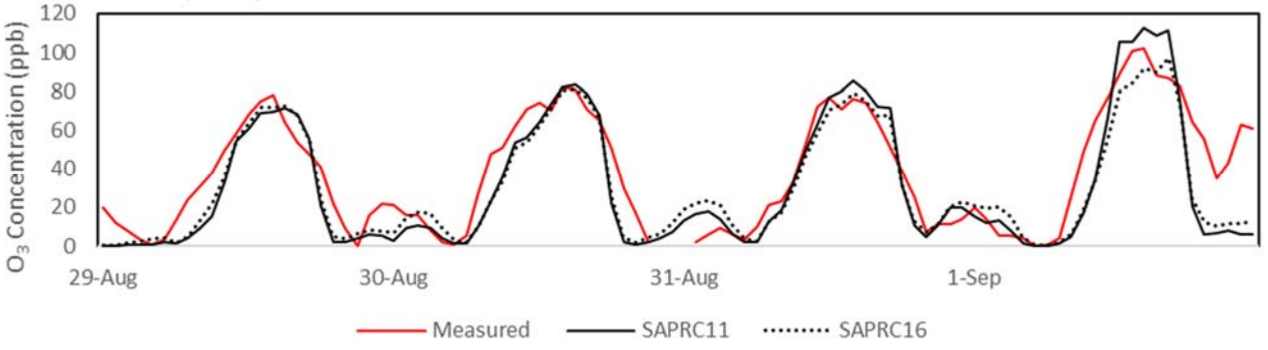

B – Bronx (NYC)

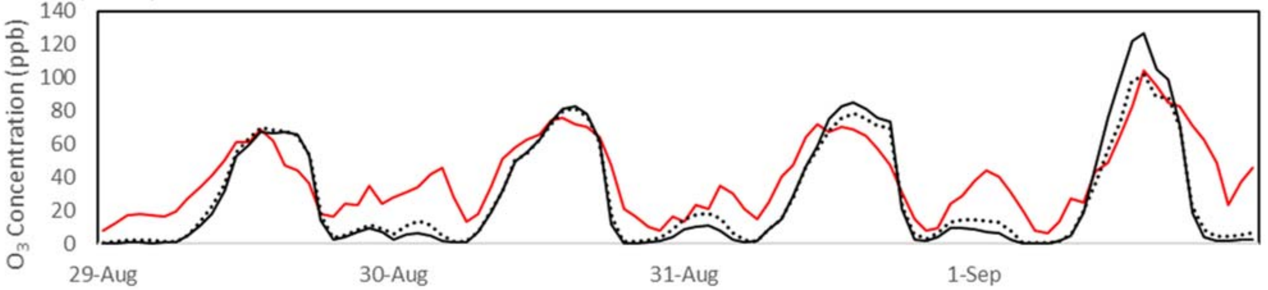

C – PHIPA

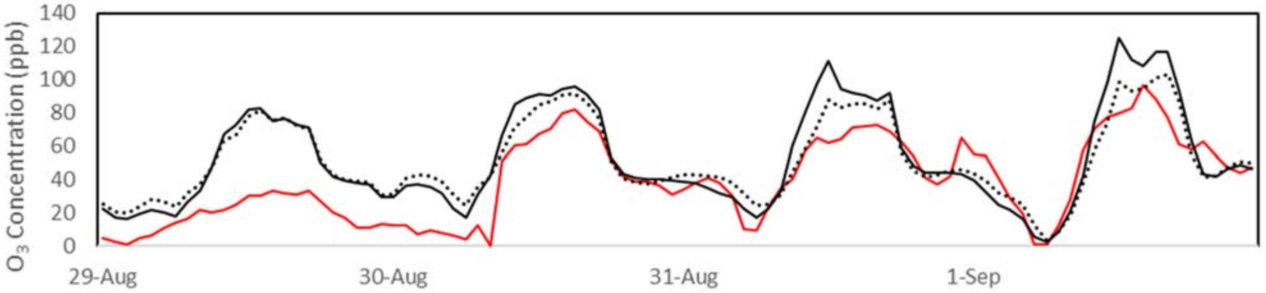

D –PHIPA 2

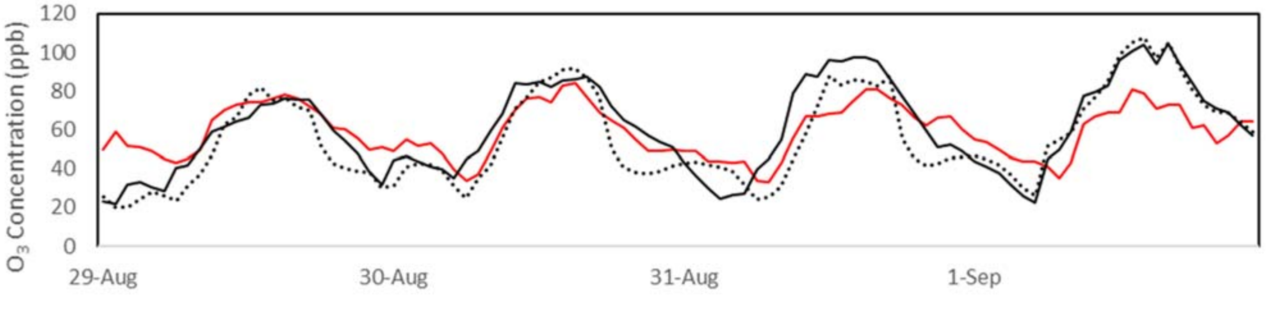

Figure 6-8: SAPRC11 vs SAPRC16 time series plots for O$_3$ (ppb) at two sites in New York City, NY and two sites in Philadelphia, PA. SAPRC11 = bold line, SAPRC16 = dashed line. Measured 1-hour O$_3$ concentration = red line.

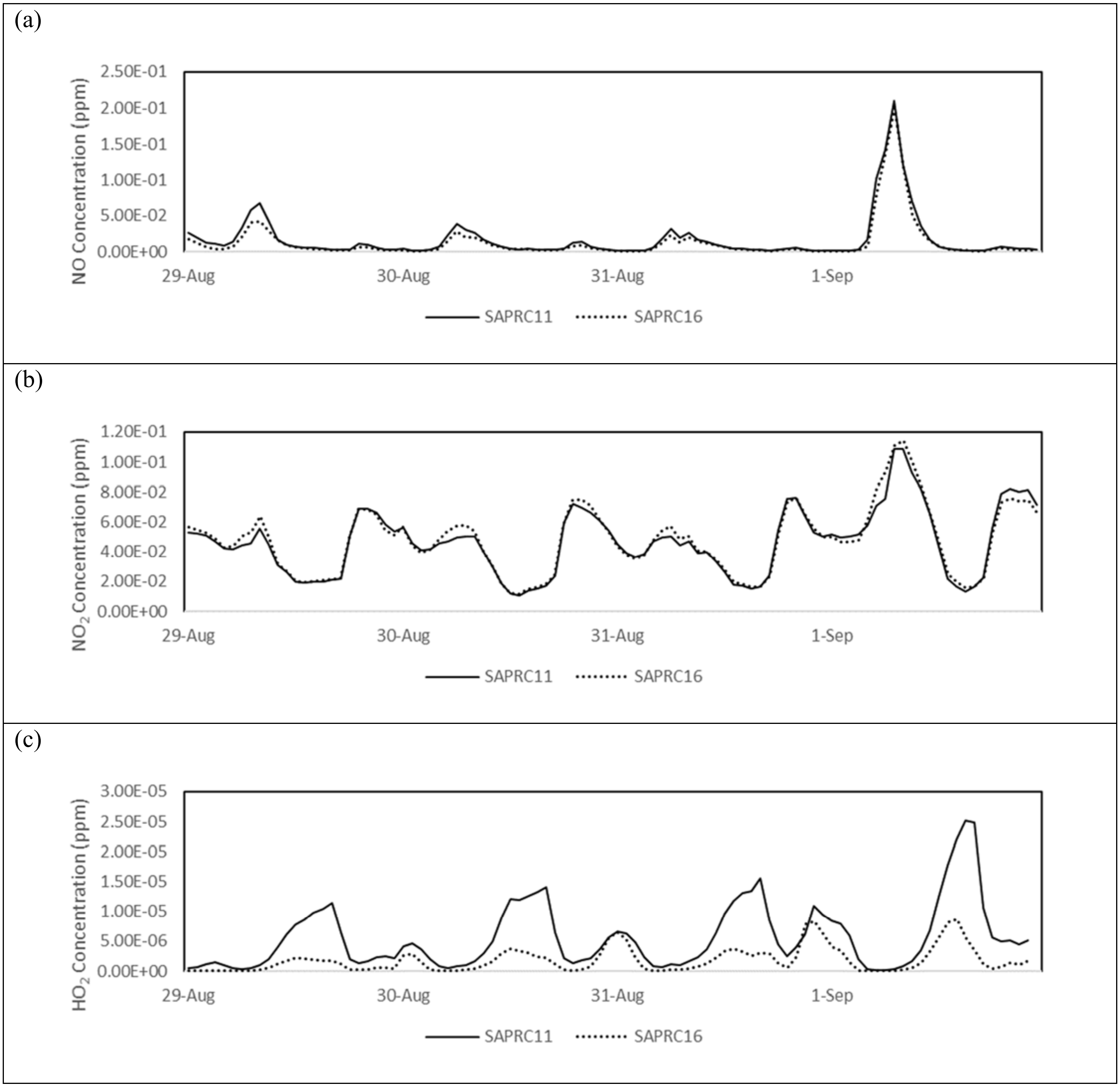

Figure 6-9: SAPRC11 vs SAPRC16 time series plots for a) NO, b) NO_2 and c) HO_2 at Queens, NY

(a) SAPRC11 NYC/PHIPA Ozone Concentration Sep 1, 2010 @1500

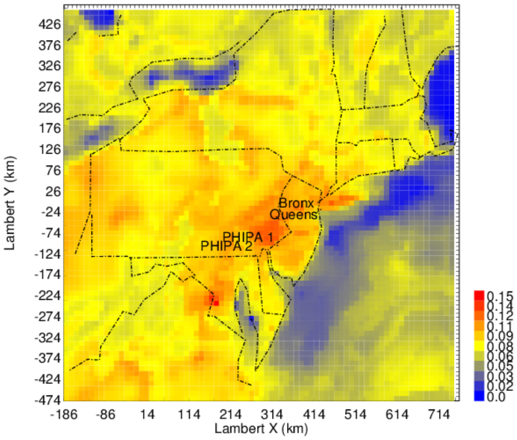

(b) SAPRC16 NYC/PHIPA Ozone Concentration Sep 1, 2010 @1500

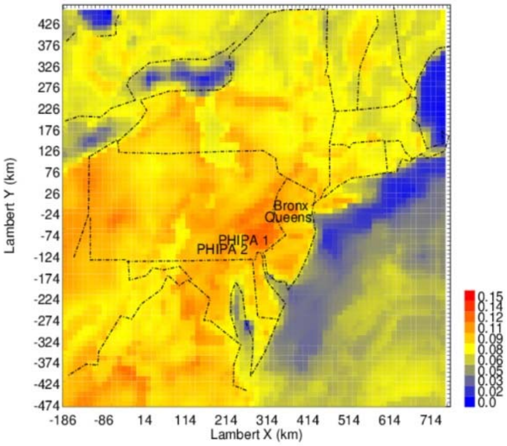

(c) SAPRC11-SAPRC16 NYC/PHIPA Ozone Concentration Sep 1, 2010 @1500

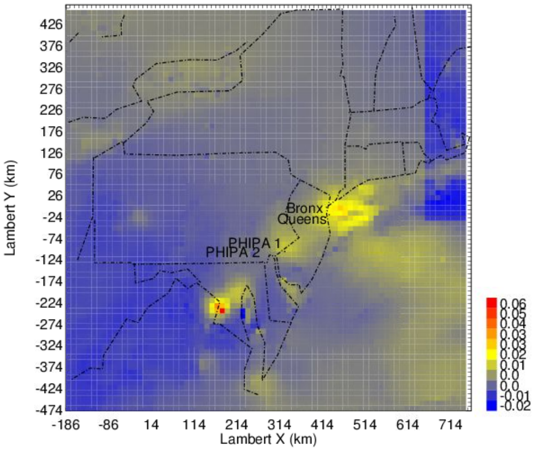

Figure 6-10: Comparison of regional ozone concentrations predicted by (a) SAPRC11 and (b) SAPRC16 on an O_3 non-attainment day in the North Eastern (NYC/Philadelphia) United States.

6.3.3 CalNex Field Campaign Analysis

Griffith et al compared HO_2 and OH radical concentrations measured during the CalNex 2010 field campaign to various model predictions [214]. In the current study, two additional simulations were performed with the SAPRC11 and SAPRC16 chemical mechanisms and the predicted HO_2 and OH concentrations were added to the comparison. Figure 6-11 illustrates the simulated vs measured values for O_3, OH and HO_2 concentrations during the 1-month long field campaign in Pasadena, CA. Measured OH and HO_2 (molec/cm^3) values varied in time throughout the 1-month field campaign and missing hourly averages are represented with a break in the time series. The mean fractional error (MFE) for O_3 predictions over the simulation period was 0.358 for SAPRC11 and 0.378 for SAPRC16. Overall, SAPRC16 under-predicts daily maximum O_3 concentrations even though total simulation O_3 MFE is within the US EPA model performance criteria.

The MFB and MFE calculated for OH and HO_2 predicted using SAPRC11 and SAPRC16 are summarized in Table 6-4. SAPRC16 significantly under-predicts HO_2 concentrations, possibly because of the new RO_2 isomerization reactions in this mechanism (see Fig 6-3 and related discussion). Additional differences between SAPRC16 and SAPRC11 may be related to changes in RO_2 + NO reactions (where RO_2 represents peroxy-radicals other than HO_2). In SAPRC11, the RO_2+NO reactions yield NO2 with a stoichiometric coefficient of 1.0. In SAPRC16, RO_2+NO reactions yield NO2 with a stoichiometric coefficient of 0.88-0.95. A sensitivity test was conducted during the CalNex episode that changed the yield of NO2 to 1.0 in all SARC16 RO_2+NO reactions. Ozone concentrations only increased by approximately 1% in this test because HO_2 is the dominant peroxy-radical (see Fig 6-3 panel captions) and so changes to the RO_2+NO pathways have little effect.

Table 6-4. Mean Fractional Bias and Mean Fractional Error for model performance of simulated OH and HO_2 with SAPRC11 and SAPRC16 compared to CalNex field campaign ambient values.

Mean Fractional Bias	**SAPRC11**	**SAPRC16**
OH	0.0267	-0.005
HO_2	-0.261	-0.931

Mean Fractional Error	**SAPRC11**	**SAPRC16**
OH	0.591	0.601
HO_2	0.723	1.129

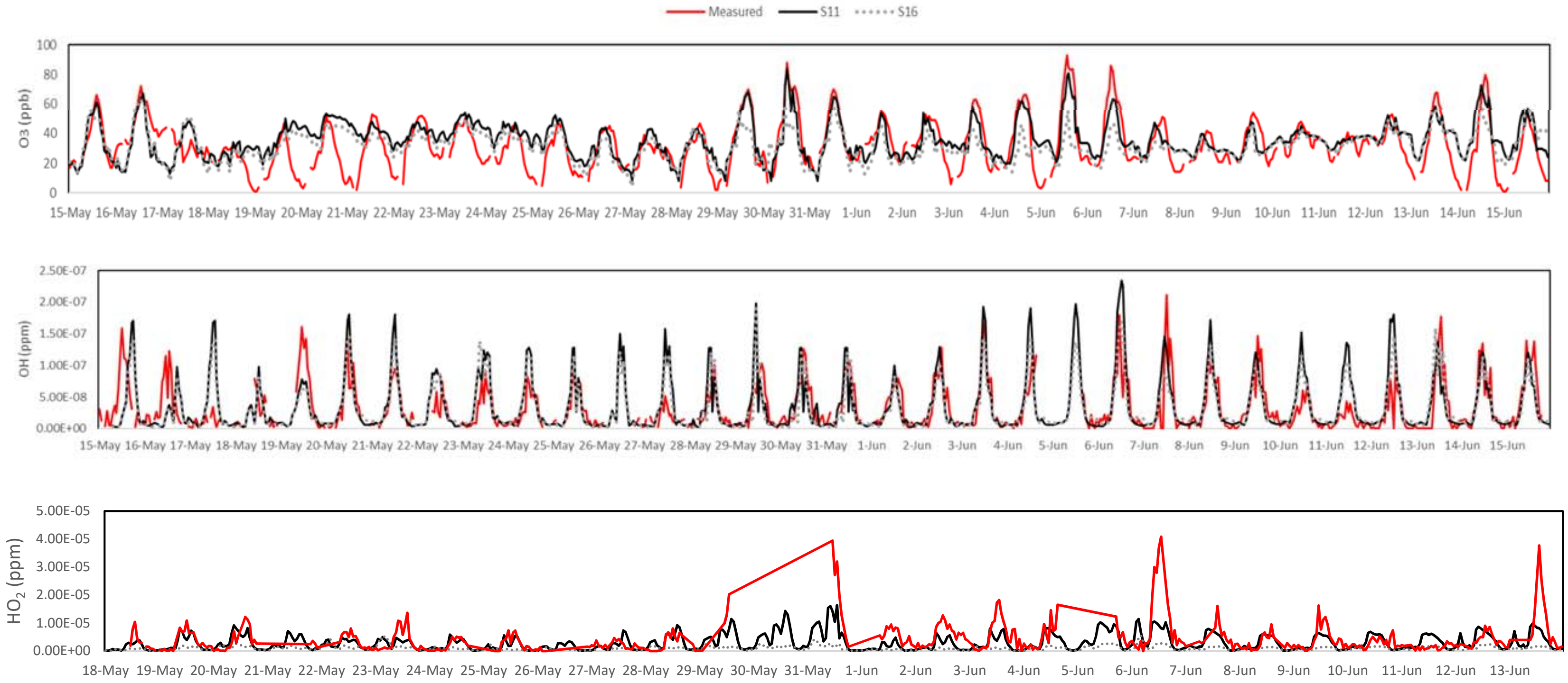

Figure 6-11: Time series of predicted and measured concentrations during the CalNex field campaign. Top figure compares measured 1-hour O_3 (red line) concentration to simulated O_3 concentration for SAPRC11(black line) and SAPRC16 (grey dashed line). Middle figure compares measured OH radical concentration (red line) to simulated OH for SAPRC11 (black line) and SAPRC16 (grey dashed line). Bottom figure compares measured HO_2 radical concentration (red line) to simulated HO_2 for SAPRC11 (black line) and SAPRC16 (grey dashed line)

6.4 Discussion

Griffith et al. compared daytime HOx measurements versus model predictions for 15 studies between 1993 and 2010 throughout the US and other locations around the world (Figure 6-1 in [208]). Eight (8) of the studies under-predicted HO_2 concentrations, some by up to a factor of 3.4 [208]. The RACM2 mechanism under-predicted HO2* concentrations during weekday simulations by up to a factor of 3, likely due to incomplete characterization of trace gases in the model [208]. The preliminary SAPRC16 mechanism evaluated in the current study appears to predict HO_2 concentrations even lower than these previous studies. Further work is required to investigate why this is the case for the SAPRC16 mechanism before widespread public adoption.

Semi-volatile reaction products predicted by the SAPRC mechanisms have been used as inputs to numerous secondary organic aerosol (SOA) models including the 2-product model developed for CMAQ [241] and the statistical oxidation model (SOM) [242]. Accurate predictions of concentrations for semi-volatile reaction products are a necessary first step in all SOA calculations. SAPRC16 improves the prediction of condensable reaction by expanding the aromatic and terpene groups that were previously aggregated in SAPRC11 as shown in Table 6-5. Figure 6-12 illustrates the time series of the aromatic SAPRC11 SOA precursor species versus the sum of the corresponding SAPRC16 SOA precursor species over a 1-week time period during the CalNex field campaign per total emissions in kmol day^{-1}. The concentrations of species "ARO1" (=ARO1 + TOLU + BENX + C2BEN + BZ123 + BZ124 + BZ135) are very similar in SAPRC16 and SAPRC11. Summed "ARO2" species (=ARO2 + OXYL + MYXL + PXYL + NAPS + STYRS) and "BENZ" (=BENZENE) react faster (lower concentrations) in SAPRC16 versus SAPRC11. This implies that ARO2 and BENZ species will produce condensable reaction products closer to the source of the precursor emissions in SAPRC16. Additional SAPRC16 SOA precursors and their time series during the CalNex episode is provided in the Supporting Information.

Measured SOA yields depend strongly on the ratio of NO/HO_2. The final SOA concentrations predicted by SAPRC16 will depend on parameters derived from fitting the SAPRC16+SOA model to results from chamber experiments conducted under low NOx/HO_2 conditions and high NOx/HO_2 conditions. The HO_2 under-predictions in SAPRC16 should be resolved before the model is used to predict ambient SOA concentrations.

A preliminary analysis of SAPRC16 was conducted using CMAQ for an episode in the SoCAB during May 2016. The May 2016 episode was chosen based on availability of a consistent emissions inventory for both SAPRC07T (SAPRC11 has not been implemented in CMAQ) and SAPRC16 in CMAQ model-ready format. CMAQ-SAPRC16 predicted lower O_3 and HO_2 concentrations compared to CMAQ-SAPRC07T. These findings are consistent with the trends predicted by the UCD-CIT 3D air quality model and suggest that the issues identified in the current study are independent of the host Chemical Transport Model (CTM). Ambient measurements are not available for HO_2 concentrations during May 2016 and computational resources were not available to apply the CMAQ-SAPRC16 model to other episodes in this study.

Table 6-5. SAPRC11 SOA precursor species, SAPRC16 disaggregated SOA precursor species and the description.

SAPRC11 lumped Species	Description	SAPRC16 lumped species	Description
ARO1	ARO1 = Aromatics with kOH < 2x104 ppm-1 min-1.	ARO1 + TOLU + BENX + C2BEN + BZ123 + BZ124 + BZ135	ARO1 = Aromatics that have kOH between 1.7 x 10^{-12} and 1.4 x 10^{-11} cm^3 $molec^{-1}$ s^{-1} TOLU = Toluene BENX = Aromatics other than benzene that have kOH between 3.4 x 10-13 and 1.7 x 10-12 cm^3 $molec^{-1}$ s^{-1} C2BEN = Ethyl Benzene BZ123 = 1,2,3-Trimethyl Benzene BZ124 = 1,2,4-Trimethyl Benzene BZ135 = 1,3,5-Trimethyl Benzene
ARO2	ARO2 = Aromatics with kOH > 2x104 ppm-1 min-1.	ARO2 + OXYL + MYXL + PXYL + NAPS + STYRS	ARO2 = Aromatics other than naphthalenes, tetralins, or indans that have kOH greater than 1.4 x 10^{-11} cm^3 $molec^{-1}$ s^{-1} OXYL = o-Xylene MXYL = m-Xylene PXYL = p-Xylene NAPS = Naphthalenes, tetralins, and indans STYRS = Aromatics other than styrene with double bonds outside of the aromatic ring.
BENZENE	Benzene	BENZ	BENZ = Benzene

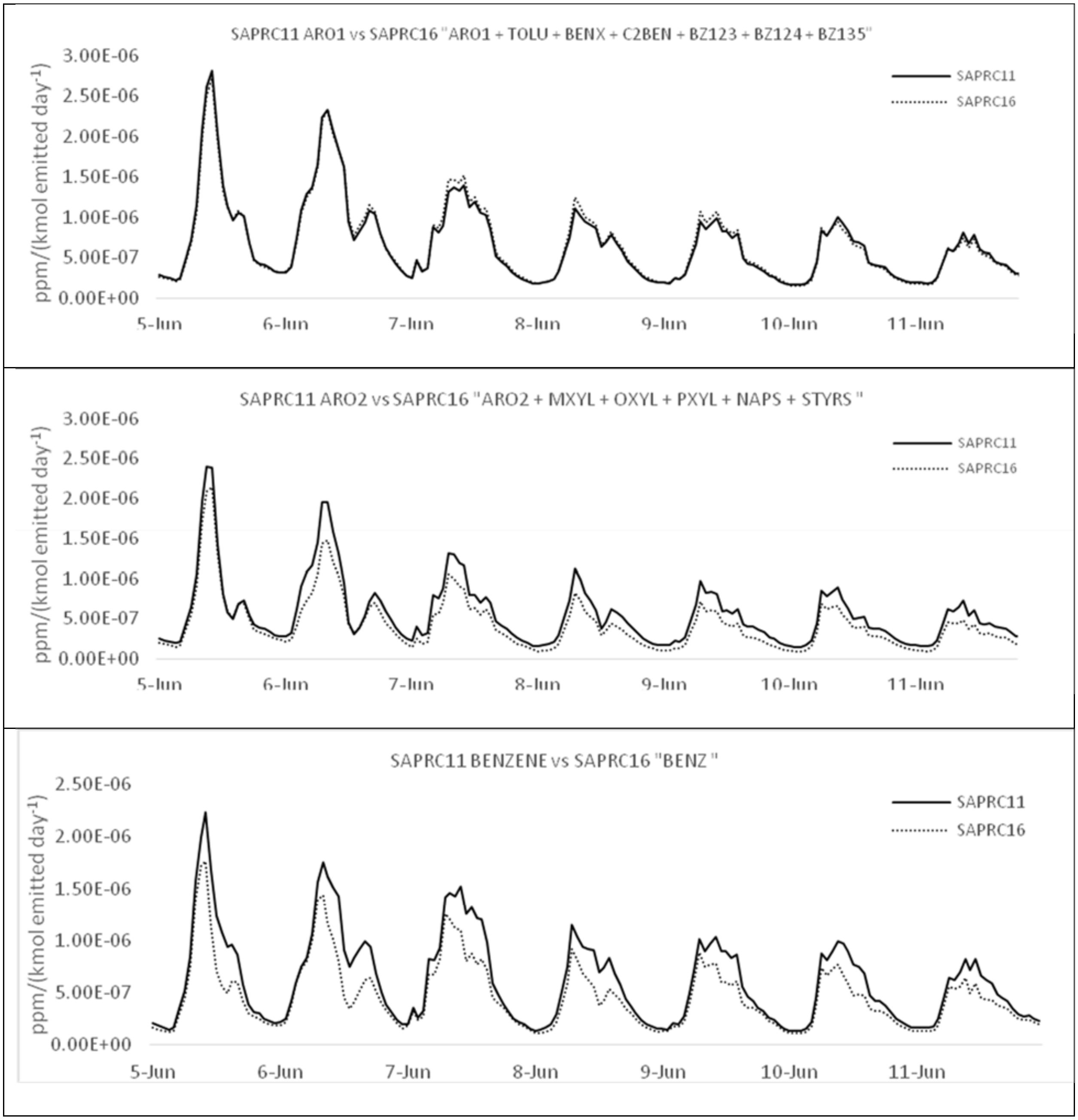

Figure 6-12: Time series of SAPRC11 SOA precursor species vs. a combined subset of SAPRC16 SOA precursor species for one (1) week during the CalNex simulation period over Pasadena, CA.

6.5 Conclusion

Ambient simulations carried out with the SAPRC16 chemical mechanism predict slightly lower peak (daily maximum) O_3 concentrations compared to results from the SAPRC11 mechanism in areas with high NOx concentrations. O_3 concentrations predicted by SAPRC16 are lower than measured values in polluted California air basins including the South Coast Air Basin (SoCAB) surrounding Los Angeles, CA and the San Joaquin Valley (SJV) on days when NOx concentrations are high and measured O_3 values are in non-attainment with the NAAQS. Model performance varies by location, with SAPRC16 generally predicting lower O_3 concentrations than SAPRC11 in the western US. Predicted O_3 concentrations in rural areas with lower NOx concentrations are similar for SAPRC16 and SAPRC11. Generally speaking, SAPRC16 O_3 predictions have slightly higher errors and biases than SAPRC11 O_3 predictions at four out of six locations investigated in the current study.

Analyzing trace radical species can help diagnose differences between SAPRC16 and SAPRC11. The two mechanisms predicted similar OH concentrations in Los Angeles but SAPRC16 significantly under predicted HO_2 concentrations in comparison to a more moderate under prediction by SAPRC11. These differences in predicted HO_2 concentrations may be related to more detailed HO_2+RO_2 reactions and RO_2 isomerization reactions in SAPRC16, but further research is required to investigate this issue. It is also worth noting that both SAPRC11 and SAPRC16 are also influenced by uncertainties in emissions and meteorology that are independent of the mechanism but can have large effects on model predictions. Future evaluations of SAPRC16 should include efforts to evaluate the accuracy of the underlying emissions inventory, prediction of HOx radicals and SOA precursors. SOA models should only be coupled to SAPRC16 after differences in predictions of HO_2 are better understood.

Differences between ozone predictions made by SAPRC16 and SAPRC11 increased as emissions decreased suggesting that the two mechanisms will predict different outcomes from emissions control programs. Further investigation needs to be performed on the SAPRC16 chemical mechanism to better understand the quenching of O_3 production and model under-prediction of HO_2 radical concentrations in regions with high NOx concentrations before this model is broadly adopted for use in the development of ozone control programs.

7 PREDICTED ANNUAL TRENDS IN ULTRAFINE PARTICLE NUMBER AND MASS CONCENTRATIONS IN CALIFORNIA

Preamble: Chapter 7 introduces a nucleation algorithm into the UCD/CIT reactive chemical transport air quality model and tests the ability of the model to predict ambient concentrations of particles with diameter greater than 10 nm (N_{10}) across California in the year 2012. Source contributions to N_{10} are predicted for different locations throughout the state. This chapter establishes the methods used in subsequent model exposure chapters in the report.

7.1 Introduction

Numerous epidemiological studies have identified positive correlations between exposure to ambient particulate matter (PM) and increased risk of respiratory and cardiovascular diseases, premature mortality and hospitalization [243-253]. Most of these studies have not fully addressed ultrafine particles (UFPs; $Dp<0.1\mu m$) because these particles make a very small contribution to total ambient PM mass [254]. Toxicity studies suggest that UFPs may be especially dangerous to human health since they have higher toxicity per unit mass [152-154] and can penatrate the lungs and enter the bloodstream and secondary organs [51]. These toxicology results are suggestive but more epidemiological evidence is required before the threat to public health from UFPs can be fully assessed.

Most previous UFP epidemiology studies are based on the number concentration of particles with diameter greater than some lower bound (typically 7 nm; N_7) measured at fixed sites using commercially-available instruments. These devices are expensive and they require regular maintence which limits the number of measurement sites that can be deployed. Translating measured N_7 into population exposure estimates is also difficult because UFP concentrations change more rapidly over shorter distances than $PM_{2.5}$ [39, 41, 255]. Land use regression (LUR) models could potentially be used to interpolate UFP concentrations between sparse measurement locations, but the atmospheric processes governing N_7 concentrations are highly non-linear and (so far) sufficient training data is not generally available for LUR models to estimate N_7 exposure over a large enough population to support a definitive epidemiology study [256]. Previous attempts to use regional reactive chemical transport models to predict N_7 in highly populated regions have focused on nucleation, yieldeding a wide range of predicted concentrations and only modest agreement with measurements when nucleation algorithms were not standardized [257-259]. Obtaining accurate exposure estimates to N_7 in highly populated regions therefore remains a major challenge in UFP epidemiological studies.

Recent work has examined UFP mass ($PM_{0.1}$) as an alternative metric for UFP exposure, and demonstrated that $PM_{0.1}$ can be predicted with reasonable accuracy over large populations using regional reactive chemical transport models [39, 255]. The $PM_{0.1}$ exposure fields developed using this technique have been used in multiple epidemiological studies that revealed associations with mortality [7] and pre-term birth [42, 164]. Despite the success of studies using $PM_{0.1}$, techniques that estimate N_7 exposure are still needed because a large number of ongoing UFP studies are based on N_7 and it is possible that $PM_{0.1}$ and N_7 are associated with different types of health effects.

Here we extend the previous work using regional reactive chemical transport models for UFPs to include the number concentration of particles with diamter greater than 10 nm (N_{10}) in the San Francisco Bay Area (SFBA) and the South Coast Air Basin (SoCAB) region around Los Angels which are the two most densely populated major metropolitan location in California. Source contributions to $PM_{0.1}$ and N_{10} are tracked using the University of California, Davis / California Institute of Technology (UCD/CIT) regional reactive chemical transport model with 4 km spatial resolution. Predicted concentrations during the year 2012 are compared to measurements available at 10 regional monitoring sites. The spatial distribution fields of different particle metrics (N_{10}, $PM_{0.1}$, $PM_{2.5}$) are combined with population distributions to estimate exposure. To the best of our knowledge, this is the first integrated study of both UFP number and mass using a regional reactive chemical transport model in California.

7.2 Methods

7.2.1 Air Quality Model

Simulations for the years 2015-2016 were carried out across California using the UCD/CIT regional air quality model. The UCD/CIT airshed model is a reactive 3-D chemical transport model that has been succesfully applied in numerous previous studies in the San Joaquin Valley (SJV) and the SoCAB [41, 235, 260-275]. The UCD/CIT model predicts the evolution of gas and particle phase pollutants in the atmosphere in the presence of emissions, transport, deposition, chemical reaction, and phase change as represented by Eq. (8-1)

$$\frac{\partial c_i}{\partial t} + \nabla \cdot uC_i = \nabla K \nabla C_i + E_i - S_i + R_i^{gas}(C) + R_i^{part}(C) + R_i^{phase}(C)$$

$$\frac{\partial C_i}{\partial t} + \nabla \cdot uC_i = \nabla K \nabla C_i + E_i - S_i + R_i^{gas}(C) + R_i^{part}(C) + R_i^{phase}(C)$$

$$\frac{\partial C_i}{\partial t} + \nabla \cdot uC_i = \nabla K \nabla C_i + E_i - S_i + R_i^{gas}(C) + R_i^{part}(C) + R_i^{phase}(C) \qquad (8\text{-}1)$$

where C_i is the concentration of gas or particle phase species *i* at a particular location as a function of time *t*, *u* is the wind vector, *K* is the turbulent eddy diffusivity, E_i is the emissions rate, S_i is the loss rate, R_i^{gas} is the change in concentration due to gas-phase reactions, R_i^{part} is the change in concentration due to particle-phase reactions and $R_i^{phase}$is the change in concentration due to phase change [235]. Loss rates include both dry and wet deposition. Phase change for inorganic species occurs using a kinetic treatment for gas-particle conversion [276] driven towards the point of thermodynamic equilibrium [277]. Phase change for organic species is also treated as a kinetic process with vapor pressures of semi-volatile organics calculated using the 2-product model [278].

The UCD/CIT model explicitly tracks the mass and the number concentration of particles in each size bin, with tracer species used to quantify source contributions to the primary particle mass in that bin. A moving sectional bin approach is used [270] so that particle number and mass can be explicitly conserved with particle diameter acting as the independent variable.

7.2.2 Nucleation Algorithm

Nucleation was added to the UCD/CIT model for the first time in the current study using the ternary nucleation (TN) mechanism involving H_2SO_4-H_2O-ammonia (NH_3) [279]. As was the case in previous studies using this algorithm, the resulting nucleation rate was adjusted using a tunable nucleation parameter set to 10^{-5} for new particle nucleation [280]. The Kerminen and Kulmala parameterization [281] was added in order to bridge the gap between the 1 nm particle nuclei and their appearance into the smallest size bin of the UCD/CIT model (~10 nm). Emission, transport, deposition, and coagulation of UFPs were simulated using operators developed for the model framework, leading to modification of the particle size distribution and the subsequent N_{10} concentrations.

Dynamic condensation / evaporation is not considered for nucleation mode particles because these processes act slowly on the regional scale relative to the other operators and they do not strongly alter the ground-level N_{10} outside the near-roadway environment (within 300 m or major highways). This 300 m resolution is beyond the scope of the current modeling exercidse which uses 4 km spatial resolution in the horizontal direction. The model configuration in the current study reflects the focus on regional UFP concentrations, not near-roadway UFP concentrations. Future updates to this chapter will explore the effects of dynamic condensation / evaporation calculations for nucleation mode particles but this update will not significantly affect the results of the current study.

7.2.3 Domain Configuration

The model domains used in the study are shown in Figure 6-1. The parent domain with 24 km horizontal resolution covered the entire state of California (referred to as CA_24km) and the two nested domains with 4 km horizontal resolution covered the SFBA + SJV + South Sacramento Valley air basins (referred as SJV_4km) and the SoCAB surrounding Los Angeles (referred as SoCAB_4km). The UCD/CIT model was configured with 16 vertical layers up to a height of 5 km above ground level, with 10 layers in the first 1 km. Previous studies have shown that this vertical configuration captures the air pollution system above California [39, 41, 255]. Particulate number, mass, and composition are represented in 15 size bins, with particle diameters being centered within equally spaced logarithmic size interval spanning the diameter range from 0.01 to 10µm.

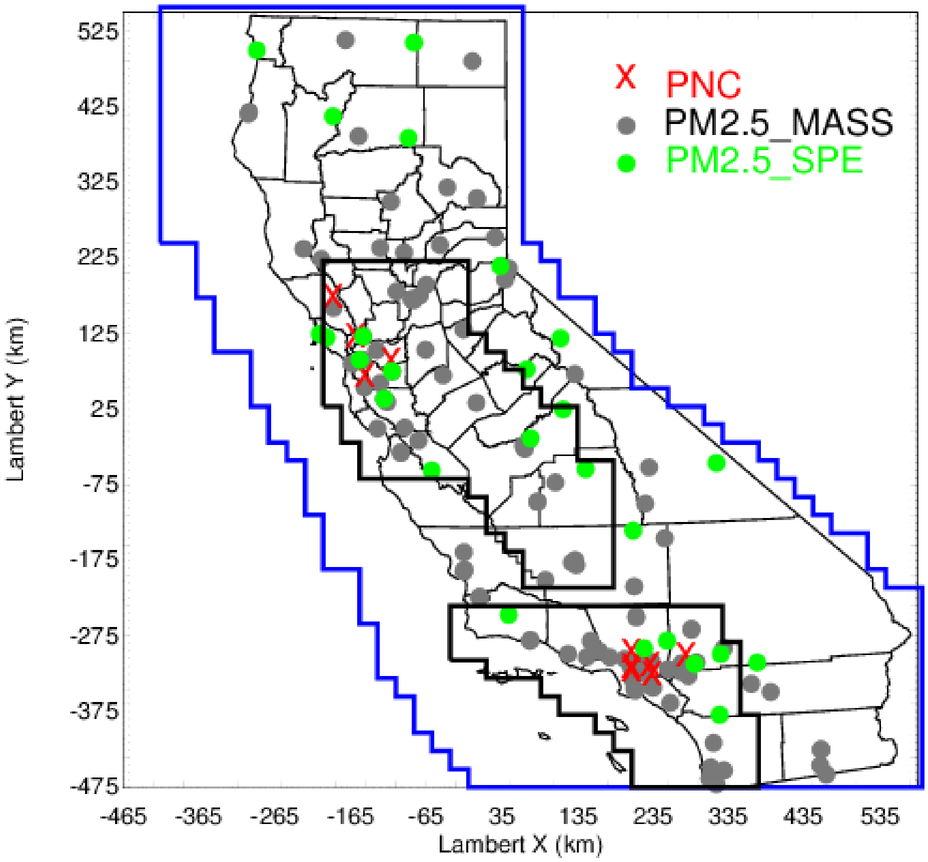

Figure 7-1: Modeling domains. Blue lines outline the CA_24 km domain, black lines outline the SoCAB_4 km (bottom) and SJV_4 km domains (top). Red crosses represent ten particle number concentration (N_7) sites (fours sites operated by staff at the Bay Area Air Quality Management District (BAAQMD) and six sites from the Multiple Air Toxics Exposure Study IV (MATES IV)). Detailed location information for the N_7 sites is listed in Table S7-3. Green dots represent BAAQMD $PM_{2.5}$ speciation network sites and the Interagency Monitoring of Protected Visual Environments (IMPROVE) sites; gray dots represent the $PM_{2.5}$ federal reference method (FRM) sites.

7.2.4 Meteorlogical Fields

Hourly meteorological fields during the modeling period were generated by the Weather Research and Forecasting (WRF) model version 3.4 with three nested domains that had horizontal resolutions of 36, 12 km and 4 km, respectively. In the present simulations, the WRF model was configured with 50 vertical layers (up to 100 hpa) and four-dimensional data assimilation (FDDA) nudging was utilized to improve the agreement between model predictions and observed meteorological patterns [282, 283]. WRF predictions for wind speed, temperature, and relative humidity were compared to measurements for seven counties in the SFBA and two counties in SoCAB (see Table S7-2). Temperature has mean bias (MB) within ~0.2 ˚C and root- mean-square errors (RMSE) between 4-5 ˚C. Wind speed has mean fraction bias (MFB) within ±0.20 and RMSE generally <2.0 m/s. This level of performance is consistent with performance of WRF in previous studies conducted in California [41, 284].

7.2.5 Emissions

The emission inventories used in the SFBA were developed by the BAAQMD for the year 2012 based on the regulatory inventory provided by the California Air Resources Board for that same year. The SFBA inventory was processed using the Sparse Matrix Operator Kernel Emissions (SMOKE)v3.7 software package provided by US EPA. SMOKE was configured to separately tag emissions from on-road gasoline vehicles, off-road gasoline vehicles, on-road diesel vehicles, off-road diesel vehicles, food cooking, biomass burning, non-residential natural gas, and all other sources. The emission inventories used in South Sacramento Valley, SJV and SoCAB were provided by the California Air Resources Board.

Measurements conducted in parallel with the current study found that particles emitted from natural gas combustion in home appliances were semi-volatile when diluted by a factor of 25 in clean air, but particles emitted from industrial sources did not evaporate under the same conditions [285]. Near-field emissions from residential natural gas sources were therefore set to zero in the current study while emissions from other natural gas combustion sources were retained at their nominal levels. SMOKE results were transformed into size-resolved emissions of particle number, mass, and composition using measured source profiles through an updated version of the emissions model described by Kleeman and Cass [286]. The PM profiles used for each source type were specified as weighted averages from each of the detailed sources within each broad category as summarized in Table S7-1. A more detailed discussion of the emissions processing has been presented in a previous study [41].

7.3 Results

7.3.1 Statistical Evaluation

According to Taylor's Hypothesis [287], it is expected that the spatial distribution of model results is more important than the temporal distribution when evaluating performance. In the current study model performance evaluations are limited to the locations where measurements were made. Therefore, the temporal distribution is also considered by comparing predicted vs. measured daily average N_7, $PM_{2.5}$ and individual $PM_{2.5}$ species mass concentrations. The evaluation data set was compiled from several measurement networks including the sites operated by staff at the Bay Area Air Quality Management District (BAAQMD), the IMPROVE sites, the MATES IV sites and FRM sites. Model performance for $PM_{2.5}$ at routine monitoring sites (Figure 7-1) generally meets the performance criteria suggest by Boylan and Russell [288] (mean fractional error (MFE) ≤ +0.75 and mean fractional bias (MFB) ≤ ±0.5) (Table S7-4). Of greatest interest in the current study, predicted N_{10} values were compared to measured N_7 (aerosol number concentrations for particle diameters ranging from 7nm-1000nm) values at four sites in the SFBA (Santa Rosa, San Pablo, Redwood City and Livermore) and six sites in SoCAB (Anaheim, Central Los Angeles, Compton, Huntington Park, Inland-valley and Rubidoux). N_7 measurements in the SFBA were made using an Environmental Particle Counter (EPC) Monitor Model 3783 (TSI Inc) while N_7 measurements in the SoCAB were made with EPC Model 3781 (TSI Inc). Both monitors can detect ultrafine particles down to 7 nm which is smaller than the first size bin of 10 nm used in model calculations. Previous studies conducted at Fresno, California, suggest that N_7 accounts for approximately 8% of N_7 [289], and so some amount of negative bias is expected when comparing predicted N_{10} to measured N_7. The evaluation results for N_{10} summarized in Table 7-1 follow this expected trend but mean fractional bias (MFB) and mean fractional error (MFE) at each comparison site still meet the performance criteria suggest by Boylan and Russell [288]. This level of performance is comparable to the results from a previous UFP number simulation conducted in Northern California using a modified version of the WRF-Chem model [290]. The good agreement between predicted and measured N_{10} builds confidence in the model skill for UFP predictions in the current study.

Table 7-1. Performance statistics for N_{10} predictions vs. N_7 at individual monitoring sites. Threshold for regulatory PM modeling applications is typically MFB< ± 0.5 and MFE < 0.75.

Location	MFB	MFE	RMSE Particles cm^{-3}
Livermore	0.02	0.25	2831
Redwood city	-0.21	0.37	5141
San Pablo	-0.38	0.51	5392
Santa Rosa	-0.19	0.39	2634
Anaheim	0.39	0.43	7834
Central LA	0.11	0.23	5505
Compton	0.25	0.31	6485
Huntington Park	0.19	0.27	9966
Inland-Valley	0.35	0.38	8494
Rubidoux	0.44	0.47	7106

7.3.2 $PM_{0.1}$ and N_{10} Source Apportionment in California

The UCD/CIT model explicitly tracks the mass and the number concentration of particles in each size bin, with tracer species used to quantify source contributions to the primary particle mass (but not number) in that bin. The floating section size bins mean that particle mass and particle number are explicitly conserved in each size bin. This enables simplified source apportionment calculations for number. In the current study, the mass contribution from each source was converted to the number contribution from that source according to Eq. (7-1)

$$number_i = mass_i / (\pi/6 * Dp^3 * \rho) \qquad (7\text{-}1)$$

where $number_i$ is the number concentration associated with source i, $mass_i$ is the mass concentrations associated with source i, Dp is the core particle diameter and ρ is the core particle density (calculated based on particle composition). Core particle diameter and core particle density were calculated by removing the condensed species from the particles to better represent the emitted composition that formed the basis for the number emissions rate. The accuracy of the particle source apportionment approach was tested by comparing the sum of the “reconstructed” particle number (eq 1) across all sources to the actual total particle number tracked by the model yielding error <10% in the current study.

Figure 7-2 and 7-3 compare the source contributions to $PM_{0.1}$ OC concentrations predicted by the UCD/CIT model and the molecular marker technique at San Pablo, East Oakland, downtown Los Angeles and Fresno during a summer month (August 2015) and a winter month (February 2016). The “others” category in the molecular marker calculation represents unresolved sources, while in the UCD/CIT model “others” represents the sum of non-residential natural gas source combustion, aircraft emissions, and the sources that were not tagged in the current study. In general, predicted source contributions to $PM_{0.1}$ OC from the molecular marker technique and the UCD/CIT model are in good agreement. Natural gas dominates $PM_{0.1}$ OC in the summer of 2015 at San Pablo, East Oakland, downtown Los Angeles and Fresno, while wood smoke and aircraft are the major sources of $PM_{0.1}$ OC in Fresno and East Oakland during the winter of 2016. The importance of ultrafine particles from natural gas combustion has not previously been recognized because these particles lack a unique chemical signature, which causes them to be lumped into the “unresolved” category in receptor-based source apportionment studies. The general agreement in the source contributions from the gasoline, diesel, wood burning, meat cooking and other source categories predicted by the UCD/CIT model and the molecular marker technique builds confidence in the accuracy of the UFP source predictions in the current study.

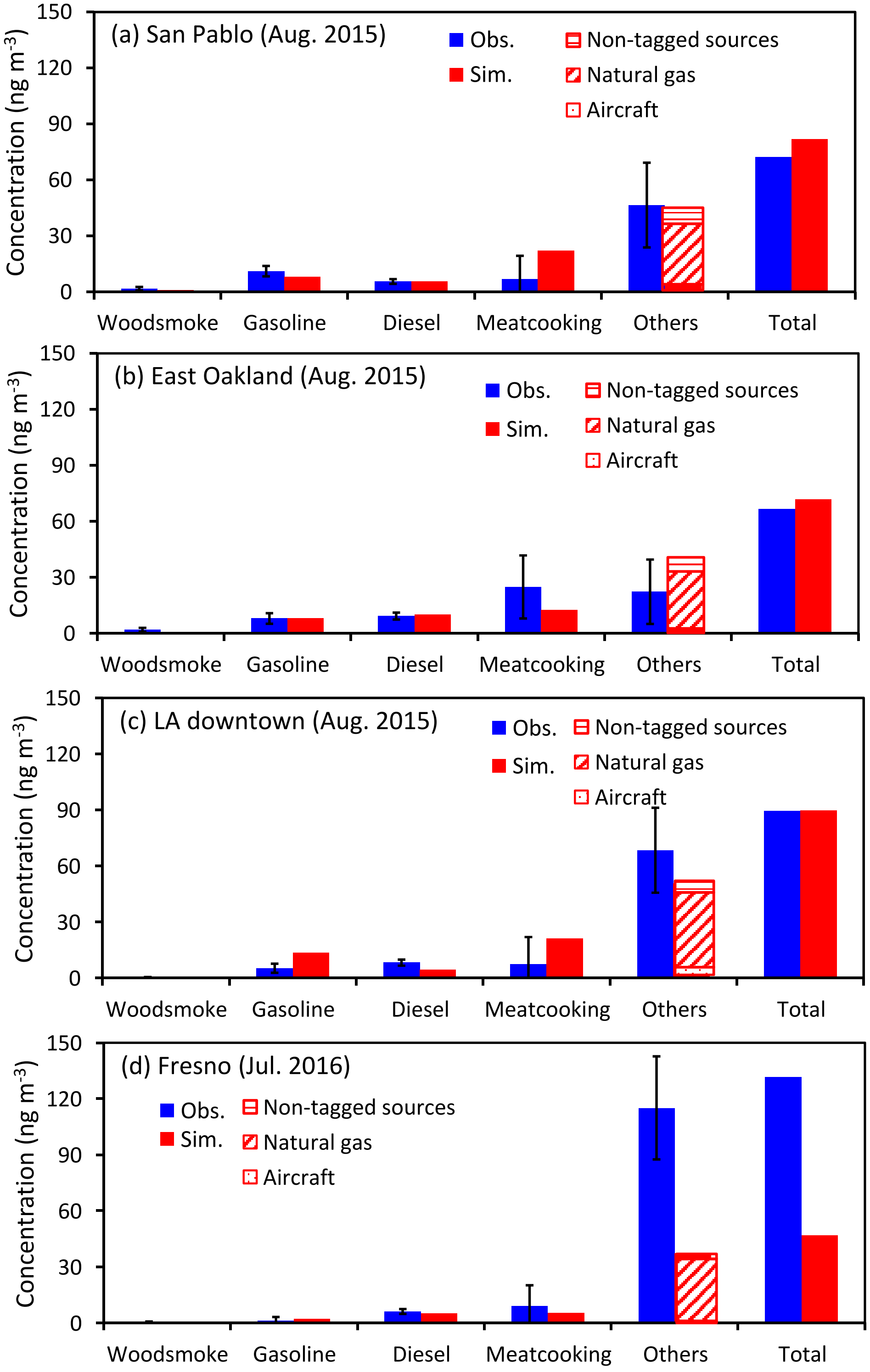

Figure 7-2: Source contribution to $PM_{0.1}$ predicted by the CMB receptor model and the UCD/CIT model at four sites in California in August 2015

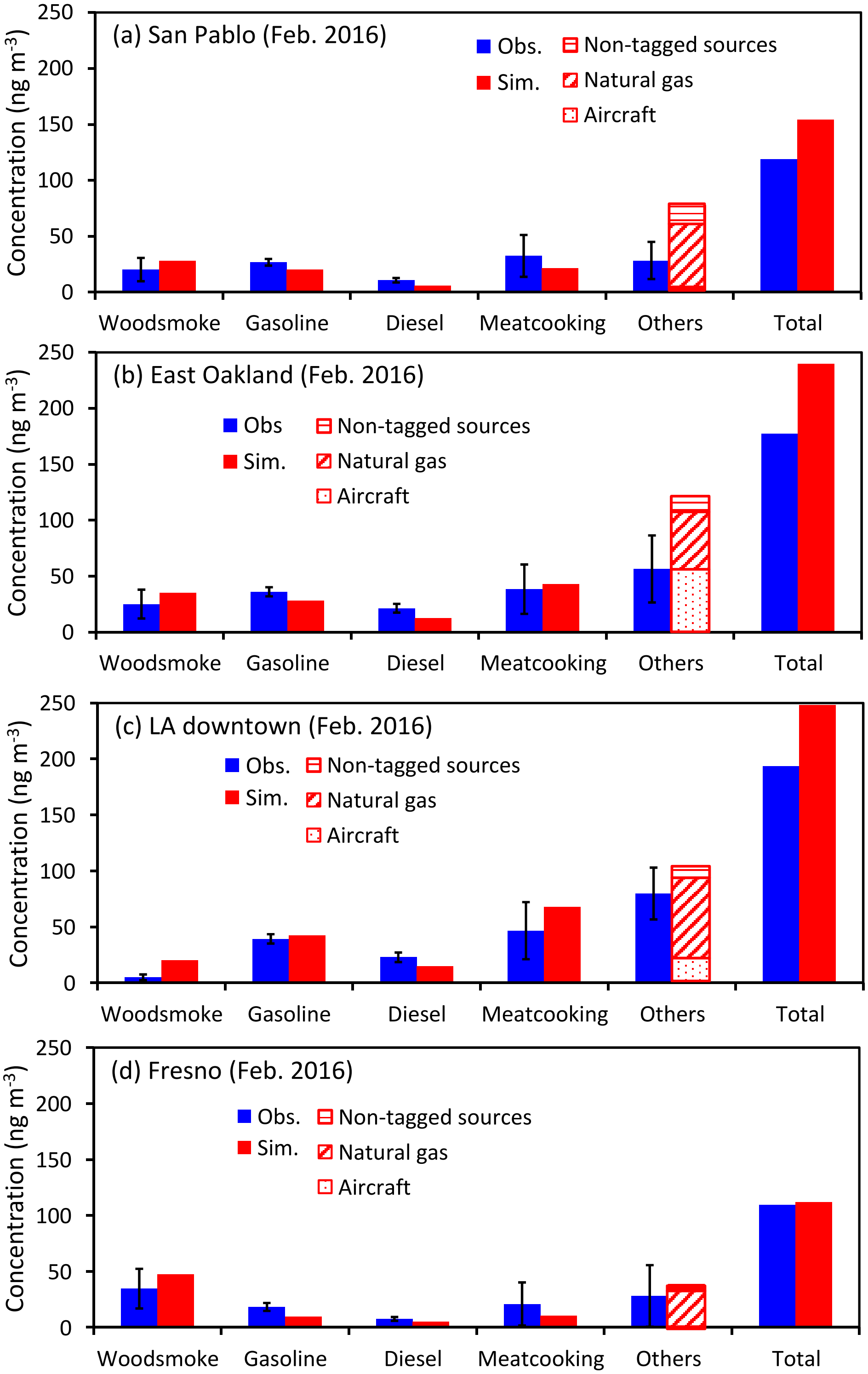

Figure 7-3: Source contribution to $PM_{0.1}$ predicted by the CMB receptor model and the UCD/CIT model at four sites in California in February 2016.

Figures 7-4 through 7-6 and Figures 7-7 through 7-9 show the seasonal variation of major source contributions to primary N_{10} and $PM_{0.1}$, respectively. The black circles in Figure 7-4 through 7-6 represent the measured N_7 at four BAAQMD sites in SFBA and six MATES sites in Los Angeles and Riverside counties. Predicted N_{10} agrees reasonably well with measured seasonal variations of N_7 at San Pablo, Redwood City, Livermore, Anaheim, Central LA, Compton and Huntington Park. The model under predicts N_7 at Santa Rosa and over predicts N_7 at Inland-Valley and Rubidoux but overall model performance statistics for N_{10} are within the guidelines for regulatory $PM_{2.5}$ applications (see Table 7-1). Nucleation contributes to summer N_{10} at all sites but makes negligible contributions to $PM_{0.1}$ concentrations. Traffic sources including gasoline- and diesel-powered vehicles make significant contributions to $PM_{0.1}$ concentrations at each measurement site depending on proximity to major freeways. Near-roadway effects on ultrafine particle concentrations are not apparent since these locations were chosen to be regional monitors and so they are more than 300 m from the nearest freeway. Predicted contributions from traffic sources are consistent with the molecular marker results illustrated in Figures 7-2 through 7-3. Traffic contributions to regional N_{10} concentrations more than 300 m away from roadways are even smaller than $PM_{0.1}$ contributions because the size distribution of particles emitted from motor vehicles peaks at 100 – 200 nm [23, 24]. Wood smoke makes strong contributions to regional $PM_{0.1}$ concentrations in central California during winter but much smaller contributions in the SoCAB because wood burning is not typically used for home heating in this region. Wood burning contributions N_{10} are less dominant in central California because the size distribution of particles emitted from wood combustion peaks at 100-300 nm [291]. The largest source of N_{10} in central California and N_{10}+$PM_{0.1}$ in the SoCAB is non-residential natural gas combustion. Industrial processes and power generation that use natural gas do not follow strong seasonal cycles and so the strength of the natural gas source contributions is somewhat constant across seasons subject to variability caused by meteorological conditions.

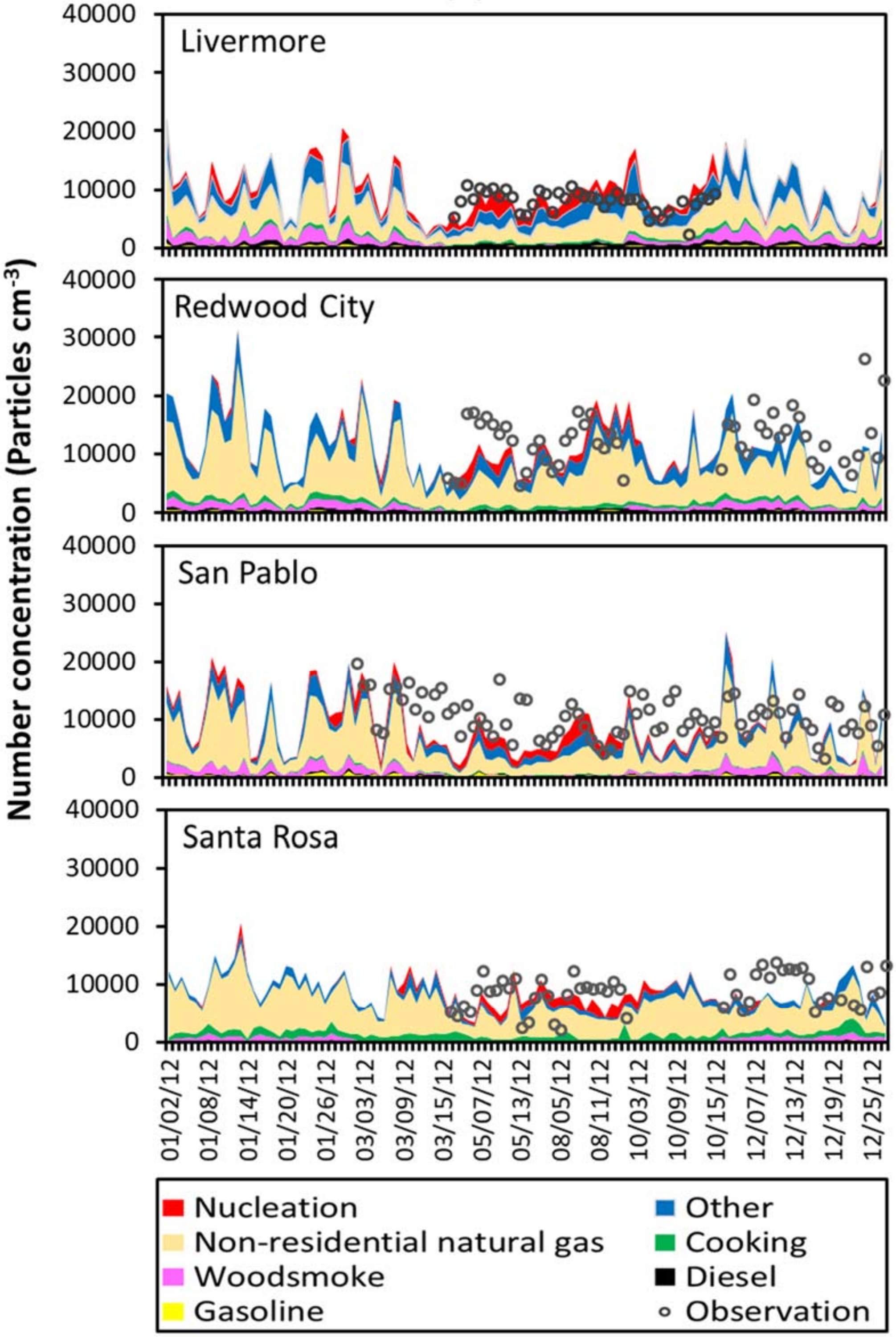

Figure 7-4: Seasonal variation of measured N_7 (black circles) and major source contributions to predicted N_{10} at Livermore, Redwood City, San Pablo and Santa Rosa, respectively.

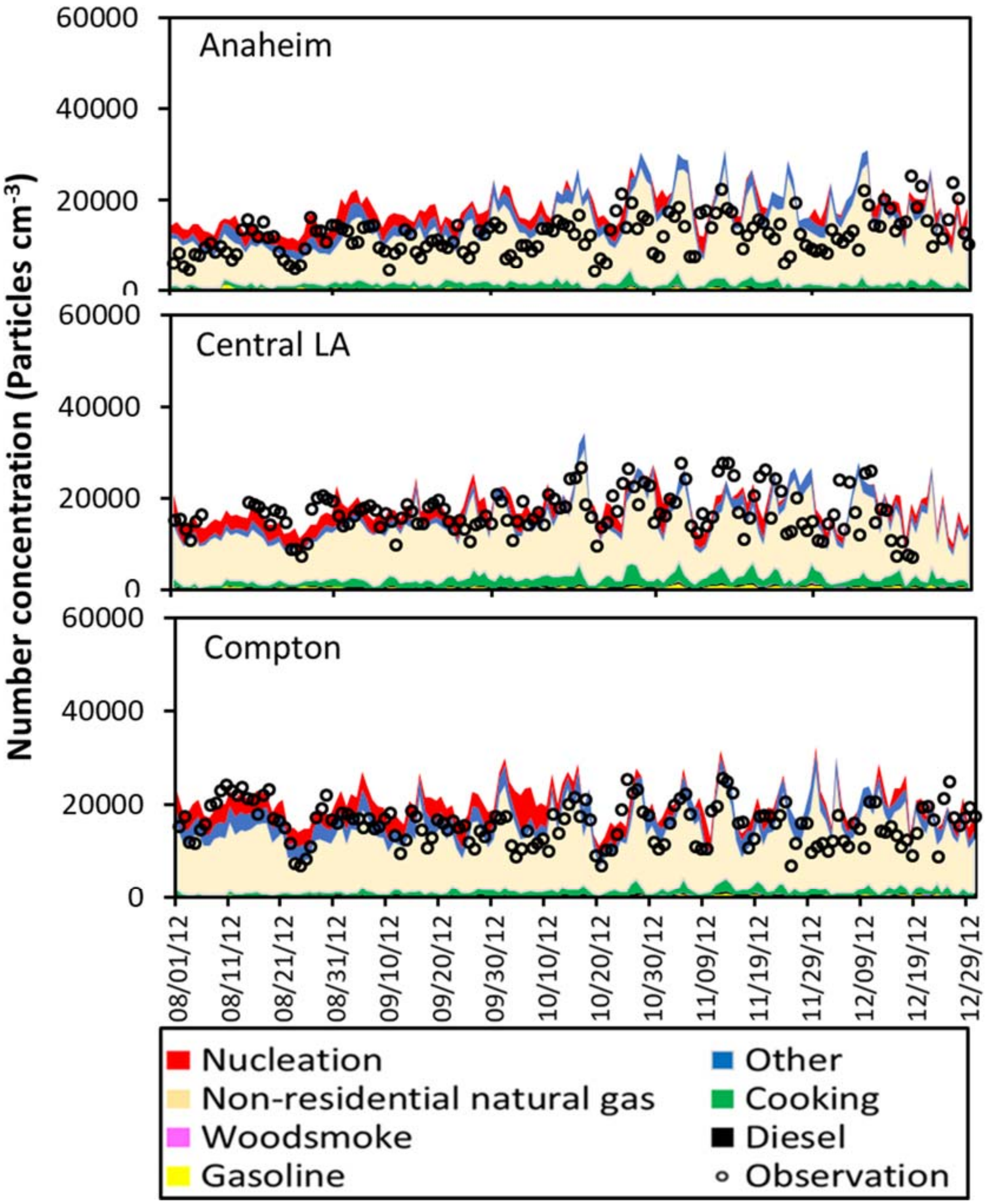

Figure 7-5: Seasonal variation of measured N_7 (black circles) and major source contributions to predicted N_{10} at Anaheim, Central LA, and Compton, respectively.

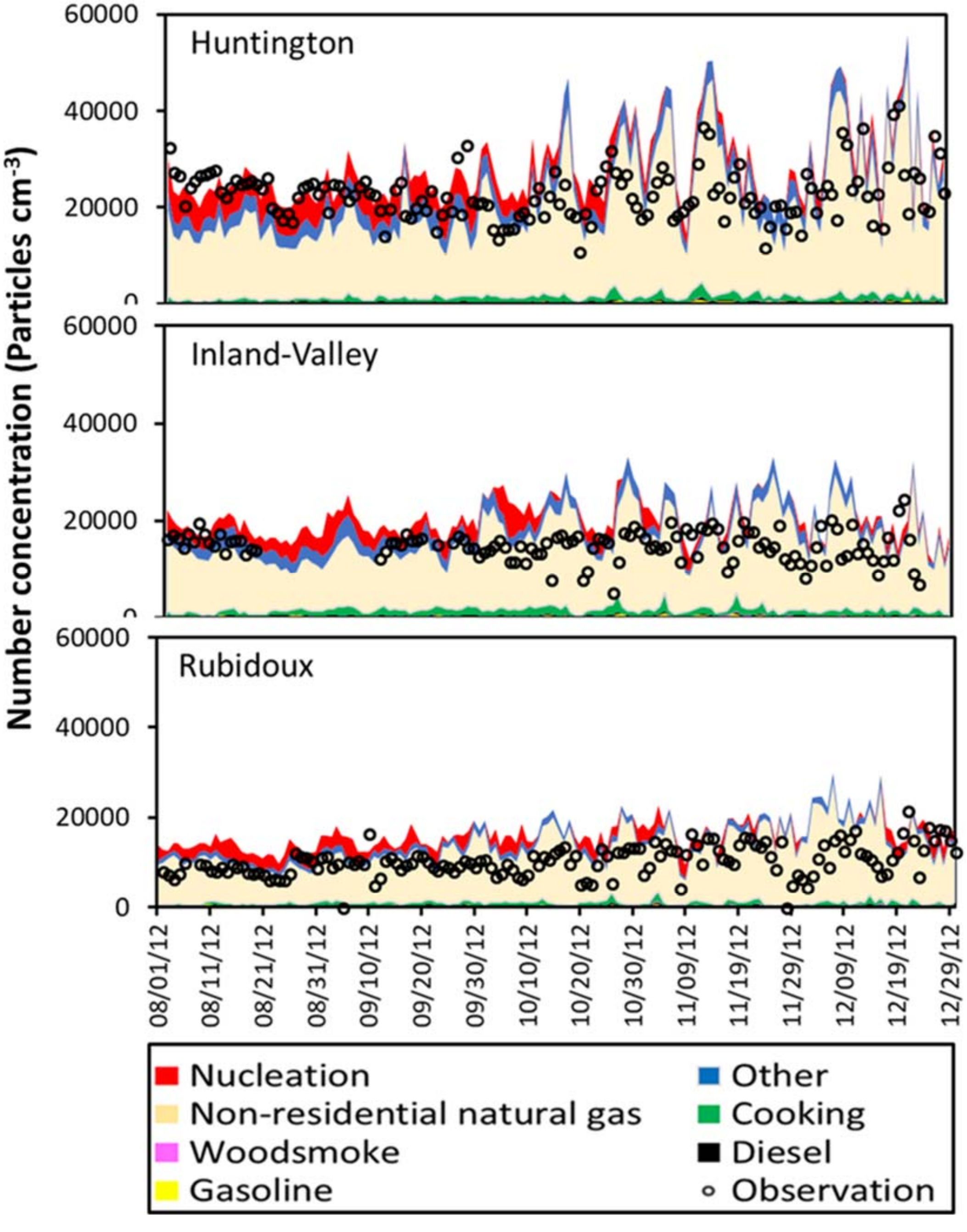

Figure 7-6: Seasonal variation of measured N_7 (black circles) and major source contributions to predicted N_{10} at Huntington Park, Inland-Valley, and Rubidoux, respectively.

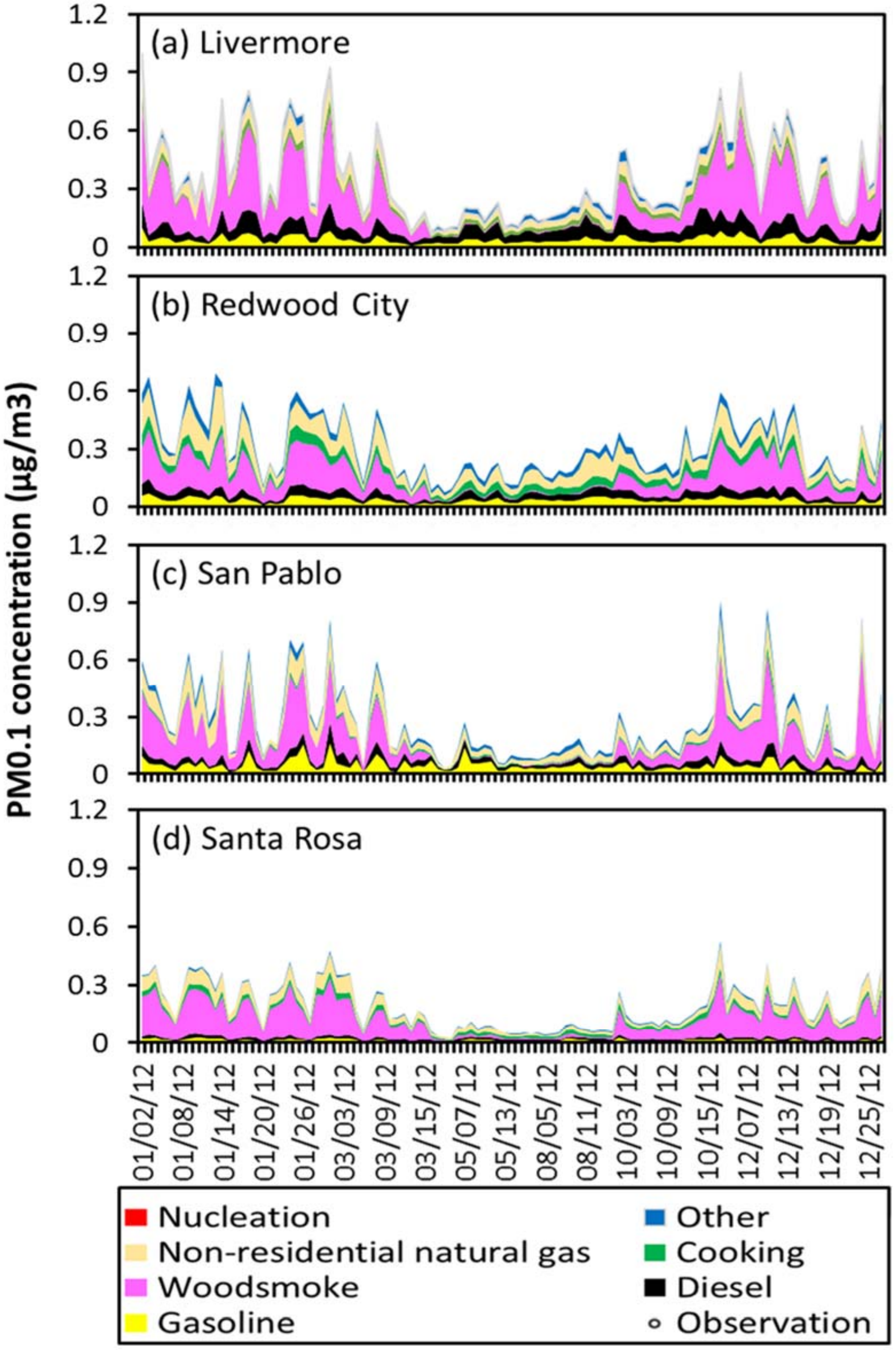

Figure 7-7: Seasonal variation of major source contributions to $PM_{0.1}$ at Livermore, Redwood City, San Pablo and Santa Rosa, respectively.

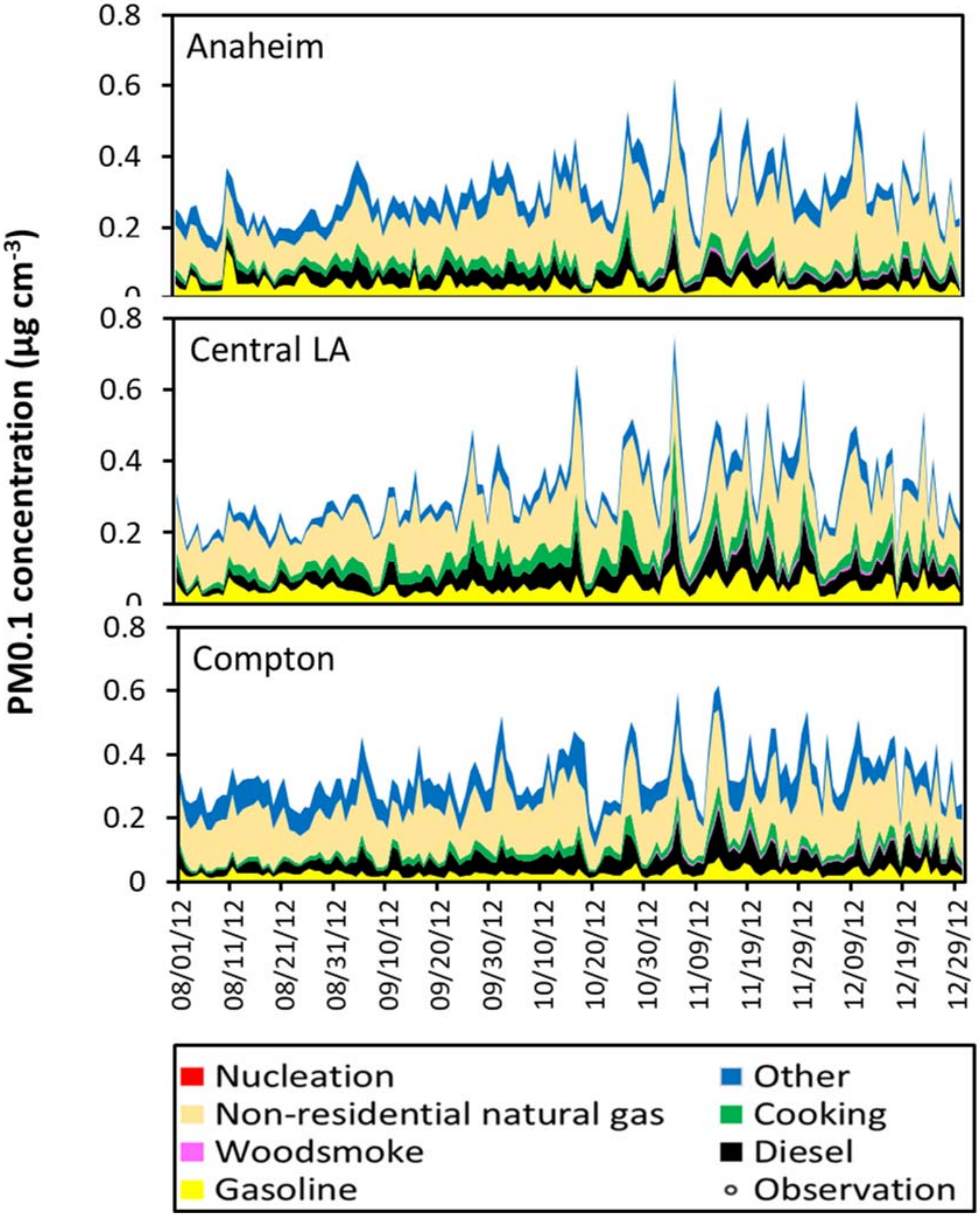

Figure 7-8: Seasonal variation of major source contributions to $PM_{0.1}$ at Anaheim, Central LA, and Compton, respectively.

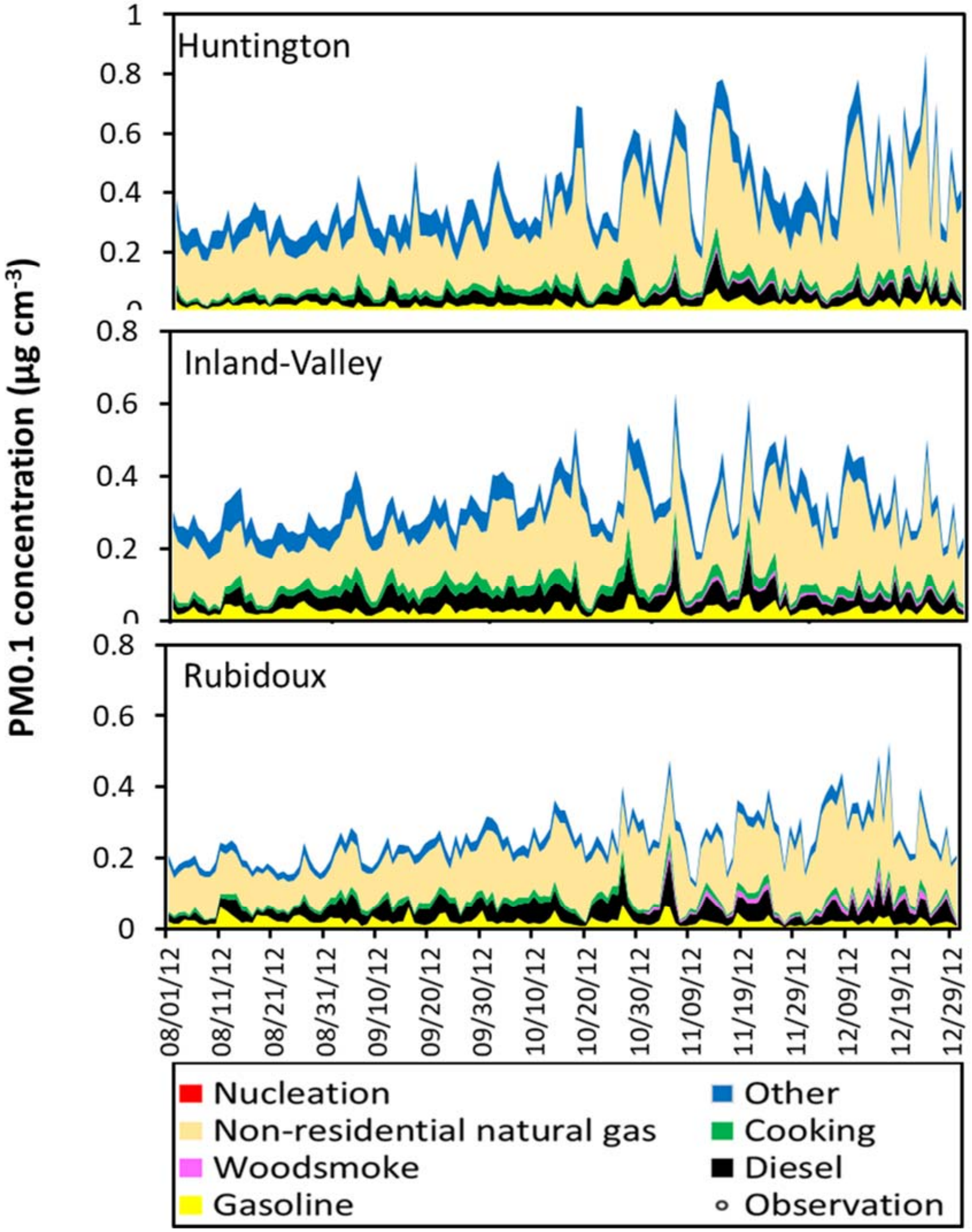

Figure 7-9: Seasonal variation of major source contributions to $PM_{0.1}$ at Huntington Park, Inland-Valley, and Rubidoux, respectively.

Figures 7-10 and Figures 7-11 show the source contributions to N_{10} and $PM_{0.1}$, respectively, averaged over the days shown in Figures 7-4 through 7-9. Non-residential natural gas combustion makes the largest predicted contribution to N_{10} at all the sites that were evaluated. Traditional sources that were tracked including meat cooking, wood smoke, and mobile (gasoline + diesel) accounted for approximately 10-20% of the predicted N_{10} at the sites selected for study. "Other" sources that were not tagged explicitly in the current study accounted for 8-28% of N_{10} across these sites. Nucleation is a significant source for of N_{10} for both BAAQMD sites and MATES sites where sulfur emissions were highest, with contributions ranging from 6-14%.

The dominant N_{10} contribution from non-residential natural gas combustion reflects the emitted particle size distribution combined with the ubiquitous use of this fuel in the SFBA and SoCAB regions. The chemical composition and size distribution information for non-residential natural gas combustion emissions used in this study was measured by Hildemann et al. [292] and Li and Hopke [293], respectively. Size distributions and volatility were further confirmed during on-going field studies conducted by the current authors [285]. The estimated non-residential natural gas combustion particle number and mass size distributions are shown in Figure S7-1 (left column). Clearly, the majority of particles from non-residential natural gas combustion are typically found in diameters <0.05 μm, while particles emitted from other sources such as wood combustion tend to have slightly larger particle diameter (with lower number concentration per unit of emitted mass).

Figures 7-11 show that wood smoke is the largest $PM_{0.1}$ source at Livermore (36%), San Pablo (35%), while non-residential natural gas combustion still makes the largest contribution to $PM_{0.1}$ at Redwood City (28%), Santa Rosa (41%) and MATES sites (42%-58%) in the SoCAB region. Contributions from cooking and mobile sources are enhanced in $PM_{0.1}$ vs. N_{10}, with the cooking source accounting for 15% of $PM_{0.1}$ at Santa Rosa and mobile sources (gasoline + diesel) accounting for 34% of $PM_{0.1}$ at the Central LA site, followed by 33% of $PM_{0.1}$ at Livermore site. The different rankings of source contributions to N_{10} and $PM_{0.1}$ can be explained by the comparison of particle number-size distribution and particle mass-size distribution for the non-residential natural gas and wood burning sources at four evaluated sites (Figure S7-1). Particles emitted from non-residential natural gas combustion and wood burning have number distributions that peak at particle diameters of 0.016-0.025 μm and 0.025-0.04 μm, respectively. Non-residential natural gas combustion and wood burning mass distributions, however, peak at particle diameters of 0.025-0.04 μm and 0.10-0.16 μm, respectively.

Figure 7-12 through 7-14 show diurnal variations of measured N_7 and predicted N_{10} averaged over days in August and December 2012. Measured N_7 diurnal patterns in August are bimodal with the first peak usually occurring at 6-7 am at four sites in SFBA and 5-6 am at six sites in Los Angeles and Riverside County and the second peak occurring between 12-3 pm. The first summer peak corresponds to morning activities including cooking and traffic "rush hours", while the second peak appears to be related to nucleation events. The predicted N_{10} diurnal variations in August were in good agreement with measurements at five out of ten sites (Livermore, San Pablo, Anaheim, Compton, and Huntington Park). The model generally predicts a biomodal diurnal profile with maximum values in reasonable agreement with measurements at these locations. The model failed to capture the mid-day nucleation event at Santa Rosa possibly due to missing SO_2 sources in the emissions inventory upwind from this site. The model overestimated mid-day peak values at Inland-valley and Rubidoux sites. In December, the measured N_7 diurnal pattern was also bimodal with the first peak around 7:00-8:00am and the second peak in the evening at around 8pm. This pattern reflects both the emissions activity and the mixing status of the atmosphere throughout the day. The predicted N_{10} concentration is in good agreement with measurements for the early morning peak but generally underestimated the evening peak possibly due to excess atmospheric mixing after sunset in the model calculations. Nucleation appears to play a small role during winter. Non-residential natural gas combustion is predicted to be the largest source of N_{10} during morning and evening peaks. The diurnal profiles of non-residential natural gas emissions are included in supplemental information (Figure S7-2). Industrial natural gas combustion emissions peak during the daytime with lower values at night. Emissions from electricity generation powered by natural gas peak in the morning and evening. Commercial natural gas combustion emissions may either peak in the morning and evening or they may follow a uniform diurnal profile depending on the specific source and location.

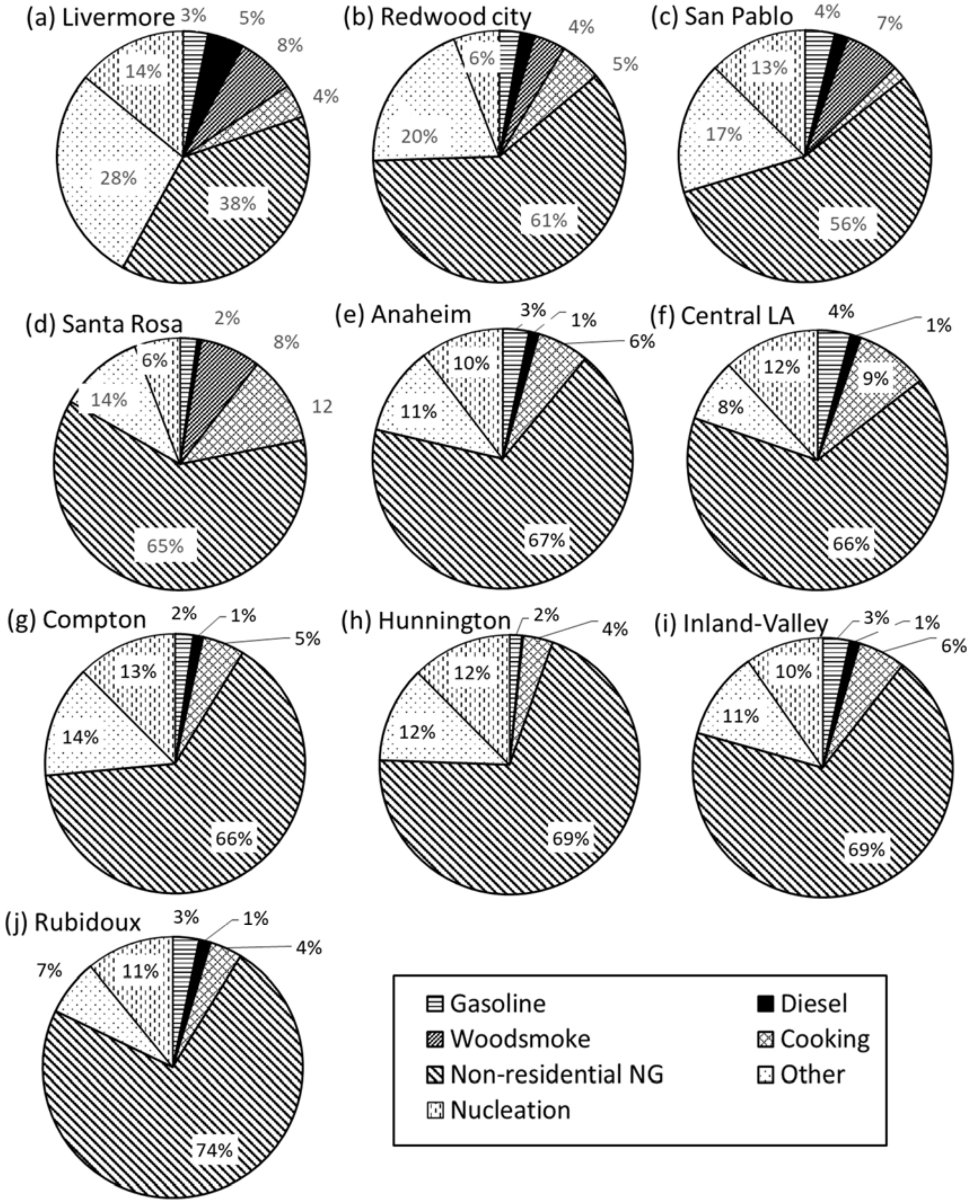

Figure 7-10: The relative source contributions to N_{10} at Livermore, Redwood City, San Pablo, Santa Rosa, Anaheim, Central LA, Compton, Huntington Park, Inland-Valley and Rubidoux, respectively. Averaging time included all days shown in Figures 4-6.

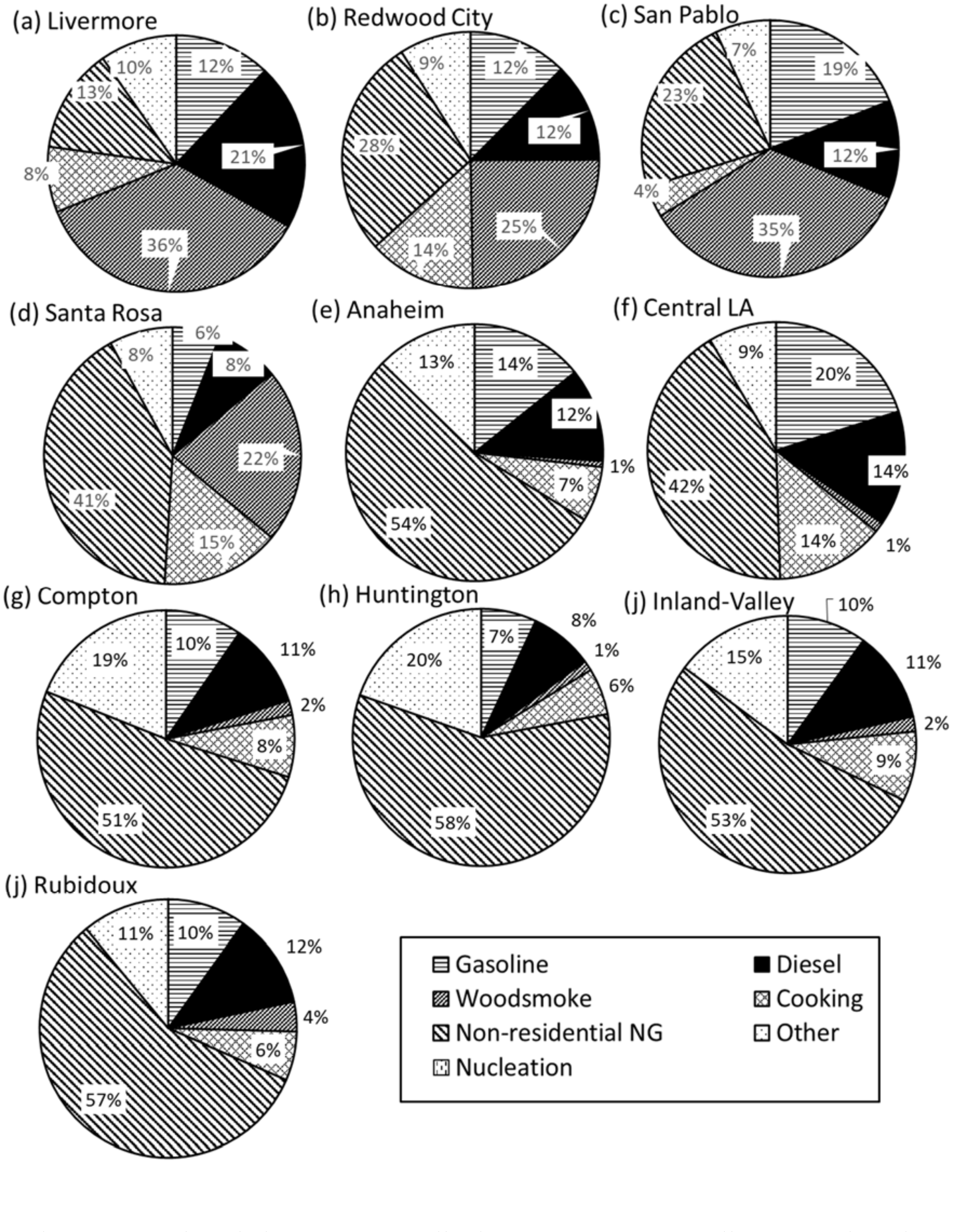

Figure 7-11: The relative source contributions to PM0.1 seasonally averaged at Livermore, Redwood City, San Pablo and Santa Rosa, Anaheim, Central LA, Compton, Huntington Park, Inland-Valley and Rubidoux, respectively. Averaging time included all days shown in Figures 7-9.

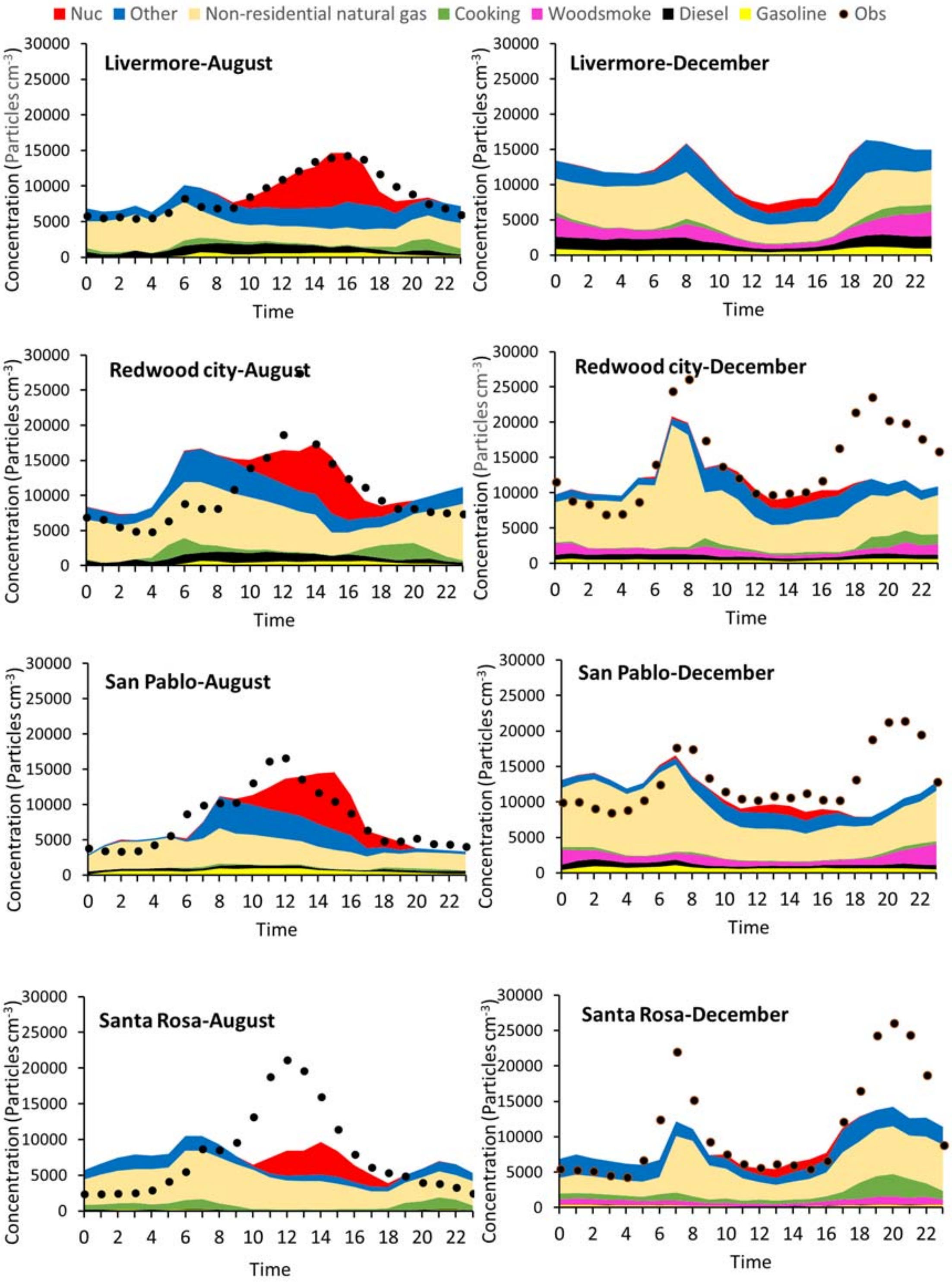

Figure 7-12: Diurnal variations of measured N_7 and predicted N_{10} averaged for August 2012 (left column) and December 2012 (right column) at Livermore, Redwood city, San Pablo and Santa Rosa.

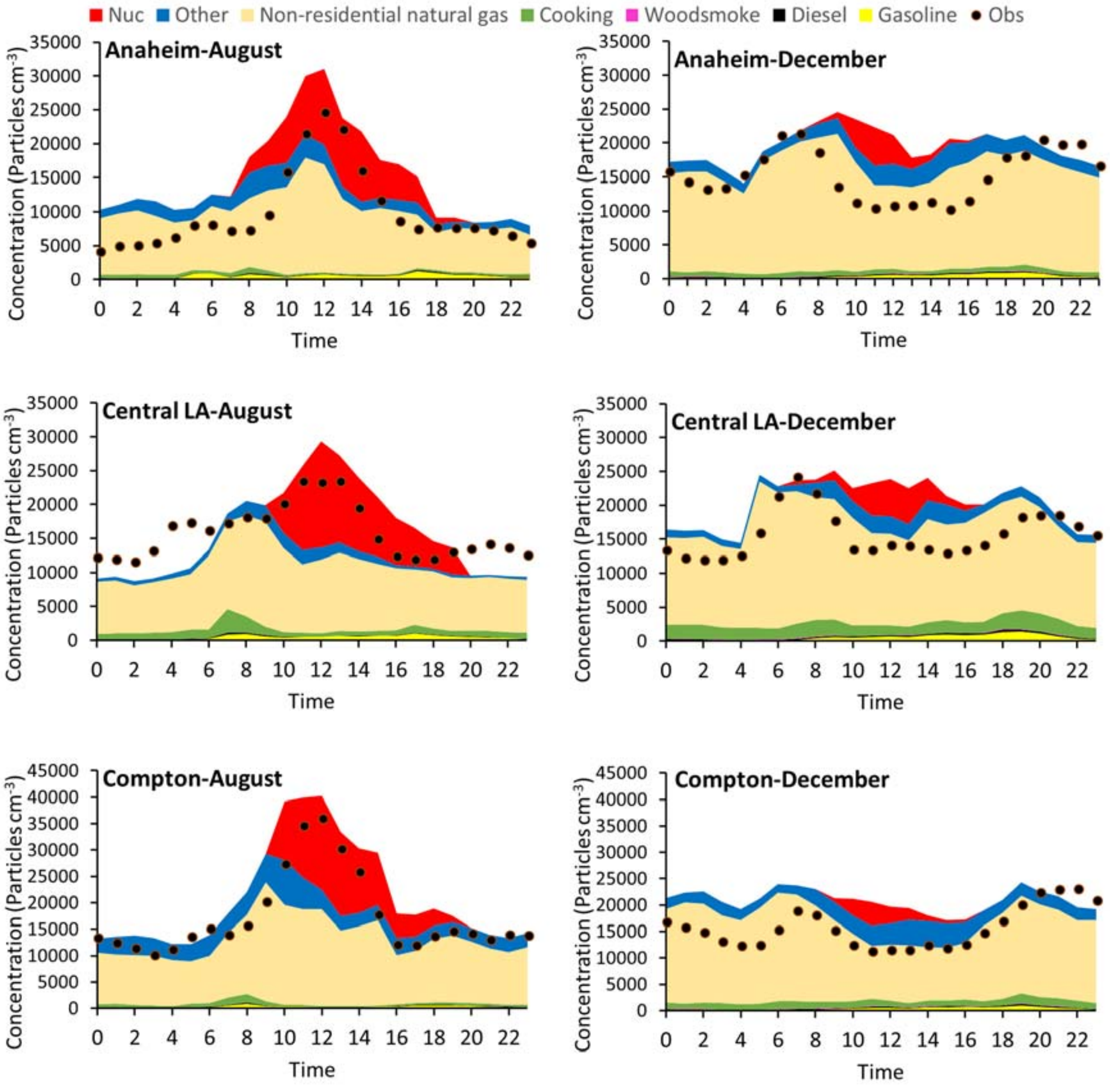

Figure 7-13: Diurnal variations of measured N_7 and predicted N_{10} averaged for August 2012 (left column) and December 2012 (right column) at Anaheim, Central LA, and Compton.

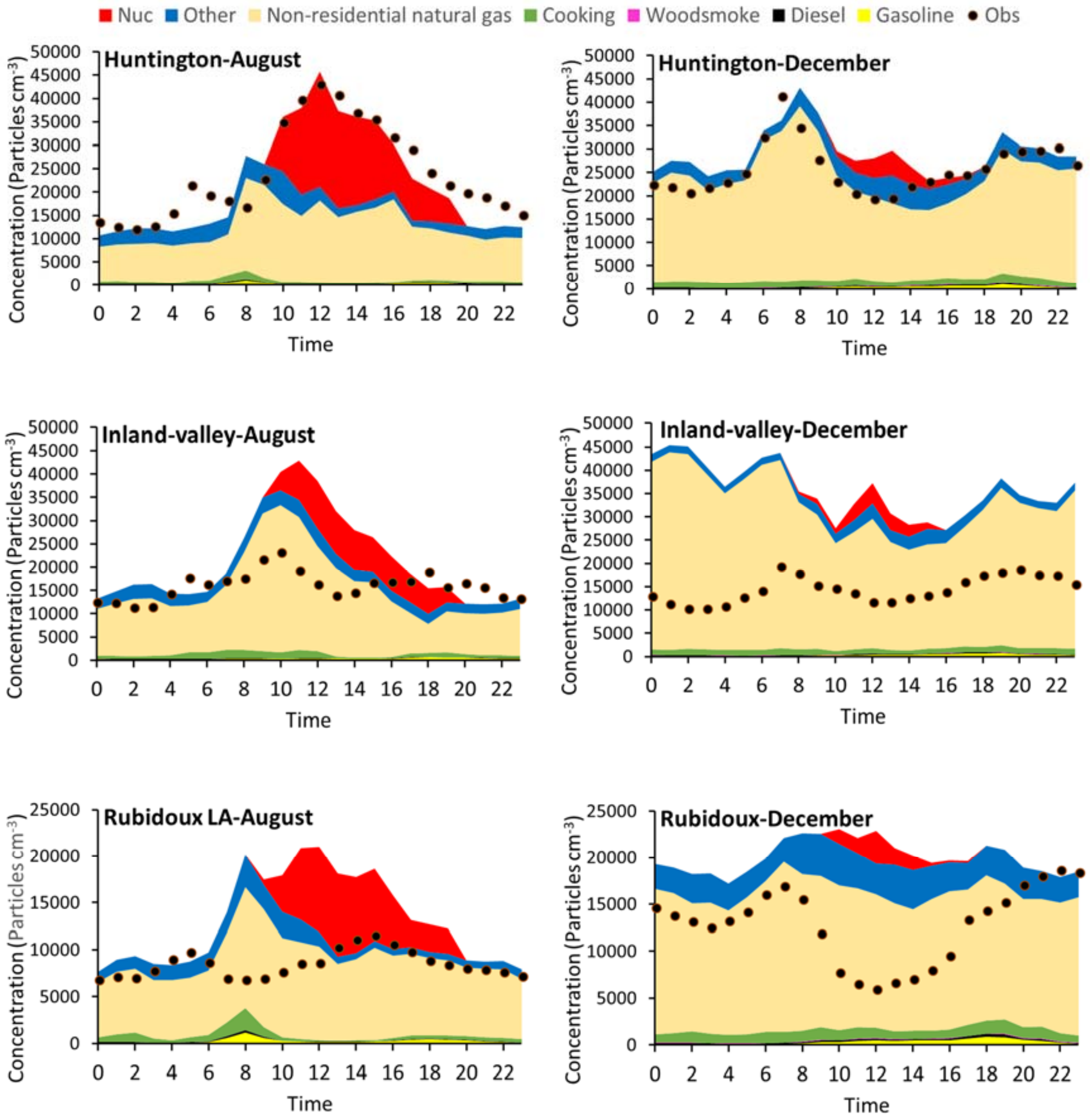

Figure 7-14: Diurnal variations of measured N_7 and predicted N_{10} averaged for August 2012 (left column) and December 2012 (right column) at Anaheim, Central LA, and Compton.

7.4 Discussion

Previous researchers have used Positive Matrix Factorization (PMF) to calculate source contributions to N_{10} [254, 294-300]. The dominant factors resolved by these studies have been traffic, urban background, secondary aerosol, wood burning and nucleation [254, 294-300]. Particles from natural gas combustion were not separately identified by PMF because they do not contain a unique chemical tracer. It is very likely that natural gas combustion particles are artificially lumped into another source (e.g. traffic) or part of the "urban background" signal identified in previous studies. Natural gas combustion is used extensively in California for electric power, industrial, commercial and residential use (Table S7-5), and so it seems plausible that this source contributes to ambient UFP concentrations.

The current UFP predictions rely on source profile measurements for wood burning, food cooking, mobile sources, and non-residential natural gas combustion [23, 24, 291, 301-312]. All of these size distributions were measured using appropriate instruments and methods by knowledgeable researchers, but some of these past studies were conducted more than a decade ago. Size distribution information for vehicles, natural gas, etc. have been added to the supplemental information (Figure S7-3). Changes in fuel composition and emissions control technology in the interim years may have altered the emitted size distributions. New measurements of particle size distributions emitted from natural gas combustion and biomethane combustion were made in parallel with the current project to confirm the source profile measurements from past studies[285]. The results of these measurements are consistent with previous size distribution results.

California has tighter air pollution standards than many other regions in the United States due to the severe air quality problems that have historically occurred in the state. California therefore has a unique mixture of fuels and emissions control technology that may affect the mixture of sources that contribute to atmospheric ultrafine particle concentrations. Venecek et al. [313] recently used the UCD/CIT air quality model with the 2011 National Emissions inventory to calculate source contributions to $PM_{0.1}$ in 39 major cities across the United States during peak summer photochemical smog episodes in the year 2010. The findings from this study show that natural gas combustion is a major source of ultrafine particles in the regional atmosphere over urban areas across the United States. The public health questions associated with ultrafine particles emitted by natural gas combustion have wide-ranging implications. Similar levels of ultrafine particle concentrations will likely occur in other regions across the world that extensively use natural gas as a fuel source, although other sources of ultrafine particles may also make strong contributions depending on the total mix of fuels in each region.

Recent theories suggest that primary particulate matter composed of semi-volatile organic compounds may evaporate after release to the atmosphere, which may reduce ambient N_{10}. Measurements conducted in parallel with the current study confirmed that particles emitted from natural gas combustion in home appliances partially evaporated when diluted by a factor of 25 in clean air, but particles emitted from industrial sources did not evaporate under the same conditions[285]. Future work should verify the accuracy of the size and composition distributions for all natural gas combustion sources given their apparent importance for predicted N_{10}.

Evidence from both toxicology and epidemiology will be required to assess the effect of UFPs on public health. It is essential to identify and quantify UFP sources based on both mass ($PM_{0.1}$) and number N_{10} during this process [300]. An accurate comparison of both $PM_{0.1}$ and N_{10} exposure could lay the groundwork for specific assessment of health effects of UFPs and potentially more efficient control strategies for PM emission from major sources [299]. Ideally, spatial exposure patterns for N_{10}, $PM_{0.1}$, and $PM_{2.5}$ will be sufficiently unique to separate their individual effects in epidemiological studies. Regression statistics for different metrics were calculated by using all grid cells in the model domain of the current study. The correlations between the various particle metrics were: $R^2(PM_{2.5}$ vs. $N_{10})=0.35$, $R^2(PM_{2.5}$ vs. $PM_{0.1})=0.63$, $R^2(PM_{0.1}$ vs. $N_{10})=0.75$. It seems likely that future epidemiological studies will be able to differentiate between the effects of $PM_{2.5}$ and N_{10} based on the low R^2 value. The potential for comparisons between $PM_{2.5}$ and $PM_{0.1}$ is less clear cut, but previous work helps understand what may be possible. Ostro et al.[247] compared the associations between IHD mortality and $PM_{2.5}$ vs. $PM_{0.1}$ in the California Teachers Study (CTS) cohort. Associations between IHD mortality and the sum of $PM_{2.5}$ mass (p-value=0.001) were stronger than associations between IHD mortality and the sum of $PM_{0.1}$ mass (p-value=0.01) but individual components of mass (EC, OC, Cu, etc) all had stronger associations with IHD mortality in the $PM_{0.1}$ size fraction than the $PM_{2.5}$ size fraction.

The current study focuses on outdoor exposure to UFPs that may be useful in future epidemiological studies. Indoor or in-vehicle exposure to UFPs can also be significant [314-318] but characterizing these micro-environments is beyond the scope of the current manuscript.

7.5 Conclusions

The UCD/CIT regional chemical transport model has been updated with a nucleation algorithm and combined with the existing size-resolved source profiles of particlualte matter emissions to predict regional source contributions to airborne particle number concentration (N_{10}) and airborne particulate ultrafine mass ($PM_{0.1}$). Predicted 24-hour average N_{10} is in good agreement with measured N_7 at ten sites across California in summer (Aug) and winter (Dec). Predicted diurnal variation of N_{10} is in reasonable agreement with measured concentrations but uner-predicts early evening peaks in the winter due to the failure of meteorological calculations to capture the suppressed mixing in the atmosphere at these times. Predicted $PM_{0.1}$ source contributions are in good agreement with $PM_{0.1}$ source contributions measured in a molecular marker study at four sites across California in summer (Aug) and winter (Dec) months. Natural gas combustion is the largest source of regional N_{10} at all locations outside of the immediate vicinity of other major combustion sources. Nucleation contributed to particle number during the summer months at midday but did not dominate N_{10} concentrations. Likewise, traffic sources contributed to N_{10} but did not dominate over regions more than 300 m away from freeways. Combustion sources such as wood burning, food cooking, and mobile sources made stronger contributions to $PM_{0.1}$ at heavily urbanized locations. Wood burning for home heating had strong seasonal patterns with peak concentrations in winter while other sources contributed more consistently throughout the seasons. Nucleation made a negligible contribution to $PM_{0.1}$ over the urban areas at the focus of the current study.

The current study identifies natural gas combustion as a major source of ultrafine particle number and mass concentrations in urban regions throughout California. The health implications of these natural gas combustion particles should be investigated in future epidemiology studies.

7.6 Appendix

Table S7-1. PM profiles used for each source type were specified as weighted averages from each of the detailed sources within each broad category

Source Type	PM Source Profile
On-road gasoline vehicles	10% Non-catalyst vehicle + 90% Catalyst Vehicle
Off-road gasoline vehicles	100% Non-catalyst vehicle
On-road diesel vehicles	100% On-road diesel vehicle
Off-road diesel vehicles	90% 1970's diesel vehicle + 7% 1980's diesel vehicle + 3% on-road diesel vehicle
Food Cooking	85% meat frying + 15% charbroiling
Biomass burning	95% residential wood smoke + 5% waste burning
Natural gas combustion	100% natural gas combustion
Other	70% construction & demolition + 10% paved road travel + 4% farming ops + 3% brake wear + 2% cattle feedlot + 2% mining ops + 1% process heaters + 1% cement manufacturing + 3% wood processing + 1% solid waste disposal + 2% mineral processing + 1% asphalt production + 1% organic solvent

Table S7-2. Meteorology evaluation metrics for the entire simulation period in SFBA counties (Alameda (ALA) county, Contra Costa (CC) county, Napa (NAP) county, San Francisco (SF) county, Santa Clara (SCL) county, San Mateo (SM) county, Solano (SOL) county) and two counties in Southern California (Los Angeles county (LA) and Riverside county (RV)).

	Temperature ˚C		Wind			Relative Humidity		
County	MB	RMSE	MFB	MFE	RMSE m/s	MFB	MFE	RMSE %
ALA	0.21	4.02	-0.05	0.56	1.39	-0.28	0.39	28.81
CC	0.14	4.36	0.03	0.62	1.63	-0.33	0.47	31.16
NAP	0.12	4.25	0.05	0.59	1.71	-0.38	0.49	35.96
SF	0.11	4.14	-0.08	0.64	2.14	-0.33	0.46	35.49
SCL	0.16	4.23	-0.08	0.57	1.62	-0.28	0.42	30.42
SM	0.15	5.49	-0.05	0.6	1.75	-0.26	0.43	32.49
SOL	0.13	4.67	0.10	0.56	1.37	-0.36	0.47	35.23
LA	0.10	3.91	-0.12	0.58	1.66	-0.14	0.35	27.31
RV	0.12	4.34	0.07	0.59	1.28	-0.11	0.38	26.28

Table S7-3. Locations of N_7 for measurement sites used in the analysis

Station name	Address	Latitude	Longitude
Anaheim	1630 Pampas Ln Anaheim, CA 92802	33.83	-117.94
Central LA	1630 North Main Street, Los Angeles, CA 90012	34.07	-118.23
Compton	700 North Bullis Rd Compton, CA 90221	33.90	-118.21
Hunnington Park	6301 S. Santa Fe Ave. 90221	33.87	-118.22
Inland Valley	14360 Arrow Highway	34.11	-117.96
Rubidoux	5891 Mission Blvd Riverside, CA 92509	34.00	-117.42
Livermore	793 Rincon Avenue, Livermore, CA 94551	37.69	-121.78
San Pablo	1865 Rumrill Boulevard, San Pablo, CA 94806	37.96	-122.36
Redwood City	897 Barron Avenue, Redwood City, CA 94063	37.48	-122.20
Santa Rosa	837 5th Street, Santa Rosa, CA 95404	38.44	-122.71

Table S7-4. Statistics of $PM_{2.5}$ and $PM_{2.5}$ species

	MASS $PM_{2.5}$	EC $PM_{2.5}$	OC $PM_{2.5}$	Nitrate	Sulfate	Ammonium
MFB	-0.11	-0.18	-0.32	-0.2	-0.41	0.22
MFE	0.26	0.32	0.46	0.51	0.6	0.49

Table S7-5. Ultrafine PM emission inventory from natural gas combustion in the commercial, industrial and electricity sectors for the entire SoCAB region and SFBA region during the summer and winter months.

		Electricity short tons/day	Industrial short tons/day	Commercial short tons/day
SoCAB	Summer	1.95	0.57	0.69
	Winter	2.02	0.58	0.93
SFBA	Summer	0.18	0.07	0.88
	Winter	0.19	0.25	1.50

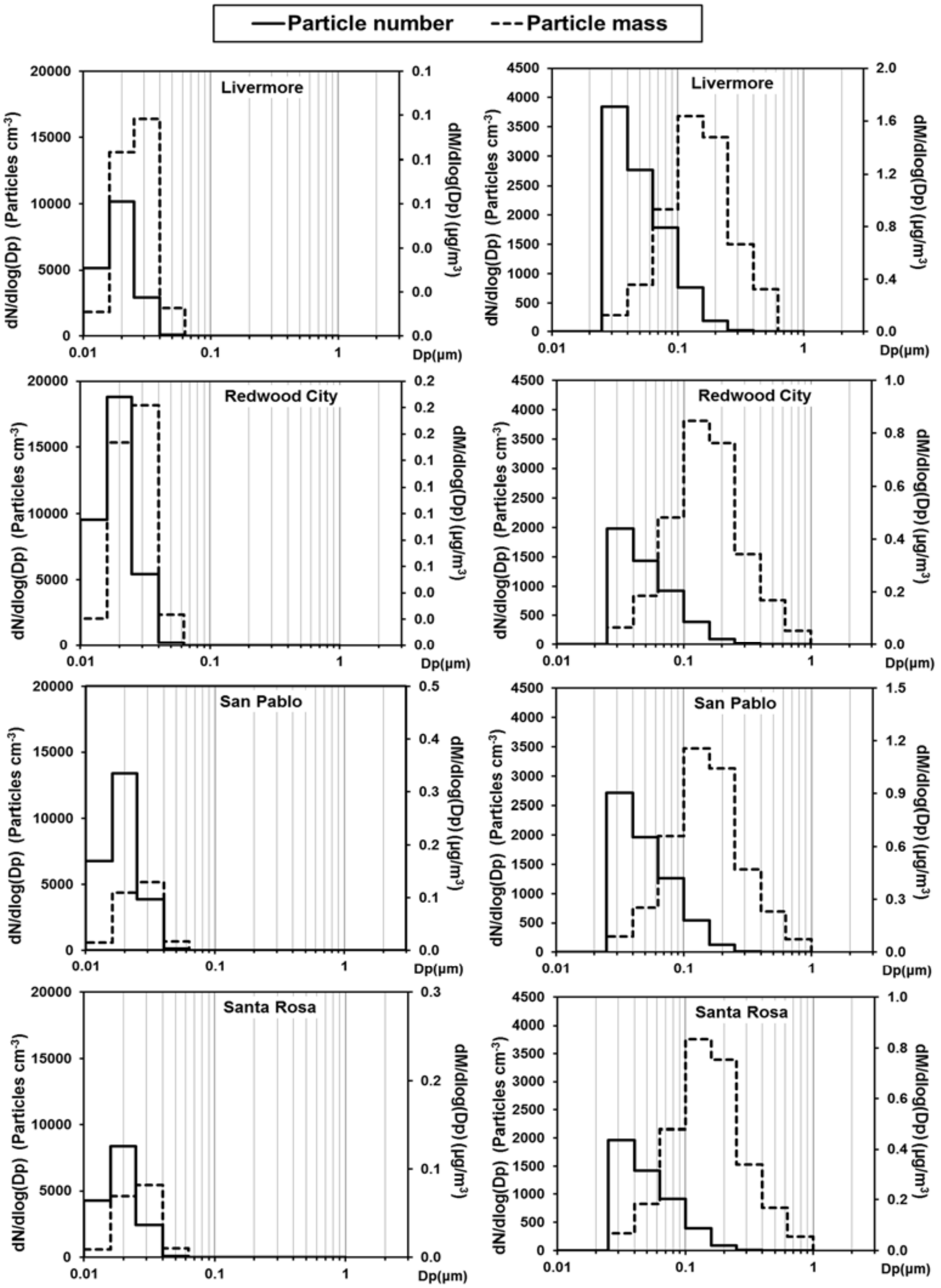

Figure S7-1: Particle number-size distribution and particle mass-size distribution for natural gas combustion (left panel) and wood burning sources (right panel) at four evaluated sites in SFBA.

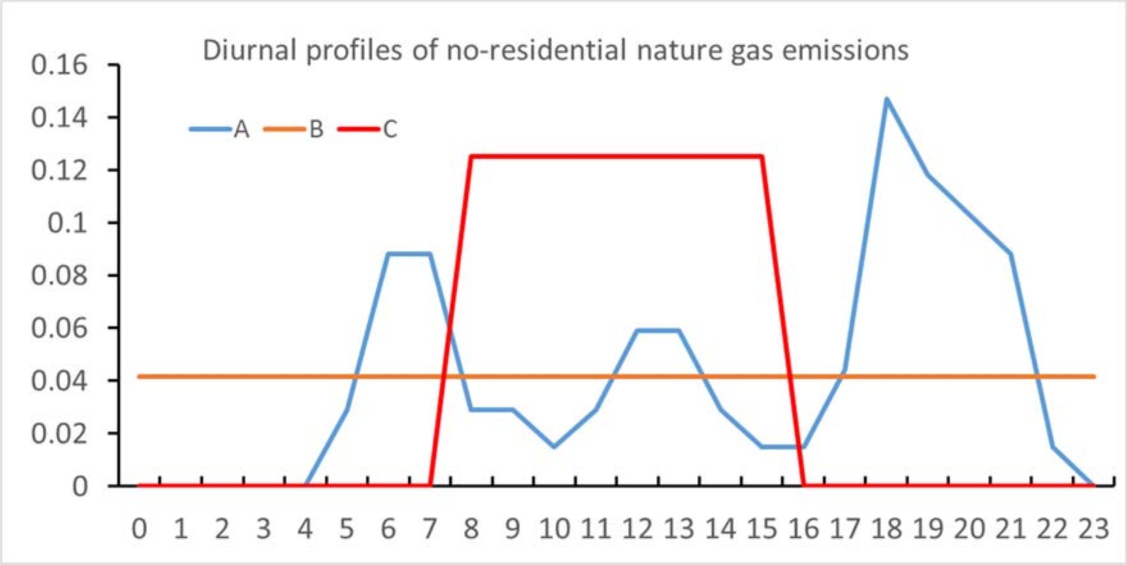

Figure S7-2: Diurnal profiles of non-residential natural gas combustion emissions.

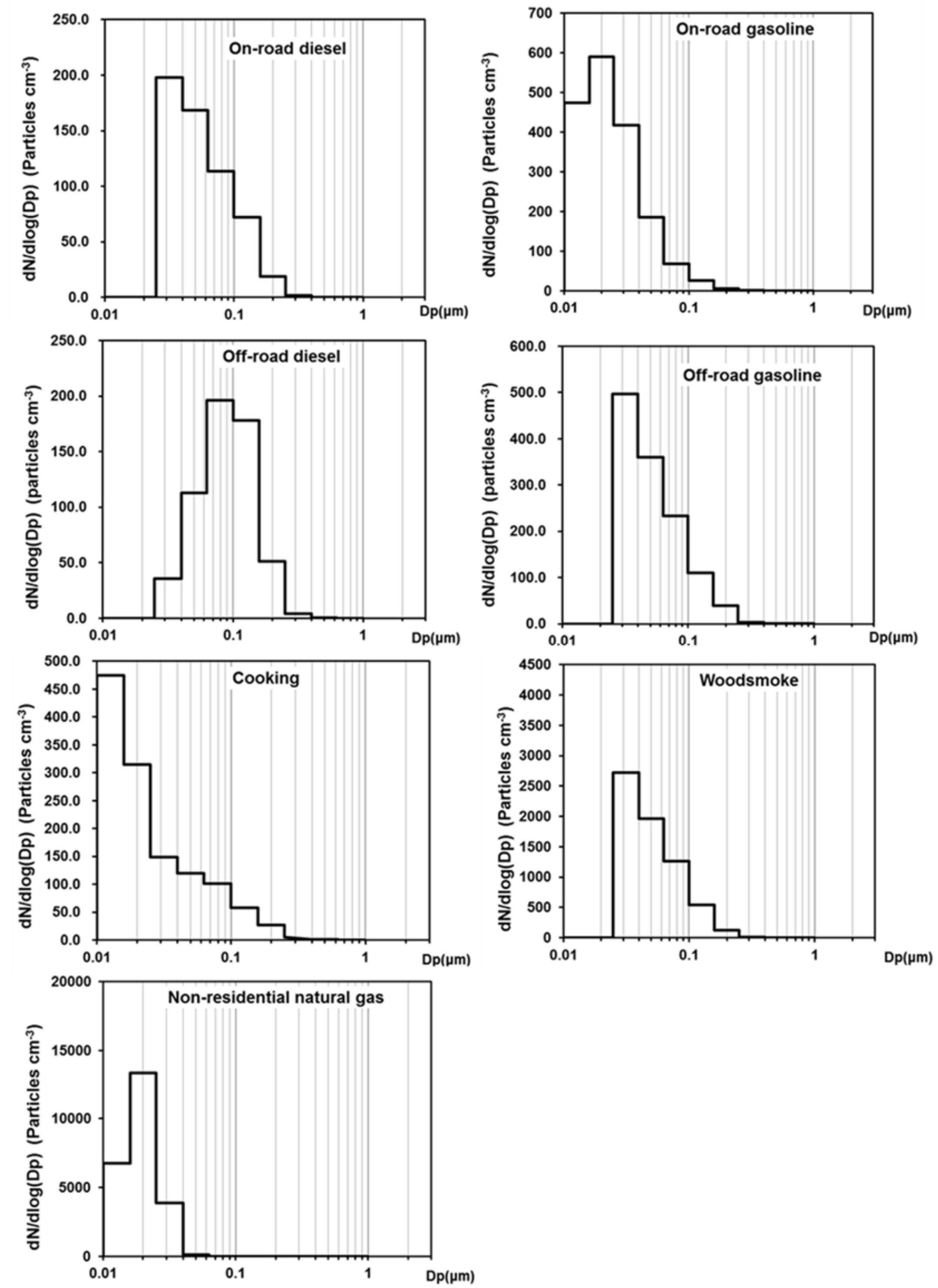

Figure S7-3: Particle size distributions of major sources calculated by UCD/CIT model at San Pablo.

8 SOURCE CONTRIBUTIONS TO ULTRAFINE PARTICLE MASS ($PM_{0.1}$) CONCENTRATIONS IN CALIFORNA PREDICTED BY RECEPTOR-ORIENTED MODELS VS. SOURCE-ORIENTED MODELS

Preamble: Chapter 8 compares predictions of $PM_{0.1}$ made by the UCD/CIT model to concentrations measured during the comprehensive year of sampling conducted in 2015-2016 as summarized in Chapters 3-5. $PM_{0.1}$ source contributions predicted by the UCD/CIT model are compared to measured source contributions calculated using the Chemical Mass Balance (CMB) model as discussed in Chapter 5. Final UCD/CIT predictions are resolved by chemical species, source contributions, and total concentrations.

8.1 Introduction

In 1998, the U.S. National Research Council identified airborne ultrafine particles (UFPs) ($Dp<0.1$ μm) as a research priority to better protect public health from the harmful effects of air pollution [2]. Twenty years later, numerous laboratory studies have confirmed the hypothesis that UFPs are toxic [50] but the epidemiological evidence for the health effects of UFPs has been less conclusive due to inconsistencies in exposure metrics and suitable exposure assessment methods [50]. The choice of different UFP metrics (number vs. surface area vs. mass) and the presence of sharp spatial gradients in exposure fields for each of these metrics make it difficult to accurately characterize exposure to UFPs using central site monitors. More recent studies have addressed this complexity by using source-oriented Regional Chemical Transport Model (RCTM) calculations to fill in the gaps between measured UFP concentrations [39-41]. Epidemiological studies based on these calculated long-term exposures have identified robust associations between UFP and increased hazard ratios for death by ischemic heart disease [7] and robust associations between UFP and birth outcomes [8, 42] in California.

RCTMs are based on the fundamental equations of fluid mechanics, chemistry, and physics. Some of the atmospheric processes represented by these models are still areas of active research. The input data required for the RCTM calculations is complex, including a full description of the upwind boundary conditions, local emissions, meteorology, and land surface characteristics over the region of interest. Given the uncertainty inherent in the RCTM formulations and input data, predictions must be rigorously compared to independent measurements in order to confirm that theories, assumptions, and input data are sufficiently accurate for each exposure analysis. Comparisons between measured vs. predicted concentrations played a critical role in the recent successful epidemiological studies based on predicted UFP exposure fields [39-41].

The number concentration of particles with diameter larger than 7 nm (N_7) is the most commonly measured feature of atmospheric UFPs. N_7 concentrations are dominated by particles with $Dp<50$nm and so this metric is unique to the ultrafine particle size fraction. Additional UFP exposure metrics may also be equally relevant since they form the basis for potential mechanisms of injury. Surface area is an important metric because of the increased bio-availability of toxic compounds adsorbed onto the surface of UFPs. Likewise, UFP mass ($PM_{0.1}$) is a key metric due to the ability of UFPs to translocate across cell membranes and deliver doses of toxic chemicals to regions of the body that will not be reached by larger particles. UFP surface area and $PM_{0.1}$ mass tend to be correlated in space and time while N_7 follows different patterns. Thus, separate studies are required to fully evaluated exposure to N_7 vs. UFP surface area & $PM_{0.1}$.

For those UFP studies that focus on $PM_{0.1}$, receptor-oriented source apportionment techniques can be used to further evaluate the accuracy of RCTM predictions. Receptor-oriented $PM_{0.1}$ source apportionment techniques are based on the statistical models developed for $PM_{2.5}$. The chemical composition of $PM_{0.1}$ is analyzed to quantify unique molecular markers for individual sources or to characterize patterns in time that can be related back to source signatures [18, 20, 25, 94, 155]. The source contributions to $PM_{0.1}$ calculated using the measured concentrations can be compared to the source contributions predicted by source-oriented RCTMs to confirm that the model calculations are predicting the right concentrations for the right reasons.

Past comparisons between source-oriented RCTM predictions and receptor-oriented source apportionment studies for $PM_{0.1}$ have focused on intensive studies carried out over times ranging from a few weeks to a few months in limited geographical regions. A broader comparison between source-oriented RCTMs and receptor-oriented $PM_{0.1}$ source apportionment spanning a full annual cycle across California's major polluted air basins would more comprehensively evaluate the accuracy of the RCTM predictions.

The purpose of this study is to apply a source-oriented RCTM to predict the major primary particle source contributions to $PM_{0.1}$ across California and to compare those predictions to receptor-oriented source apportionment predictions based on measured concentrations. The source-oriented UCD/CIT model was used to predict daily average $PM_{0.1}$ mass and source contributions in California from August 2015-July 2016 with 4km resolution. Comparisons are made to $PM_{0.1}$ measurements made at four locations across California to provide an independent evaluation of the model accuracy. Seasonal-average receptor-oriented source apportionment calculations are performed on measurement data using the Chemical Mass Balance (CMB) model to fully evaluate the UCD/CIT source predictions to $PM_{0.1}$. The rigorous comparison of the two $PM_{0.1}$ exposure predictions will provide guidance about the most robust UFP exposure metrics in future epidemiological studies.

8.2 Methods

8.2.1 Receptor-Oriented Chemical Mass Balance Receptor Model

The Chemical Mass Balance (CMB) receptor model uses measured source concentration profiles for primary particulate matter to identify source contributions to airborne particulate matter at an ambient receptor location [171, 173-175]. $PM_{0.1}$ source composition profiles in the current are mainly based on a series of molecular markers including cholesterol (meat cooking); levoglucosan (biomass combustion); 17α(H)-21β(H)-30-Norhopane, 17α(H)-21β(H)-Hopane and αββ20R-C29-ethylcholestane (motor oil); and benzo[ghi]perylene and coronene (gasoline fuel combustion products) [18, 43]. These markers are dominated by specific individual sources with atmospheric lifetimes sufficiently long to make them useful in urban/regional source apportionment studies (1-2 days).

Traditional applications of the CMB model assume that the chemical species used in source profiles do not undergo chemical transformation between the emissions source and the receptor site and that the primary PM tracked by the calculation does not partition between the gas and particle phases. The results shown in Chapter 5 of the current study [319] show that long-term $PM_{0.1}$ source apportionment results across four cities in California can only be explained when gas-particle partitioning and chemical reactions are accounted for in the CMB calculations. The $PM_{0.1}$ source apportionment calculations discussed in the current chapter include this more complex treatment for semi-volatile reactive behavior.

The full set of $PM_{0.1}$ source profiles and the results over an annual cycle across locations are presented in Chapter 5.

8.2.2 Source-Oriented Air Quality Model

Simulations for the years 2015-2016 were carried out across California using the source-oriented UCD/CIT regional air quality model. The UCD/CIT airshed model is a reactive 3-D chemical transport model that predicts the evolution of gas and particle phase pollutants in the atmosphere in the presence of emissions, transport, deposition, chemical reaction, and phase change as represented by Eq. (8-1)

$$\frac{\partial C_i}{\partial t} + \nabla \cdot uC_i = \nabla K \nabla C_i + E_i - S_i + R_i^{gas}(C) + R_i^{part}(C) + R_i^{phase}(C)$$

$$\frac{\partial C_i}{\partial t} + \nabla \cdot uC_i = \nabla K \nabla C_i + E_i - S_i + R_i^{gas}(C) + R_i^{part}(C) + R_i^{phase}(C)$$

$$\frac{\partial C_i}{\partial t} + \nabla \cdot uC_i = \nabla K \nabla C_i + E_i - S_i + R_i^{gas}(C) + R_i^{part}(C) + R_i^{phase}(C) \tag{8-1}$$

where C_i is the concentration of gas or particle phase species *i* at a particular location as a function of time *t*, *u* is the wind vector, *K* is the turbulent eddy diffusivity, E_i is the emissions rate, S_i is the loss rate, R_i^{gas} is the change in concentration due to gas-phase reactions, R_i^{part} is the change in concentration due to particle-phase reactions and $R_i^{phase}$is the change in concentration due to phase change [320]. Loss rates include both dry and wet deposition. Phase change for inorganic species occurs using a kinetic treatment for gas-particle conversion [276] driven towards the point of thermodynamic equilibrium [277]. Phase change for organic species is also treated as a kinetic process with vapor pressures of semi-volatile organics calculated using the 2-product model [278].

The UCD/CIT model explicitly tracks the mass and the number concentration of particles in each size bin, with tracer species used to quantify source contributions to the primary particle mass in that bin. A moving sectional bin approach is used [270] so that particle number and mass can be explicitly conserved with particle diameter acting as the dependent variable.

The emissions of particle source tracers are empirically set to be 1 % of the total mass of primary particles emitted from each source category, so they do not significantly change the particle radius and the dry deposition rates. For a given source, the simulated concentration of artificial tracer directly correlates with the amount of PM mass emitted from that source in that size bin. The corresponding number concentration attributed to that source can be calculated using Eq. (8-2)

$$num_i = \frac{tracer_i \times 100}{\frac{\pi}{6} Dp^3 \rho}$$

where $tracer_i$ represents the artificial tracer mass in size bin *i*, *Dp* is the core particle diameter, and ρ is the core particle density. Core particle properties are calculated by removing any condensed species to better represent the properties of the particles when they were emitted to the atmosphere. More details describing the source apportionment technique in UCD/CIT model are provided in the previous studies [41, 260, 261, 321-323].

A total of 50 particle-phase chemical species are included in each of 15 discrete particle size bins that range from 0.01-10 µm particle diameter [235]. Artificial source tags are used to quantify source contributions to the primary particle mass for a specific bin size, therefore allowing for the direct contribution of each source of $PM_{2.5}$ and $PM_{0.1}$ mass to be determined. Gas-phase concentrations of oxides of nitrogen (NOx), volatile organic compounds (VOCs), oxidants, ozone, and semi-volatile reaction products were predicted using the SAPRC-11 chemical mechanism [230].

8.2.3 Domain Configuration

UCD/CIT simulations were configured using a one-way nesting technique with a parent domain of 24 km horizontal resolution that covered the entire state of California and a nested domain with 4 km horizontal resolution that covered the San Joaquin Valley (SJV) and the South Coast Air Basin (SoCAB). Chapter 7 illustrates the model domain configuration. Calculations used 15 telescoping vertical layers up to a top height of 5km.

8.2.4 Meteorological Fields

Meteorological fields were simulated with the Weather Research & Forecast (WRF) model v3.4 configured with three nested domains centered at 37° N, 120.5° W. The outer domain was divided into 60 × 60 grid cells with 36-km horizontal resolution. The second domain was divided into 112 × 121 grid cells with 12-km resolution. The inner-most domain was divided into 298 × 277 grid cells with 4-km resolution, which covers all of California. The 31 vertical layers from the ground level to the top pressure of 100 hPa were used for all grids. The meteorological initial and boundary conditions were taken from North American Regional Reanalysis (NARR), which has a spatial resolution of 32 km and a temporal resolution of 3 h. The Yonsei University (YSU) boundary layer vertical diffusion scheme was adopted in this study. Four-dimensional data assimilation (FDDA) was applied to anchor model predictions to observed meteorological patterns. The surface friction velocity (u*) was increased by 50% to correct for positive bias during low wind speed events that produce the highest pollution episodes.

8.2.5 Emissions

The emission inventories used in the current study were provided by the California Air Resources Board for the years 2014 and 2015. Day-specific meteorological information from the WRF model was used with the Model of Emission of Gases and Aerosols from Nature (MEGAN) [324] to estimate day-specific biogenic emissions. The gridded geo-referenced emission factors and land cover variables required for MEGAN calculations were created using the MEGANv2.1 pre-processor tool and the ESRI_GRID leaf area index and plant functional type files available at the Community Data Portal [325]. Daily values of wildfire emissions were generated using the Global Fire Emissions Database (GFED) [237]. Residential wood smoke emissions were updated by considering POA evaporation and wood burning control policies applied in California [326]. These updates reduced the effective residential wood smoke primary organic aerosol (POA) emissions by 50% in all years compared to the basecase inventories, and better represent long-term trends in wood smoke emissions. Mobile source emissions were scaled in 69 regions throughout California based on the Emissions Factor (EMFAC) v2014 using day-specific meteorology from WRF. The source profile for aircraft emissions was updated based on recent measurements. The particulate matter emissions from residential natural gas combustion were set to zero under the assumption that these particles evaporated upon dilution in the atmosphere. Subsequent direct measurements of natural gas combustion emissions at increasing dilution factors revealed that the ultrafine particles emitted by this source will not completely evaporate [193] but this change could not be incorporated into the current study given the long time required for the simulations. Basecase fugitive dust emissions were replaced by an online dust model [327] based on the wind speed, and soil moisture predicted by the WRF model. This change corrects the positive bias in dust emissions and PM2.5 mass noted by Hu et al. [39, 328].

8.2.6 Boundary Conditions

The gas and particle phase initial and hourly varying boundary conditions for the UCD/CIT model were taken from the global model MOZART-4/NCEP (a model for ozone and related chemical Tracers). Additional details of MOZART simulations are provided by Emmons et al. [329].

8.3 Results

8.3.1 Source-Oriented Model Performance Evaluation

Measured concentrations for criteria air pollutants are compared to predicted daily-average concentrations over a 17 year period from 2000 – 2016 in Chapter 9. This long-term analysis encompasses the one year simulation period (August, 2015-July, 2016) used in the current Chapter.

Section 9.3.1 summarizes the results of these comparisons for individual species. Looking across the full 17 year period, $PM_{2.5}$ species and gas species were found to be in reasonable agreement with measured ambient concentrations, with an overall MFB within ± 0.5 and MFE < 0.75 meeting the criteria typically used for regulatory $PM_{2.5}$ modeling applications. The available measured number concentrations of airborne particles with diameter greater than 7 nm (N_7) were also found to have acceptable agreement with predicted number concentrations of particles with diameter greater than 10 nm (N_{10}).

In the current chapter, model predictions are compared to the measured UFP mass ($PM_{0.1}$) collected over twelve months at three cities in California: Los Angeles, East Oakland, San Pablo, and over six months at Fresno. A description of the measurement locations and sampling method is provided in Chapter 5. The performance statistics in Table 8-1 show that predicted $PM_{0.1}$ EC and $PM_{0.1}$ OC concentrations are in good agreement with measurements at San Pablo, East Oakland and Los Angeles with MFB within ± 0.5 and MFE < 0.75. Predicted $PM_{0.1}$ EC concentrations are significantly lower than measured values at Fresno, possibly because of construction activities immediately around the sampling location that were not represented in the emissions inventory.

Table 8-1. MFB and MFE for PM0.1 EC and PM0.1 OC in 2015-2016.

Location (Date Range)	**UFP Metric**	**MFB**	**MFE**
$PM_{0.1}$ Evaluations			
San Pablo (2015.07-2016.07)	$PM_{0.1}$OC	0.21	0.41
	$PM_{0.1}$ EC	-0.15	0.45
East Oakland (2015.07-2016.07)	$PM_{0.1}$OC	0.41	0.48
	$PM_{0.1}$ EC	-0.29	0.54
Los Angeles (2015.08-2016.07)	$PM_{0.1}$OC	0.29	0.45
	$PM_{0.1}$ EC	-0.23	0.47
Fresno (2015.12-2016.07)	$PM_{0.1}$OC	-0.29	0.37
	$PM_{0.1}$ EC	-1.60	1.62

Figure 8-1 shows predicted $PM_{0.1}$ EC+OC concentrations are in good agreement with measured values at all times and locations except Fresno. The model consistently under-predicted $PM_{0.1}$ OC and EC concentrations at Fresno indicating that the potential emissions bias was a factor over the entire study period. This issue is not apparent at the other measurement locations, with generally good agreement observed over the annual study cycle. The model calculations correctly predict seasonal trends, with higher concentrations in the winter months and lower concentrations in the summer months. These seasonal trends reflect the increased fuel combustion for winter heating combined with reduced atmospheric mixing in winter. The general agreement between model predictions and measurements at three out of four measurement sites increases confidence in the source apportionment analysis of ultrafine PM carried out in the current study.

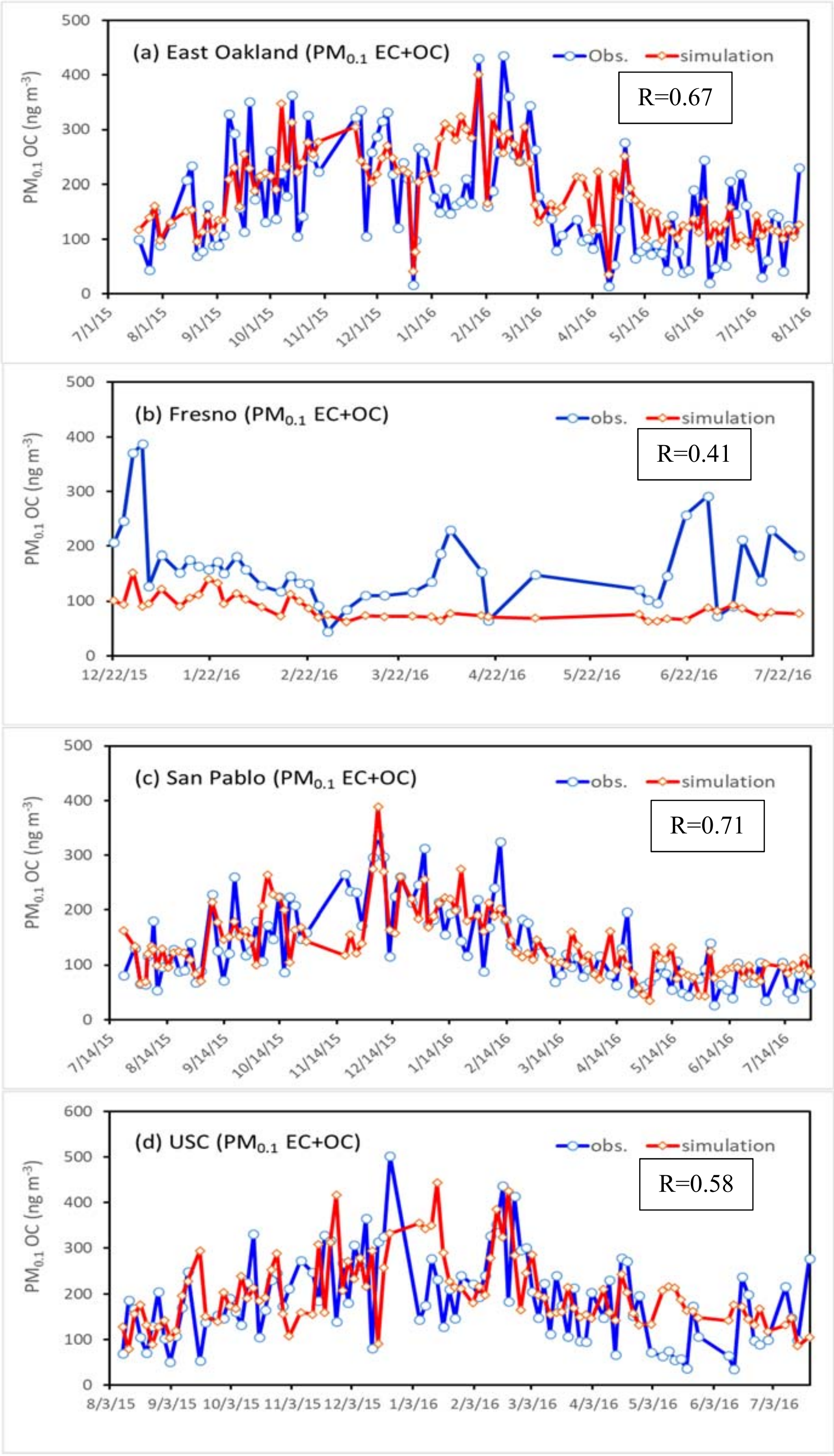

Figure 8-1 Predicted VS. measured PM$_{0.1}$ EC+OC at San Pablo, Fresno, East Oakland, and LA downtown during the sampling period.

8.3.2 *Comparison between source-oriented UCD/CIT vs. receptor-oriented CMB results*

Figures 8-2 and 8-3 summarize the comparison between the annual-average source contributions to $PM_{0.1}$ OC and $PM_{0.1}$ EC concentrations predicted by the UCD/CIT model and the CMB model at San Pablo (SP), East Oakland (EO), LA downtown (LA) and Fresno sites (FR). Source contributions to $PM_{0.1}$ OC and $PM_{0.1}$ EC predicted by the UCD/CIT model and the CMB model are generally in good agreement. Food Cooking and mobile sources (gasoline + diesel) are the largest two $PM_{0.1}$ OC sources at San Pablo, East Oakland and LA downtown. The regions surrounding these sites have the highest population density in California leading to intensive emissions from local mobile, residential, and commercial sources. Residential wood combustion dominates $PM_{0.1}$ OC at the Fresno site, followed by food cooking. Diesel engine contributions to $PM_{0.1}$ OC predicted by the UCD/CIT model are lower than the values predicted by the CMB model at Fresno reflecting the uncertainty in the emissions inventory for this source type in Fresno region.

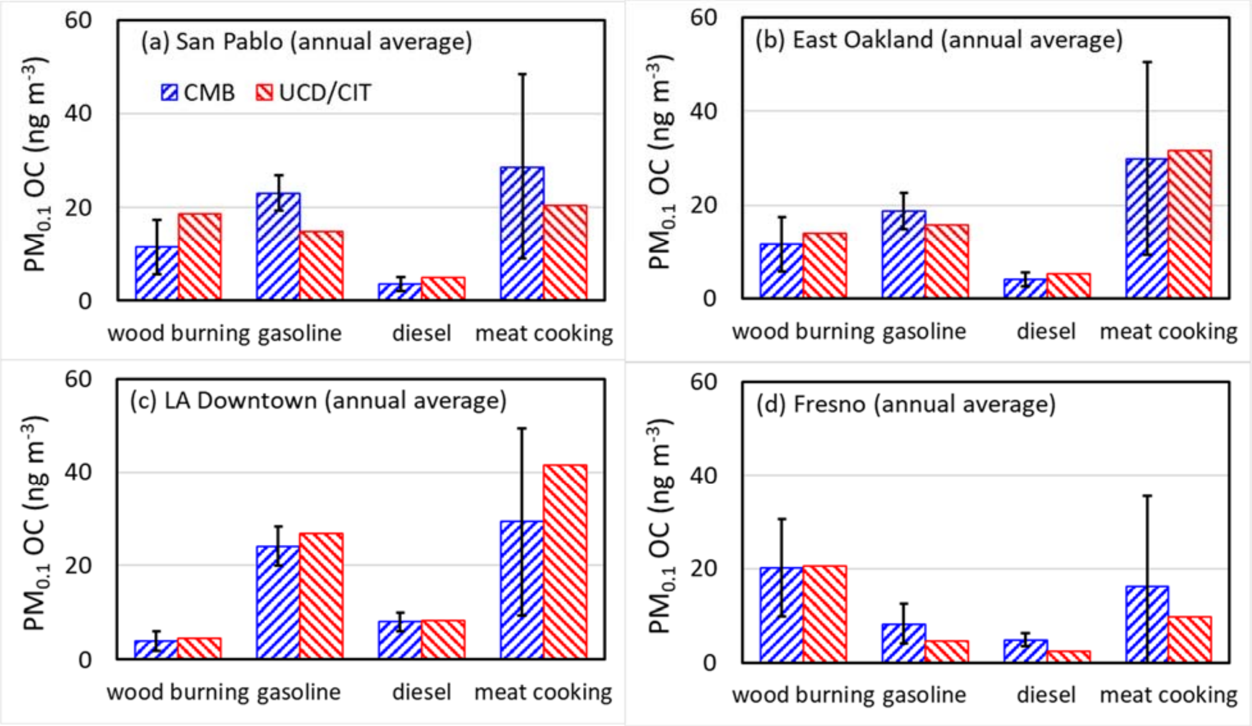

Figure 8-2 Predicted annual-average $PM_{0.1}$ OC source contributions at San Pablo, East Oakland, LA Downtown, and Fresno. Error bar represents uncertainty in CMB results.

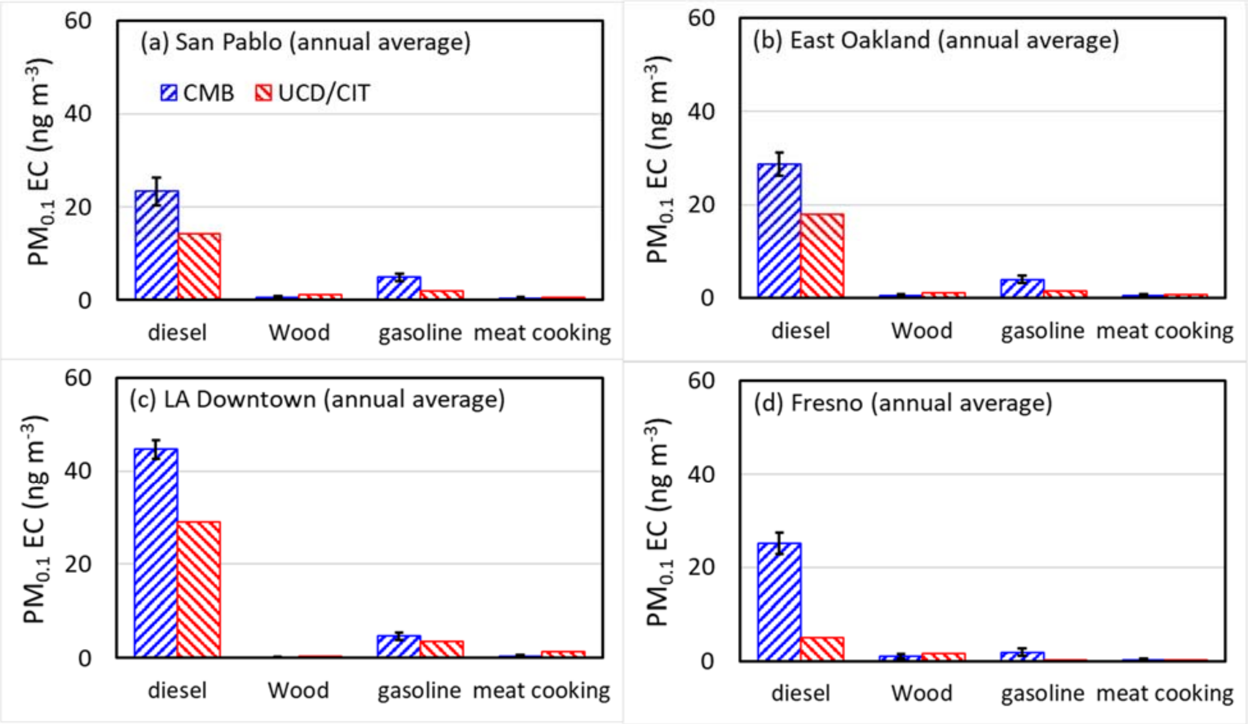

Figure 8-3 Predicted annual-average $PM_{0.1}$ EC source contributions at San Pablo, East Oakland, LA Downtown, and Fresno. Error bar represents uncertainty in CMB results.

Figures 8-4 through 8-7 show seasonal source contributions to $PM_{0.1}$ OC at the individual measurement sites. Seasonal trends in $PM_{0.1}$ from wood burning predicted by UCD/CIT model are similar to those calculated using the CMB model. Wood burning $PM_{0.1}$ concentrations peak in winter when heating demand increases and atmospheric mixing height decreases. $PM_{0.1}$ associated with all sources increase during the winter due to this reduced mixing effect but the magnitude of the winter enhancement is not as great since these other sources have relatively constant activity through the entire year as opposed to the increased activity of wood combustion during the winter.

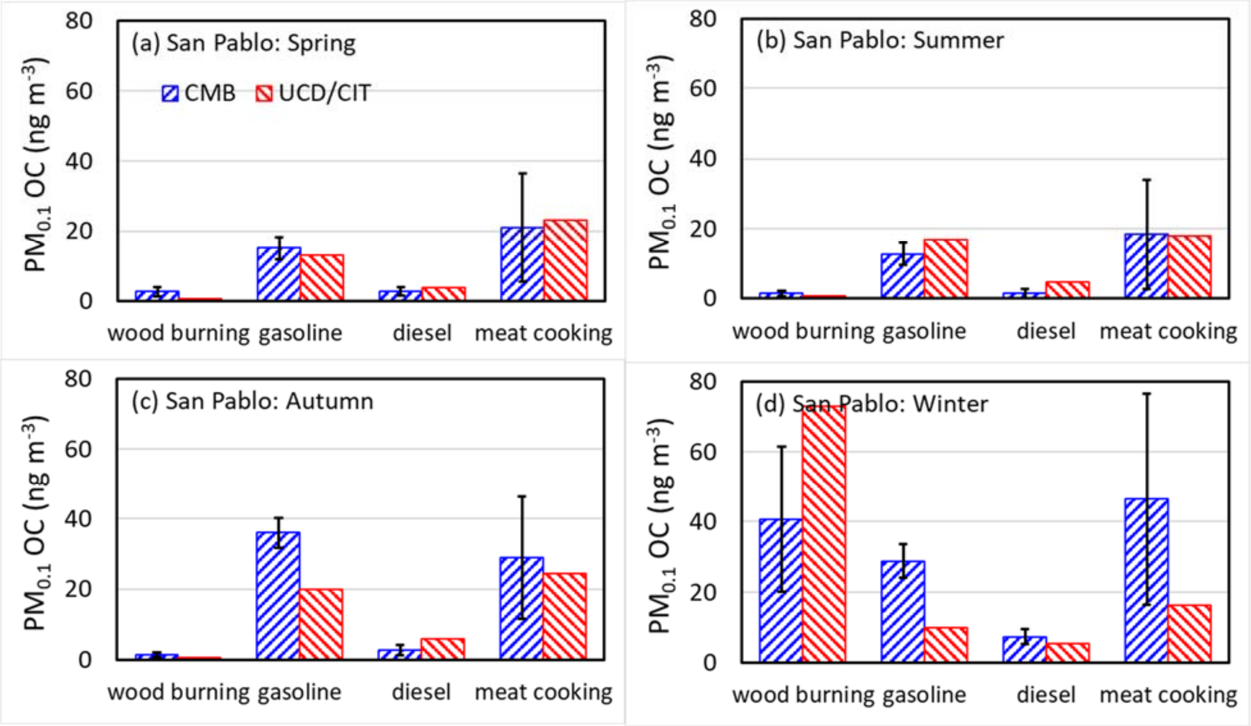

Figure 8-4 Source contributions to $PM_{0.1}$ OC predicted by the UCD/CIT model and the CMB model as a function of season at the San Pablo site

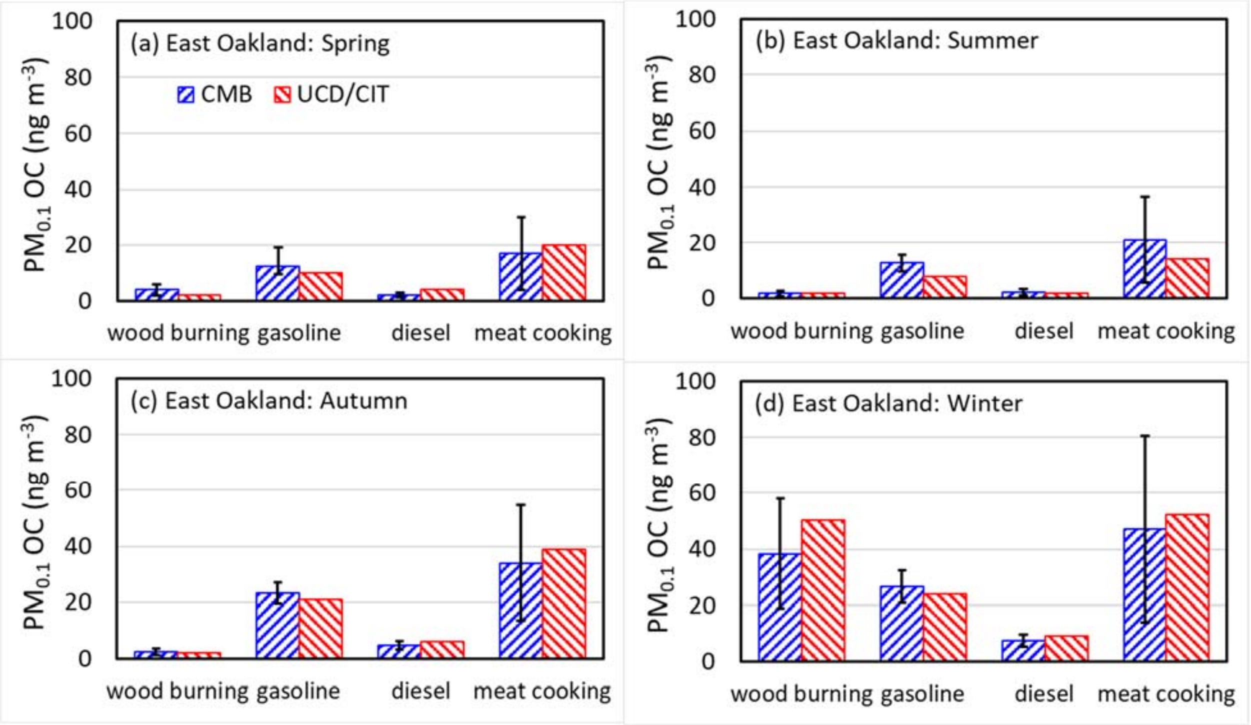

Figure 8-5 Source contributions to $PM_{0.1}$ OC predicted by the UCD/CIT model and the CMB model as a function of season at the East Oakland site

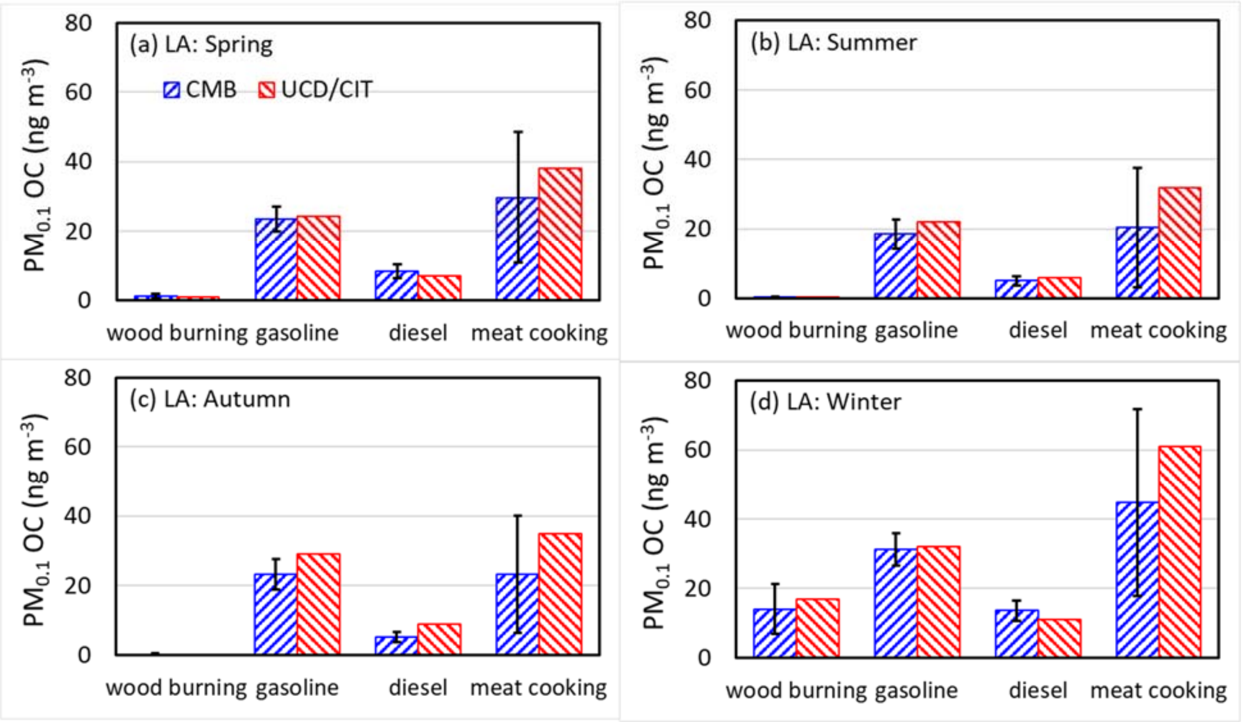

Figure 8-6 Source contributions to $PM_{0.1}$ OC predicted by the UCD/CIT model and the CMB model as a function of season at the central Los Angeles site

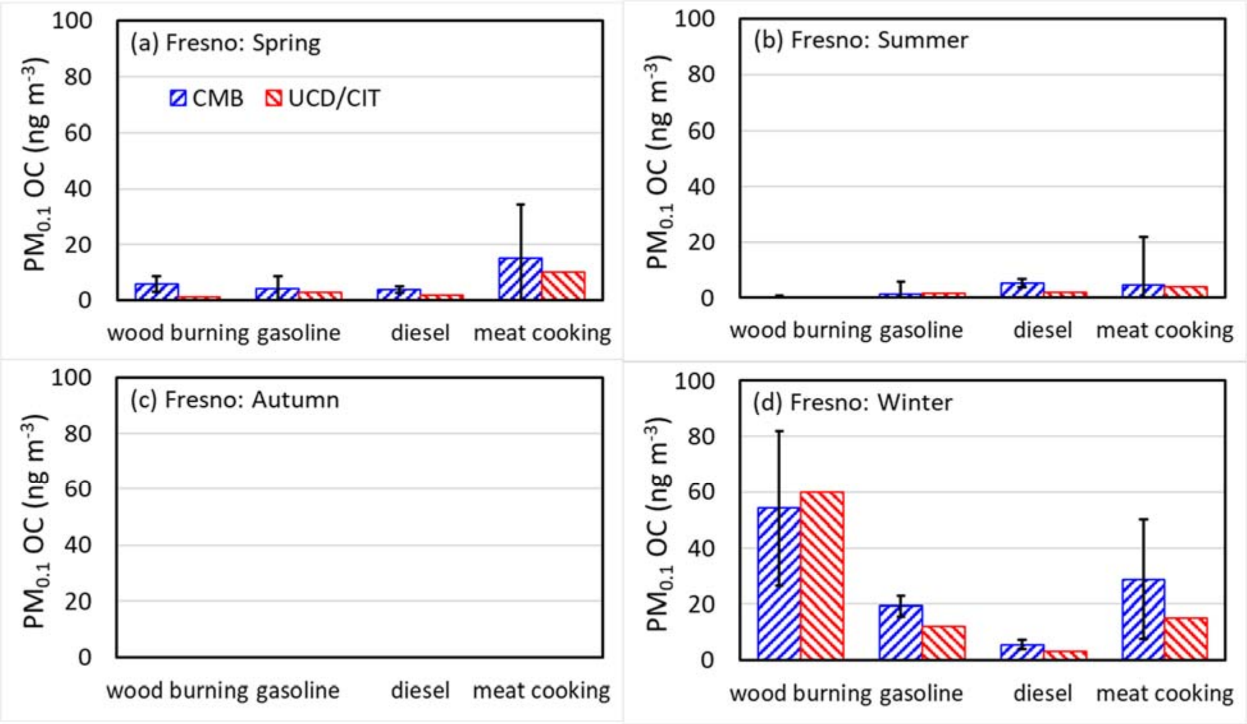

Figure 8-7 Source contributions to $PM_{0.1}$ OC predicted by the UCD/CIT model and the CMB model as a function of season at the Fresno site

Figures 8-8 through 8-11 show seasonal source contributions to $PM_{0.1}$ EC at the individual measurement sites. Diesel engines are predicted to be the single largest source of $PM_{0.1}$ EC in both CMB and UCD/CIT calculations, accounting for +70% of the total $PM_{0.1}$ EC concentration. Diesel contributions predicted by UCD/CIT model are lower than the values estimated by CMB model, especially during the winter months. It should be noted that the CMB calculations assume that any EC not attributed to gasoline fuel combustion, motor oil, food cooking, and biomass combustion must be associated with diesel engine exhaust. This has the potential to over-estimate the diesel $PM_{0.1}$ EC concentrations in CMB calculations if other sources of EC are present in the real atmosphere.

There are two immediate explanations for the under-prediction of diesel $PM_{0.1}$ EC by the UCD/CIT model displayed in Figures 8-8 through 8-11. It is possible that the WRF meteorological model over-predicted wind speeds more severely during winter stagnation events than summer stagnation events. The over-predicted wind speeds would provide too much dilution leading to an under-prediction of the $PM_{0.1}$ EC concentrations. Similar concentration biases would develop for other pollutants in this case, but a consistent pattern of $PM_{0.1}$ OC under-predictions is not apparent in Figures 8-4 through 8-7. A second explanation is that there is some other source of $PM_{0.1}$ EC present in winter that is not represented in emissions inventories. Possible sources that could emit more $PM_{0.1}$ EC during colder winter months include gasoline-powered vehicles that have significantly higher cold-start emissions than hot-running emissions. A comprehensive exploration of these issues is beyond the scope of the current project, but they will be investigated in future studies.

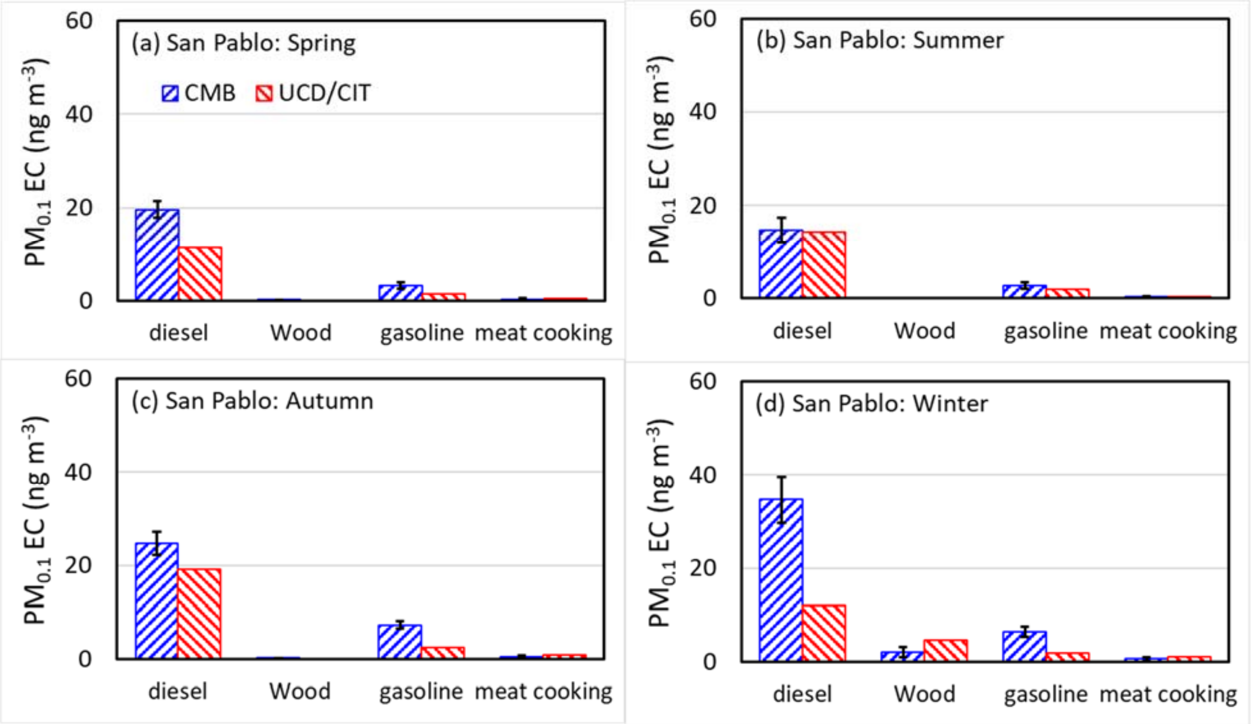

Figure 8-8 Source contributions to $PM_{0.1}$ EC predicted by the UCD/CIT model and the CMB model as a function of season at the San Pablo site

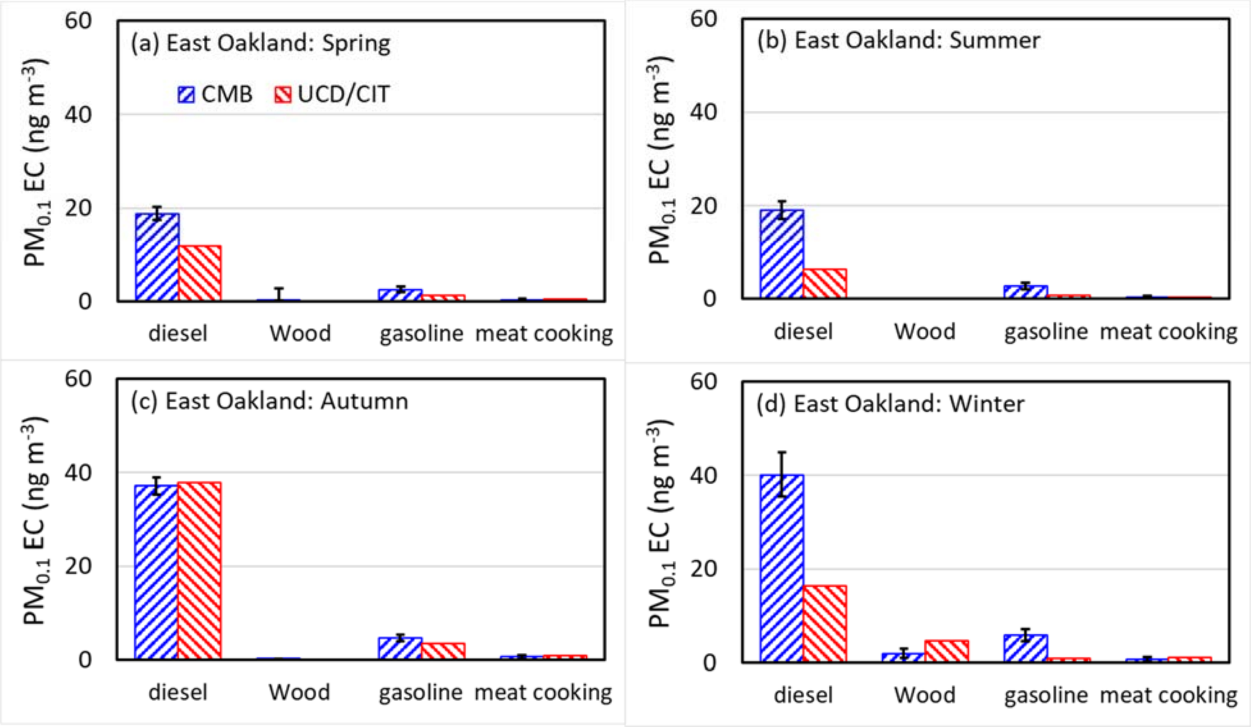

Figure 8-9 Source contributions to $PM_{0.1}$ EC predicted by the UCD/CIT model and the CMB model as a function of season at the East Oakland site

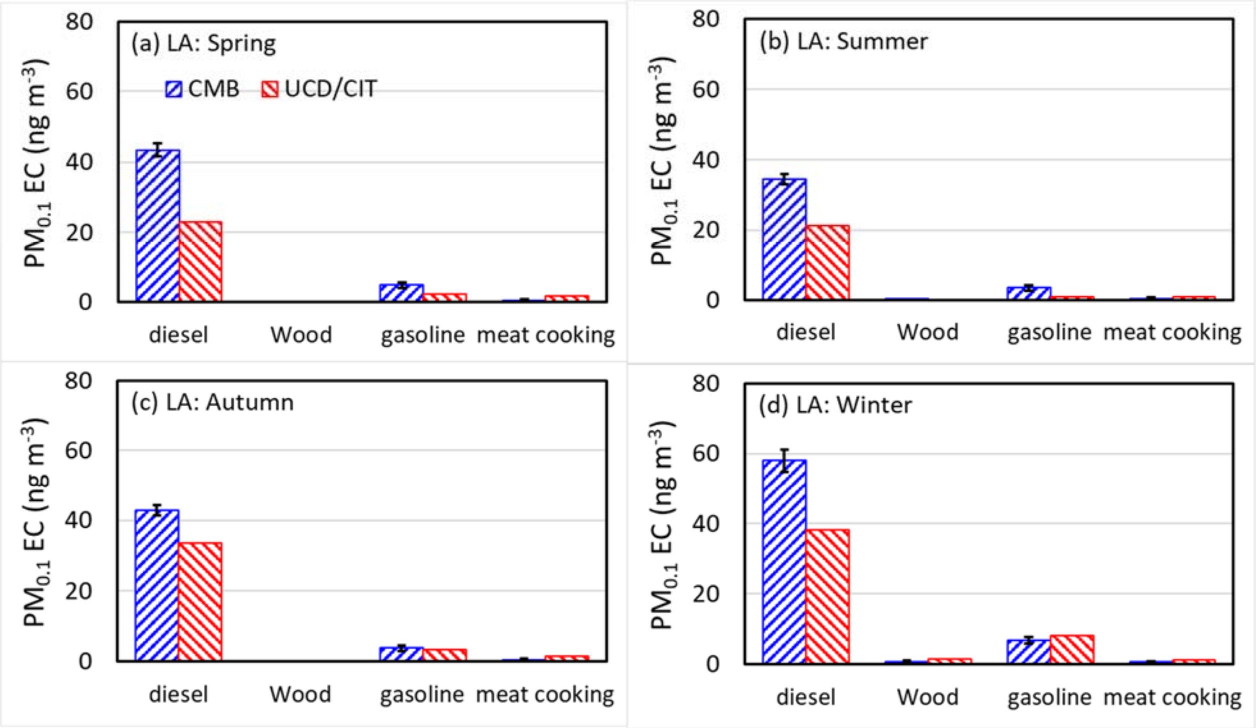

Figure 8-10 Source contributions to PM$_{0.1}$ EC predicted by the UCD/CIT model and the CMB model as a function of season at the LA downtown site

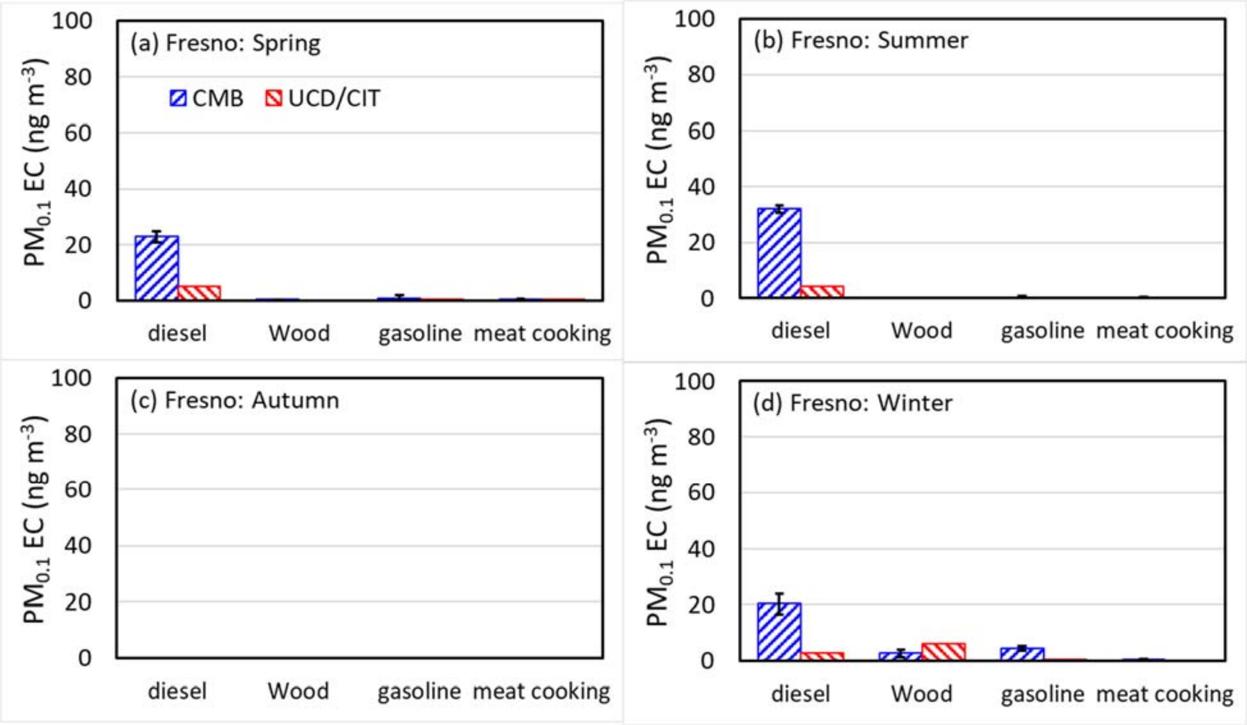

Figure 8-11 Source contributions to PM$_{0.1}$ EC predicted by the UCD/CIT model and the CMB model as a function of season at the Fresno site

Despite the issues identified for winter $PM_{0.1}$ EC concentrations, the general agreement in the source contributions from the mobile, wood burning and meat cooking source categories predicted by the UCD/CIT and the CMB method provides confidence in the accuracy of the UCD/CIT source appointments results.

8.3.3 Temporal Variation of $PM_{0.1}$ Source Contributions

Figure 8-14 show the monthly variation of nine types of major source contributions to primary $PM_{0.1}$ mass concentrations at the LA downtown and San Pablo sites. Natural gas combustion is the biggest primary PM source at LA downtown and San Pablo sites, with higher values during the cold months and lower values in the warm months. Wood smoke is the second largest source at San Pablo site during the winter months. Wood smoke concentrations decrease sharply in spring, summer, and fall months. Mobile source (gasoline + diesel) is the second largest source at LA downtown site, followed by food cooking. The different ranking of source contributions to ultrafine particles at Los Angeles and San Pablo may be informative for health-source apportionment studies at a regional or larger scale.

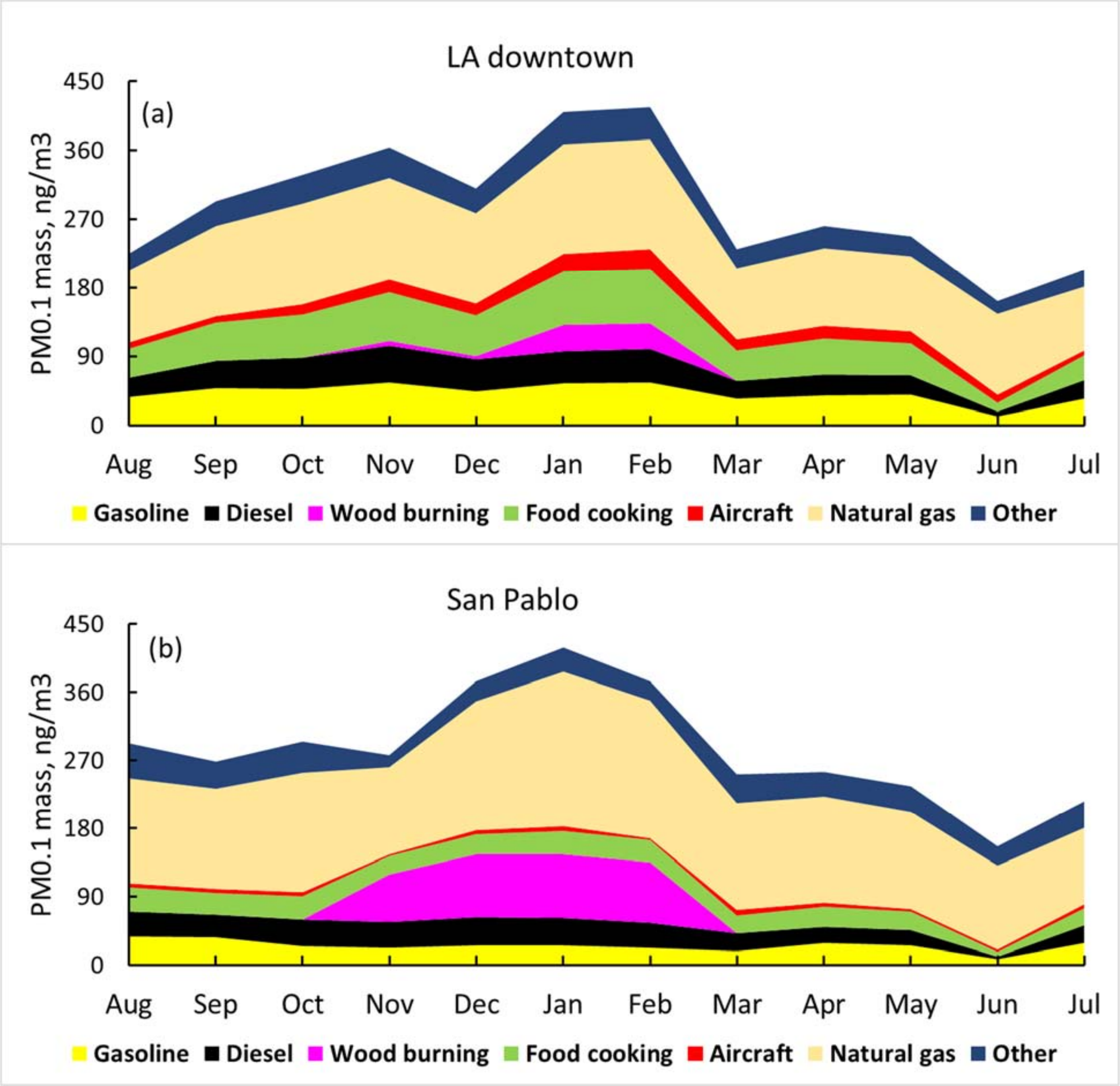

Figure 8-12 Monthly variations of predicted source contributions from nine major sources to primary $PM_{0.1}$ *mass at the LA downtown and San Pablo sites.*

8.3.4 Spatial Distribution of $PM_{0.1}$ *Source Contributions*

Figure 8-16 shows predicted source contributions to yearly average $PM_{0.1}$ concentrations. The spatial patterns of $PM_{0.1}$ concentrations associated with different sources varies significantly. $PM_{0.1}$ from on-road mobile (figure 8-16a) and on-road diesel (figure 8-16c) sources follows the pattern of major transportation corridors, with the highest values predicted in urban areas such as San Francisco and Los Angeles. $PM_{0.1}$ from off-road engines (figure 8-16b and figure 8-16d) are also high in urban areas, especially around construction projects. Wood burning $PM_{0.1}$ is concentrated in the urban residential areas of northern California and the coastal areas of Southern California. Wildfires do not dominate the long-term average biomass combustion $PM_{0.1}$ concentrations during the current study period, although increased wildfire activity in the future could alter this pattern. Food cooking $PM_{0.1}$ is mainly located in the urban area of San Francisco and Los Angeles which have the highest population density in California. Aircraft $PM_{0.1}$ is concentrated around major military airports in California with lower concentrations around civilian airports. This pattern reflects the continued use of military jet fuel with higher sulfur content than civilian jet fuel. Natural gas combustion $PM_{0.1}$ concentrations peak in the region around natural gas power plants and in urban areas of San Francisco and Los Angeles that have numerous commercial and industrial sources. The $PM_{0.1}$ source apportionment fields provide useful exposure estimates for future epidemiological studies.

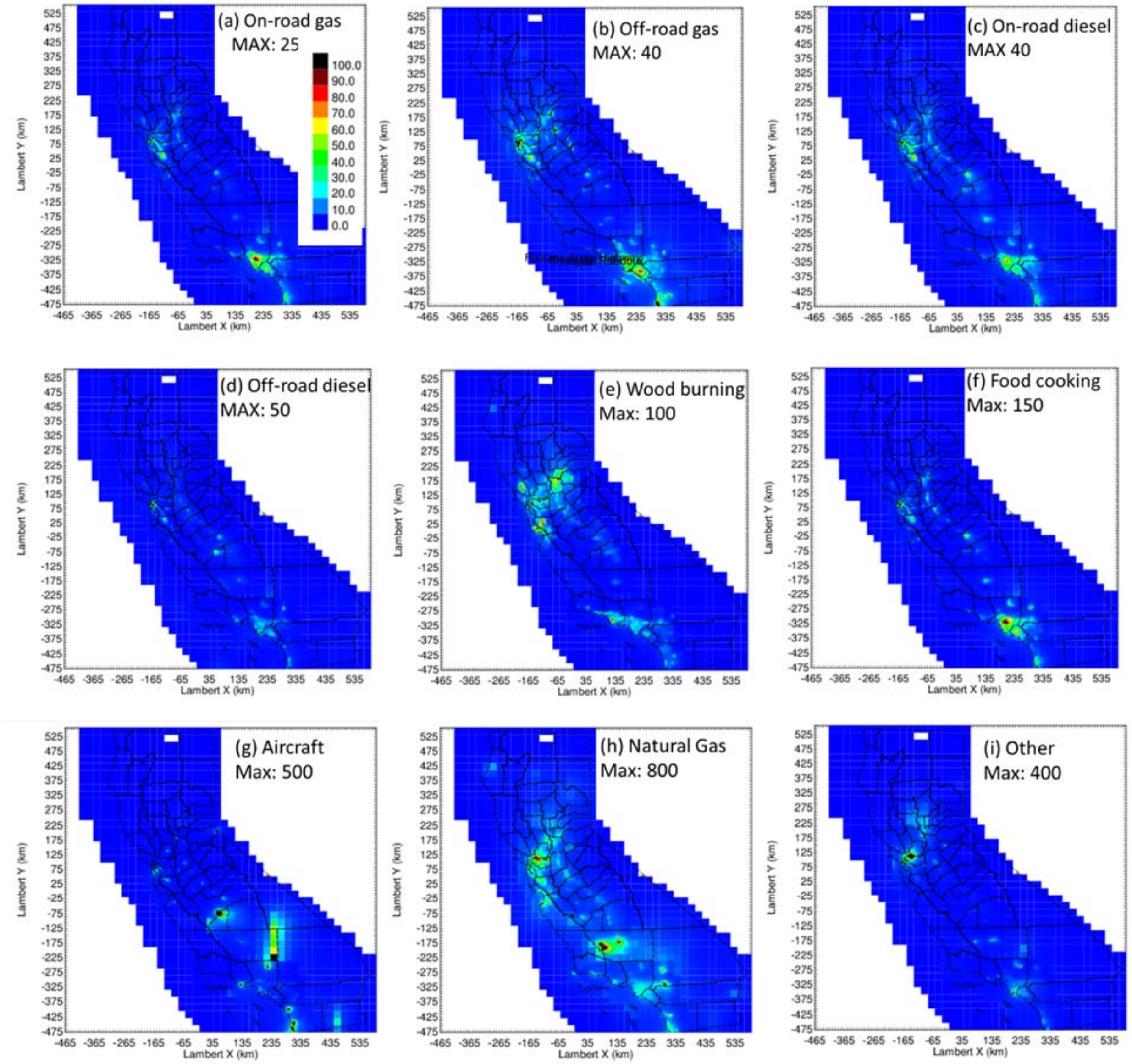

Figure 8-13 Predicted source contributions to annual-average $PM_{0.1}$ concentrations in 2015-16. The color scales indicate the percentage of the maximum concentrations displayed in the title of each panel. Units are (ng m^{-3}).

8.4 Conclusions

The UCD/CIT air quality model was used to predict $PM_{0.1}$ concentrations over California for a one year period (August 2015-July 2016) with 4km spatial resolution. Predicted concentrations were compared to measurements made at four monitoring sites in major cities across the state. Absolute concentrations of $PM_{0.1}$ OC and $PM_{0.1}$ EC meet the performance guidelines normally required for regulatory modeling of $PM_{2.5}$. The source contributions to $PM_{0.1}$ mass predicted by the UCD/CIT model are in general agreement with the source contributions calculated from measured concentrations using the CMB model. The seasonal trends in source contributions to $PM_{0.1}$ OC are also generally predicted correctly, but there is evidence that the UCD/CIT model does not capture all of the source contributions to $PM_{0.1}$ EC during the winter season.

The UCD/CIT air quality model quantified nine sources of primary $PM_{0.1}$ mass across California compared to only four sources resolved by CMB calculations. The UCD/CIT predictions may therefore suggest the identity of the unresolved sources in the CMB calculations for $PM_{0.1}$. Leading candidates for these missing $PM_{0.1}$ sources include natural gas combustion and aircraft emissions. Both the UCD/CIT and CMB models predict that mobile sources are an important but not dominant source of $PM_{0.1}$ in California. Wood burning, food cooking and natural gas combustion all make significant contributions to regional $PM_{0.1}$ concentrations.

Overall, the general agreement between the UCD/CIT and CMB model calculations across three major urban areas builds confidence that the $PM_{0.1}$ exposure fields predicted by the UCD/CIT model will provide reasonable accurate exposure assessments for future epidemiological studies.

9 PREDICTED LONG-TERM TRENDS IN ULTRAFINE PARTICLE NUMBER AND MASS CONCENTRATIONS IN CALIFORNIA: 2000-2016

Preamble: Chapter 9 summarizes predictions made by the UCD/CIT model for long-term trends in regional ultrafine particle concentrations in California. Predictions are resolved by chemical species, source contributions, and total concentrations. Comparisons are made to the historical measurements summarized in Chapter 2.

9.1 Introduction

Despite the identification of airborne ultrafine particles (UFPs; $Dp<0.1$ μm) as a high-priority research topic over 20 years ago [2], the public health threat associated with UFPs is still not in clear focus. UFPs are toxic in laboratory tests [152-154] but the evidence from past epidemiological studies is not conclusive [50]. New exposure methods [39-41] have addressed some of the difficulties associated with UFPs, and more recent epidemiological studies have consistently found increased risk of adverse health outcomes associated with UFPs [7, 8, 42]. Thus, it appears that UFPs play a role in the overall health risks associated with air pollution. The exposure patterns and long-term trends associated with UFPs therefore merit consideration.

Air quality in California and across the United States has steadily improved over the past decades due to the success of emissions control programs. $PM_{2.5}$ concentrations have decreased at a rate of XX% yr^{-1} in California since the year ~2000 when consistent network monitoring began, but a comparable record of network measurements for UFP concentrations is not available. The review and analysis of intensive field campaigns presented in Chapter 2 suggests that there are important long-term trends in ambient UFP concentrations that are changing exposure fields and potential health effects. The public health consequences of these trends can only be evaluated if exposure fields are developed to properly represent these trends.

The purpose of this chapter is to predict long-term trends in UFP concentrations between the years 2000 – 2016 using the techniques developed to estimate exposure fields in recent successful epidemiological studies [39-41]. Daily-average UFP concentrations are predicted over the 17 year study period using a regional chemical transport model (RCTM) with 4km resolution. Predicted concentrations are compared to the historical record of intensive UFP measurements and to a full year of 3-day average UFP measurements made at four monitoring sites in 2015 - 2016. The accuracy of predicted total UFP concentrations and source-resolved UFP concentrations are evaluated during periods when measurements are available. The long-term trends in UFP concentrations are then discussed along with implications for public health.

9.2 Methods

9.2.1 Air Quality Model

Simulations for the years 2015-2016 were carried out across California using the source-oriented UCD/CIT regional air quality model that predicts the evolution of gas and particle phase pollutants in the atmosphere in the presence of emissions, transport, deposition, chemical reaction, and phase change (condensation/evaporation/nucleation). Section 8.2 provides a detailed description of the model formulation, the general input data, and the configuration for the regional UFP simulations. Details specific to the long-term UFP simulations are summarized in the following sections.

9.2.2 Anchor Year Inventories

Basecase emissions inventories were provided by the California Air Resources Board for the anchor years 2000, 2010, and 2015. General area and point source emissions are resolved by month of year and day of week to capture important seasonal and day-of-week patterns. The twenty largest sources of ultrafine particulate matter emissions were identified within each of these inventories and emissions in intermediate years were interpolated in time for each of these major sources. Emissions from minor sources were assigned using values from the preceding anchor year except as noted in the sections below.

9.2.3 Mobile Source Emissions

Mobile source emissions were scaled in 69 regions throughout California based on the Emissions Factor (EMFAC) v2014 using day-specific meteorology from WRF. Scaling factors were derived for each EMFAC region by comparing results from the anchor year to results from the target year. These factors simultaneously account for emissions changes caused by the evolving vehicle fleet distribution and emissions changes caused by day-specific meteorology. The unique scaling factors for each of the 69 EMFAC regions were applied to all of the 4km model grid cells contained in that region. The anchor year mobile source inventories were selected based on month of year and day-of-week to appropriately represent time trends.

Gas Direct Injection (GDI) gasoline vehicles were assumed to penetrate the light duty vehicle fleet starting in 2007 based on market share information. GDI vehicles have higher PM emissions rates and higher EC content than corresponding PFI vehicles. EMFAC accounts for the change in PM emissions rates associated with GDI adoption but not for the resulting change in the composition of emitted particles. In the current study, modified PM emissions profiles for on-road gasoline vehicles were constructed for each simulation year using measurements from Port Fuel Injection (PFI) and GDI vehicles weighted by market share.

9.2.4 Diesel Particle Filters

Diesel particle filters (DPFs) reduce particulate matter emissions from diesel engines by +98% by oxidizing all of the carbonaceous material contained in the particles [330]. The EMFAC v2014 model was used to scale on-road diesel emissions to account for the adoption of DPFs using the procedures described in the previous section. EMFAC describes PM emissions rates but does not account for the change in the composition of emitted particles. The PM emissions from diesel engines equipped with a DPF have low carbon content and higher concentrations of residual components such as sulfate [330]. These changes are important when viewed per unit of emitted PM mass, but fleet average emissions profiles are dominated by the diesel vehicles that do not have DPFs installed. The majority of the effect from DPF adoption was therefore captured by the EMFAC scaling, with a minor contribution from the altered diesel PM profile for the residual ~2% of PM emissions.

9.2.5 Residential Wood Burning

The San Joaquin Valley Unified Air Pollution Control District (SJVUAPCD) implemented programs to curtail wood burning in communities with natural gas service below 3000 feet elevation beginning in the year 2003. The Bay area Air Quality Management District (BAAQMD) adopted a wood burning device rule in 2008. The Sacramento Metropolitan Air Quality Management District (SMAQMD) also enacted curtailment programs for wood burning between 2008-2011. The effectiveness of these programs is difficult to assess and so the resulting changes to the wood burning emissions inventory are uncertain.

In the current study, a multi-linear regressions model was developed to predict wood burning emissions between 2003-2009 based on measured temperature, humidity, and natural gas consumption. Ambient $PM_{2.5}$ potassium (K) measurements were used as an indicator for wood smoke concentrations. The model assumes that heating load is correlated to meteorological conditions and that heat is only supplied by natural gas or by wood combustion. The seasonal-average scaling factors predicted by the regression model were applied to the year 2000 wood burning emissions as summarized in Table 9-1 below. Wood smoke emissions are predicted to decline gradually in the initial years of the curtailment program with eventual decreases of approximately 90% in the later years.

Table 9-1. Wood burning scaling factors applied to year 2000 emissions for each target year.

Target Year	Scaling Factor Applied to Year 2000 Emissions*
2000-2002	1.00
2003	0.86
2004	0.93
2005	0.52
2006	0.25
2007	0.02
2008	0.12
2009	0.12

*Scaling factors reflect both the meteorological conditions for the indicated year and the effectiveness of curtailment efforts.

The $PM_{0.1}$ measurements and source apportionment studies summarized in Chapter 5 strongly suggest that particulate organic carbon emitted from biomass combustion is semi-volatile, with roughly 50% of the emissions evaporating under typical ambient conditions. In the current study, the OC emitted in wood smoke was reduced by 50% to represent the effects of this evaporation process. These reductions are combined with the overall wood smoke emissions reductions summarized in Table 9-1 since the potassium concentrations used to derive the regression equations are non-volatile and therefore reflect only the wood burning activity level, not the subsequent gas-particle partitioning of the exhaust particles. The 50% of the residual wood smoke OC that did not evaporate after atmospheric dilution was assumed to be non-volatile in the UCD/CIT calculations.

9.2.6 Wildfires

Daily values of wildfire emissions were generated using the Global Fire Emissions Database (GFED) [237]. Wildfire emissions were assigned the same particle size and composition distribution as routine biomass combustion. Typical wildfire plumes rise to 6-10 km in the atmosphere depending on the intensity of the fire and the local meteorological conditions [331]. Wildfire plumes were injected at the top of the model domain at a height of approximately 5 km in the current simulations. Future studies will evaluate the sensitivity of the plume-rise treatment but this analysis is beyond the scope of the current report.

9.2.7 Natural Gas Combustion

Natural gas combustion exhaust was tracked separately in model calculations to quantify the contributions that this source makes to ambient ultrafine particulate matter. Natural gas combustion emissions were scaled each year based on statewide consumption data available from the United States Energy Information Administration (www.eia.gov). Figure 9-1 summarizes the natural gas combustion scaling factors applied to the year 2000 emissions to represent the years 2000-2009. Residential and Commercial / Industrial natural gas combustion emissions both peak during the colder winter months. Residential natural gas combustion emissions decrease significantly during warmer summer months due to the decline in heating demand. Commercial / industrial natural gas combustion emissions also decrease during the summer but not as severely as residential emissions. Natural gas combustion emissions for electricity production increase during the summer as demand for air conditioning increases with warmer temperatures.

Natural gas combustion emissions in years 2010 and later were represented using the month of year and day of week emissions presented in the preceding anchor emissions inventory.

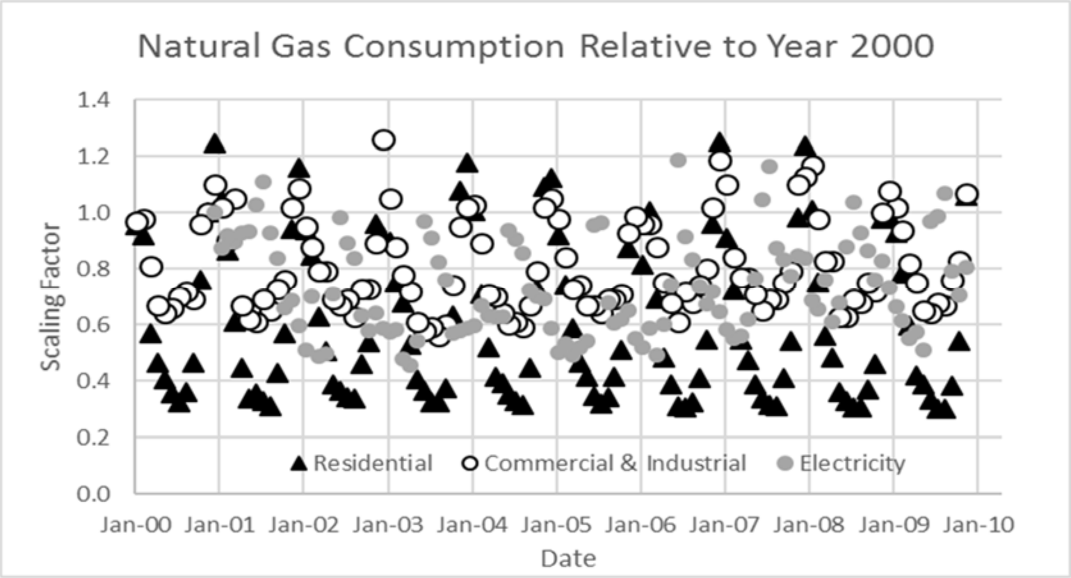

Figure 9-1: Natural gas combustion scaling factors applied to year 2000 emissions for each target year. Information from the United States Energy Information Administration.

The size distribution of natural gas combustion emissions was measured in laboratory experiments to confirm the accuracy of the source profiles used in model calculations [193]. Emissions dilution experiments indicated that residential natural gas combustion particles will partially evaporate after release to the atmosphere. Residential natural gas combustion particle emissions were reduced by 70% to represent the effects of this evaporation process. The residual natural gas combustion OC was assumed to be non-volatile in the UCD/CIT model calculations.

9.2.8 Soil NOx

Candidate soil NOx emissions were included in the calculations based on a biogeochemical model combined with fertilizer application rates [332]. Soil NOx emissions varied by month of the year based on the effects of temperature on the biogeochemical cycle. Sensitivity studies carried out across years between 2000 – 2015 indicate the inclusion of soil NOx emissions improves the accuracy of model predictions for gas phase ozone and particulate nitrate [333].

9.3 Results

9.3.1 Model Performance Evaluation

Mean fractional bias (MFB) and mean fractional error (MFE) were calculated to evaluate UCD/CIT model performance in space and time for key gas-phase species and particle-phase species in multiple size fractions.

$$\mathrm{MFB} = \frac{2}{N}\sum_{i=1}^{N}\frac{(Pred_{x,t}^{i}-Obs_{x,t}^{i})}{(Pred_{x,t}^{i}+Obs_{x,t}^{i})} \tag{1}$$

$$\mathrm{MFE} = \frac{2}{N}\sum_{i=1}^{N}\frac{|Pred_{x,t}^{i}-Obs_{x,t}^{i}|}{(Pred_{x,t}^{i}+Obs_{x,t}^{i})} \qquad (2)$$

Boylan and Russell [288] proposed concentration-dependent MFB and MFE performance goals and criteria. Performance goals define the maximum level of accuracy that a model can be expected to achieve. Performance criteria define the acceptable level of accuracy for standard $PM_{2.5}$ modeling applications (MFB< ± 0.5 and MFE < 0.75).

Figures 9-2 and 9-3 show the MFB and MFE values for $PM_{2.5}$ mass, $PM_{2.5}$ EC, $PM_{2.5}$ OC, $PM_{2.5}$ nitrate, $PM_{2.5}$ sulfate, $PM_{2.5}$ ammonium, and gaseous species of O_3, CO, NO, NO_2, and SO_2 using daily, monthly, and yearly averages across all sites in the 4 km domains during the entire 17-year study period. The factors that affect the accuracy of the predicted concentrations for these species also affect the accuracy of the predicted concentrations for ultrafine particles. Daily-average concentrations of all species except SO_2 and sulfate have MFBs within ± 0.5 and MFE less than 0.75, indicating acceptable agreement between predictions and measurements. SO_2 has relatively high MFB of −0.55 and high MFE of 0.76, indicating that this species is consistently under-predicted. Likewise, sulfate is under-predicted indicating that emissions of sulfur-containing species are likely biased low. Sulfate is a minor constituent of ultrafine particulate matter $PM_{0.1}$ in California [16] and so this issue does not weaken the utility of the long-term $PM_{0.1}$ predicted concentration fields.

Previous studies have found that longer averaging times reduce the influence of extreme events and short-term variability in emissions leading to better agreement between predicted and measured values [39, 41]. These trends are apparent in the results summarized in Figures 9-2 and 9-3 of the current study. The MFB and MFE values for particle matter and gaseous species improve as averaging time increases from daily to monthly to annual averages.

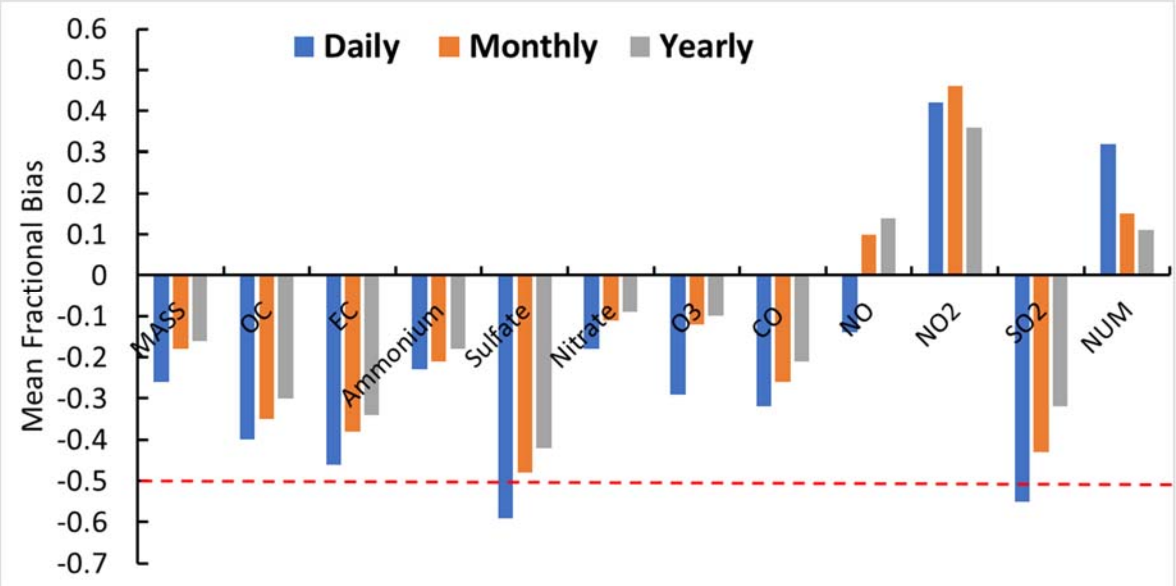

Figure 9-2: Mean Fractional Bias (MFB) of $PM_{2.5}$ mass, individual $PM_{2.5}$ species, key gaseous species, and N_{10} (particle number)

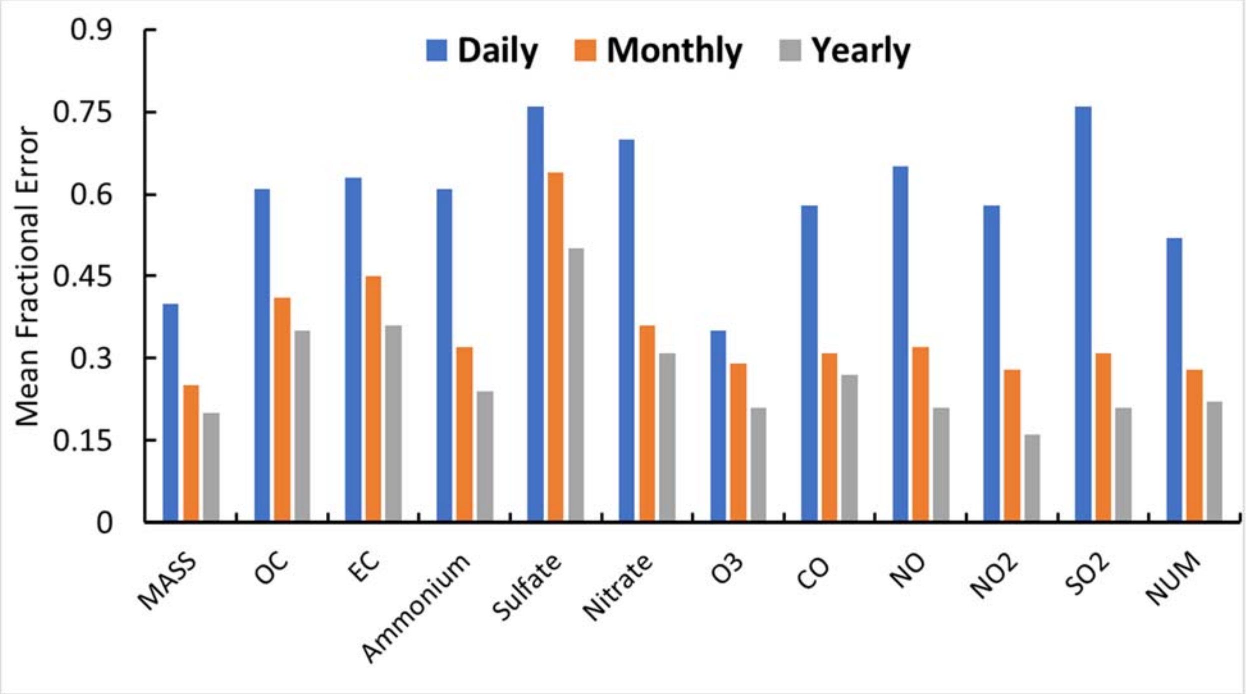

Figure 9-3: Mean Fractional Error (MFE) of $PM_{2.5}$ mass, individual $PM_{2.5}$ species, key gaseous species, and N_{10} (particle number)

Measurements of ultrafine particle concentrations between the years 2000-2016 were assembled from short-term field campaigns to evaluate the accuracy of the long-term ultrafine particle predictions. This measurement dataset is not as complete as the continuous $PM_{2.5}$ and gaseous monitoring data, but it still provides some ability to check the accuracy of model predictions across the entire seventeen year study period. The overall performance statistics for $PM_{0.1}$ EC, $PM_{0.1}$ OC, and N_{10} are summarized in Table 9-2. The mean fractional bias (MFB) and mean fractional error (MFE) meets the threshold required for regulatory modeling of $PM_{2.5}$ (MFB< ± 0.5 and MFE < 0.75) at all times and locations except for an unexplained under-prediction in $PM_{0.1}$ EC concentrations at Fresno during 2015-16. As discussed in Chapter 5, local construction activities around the sampling site may have influenced the measurements at this location. The acceptable agreement between predicted and measured $PM_{0.1}$ EC, $PM_{0.1}$ OC, and N_{10} builds confidence in the model skill for ultrafine particle predictions at all times and locations in the current study.

Table 9-2. MFB and MFE for $PM_{0.1}$ OC, $PM_{0.1}$ EC, and N_{10}

Location (Date Range)	**UFP Metric**	**MFB**	**MFE**
$PM_{0.1}$ Evaluations			
San Pablo (2015-16)	$PM_{0.1}$OC	0.21	0.41
	$PM_{0.1}$ EC	-0.15	0.45
East Oakland (2015-16)	$PM_{0.1}$OC	0.41	0.48
	$PM_{0.1}$ EC	-0.29	0.54
Los Angeles (2015-16)	$PM_{0.1}$OC	0.29	0.45
	$PM_{0.1}$ EC	-0.23	0.47
Fresno (2015-16)	$PM_{0.1}$OC	-0.29	0.37
	$PM_{0.1}$ EC	-1.60	1.62
Sacramento (2010)	$PM_{0.1}$OC	0.45	0.71
	$PM_{0.1}$ EC	0.49	0.73
Fresno, Westside (2006-09)	$PM_{0.1}$OC	0.28	0.47
	$PM_{0.1}$ EC	0.35	0.52
Bakersfield, Modesto, Sacramento, Davis (2000)	$PM_{0.1}$OC	0.5	0.57
	$PM_{0.1}$ EC	0.32	0.48
N_{10} Evaluations			
Anaheim (2012-2015)	N_{10}	0.19	0.34
Central Los Angeles (2012-15)	N_{10}	0.28	0.52
Fontana (2012-15)	N_{10}	0.34	0.63
Rubidoux (2012-15)	N_{10}	0.29	0.54

9.3.2 Long-Term UFP Trends

Long term trends of predicted and measured $PM_{0.1}$ EC and $PM_{0.1}$ OC are shown in Figures 9-4 and 9-5. Predicted $PM_{0.1}$ EC and $PM_{0.1}$ OC concentrations agree reasonably well with measurements at most of sites, except at Sacramento where predicted values are greater than measurements. This over-prediction suggests a possible positive bias in emissions at this location. Both predicted and measured concentrations of $PM_{0.1}$ EC and $PM_{0.1}$ OC decline over the years 2000 - 2016. This trend reflects the factors discussed in Chapter 2.2 including adoption of improved technology for motor vehicles, clean truck programs around shipping ports, curtailment of wood combustion during winter stagnation events, reduced sulfur concentrations in shipping fuels, and emissions reduction activities around airports.

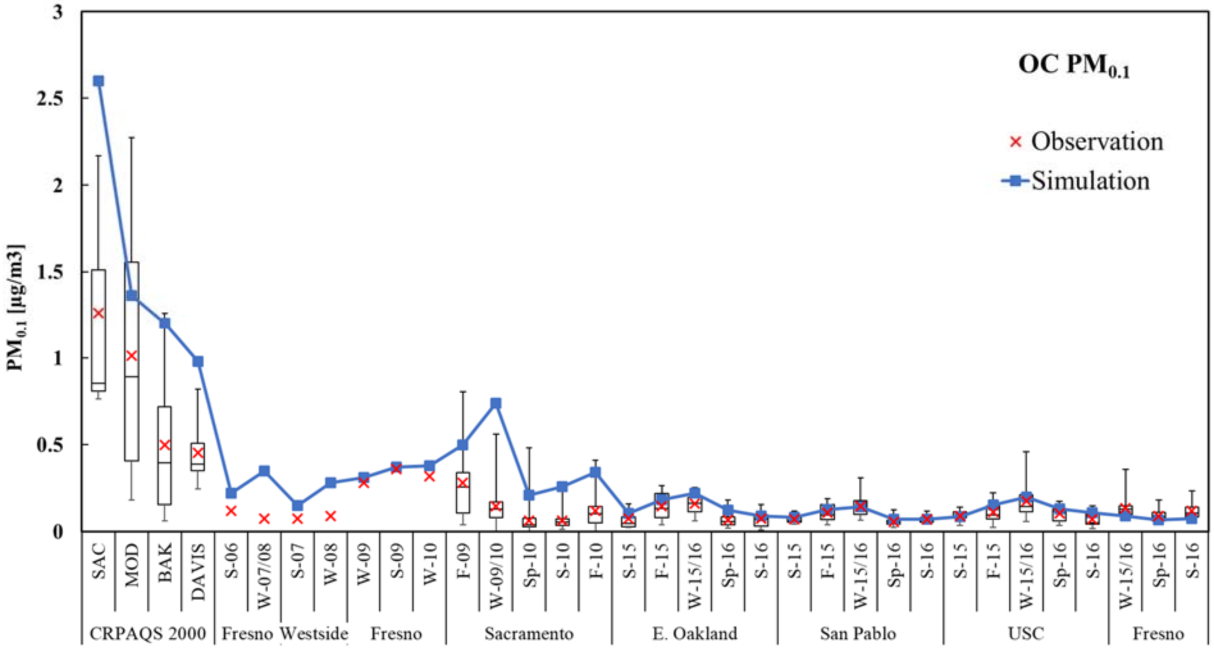

Figure 9-4: Average predicted and measured $PM_{0.1}$ OC concentration from 2000 to 2016 at locations where measurements were made in California.

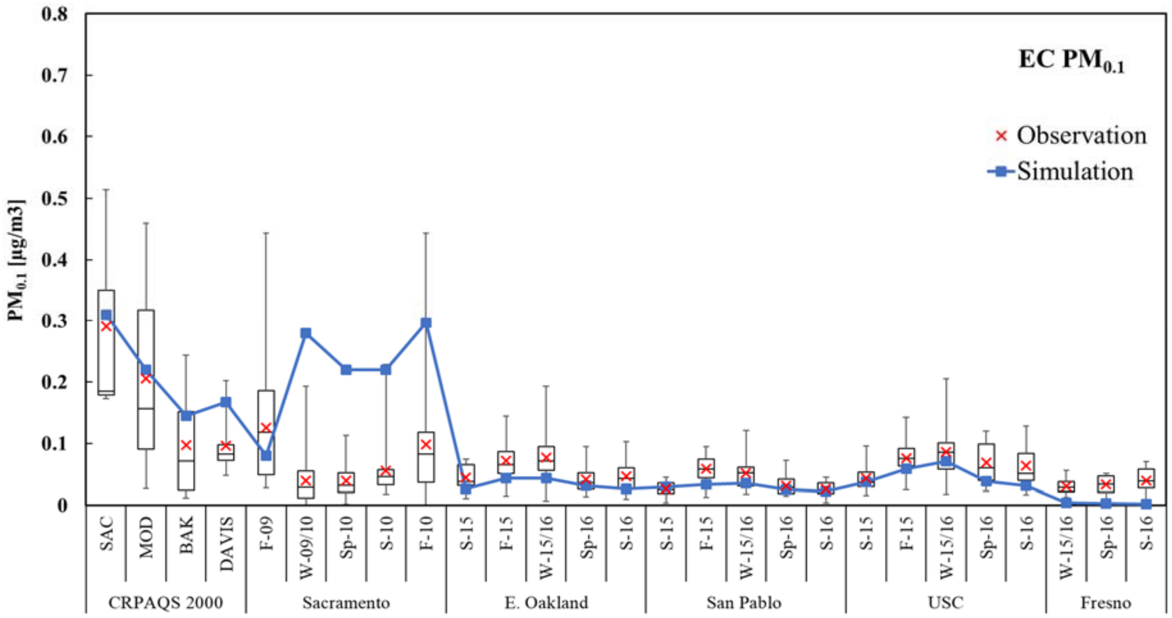

Figure 9-5: Average predicted and measured $PM_{0.1}$ EC concentration from 2000 to 2016 at locations where measurements were made in California.

Predicted (N_{10}) and measured (N_7) annual-average particle number concentrations at Fontana, and Rubidoux are shown in Figure 9-6. Consistent N_7 measurements spanning a full year are available in the years 2001 and 2012 – 2016 but are sparse between the years 2002 – 2011. Predicted annual-average particle number concentrations are in good agreement with measured annual-average particle number concentrations during the years when measurements are available. Long term trends are difficult to assess from the measurements with only a single year in 2001, but the overall trend appears to be downward in agreement with the $PM_{0.1}$ results illustrated in Figures 9-6.

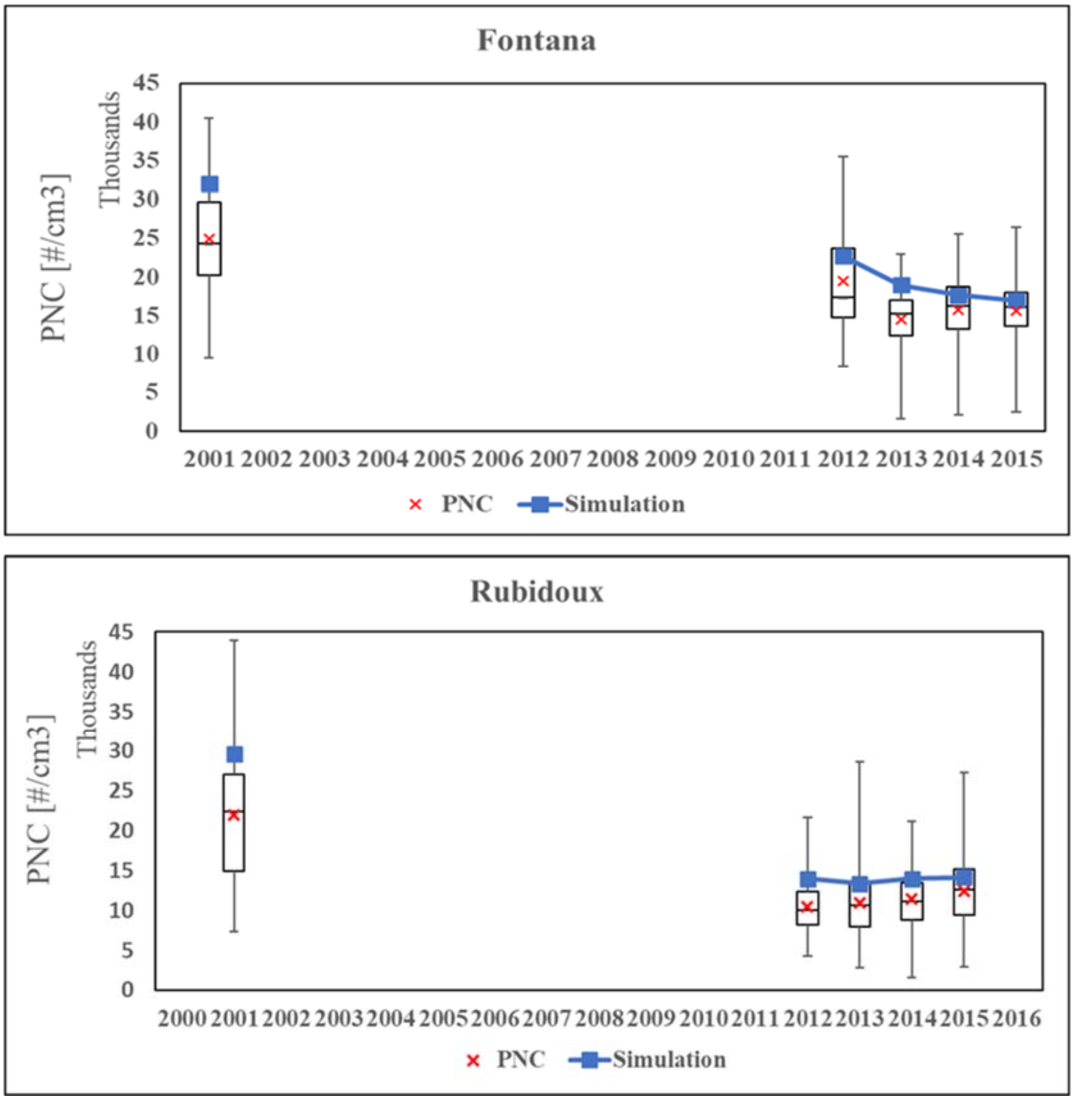

Figure 9-6: Predicted and measured particle number concentration (PNC) at Fontana and Rubidoux sites in Southern California.

Figures 9-7 through 9-8 show the predicted time trend for major source contributions to primary $PM_{0.1}$ mass and N_{10} at Los Angeles, Fresno and Sacramento from 2000-2016. At Fresno and Sacramento, wood smoke contributes strongly to $PM_{0.1}$ mass (> 40%) in winter months from 2000-2003. After 2003, wood smoke contributions to $PM_{0.1}$ mass decrease in the winter months due to the implementation of wood burning control policies (see Section 9.2.5). The $PM_{0.1}$ mass and N_{10} contribution from mobile sources (gasoline and diesel) decreases from 2000 to 2016, reflecting the penetration of newer / cleaner vehicles into the fleet. Natural gas combustion is a very significant source of $PM_{0.1}$ mass and N_{10} at all locations. Natural gas combustion is the largest source of $PM_{0.1}$ mass at Sacramento with sharp declines during the year 2007, possibly due to the effects of the economic downturn that started in that year.

Figure 9-8 shows that natural gas combustion is the single largest predicted primary N_{10} source at all three sites. N_{10} decreases significantly after 2007 at Los Angeles due to reduced contributions from natural gas combustion. $PM_{0.1}$ and N_{10} contributions from food cooking increase at Los Angeles and Sacramento sites, with food cooking accounting for 30% of total primary PM0.1 mass after the year 2010 in Los Angeles.

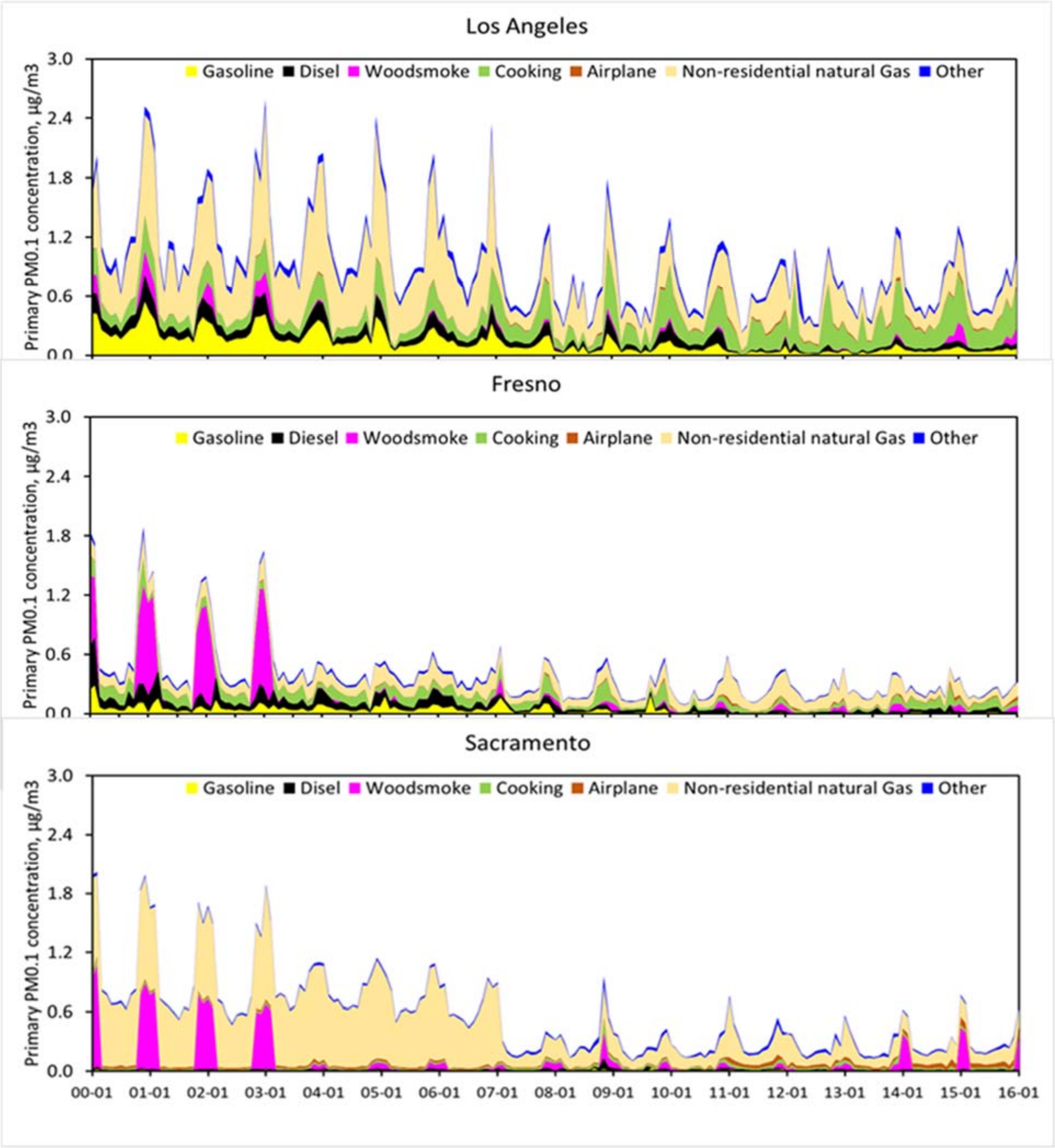

Figure 9-7: Predicted source contributions to primary $PM_{0.1}$ mass from 2000-2016 at Los Angeles, Fresno and Sacramento

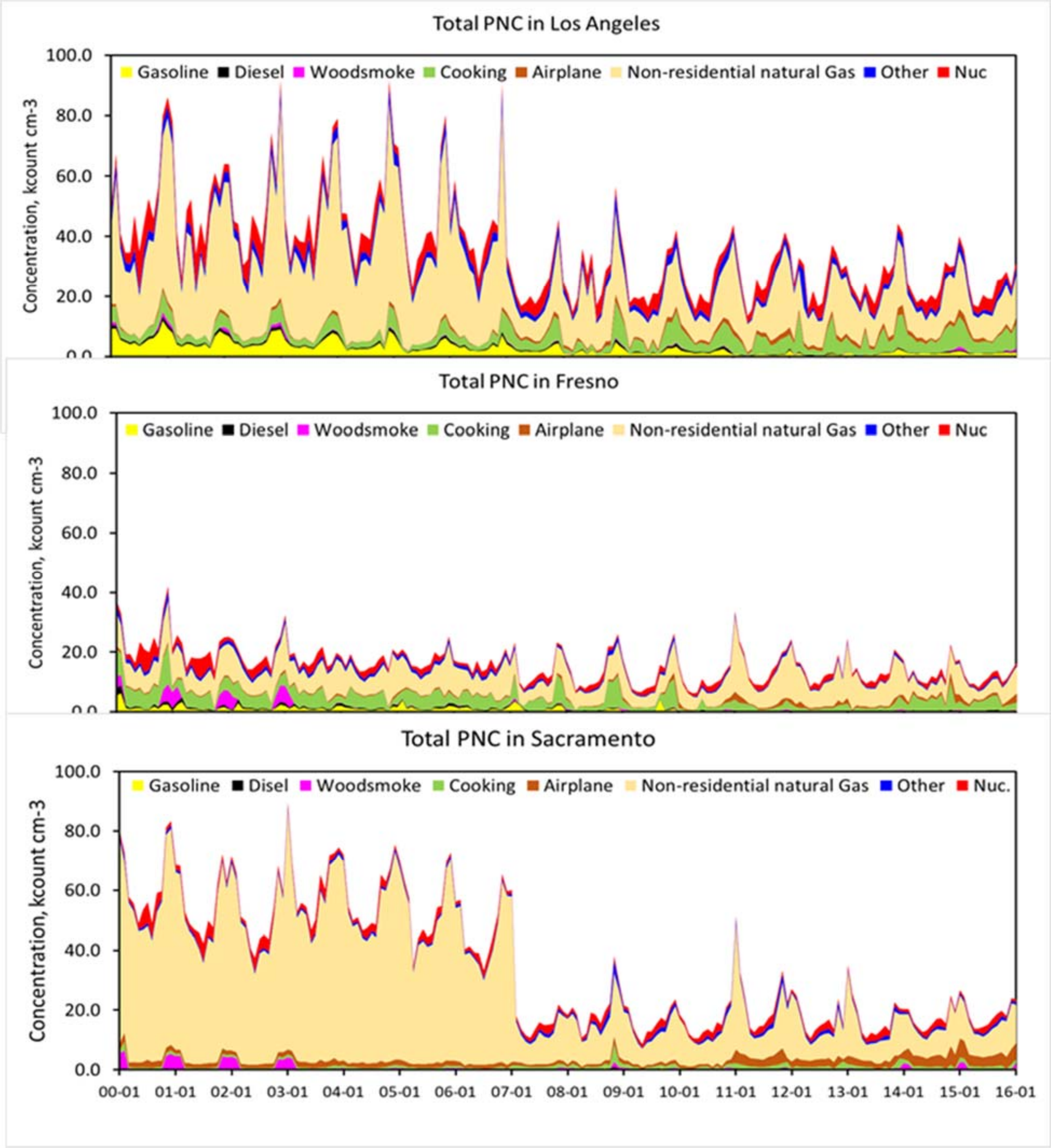

Figure 9-8: Predicted source contributions to primary N_{10} from 2000-2016 at Los Angeles, Fresno and Sacramento

Figure 9-9 shows the predicted time trend for major source contributions to primary $PM_{2.5}$ mass at Los Angeles, Fresno, and Sacramento from 2000 – 2016. A comparison of Figures 9-7 and 9-9 show that the different sources dominate $PM_{0.1}$ mass and $PM_{2.5}$ mass. Most notably, natural gas combustion is predicted to be a strong source of primary $PM_{0.1}$ mass but a relatively minor source of $PM_{2.5}$ mass. Food cooking plays a larger role in $PM_{2.5}$ mass across all sites, reflecting the fact that food cooking particles have an emissions size distribution that peaks at approximately 300 nm (ie only the tail of the distribution contributions to ultrafine particles). Seasonal trends and long-term trends for major sources generally have similar effects on ultrafine particle concentrations and $PM_{2.5}$.

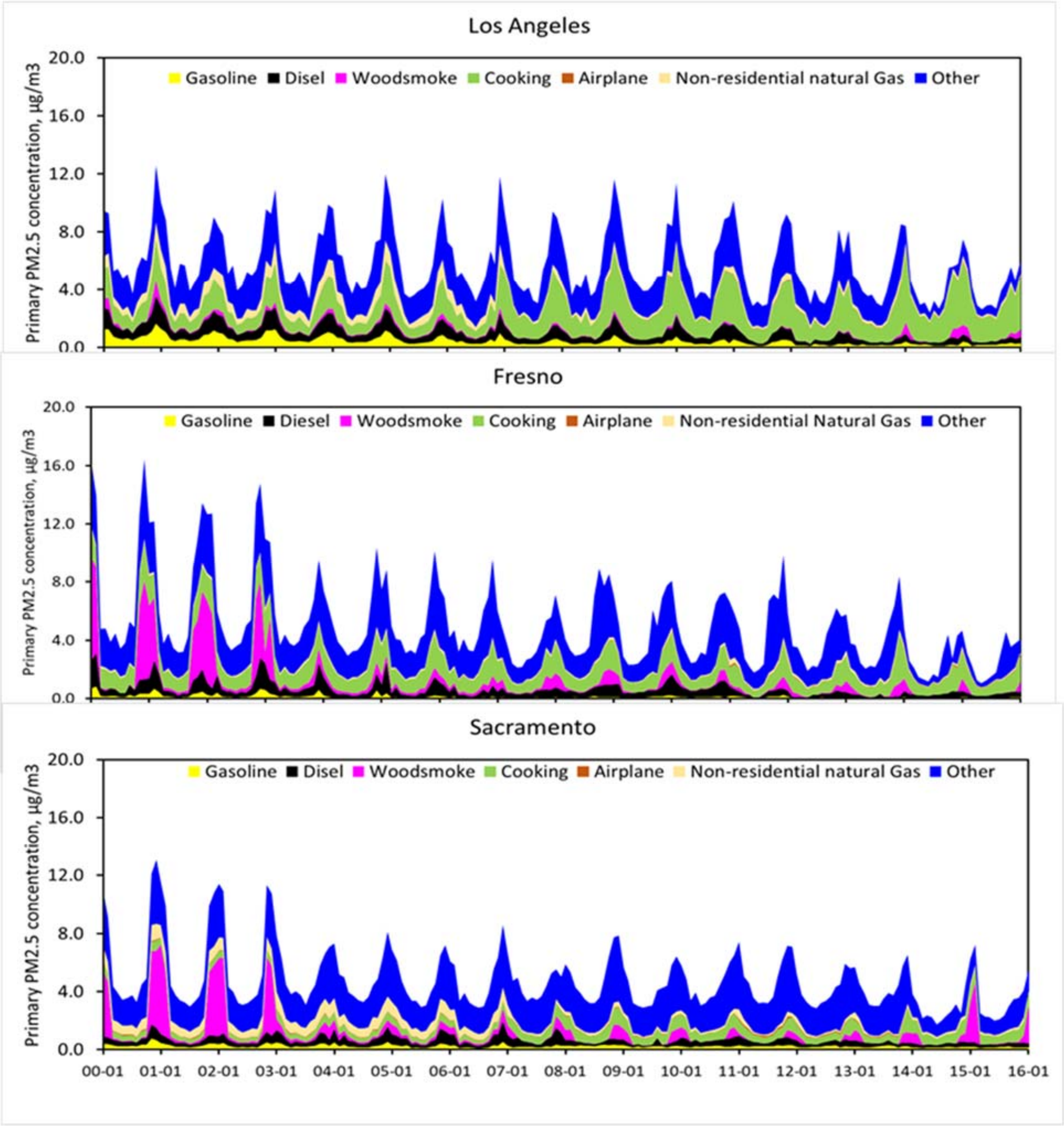

Figure 9-9: Predicted source contributions to primary $PM_{2.5}$ mass from 2000-2016 at Los Angeles, Fresno and Sacramento

9.4 Discussion

Despite the acceptable performance of model calculations in the current study, the majority of the MFE values displayed in Figure 9-2 are less than zero, indicating that concentrations are consistently under-predicted across the measurement sites. One possible explanation for this pattern is that wind speeds are over-predicted by the WRF meteorological model during stagnation events leading to excess dilution for primary emissions. Figure 9-10 illustrates the calculated mean fractional bias in wind speed predictions as a function of measured wind speed for locations averaged across the South Coast Air Basin (SC) and the San Joaquin Valley (SJV) during the years 2000-2009. Results are shown for the current study and for the previous simulations by Hu et al. (2015). Mean fractional bias increases in more stagnant episodes, reaching a value of almost 1.0 over-prediction in the South Coast Air Basin for stagnation events with measured wind speeds below 0.5 m/sec. The bias in the current study is consistently 5-10% higher than the bias in the predictions by Hu et al. (2015) due to differences in the configuration of the WRF model in the two studies.

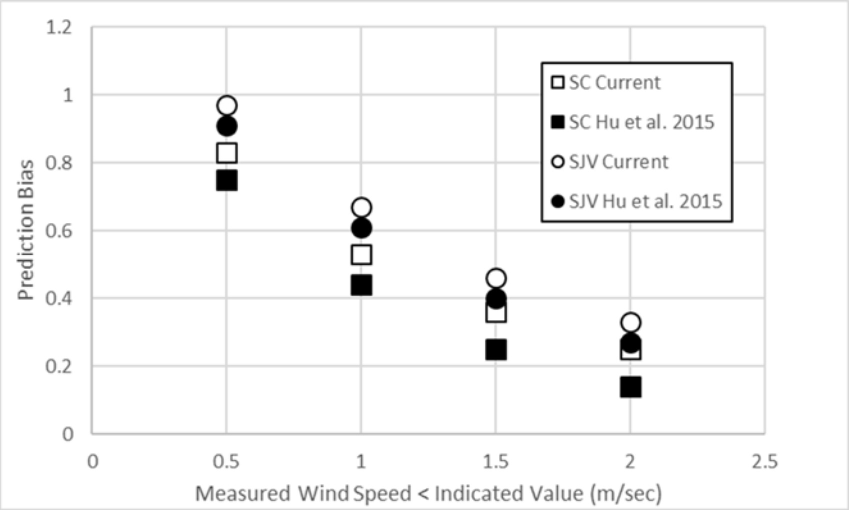

Figure 9-10: Mean fraction bias in predicted wind speeds as a function of measured wind speed in the years 2000-2009 in the South Coast (SC) and San Joaquin Valley (SJV). Perfect agreement between predictions and measurements yields a mean fraction bias of 0.

9.5 Conclusions

Concentration fields for $PM_{0.1}$ and N_{10} were predicted over a 17 year period (from 2000 to 2016) in California at 4 km horizontal resolution and hourly time resolution. Calculations were performed using the UCD/CIT reactive chemical transport model that simultaneously predicts criteria pollutant concentrations allowing for a comprehensive evaluation of model performance. Predicted concentrations of ozone, NO, NO_2, CO, $PM_{2.5}$ mass, $PM_{2.5}$ nitrate, and $PM_{2.5}$ ammonium ion meet standard modeling performance criteria ($MFB < \pm 0.5$) when compared to daily, monthly and yearly averaged measurements. Predicted $PM_{2.5}$ sulfate concentrations do not meet target performance metrics due to missing sulfur emissions, but sulfate is know to be a minor component of $PM_{2.5}$ and $PM_{0.1}$ based on past measurements in California. Most importantly in the current application, predicted N_{10}, $PM_{0.1}$ EC and $PM_{0.1}$ OC meet the performance criteria for the periods when measurements are available.

Long-term source appointment results predict that mobile source contributions to N_{10} and $PM_{0.1}$ mass have significantly decreased from 2000-2016 due to the adoption of cleaner vehicles into the on-road fleet. Wood smoke contributions to N_{10} and $PM_{0.1}$ mass have also decreased significantly due to curtailment efforts on residential wood combustion for home heating after the year 2003. In contrast, food cooking source contributions to N_{10} and $PM_{0.1}$ have remained constant or even increased with increasing population over the 17 year study period. Natural gas combustion makes significant contributions to N_{10} and $PM_{0.1}$ mass at all urban locations across California over the entire 17 year study period.

Overall, N_{10}, $PM_{0.1}$ OC, $PM_{0.1}$ EC, and $PM_{2.5}$ mass all decreased over the years 2000 – 2016 in urban areas across California due to the implementation of emissions control policies. The dataset generated by this study will be provide useful exposure estimates for fine and ultrafine particle concentrations in California. Major remaining uncertainties in the exposure estimates are related to an incomplete understanding of the emissions strength and volatility of natural gas combustion emissions, and secondary organic aerosol (SOA) formation mechanisms.

10 HIGH SPATIAL-RESOLUTION (1KM) PREDICTIONS FOR ULTRAFINE PARTICLE CONCENTRATIONS IN CALIFORNIA

Preamble: Chapter 10 summarizes predictions of regional patterns in ultrafine particle concentrations in California using regional grid model calculations applied with 1km spatial resolution. Predictions are resolved by chemical species, source contributions, and total concentrations. Comparisons are made to the measurements that overlap with the simulation periods.

10.1 Introduction

Air pollution standards designed to protect public health are based on the weight of evidence from both toxicology and epidemiology. Developing accurate exposure estimates for robust epidemiological studies of ultrafine particles (UFPs) is difficult because sharp spatial gradients limit the usefulness of central site monitors. Landuse regression models have not been fully developed for UFPs and so more fundamental physics-based models have been employed to estimate UFP exposure. Gaussian dispersion models such as CALINE, CALPUFF, and AERMOD have been used to calculate exposure to UFP in near roadway environments. These models typically calculate the near-roadway exposure but cannot accurately represent the complex evolution of the UFP further afield as condensation/evaporation and coagulation happen over longer timescales. Regional chemical transport models have been applied to predict long-term UFP exposure fields but the 4 km spatial resolution demonstrated to date raises the issue of exposure misclassification (although it could be argued that studies using central site monitors to represent exposures more than 4km away have equal or higher exposure misclassification).

The purpose of this chapter is to explore the benefits of using a chemical transport model to predict UFP exposure fields at 1 km spatial resolution for over multiple years in California. The changes needed to the UFP modeling system for 1 km modeling will be described. The accuracy of pollutant concentrations predicted at 1 km resolution and 4km resolution will then be compared. Finally, noteworthy changes in exposure concentrations predicted at 1 km and 4 km resolution will be evaluated and the underlying causes will be discussed.

10.2 Methods

The air quality models and input data used for 1 km simulations have been described in previous chapters except where updates were needed to handle the increased resolution. Unique aspects of the 1 km simulations are summarized in the sections below.

10.2.1 Meteorological Fields

Hourly meteorology inputs to drive the regional chemical transport model over the years 2000 through 2002 were simulated using the Weather Research and Forecasting (WRF) v3.4 model (www.wrf-model.org). WRF was configured with six-nested domains centered at 37° N, 120.5°

W as shown in Figure 10-1. The coarse outer domain (D01) was divided into 60 × 60 grid cells of 36-km horizontal resolution. The second domain (D02) was divided into 112 × 121 grid cells of 12-km resolution. The third domain (D03) had 4-km resolution and was divided into 298 × 277 grid cells. D03 covers all of California and this domain provided inputs for the 4 km model calculations discussed in preceding chapters. For the 1 km simulations, three additional nested domains were specified: D04 (San Francisco and Sacramento 217 x 235), D05 (Fresno 113 x 105 – not used), and D06 (South Coast Air Basin 257 × 165). The same 31 vertical layers from the ground level to the top pressure of 100 hPa were used for all domains. Initial and boundary conditions for meterological simulations were taken from North American Regional Reanalysis (NARR), which has a spatial resolution of 32 km and a temporal resolution of 3 h. The Yonsei University (YSU) boundary layer vertical diffusion scheme [334] and Pleim-Xiu land surface scheme [335] were adopted in this study. Four-dimensional data assimilation was applied to anchor the model predictions to observed meteorological patterns. Surface friction velocity (u*) was increased by 50% to correct bias during the events with low surface winds that produce the highest pollutant concentrations.

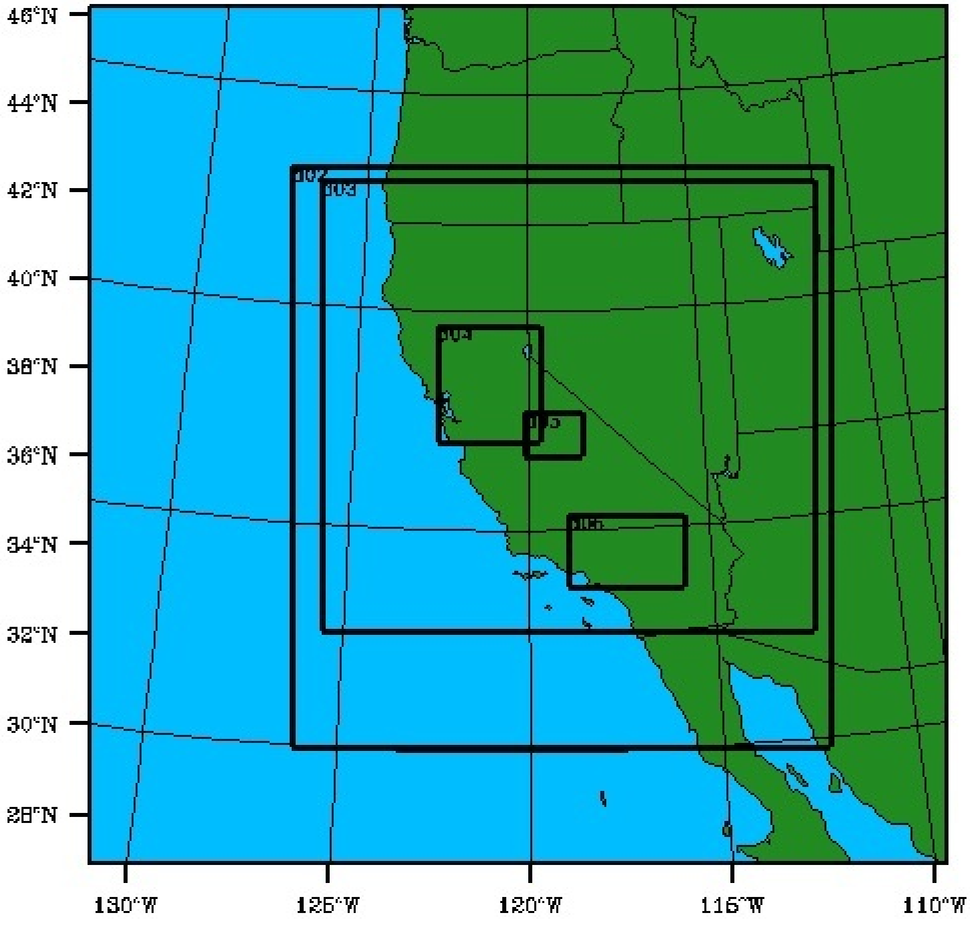

Figure 10-1: WRF domain configuration for 1km simulations. D04, D05, and D06 are the three smallest rectangles.

10.2.2 Mobile Source Emissions

Mobile source emissions are calculated using the fuel-based gridded inventory at 1 km resolution by McDonald et al. [336] for the year 2005. This inventory provides space- and time-varying values of gasoline and diesel fuel consumption (mass of fuel burned per unit time) by on-road vehicles. McDonald and Harley [337] report that gasoline and diesel fuel sales in the San Francisco bay area air basin decreased by 10.5% and 8.1%, respectively, between the years 2005 and 2010. The 2005 gridded fuel-based inventory is scaled accordingly to account for fuel use changes between years 2005 and 2010. Similar corrections are made for the SoCAB inventory in 2010.

The EMFAC model was used to calculate emission factors (mass of pollutant emitted per mass of fuel burned) for the pollutants listed in Table 10-1 and Table 10-2 for summer and winter, respectively. Fuel consumption values from the fuel-based inventory are multiplied by these emission factors to obtain emission rates (mass of pollutant emitted per unit time).

Table 10-1. EMFAC summer emission factors (mass of pollutant emitted per mass of fuel burned) for the year 2010. Values in parenthesis were measured in 2010 at the Caldecott tunnel, CA and are provided for comparison.

Pollutant	San Francisco Bay Area		South Coast Air Basin		
	Gasoline Engines	Diesel Engines	Gasoline Engines	Diesel Engines	Units
CO_2	3.0 (3.0)[a]	3.1 (3.2)[a]	2.95	3.2	kg kg^{-1}
CO	29 (14.3)[b]	5.1 (8)[c]	24.5	6.8	g kg_{-1}
NO_x	2.7 (1.9)[b]	24 (28)[c]	2.3	24.8	g kg_{-1}
SO_x	30	30	29.5	29.3	mg kg^{-1}
NMOC (exhaust)	1.4	1.2	1.2	1.6	g kg_{-1}
NMOC (evaporative)	1.6	0	1.5	0	g kg_{-1}
PM_{25}	27 (38)[b]	650	25.5	744	mg kg^{-1}

[a]: values calculated from carbon content of fuels reported by [338]; [b]: values from [339]
[c]: values from [340]

Table 10-2. EMFAC winter emission factors (mass of pollutant emitted per mass of fuel burned) for on-road sources for the year 2010. Values in parenthesis were measured in 2010 at the Caldecott tunnel, CA and are provided for comparison.

Pollutant	San Francisco Bay Area		South Coast Air Basin		
	Gasoline Engines	Diesel Engines	Gasoline Engines	Diesel Engines	Units
CO$_2$	3.0 (3.0)[a]	3.1 (3.2)[a]	2.95	3.2	kg kg^{-1}
CO	34 (14.3)[b]	5.2 (8)[c]	25.1	7.1	g kg$_{-1}$
NO$_x$	3.6 (1.9)[b]	25 (28)[c]	2.6	25.8	g kg$_{-1}$
SO$_x$	30	30	29.8	29.3	mg kg^{-1}
NMOC (exhaust)	1.9	1.2	1.3	1.6	g kg$_{-1}$
NMOC (evaporative)	1.5	0	1.7	0	g kg$_{-1}$
PM$_{25}$	29 (38)[b]	660	26.0	751	mg kg^{-1}

[a]: values calculated from carbon content of fuels reported by [338]; [b]: values from [339]
[c]: values from [340]

The EMFAC model does not provide emission data for ammonia. Ammonia emissions were estimated by multiplying NOx emission estimates by observed NH$_3$ to NOx ratios in gasoline and diesel vehicles exhaust plumes. The Fuel Efficiency Automobile Test (FEAT) Data Center reports emission measurements from on-road studies conducted at a variety of locations and time. At each location, the mol fractions of CO, CO$_2$, HC, NO, SO$_2$, NH$_3$, and NO$_2$ in the exhaust plumes of passing vehicles are measured using remote sensing techniques. We use data reported for California sites (Table 10-3 and Tale 10-4) and collected for 5 years centered on the year 2010 to calculate average NH3 to NOx emission ratios. Five years of data are used in order to increase the number of data points used in the calculations. Estimated NH3 to NOx emission mass ratios are 0.19 for on-road gasoline vehicles and 0.0092 for on-road diesel vehicles.

Table 10-3. Measurement sites from the Fuel Efficiency Automobile Test Data used to calculate NH_3 to NO_x emission ratios for on-road vehicles in the SoCAB.

	Site	Years in the range 2008 to 2012 with available data
Gasoline:	West Los Angeles, LaBrea Boulevard	2008
	Van Nuys	2010
	San Jose	2008
	Fresno	2008
Diesel:	Port of Los Angeles	2008, 2009, 2010, 2012
	Orange County, Riverside Freeway	2008, 2009, 2010, 2012

Table 10-4. Measurement sites from the Fuel Efficiency Automobile Test Data used to calculate NH_3 to NO_x emission ratios for on-road vehicles in the San Francisco Bay Area.

	Site	Years in the range 2008 to 2012 with available data
Gasoline:	San Jose	2008
	Fresno	2008
	West Los Angeles, LaBrea Boulevard	2008
	Van Nuys	2010
Diesel:	Port of Los Angeles	2008, 2009, 2010, 2012
	Orange County, Riverside Freeway	2008, 2009, 2010, 2012

Diurnal profiles from McDonald et al. [336] were used to distribute emissions in time, separately for gasoline and diesel (Figure 10-2). Separate diurnal profiles were used for the following day-of-week scenarios, as reported by McDonald et al. [336]: Monday through Thursday, Friday, Saturday, and Sunday. Daily emission totals were also scaled for each season and each day-of-week scenario, using values reported by McDonald et al. [336]. For example, the gasoline-related CO2 emission total on a Monday is different from the gasoline-related CO2 emission total on a Saturday. Seasonal scaling factors were calculated using data for June through August (summer) and December through February (winter). McDonald et al. [336] provide separate profiles for urban and rural roadway segments but urban profiles were used everywhere to avoid discontinuities where urban grid cells are adjacent to rural grid cells. Fuel densities (gasoline: 741 $g\ L^{-1}$; diesel: 850 $g\ L^{-1}$) reported by Gentner et al. [338] are used for conversion between volumes and masses of fuel.

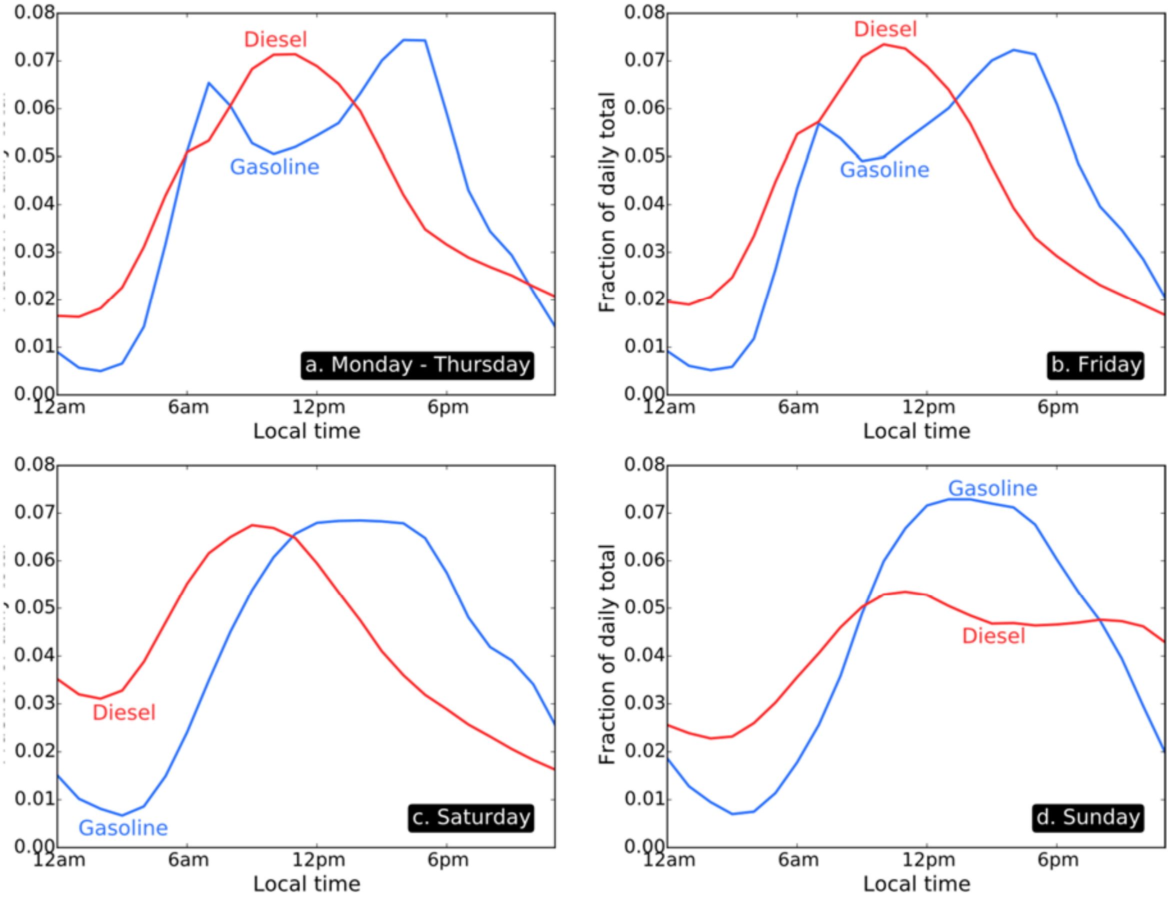

Figure 10-2: Diurnal emission profiles of on-road vehicle emissions from McDonald *et al.* [336].

10.2.3 Area Source Emissions

Area-source emissions with spatial resolution of 1 km were created for major UFP sources using spatial surrogates processed with the "Spatial Allocator" software maintained by US EPA.

Off-road gasoline emissions used spatial surrogate 620 (service and commercial employment; 11% of emissions) and spatial surrogate 630 (service and commercial employment at schools, golf courses, and cemeteries; 60% of emissions). Spatial surrogate 620 was created from information provided by Metropolitan Planning Organizations (MPOs) / Council of Governments (COGs) throughout California. Spatial surrogate 630 was obtained directly from ARB at 1km resolution since the corresponding shapefile contained proprietary information.

Off-road diesel engines used spatial surrogate 490 (rail lines; 60% of emissions) and 500 (rail yards; 11% of emissions).

Aircraft emission were processed differently for the San Francisco and Sacramento domains compared to the Los Angeles domain. Sacramento and San Francisco aircraft emissions were represented as area sources while Los Angeles aircraft emissions were represented as point sources. For the Sacramento and San Francisco domains, surrogate 382 (military aircraft), 140 (commercial airports), and 100 (all airports) were used to allocate all the aircraft emission. Data sources and reference years are shown in Table 10-5 below. Emissions were scaled to target simulation years using emissions projections by Summary Category from CARB available at https://www.arb.ca.gov/app/emsinv/fcemssumcat/fcemssumcat2016.php.

Aircraft emissions in the Los Angeles domain were created by reprocessing CARB aircraft emissions with county-level resolution for the year 2016 through SMOKE at 1km spatial resolution. Scaling factors were then applied to estimate emissions in the years 2000 through 2002 using the emissions projections by Summary Category referenced above.

Table 10-5. Data source for 1km aircraft emissions.

domain	Emission type	Surrogate /emission	percentage	Data Source
SAC, SFBA	area	382 - MILITARY_ AIRCRAFT	~54%	http://www.dot.ca.gov/hq/tsip/gis/datalibrary/Metadata/Airp_military.html
		140 - Comm_ Airports	~40%	http://www.dot.ca.gov/hq/tsip/gis/datalibrary/Metadata/Airports.html
		100 – all Airports	~remaining	http://ais-faa.opendata.arcgis.com/datasets/e747ab91a11045e8b3f8a3efd093d3b5_0
LA	point	2016 Point source downscaling to 2000/ 2001/ 2002	~100%	ARB 2016 inventory, run through SMOKE at 1km resolution

The majority of the natural gas combustion emission are released by point sources that can be represented at any spatial resolution needed. The largest area sources of natural gas combustion emissions are represented by spatial surrogate 620 (service and commercial employment) and spatial surrogate 530 (residential heating). Surrogate 620 is also used to regrid type 2 off-road gasoline emissions as descrbed above. Spatial surrogate 530 was created from shapefile “residential fuel” provided by CARB.

10.3 Results

10.3.1 Meteorological Fields

Table 10-6 summarizes the performance of the WRF simulations over the years 2000-2002 at 4km spatial resolution.

Table 10-6. WRF performance metrics for the years 2000-2002 at 4km spatial resolution.

	Temperature					Wind					Relative Humidity				
Basin	AveObs ºC	AveSim ºC	MFB -	MFE -	RMSE ºC	AveObs m/s	AveSim m/s	MFB -	MFE -	RMSE m/s	AveObs %	AveSim %	MFB -	MFE -	RMSE %
GBV	13.95	11.2	-0.17	0.24	5.02	2.71	2.29	-0.03	0.63	2.31	34.21	43.23	0.24	0.4	20.32
LC	13.95	12.7	0.02	0.38	4.41	3.12	2.09	-0.25	0.63	2.36	60.5	66.16	0.12	0.34	23.05
LT	7.31	6.44	-0.06	0.35	3.44	1.41	2.03	0.29	0.57	1.25	54.59	61.01	0.11	0.33	21.41
NC	12.47	12.11	0.03	0.31	3.98	2.48	1.99	-0.05	0.65	2.14	68.19	69.39	0.04	0.28	21.42
NCC	13.65	13.5	-0.01	0.33	4.75	2.11	2.01	0.04	0.61	1.62	73.38	71.15	-0.02	0.28	23.17
NEP	9.95	9.4	0.05	0.28	4.23	2.43	1.94	-0.14	0.63	1.85	57.43	59.94	0.05	0.31	20.45
MD	17.83	16.11	-0.1	0.28	4.39	3.25	2.59	-0.1	0.62	2.46	39.35	48.32	0.21	0.41	22.37
MC	12.75	11.65	-0.04	0.26	4.05	1.99	1.84	0.05	0.61	1.64	57.28	62.26	0.1	0.31	20.64
SC	16.58	15.4	-0.05	0.25	4.09	2.33	1.9	-0.07	0.61	2.03	61.41	65.16	0.07	0.32	22.86
SCC	14.24	13.91	0	0.3	5.03	2.31	2.18	0.08	0.63	1.94	69.23	69.46	0.01	0.3	23.15
SD	15.79	15.13	-0.04	0.33	5.57	1.82	2.31	0.25	0.64	1.72	67.01	67.58	0.03	0.3	21.97
SFB	13.89	13.77	-0.01	0.32	4.65	2.44	1.98	-0.02	0.67	2.26	72.99	71.41	-0.02	0.25	21.03
SJV	15.71	15.08	-0.03	0.32	4.9	1.9	1.89	0.06	0.6	1.54	61.44	61.49	0	0.29	20.7
SS	23.15	21.81	-0.1	0.29	6.06	2.23	2.29	0.04	0.67	2.1	42.63	45.19	0.04	0.39	22.19
SV	15.41	14.88	-0.03	0.29	4.45	2.14	1.95	0	0.6	1.67	62.27	62.34	0	0.27	18.82
CA	14.83	14.08	-0.03	0.3	4.7	2.26	2.04	0.01	0.62	1.91	61.3	63.11	0.05	0.31	21.51

10.3.2 PM$_{2.5}$ – Los Angeles

Table 10-7 summarizes the performance statistics Mean Fractional Bias (MFB) and Mean Fractional Error (MFE) for PM$_{2.5}$ concentrations predicted at central Los Angeles between the years 2000 through 2002. The measurement record at this site is incomplete over the simulation period and so only 25 comparison days over seven months are available for the analysis. Simulations conducted with 1km spatial resolution have better performance for all PM$_{2.5}$ metrics other than Cu and Na. PM$_{2.5}$ mass, EC, OC, sulfate, iron, and manganese are all simulated more accurately at the higher spatial resolution.

Table 10-7. Performance statistics at central Los Angeles for calculations run at 1km and 4km spatial resolution.

				Daily Comparison n = 25						
resolution		PM2.5 MASS	PM2.5 EC	PM2.5 OC	PM2.5 Nitrat	PM2.5 Sulfate	PM2.5 Cu	PM2.5 Fe	PM2.5 Mn	PM2.5 Na
1km	MFB	7.18%	-17.20%	-59.03%	-36.96%	9.09%	-110.36%	19.39%	-10.95%	-150.39%
	MFE	45.44%	49.27%	65.98%	57.84%	63.37%	110.46%	49.89%	56.56%	150.39%
4km	MFB	-35.18%	-59.40%	-69.76%	-109.58%	-35.50%	-20.59%	32.25%	-19.38%	-149.25%
	MFE	52.29%	64.39%	71.37%	114.04%	68.15%	56.23%	57.84%	55.97%	149.25%
				Monthly Comparison n = 7						
resolution		PM2.5 MASS	PM2.5 EC	PM2.5 OC	PM2.5 Nitrat	PM2.5 Sulfate	PM2.5 Cu	PM2.5 Fe	PM2.5 Mn	PM2.5 Na
1km	MFB	18.60%	-4.27%	-46.16%	-26.93%	18.55%	-114.88%	35.14%	4.60%	-137.80%
	MFE	33.18%	20.59%	46.16%	33.69%	55.50%	114.88%	35.14%	34.11%	137.80%
4km	MFB	-52.32%	-78.46%	-82.17%	-115.41%	-50.68%	-53.96%	2.83%	-40.33%	-152.28%
	MFE	56.09%	78.46%	82.17%	115.41%	73.47%	59.09%	59.98%	43.74%	152.28%

Figure 10-3 illustrates the time series of predicted and measured $PM_{2.5}$ concentrations at central Los Angeles during the years 2000 through 2002. Predicted and measured $PM_{2.5}$ mass, EC, and OC all peak during the winter months. Simulations carried out at 1km spatial resolution more accurately predict the highest winter concentrations while simulations carried out with 4km spatial resolution consistently under-predict winter concentrations.

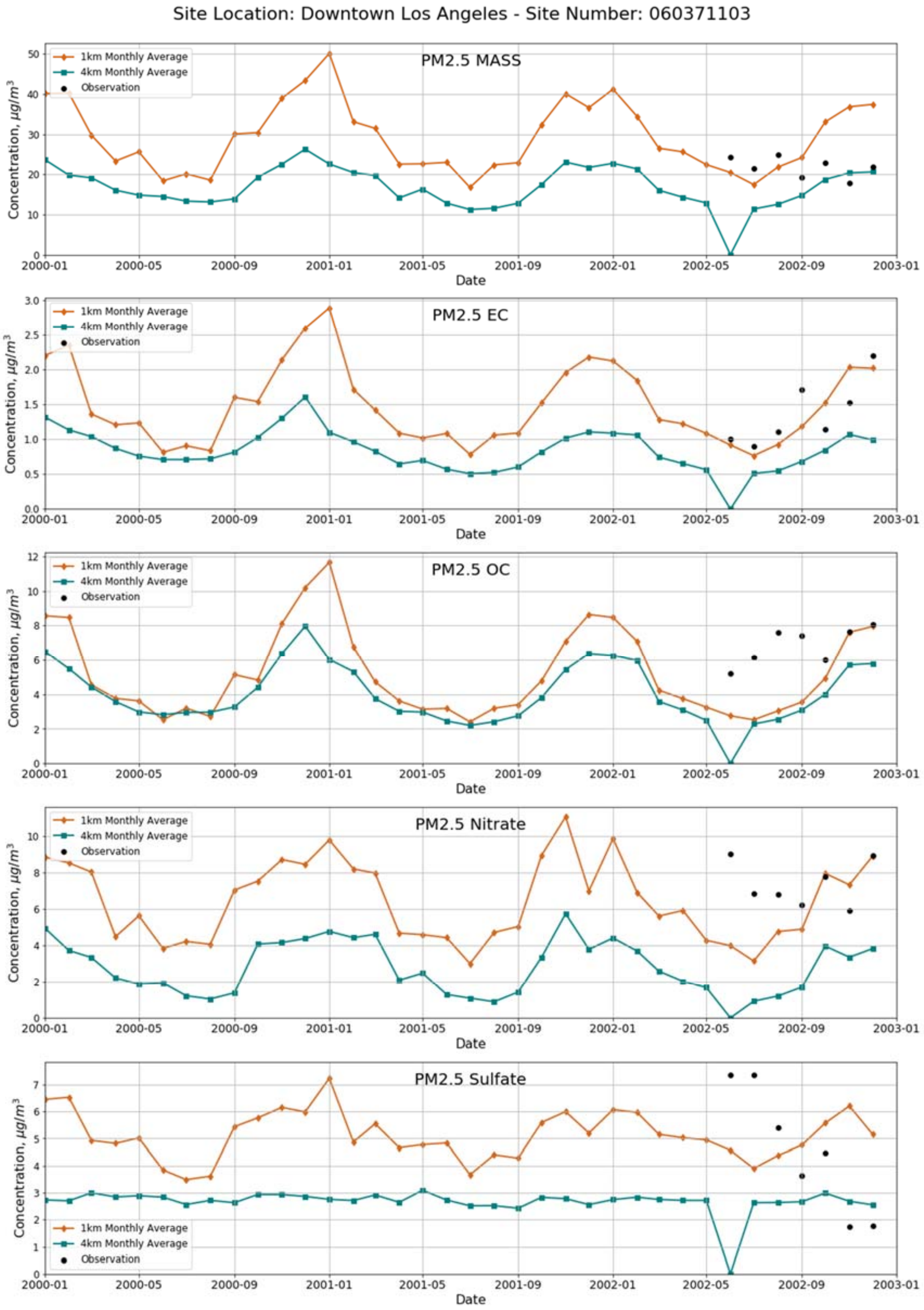

Figure 10-3: Time series of $PM_{2.5}$ concentrations predicted at central Los Angeles using 1km spatial resolution and 4km spatial resolution.

Figures 10-4 and 10-5 illustrate the $PM_{2.5}$ concentrations over the South Coast Air Basin surrounding Los Angeles averaged over the years 2000 through 2002. Separate panels are shown for total mass, EC, OC, Cu, Mn, Fe, nitrate (NO_3^-), sulfate (SO_4^{2-}), anthropogenic SOA (SOA_A), and biogenic SOA (SOA_B) at both 1km and 4km resolution. Both simulations predict that the highest $PM_{2.5}$ mass concentrations occur in a concentrated region around the Port of Los Angeles, but the 1km simulation has reduced numerical diffusion which results in higher predicted concentrations (Figure 10-4 a and b). The remaining $PM_{2.5}$ mass fields away from the Port are generally smooth with little obvious additional detail revealed by the increased spatial resolution.

The $PM_{2.5}$ EC fields predicted at 1km spatial resolution have greater spatial detail compared to the corresponding fields predicted at 4km spatial resolution (Figure 10-4 c and d). The major freeways in the SoCAB can be individually resolved using 1km resolution while the 4km resolution results appear to be more uniformly distributed across the entire region. These results suggest that traffic exposure fields benefit from the increased spatial resolution, and components dominated by traffic sources (such as EC) are more accurately resolved by 1km simulations.

$PM_{2.5}$ OC fields predicted at 1km and 4km spatial resolution are similar with the exception that numerical diffusion greatly reduces OC concentrations at the Port of Los Angeles in the 4km simulations (Figure 10-4 e and f). Traffic is not the dominant source of regional $PM_{2.5}$ OC in the SoCAB and the increased spatial resolution for other important sources does not strongly resolve additional details if the sources themselves are uniformly distributed.

$PM_{2.5}$ Cu fields predicted at 1km and 4km resolution are very different (Figure 10-4 g and h). Further analysis of the model configuration revealed that the tire dust and brake wear emissions were mistakenly left out of the 1km simulations, causing lower concentrations and altered spatial patterns for $PM_{2.5}$ Cu. The omission of brake wear also affects $PM_{2.5}$ Fe predictions at 1km spatial resolution (Figure 10-5 a and b). Table 10-7 above confirms the degraded performance for Cu, and this element will not be discussed further in the current analysis. Future simulations at 1km spatial resolution will include tire and brake wear.

$PM_{2.5}$ Mn fields predicted at 1km and 4km resolution are similar with the exception of increased numerical diffusion around the Port of Los Angeles in the 4km results (Figure 10-4 i and j). These trends are similar to the behavior exhibited by OC.

$PM_{2.5}$ nitrate, anthropogenic SOA, and biogenic SOA fields predicted at 1km and 4km resolution are similar with the exception that nitrate and anthropogenic SOA concentrations are slightly higher in the 1km simulations due to differences in the mobile source emissions inventory estimated using fuel consumption data [337] compared to the original mobile inventory developed by CARB. This absence of fine-scale spatial patterns in the secondary pollutant fields is expected since they are formed by regional processes that operate over large spatial scales. $PM_{2.5}$ sulfate fields behave more like primary pollutants since the highest concentrations are dominated by primary emissions at the Port of Los Angeles. Simulations performed at 4km resolution have increased numerical diffusion resulting in lower concentrations around sulfate point sources.

Figures 10-6 and 10-7 illustrate the source contributions to primary $PM_{2.5}$ mass over the South Coast Air Basin surrounding Los Angeles averaged over the years 2000 through 2002. The results confirm that on-road traffic sources are resolved more accurately by the increased spatial resolution of the 1km simulations. It is noteworthy that the 1km simulations predict the highest concentration of on-road gasoline primary $PM_{2.5}$ along the major freeways that run parallel to the coastline while the 4km simulations peak in central Los Angeles. Likewise, the 1km simulations predict the highest concentration of on-road diesel primary $PM_{2.5}$ along the major freeway moving north from the Port of Los Angeles while the 4km simulations once again peak in central Los Angeles. These different spatial patterns may impact the hazard ratios assigned to each source during epidemiological analysis.

The spatial fields for off-road gasoline, off-road diesel, wood smoke, food cooking, and natural gas combustion are not significantly enhanced with additional spatial details in the 1km simulations. These spatial surrogates used to represent the underlying sources are approximately uniformly distributed at 1km resolution and so increasing the spatial resolution of the model simulations does not result in new exposure patterns.

The fields for primary $PM_{2.5}$ contributions from airports clearly show the signature for the Los Angeles International Airport (LAX) in the 1km simulations because emissions were calculated from the 2016 CARB aircraft emissions inventory which yields very different results than the original year 2000 CARB aircraft emissions inventory.

The fields for primary $PM_{2.5}$ contributions from "other sources" produced by the 1km and 4km simulations differ due to the omission of brake and tire wear emissions in the 1km simulations.

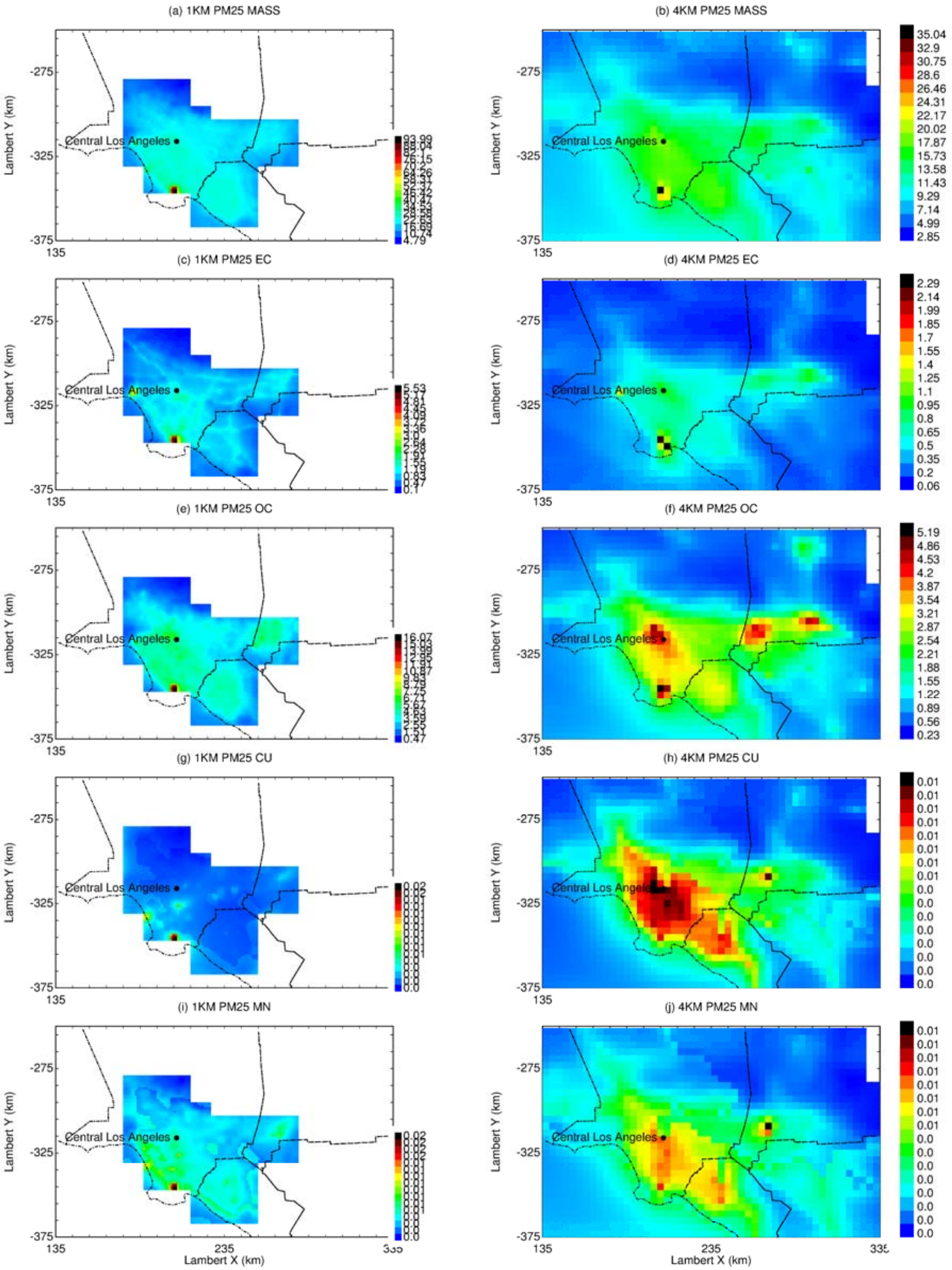

Figure 10-4: Average PM2.5 concentrations predicted in Los Angeles for the years 2000 through 2002 using 1km spatial resolution (left column) and 4km spatial resolution (right column).

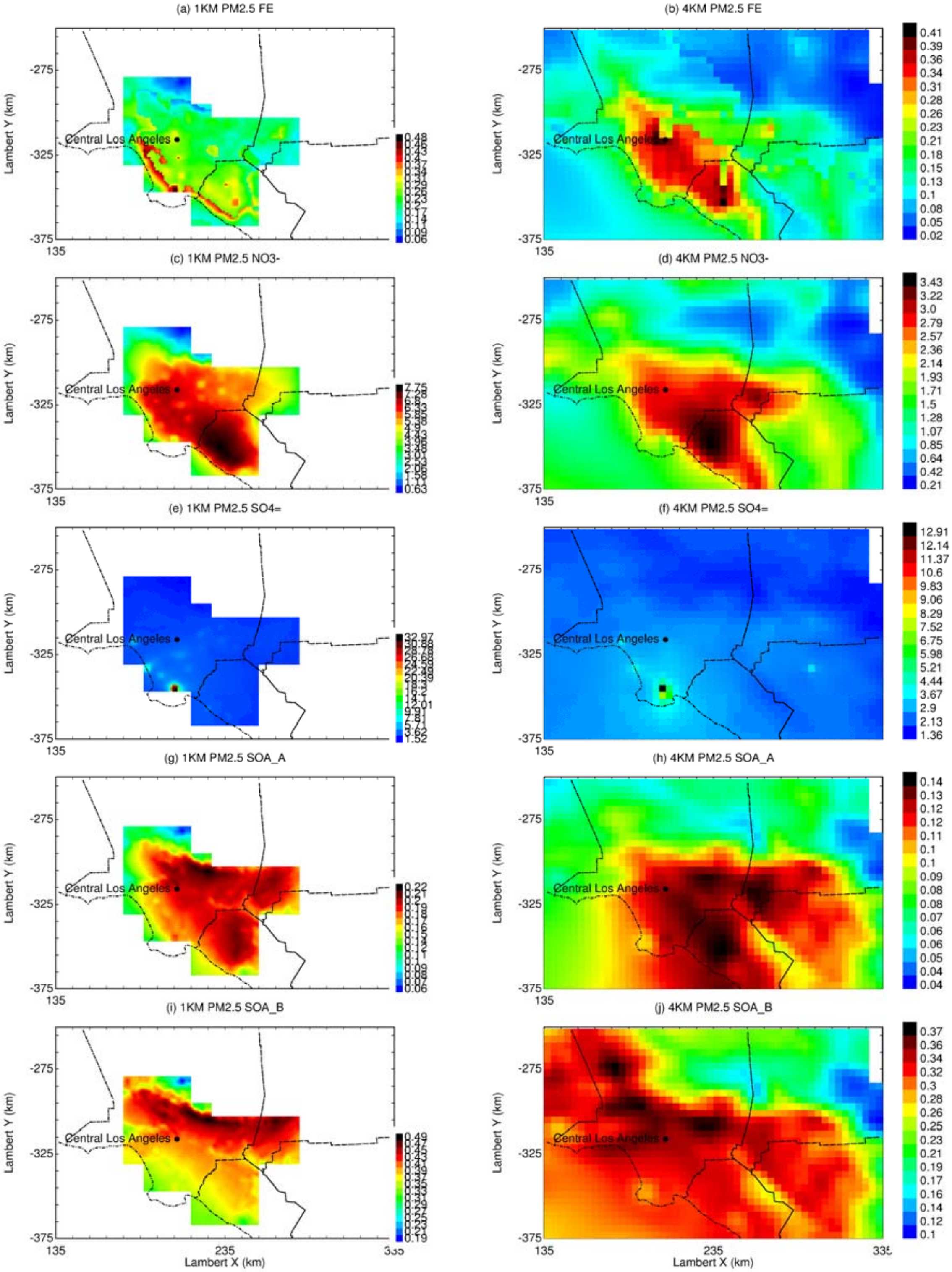

Figure 10-5: Average PM2.5 concentrations predicted in Los Angeles for the years 2000 through 2002 using 1km spatial resolution (left column) and 4km spatial resolution (right column).

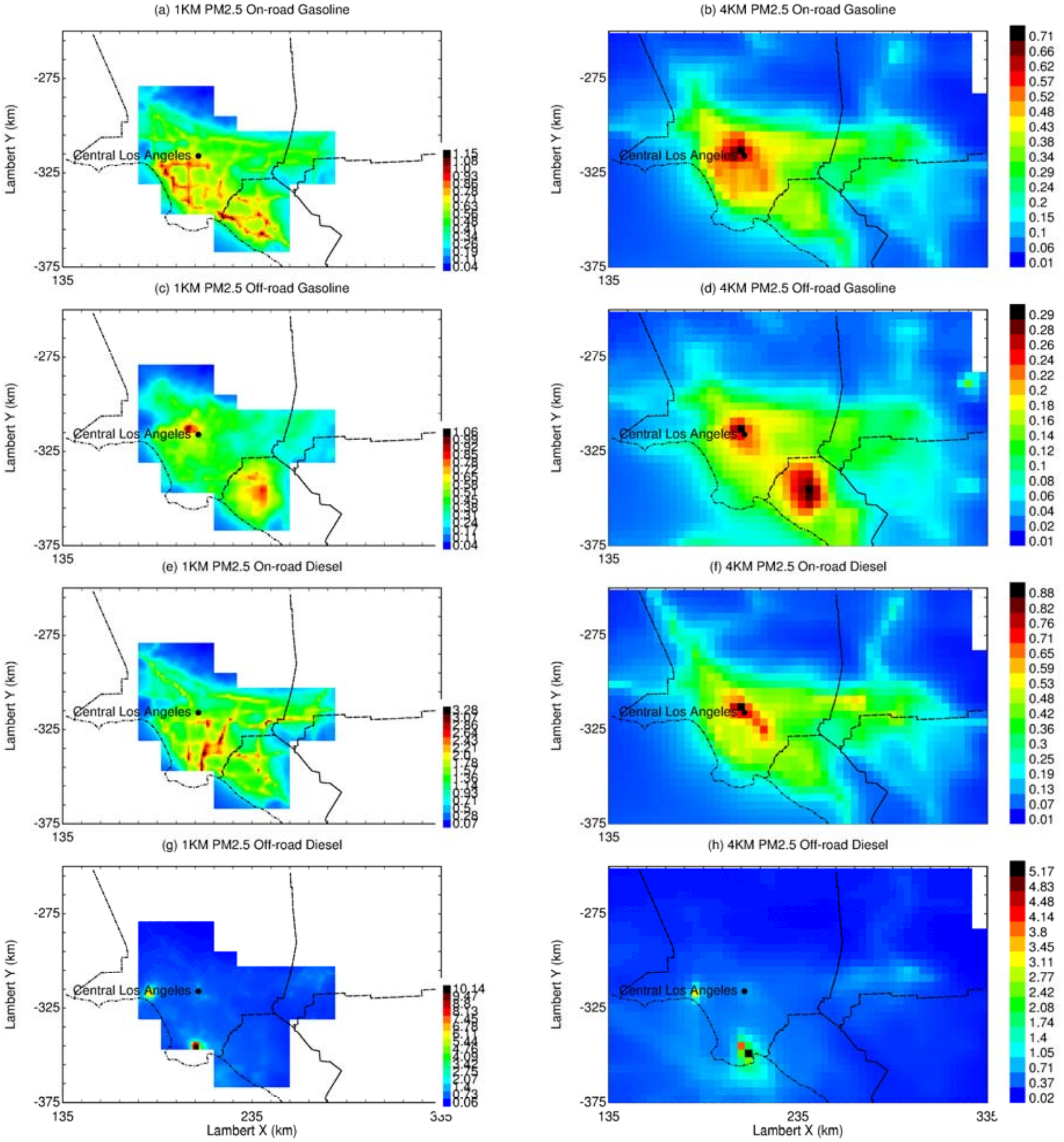

Figure 10-6: Average PM2.5 source contributions predicted in Los Angeles for the years 2000 through 2002 using 1km spatial resolution (left column) and 4km spatial resolution (right column).

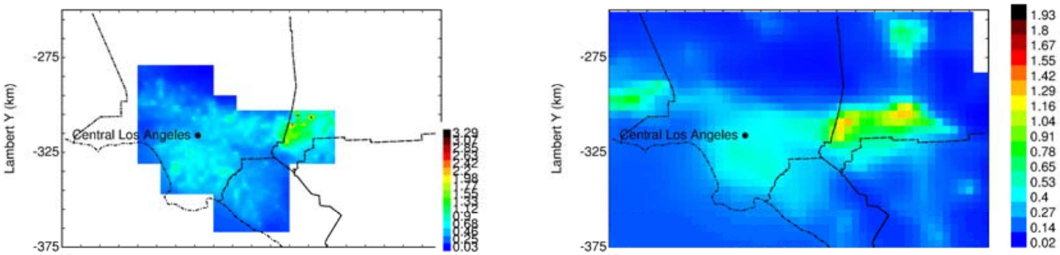
(a) 1KM PM2.5 Wood Smoke

(b) 4KM PM2.5 Wood Smoke

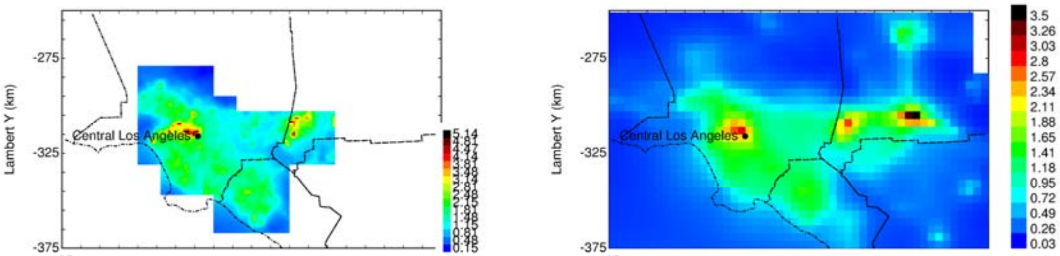
(c) 1KM PM2.5 Food Cooking

(d) 4KM PM2.5 Food Cooking

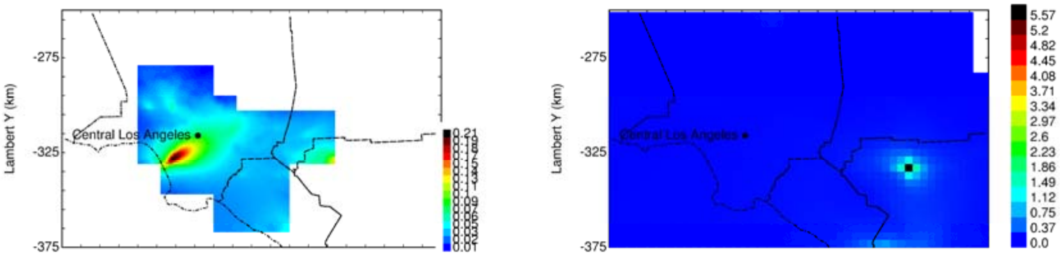
(e) 1KM PM2.5 Aircraft

(f) 4KM PM2.5 Aircraft

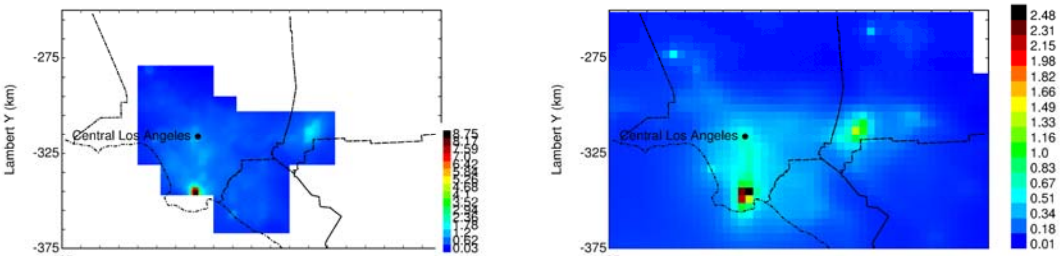
(g) 1KM PM2.5 Natural Gas

(h) 4KM PM2.5 Natural Gas

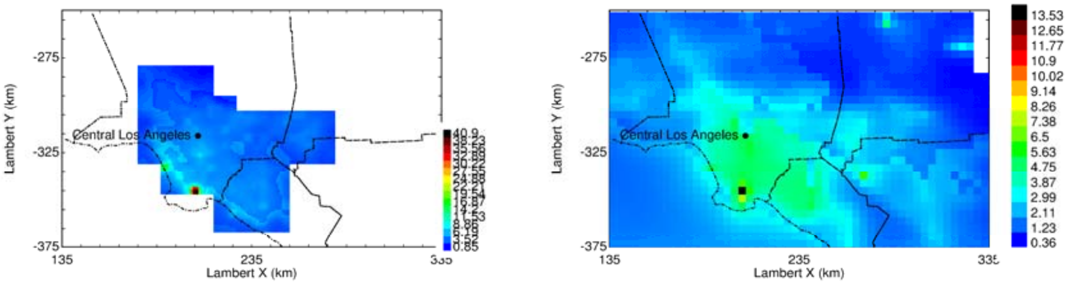
(i) 1KM PM2.5 Other

(j) 4KM PM2.5 Other

Figure 10-7: Average PM2.5 source contributions predicted in Los Angeles for the years 2000 through 2002 using 1km spatial resolution (left column) and 4km spatial resolution (right column).

10.3.3 PM$_{2.5}$ – San Francisco Bay Area

Table 10-8 summarizes PM$_{2.5}$ performance statistics for simulations at the San Jose monitoring site within the San Francisco Bay Area during the years 2000 through 2002. MFB and MFE are improved for PM$_{2.5}$ EC, OC, nitrate, Fe, and Mn when the model spatial resolution is increased to 1km, but performance statistics for PM$_{2.5}$ mass, sulfate, and Cu are degraded at the higher spatial resolution. These trends reflect the increased accuracy of the predicted mobile source contributions to PM$_{2.5}$ combined with the omission of brake and tire wear emissions in the 1km simulations as discussed in Section 10.3.2.

Table 10-8. Performance statistics at San Jose for 1km and 4km spatial resolution.

				Daily Comparison						
resolution		PM2.5 MA	PM2.5 EC	PM2.5 OC	PM2.5 Nit	PM2.5 Sul	PM2.5 Cu	PM2.5 Fe	PM2.5 Mn	PM2.5 Na
1km	MFB	34.42%	-34.40%	-17.21%	-42.03%	63.54%	-133.92%	57.99%	38.93%	-179.14%
	MFE	50.33%	49.69%	45.51%	95.45%	75.11%	137.52%	73.23%	70.57%	179.14%
4km	MFB	21.96%	-42.07%	-24.93%	-54.10%	53.18%	33.78%	71.13%	47.09%	-175.80%
	MFE	48.18%	56.32%	46.88%	93.48%	69.32%	64.92%	86.62%	76.66%	175.80%
				Monthly Comparison						
resolution		PM2.5 MA	PM2.5 EC	PM2.5 OC	PM2.5 Nit	PM2.5 Sul	PM2.5 Cu	PM2.5 Fe	PM2.5 Mn	PM2.5 Na
1km	MFB	37.46%	-31.38%	-13.45%	-34.82%	61.06%	-147.50%	57.57%	42.64%	-186.44%
	MFE	38.09%	39.75%	40.27%	61.27%	61.06%	147.50%	62.15%	51.67%	186.44%
4km	MFB	23.79%	-46.99%	-25.69%	-71.43%	51.92%	32.04%	74.62%	55.47%	-182.38%
	MFE	26.21%	50.29%	40.39%	86.73%	52.19%	36.87%	75.10%	60.28%	182.38%

Figure 10-8 illustrates the time series of predicted and measured PM$_{2.5}$ concentrations at San Jose during the years 2000 through 2002. Similar to the results for central Los Angeles discussed in Section 10.3.2, predicted and measured PM$_{2.5}$ mass, EC, and OC all peak during the winter months. Concentrations predicted using 1km spatial resolution are generally slightly higher than concentrations predicted with 4km spatial resolution, especially during peak events in winter periods. The increased concentrations reflect reduced numerical diffusion in simulations with higher spatial resolution as well as increased emissions from mobile sources calculated using fuel-consumption data [337].

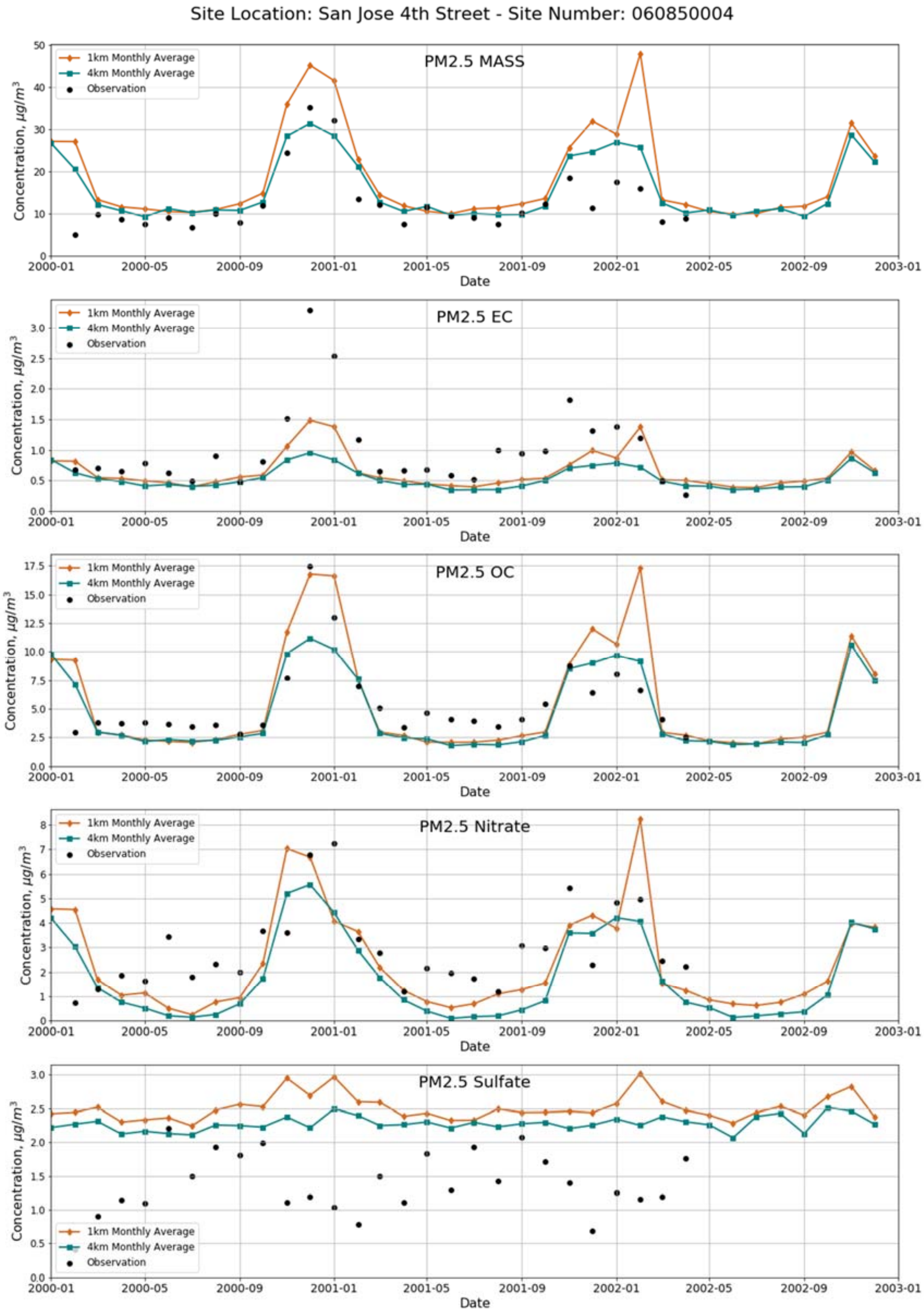

Figure 10-8: Time series of $PM_{2.5}$ concentrations predicted at central Los Angeles using 1km spatial resolution and 4km spatial resolution.

Figures 10-9 and 10-10 display the $PM_{2.5}$ concentration fields over the San Francisco Bay Area averaged over the years 2000 through 2002. The left panels in each figure display simulation results at 1km spatial resolution while the right panel in each figure displays results at 4km spatial resolution. Predicted $PM_{2.5}$ mass fields appear similar at 1km and 4km resolution (Figure 10-9 a and b). Peak concentrations around point sources are higher in 1km simulations because of the reduced numerical diffusion.

Predicted $PM_{2.5}$ EC concentration fields once again show the greatest enhancement when in simulations carried out at 1km spatial resolution compared to 4km spatial resolution (Figures 10-9 c and d). Individual traffic corridors can be resolved at the higher spatial resolution allowing for increased accuracy in the related exposure fields. $PM_{2.5}$ OC fields are relatively smooth at both 1km and 4km spatial resolution reflecting the more uniform distribution of primary OC emissions sources across the urban region (Figure 10-9 e and f). Similarly, $PM_{2.5}$ Mn fields show little change between 1km and 4km resolution (Figure 10-9 i and j).

Predicted $PM_{2.5}$ nitrate, anthropogenic SOA (SOA_A) and biogenic SOA (SOA_B) fields over the SFBA are similar at 1km and 4km resolution due to the secondary formation processes that dominate these components. Nitrate and anthropogenic SOA concentrations predicted in 1km simulations are slightly higher than concentrations predicted in the 4km simulations due to differences in the mobile source emissions inventory as discussed in Section 10.3.2. Predicted $PM_{2.5}$ sulfate concentrations are similar in 1km and 4km simulations because the sulfate point sources are represented at 4km resolution in the 1km simulations. It was not possible to completely remap all area sources in the emissions inventory to 1km resolution.

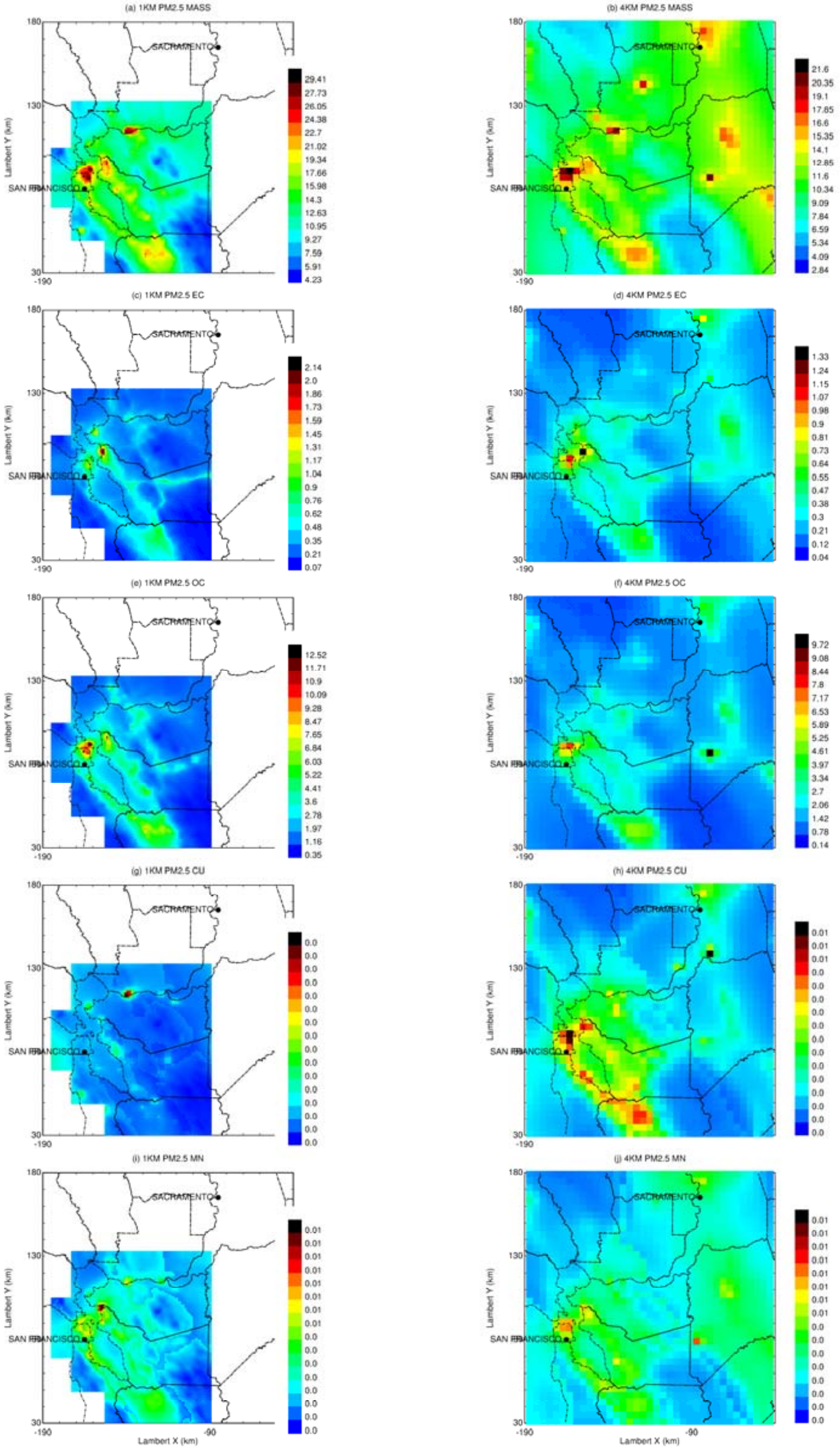

Figure 10-9: Average PM2.5 concentrations predicted in San Francisco for the years 2000 through 2002 using 1km spatial resolution (left column) and 4km spatial resolution (right column).

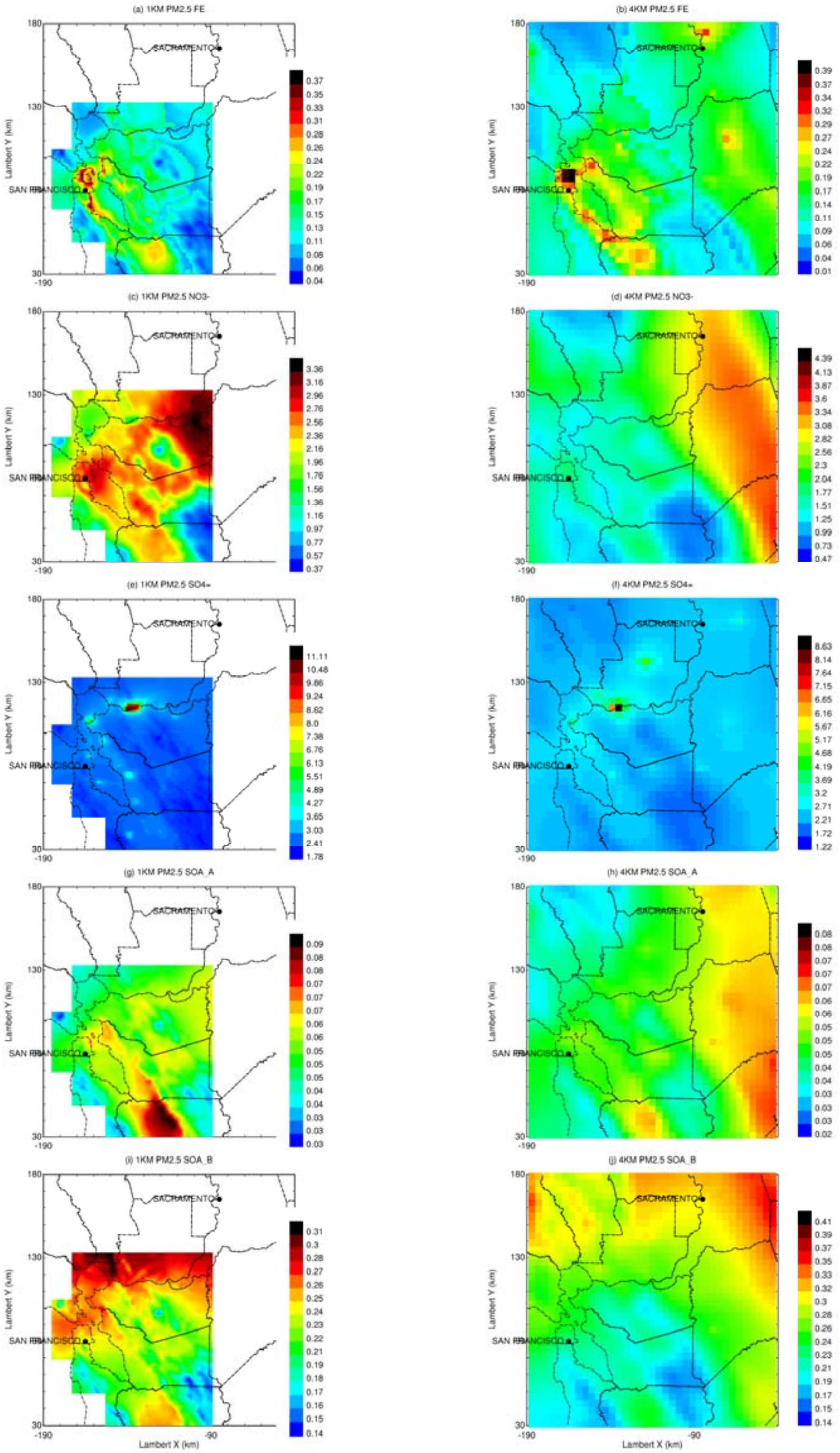

Figure 10-10: Average $PM_{2.5}$ concentrations predicted in San Francisco for the years 2000 through 2002 using 1km spatial resolution (left column) and 4km spatial resolution (right column).

Figures 10-11 and 10-12 display the predicted source contributions to primary $PM_{2.5}$ over the San Francisco Bay Area during the years 2000 through 2002. The left panel of each figure displays results simulated at 1km spatial resolution while the right panel displays results simulated at 4k spatial resolution. Contributions from on-road gasoline and diesel vehicles are resolved with finer spatial resolution in the 1km simulations compared to the 4km simulations. Contributions from off-road gasoline and diesel sources are not generally improved at higher model resolution because the underlying spatial surrogates used to allocate these emissions are only approximate.

Primary $PM_{2.5}$ contributions from point sources are more concentrated in the 1km simulations due to reduced numerical diffusion in these model predictions. This results in more concentrated $PM_{2.5}$ concentrations associated with wood combustion, aircraft emissions, and natural gas combustion.

The increased spatial resolution of the 1km emissions identifies a potential error in the allocation of restaurant food cooking emissions shown in Figure 10-12 c and d. The highest food cooking emissions are located at Treaure Island in the San Francisco Bay, but this location is lightly populated and it does not have an unusually high concentration of restaurants. This may reflect an error in the original 2000 emissions that was not corrected in the current work because the restaurant area source emissions within each of the original 4km grid cells were allocated to the most appropriate 1km grid cells within that 16 km^2 area but not reallocated outside that zone.

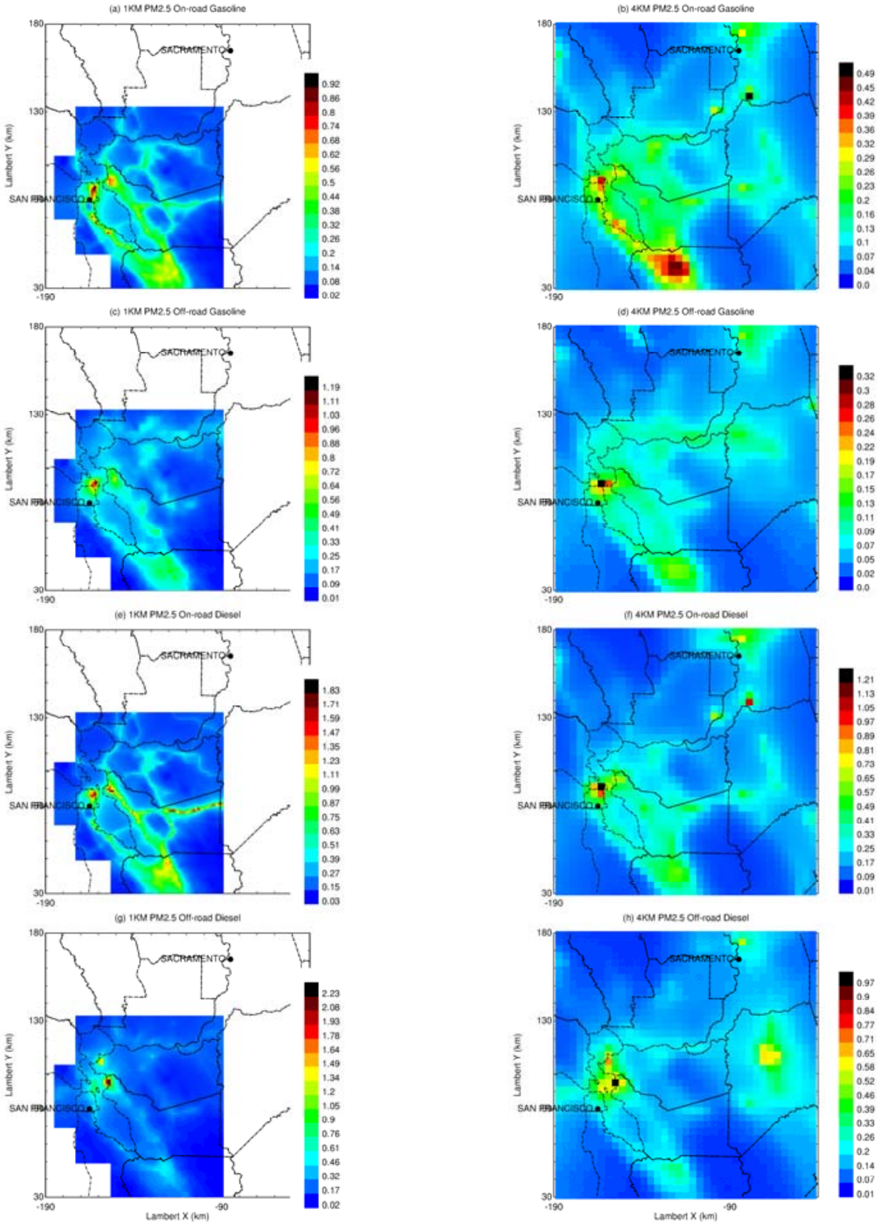

Figure 10-11: Average $PM_{2.5}$ source contributions predicted in San Francisco for the years 2000 through 2002 using 1km spatial resolution (left column) and 4km spatial resolution (right column).

(a) 1KM PM2.5 Wood Smoke (b) 4KM PM2.5 Wood Smoke

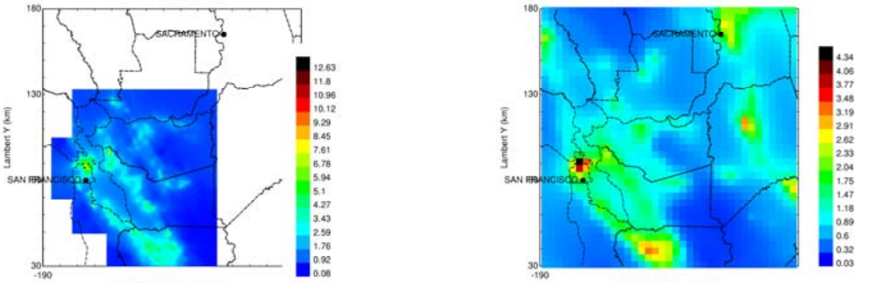

(c) 1KM PM2.5 Food Cooking (d) 4KM PM2.5 Food Cooking

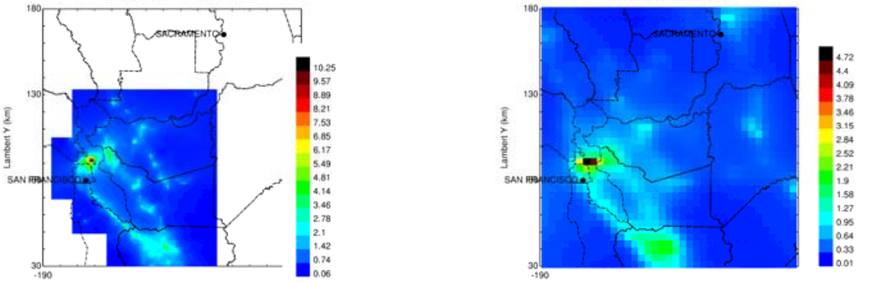

(e) 1KM PM2.5 Aircraft (f) 4KM PM2.5 Aircraft

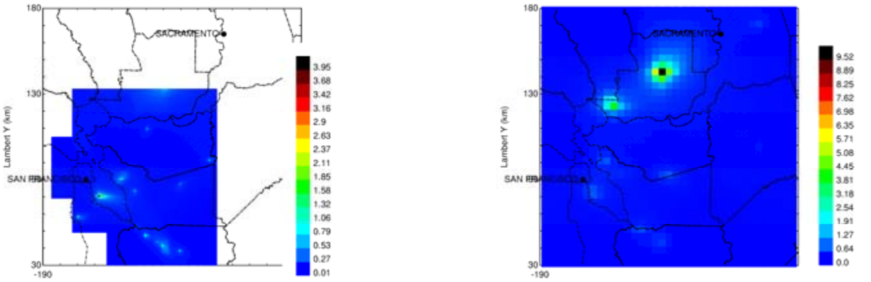

(g) 1KM PM2.5 Natural Gas (h) 4KM PM2.5 Natural Gas

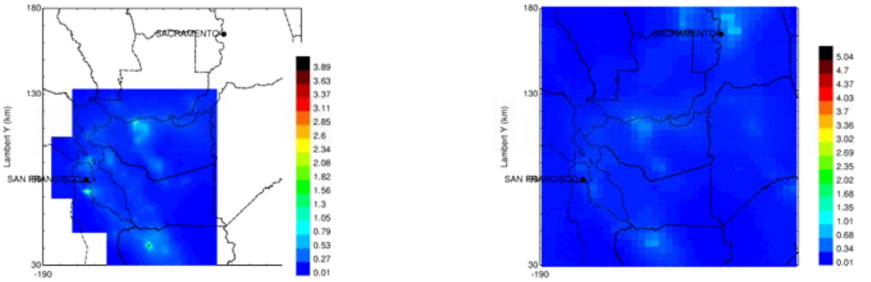

(i) 1KM PM2.5 Other (j) 4KM PM2.5 Other

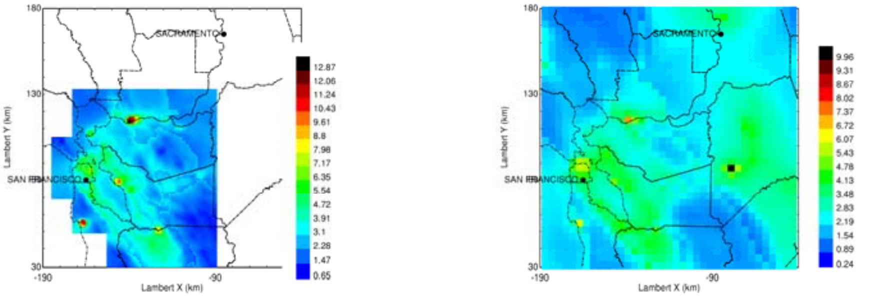

Figure 10-12: Average $PM_{2.5}$ source contributions predicted in San Francisco for the years 2000 through 2002 using 1km spatial resolution (left column) and 4km spatial resolution (right column).

10.3.4 $PM_{2.5}$ – Sacramento

Table 10-9 summarizes $PM_{2.5}$ performance statistics for simulations at the downtown Sacramento monitoring site during the years 2000 through 2002. MFB and MFE are slightly improved for $PM_{2.5}$ EC, OC, nitrate, Fe, and Mn when the model spatial resolution is increased to 1km, but performance statistics for $PM_{2.5}$ mass, sulfate, and Cu are degraded at the higher spatial resolution. These trends are similar to the results obtained at San Jose and once again reflect the increased accuracy of the predicted mobile source contributions to $PM_{2.5}$ combined with the omission of brake and tire wear emissions in the 1km simulations as discussed in Section 10.3.2.

Table 10-9. Performance statistics at downtown Sacramento for calculations run at 1km and 4km spatial resolution.

				Daily Comparison					
resolution		PM2.5 MA	PM2.5 EC	PM2.5 OC	PM2.5 Nit	PM2.5 Sul	PM2.5 Cu	PM2.5 Fe	PM2.5 Mn
1km	MFB	14.83%	-30.73%	-90.88%	-35.02%	66.72%	-119.32%	80.48%	60.80%
	MFE	46.57%	52.93%	95.14%	99.87%	77.83%	120.67%	96.04%	84.31%
4km	MFB	4.82%	-37.59%	-101.52%	-38.90%	57.29%	-20.17%	83.50%	61.49%
	MFE	43.00%	50.70%	104.62%	78.15%	77.89%	68.42%	102.10%	86.38%
				Monthly Comparison					
resolution		PM2.5 MA	PM2.5 EC	PM2.5 OC	PM2.5 Nit	PM2.5 Sul	PM2.5 Cu	PM2.5 Fe	PM2.5 Mn
1km	MFB	16.15%	-17.83%	-84.46%	-7.43%	72.41%	-139.57%	88.08%	67.88%
	MFE	34.21%	41.06%	90.64%	45.74%	72.41%	139.57%	88.08%	67.88%
4km	MFB	6.69%	-24.99%	-94.64%	-18.81%	69.85%	-32.11%	94.11%	70.22%
	MFE	27.26%	38.61%	94.64%	52.99%	69.85%	38.46%	94.11%	70.22%

Figure 10-13 illustrates the time series of predicted and measured $PM_{2.5}$ concentrations at downtown Sacramento during the years 2000 through 2002. Similar to the results for central Los Angeles discussed in Section 10.3.2, predicted and measured $PM_{2.5}$ mass, EC, and OC all peak during the winter months. Concentrations predicted using 1km spatial resolution are generally slightly higher than concentrations predicted with 4km spatial resolution, especially during peak events in winter periods. These increased concentrations reflect the reduced numerical diffusion at increased spatial resolution and the higher mobile source emissions calculated using the fuel-based inventory methods [337].

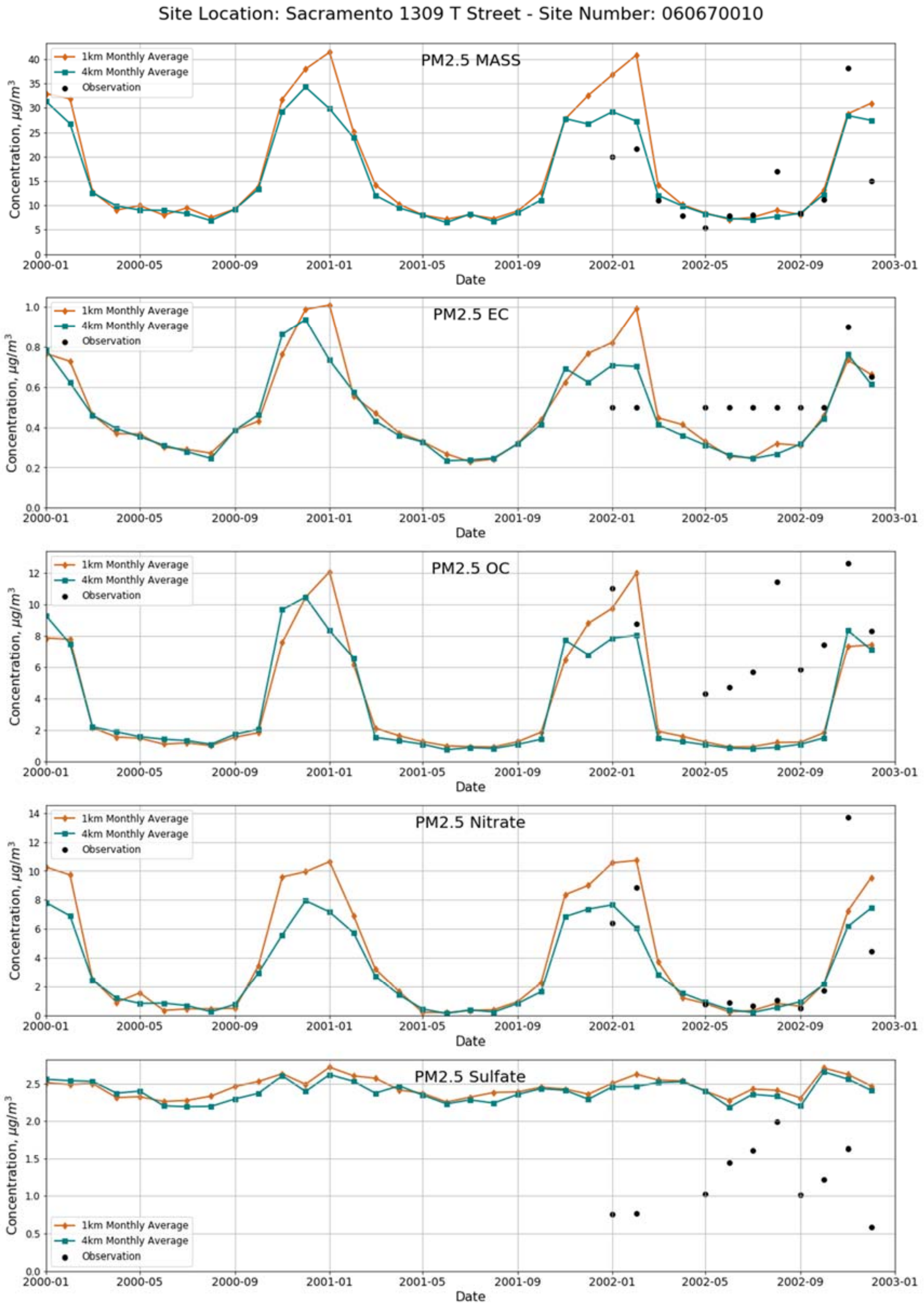

Figure 10-13: Time series of $PM_{2.5}$ concentrations predicted at downtown Sacramento using 1km spatial resolution and 4km spatial resolution.

Figures 10-14 and 10-15 display predicted $PM_{2.5}$ concentrations over Sacramento averaged between the years 2000 through 2002. The left panel of each figure displays results at 1km resolution while the right panel displays results at 4km resolution. The trends observed over Sacramento generally match the trends discussed previously for the San Francisco Bay Area and Los Angeles. $PM_{2.5}$ species emitted by point sources have higher concentrations around those sources when simulated at higher spatial resolution due to less numerical diffusion. $PM_{2.5}$ EC is better resolved due to the improved ability to capture the spatial trends of the highway network, but $PM_{2.5}$ OC has significant contributions from area sources that continue to produce uniform spatial distributions over the entire urban area. Secondary $PM_{2.5}$ nitrate and SOA is uniformly distributed in space due to the regional secondary chemistry that produces these pollutants in the upper atmosphere and then mixes them to the earth's surface during the daytime hours. Predicted $PM_{2.5}$ nitrate and SOA_A concentrations were higher in the 1km simulations than in the 4km simulations due to higher mobile source emissions estimated using fuel consumption methods [337].

Figures 10-16 and 10-17 display predicted primary $PM_{2.5}$ source contributions over Sacramento during the study period. On-road sources and point sources benefit from the increased spatial resolution, but area sources do not generally show significant enhanced features.

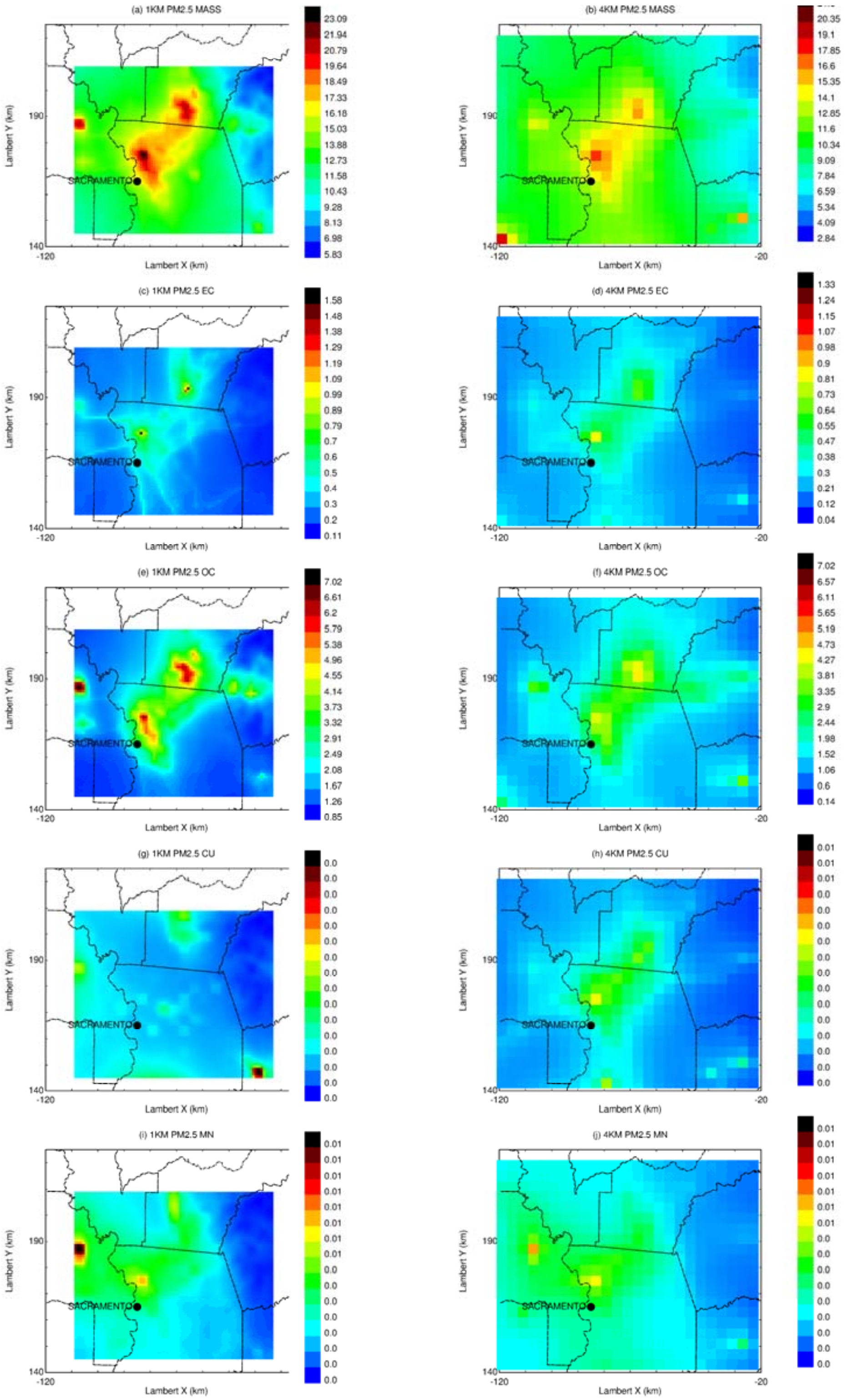

Figure 10-14: Average PM2.5 concentrations predicted in Sacramento for the years 2000 through 2002 using 1km spatial resolution (left column) and 4km spatial resolution (right column).

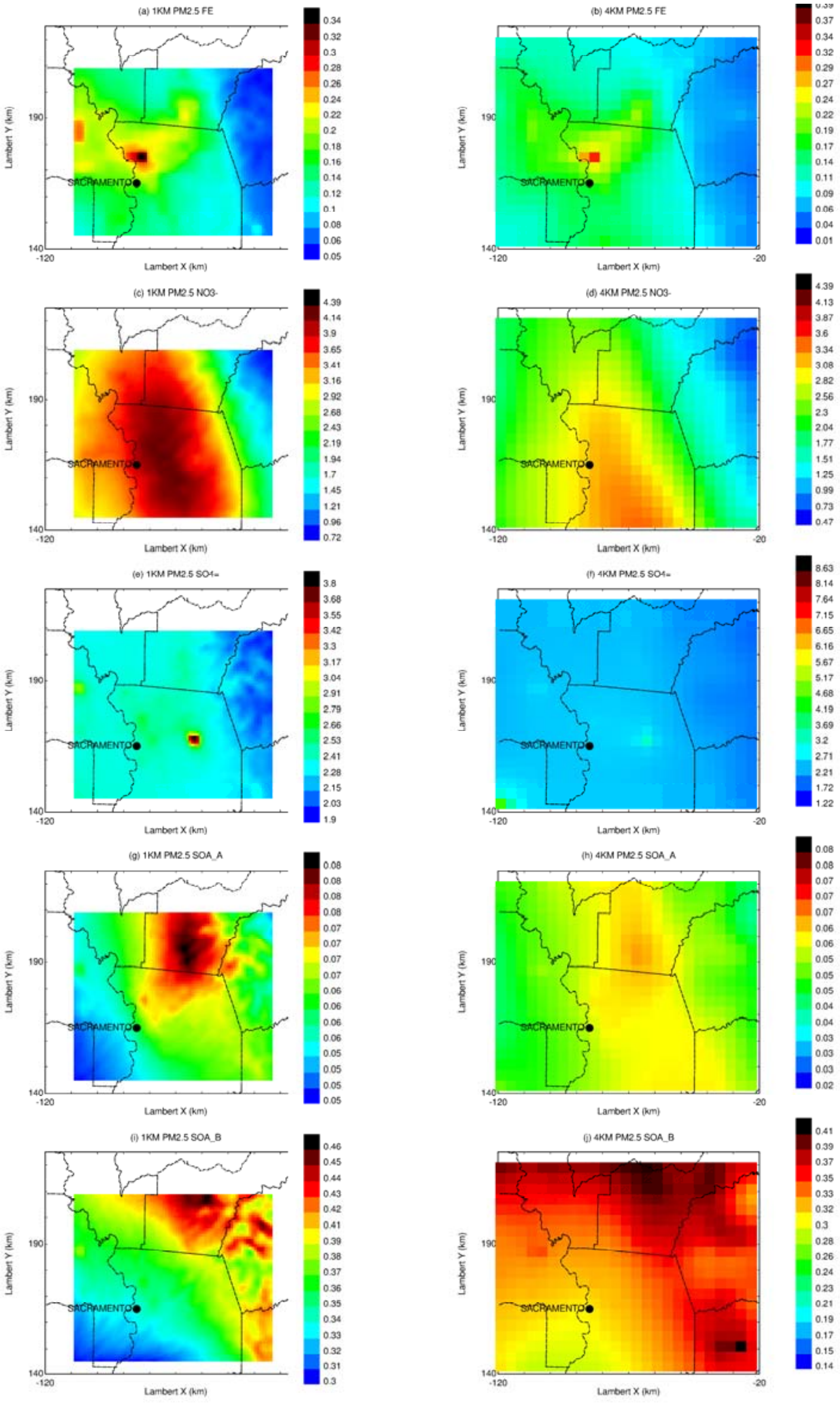

Figure 10-15: Average PM2.5 concentrations predicted in Sacramento the years 2000 through 2002 using 1km spatial resolution (left column) and 4km spatial resolution (right column).

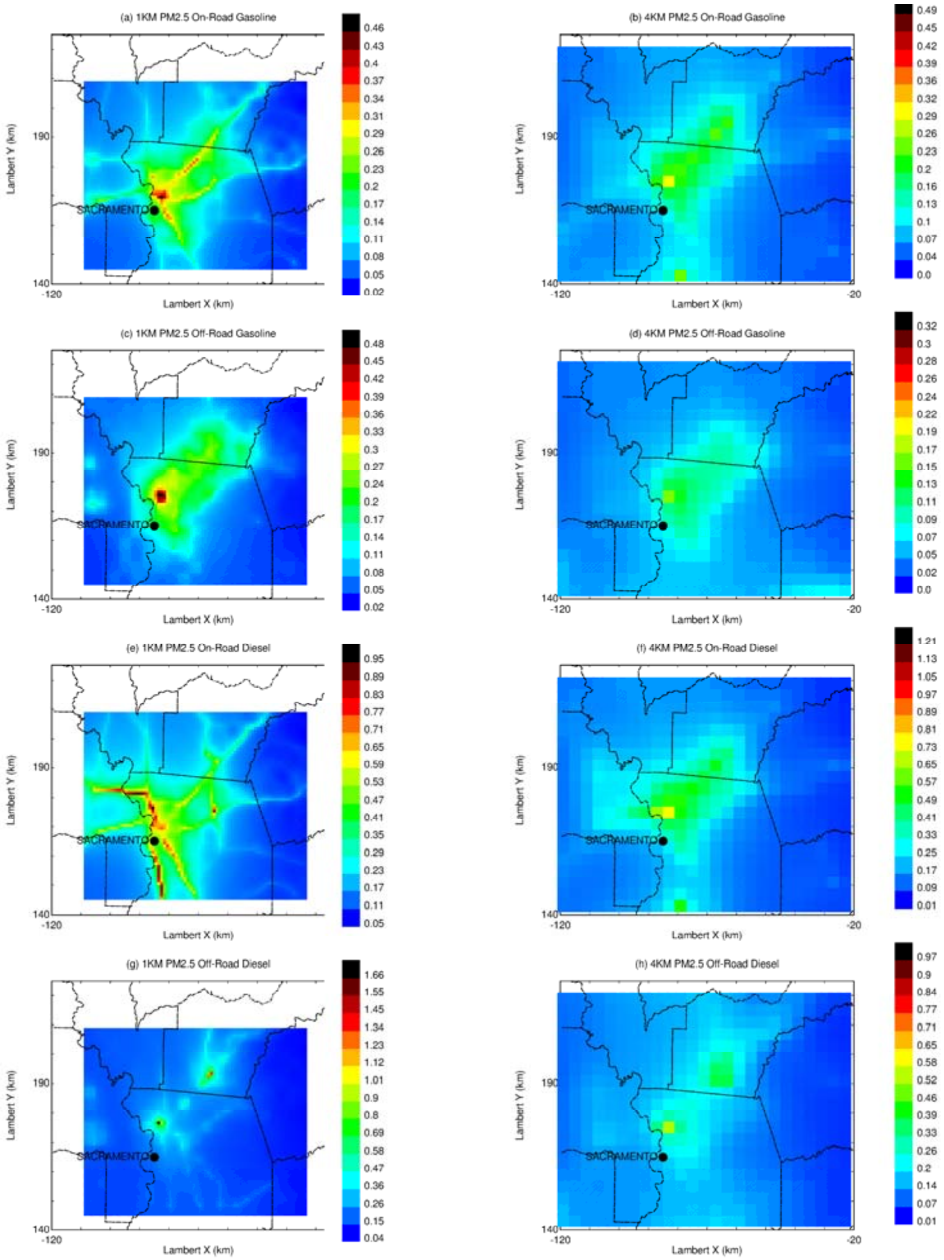

Figure 10-16: Average $PM_{2.5}$ source contributions predicted in Sacramento the years 2000 through 2002 using 1km spatial resolution (left column) and 4km spatial resolution (right column).

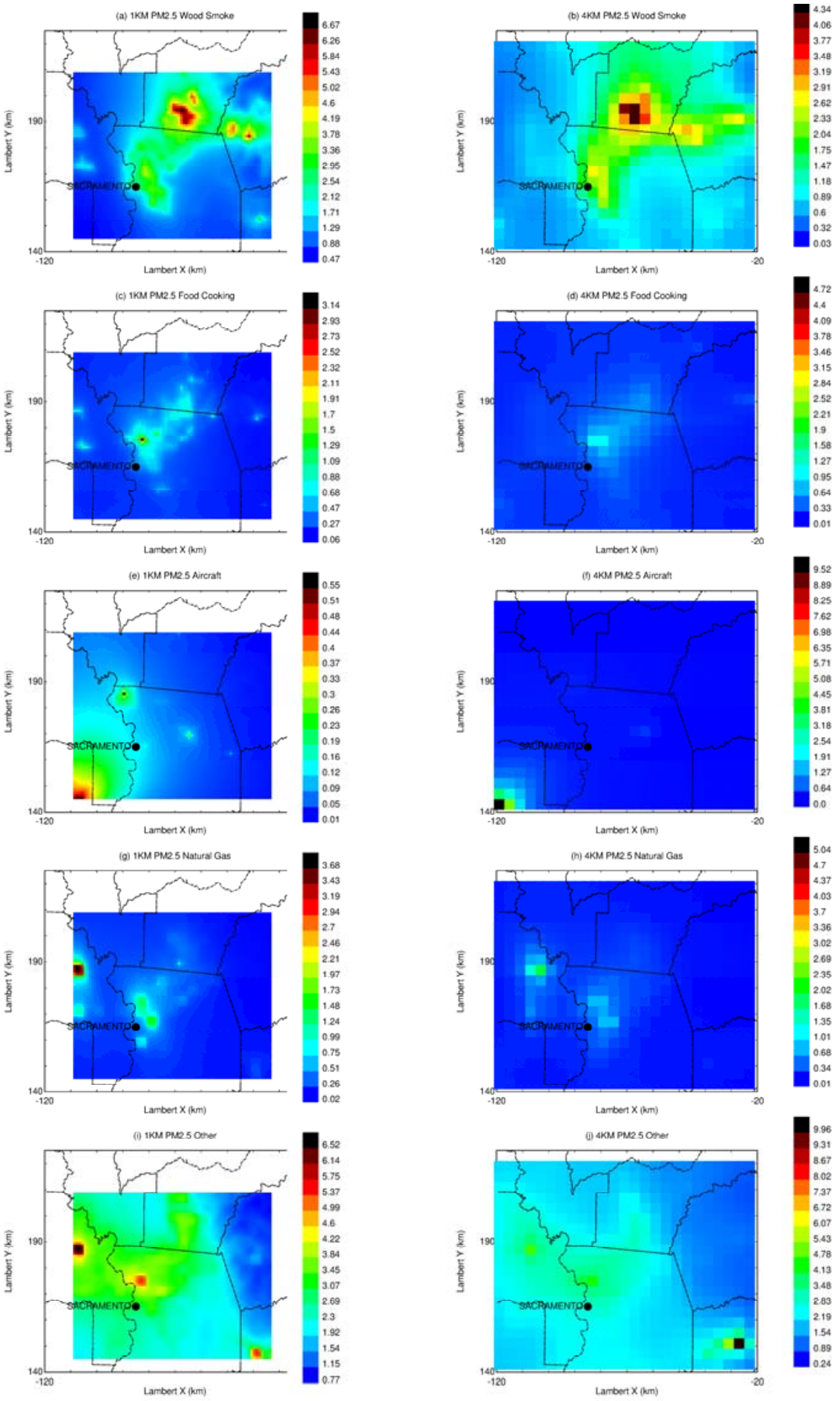

Figure 10-17: Average $PM_{2.5}$ source contributions predicted in Sacramento the years 2000 through 2002 using 1km spatial resolution (left column) and 4km spatial resolution (right column).

10.3.5 $PM_{0.1}$ – Los Angeles

Figures 10-18 and 10-19 illustrate the $PM_{0.1}$ concentrations over the South Coast Air Basin surrounding Los Angeles averaged over the years 2000 through 2002. Figures 10-20 and 10-21 display source contributions to primary $PM_{0.1}$ over this same time period. The left panel of each figure displays 1km simulation results while the right panel displays 4km simulation results. The trends illustrated in each figure are generally similar to those discussed for $PM_{2.5}$ concentrations in Section 10.3.2. Thus, it appears that the main effects of increased spatial resolution are related to physical transport processes that affect all particle size fractions approximately equally.

The size distribution of particles emitted from tire and brake wear in the current study does not extend into the ultrafine particle size range. As a result, the lack of the tire and brake wear emissions from the 1km simulations does not affected the predicted spatial distribution of $PM_{0.1}$ Cu, Fe, or "Other Sources". Predicted $PM_{0.1}$ concentration fields for each of these components or sources is generally consistent between simulations using 1km and 4km spatial resolution.

The particle size distribution for aircraft emissions is primarily in the ultrafine size range and so the differences between 1km and 4km simulations are very similar for $PM_{0.1}$ and $PM_{2.5}$ size fractions. As discussed in Section 10.3.2, the updated emissions in the 1km simulations are considered to be more accurate than the emissions in the original year 2000 emissions inventory.

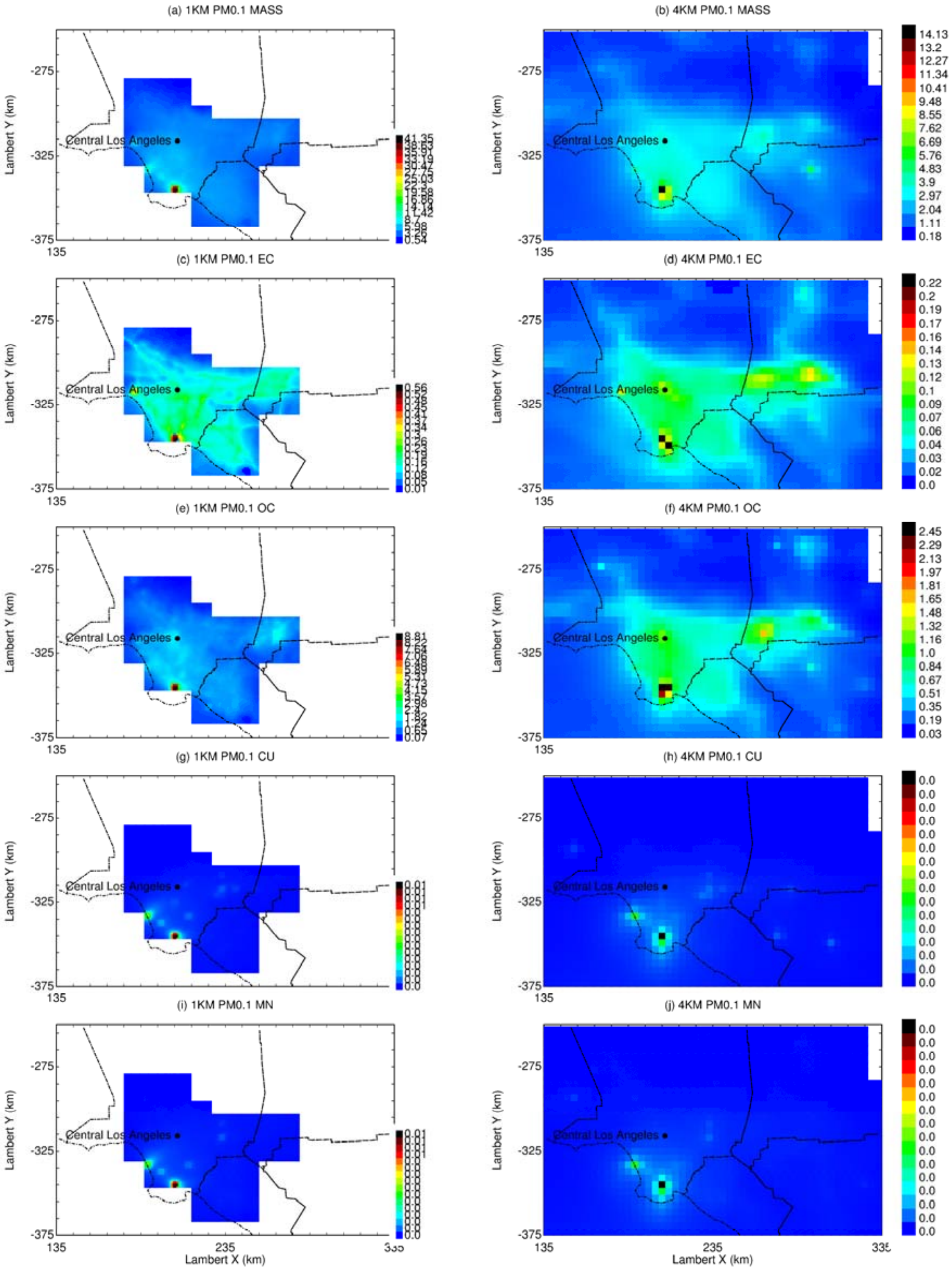

Figure 10-18: Average $PM_{0.1}$ concentrations predicted in Los Angeles for the years 2000 through 2002 using 1km spatial resolution (left column) and 4km spatial resolution (right column).

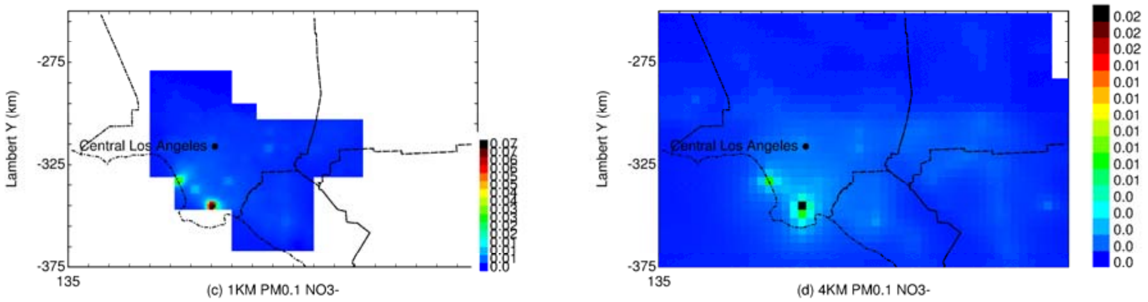
(a) 1KM PM0.1 FE

(b) 4KM PM0.1 FE

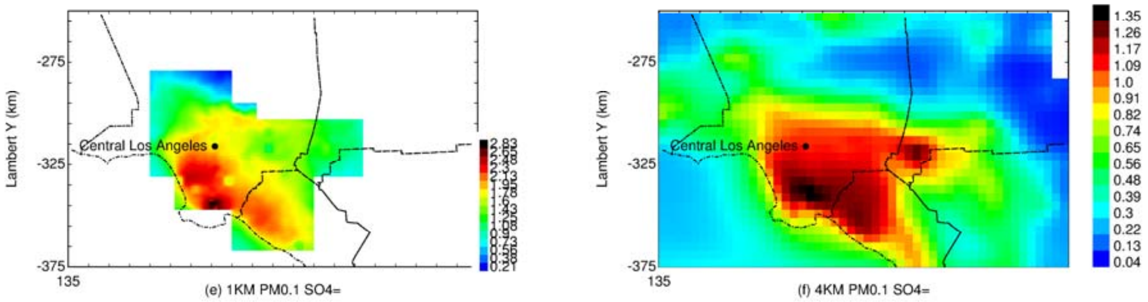
(c) 1KM PM0.1 NO3-

(d) 4KM PM0.1 NO3-

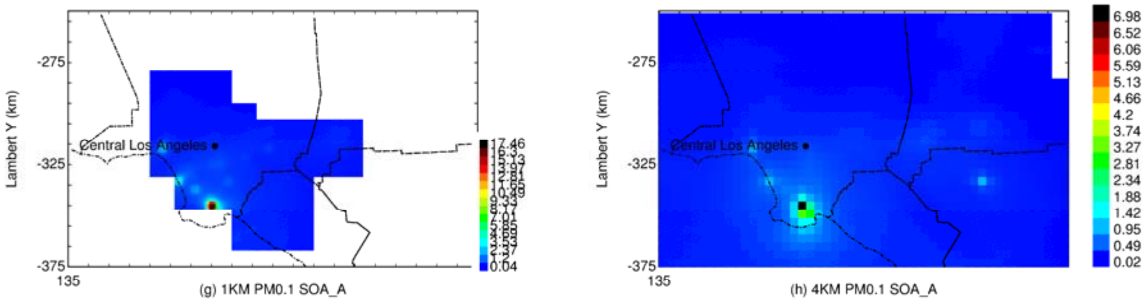
(e) 1KM PM0.1 SO4=

(f) 4KM PM0.1 SO4=

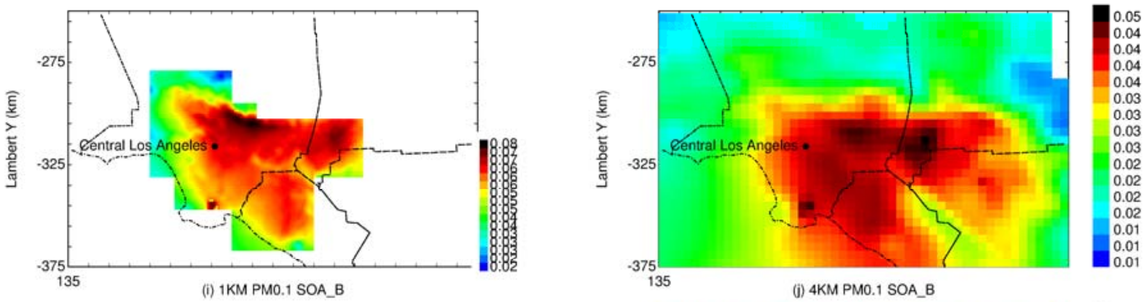
(g) 1KM PM0.1 SOA_A

(h) 4KM PM0.1 SOA_A

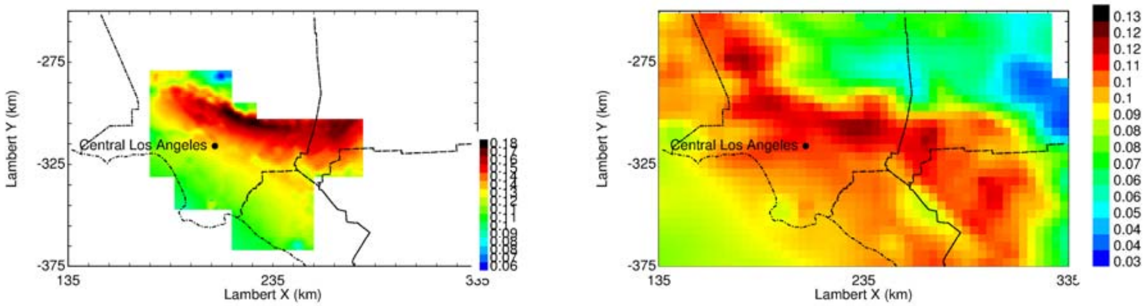
(i) 1KM PM0.1 SOA_B

(j) 4KM PM0.1 SOA_B

Figure 10-19: Average $PM_{0.1}$ concentrations predicted in Los Angeles for the years 2000 through 2002 using 1km spatial resolution (left column) and 4km spatial resolution (right column).

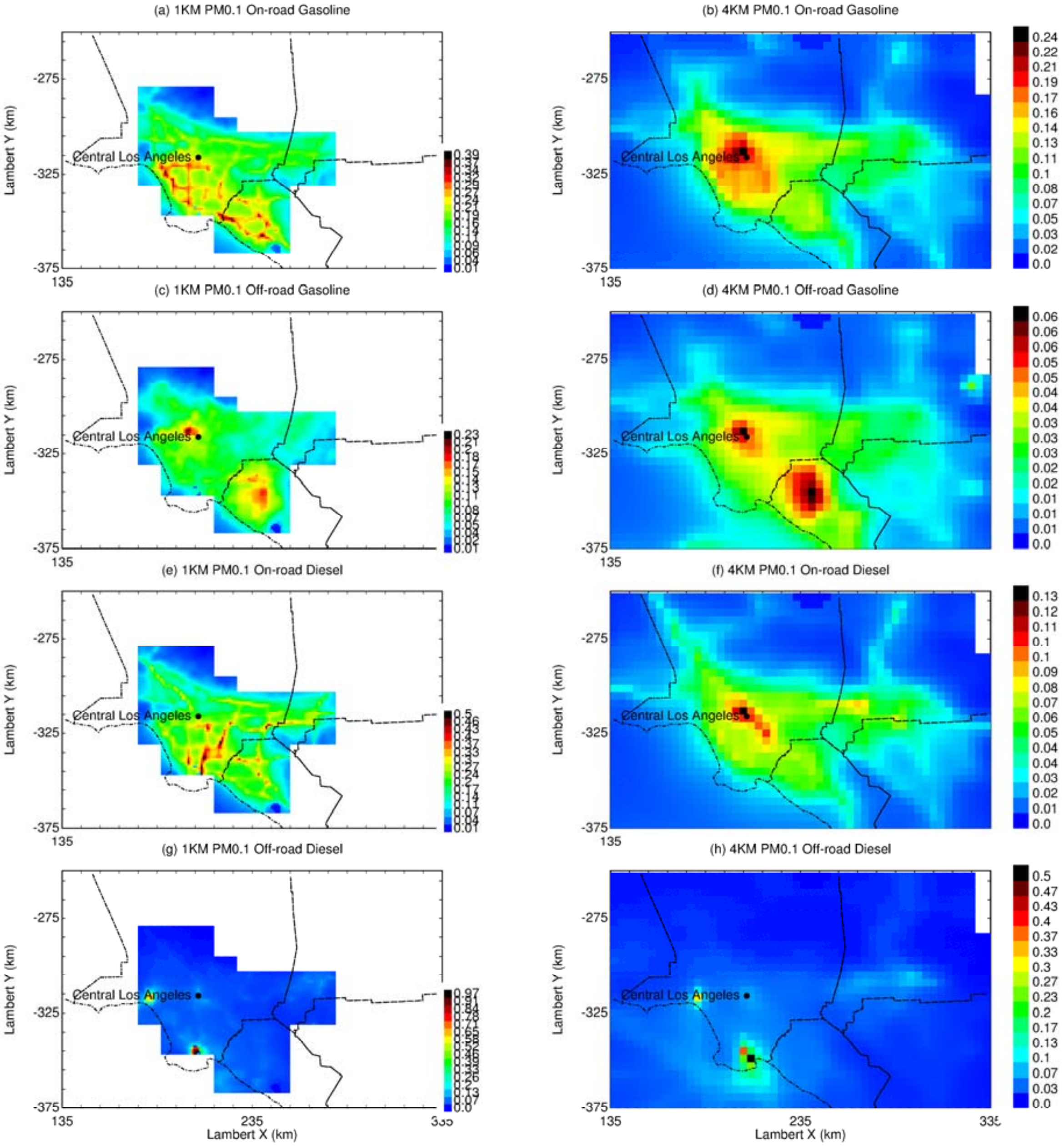

Figure 10-20: Average PM$_{0.1}$ source contributions predicted in Los Angeles for the years 2000 through 2002 using 1km spatial resolution (left column) and 4km spatial resolution (right column).

(a) 1KM PM0.1 Wood Smoke (b) 4KM PM0.1 Wood Smoke

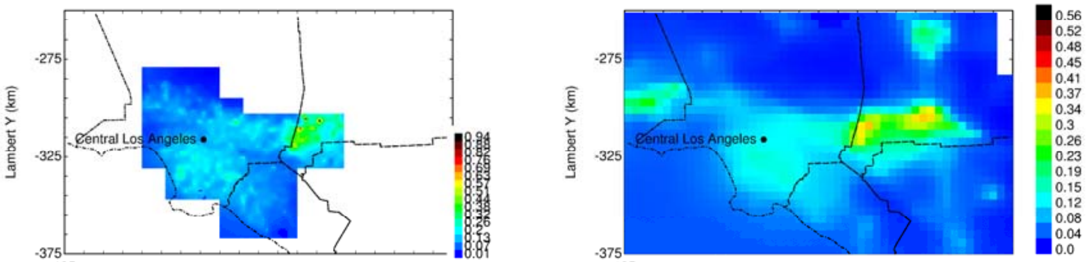

(c) 1KM PM0.1 Food Cooking (d) 4KM PM0.1 Food Cooking

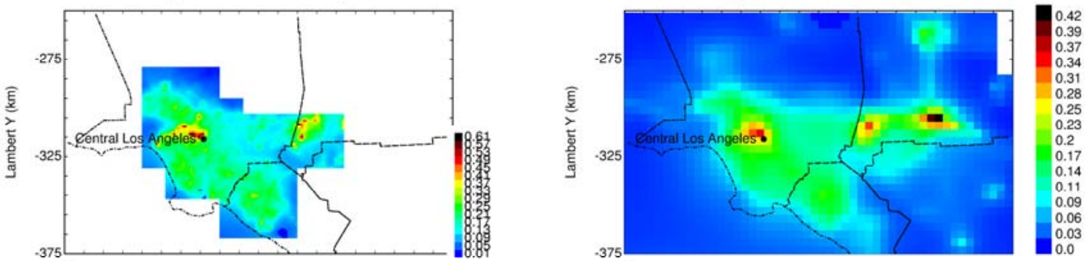

(e) 1KM PM0.1 Aircraft (f) 4KM PM0.1 Aircraft

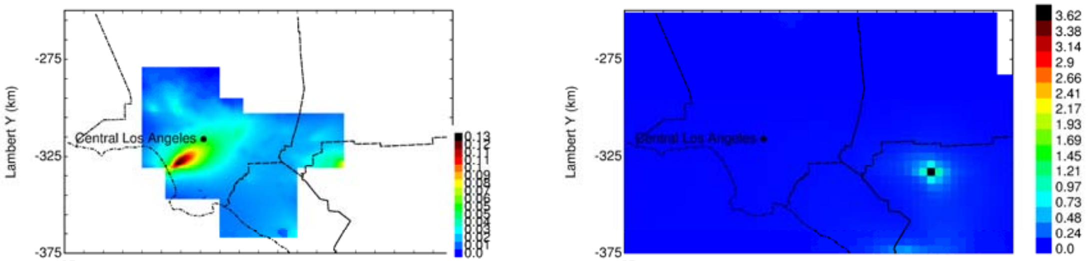

(g) 1KM PM0.1 Natural Gas (h) 4KM PM0.1 Natural Gas

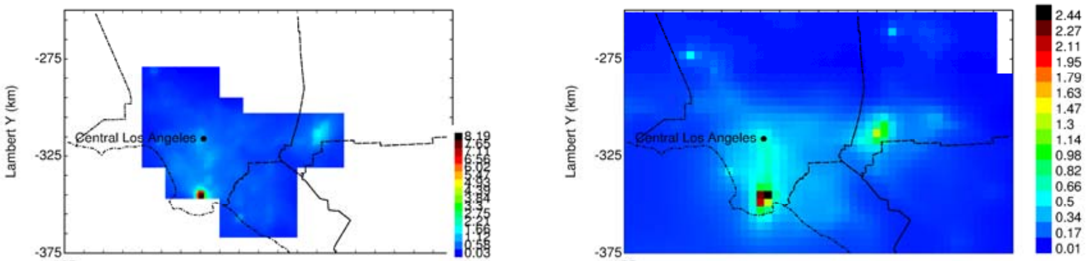

(i) 1KM PM0.1 Other (j) 4KM PM0.1 Other

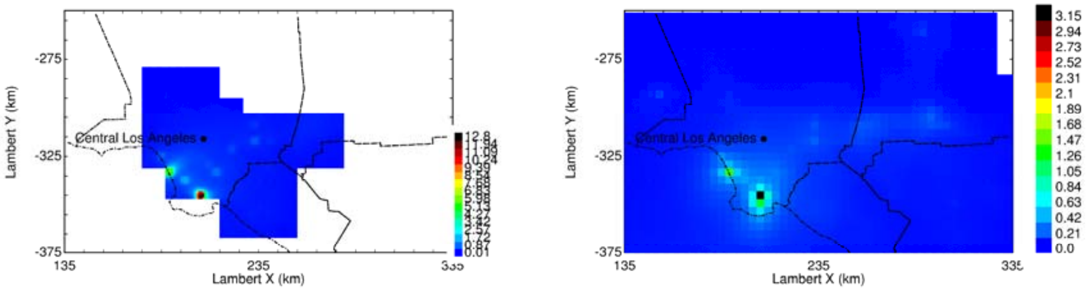

Figure 10-21: Average $PM_{0.1}$ source contributions predicted in Los Angeles for the years 2000 through 2002 using 1km spatial resolution (left column) and 4km spatial resolution (right column).

10.3.6 $PM_{0.1}$ – San Francisco Bay Area

Figures 10-22 and 10-23 illustrate the $PM_{0.1}$ concentrations over the San Francisco Bay Area durng the years 2000 through 2002. Figures 10-24 and 10-25 display source contributions to primary $PM_{0.1}$ over this same time period. The left panel of each figure displays 1km simulation results while the right panel displays 4km simulation results. The trends illustrated in each figure are generally similar to those discussed for $PM_{2.5}$ concentrations in Section 10.3.3. Mobile and point sources have enhanced concentrations in the 1km simulations but area sources do not show major changes compared to 4km simulations. Once again, $PM_{0.1}$ Cu, Fe, or “Other Sources” predicted at 1km resolution and 4km resolution are in general agreement because the size distribution for tire and brake wear does not extend into the ultrafine size fraction.

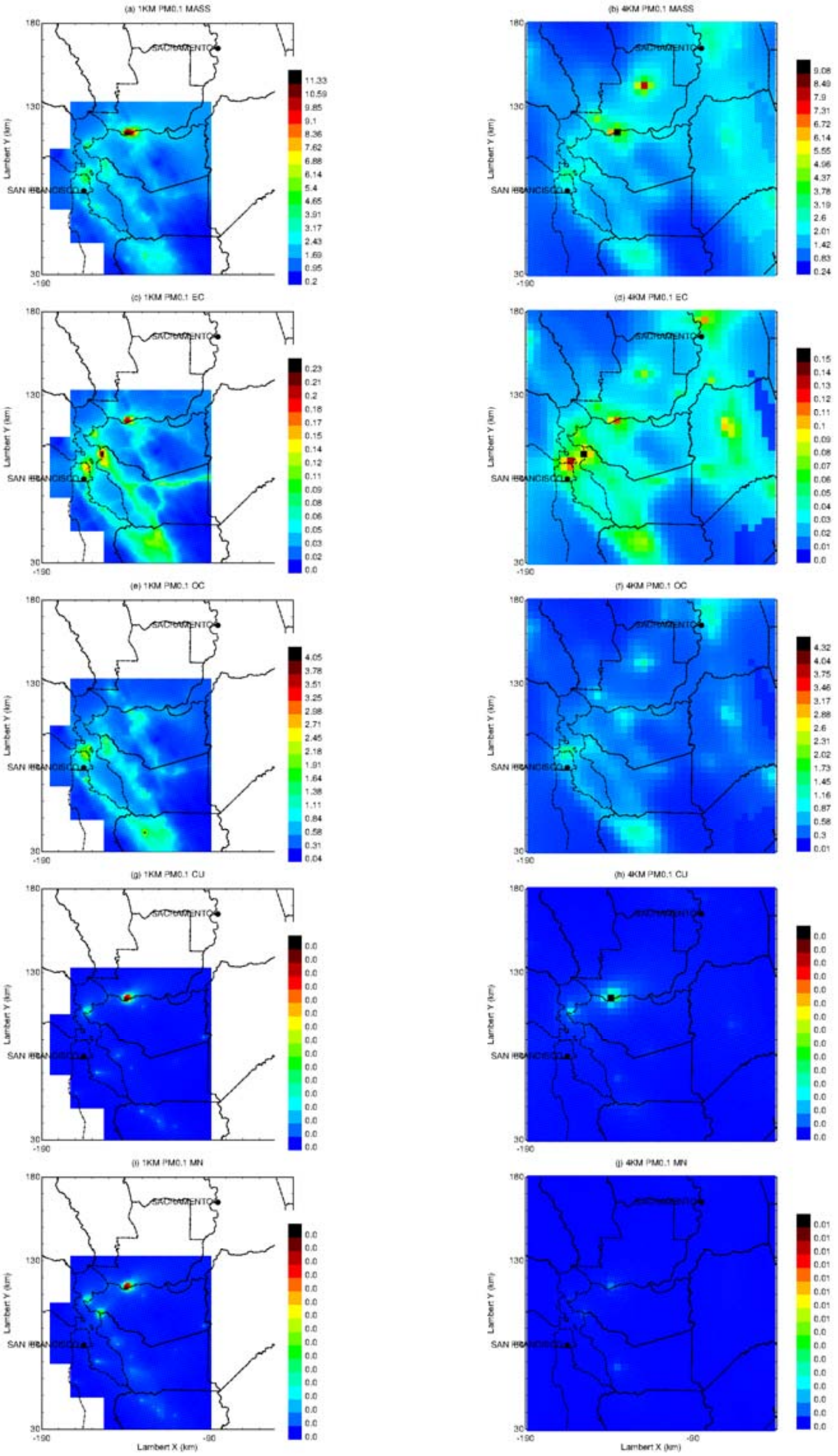

Figure 10-22: Average $PM_{0.1}$ concentrations predicted in San Francisco for the years 2000 through 2002 using 1km spatial resolution (left column) and 4km spatial resolution (right column).

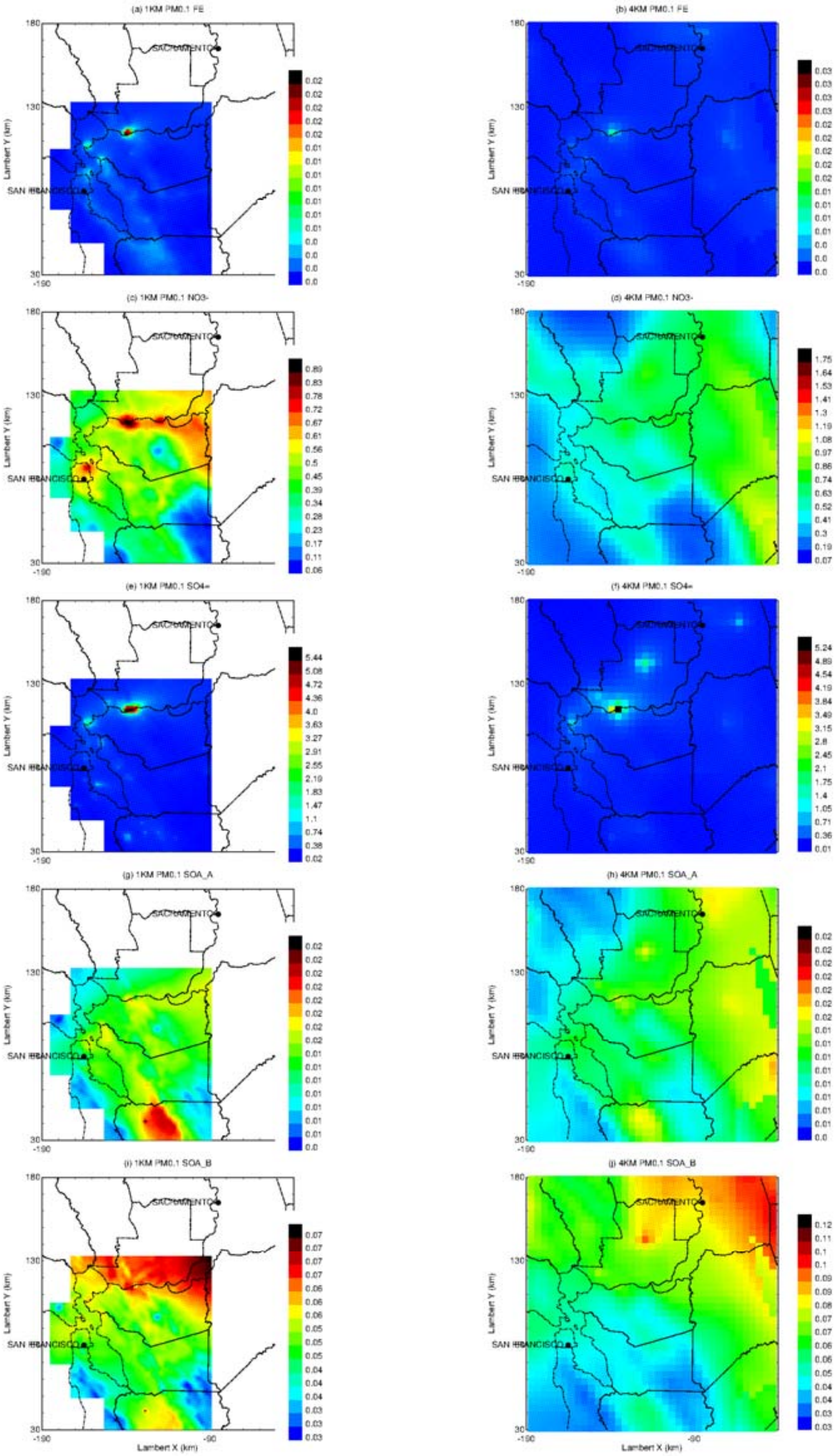

Figure 10-23: Average $PM_{0.1}$ concentrations predicted in San Francisco for the years 2000 through 2002 using 1km spatial resolution (left column) and 4km spatial resolution (right column).

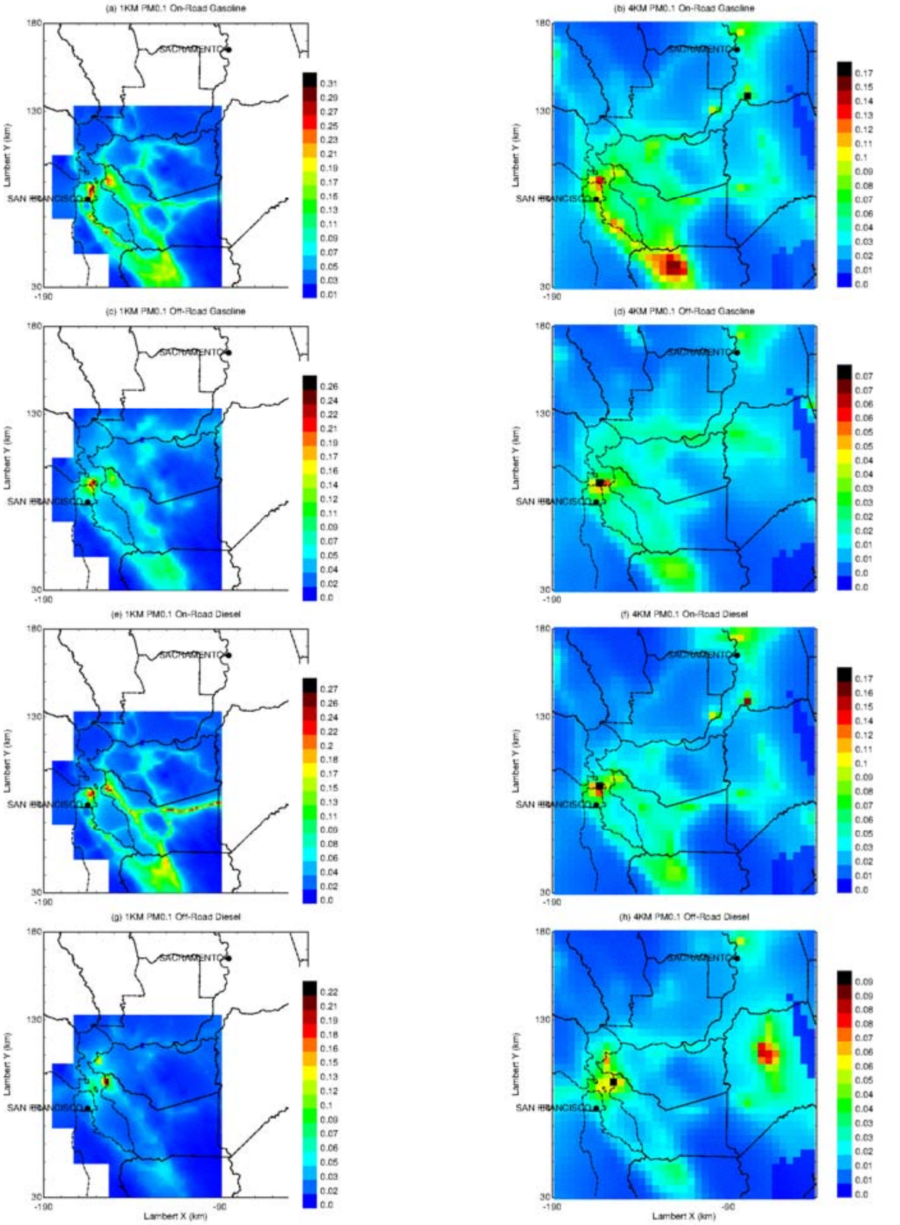

(a) 1KM PM0.1 On-Road Gasoline

(b) 4KM PM0.1 On-Road Gasoline

(c) 1KM PM0.1 Off-Road Gasoline

(d) 4KM PM0.1 Off-Road Gasoline

(e) 1KM PM0.1 On-Road Diesel

(f) 4KM PM0.1 On-Road Diesel

(g) 1KM PM0.1 Off-Road Diesel

(h) 4KM PM0.1 Off-Road Diesel

Figure 10-24: Average $PM_{0.1}$ source contributions predicted in San Francisco for the years 2000 through 2002 using 1km spatial resolution (left column) and 4km spatial resolution (right column).

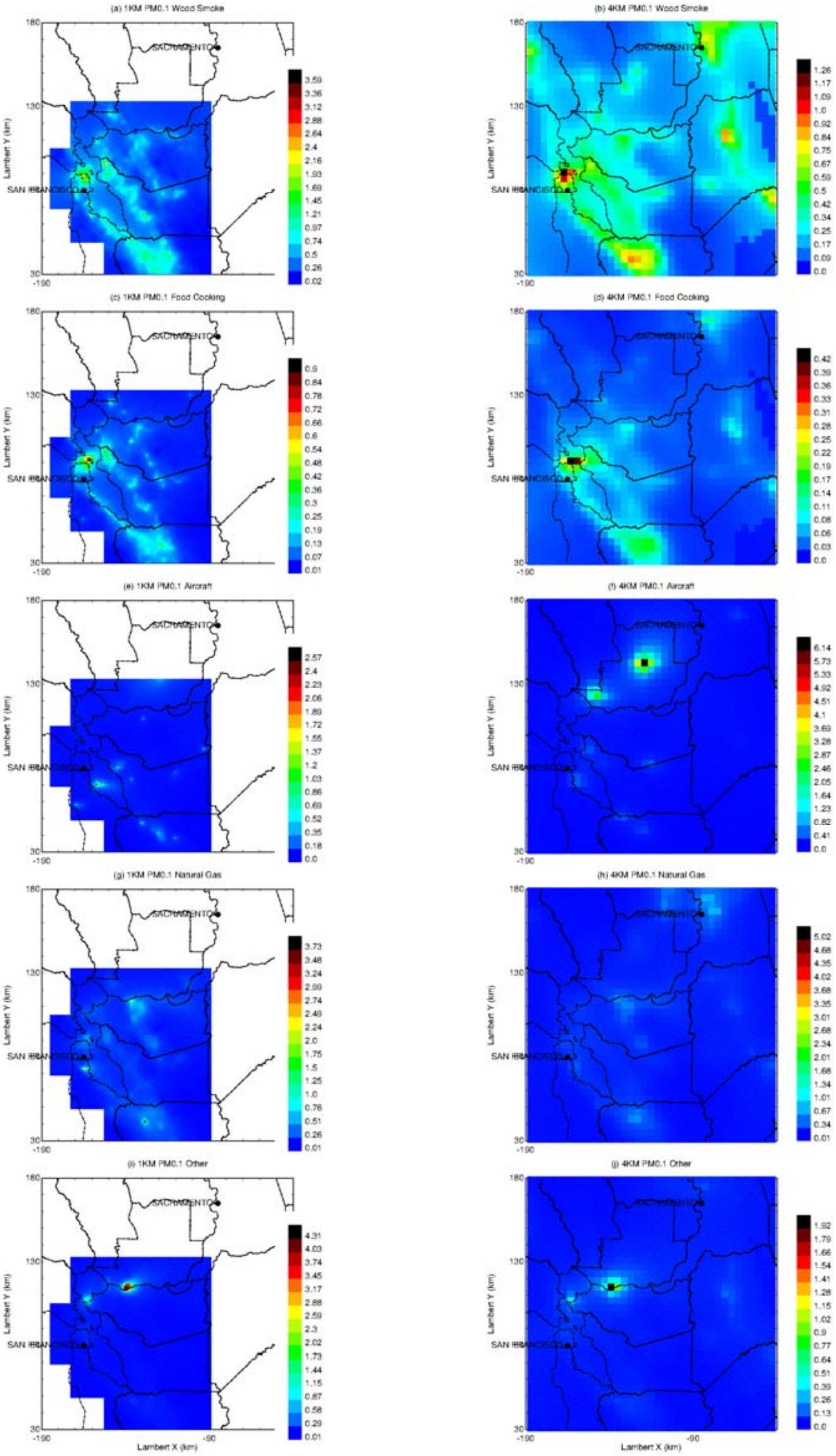

Figure 10-25: Average $PM_{0.1}$ source contributions predicted in San Francisco for the years 2000 through 2002 using 1km spatial resolution (left column) and 4km spatial resolution (right column).

10.3.7 $PM_{0.1}$ – Sacramento

Figures 10-26 and 10-27 illustrate the $PM_{0.1}$ concentrations over the San Francisco Bay Area during the years 2000 through 2002. Figures 10-28 and 10-29 display source contributions to primary $PM_{0.1}$ over this same time period. The left panel of each figure displays 1km simulation results while the right panel displays 4km simulation results. The trends illustrated in each figure are generally similar to those discussed for $PM_{2.5}$ concentrations in Section 10.3.3. Mobile and point sources have enhanced concentrations in the 1km simulations but area sources do not show major changes compared to 4km simulations. Once again, $PM_{0.1}$ Cu, Fe, or "Other Sources" predicted at 1km resolution and 4km resolution are in general agreement because the size distribution for tire and brake wear does not extend into the ultrafine size fraction.

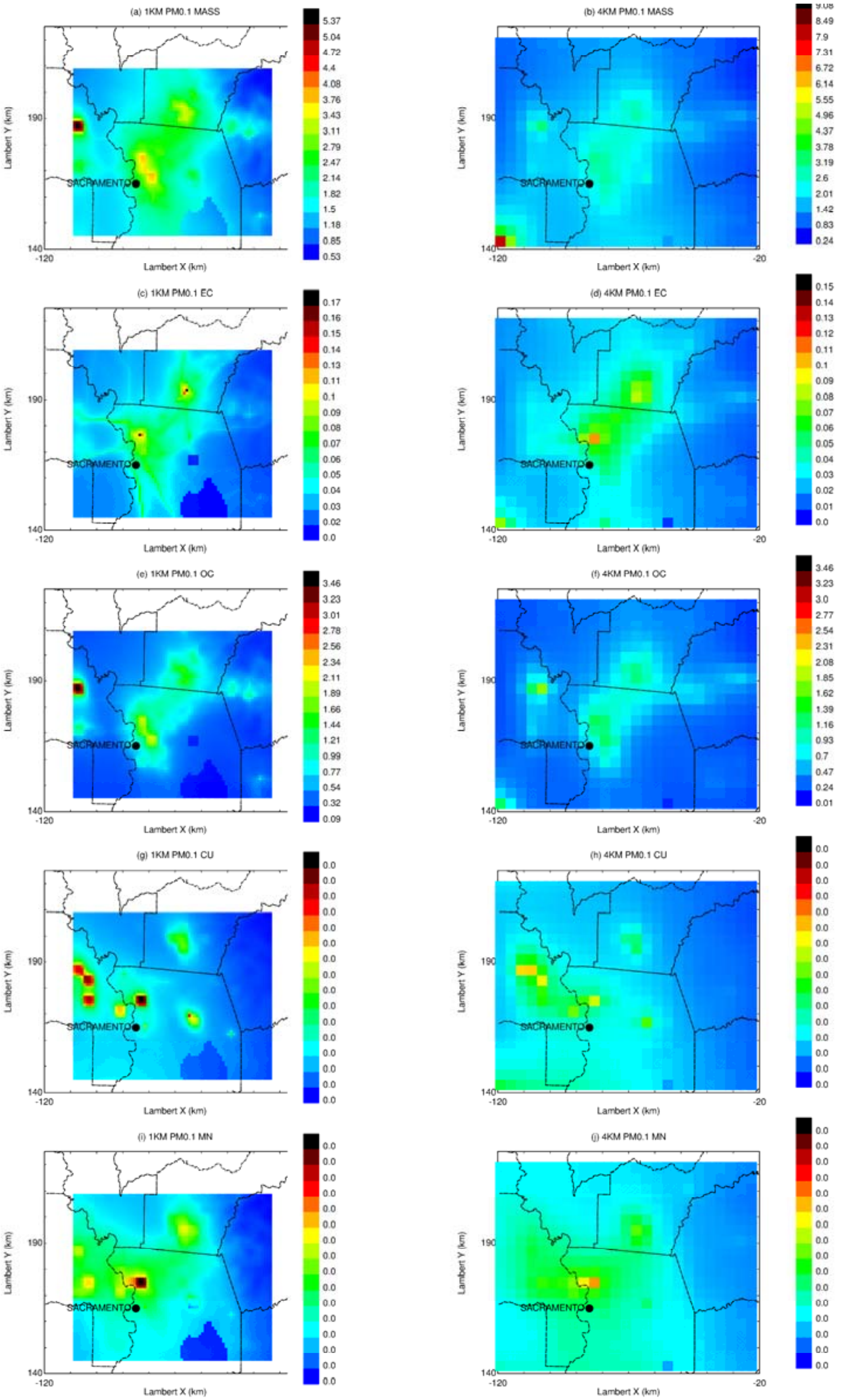

Figure 10-26: Average $PM_{0.1}$ concentrations predicted in Sacramento for the years 2000 through 2002 using 1km spatial resolution (left column) and 4km spatial resolution (right column).

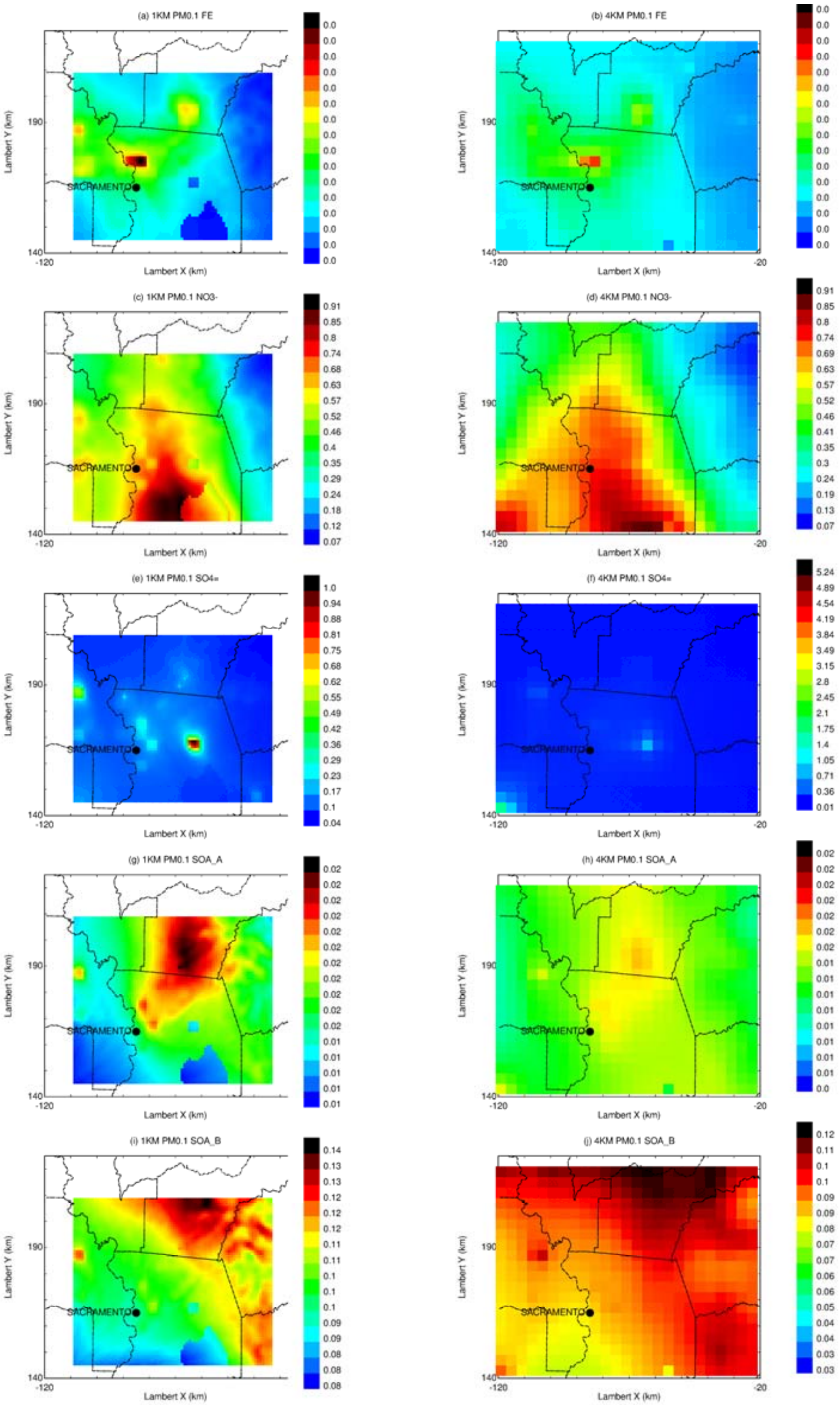

Figure 10-27: Average PM0.1 concentrations predicted in Sacramento for the years 2000 through 2002 using 1km spatial resolution (left column) and 4km spatial resolution (right column).

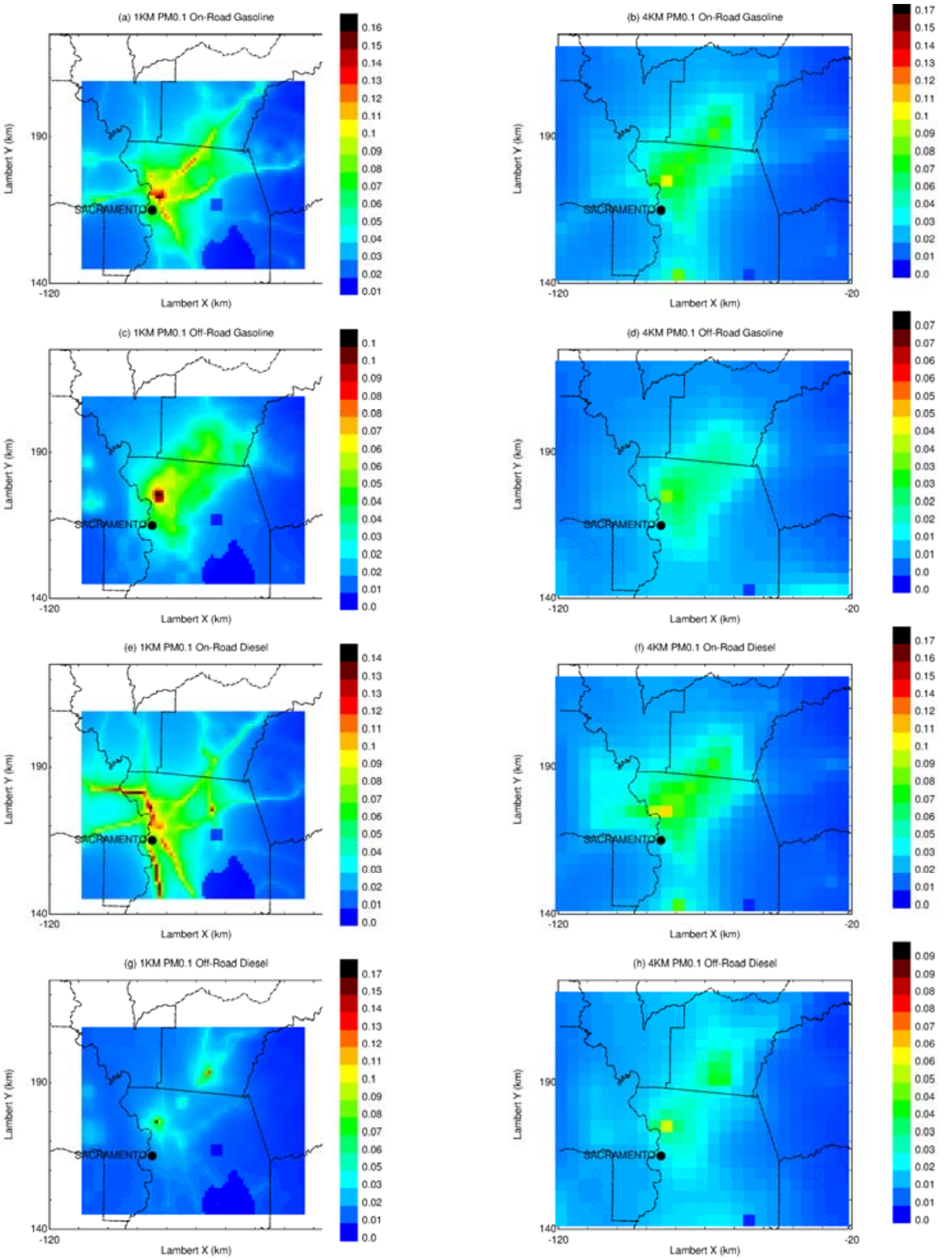

Figure 10-28: Average $PM_{0.1}$ source contributions predicted in Sacramento for the years 2000 through 2002 using 1km spatial resolution (left column) and 4km spatial resolution (right column).

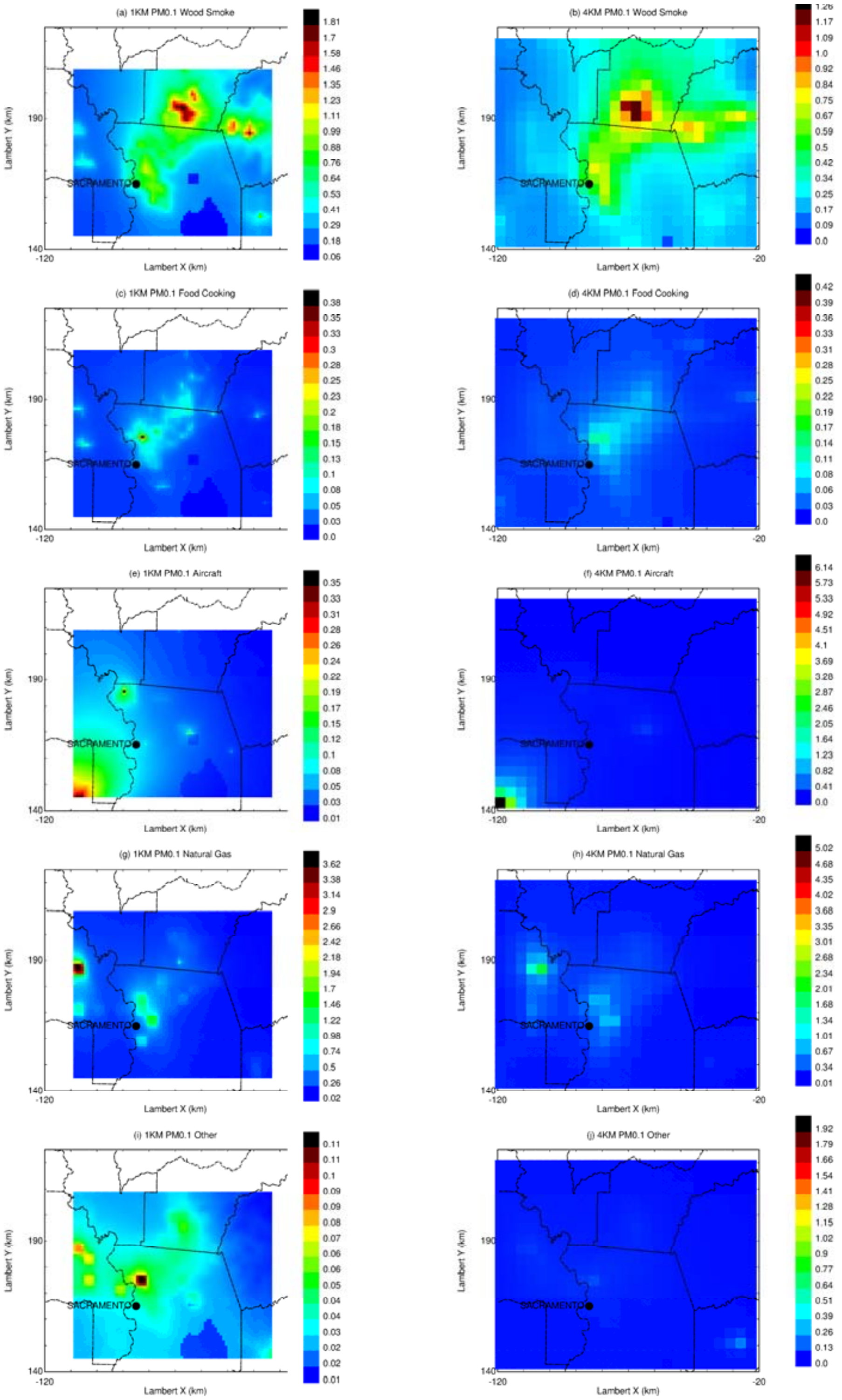

Figure 10-29: Average $PM_{0.1}$ source contributions predicted in Sacramento for the years 2000 through 2002 using 1km spatial resolution (left column) and 4km spatial resolution (right column).

10.4 Conclusions

Emissions inventories with 1km spatial resolution were created for the South Coast Air Basin, San Francisco Bay Area, and Sacramento for the years 2000 through 2002. Mobile source emissions with 1km resolution were estimated using a fuel-consumption approach that produced slightly higher total emissions of PM and NOx compared to the standard mobile source emissions inventory produced by CARB. Major area source emissions with 1km resolution were re-gridded using updated spatial surrogates that refined the location of the emissions within each 4km grid cells in the original emissions inventory produced by CARB (leaving the grid-wide total emissions unchanged). Major point source emissions were specified in the 1km grid cell where the facility was located.

Statistical analysis indicates that increasing the model resolution from 4km to 1km increases the accuracy of $PM_{2.5}$ predictions related to mobile sources. The spatial distribution of mobile source pollutant concentrations at 1km resolution follows the location of major highways but these concentrations have a uniform distribution lacking finer spatial detail when simulated with 4km resolution. Likewise, $PM_{0.1}$ predictions at 1km resolution can resolve major freeways in all domains while predictions at 4km resolution produce more uniform regional concentrations.

The concentration field around point sources is more focused in simulations that use 1km spatial resolution compared to 4km resolution. Point source emissions are distributed uniformly throughout the grid cell they are emitted into in a process call "numerical diffusion" that is an unavoidable feature of the Eulerian grid modeling approach. The calculations carried out at 1km spatial resolution show that actual atmospheric diffusion is relatively slow and the numerical diffusion inherent in the 4km calculations likely under-estimates the true concentration field around point sources. The net effect of this numerical diffusion on population exposure may be minimal because only a small fraction of the total population lives within 4km of a major point source. Numerical diffusion may be more important when considering air pollution impacts for segments of the population in lower socio-economic classes since these groups may be attracted to the regions around point sources by lower housing prices.

$PM_{2.5}$ predictions related to area sources are not strongly affected by increasing the model resolution from 4km to 1km. The spatial surrogates used to allocate area source emissions are reasonably accurate when viewed from a statewide perspective but they lack detail at finer spatial resolution approaching 1km. Spatial surrogates used to allocate many area emissions are relatively uniform over urban areas in California leading to uniform emissions and uniform concentration fields irrespective of the increased resolution of the calculations.

Concentration fields for secondary pollutants including particulate nitrate and secondary organic aerosol do not exhibit finer spatial details when simulations are performed at 1km resolution compared to 4km resolution. The processes that form secondary pollutants occur in a mixed zone of the troposphere which inherently removes fine-scale spatial gradients.

The slightly higher mobile source emissions rates in the fuel-based inventory at 1km resolution produce higher concentrations of secondary $PM_{2.5}$ and $PM_{0.1}$ components including nitrate and anthropogenic secondary organic aerosol. These increased concentrations also contribute to the improved performance of the model calculations carried out at 1km spatial resolution. While not the focus of the current analysis, this finding suggests that some of the model under-predictions noted in Sections 7, 8, and 9 may be related to uncertainty in mobile source emissions estimates.

The spatial distribution of primary $PM_{2.5}$ and primary $PM_{0.1}$ differs in 1km compared to 4km simulations for both gasoline and diesel vehicles. These changes are caused by different spatial allocation methods used in the mobile source emissions inventory rather than the increased resolution of the model calculations. The uncertainty in the spatial pattern of the mobile source exposure fields has implications for the uncertainty of subsequent epidemiological analysis.

11 PREDICTED ULTRAFINE PARTICULATE MATTER SOURCE CONTRIBUTIONS ACROSS PEAK SUMMER AIR POLLUTION EVENTS THROUGHOUT THE CONTINENTAL UNITED STATES

Preamble: Chapter 11 extends the methods for ultrafine particle predictions developed for California across the entire continental United States focusing on the peak photochemical episode occurring in 39 major cities in the year 2010. Predictions are resolved by chemical species, source contributions, and total concentrations. Note that Chapter 11 is outside the scope of the current project and is carried out as a demonstration study to examine how the results in California compare to the results in the rest of the US. The peak summer photochemical period was chosen partly based on scientific interest (summer PM concentrations are highest in much of the US) and partly out of convenience (the meteorological fields and emissions had already been created for a separate project). Future studies will extend this analysis to a full annual cycle.

11.1 Introduction

Airborne particulate matter (PM) has been linked with premature mortality and numerous other health risks in cities across the world (see for example references [248, 341-347]). Despite years of progress [348], PM concentrations in many urban regions in the U.S. still exceed health-based standards resulting in an increase of non-accidental mortality [342, 349]. Toxicology testing suggests that ultrafine particles with diameter < 0.1 μm may be the most harmful size fraction within $PM_{2.5}$ [7, 350-353]. Initial attempts to analyze ultrafine particles in epidemiology studies have used particle number concentration as a surrogate for ultrafine particle exposure, but this approach has not found consistent relationships with health effects [7]. In contrast, a recent epidemiology study based on ultrafine particle mass ($PM_{0.1}$) found significant associations with premature mortality [7]. In addition, ultrafine (UF) mass concentrations are highly correlated with particle surface area and can be a good metric for the potential exposure to UF particles [7, 155]. Follow-up studies have also found significant associations between $PM_{0.1}$ and reproductive outcomes including low birth weight and preterm birth [8, 354]. These findings have biological plausibility, since ultrafine particles may cross cell membranes and interfere with internal cell function [51]. Ultrafine particles have greater surface area-per volume due to the small particle diameter making it more available for chemical reaction. Ultrafine particles can also translocate into the bloodstream. Ultrafine particles can therefore have a larger impact when deposited deep into the lung cavity where they are not easily removed [153, 350].

A monitoring network for PM_{10} and $PM_{2.5}$ has been operating throughout the continental U.S. for almost 20 years. Multiple studies have performed source apportionment calculations for coarse and fine PM using these measurements [25, 355-357]. In contrast, measurements of $PM_{0.1}$ are limited to focused field campaigns lasting for short time periods with even fewer studies attempting source apportionment calculations [18]. Multiple barriers have prevented the widespread deployment of $PM_{0.1}$ monitoring networks including (i) the low concentration of $PM_{0.1}$ mass, which challenges the detection limits of analytical methods, (ii) the artifacts associated with collecting $PM_{0.1}$ samples, (iii) the additional workload involved in operating the collection devices, and (iv) the sharp spatial gradients of $PM_{0.1}$ concentrations. Expensive investments in $PM_{0.1}$

monitoring are unlikely to occur without compelling evidence linking $PM_{0.1}$ to public health. Early epidemiological studies for $PM_{0.1}$ must therefore use some other technique besides direct measurements to calculate population exposure.

Various methods such as the source-resolved PMCAMx chemical transport model, the chemical mass balance (CMB) model, photochemical box models and land use regression (LUR) models have been used to track source contributions to primary organic matter, elemental carbon and in some cases particle number concentration over areas in the Eastern U.S. and parts of Europe and Asia [358-365]. However, these methods are limited in one or more aspects of their ability to predict population exposure to ultrafine particles over large analysis domains. Source resolved models, such as PMCAMx, have been used to resolve composition for particle number concentration in the Eastern U.S. but not for $PM_{0.1}$ [359]. CMB models need measurements of specific molecular markers at numerous sites to resolve the sharp spatial gradients of ultrafine particle source contributions. LUR models need comprehensive measurements that act as training data sets in order to extend throughout a modeling domain [358].

Hu et al. [39] calculated population exposure to $PM_{0.1}$ in California using a regional source-oriented chemical transport model supported by measured profiles for particle size and composition of particles emitted by dominant sources. Predictions were compared to all available fine and ultrafine particle measurements over the period 2000-2010 with good agreement observed for the dominant chemical components of $PM_{0.1}$ mass including organic aerosol, elemental carbon, and numerous trace metals [39]. The 4km spatial resolution used in these calculations supported multiple epidemiological studies based on spatial gradients of exposure [7, 8]. These encouraging results motivate the expansion of the $PM_{0.1}$ exposure technique to other locations.

Here we use the Eulerian source-oriented UCD/CIT chemical transport model to predict the concentration of $PM_{0.1}$ in thirty-nine urban regions throughout the U.S. during summer pollution events in 2010. The calculation tracks contributions from fifteen (15) primary particle sources through a simulation of all major atmospheric processes while retaining information about particle size, composition and source origin [39]. The results of this calculation reveal U.S. national trends in $PM_{0.1}$ concentrations for the first time and suggest locations where the differential health effects of $PM_{0.1}$ and $PM_{2.5}$ can best be studied.

11.2 Methods

11.2.1 Simulation Dates

The thirty-nine cities that have previously been used in air pollution studies across the continental U.S. [366-368] were selected as the focus locations for the current analysis. Simulations within each target city were carried out during peak summer air pollution events in 2010. The modeling year is aligned with census datasets that can be used to construct population exposure estimates. In addition, this study builds on previous work that examined the maximum photochemical periods in 2010 ([367, 368]). The dates selected were based on initial investigation of measured 1-hr ozone concentrations across all monitors in a core-based statistical area (CBSA). A CBSA is defined as a U.S. geographical area that consists of one or more counties anchored by an urban center of at least 10,000 people plus adjacent counties that have a high degree of social and economic integration with the core as measured through commuting [369]. More simulations covering a broader range of dates will be performed in future studies but are currently beyond the scope of this project.

The selected air pollution events within each CBSA typically had measured 1-hr maximum ozone (O_3) concentrations greater than 70 ppb. Regional pollution events caused by atmospheric stagnation were selected whenever possible as opposed to special events caused by unusual occurrences such as wildfires that affected only one city at a time. Figure 11-1 illustrates the average 1-hr maximum ozone concentration across all monitors within each CBSA during the selected regional events. Simulation periods are organized in chronological order for the year 2010 and cities within the same geographical region are grouped together. Measured 24-hr $PM_{2.5}$ concentrations during peak summer pollution events ranged between 3.2-30 μg/m^3 depending on the location. The aggregation of these events across the U.S. enables a comparison of typical summer time air pollution episodes within different cities.

The simulation dates in each city are listed in Table 11-1 and a map of the city locations is shown in Figure 11-2. The aggregation of these events across the U.S. enables a comparison of typical summer time air pollution episodes within different cities.

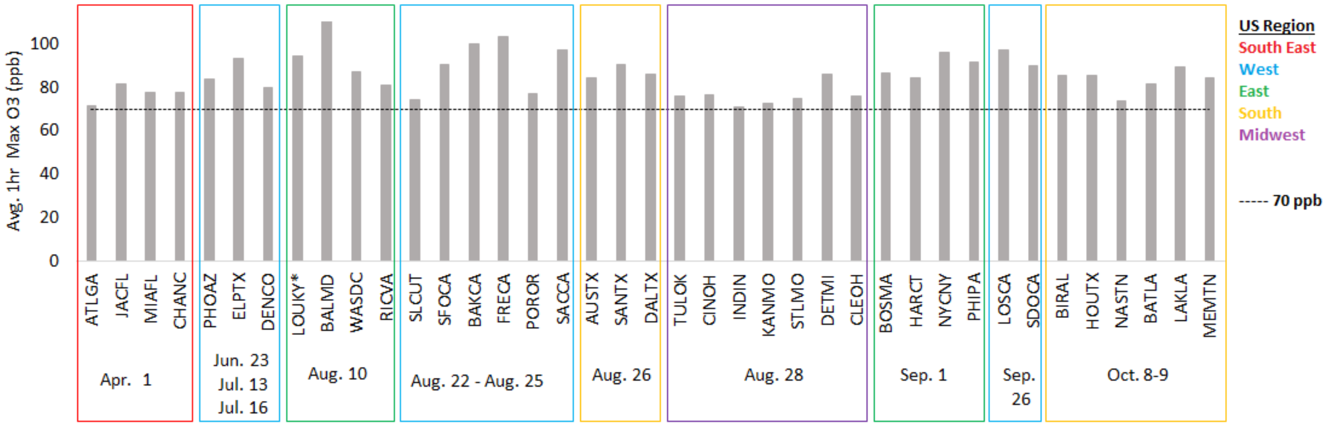

Figure 11-1: Average 1-hr Maximum O3 across all monitors in each domain. Cities are grouped by corresponding extreme O3 date (with O3 avg. > 70 ppb) and U.S. geographical region.

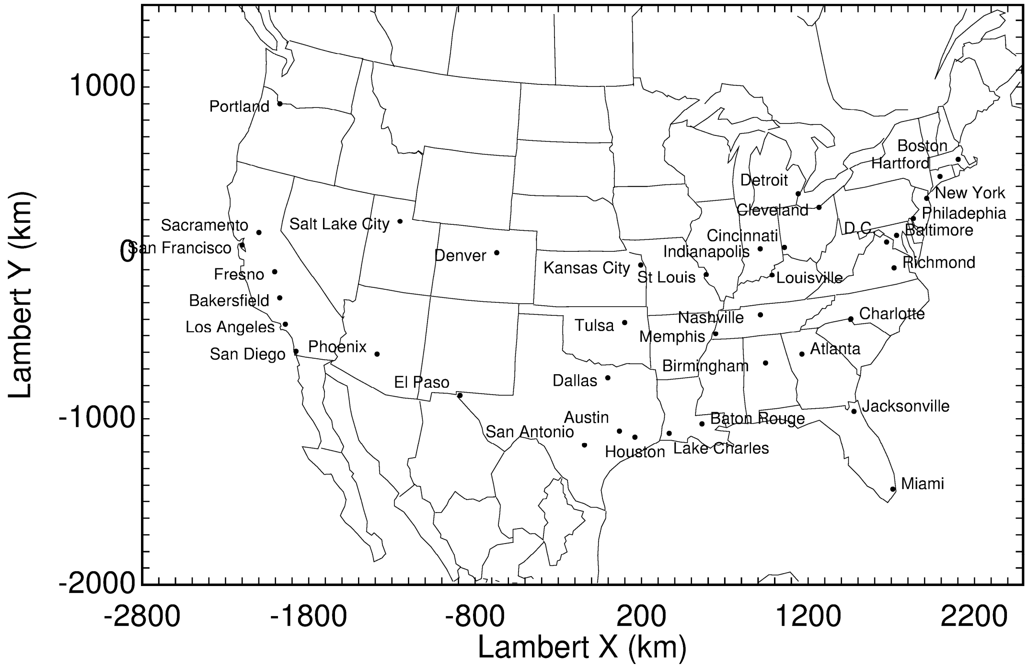

Figure 11-2: Map of 39 cities used for UFP calculations throughout the continental U.S

Table 11-1. City, City Code, Simulation Date, 2010 Population and Geographical Region

City	City Code	2010 Simulation Date^{+}	2010 Population	US Geographical Region
Atlanta	ATLGA	March 29 - April 1	422765	South East
Austin	AUSTX	August 23 - August 26	815260	South
Bakersfield	BAKCA	August 23 - August 26	348938	West
Baltimore	BALMD	August 7 - August 10	621210	East Coast
Baton Rouge	BATLA	October 6 - October 9	229584	South
Birmingham	BIRAL	October 6 - October 9	212107	South East
Boston	BOSMA	August 29 - September 1	620451	East Coast
Charlotte	CHANC	March 30 - April 2	738710	South East
Cincinnati	CINOH	August 25 - August 28	296904	Midwest
Cleveland	CLEOH	August 25 - August 28	396009	Midwest
Dallas	DALTX	August 23 - August 26	1201000	South
Denver	DENCO	July 13 - July 16	603421	West
Detroit	DETMI	August 25 - August 28	711299	Midwest
El Paso	ELPTX	July 11 - July 14	651665	West
Fresno	FRECA	August 23 - August 26	497090	West
Hartford	HARCT	August 29 - September 1	125312	East Coast
Houston	HOUTX	October 6 - October 9	2103000	South
Indianapolis	INDIN	August 25 - August 28	830952	Midwest
Jacksonville	JACFL	March 29 - April 1	823291	South East
Kansas City	KANMO	August 25 - August 28	460639	Midwest
Lake Charles	LAKLA	October 6 - October 9	72268	South
Los Angeles	LOSCA	September 23 - September 26	3796000	West
Louisville	LOUKY	August 7 - August 10	300000	Midwest
Memphis	MEMTN	October 6 - October 9	647609	Midwest
Miami	MIAFL	March 30 - April 2	400769	South East
Nashville	NASTN	October 7 - October 10	1800000	Midwest
New York City	NYCNY	August 29 - September 1	8190000	East Coast
Philadelphia	PHIPA	August 27 - August 30	1529000	East Coast
Phoenix	PHOAZ	June 19 - Jun3 22	1449000	West
Portland	POROR	August 23 - August 26	585286	West
Richmond	RICVA	August 7 - August 10	204351	East Coast
Sacramento	SACCA	August 22 - August 25	466488	West
Salt Lake City	SLCUT	August 18 - August 21	186505	West

City	City Code	2010 Simulation Date^{+}	2010 Population	US Geographical Region
San Antonio	SANTX	August 23 - August 26	1334000	South
San Diego	SDOCA	September 23 - September 26	1306000	West
San Francisco	SFOCA	August 22 - August 25	805704	West
St. Louis	STLMO	August 25 - August 28	319257	Midwest
Tulsa	TULOK	August 25 - August 28	392443	Midwest
Washington DC	WASDC	August 7 - August 10	604453	East Coast

11.2.2 Model Description

The UCD/CIT model predicts the evolution of gas and particle phase pollutants in the atmosphere in the presence of emissions, transport, deposition, chemical reaction and phase change [235] as represented by Eq. (1)

$$\frac{\partial C_i}{\partial t} + \nabla \cdot uC_i = \nabla K \nabla C_i + E_i - S_i + R_i^{gas}(C) + R_i^{part}(C) + R_i^{phase}(C)$$

$$\frac{\partial C_i}{\partial t} + \nabla \cdot uC_i = \nabla K \nabla C_i + E_i - S_i + R_i^{gas}(C) + R_i^{part}(C) + R_i^{phase}(C)$$

$$\frac{\partial C_i}{\partial t} + \nabla \cdot uC_i = \nabla K \nabla C_i + E_i - S_i + R_i^{gas}(C) + R_i^{part}(C) + R_i^{phase}(C) \qquad \text{(E1)}$$

where C_i is the concentration of gas or particle phase species i at a particular location as a function of time t, u is the wind vector, K is the turbulent eddy diffusivity, E_i is the emissions rate, S_i is the loss rate, R_i^{gas} is the change in concentration due to gas-phase reactions, R_i^{part} is the change in concentration due to particle-phase reactions and R_i^{phase} is the change in concentration due to phase change [235]. Loss rates include both dry and wet deposition. Phase change for inorganic species occurs using a kinetic treatment for gas-particle conversion [276] driven towards the point of thermodynamic equilibrium [277]. Phase change for organic species is also treated as a kinetic process with vapor pressures of semi-volatile organics calculated using the 2-product model [278]. More sophisticated approaches for secondary organic aerosol (SOA) formation [242] were also tested in the current study but these required a larger number of assumptions and they did not produce higher SOA concentrations in the $PM_{0.1}$ size fraction.

Nucleation was included in the model using the ternary nucleation (TN) mechanisms involving H_2SO_4-H_2O-ammonia (NH_3) [279]. This mechanism has been applied in previous studies and similar adjustment of the nucleation rate was achieved using a tunable nucleation parameter set to

10^{-5} for new particle nucleation [370] . Yu et al (2018) used a similar approach to predict particle number concentrations across California in 2012. Yu et al found good agreement of daily predictions of N_{10} and $PM_{0.1}$ source contributions compared to results that used receptor based studies [370].

Kuwayama et al (2013) found that UF mass concentrations are highly correlated with particle surface area and serve as a good metric for the potential exposure to UF particles [155]. Nucleation increases the concentration of the smallest particles in the atmosphere which increases the surface-area to volume ratio increases the realism of the simulated UFP distribution in the atmosphere. Model spatial resolution was 4km over the 4.2 million km^2 of simulated urban areas and so near-roadway concentrations of ultrafine particles on spatial scales of ~0.1 km will not be presented.

A total of 50 particle-phase chemical species are included in each of 15 discrete particle size bins that range from 0.01-10 µm particle diameter [235]. Artificial source tags are used to quantify source contributions to the primary particle mass for a specific bin size, therefore allowing for the direct contribution of each source of $PM_{2.5}$ and $PM_{0.1}$ mass to be determined. Gas-phase concentrations of oxides of nitrogen (NOx), volatile organic compounds (VOCs), oxidants, ozone, and semi-volatile reaction products were predicted using the SAPRC-11 chemical mechanism [230].

11.2.3 Model Inputs

Anthropogenic emissions were generated using the Sparse Matrix Operator Kernel Emissions (SMOKEv3.7) modeling system applied to the 2011 National Emissions Inventory. Emissions from each of the four major source sectors (area, mobile, non-road and point were tagged to create fifteen (15) different emissions groups: on road diesel, on road gasoline, off road diesel, off road gasoline, biomass, food cooking, natural gas combustion, process heaters, distillate oil, aviation, cement, coal, steel foundries, paper products and all other emissions. Size and composition-resolved source profiles were then assigned to the PM emissions within each of these groups using the UCD/CIT emissions processor based on the most recent measurements available in the literature [291, 371, 372]. Some of the fifteen (15) source categories were represented using weighted average source profiles from multiple sources as described in the Appendix Table S11-2.

Daily values for 2010 wildfire emissions were generated using the Global Fire Emissions Database (GFED) [237]. Biogenic emission rates were generated using the Model of Emissions of Gases and Aerosols from Nature (MEGANv2.1). The gridded geo-referenced emission factors and land cover variables required for MEGAN calculations were created using the MEGANv2.1 pre-processor tool and the ESRI_GRID leaf area index and plant functional type files available at the Community Data Portal [325].

Meteorology parameters used to drive the UCD/CIT CTM and MEGANv2.1 biogenic emissions were generated using the Weather Research and Forecasting model (WRFv3.6) and WRF preprocessing system (WPSv3.6). Meteorological fields were created within 3 nested domains with horizontal resolutions of 36km, 12km, and 4km, respectively. Each domain had 31 telescoping vertical levels up to a top height of 12km. Four-dimensional data assimilation (FDDA) or "FDDA nudging" was used to anchor meteorological predictions to measured values (Hu et al., 2010). Meteorological data and gridded map projections needed for 2010 emissions modeling were taken from the corresponding WRF simulations using the meteorology-chemistry interface processor (MCIP).

11.2.4 Supporting Measurements

Ambient hourly ozone measurements and daily $PM_{2.5}$ measurements were obtained from the EPA AQS API / Query AirData [373]. Model predictions are compared to these measurements to build confidence in the accuracy of the overall modeling system since $PM_{0.1}$ measurements are not available during any of the peak summer pollution events studied here.

11.3 Results

Predicted 1-hr ozone and maximum 1-hr NO_2, SO_2 and CO concentrations were compared to measurements at all available monitors within each CBSA to indirectly evaluate the accuracy of the emissions inventories and meteorology fields. Many of the sources that emit ozone precursors also emit ultrafine particles. Likewise, meteorological parameters including wind speed and mixing depth influence the concentrations of all pollutants including ultrafine particles. Successful predictions of gas phase and particle phase species are therefore necessary steps in the accurate prediction of ultrafine particle concentrations during summer photochemical smog episodes. Figure 11-3 illustrates the mean fractional bias (MFB) and mean fractional error (MFE) for predicted gas phase species against measured values for each monitor within a specific modeling domain. All monitor information for the 39 cities are shown in the supplemental information Tables S11-3 through S11-7.

Predicted 24-hr $PM_{2.5}$ concentrations were also compared to measurements at all available monitors within each target CBSA. Many of the combustion sources that emit primary particles within the $PM_{2.5}$ size fraction also emit $PM_{0.1}$ and their precursors. The Chemical Speciation Monitoring Network (CSN) operated by the U.S. Environmental Protection Agency (EPA) measures $PM_{2.5}$ mass and chemical composition at more than 260 sites throughout the U.S. including many of the 39 cities studied in the current analysis [374]. Figure 11-4 illustrates the MFB and MFE for 24-hr average predicted $PM_{2.5}$ concentrations against measured 24-hr average $PM_{2.5}$ concentrations at each available monitor over the specific simulation period. Full monitor information including latitude, longitude and total # of available measurements for comparison within the simulation period is shown in the supporting information Tables S11-3 through S11-7.

Table 11-2 summarizes the total number of available monitors for comparison of measured values vs. predicted values for each of the gas phase species (CO, SO2, NO2 and Ozone) and $PM_{2.5}$. EPA model performance recommendations based on Boylan and Russell (2006) note the criteria for MFB and MFE to be +/- 0.60 and 0.75, respectively [288]. The last two columns of Table 11-2 display the percentage of measured vs. predicted comparisons that met the EPA criteria for MFE and MFB over the entire U.S. modeling domain. In general, over 95% of all locations across all modeling simulations met EPA criteria for prediction of gas phase and particle phase species.

Elemental carbon (EC) and organic compounds (OC) are the chemical components most relevant for both the $PM_{2.5}$ and the $PM_{0.1}$ size fractions. Figure 11-5 illustrates predicted vs. measured 24-hr $PM_{2.5}$ EC and OC concentrations for all 39 cities. In general, the model slightly under predicts $PM_{2.5}$ EC, OC, and mass with regression slopes ranging from 0.62 for EC to 0.97 for OC. The negative bias in model predictions may stem from the 4km spatial averaging inherent in the calculations vs. the influence of sources closer than 4 km to the measurement site in the urban environment such as highways, restaurants, etc. This trend is reflected in the performance of ozone predictions during the evening hours for Los Angeles and New York City (Appendix Figure S11-1), where measured ozone concentrations likely falls to zero due to titration from nearby NOx emissions while predicted ozone concentrations remain greater than zero due to dilution of NOx emissions within 4 km grid cells. The MFB and MFE for $PM_{2.5}$ predictions are summarized in the Appendix Table S11-4.

$PM_{0.1}$ measurements are not available for model evaluation in the 39 cities across the U.S. in 2010 at the core of the current study, but measurements are available in California in the years 2015 and 2016 that can serve to evaluate similar modeling procedures. Yu et al. [370] compared $PM_{0.1}$ concentrations in Los Angeles, Fresno, East Oakland, and San Pablo, California predicted using the UCD/CIT air quality model to receptor-based source apportionment calculations based on measured concentrations of molecular markers in the ultrafine particle size fraction [375]. Good agreement (MFE less than ±0.5 and MFB less than 0.75) was found between predictions from these two independent techniques for $PM_{0.1}$ concentrations associated with gasoline engines, diesel engines, food cooking, wood burning, and “other sources”. Further details of this comparison are provided in Chapter 8 of the current report. This evaluation of the modeling procedures builds confidence in the $PM_{0.1}$ source predictions across the U.S. in the current study.

Figure 11-6 illustrates a composite representation of $PM_{2.5}$ and $PM_{0.1}$ mass across the U.S. during the summer pollution episodes listed in Table 11-1. The spatial plot in Figure is constructed using the intermediate 12km simulation results from multiple simulations stitched together to cover a broader geographical area. Regional $PM_{0.1}$ concentrations reach a maximum value of 5 $\mu g\ m^{-3}$ in a few isolated grid cells with wildfires but concentrations generally exceed 2 $\mu g\ m^{-3}$ in major urban regions across the U.S. including Los Angeles, the San Francisco Bay Area, Houston, Miami, and New York. The comparison between $PM_{2.5}$ mass (Figure a) and $PM_{0.1}$ mass (Figure b) shows that predicted $PM_{0.1}$ spatial gradients are sharper with less regional contributions between “hot spots”. Locations in the Midwestern and Eastern U.S. outside of cities with high $PM_{2.5}$ concentrations due to secondary formation (sulfate and secondary organic aerosol) did not have corresponding high concentrations of $PM_{0.1}$. Most major urban centers had noticeable peaks of both $PM_{2.5}$ and $PM_{0.1}$. This pattern presents a challenge for epidemiological studies seeking to differentiate the effects of $PM_{2.5}$ and $PM_{0.1}$ because the locations with differential exposure (high $PM_{2.5}$ but low $PM_{0.1}$) have low population density, which will reduce the power of the analysis.

The UCD/CIT model explicitly tracks source contributions to particle mass in each size bin using artificial source tags. Pie charts of $PM_{2.5}$ and $PM_{0.1}$ source contributions are illustrated in Figure 11-6 for selected major cities. Pie charts for $PM_{0.1}$ source contributions in all 39 U.S. cities are shown in Figure . The detailed source profiles within each city are based on the nested 4km simulation results during the pollution events listed in Table 11-1. Source contribution spatial plots for the entire U.S. are shown in the supplemental information Figure S11-3 through S11-6 and pie charts for $PM_{2.5}$ source contributions in all 39 U.S. cities are shown in the supplemental information Figure S11-7. On-road gasoline and diesel vehicles made significant contributions to regional $PM_{0.1}$ in all 39 cities even though peak contributions within 0.3 km of the roadway were not resolved by the 4 km grid cells. Food cooking also made significant contributions to $PM_{0.1}$ in all cities but biomass combustion was only important in locations impacted by summer wildfires. Aviation was a significant source of $PM_{0.1}$ in cities that had airports within their urban footprints. Industrial sources including cement manufacturing, process heating, steel foundries, and paper & pulp processing impacted their immediate vicinity but did not significantly contribute to $PM_{0.1}$ concentrations in any of the target 39 cities. Natural gas combustion made significant contributions to $PM_{0.1}$ concentrations due to the widespread use of this fuel for residential, commercial, and industrial applications. Natural gas combustion contributions were especially significant in locations with high levels of industrial use such as chemical refineries or in locations with significant levels of natural gas fired power plants.

The major sources of primary $PM_{0.1}$ and $PM_{2.5}$ were notably different in many cities (compare Figure a and Figure b). The sources that contribute most strongly to $PM_{2.5}$ are on road diesel, gasoline, food cooking, coal and “other” which includes break and tire wear from mobile sources and dust. Natural gas combustion makes minor contributions to primary $PM_{2.5}$ mass since particles from this source have a mass distribution peaking at ~0.05 μm particle diameter [376] with all of the emitted mass in the $PM_{0.1}$ size fraction. In contrast, other combustion sources using more complex fuels such as on-road vehicles have a mass distribution peaking at ~0.1 μm with at least half the emitted mass outside the $PM_{0.1}$ size fraction [371, 372]. Likewise, food cooking contributes strongly to $PM_{2.5}$ concentrations but the emitted particle mass distribution peaks at 0.2 μm with the majority of the mass outside the $PM_{0.1}$ size fraction.

Biomass combustion did not make a strong impact to overall $PM_{0.1}$ due to the time period of the episodes selected. Residential wood combustion is not typically a strong source in the summer due to the warmer temperatures however in the winter time biomass would most likely be a dominant source.

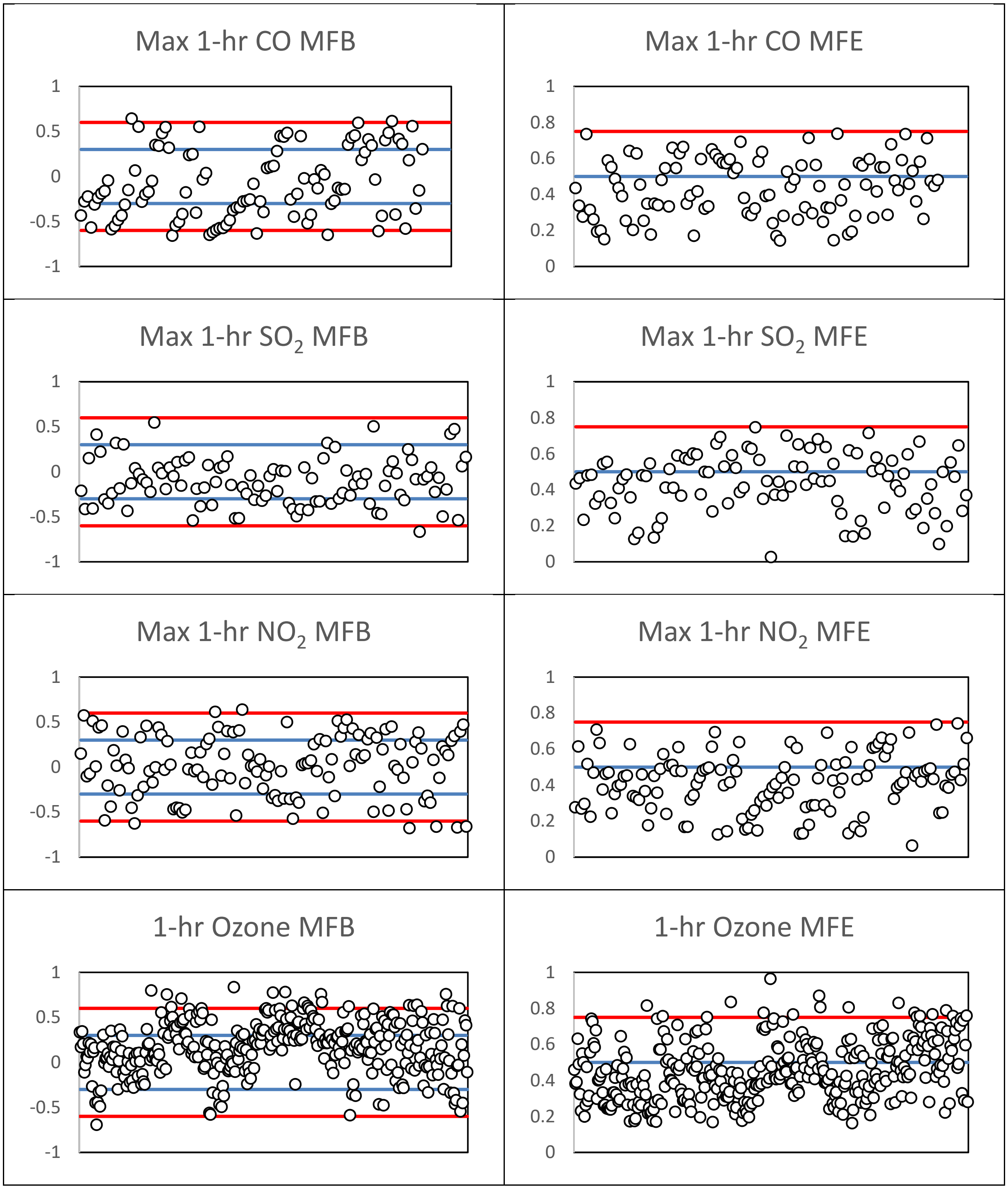

Figure 11-3: Model performance statistics for predicted major gas phase species. Red lines represents EPA criteria and blue line represents EPA goal. Mean fractional bias and mean fractional error were calculated for available measurements again predictions at every monitor in the CBSA region based of the U.S. EPA AQ datamart. Monitor latitude and longitude, name, MFB and MFE value available for all species in Appendix.

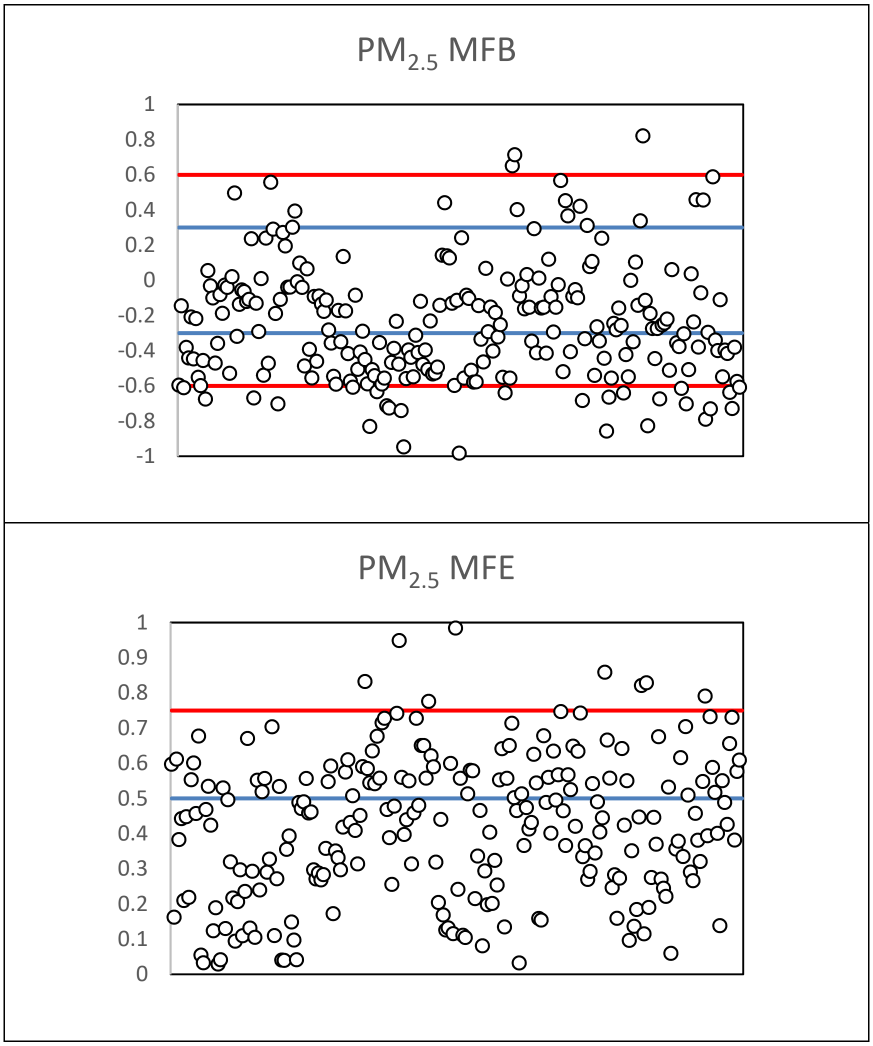

Figure 11-4: Model performance statistics for predicted PM$_{2.5}$ against measured values. Red line represents EPA criteria and blue line represents EPA goal. Mean fractional bias and mean fractional error were calculated for available measurements against predictions at every monitor in the CBSA region based of the U.S. EPA AQ DataMart. Monitor latitude and longitude, name, MFB and MFE value available for all species in Appendix.

Table 11-2. Percent of predictions throughout entire U.S. domain that met performance goals.

Species	Total Number of Monitors within 4km modeling domain for Comparison to Predicted Values	% that met 0.75 MFE Criteria	% that met ±0.60 MFB Criteria
CO	110	100%	92.7%
SO2	102	100%	99%
NO2	130	100%	94.6%
Ozone	348	94.8%	94.2%
$PM_{2.5}$	234	96.1%	90.5%

(a) Organic Carbon

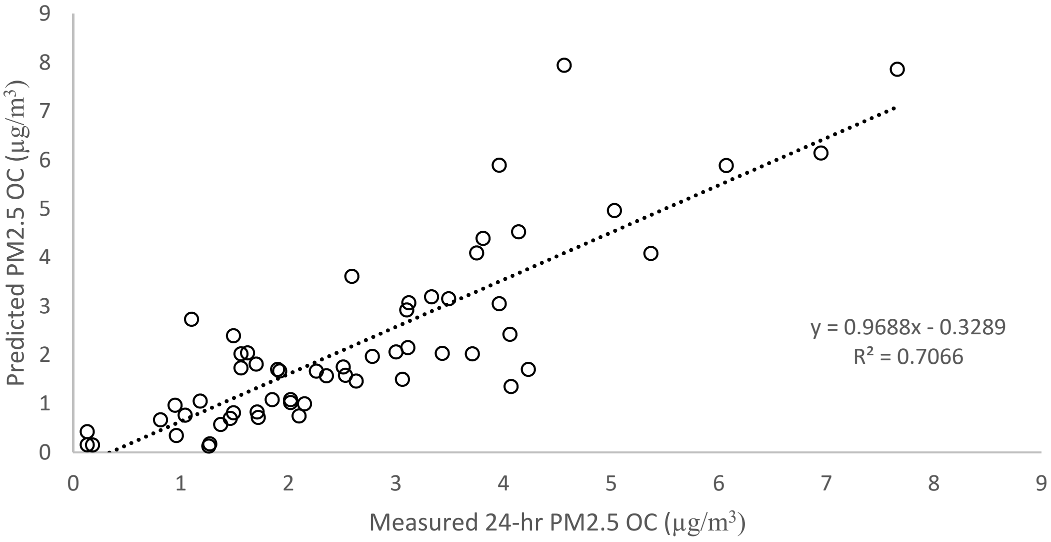

(b) Elemental Carbon

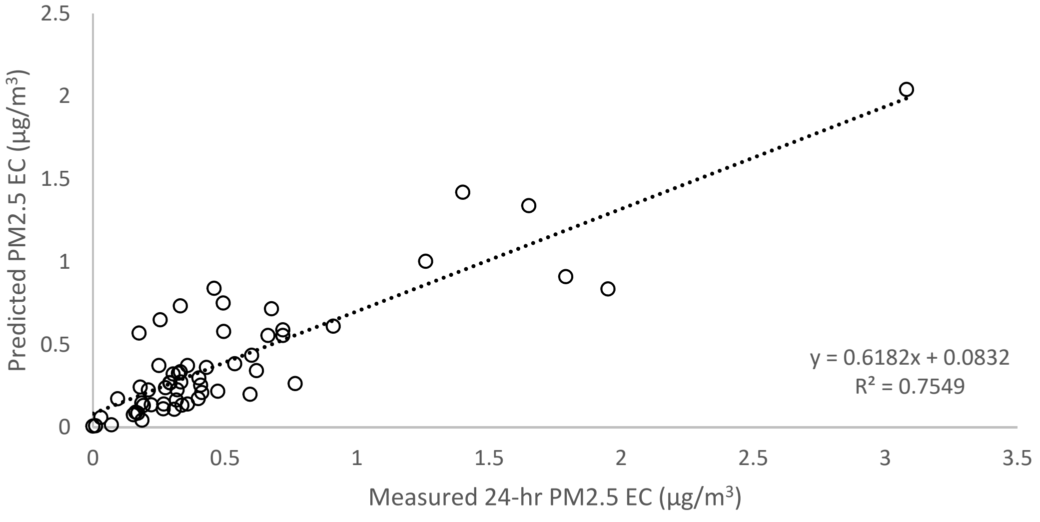

Figure 11-5: Predicted vs. Measured (a) Organic Carbon and (b) Elemental Carbon (μg m-3)

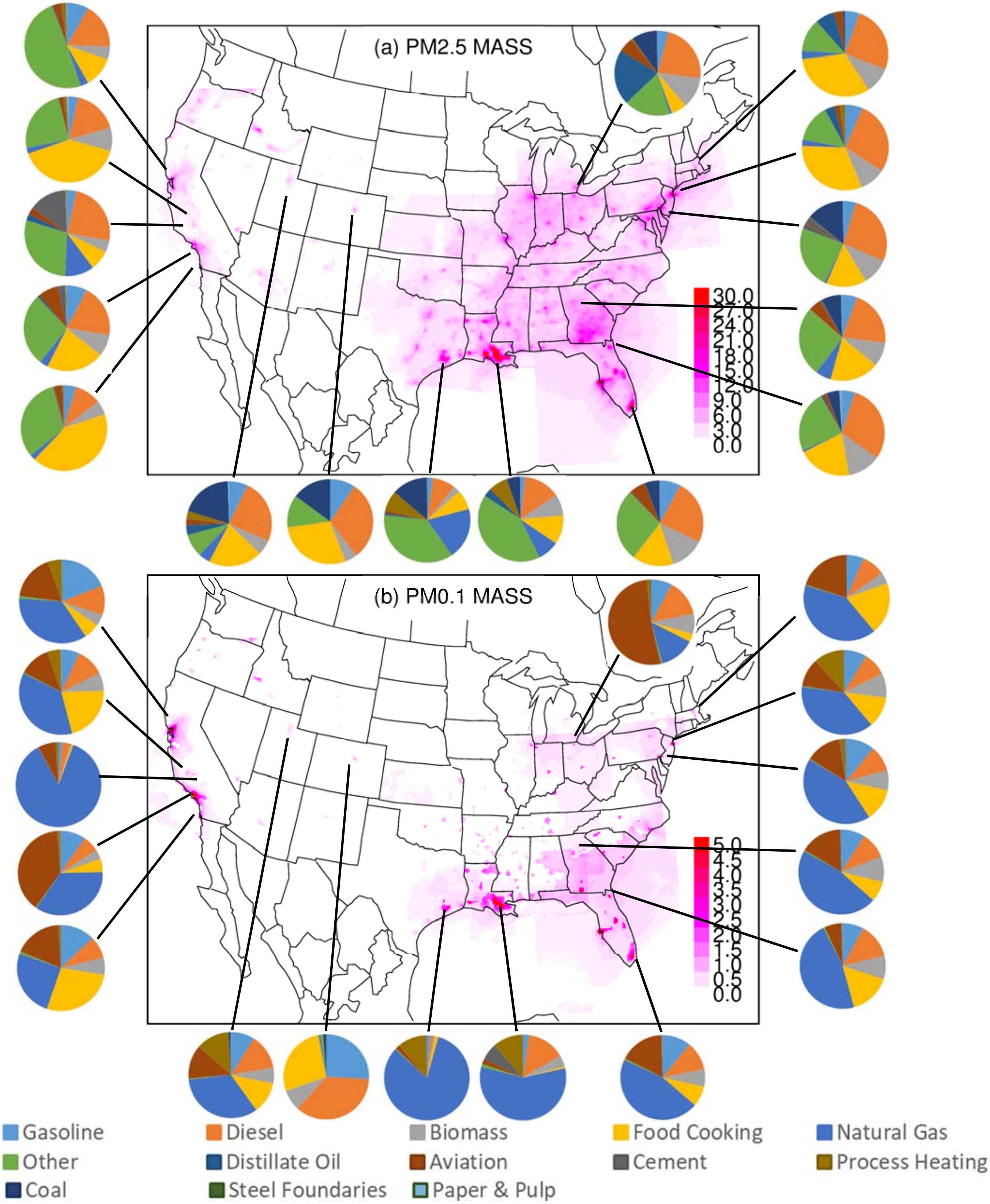
(a) PM2.5 MASS
30.0
27.0
24.0
21.0
18.0
15.0
12.0
9.0
6.0
3.0
0.0
(b) PM0.1 MASS
5.0
4.5
4.0
3.5
3.0
2.5
2.0
1.5
1.0
0.5
0.0
Gasoline
Diesel
Biomass
Food Cooking
Natural Gas
Other
Distillate Oil
Aviation
Cement
Process Heating
Coal
Steel Foundaries
Paper & Pulp

Figure 11-6: (a) $PM_{2.5}$ and (b) $PM_{0.1}$ 24-hr average mass (µg m-3) during summer air pollution event. Scale drawn to highlight all areas of US. Actual Max for (a) = 109.28 µg/m3 (b) = 7.71 µg/m3.

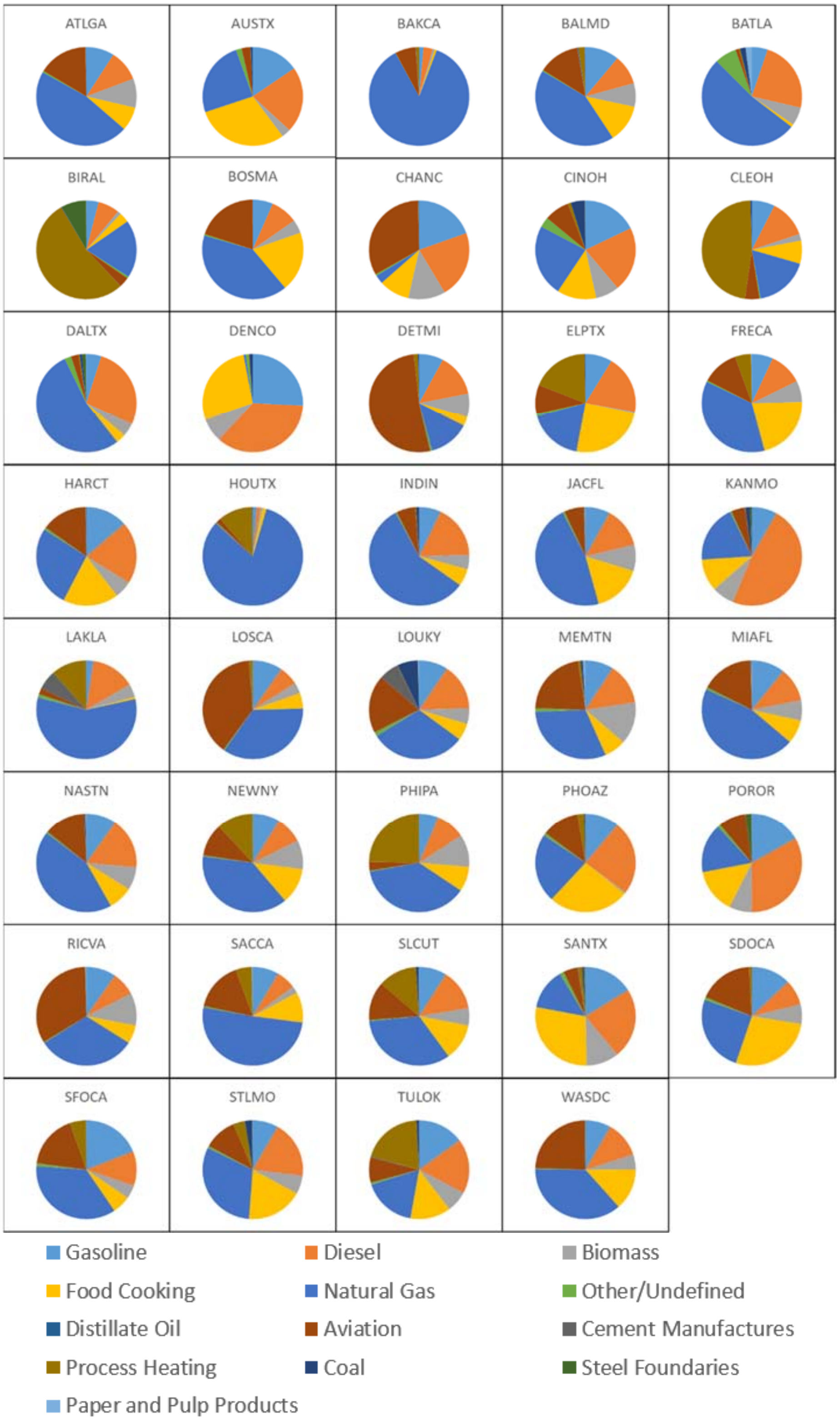

Figure 11-7: PM$_{0.1}$ source contribution for 39 cities across the continental US

(a) PM$_{2.5}$

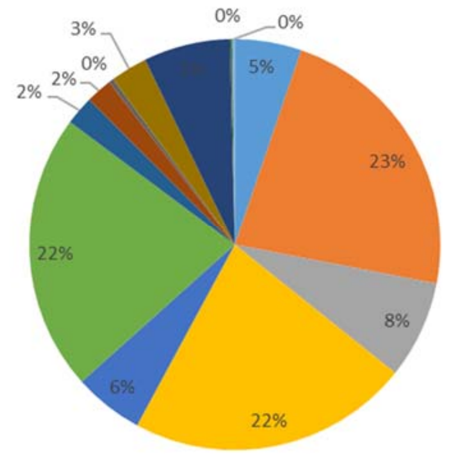

(b) PM$_{0.1}$

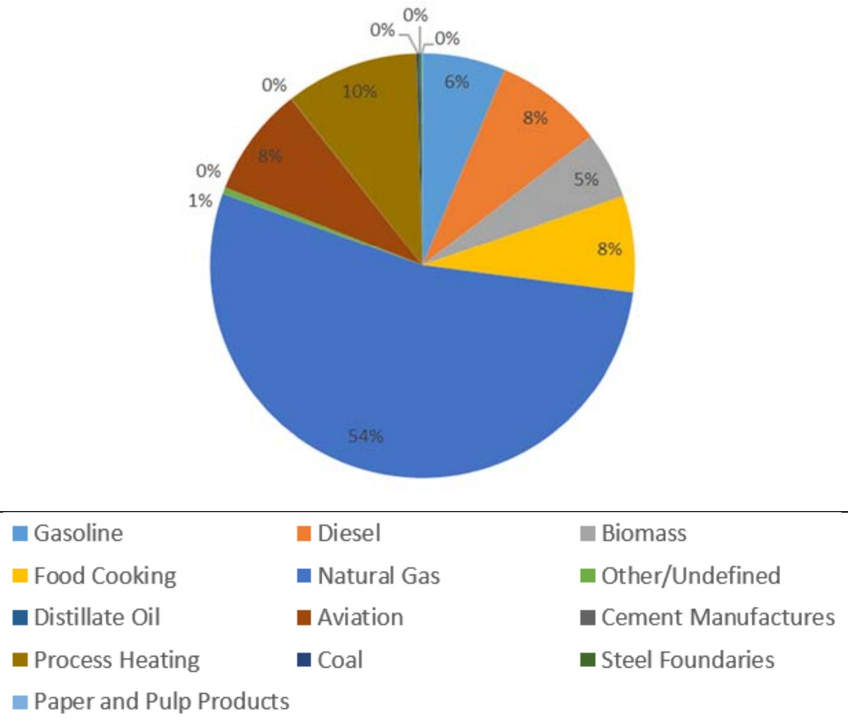

Figure 11-8: Population weighted average source contribution across the 39 major cities in the continental U.S. for (a) PM$_{2.5}$ and (b) PM$_{0.1}$

11.4 Discussion

Figure 11-8 illustrates the population-weighted average $PM_{0.1}$ source contributions across all 39 study cities shown in Table 11-1. This calculation highlights the importance of natural gas combustion particles in the $PM_{0.1}$ size fraction and the minor role that these natural gas combustion particles play in the $PM_{2.5}$ size fraction. Natural gas typically consists of +93% methane with the balance of the fuel made up by higher molecular weight alkanes and trace impurities. In addition to background sulfur compounds in the natural gas, sulfur-containing odorants such as mercaptans are commonly added to aid in leak detection. The current predictions are based on source profile measurements for wood burning, food cooking, mobile source and non-residential natural gas combustion determined by multiple peer-reviewed studies (Taback et al. 1979, Cooper 1989, Houck et al. 1989, Hildemann et al. 1991a, Hildemann et al. 1991b, Harley et al. 1992, Schauer et al. 1999a, Schauer et al. 1999b, Kleeman et al. 2000, Schauer et al. 2001, Schauer et al. 2002a, Schauer et al. 2002b, Robert et al. 2007a, Robert et al. 2007b, Kleeman et al. 2008). In addition, new measurements made by Xue et al (2018) were conducted in parallel of the current study to confirm the particle size distribution of natural gas and biomethane combustion of measurements from past studies. The results from Xue et al. are in good agreement with the profiles currently being used [375].

Natural gas combustion does not emit high amounts of particulate matter per J of energy in the fuel, but the widespread use of natural gas suggests that it could still contribute significantly to ambient $PM_{0.1}$ concentrations. Natural gas combustion accounted for 29% of total U.S. energy consumption in 2016 [377]. In contrast, gasoline combustion accounted for 17% of U.S. energy consumption and diesel fuel combustion accounted for approximately 6% of U.S. energy consumption in 2016. Gasoline and diesel fuel combustion in motor vehicles also emit most particles in the size fraction larger than $PM_{0.1}$ [371, 372] whereas natural gas combustion emits particles entirely within the $PM_{0.1}$ size fraction [376]. Taken together, these facts support the potential importance of natural gas combustion for ambient $PM_{0.1}$ concentrations and the primary difference between the $PM_{2.5}$ and $PM_{0.1}$ source compositions.

The five (5) states with the highest consumption of natural gas in 2016 were Texas (14.7%), California (7.9%), Louisiana (5.7%), New York (5%), and Florida (4.8%). These consumption patterns are reflected in the natural gas distribution system (Figure 11-9a) and the predicted $PM_{0.1}$ concentration field associated with natural gas combustion (Figure 11-9b). Natural gas end-use included electric power generation (36%), industrial applications (34%), residential use (16%), commercial use (11%), and transportation (3%).

Lane et al. (2007) used a source-resolved version of PMCAMx and individual emission inventories to determine source contributions of primary organic material ($POM_{2.5}$) [358]. Lane et al. note that $POM_{2.5}$ associated with natural gas sources ranged from 0.1 to 0.8 $\mu g/m^3$. Chang et al in 2004 measured emitted particle size distributions for gas-fired stationary combustion that fell between 10-100nm [376]. The combination of these two results indicates that the natural gas mass component of $POM_{2.5}$ predicted by Lane et al. is consistent with the magnitude of the $PM_{0.1}$ mass associated with natural gas combustion found in the current study. Lane et al. were not studying $PM_{0.1}$ and so the major role of natural gas combustion in this size fraction was not identified.

Posner and Pandis (2015) utilized PMCAMx with the LADCO 2001 BaseE source-resolved mass emissions inventory for a July 2001 prediction of N_{10} over the Eastern U.S. with 36 km resolution [359]. Posner and Pandis used a "zero-out" method in combination with source-specific size distribution to study the percent contribution of six major sources (on road gasoline, industrial, non-road diesel, on road diesel, biomass and dust) of N_{10}. They found that N_{10} was made up of 36% on-road gasoline, 31% industrial, 18% non-road diesel, 10% on-road diesel, 1% biomass burning and 4% long-range transport [359]. The emissions particle number inventory was normalized based on PM10 mass from each source and particle emissions from natural gas combustion sources were assumed negligible, which effectively removed natural gas sources from the simulation. This has minor effects on $PM_{2.5}$ and PM_{10} predictions, but the results of the current study suggest that natural gas combustion contributions significantly to ultrafine particle concentrations.

(a) Natural Gas Compressor Stations and Pipelines throughout the U.S. (Map courtesy of U.S. Energy Information Administration)

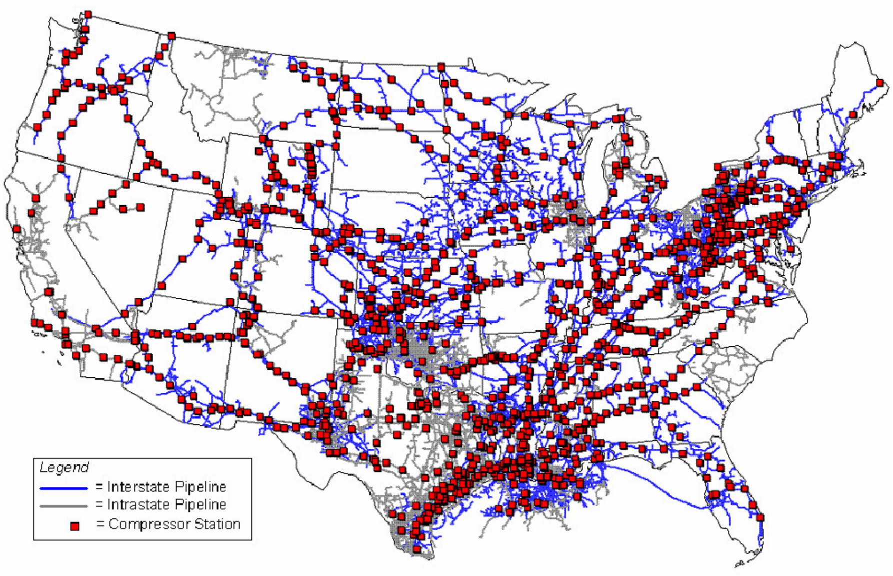

(b) UCD/CIT CTM Field Plot of $PM_{0.1}$ from Natural Gas combustion sources

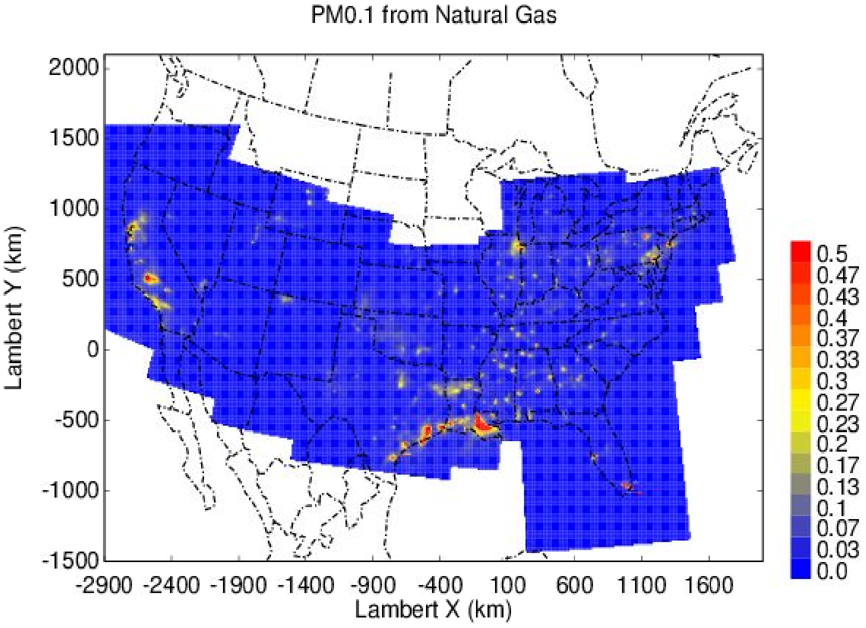

Figure 11-9 (a) Natural Gas compressor stations and pipelines across the U.S. and (b) $PM_{0.1}$ Natural Gas combustion concentrations (μg m-3).

Future epidemiological studies may be able to differentiate $PM_{0.1}$ and $PM_{2.5}$ health effects by contrasting cities with different predicted ratios of $PM_{0.1}$ / $PM_{2.5}$. Figure 11-10 illustrates the correlation between predicted $PM_{2.5}$ and $PM_{0.1}$ concentrations in the 39 cities considered in the current analysis while Figure 11-11 illustrates a sorted bar chart that displays the ratio of $PM_{0.1}$/$PM_{2.5}$ for each city. Cities with higher $PM_{0.1}$ / $PM_{2.5}$ ratios include Houston TX, Los Angeles CA, Birmingham AL, Charlotte NC, and Bakersfield CA. Cities with lower $PM_{0.1}$ to $PM_{2.5}$ ratios include Lake Charles LA, Baton Rouge LA, St. Louis MO, Baltimore MD, and Washington DC. Measurements should be conducted in these locations to verify the contrast in $PM_{0.1}$ / $PM_{2.5}$ concentrations in preparation for future exposure analysis.

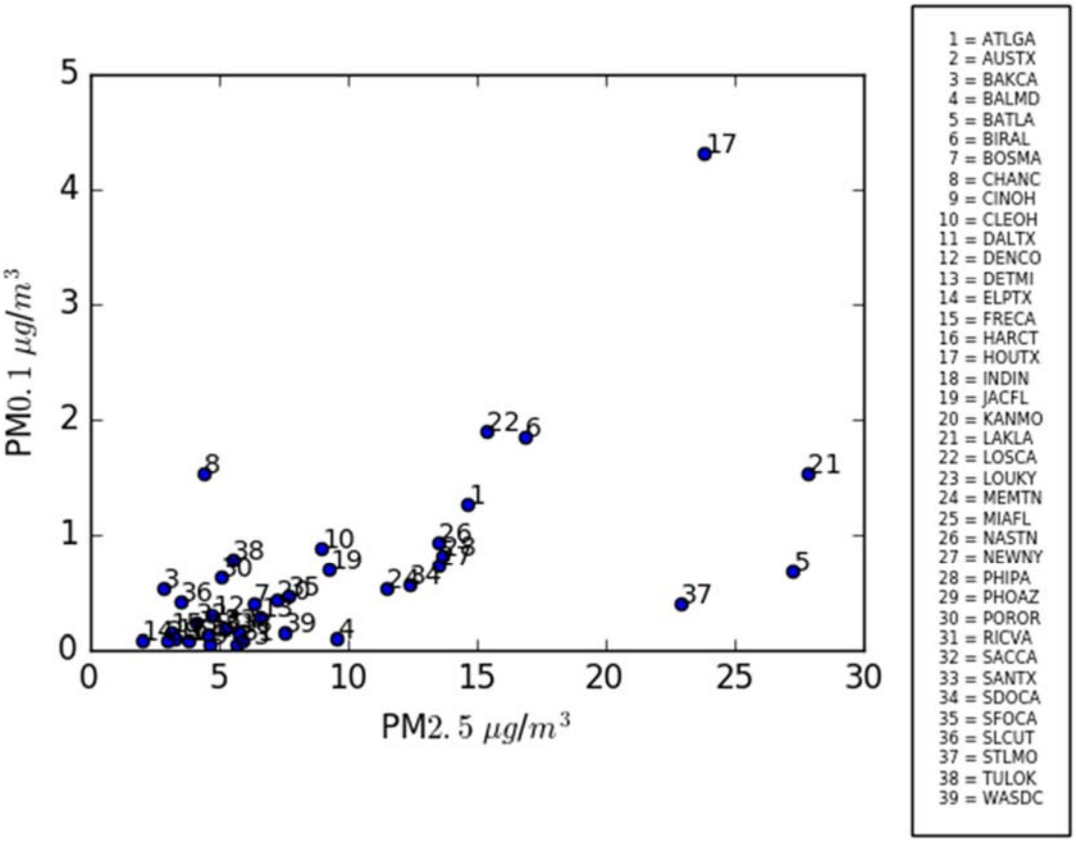

Figure 11-10 Scatter plot showing correlation between 24-hr average $PM_{2.5}$ and $PM_{0.1}$ for the 39-cities.

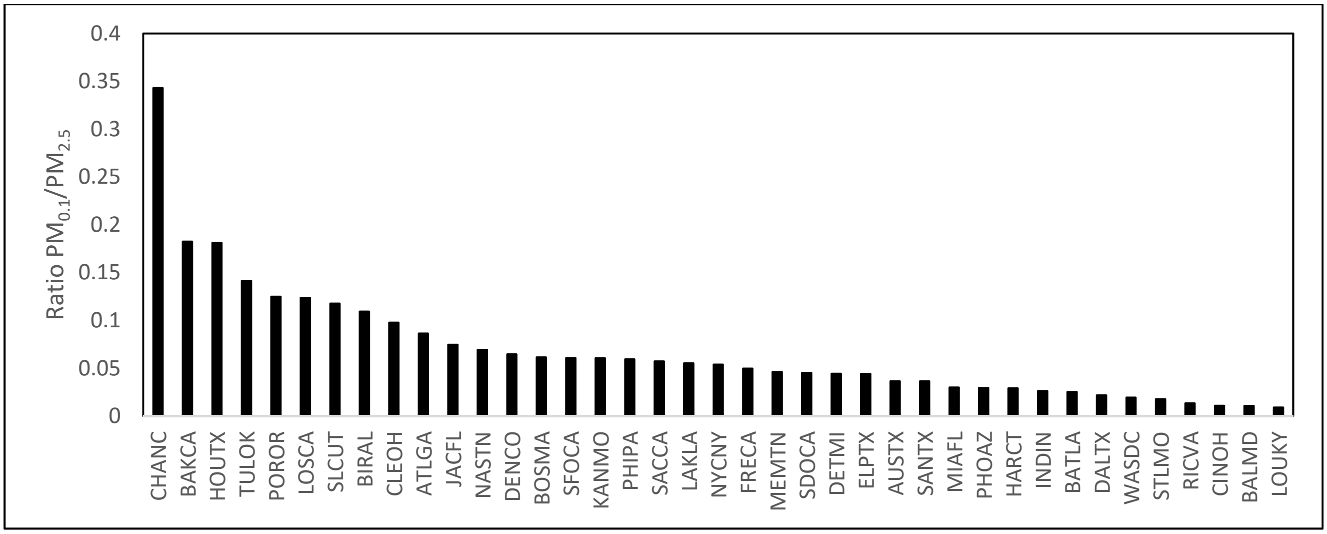

Figure 11-11: Sorted bar chart showing $PM_{0.1}/PM_{2.5}$ ratio in descending order for each city

Future epidemiological studies may also be able to use the contrast in $PM_{0.1}$ source contributions between different cities to separately identify health effects. In the current study, the similarity in $PM_{0.1}$ source contributions between cities was calculated as a dot product. The source contribution for $PM_{0.1}$ and $PM_{2.5}$, represented in the supporting information tables S11-7 through S11-16, were used as source contribution vectors for each city with 13 elements set equal to the normalized percent contribution from each source. The dot product of each city source-vector with other city source-vectors was then calculated using eq. (2)

$$\vec{a} \cdot \vec{b} = \|\vec{a}\|\|\vec{b}\|\cos(\theta) \qquad \text{(E2)}$$

where $\vec{a}$ is the vector of city i, $\vec{b}$ is the vector of source for city j, $\|\vec{a}\|$ is the magnitude of city i, $\|\vec{b}\|$ is the magnitude of the vector for city j and θ is the angle between the two vectors ranging from 0 to 90º. $cos(\theta)$ quantifies the similarity in source contributions between the two cities. Rearranging Eq. (2) $cos(\theta)$ can be solved using Eq. (3)

$$\cos(\theta) = \left(\frac{\vec{a} \cdot \vec{b}}{\|\vec{a}\|\|\vec{b}\|}\right) \qquad \text{(E3)}$$

$\cos(\theta)$ ranges between zero (0) for no correlation to one (1) for perfect correlation between the source vectors. Figure 11-12 illustrates the value of $cos(\theta)$ calculated for city comparisons for $PM_{0.1}$ (lower left) and $PM_{2.5}$ (upper right) source-vectors. The cities were arranged by region, labeled by corresponding city code defined in Table 11-1 and starting from East, South East, South, Midwest and West in order to observe any geographical patterns. $PM_{2.5}$ source-vectors were found to be slightly more homogenous across all U.S. cities than $PM_{0.1}$ source vectors. Regional clusters with similar source contributions are apparent, especially on the East Coast where cities are closer in proximity to one another. Few regional clusters were observed for $PM_{0.1}$ source vectors, suggesting that emissions control programs may need to be tailored to each specific city. Natural gas combustion is prevalent in many locations, but the remaining sources of ultrafine particles vary strongly with location.

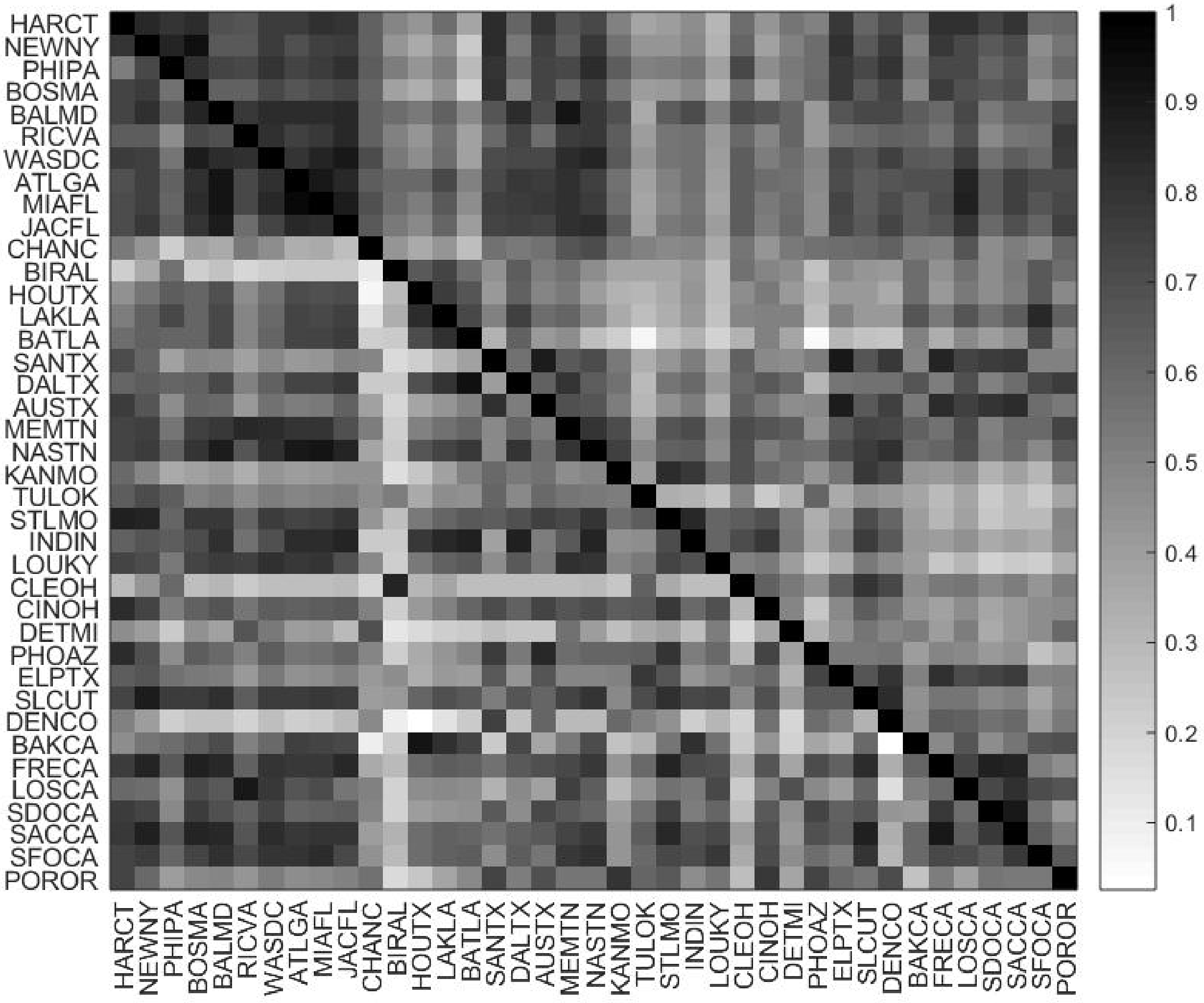

Figure 11-12: Normalized dot product between the 13 source types and each city code for $PM_{2.5}$ (upper right) and $PM_{0.1}$ (lower left). The scale represents 100% (black) to 0% (white) correlation. Cities are organized by region in the following order: East, South East, South, MidWest, West

11.5 Conclusion

The UCD/CIT regional chemical transport model was used to predict source contributions to $PM_{0.1}$ across the continental U.S. during peak photochemical smog periods during the year 2010. Model performance for $PM_{2.5}$ and ozone predictions met the recommendations for regulatory applications building confidence in the emissions inputs and meteorological fields used to drive the calculations. Similar model exercises carried out for episodes in California in 2015 and 2016 find good agreement between predicted $PM_{0.1}$ source contributions and receptor-based $PM_{0.1}$ source contributions calculated using measured concentrations of molecular markers [370]. In the current study, regional $PM_{0.1}$ concentrations exceeded 2 $\mu g\ m^{-3}$ during summer pollution episodes in major urban regions across the U.S. including Los Angeles, the San Francisco Bay Area, Houston, Miami, and New York. Predicted $PM_{0.1}$ spatial gradients were sharper than predicted $PM_{2.5}$ spatial gradients due to the dominance of primary aerosol in $PM_{0.1}$. This finding suggests that $PM_{0.1}$ measurement networks needed to support epidemiology must be denser than comparable $PM_{2.5}$ measurement networks. Non-residential natural gas combustion was identified as a major source of $PM_{0.1}$ across all major cities in the United States. On-road gasoline and diesel vehicles contributed on average 14% to regional $PM_{0.1}$ even though peak contributions within 0.3 km of the roadway were not resolved by the 4 km grid cells. This is consistent with other studies that have found an exponential decrease in ultrafine particle concentrations outside of major roadways [360] due to dilution and evaporation of UFPs. Food cooking also made significant contributions to $PM_{0.1}$ in all cities but biomass combustion was only important in locations impacted by summer wildfires. Aviation was a significant source of $PM_{0.1}$ in cities that had airports within their urban footprints. The major sources of primary $PM_{0.1}$ and $PM_{2.5}$ were notably different in many cities. Future epidemiological studies may be able to differentiate $PM_{0.1}$ and $PM_{2.5}$ health effects by contrasting cities with different ratios of $PM_{0.1}$ / $PM_{2.5}$ sources.

11.6 Appendix

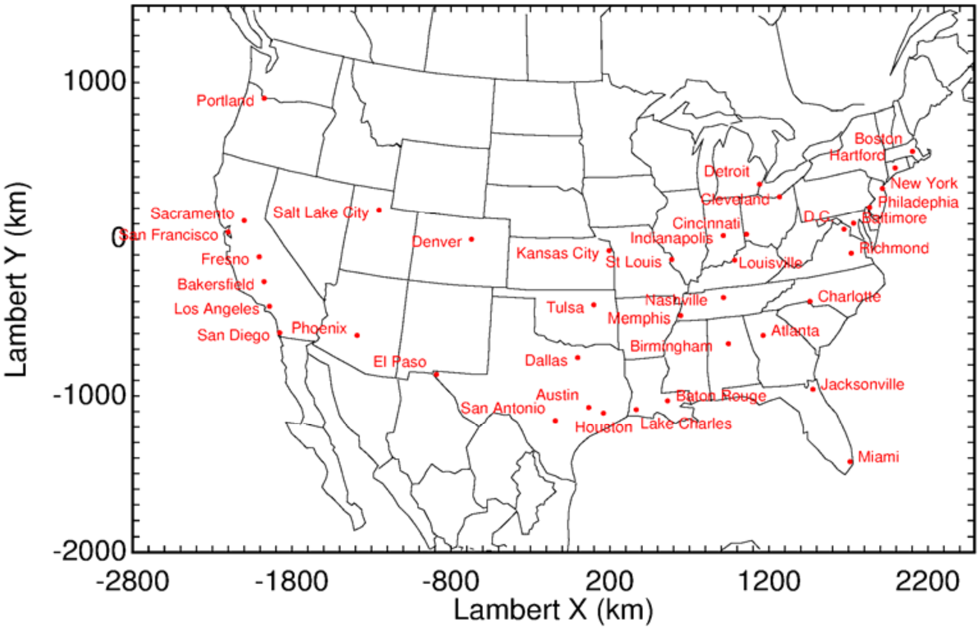

Figure S1. Map of Continental United States and 39 cities of interest

Table S11-1. Weighted source profile combinations

Source Type	Source Weight
Onroad Gasoline	10% Non-catalyst vehicle + 90% Catalyst Vehicle
Offroad Gasoline	100% Non-catalyst vehicle
Onroad Diesel	100% On-road diesel exhaust
Offroad Diesel	90% Diesel Exhaust from 1970's vehicle + 7% Diesel Exhaust from 1980's vehicle + 3% on-road diesel exhaust
Biomass Burning	90% Residential Wood Combustion + 5% Wildfire + 5% Waste burning
Food Cooking	85% Meat Frying + 15% Charbroiling
Natural Gas	100% Natural Gas Combustion
Distillate Oil	100% Distillate Fuel combustion
Aviation	100% Aircraft Jet Fuel
Cement Manufactures	100% Cement Kiln Gas Combustion
Process Heaters	100% Process Heaters
Coal	100% Coal Combustion
Steel Foundries	50% Steel Electric Arc Furnace + 50% Cast Iron Copper
Pulp and Paper mills	100% Wood Processing
Other	75% construction & demolition + 10% paved road travel + 4% farming ops + 3% brake wear + 2% cattle feedlot + 2% mining ops + 1% solid waste disposal + 1% mineral processing + 1% asphalt production + 1% organic solvent

S1. Quality Assurance – Measured vs Predicted Ozone

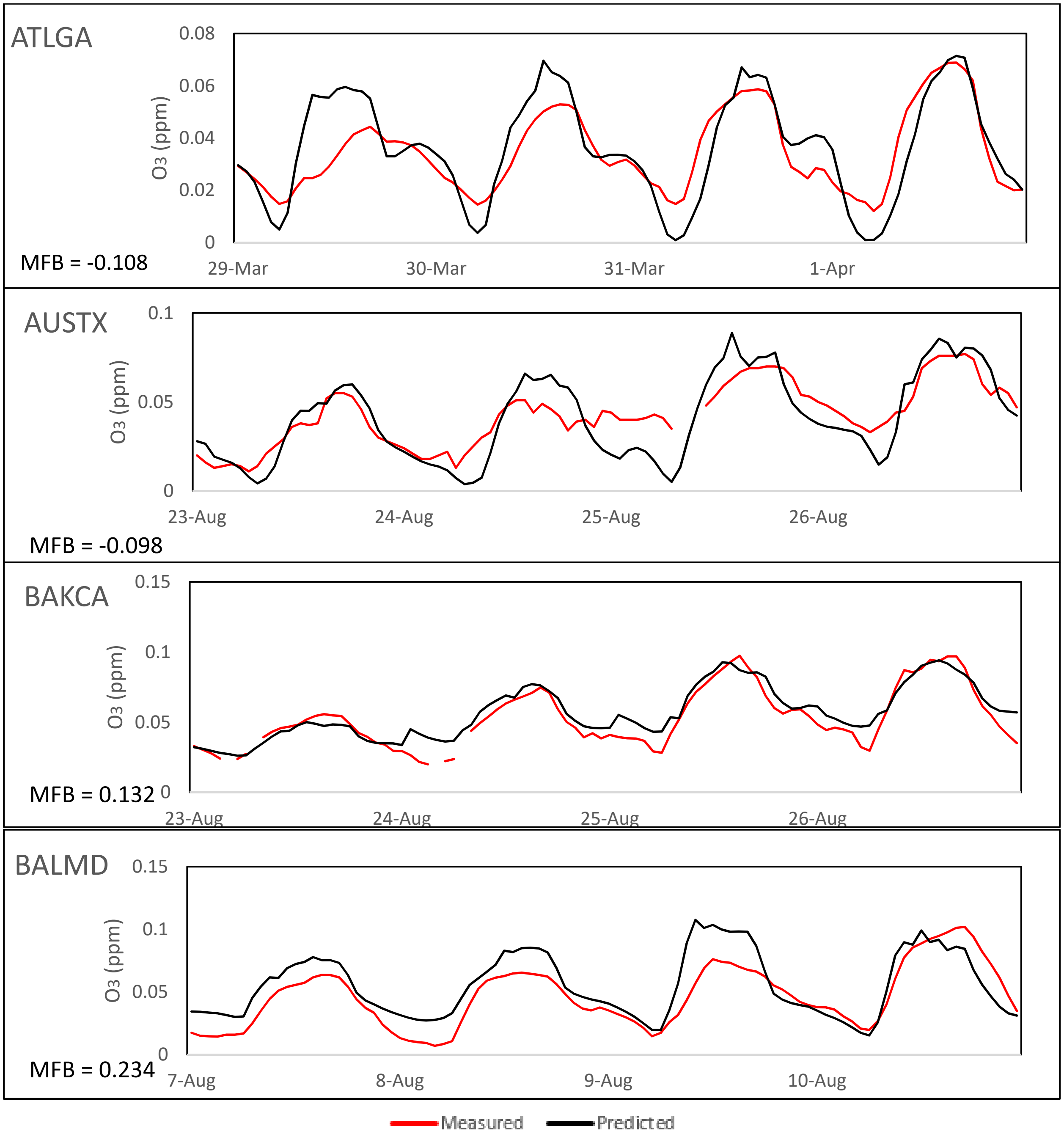

Figure S2. Time series plots of Measured (Red) vs Predicted (black) 1-hr ozone for each average city scenario throughout the U.S.

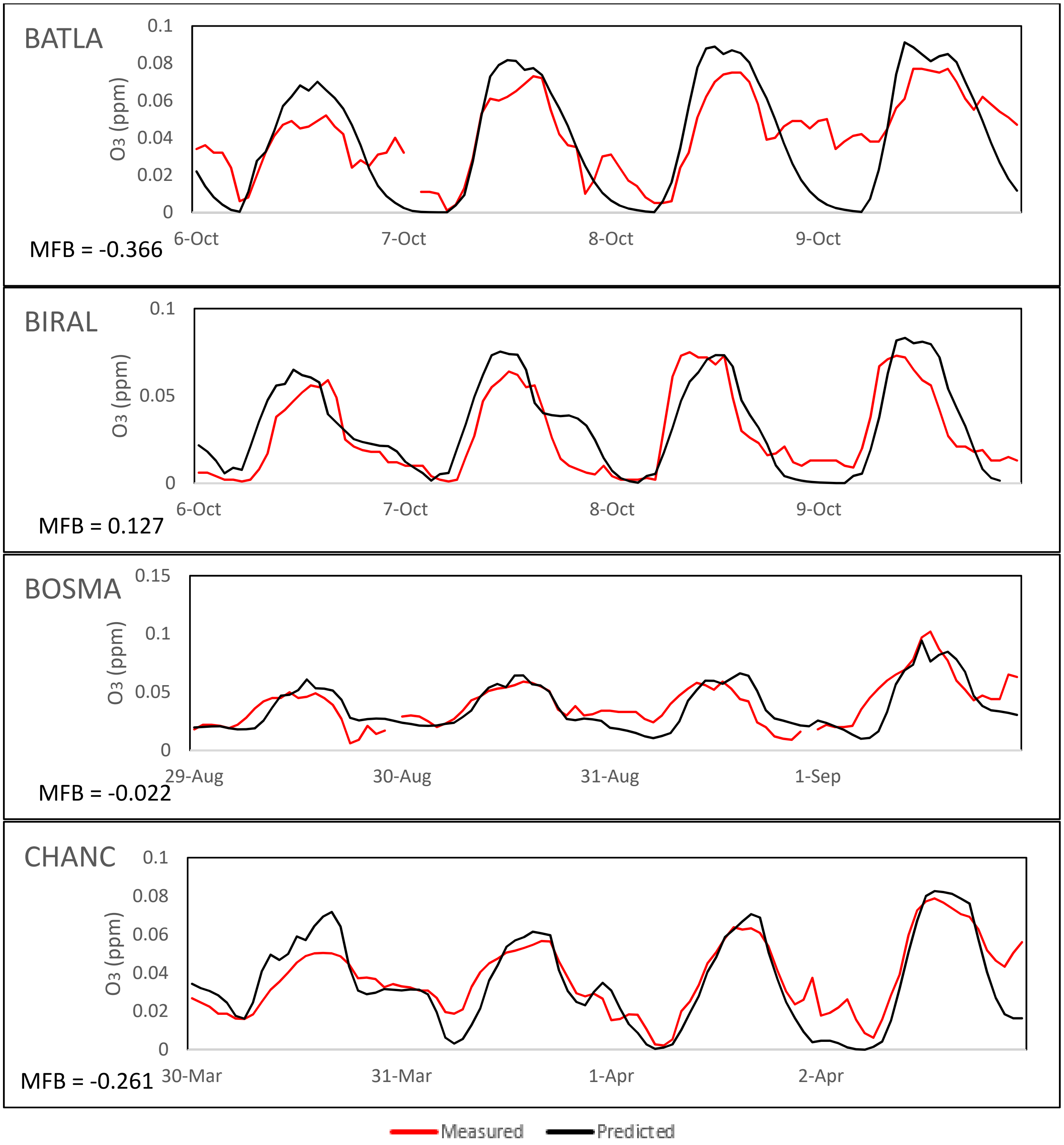

Figure S2 continued. Time series plots of Measured (Red) vs Predicted (black) 1-hr ozone for each average city scenario throughout the U.S.

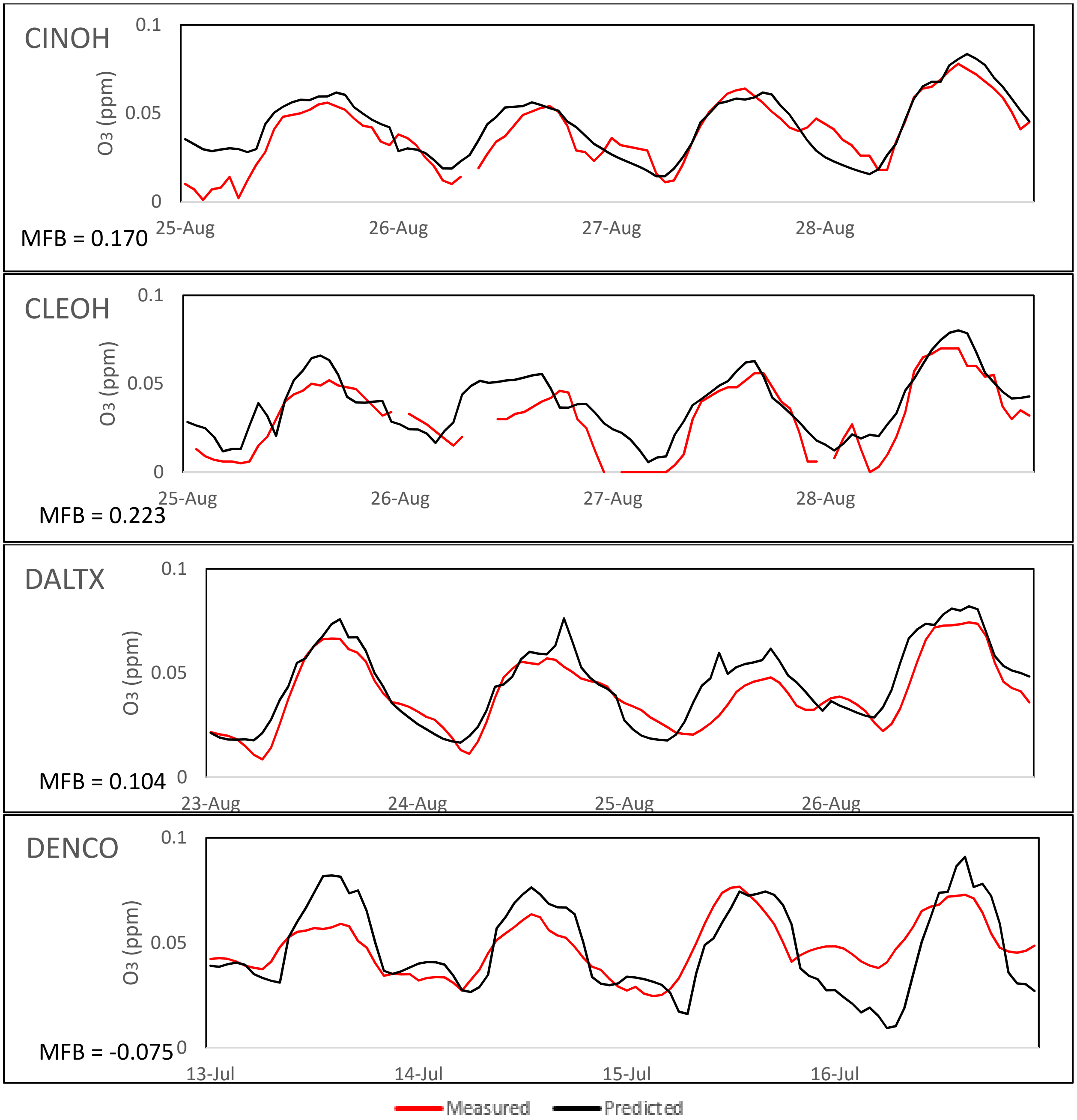

Figure S2 continued. Time series plots of Measured (Red) vs Predicted (black) 1-hr ozone for each average city scenario throughout the U.S.

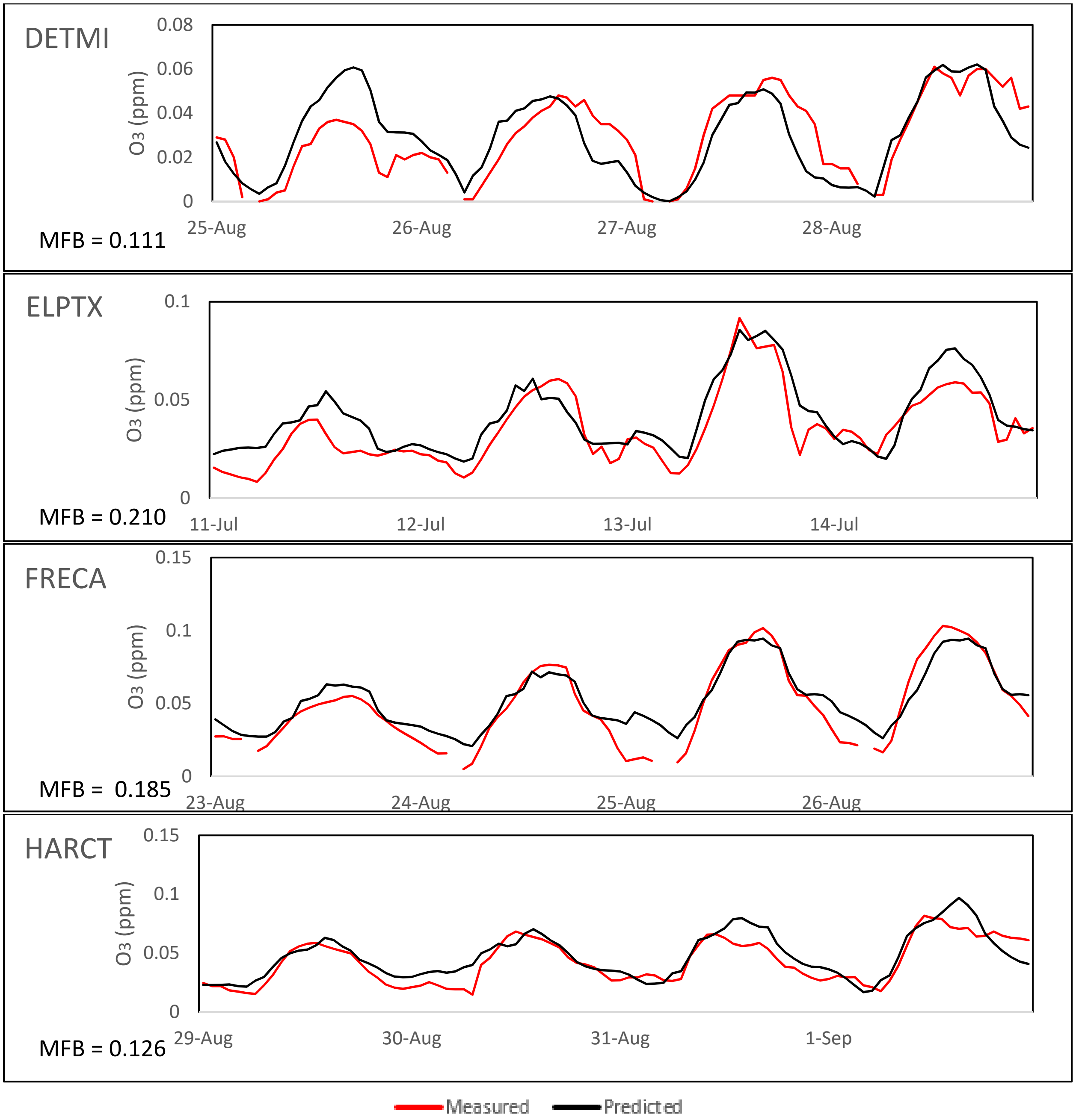

Figure S2 continued. Time series plots of Measured (Red) vs Predicted (black) 1-hr ozone for each average city scenario throughout the U.S.

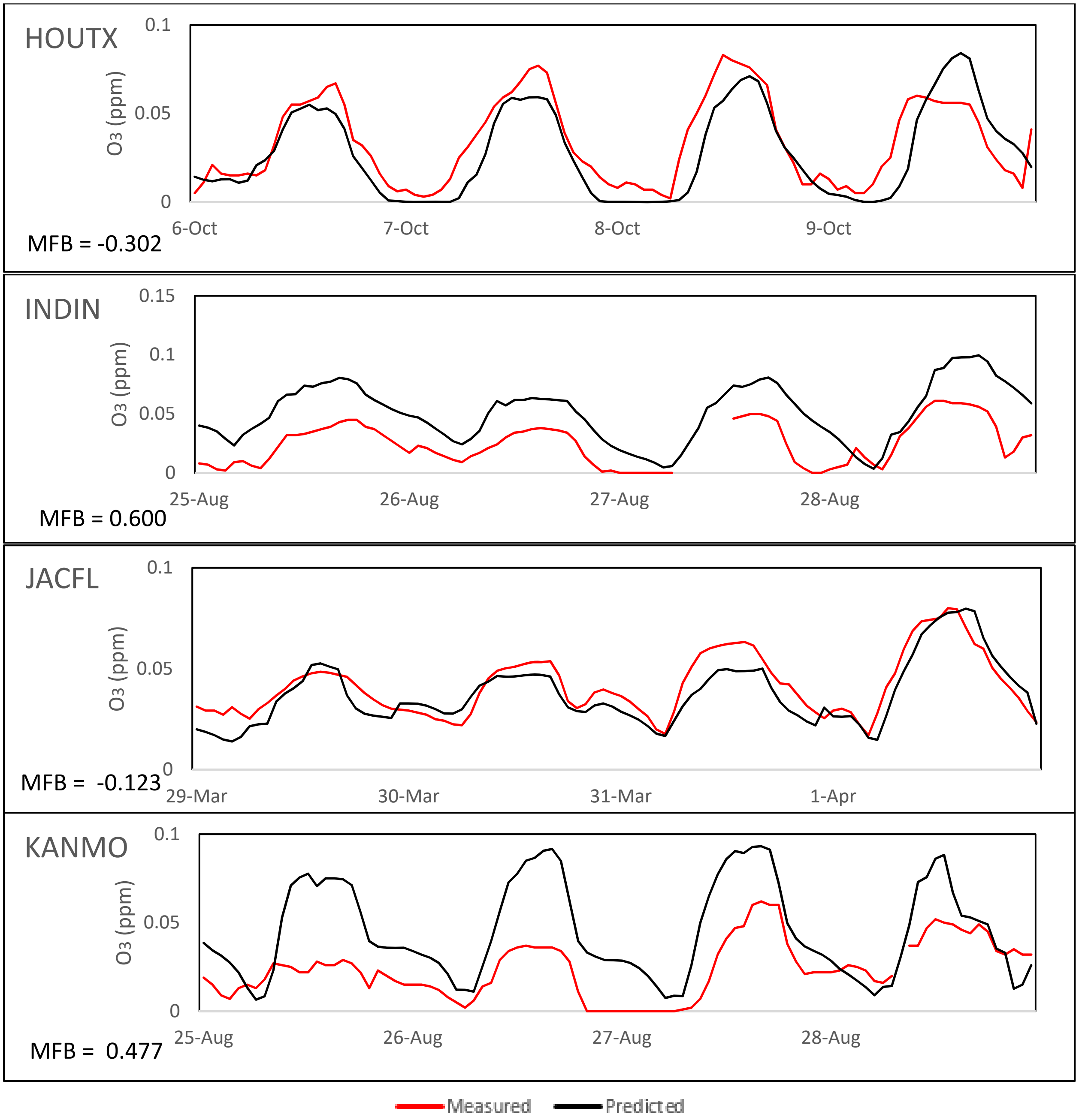

Figure S2 continued. Time series plots of Measured (Red) vs Predicted (black) 1-hr ozone for each average city scenario throughout the U.S.

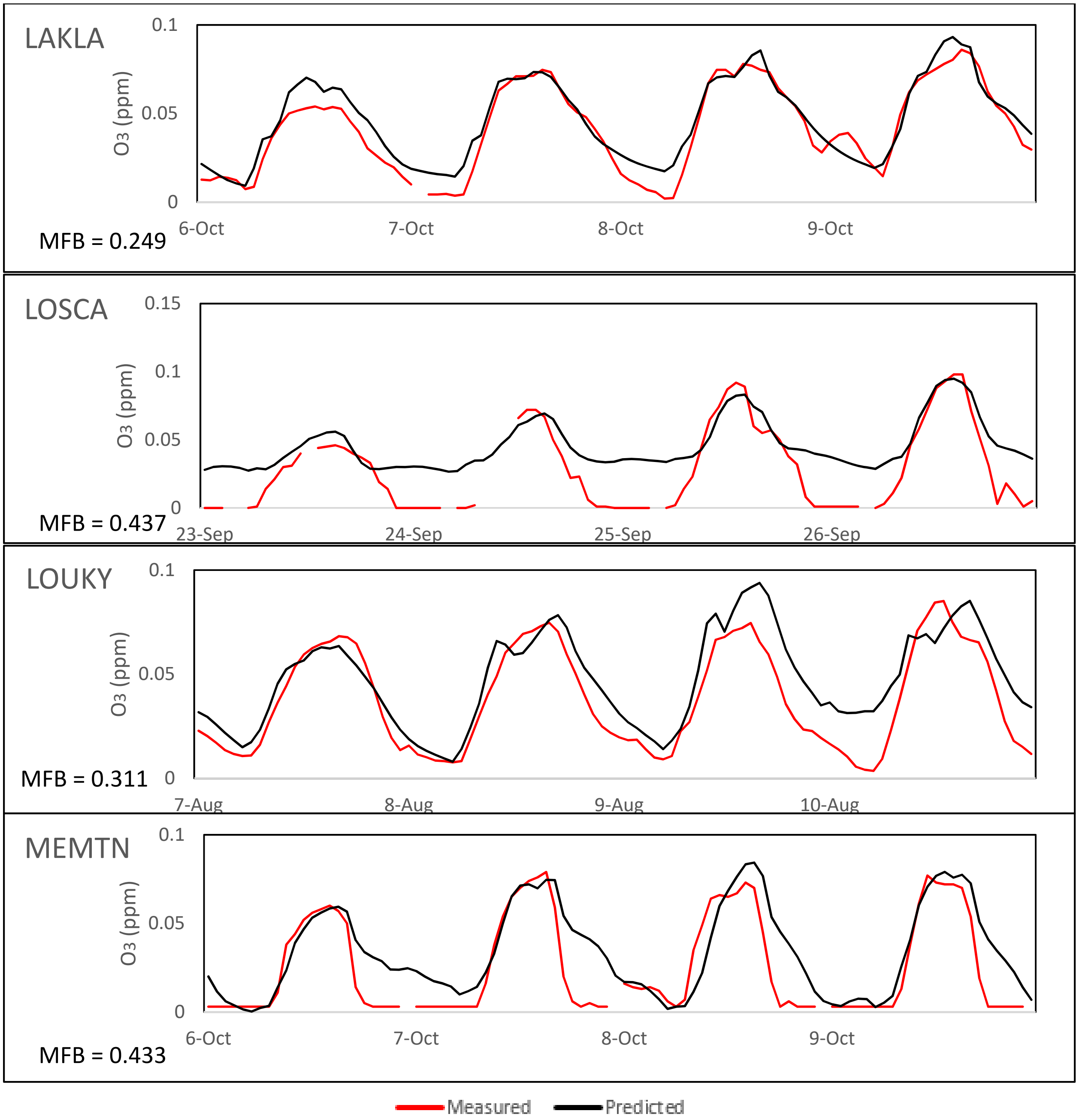

Figure S2 continued. Time series plots of Measured (Red) vs Predicted (black) 1-hr ozone for each average city scenario throughout the U.S.

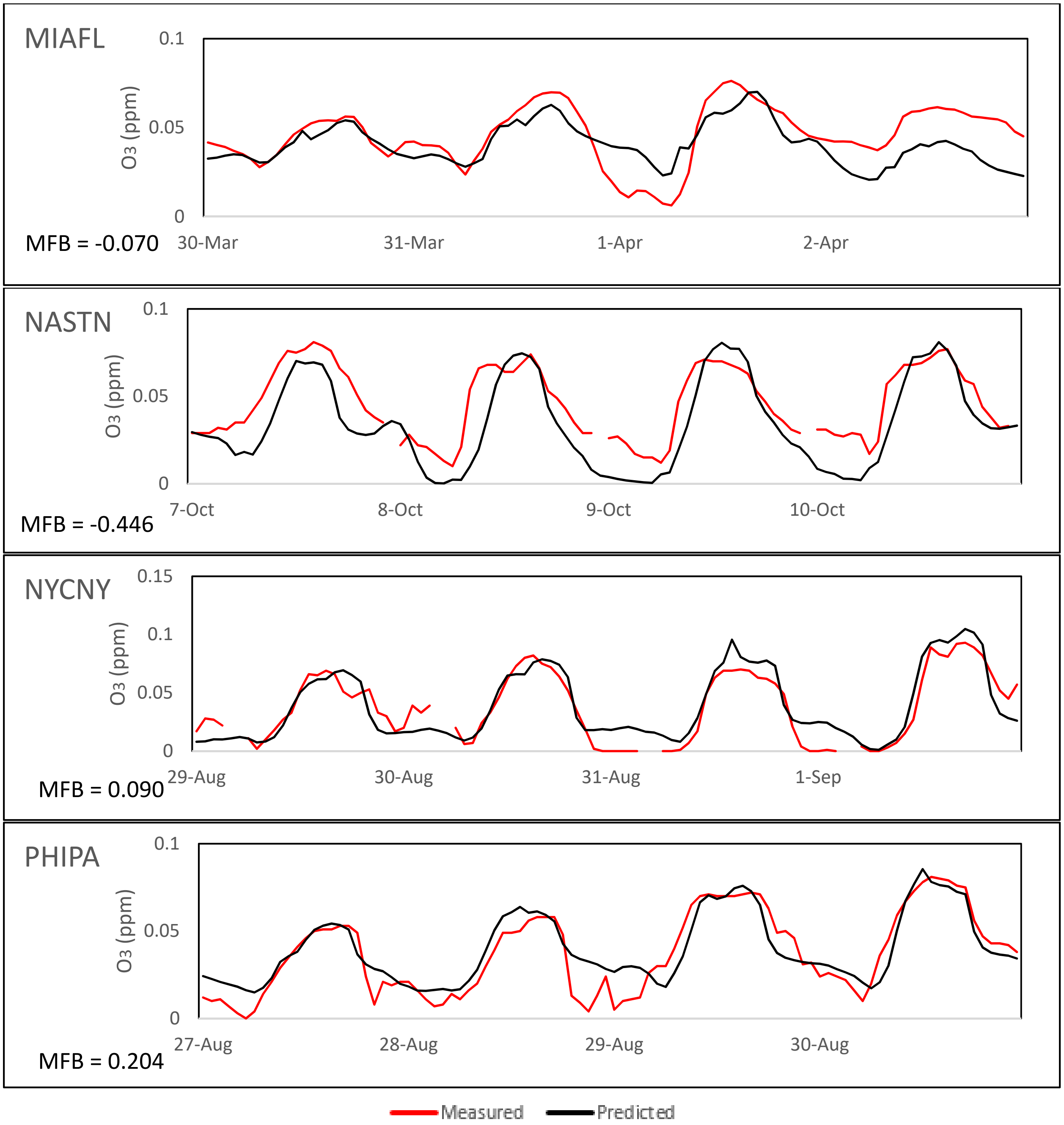

Figure S2 continued. Time series plots of Measured (Red) vs Predicted (black) 1-hr ozone for each average city scenario throughout the U.S.

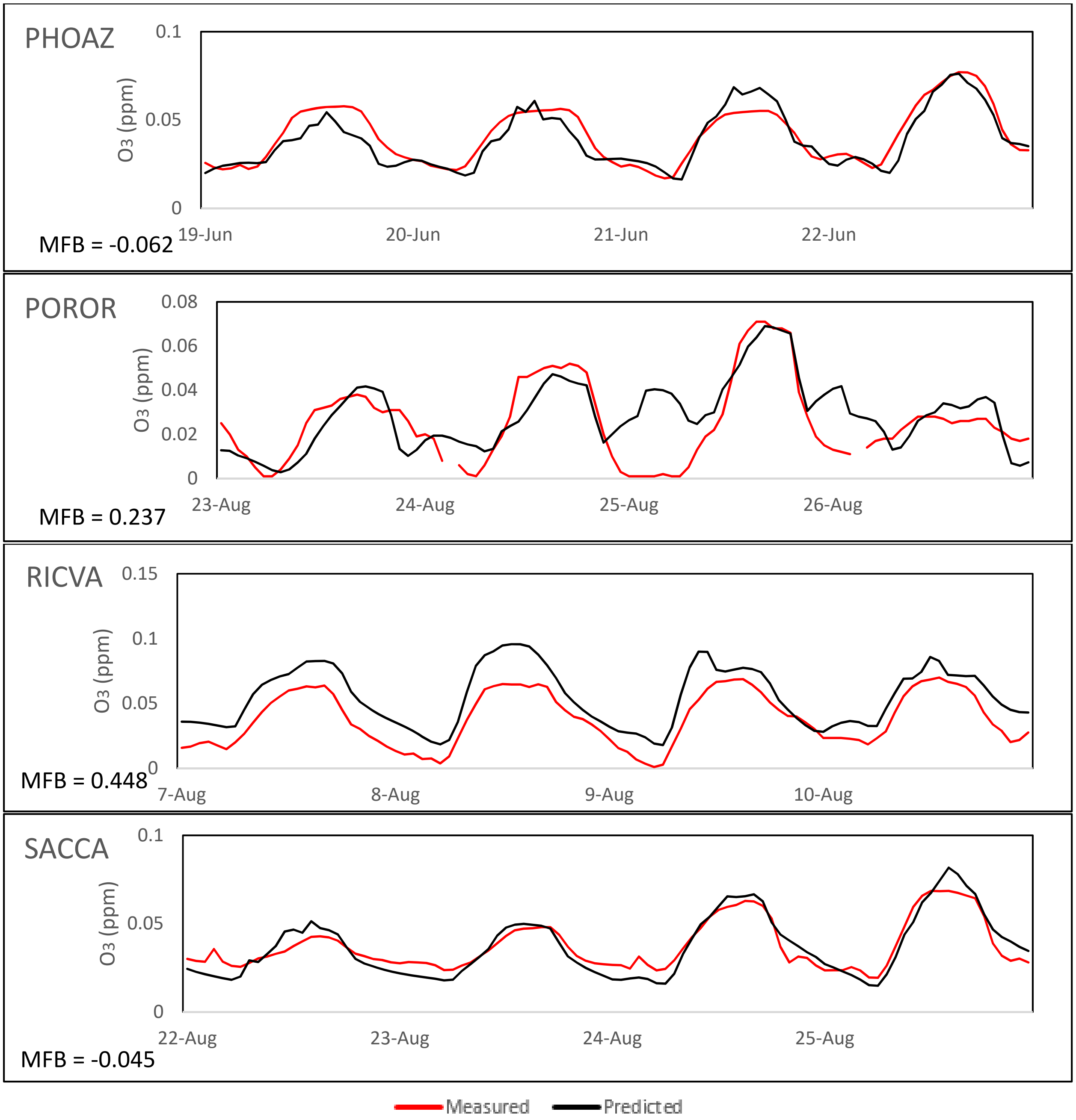

Figure S2 continued. Time series plots of Measured (Red) vs Predicted (black) 1-hr ozone for each average city scenario throughout the U.S.

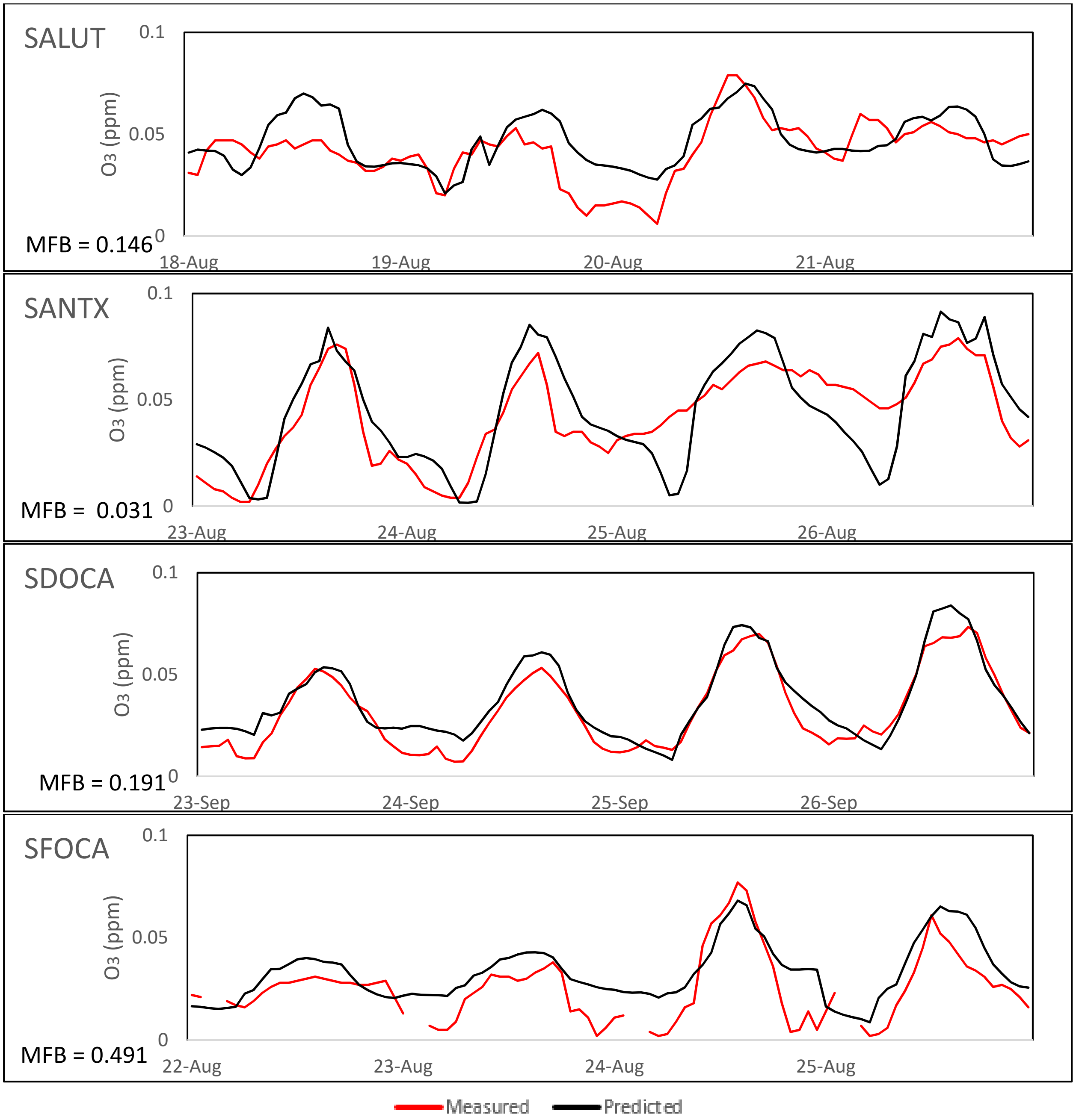

Figure S2 continued. Time series plots of Measured (Red) vs Predicted (black) 1-hr ozone for each average city scenario throughout the U.S.

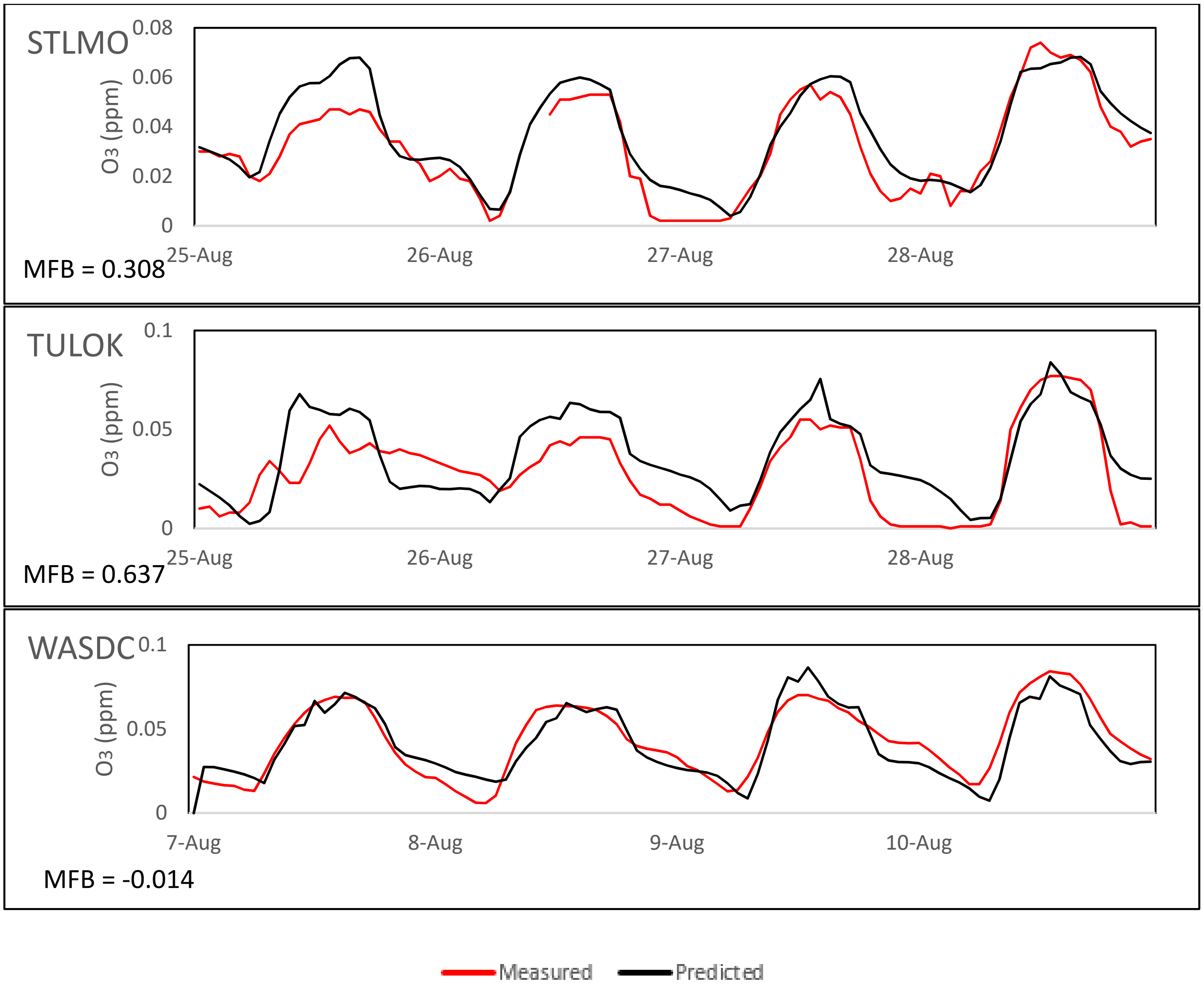

Figure S2 continued. Time series plots of Measured (Red) vs Predicted (black) 1-hr ozone for each average city scenario throughout the U.S.

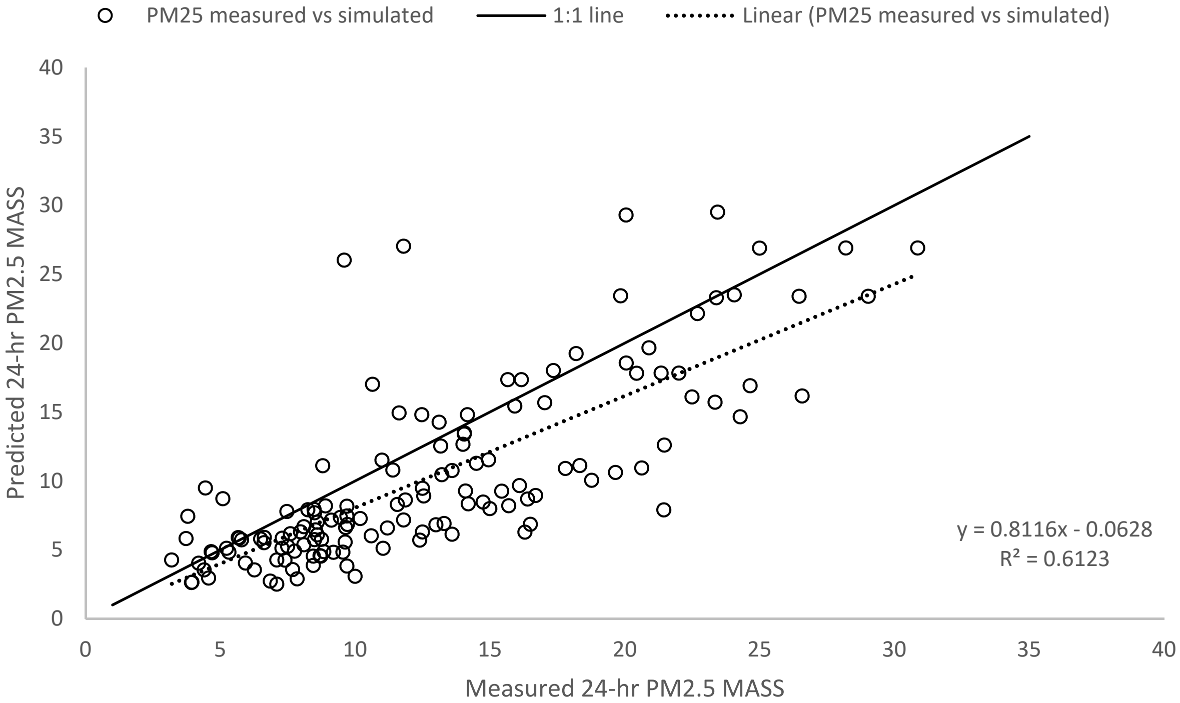

Figure S3. Predicted vs Measured 24-hr average $PM_{2.5}$ Mass (μg/m^3) for all 39 cities. R^2 value of 0.612 and slope coefficient of 0.8116.

Table S11-2. Model Performance Statistics. MFB = Mean Fractional Bias and MFE = Mean Fractional Error. EPA modeling criteria MFE < 0.67, RMSE = Root Mean Square Error.

	1-hr Ozone			**24-hr avg** $PM_{2.5}$		
City	**MFB**	**MFE**	**RMSE (ppm)**	**MFB**	**MFE**	**RMSE ($\mu g/m^3$)**
ATLGA	-0.108	0.367	0.011	-0.379	0.379	2.271
AUSTX	-0.098	0.415	0.016	-0.616	0.616	3.862
BAKCA	0.132	0.232	0.013	-0.334	0.339	2.952
BALMD	0.234	0.325	0.017	-0.034	0.143	3.293
BATLA	-0.366	0.65	0.019	0.221	0.224	2.436
BIRAL	0.127	0.576	0.018	-0.431	0.486	2.552
BOSMA	-0.022	0.313	0.013	-0.196	0.237	4.169
CHANC	-0.261	0.416	0.011	0.113	0.385	1.820
CINOH	0.17	0.307	0.011	-0.481	0.501	1.363
CLEOH	0.223	0.294	0.011	-0.208	0.208	1.648
DALTX	0.104	0.2	0.009	-0.336	0.336	4.092
DENCO	-0.075	0.238	0.013	-0.205	0.213	1.879
DETMI	0.111	0.46	0.012	-0.336	0.659	2.690
ELPTX	0.21	0.285	0.011	-0.632	0.632	2.965
FRECA	0.185	0.259	0.012	-0.665	0.665	3.890
HARCT	0.126	0.196	0.010	-0.658	0.658	2.116
HOUTX	-0.302	0.466	0.014	0.111	0.388	2.163
INDIN	0.6	0.635	0.023	-0.315	0.315	1.374
JACFL	-0.123	0.194	0.008	-0.52	0.533	5.961
KANMO	0.477	0.592	0.027	-0.465	0.465	2.491
LAKLA	0.249	0.299	0.009	0.426	0.426	6.713
LOSCA	0.437	0.442	0.016	-0.332	0.332	1.388
LOUKY	0.311	0.344	0.014	-0.116	0.236	3.242
MEMTN	0.433	0.614	0.017	-0.263	0.263	1.328
MIAFL	-0.07	0.283	0.013	-0.512	0.527	3.295
NASTN	-0.446	0.604	0.017	-0.145	0.145	0.961
NYCNY	0.09	0.29	0.011	-0.438	0.438	4.482
PHIPA	0.204	0.334	0.010	-0.138	0.152	1.420
PHOAZ	-0.062	0.194	0.011	-0.065	0.065	0.525
POROR	0.237	0.549	0.014	-0.004	0.363	0.940
RICVA	**0.448**	**0.451**	**0.018**	**-1.053**	**1.053**	**7.785**
SACCA	-0.045	0.122	0.005	0.04	0.04	0.190
SALUT	0.146	0.269	0.013	-0.385	0.385	2.186
SANTX	0.031	0.395	0.016	-0.629	0.629	3.755
SDOCA	0.191	0.302	0.009	-0.437	0.437	1.988

	1-hr Ozone			**24-hr avg** $PM_{2.5}$		
SFOCA	0.491	0.522	0.013	-0.244	0.244	1.982
STLMO	0.308	0.368	0.011	0.468	0.509	3.777
TULOK	**0.637**	**0.739**	**0.015**	**-0.25**	**0.25**	**1.320**
WASDC	-0.014	0.232	0.009	-0.071	0.117	2.985
Average	0.126	0.379	0.013	-0.27	0.384	2.724

MFB was calculated using equation 1:

$$\mathrm{MFB} = \frac{2}{N}\sum_{i=1}^{N}\frac{(Pred_{x,t}^{i}-Obs_{x,t}^{i})}{(Pred_{x,t}^{i}+Obs_{x,t}^{i})} \tag{1}$$

MFE was calculated using equation 2:

$$\mathrm{MFE} = \frac{2}{N}\sum_{i=1}^{N}\frac{|Pred_{x,t}^{i}-Obs_{x,t}^{i}|}{(Pred_{x,t}^{i}+Obs_{x,t}^{i})} \tag{2}$$

RMSE was calculated using equation 3:

$$RMSE = \sqrt{\frac{\sum_{i=1}^{n}(Pred_{x,t}^{i}-Obs_{x,t}^{i})^2}{n}} \tag{3}$$

Figures S4-S7 compares $PM_{2.5}$and $PM_{0.1}$ mass contributions from the explicitly tracked sources. In many cases, hot-spots were predicted that over-whelmed contributions in other areas. The concentration scales in Figures S4-S7 were adjusted to better view the broad impacts from all sources throughout the 12km-continental US grid. On road diesel, on road gasoline and food cooking sources result in hotspots that highlight the metropolitan areas of the United States. Aviation sources highlight both metropolitan airports and Naval / Air Force bases. Various industrial sources such as cement manufacturing and wood/paper mills highlight industrial plants in the South East United states. Natural gas fueled emissions highlight metropolitan areas that utilize large quantities of natural gas and industrial areas that consume natural gas. Coal combustion emissions highlight many metropolitan areas in the Midwest that generate a large percentage of their electricity from coal-fired power stations.

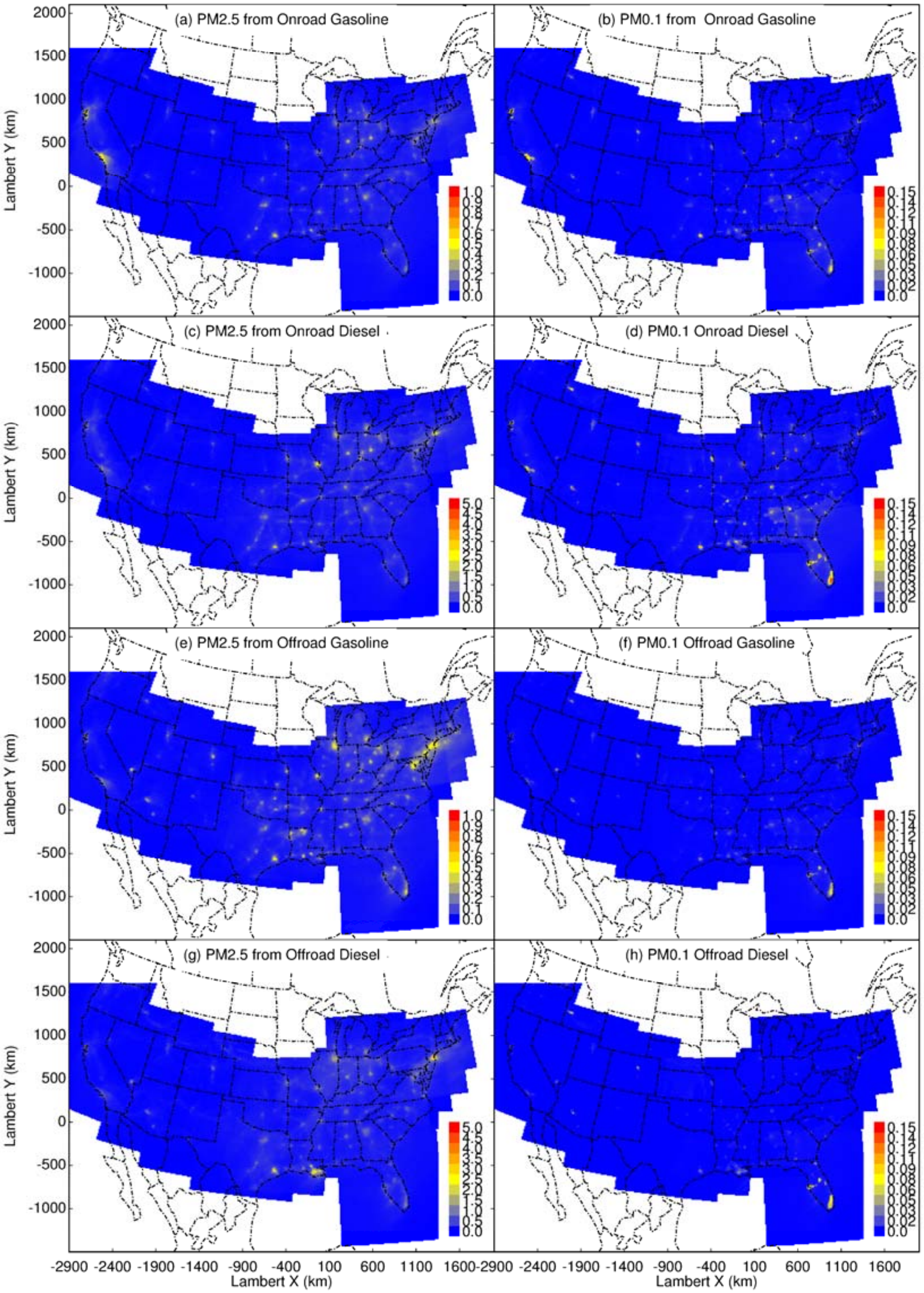

Figure S4. Field plot “snap shot” of Continental US PM$_{2.5}$ and PM$_{0.1}$ 24-hr average mass (μg/m^3) for gasoline and diesel. Scale drawn to highlight all areas of US. Actual max for (a) 0.582 μg/m^3 (b) 0.109 μg/m^3 (c) 3.365 μg/m^3 (d) 0.155 μg/m^3 (e) 0.902 μg/m^3 (f) 0.112 μg/m^3 (g) 7.534 μg/m^3 (h) 0.129 μg/m^3

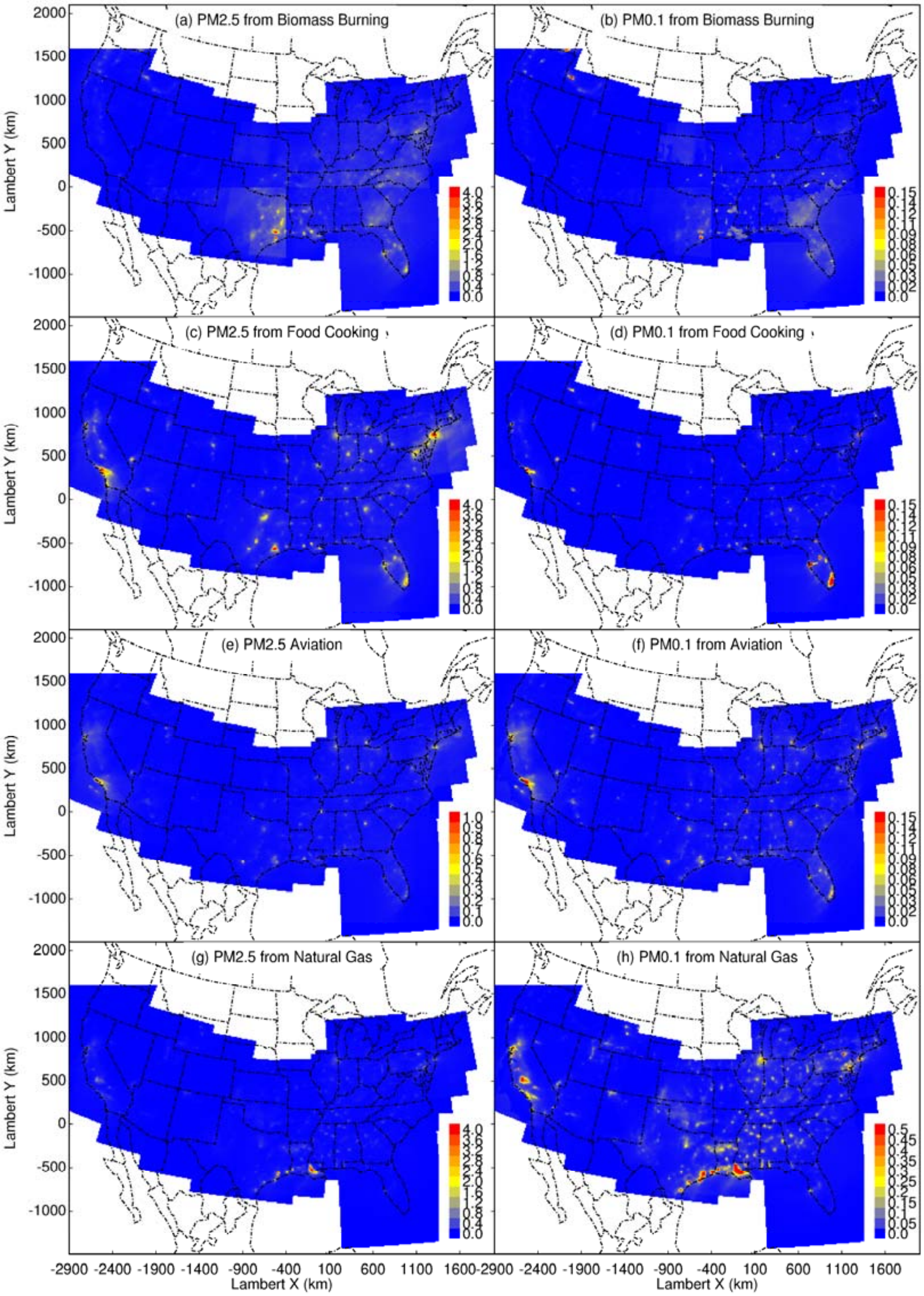

Figure S5. Field plot "snap shot" of Continental US $PM_{2.5}$ and $PM_{0.1}$ 24-hr average mass (μg/m^3) for biomass burning, food cooking, aviation, and natural gas combustion. Scale drawn to highlight all areas of US. Actual max for (a) 6.461 μg/m^3 (b) 0.388 μg/m^3 (c) 10.18 μg/m^3 (d) 0.349 μg/m^3 (e) 1.851 μg/m^3 (f) 0.556 μg/m^3 (g) 7.147 μg/m^3 (h) 3.625 μg/m^3

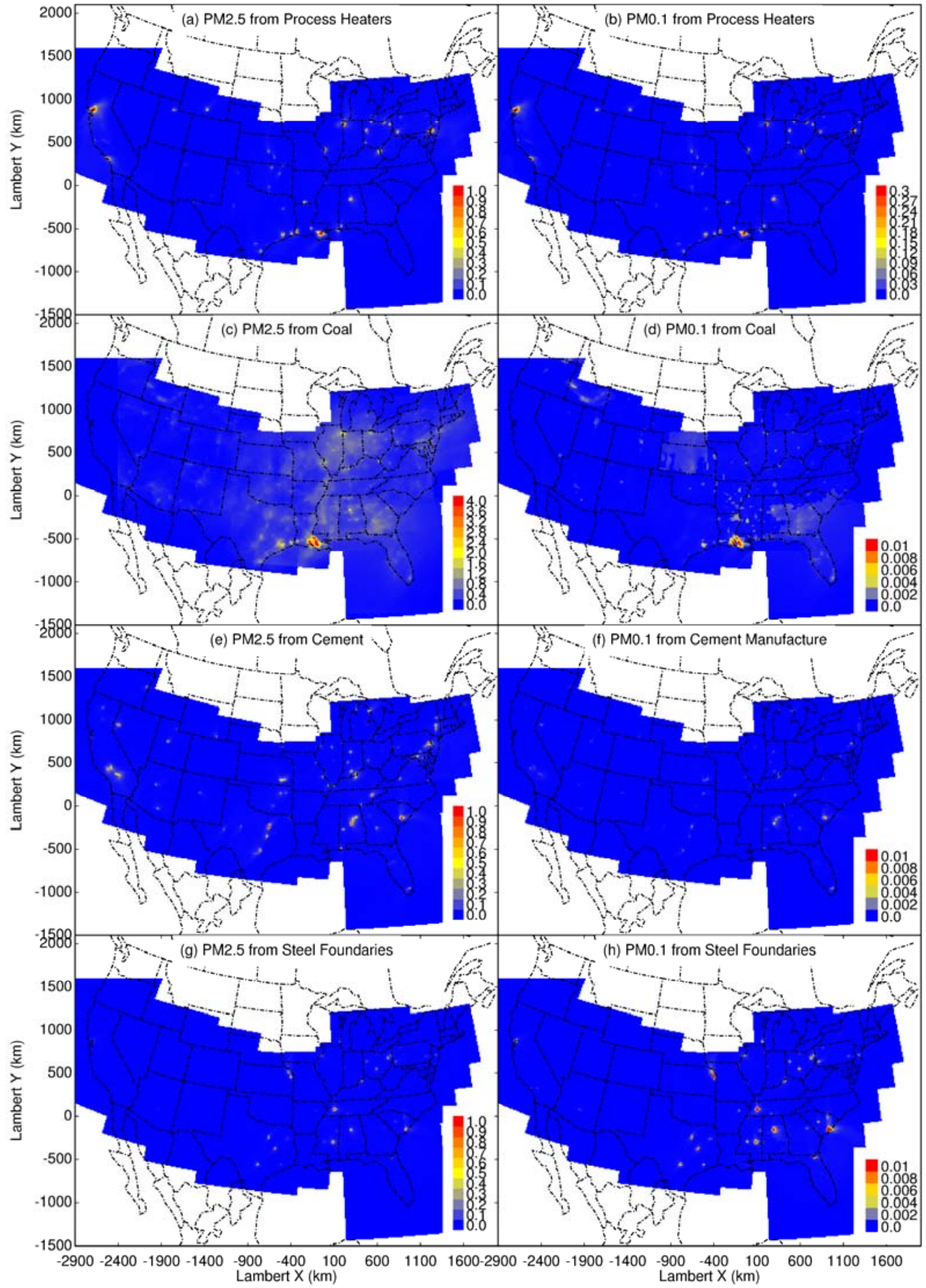

Figure S6. Field plot “snap shot” of Continental US $PM_{2.5}$ and $PM_{0.1}$ 24-hr average mass (μg/m^3) for process heaters, coal, cement, and steel foundries. Scale drawn to highlight all areas of US. Actual max for (a) 3.968 μg/m^3 (b) 1.141 μg/m^3 (c) 20.254 μg/m^3 (d) 0.040 μg/m^3 (e) 2.201 μg/m^3 (f) 1.275 μg/m^3 (g) 1.317 μg/m^3 (h) 0.0652 μg/m^3

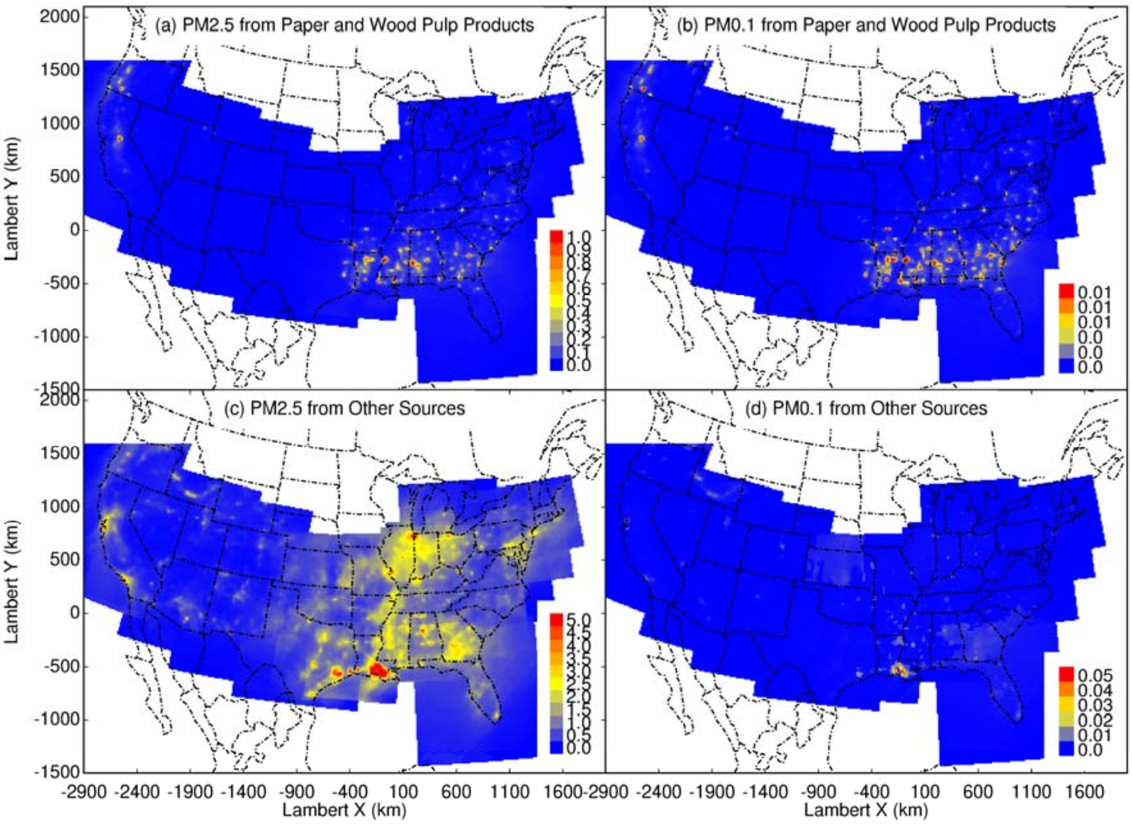

Figure S7. Field plot "snap shot" of Continental US PM$_{2.5}$ and PM$_{0.1}$ 24-hr average mass (µg/m^3) for paper and wood pulp products and "other sources". Scale drawn to highlight all areas of US. Actual max for (a) 3.968 µg/m^3 (b) 1.141 µg/m^3 (c) 84.18 µg/m^3 (d) 0.133 µg/m^3

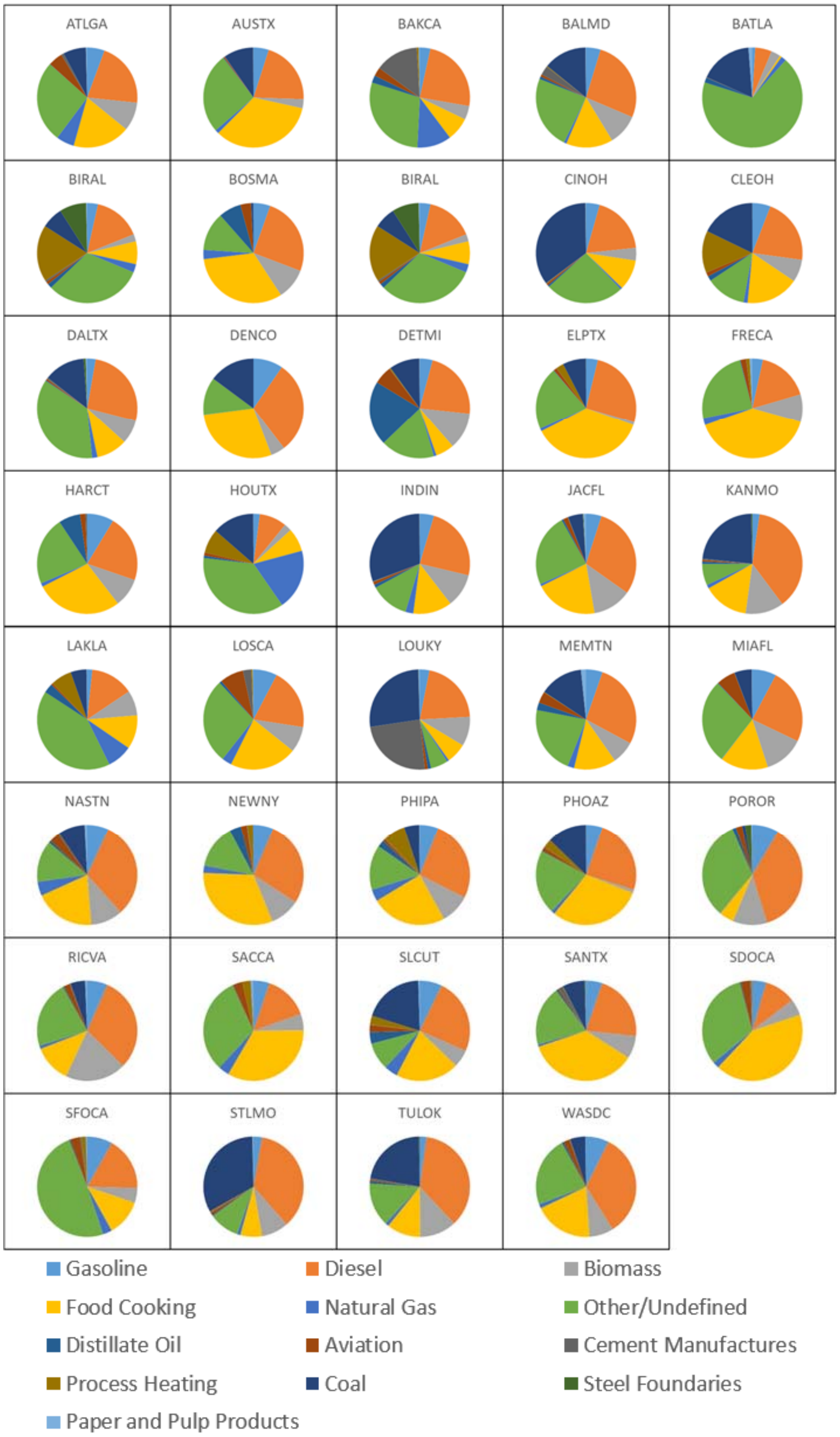

Figure S8. PM2.5 source contribution for 39 cities across the continental US

S3. PM source contribution for each city. Tables are separated by region

Table S11-3. Source contribution for $PM_{2.5}$ ($\mu g/m^3$) for the EAST

	HARCT	NEWNY	PHIPA	BOSMA	BALMD	RICVA	WASDC
Gasoline (onroad + offroad)	1.72E-01	6.59E-01	5.18E-01	2.67E-01	3.20E-01	2.14E-01	4.30E-01
Diesel (onroad + offroad)	4.32E-01	2.85E+00	2.29E+00	1.25E+00	1.82E+00	9.97E-01	1.96E+00
Biomass	1.85E-01	9.95E-01	8.32E-01	4.93E-01	6.76E-01	6.38E-01	4.61E-01
Food Cooking	5.58E-01	3.27E+00	2.11E+00	1.59E+00	1.03E+00	3.95E-01	1.11E+00
Natural Gas Combustion	2.34E-02	2.38E-01	3.28E-01	1.48E-01	5.98E-02	3.26E-02	7.93E-02
Other/Undefined	4.40E-01	1.47E+00	1.26E+00	6.16E-01	1.62E+00	7.08E-01	1.32E+00
Distillate Oil	1.39E-01	3.81E-01	1.92E-01	3.58E-01	5.73E-02	1.21E-02	3.59E-02
Aviation	3.44E-02	2.04E-01	7.63E-02	1.68E-01	5.01E-02	6.59E-02	1.17E-01
Cement Manufactures	1.08E-02	1.32E-02	1.35E-02	1.28E-03	2.03E-01	4.28E-03	6.98E-03
Process Heating	7.92E-04	1.80E-01	6.14E-01	3.34E-04	1.70E-02	2.15E-03	5.82E-03
Coal	1.33E-04	1.47E-02	4.19E-01	3.69E-02	9.50E-01	1.55E-01	2.90E-01
Steel Foundries	1.58E-04	3.93E-03	2.92E-03	5.35E-05	9.04E-04	9.08E-04	6.94E-04
Paper and Pulp Products	3.96E-04	5.34E-03	1.42E-02	1.73E-03	1.03E-02	2.12E-02	9.85E-03

Table S11-4. Source contribution for $PM_{0.1}$ ($\mu g/m^3$) for the EAST

	HARCT	NEWNY	PHIPA	BOSMA	BALMD	RICVA	WASDC
Gasoline (onroad + offroad)	9.81E-03	4.45E-02	4.03E-02	2.16E-02	7.45E-03	5.14E-03	1.21E-02
Diesel (onroad + offroad)	1.47E-02	4.47E-02	6.14E-02	2.92E-02	6.60E-03	4.18E-03	1.73E-02
Biomass	4.10E-03	4.82E-02	6.86E-02	1.46E-02	5.24E-03	5.70E-03	7.18E-03
Food Cooking	1.30E-02	6.00E-02	5.32E-02	6.51E-02	8.47E-03	3.25E-03	2.00E-02
Natural Gas Combustion	1.92E-02	1.94E-01	2.44E-01	1.36E-01	2.90E-02	1.71E-02	5.38E-02
Other/Undefined	5.42E-04	2.11E-03	2.17E-03	1.54E-03	2.58E-04	1.61E-04	4.22E-04
Distillate Oil	1.14E-12	2.41E-11	3.23E-12	1.29E-11	1.05E-12	1.34E-13	1.68E-12
Aviation	1.07E-02	5.47E-02	1.84E-02	6.68E-02	9.08E-03	1.79E-02	3.56E-02
Cement Manufactures	3.33E-05	7.24E-05	4.60E-05	4.42E-06	3.29E-04	1.25E-06	5.04E-06
Process Heating	4.20E-05	5.92E-02	1.59E-01	3.11E-05	1.29E-03	5.52E-05	1.97E-04
Coal	1.33E-04	2.13E-05	7.25E-04	9.82E-05	1.52E-04	3.53E-05	9.25E-05
Steel Foundries	1.79E-06	4.00E-04	1.10E-04	1.27E-06	2.28E-06	2.40E-06	3.37E-06
Paper and Pulp Products	4.25E-06	5.23E-05	2.56E-04	4.17E-05	5.63E-05	1.47E-04	4.57E-05

Table S11-5. Source contribution for $PM_{2.5}$ (µg/m^3) for the SOUTH EAST

	ATLGA	MIAFL	JACFL	CHANC	BIRAL
Gasoline (onroad + offroad)	4.85E-01	3.06E-01	1.59E-01	3.00E-01	5.23E-01
Diesel (onroad + offroad)	1.82E+00	9.64E-01	9.50E-01	5.47E-01	2.33E+00
Biomass	7.98E-01	5.11E-01	3.98E-01	8.72E-02	3.52E-01
Food Cooking	1.60E+00	6.10E-01	6.48E-01	2.96E-01	1.12E+00
Natural Gas Combustion	5.04E-01	4.71E-03	2.26E-02	2.22E-02	4.09E-01
Other/Undefined	2.29E+00	1.08E+00	7.50E-01	2.83E-01	4.77E+00
Distillate Oil	8.33E-03	8.83E-03	1.87E-02	1.89E-02	2.22E-01
Aviation	4.03E-01	2.40E-01	4.84E-02	3.49E-01	1.32E-01
Cement Manufactures	6.73E-02	3.37E-03	2.59E-03	6.67E-04	8.31E-02
Process Heating	2.97E-03	3.73E-04	1.50E-03	5.16E-04	2.77E+00
Coal	6.40E-01	2.21E-01	1.54E-01	8.20E-02	1.05E+00
Steel Foundries	1.90E-03	3.43E-04	6.22E-03	2.01E-03	1.31E+00
Paper and Pulp Products	3.60E-02	7.30E-03	2.69E-02	9.22E-18	5.26E-02

Table S11-6. Source contribution for $PM_{0.1}$ (µg/m^3) for the SOUTH EAST

	ATLGA	MIAFL	JACFL	CHANC	BIRAL
Gasoline (onroad + offroad)	8.16E-02	3.58E-03	2.62E-02	1.46E-01	6.62E-02
Diesel (onroad + offroad)	9.19E-02	3.69E-03	4.38E-02	1.65E-01	1.16E-01
Biomass	8.59E-02	2.23E-03	2.84E-02	8.97E-02	1.88E-02
Food Cooking	7.04E-02	2.58E-03	5.26E-02	7.40E-02	5.46E-02
Natural Gas Combustion	4.22E-01	1.51E-02	1.54E-01	2.13E-02	3.17E-01
Other/Undefined	4.53E-03	2.35E-04	2.01E-03	3.92E-03	1.01E-02
Distillate Oil	7.39E-09	7.64E-13	1.41E-09	4.62E-08	4.78E-09
Aviation	1.45E-01	5.66E-03	2.10E-02	2.46E-01	5.60E-02
Cement Manufactures	4.53E-04	3.96E-06	1.55E-05	3.09E-05	6.10E-04
Process Heating	3.98E-04	4.07E-05	2.73E-04	4.94E-04	8.97E-01
Coal	1.76E-03	4.82E-05	4.12E-04	1.60E-03	2.85E-03
Steel Foundries	8.55E-05	3.82E-06	5.16E-04	6.98E-04	1.36E-01
Paper and Pulp Products	6.11E-04	5.89E-05	5.64E-04	7.06E-18	1.53E-03

Table S11-7. Source contribution for PM$_{2.5}$ (μg/m^3) for the SOUTH

	HOUTX	LAKLA	BATLA	SANTX	DALTX	AUSTX
Gasoline (onroad + offroad)	4.26E-01	2.92E-01	1.66E-01	2.20E-01	2.22E-02	2.02E-01
Diesel (onroad + offroad)	1.83E+00	2.45E+00	9.41E-01	9.10E-01	2.14E-01	8.43E-01
Biomass	5.07E-01	1.42E+00	5.39E-01	3.12E-01	6.29E-02	1.20E-01
Food Cooking	1.58E+00	1.93E+00	1.07E-01	1.52E+00	8.14E-02	1.39E+00
Natural Gas Combustion	4.08E+00	1.43E+00	2.92E-01	2.95E-02	1.42E-02	4.83E-02
Other/Undefined	7.63E+00	7.30E+00	1.21E+01	8.17E-01	2.92E-01	1.06E+00
Distillate Oil	1.65E-01	5.38E-01	2.87E-01	2.56E-02	1.97E-03	8.27E-03
Aviation	2.01E-01	9.97E-02	1.52E-02	2.25E-02	3.81E-03	1.45E-02
Cement Manufactures	2.66E-04	1.28E-03	5.63E-04	5.31E-02	2.98E-03	4.01E-03
Process Heating	1.63E+00	1.20E+00	4.73E-03	6.44E-03	6.44E-04	4.02E-04
Coal	2.82E+00	9.03E-01	3.02E+00	3.02E-01	1.08E-01	3.94E-01
Steel Foundries	2.55E-03	1.68E-03	8.57E-04	1.44E-02	5.75E-03	8.62E-04
Paper and Pulp Products	1.30E-02	3.83E-02	2.20E-01	6.36E-03	3.84E-03	2.98E-03

Table S11-8. Source contribution for PM$_{0.1}$ (μg/m^3) for the SOUTH

	HOUTX	LAKLA	BATLA	SANTX	DALTX	AUSTX
Gasoline (onroad + offroad)	5.07E-02	2.30E-02	1.77E-02	2.78E-02	7.64E-04	2.64E-02
Diesel (onroad + offroad)	4.72E-02	1.47E-01	8.16E-02	3.97E-02	4.31E-03	3.70E-02
Biomass	2.58E-02	4.48E-02	2.06E-02	1.81E-02	6.89E-04	5.03E-03
Food Cooking	4.77E-02	6.69E-03	3.23E-03	4.89E-02	4.99E-04	5.15E-02
Natural Gas Combustion	3.20E+00	5.94E-01	1.80E-01	2.31E-02	8.48E-03	4.25E-02
Other/Undefined	1.45E-02	1.19E-02	2.45E-02	2.38E-03	3.42E-04	3.13E-03
Distillate Oil	2.38E-10	1.10E-10	3.25E-09	4.83E-14	8.67E-16	1.92E-14
Aviation	6.32E-02	2.05E-02	3.67E-03	8.01E-03	3.87E-04	4.90E-03
Cement Manufactures	9.34E-07	6.53E-02	1.97E-06	3.02E-04	4.38E-06	1.52E-05
Process Heating	4.30E-01	1.17E-01	1.40E-03	2.13E-03	4.84E-05	5.07E-05
Coal	5.35E-03	1.47E-03	6.13E-03	8.79E-04	1.26E-04	1.16E-03
Steel Foundries	1.39E-04	7.42E-05	3.62E-05	9.41E-04	1.86E-04	4.40E-05
Paper and Pulp Products	2.68E-04	6.50E-04	7.01E-03	1.35E-04	3.51E-05	3.98E-05

Table S11-9. Source contribution for PM$_{2.5}$ (µg/m^3) for the MIDWEST

	MEMTN	NASTN	KANMO	TULOK	STLMO	INDIN	LOUKY	CLEOH	CINOH	DETMI
Gasoline	4.83E-01	7.55E-01	1.37E-01	1.04E-01	1.45E-03	1.90E-01	1.03E-01	3.79E-01	1.14E-01	2.20E-01
Diesel	2.49E+00	3.45E+00	2.20E+00	1.67E+00	1.87E-02	9.98E-01	6.95E-01	1.37E+00	4.91E-01	1.20E+00
Biomass	6.71E-01	1.13E+00	7.27E-01	5.52E-01	4.57E-03	4.49E-01	3.14E-01	4.68E-01	1.07E-01	6.32E-01
Food Cooking	1.23E+00	2.13E+00	8.62E-01	5.10E-01	3.66E-03	5.19E-01	2.16E-01	1.10E+00	2.56E-01	3.18E-01
Natural Gas Combustion	1.95E-01	4.93E-01	6.94E-02	5.27E-02	5.52E-04	1.04E-01	2.28E-02	8.54E-02	1.58E-02	4.66E-02
Other/Undefined	1.99E+00	1.47E+00	4.03E-01	6.56E-01	5.12E-03	5.17E-01	1.82E-01	8.28E-01	6.59E-01	9.20E-01
Distillate Oil	2.23E-01	7.83E-02	4.76E-02	3.61E-02	1.92E-04	4.29E-02	3.48E-02	1.02E-01	1.47E-02	1.11E+00
Aviation	3.29E-01	3.61E-01	3.14E-02	2.38E-02	4.47E-04	3.77E-02	3.21E-02	8.40E-02	1.62E-02	3.15E-01
Cement Manufactures	1.61E-03	3.83E-02	2.30E-02	1.75E-02	9.59E-05	6.08E-03	8.00E-01	7.01E-04	3.45E-03	4.94E-03
Process Heating	1.26E-02	8.20E-04	5.30E-04	4.02E-04	1.85E-04	3.44E-03	9.09E-04	8.74E-01	3.56E-03	1.72E-02
Coal	1.27E+00	9.41E-01	1.35E+00	1.02E+00	1.72E-02	1.27E+00	8.89E-01	1.14E+00	9.11E-01	5.17E-01
Steel Foundries	1.69E-04	1.84E-03	1.95E-02	1.48E-02	4.31E-05	2.04E-03	2.50E-03	5.54E-04	2.07E-03	1.74E-03
Paper and Pulp Products	1.49E-01	8.73E-02	7.54E-04	5.73E-04	1.65E-04	3.38E-03	1.32E-02	1.92E-03	3.71E-03	5.96E-03

Table S11-10. Source contribution for $PM_{0.1}$ ($\mu g/m^3$) for the MIDWEST

	MEMTN	NASTN	KANMO	TULOK	STLMO	INDIN	LOUKY	CLEOH	CINOH	DETMI
Gasoline	4.40E-02	8.37E-02	2.66E-02	5.57E-02	9.43E-05	9.44E-03	2.82E-03	5.52E-02	4.81E-03	2.08E-02
Diesel	6.53E-02	1.44E-01	1.58E-01	6.69E-02	2.13E-04	2.34E-02	4.56E-03	9.21E-02	5.74E-03	3.72E-02
Biomass	6.70E-02	6.51E-02	2.35E-02	2.62E-02	6.87E-05	6.29E-03	1.57E-03	1.63E-02	2.05E-03	2.03E-02
Food Cooking	3.40E-02	6.83E-02	3.46E-02	4.90E-02	2.08E-04	7.63E-03	1.67E-03	5.62E-02	3.44E-03	8.01E-03
Natural Gas Combustion	1.50E-01	3.74E-01	6.19E-02	6.47E-02	3.54E-04	7.69E-02	9.32E-03	1.31E-01	6.38E-03	3.53E-02
Other/Undefined	5.80E-03	4.36E-03	1.53E-03	2.62E-03	8.09E-06	5.35E-04	4.11E-04	2.53E-03	9.00E-04	1.63E-03
Distillate Oil	3.97E-12	5.49E-11	1.20E-11	9.81E-12	1.17E-14	4.55E-09	6.06E-15	5.34E-08	3.48E-09	4.23E-09
Aviation	1.07E-01	1.16E-01	1.47E-02	3.06E-02	1.23E-04	8.19E-03	5.72E-03	3.48E-02	2.20E-03	1.37E-01
Cement Manufactures	4.82E-06	1.98E-04	1.34E-04	1.60E-03	1.77E-07	9.16E-06	1.92E-03	3.61E-06	3.82E-06	1.37E-05
Process Heating	3.88E-03	9.50E-05	1.50E-04	7.39E-02	4.26E-05	3.04E-04	4.36E-05	3.52E-01	2.62E-04	3.45E-03
Coal	3.71E-03	2.78E-03	5.14E-03	3.21E-03	2.71E-05	1.31E-03	2.01E-03	3.50E-03	1.24E-03	9.16E-04
Steel Foundries	5.41E-06	5.17E-05	1.81E-03	9.08E-05	8.81E-07	3.48E-05	2.40E-05	2.90E-05	2.49E-05	4.09E-05
Paper and Pulp Products	4.00E-03	2.53E-03	2.28E-05	4.26E-05	1.02E-06	2.22E-05	1.02E-04	3.88E-05	2.15E-05	1.12E-04

Table S11-11. Source contribution for $PM_{2.5}$ ($\mu g/m^3$) for the WEST

	PHOAZ	ELPTX	SLCUT	DENCO	BAKCA	FRECA	LOSCA	SDOCA	SACCA	SFOCA	POROR
Gasoline	1.13E-01	6.43E-02	2.07E-01	3.69E-01	1.32E-02	9.04E-02	1.01E+00	2.11E-01	1.18E-01	1.60E-01	1.72E-01
Diesel	5.16E-01	4.32E-01	7.05E-01	1.16E+00	9.36E-02	4.52E-01	2.39E+00	4.75E-01	3.33E-01	3.38E-01	7.44E-01
Biomass	2.27E-02	1.51E-02	1.64E-01	1.76E-01	1.70E-02	2.36E-01	7.09E-01	2.50E-01	1.22E-01	9.34E-02	2.24E-01
Food Cooking	6.33E-01	6.27E-01	5.91E-01	1.11E+00	2.92E-02	1.07E+00	2.36E+00	1.99E+00	7.72E-01	2.30E-01	9.69E-02
Natural Gas Combustion	2.35E-02	1.56E-02	1.26E-01	2.17E-03	4.25E-02	5.81E-02	4.77E-01	9.49E-02	8.04E-02	5.71E-02	4.71E-03
Other/Undefined	4.37E-01	3.43E-01	2.56E-01	4.68E-01	1.12E-01	6.40E-01	2.89E+00	1.50E+00	7.19E-01	9.67E-01	6.51E-01
Distillate Oil	4.05E-03	2.70E-03	1.07E-01	5.14E-04	9.14E-03	6.24E-03	7.34E-02	1.50E-02	4.58E-03	7.08E-03	2.38E-02
Aviation	2.65E-02	1.77E-02	6.69E-02	6.24E-04	1.07E-02	4.75E-02	4.29E-01	1.44E-01	7.00E-02	6.16E-02	4.13E-02
Cement Manufactures	6.83E-04	4.55E-04	3.58E-03	1.14E-04	5.38E-02	1.25E-03	2.94E-02	1.88E-02	5.82E-04	7.79E-03	7.43E-05
Process Heating	6.19E-02	4.13E-02	8.35E-02	2.11E-04	2.33E-03	2.83E-02	9.31E-02	1.15E-02	6.21E-02	2.92E-02	1.86E-05
Coal	2.68E-01	1.27E-01	5.69E-01	5.73E-01	4.46E-07	2.33E-06	2.71E-06	1.81E-06	1.56E-06	2.44E-06	2.01E-02
Steel Foundries	1.28E-03	8.54E-04	1.77E-06	7.14E-08	4.30E-05	9.43E-04	3.91E-03	1.59E-04	1.19E-03	9.04E-04	3.89E-02
Paper and Pulp Products	2.98E-04	1.99E-04	1.36E-02	3.74E-05	1.45E-03	2.26E-02	1.16E-02	2.33E-03	2.01E-02	8.20E-03	7.05E-03

Table S11-12. Source contribution for $PM_{2.5}$ ($\mu g/m^3$) for the WEST

	PHOAZ	ELPTX	SLCUT	DENCO	BAKCA	FRECA	LOSCA	SDOCA	SACCA	SFOCA	POROR
Gasoline	7.06E-03	7.06E-03	3.42E-02	7.08E-02	6.81E-04	9.56E-03	8.45E-03	4.56E-02	1.66E-02	2.53E-02	4.67E-02
Diesel	1.57E-02	1.57E-02	5.15E-02	9.87E-02	1.41E-03	1.51E-02	5.44E-03	2.97E-02	1.26E-02	1.50E-02	9.33E-02
Biomass	3.22E-04	3.22E-04	2.21E-02	2.16E-02	3.12E-04	9.83E-03	3.13E-03	2.30E-02	4.40E-03	5.86E-03	2.03E-02
Food Cooking	1.68E-02	2.01E-02	4.61E-02	7.53E-02	3.00E-04	2.98E-02	4.48E-03	9.87E-02	1.95E-02	7.94E-03	4.07E-02
Natural Gas Combustion	1.45E-02	1.45E-02	1.28E-01	1.94E-03	4.09E-02	5.07E-02	3.06E-02	9.00E-02	9.97E-02	4.73E-02	4.51E-02
Other/Undefined	5.99E-04	6.07E-04	1.45E-03	2.64E-03	3.83E-05	6.18E-04	3.23E-04	3.34E-03	8.62E-04	1.30E-03	2.79E-03
Distillate Oil	6.88E-13	6.88E-13	9.31E-09	2.33E-12	1.92E-09	4.55E-08	3.28E-08	9.26E-07	4.54E-10	2.43E-08	4.98E-11
Aviation	7.77E-03	7.77E-03	4.86E-02	2.54E-04	3.16E-03	1.67E-02	3.39E-02	6.33E-02	3.17E-02	2.34E-02	2.46E-02
Cement Manufactures	7.53E-07	7.53E-07	2.60E-05	7.74E-07	7.07E-05	3.26E-06	7.62E-05	1.13E-04	2.34E-06	4.04E-05	8.42E-07
Process Heating	1.40E-03	1.52E-02	4.83E-02	5.43E-05	4.45E-04	7.19E-03	9.31E-04	3.14E-03	1.02E-02	6.94E-03	6.33E-06
Coal	2.33E-04	2.25E-04	3.23E-03	3.23E-03	5.44E-07	9.90E-13	3.16E-13	5.86E-12	1.84E-14	1.32E-12	8.64E-05
Steel Foundries	4.13E-05	4.13E-05	1.23E-07	5.61E-09	9.13E-07	4.12E-05	3.83E-06	1.04E-05	3.40E-05	4.58E-05	5.48E-03
Paper and Pulp Products	4.98E-06	4.98E-06	7.40E-04	1.06E-06	9.96E-06	3.53E-04	4.31E-05	4.66E-05	6.07E-04	9.48E-05	2.89E-04

12 ASSOCIATIONS BETWEEN MORTALITY AND ULTRAFINE PARTICLE CONCENTRATIONS, SPECIES, AND SOURCES IN CALIFORNIA

Preamble: Chapter 12 performs a preliminary epidemiological analysis using the exposure fields developed in Chapters 7-10 combined with the California Teachers Study (CTS) cohort. Hazard ratios are resolved for multiple health endpoints using different models constructed from features of the ultrafine and fine particle exposure fields.

12.1 Introduction

Ultrafine particles (UFP, particles less than 0.1 μm) are thought to have significant toxicity because their small size and large numbers result in high surface area which makes it easier for the body to adsorb these particles and any potentially toxic chemicals attached to them. The Task Force statement from the American Academy of Allergy, Asthma & Immunology [378] indicates several other factors that may enhance the consequence of exposures to UFP and make them more difficult to study. These factors include: the small size of UFP helping them to evade traditional host defenses and also enable translocation into other organs; the variation in composition of the UFP surface over time and space; their spatial heterogeneity; their high retention rate and penetration into the lungs; and finally, while improvements in engine technology have reduced emissions of PM in general, UFP can still be formed from vapor condensation and can generate reactive organic species. The UFP exposures are likely to directly impact the airways and, through various pathways, the heart and brain [50]. Of note for our study, the particles or their chemical constituents can ultimately trigger a systemic inflammatory response resulting in increases in markers such as C-reactive protein (CRP), that are important predictors of cardiovascular disease and death [379]. To date, animal and human experimental studies provide evidence for cardiovascular and other adverse outcomes. These studies have reported effects on lung function changes, airway inflammation, allergic responses, altered heart rate and heart rate variability, accelerated atherosclerosis, and increased markers of brain inflammation [50]. However, the findings among these studies and in comparison to epidemiologic studies are inconsistent. The inconsistency may be due to the variation in study sample and design. In addition, there is difficulty in reproducing UFP exposures in the laboratory similar to real world ambient exposures. Specifically, there are differences between the size range of UFP examined in experimental studies and those in the epidemiologic studies. In the experimental studies UFPs are either re-aerosolized off filters or concentrated from ambient particles (CAPs). The CAP UFPs include particle sizes just under 300 nm and it's possible that larger particles are included within the re-aerosolized particles. Regarding epidemiologic studies, there is not always the clear delineation of particles less than 0.1 μm because some studies use particle number counts which have no upper cutoff of size range. While a majority of the particles will be less than 0.1 μm, larger particles will be included in the exposure metric, therefore, it is not strictly a UFPP exposure. Finally, there are major difficulties in measuring and thereby conducting studies of long-term exposure, either experimentally or in epidemiologic studies. In addition, even when UFP are measured, they are often highly correlated with other pollutants such as $PM_{2.5}$, NO_2, and EC.

Epidemiologic studies have been difficult to conduct due to the problem of accurately measuring exposure to UFP given their significant spatial heterogeneity and their high correlation with other pollutants such as nitrogen dioxide (NO_2) and $PM_{2.5}$. Panel studies, where a pre-selected cohort are followed over a period of time with repeated measures and individual exposure measurements, have provided important evidence of health effects. For example, earlier studies by Delfino et al. [380, 381] examined both outdoor and indoor UFP exposures on elderly subjects with a history of heart disease. Several different biomarkers were recorded over multiple months and the studies have reported fairly consistent effects on inflammatory markers such as IL-6 and CRP. A more recent study in Liu et al. [382] recruited 100 subjects living in the Taipei metropolitan area. UFP were measured outside of the homes and in various indoor locations. UFP exposure was associated with increases in diastolic and systolic blood pressure and CRP, and decreases in FEV_1. This suite of associations were not observed for $PM_{2.5}$, PM10, NO_2 or ozone. Extrapolating the findings of these panel studies to the general population, however, is difficult and again, they only measure short-term (i.e. daily) exposures.

Short-term exposure epidemiological studies of the general population have been undertaken but with difficulties in accurately measuring exposure to UFP. Typically the study design involves a time-series study of daily changes of UFP in a city with only one, or a few UFP monitors. A review of these studies by HEI [50] indicates that the findings regarding effects on cardiovascular or respiratory mortality have been inconsistent, likely due to the difficulty in measuring exposure. Where studies have measured UFP, few have actually assessed whether the effects associated with UFP are independent of other pollutants. When they have, the effects of UFP have not been consistently discernible from those of other pollutants with which they often occur or share similar sources. In more recent studies since the HEI review, Stafoggia et al. [383] and Lanzinger et al. [384, 385] conducted studies of the effects of daily or multi-day exposures to UFP on hospital admissions and mortality. Each study used multiple European cities and combined the results in a meta-analysis. For each city, a single monitor was used to estimate UFP concentrations. Generally, a weak or no association was reported from these studies. Most of these studies used particle number counts as their exposure metric.

There have been only a few studies of long-term exposure to UFP. In our previous study [7] we reported multiple associations between UFP mass and constituents with IHD. UFP concentrations were estimated using a chemical transport model similar to the one used in the current study. Among other long-term exposure studies, Corlin et al. [386] examined exposure to UFP and markers of cardiovascular disease among a cohort of 1499 Puerto Ricans living in Eastern Massachusetts. Particle counts were estimated using a LUR which only explained 37% of the variance in UFP. Participants were examined three times over a six period and assigned an UFP exposure for the one year prior to the examination. The study reported associations between UFP and CRP but not with blood pressure and the findings were not consistent.

Downward et al. [387] examined long-term exposures to UFP with a prospective cohort of 34,000 Dutch citizens. Exposures were based on a LUR that explained 50% of the spatial variance of UFP which was assigned to each participant's residence at baseline. Cardiovascular outcomes were obtained from local and national registries. The results indicated an association between UFP and first events of total cardiovascular cases, myocardial infarction and heart failure, but not of stroke. Interestingly, $PM_{2.5}$ was not associated with these endpoint. In two pollutant models, the association with UFP remained after $PM_{2.5}$ or NO2 were added to the model.

Our data provide a significant advancement in the understanding of the potential impacts of ultrafine particles. As indicated above, the correlations between our estimated versus available measured concentrations are very high for mass and several species. We have estimated $PM_{2.5}$ and UFP concentrations over a 10 year period (2000-2009) and linked these concentrations with monthly residential history at a 4k grid resolution. Our cohort of current and retired teachers provides data on most important risk factors for mortality, has low and similar occupational exposure and very low current smoking rates (<5%). These factors reduce the likelihood of significant residual confounding of the air pollution effect. It remains a significant challenge, however, to isolate and identify the independent impact of each constituent of $PM_{2.5}$ or UFP. As described above, uncertainties remain in the chemical transport model and certain constituents are very highly correlated since they are generated from the same sources. Nevertheless, we are able to add to the limited available evidence regarding the health impacts of long term exposure to ultrafine particles. Below we describe our study that examines the association between various mortality outcomes and both $PM_{2.5}$ and UFP mass, constituents and sources.

12.2 Methods

12.2.1 Data

The CTS is a prospective study of 133,479 current and former female teachers and administrators who completed baseline questionnaires mailed to them in 1995 to investigate the incidence of breast cancer in public school teachers and administrators, as described in detail in Bernstein et al. (2002). Subsequent questionnaires were mailed to CTS participants in 1997 and 2000. The design and on-going follow-up of the CTS cohort is a multi-institutional collaboration involving researchers with diverse and complementary areas of expertise. Record linkage is conducted annually to mortality files administered by the California Department of Public Health. In addition, residential addresses of each CTS participant were updated annually for the mailing of newsletters. The cohort is multi-ethnic but primarily non-Hispanic white (86.7%) and born in the United States (93.6%). For this study, we used cohort follow-up data from January 2001 through December 2011. Women under age 30 at the start of the study were excluded in order to focus on mid-life and older women. Use of data on human subjects in the main CTS cohort study was reviewed and initially approved by the California Committee for the Protection of Human Subjects, Health and Human Services Agency, and by the institutional review boards (IRB) for each participating institution in June 1995 and annually thereafter. Informed consent was obtained upon entry into the cohort.

12.2.2 Health outcomes

In this analysis, we focused on associations between long-term exposures and mortality. Deaths were assigned codes based on the International Classification of Diseases, volume 10 (ICD-10) for the following outcomes: all-cause deaths excluding those with an external cause (A00-R99), cardiovascular (CV) deaths (I00-I99), Ischemic heart disease (IHD) deaths (I20-I25), pulmonary deaths (C34, J00-J98) and stroke (I61-I64, 431-436). Person-days at risk were calculated as the number of days starting from January 1, 2001 until the earliest of three dates: (i) the date of death;

(ii) a move out of California for at least four months; or (iii) June 30, 2011, the end of follow-up for this analysis. If a woman moved out of state for less than four months exposures during that time were not included in the calculations of the long-term average.

12.2.3 Air pollution exposure estimates

The UCD/CIT chemical transport model was used to estimate ground-level concentrations of $PM_{2.5}$ and UFP mass, constituents and sources over the major population regions in California using a 4-km grid resolution for most of the state from January, 2000 through December, 2009. The mass estimates include both primary and secondary particles. Based on previous studies and our own prior study results, we examined a subset of species including Cu, Fe, Mn, EC, OC, nitrate, ammonium ion, anthropogenic and biological secondary organics (SOAa and SOAb, respectively), "other" metals, and "other" species. Note there is no nitrate or ammonium ion in the UFP. The primary sources used in the analysis include on-road diesel, off-road diesel, on-road gas, off-road gas, wood smoke, meat cooking, aircraft, natural gas combustion and "other" anthropogenic which include ship emissions, dust, tire and brake wear and others.

Ultimately, the exposure metrics were combined with the updated addresses. Monthly individual exposure estimates were developed through spatial linkage of the geocoded residential addresses. All residences within a given grid in a given month were assigned the modeled pollutant value for that grid for that period. The average long-term pollution exposure for a participant was obtained by calculating the mean of her monthly averages. At the time of each death, the long-term average for each individual remaining in the cohort was recalculated, allowing comparison between the decedent's long-term average exposure and those of the members remaining in the risk set.

12.2.4 Covariates

The individual-level covariates included as explanatory variables in the regression models were based on previous results from air pollution studies for this cohort [388]. Specifically, the covariates included twenty individual-level covariates (a total of 58 terms): age (divided into two-year categories between ages 30 and 79, three-year categories between ages 80 and 88, and one category for women aged 89 and older); race (non-Hispanic White, other (African-American, Hispanic, Asian, Pacific Islander, and Native American) or unknown); marital status (married/living with partner, not married, and unknown); smoking status (never, former, and current smokers) and pack-years of smoking (continuous variable for former and current smokers); second-hand smoke exposure (none, household exposure, unknown); body mass index (BMI) (16-19 kg/m^2, 20-24, 25-29, 30-39, 40-55); lifetime physical activity (tertiles, unknown); alcohol consumption (beer (no/yes/unknown), wine (no/yes/unknown), liquor (no/yes/unknown)); average daily dietary intake of fat (tertiles, unknown), fiber (tertiles, unknown), and calories (tertiles, unknown); menopausal status and hormone replacement therapy use combined (pre-menopausal, peri/post-menopausal and no HT use, peri/post menopausal and past HT use, peri/post-menopausal and current use of estrogen, peri/post-menopausal and current use of estrogen plus progestin, and unknown menopausal status or HT use; family history of myocardial infarction (yes/no) or stroke (yes/no); and use of blood pressure medication (low, medium, high, unknown) or aspirin (low, medium, high, unknown). Data on all individual-level variables except marital status (which was assessed in the 2000 questionnaire) were obtained from the baseline questionnaire.

We also included six Census-derived contextual (neighborhood) variables including income (median household income), proportion of residents living below the poverty line, education (percent with college degree), population size, racial composition (percent white, percent black, percent Hispanic) and unemployment (percent unemployed). These variables were derived from the 2000 census at the block group level based on the subject's residence at the time of the baseline questionnaire. These variables represent social, economic, and environmental settings at a group level that may be associated with disease outcomes at the individual level. As such, they may provide additional control for residual confounding.

12.2.5 Statistical methods

We fitted Cox proportional hazards models to estimate hazard ratios (HRs) and 95% confidence intervals (CIs) for associations between each pollutant and the outcomes of interest. We examined each pollutant with a separate regression model adjusted for the covariates described above. The Cox model was stratified by age and race/ethnicity. To ensure that we would be examining associations with chronic rather than acute exposures, study exposures began in January 2000 and ended in 2009 while the cohort follow-up began in January 2001 and continued through December 2011. We analyzed the CTS data using time-dependent pollution metrics in which the exposure estimates for everyone remaining alive in the risk set were recalculated each month. This enabled a comparison of their average exposures up to that time with that of the individual who had died. In this way, decedents and survivors comprising the risk set had similar periods of pollution exposure, without subsequent pollution trends influencing the surviving women's exposure estimates.

We examined the association between the mortality endpoints and both $PM_{2.5}$ and UFP mass and each of their individual constituents and sources. Several sensitivity analyses were conducted. To examine the strength of association for $PM_{2.5}$ versus UFP, we examined two pollutant models that include both $PM_{2.5}$ and UFP terms for mass and a subset of constituents. We also examined models with both a single constituent and mass in the same regression. The latter sensitivity analyses is an attempt to isolate the independent effect of the individual constituents of UFP after controlling for the effect of mass. Mostofsky et al. [389] reviewed several statistical methods to address the difficult issue of determining individual pollutant effects, and each has its own limitations. The approach we used serves to control for the effect of mass as well as constituents that are highly correlated with it, thereby reducing their influence on the single constituent in the model. However, since there is high inter-correlation among the constituents, a single term may still actually represent many covarying constituents. Finally, we examined the impacts of UFP EC solely from mobile sources and the impacts of $PM_{2.5}$ EC greater and less than 0.1 μm.

12.3 Results

Of the 133,479 women who completed a baseline questionnaire, 38,365 were excluded for several reasons including: no $PM_{2.5}$ or UFP pollution data, lack of residential information, death or moved out of the area before the start of the follow-up, missing covariate data or less than 6 months of pollution values during the year 2000. Ultimately, 88,159 women were included in the full study. The characteristics of the included versus excluded participants are summarized in Appendix I to Chapter 12.

A total of 10,830 natural deaths occurred during the follow-up from January 2001 through December 2011; of these, 4,069, 1,741 1,552 and 699 deaths were due to CV, IHD, pulmonary diseases and stroke, respectively. As indicated in Table 12-1, the average age of eligible cohort members at the start of follow-up was 57 years, 86% of these women were non-Hispanic white and under 5% were current smokers. About half of the cohort were married or living with a partner.

Table 12-1. Descriptive statistics for health and covariate variables for women in the analysis.

Covariate	Percentage or mean ± SD
Age at January 2001 (yr)	57.2 ± 14.0
Race (% non-Hispanic white)	86.0
Smoking status (%):	
Never smoker	68.3
Former smoker	27.0
Current smoker	4.7
Total pack-years	14.8 ± 17.3
Adult second-hand smoke exposure (%)	48.4
BMI (kg/m^2)	24.9 ± 5.1
Married/living with partner (%)	45.5
Non-drinker	32.2
Menopausal status and HT use (%):	
Premenopausal	40.2
Peri/postmenopausal and no hormone therapy use	12.4
Peri/postmenopausal and current/past hormone therapy use	34.2
Unknown menopausal status/hormone therapy use	13.2
Dietary fat (g/d)	56.0 ± 26.7
Dietary fiber (g/d)	15.1 ± 6.4
Dietary calories (kcal/d)	1,589.4 ± 555.2
Physical activity (h/wk)	4.4 ± 4.0
Family history of heart disease (%)	45.5
Taking hypertension medication/aspirin (%)	33.1

All characteristics were reported on baseline questionnaire, except marital status which was reported on the 2000 questionnaire.

Tables 12-2 provides the descriptive statistics for the $PM_{2.5}$ concentrations of mass (mean = 11.45 $\mu g/m^3$) and constituents and sources used in the study while Table 12-3 summarizes the distribution for the UFP concentrations for mass (mean = 0.68 $\mu g/m^3$) constituents and sources. The correlation among the $PM_{2.5}$ and UFP constituents are displayed in Tables 12-4 and 12-5. For both particle sizes, the correlations among the constituents are moderate to high. For example, for $PM_{2.5}$(EC), the correlations range from 0.89 (with Cu and OC) to 0.35 (with SOAb). $PM_{2.5}$ (SOAa) has the highest correlation (0.71) with Cu and lowest with "Other" constituents (0.30). Likewise for UFP(EC), the highest correlation is with OC (0.91) and lowest with SOAb (0.33). SOAa has only moderate correlation with "Other" constituents. The correlations between the $PM_{2.5}$ versus $PM_{0.1}$ species are summarized in Appendix II to Chapter 12. High correlations are observed between many of the species pairs.

Table 12-2. Distribution of $PM_{2.5}$ particle mass, species and sources ($\mu g/m^3$)

Pollutant	$PM_{2.5}$ **Mean**	**Minimum**	**25th percentile**	**Median**	**75th percentile**	**Maximum**
Mass	11.45	3.09	9.33	11.42	13.53	36.19
Cu	0.003	0.0001	0.001	0.002	0.004	0.02
Fe	0.18	0.03	0.13	0.17	0.22	0.63
N(V)	2.14	0.05	1.52	2.03	2.73	9.37
N(-III)	1.48	0.43	1.25	1.45	1.71	4.00
Mn	0.003	0.001	0.002	0.003	0.004	0.07
NA	0.03	0.001	0.01	0.02	0.04	0.12
EC	0.36	0.05	0.24	0.33	0.48	2.55
OC	1.88	0.22	1.24	1.79	2.42	11.00
Other[a)]	1.19	0.17	0.90	1.17	1.45	6.54
Metals[b)]	0.35	0.06	0.26	0.35	0.44	1.17
SOAb [c)]	0.33	0.03	0.26	0.34	0.37	1.60
SOAa [c)]	0.08	0.02	0.05	0.08	0.11	0.25
Sources of primary particles						
On road gas	0.16	0.001	0.08	0.13	0.22	0.83
Off road gas	0.07	0.003	0.04	0.06	0.10	0.37
On road diesel	0.26	0.02	0.15	0.24	0.35	1.39
Off road diesel	0.25	0.01	0.12	0.19	0.33	5.70
Wood smoke	0.56	0.00001	0.20	0.40	0.77	9.58
Meat cooking	0.73	0.03	0.33	0.59	1.06	6.24
Aircraft	0.07	0.003	0.02	0.03	0.06	9.02
Natural gas combustion	0.17	0.01	0.08	0.13	0.24	3.58
Other anthropogenic	2.61	0.43	1.93	2.63	3.24	14.38
Primary $PM_{2.5}$ Mass	4.88	0.62	3.48	4.79	6.17	23.29

a) Includes shipping, dust, brake and tire wear, solvent use; b) Metals besides Cu, Fe, and Mn

c) SOAb = Secondary organics, biological; SOAa = secondary organics, anthropological

Table 12-3. Distribution of UFP particle mass, species and sources (µg/m^3)

Pollutant	**UFP Mean**	**Minimum**	**25th percentile**	**Median**	**75th percentile**	**Maximum**
Mass	0.68	0.06	0.45	0.65	0.87	5.47
Cu	0.00002	0.0000007	0.000005	0.000009	0.00003	0.002
Fe	0.001	0.0002	0.0007	0.001	0.001	0.03
Mn	0.00004	0.000003	0.00002	0.00002	0.00004	0.01
NA	0.0002	0.00001	0.00009	0.0002	0.0003	0.003
EC	0.04	0.002	0.02	0.03	0.05	0.23
OC	0.39	0.02	0.23	0.36	0.52	3.13
Other[a)]	0.05	0.003	0.02	0.04	0.06	2.82
Metals[b)]	0.01	0.001	0.01	0.01	0.02	0.38
SOAb [c)]	0.09	0.01	0.07	0.10	0.11	0.51
SOAa [c)]	0.02	0.003	0.01	0.02	0.03	0.08
Sources of primary particles						
On road gas	0.05	0.001	0.02	0.04	0.07	0.28
Off road gas	0.01	0.0004	0.01	0.01	0.02	0.10
On road diesel	0.04	0.002	0.02	0.03	0.05	0.28
Off road diesel	0.02	0.001	0.01	0.02	0.03	0.54
Wood smoke	0.16	0.0000	0.05	0.11	0.22	3.12
Meat cooking	0.08	0.002	0.03	0.06	0.11	0.71
Aircraft	0.04	0.002	0.01	0.02	0.04	5.51
Natural gas combustion	0.16	0.01	0.08	0.12	0.23	3.57
Other anthropogenic	0.06	0.004	0.02	0.04	0.08	3.86
Primary UFP Mass	0.63	0.03	0.37	0.59	0.82	7.56

a) Includes shipping, brake and tire wear, solvent use; b) Metals besides Cu, Fe, and Mn

c) SOAb = Secondary organics, biological; SOAa = secondary organics, anthropological

Table 12-4. Spearman correlations among $PM_{2.5}$ species

$PM_{2.5}$ **Species**	**Mass**	**Cu**	**Fe**	**Nit**	**Ammo**	**Mn**	**EC**	**OC**	**Other**	**Metals**	**SOAb**
Mass	1.00										
Cu	0.70	1.00									
Fe	0.91	0.82	1.00								
Nitrate	0.81	0.40	0.69	1.00							
Ammo	0.89	0.501	0.75	0.96	1.00						
Mn	0.92	0.79	0.98	0.69	0.77	1.00					
EC	0.84	0.89	0.83	0.50	0.62	0.83	1.00				
OC	0.84	0.78	0.81	0.47	0.57	0.80	0.89	1.00			
Other	0.87	0.48	0.80	0.65	0.75	0.83	0.66	0.67	1.00		
Metals	0.94	0.66	0.96	0.74	0.80	0.96	0.75	0.78	0.89	1.00	
SOAb	0.37	0.36	0.37	0.45	0.43	0.37	0.35	0.20	0.17	0.29	1.00
SOAa	0.58	0.71	0.60	0.57	0.60	0.57	0.62	0.43	0.30	0.47	0.52

Table 12-5. Spearman correlations among UFP species

UFP Species	**Mass**	**Cu**	**Fe**	**Mn**	**EC**	**OC**	**Other**	**Metals**	**SOAb**
Mass	1.00								
Cu	0.59	1.00							
Fe	0.85	0.64	1.00						
Mn	0.74	0.82	0.88	1.00					
EC	0.92	0.68	0.86	0.80	1.00				
OC	0.98	0.56	0.81	0.72	0.91	1.00			
Other	0.70	0.67	0.69	0.69	0.68	0.63	1.00		
Metals	0.96	0.65	0.86	0.80	0.88	0.94	0.76	1.00	
SOAb	0.30	0.45	0.36	0.32	0.33	0.23	0.18	0.22	1.00
SOAa	0.46	0.64	0.53	0.49	0.51	0.41	0.45	0.43	0.72

Note: Nit= Nitrate; Ammo = Ammonium Ion; Metals = Other Metals

Table 12-6 summarizes the regression results for $PM_{2.5}$ with all-cause, CV and IHD mortality. Pulmonary and stroke mortality are not included since there was no evidence of an association between these outcomes and either $PM_{2.5}$ or UFP mass and constituents. For all-cause mortality, associations were observed only with $PM_{2.5}$ mass and EC with more modest associations ($P < 0.10$) for OC and "other" species. EC, "other" and SOA were associated with cardiovascular mortality. For IHD, associations were observed for mass and many of the constituents including Cu, Fe, nitrate, ammonium ion, EC, metals and SOAa and SOAb. In the analysis of sources, for all-cause mortality an association was demonstrated only for EC, with a modest association for natural gas combustion. For IHD, positive associations were observed for all four mobile sources, meat cooking, natural gas combustion, and other anthropogenic sources. Of note, EC was associated with all three endpoint and appeared to be the most robust of the estimates.

Table 12-6. Hazard ratios (HR) for $PM_{2.5}$ mass, constituents and sources ($\mu g/m^3$)

		All-cause mortality # deaths=10,830		**CV mortality # deaths=4,069**		**IHD mortality # deaths=1,741**	
	IQR	**HR (95% CI)**	**p value**	**HR (95% CI)**	**p value**	**HR (95% CI)**	**p value**
Pollutant							
Mass	4.20	1.03 (1.00, 1.06)	.0916	1.04 (0.99, 1.09)	.1118	1.09 (1.01, 1.17)	.0232
Cu	0.002	1.01 (0.98, 1.04)	.5569	1.03 (0.98, 1.08)	.2650	1.13 (1.05, 1.22)	.0011
Fe	0.10	1.01 (0.98, 1.04)	.4083	1.03 (0.98, 1.08)	.2252	1.10 (1.02, 1.19)	.0124
Nitrate	1.21	1.01 (0.98, 1.04)	.4829	1.04 (0.99, 1.09)	.1397	1.08 (1.00, 1.16)	.0420
Ammonium ion	0.46	1.01 (0.98, 1.04)	.3749	1.04 (0.99, 1.09)	.1136	1.09 (1.01, 1.17)	.0182
Mn	0.002	1.00 (0.98, 1.03)	.7908	1.03 (0.99, 1.06)	.1360	1.04 (1.00, 1.09)	.0575
EC	0.24	1.03 (1.00, 1.06)	.0238	1.05 (1.00, 1.10)	.0334	1.12 (1.05, 1.20)	.0010
OC	1.18	1.03 (1.00, 1.05)	.0565	1.01 (0.97, 1.06)	.5223	1.03 (0.97, 1.10)	.3294
Other	0.55	1.02 (1.00, 1.05)	.0566	1.04 (1.00, 1.08)	.0650	1.04 (0.98, 1.11)	.1768
Metals	0.18	1.02 (0.99, 1.05)	.2369	1.03 (0.98, 1.09)	.1844	1.08 (1.00, 1.16)	.0435
SOA bio	0.11	1.00 (0.97, 1.03)	.9723	1.09 (1.03, 1.15)	.0031	1.24 (1.14, 1.35)	.0000
SOA anthro	0.06	1.01 (0.98, 1.05)	.5101	1.06 (1.00, 1.13)	.0559	1.20 (1.10, 1.32)	.0001
Sources							
On road gas	0.14	1.01 (0.98, 1.03)	.6346	1.02 (0.98, 1.06)	.3612	1.09 (1.03, 1.16)	.0042
Off road gas	0.06	1.01 (0.99, 1.04)	.3012	1.02 (0.98, 1.07)	.3371	1.09 (1.02, 1.16)	.0068
On road diesel	0.20	1.03 (1.00, 1.06)	.0388	1.04 (0.99, 1.08)	.1161	1.09 (1.02, 1.16)	.0134

		All-cause mortality # deaths=10,830		**CV mortality # deaths=4,069**		**IHD mortality # deaths=1,741**	
	IQR	**HR (95% CI)**	**p value**	**HR (95% CI)**	**p value**	**HR (95% CI)**	**p value**
Off road diesel	0.20	1.01 (0.99, 1.03)	.1729	1.03 (1.00, 1.06)	.0884	1.07 (1.03, 1.11)	.0011
Wood smoke	0.57	1.01 (1.00, 1.03)	.1396	0.99 (0.96, 1.01)	.3294	0.94 (0.89, 0.98)	.0047
Meat cooking	0.73	1.01 (0.99, 1.04)	.3243	1.03 (0.98, 1.07)	.2576	1.07 (1.00, 1.14)	.0368
Aircraft	0.04	1.00 (1.00, 1.01)	.2283	1.00 (1.00, 1.01)	.3646	1.00 (0.99, 1.01)	.9459
Natural gas	0.15	1.02 (1.00, 1.04)	.0610	1.02 (0.99, 1.06)	.1722	1.08 (1.03, 1.12)	.0011
Other anthro	1.31	1.02 (1.00, 1.06)	.1014	1.04 (0.99, 1.09)	.0944	1.09 (1.02, 1.18)	.0141
Netprime	2.49	1.03 (1.00, 1.06)	.0602	1.05 (1.00, 1.10)	.0586	1.12 (1.04, 1.20)	.0021
Primary Mass	2.69	1.03 (1.00, 1.06)	.0312	1.03 (0.99, 1.08)	.1831	1.06 (0.99, 1.14)	.0830

Netprime = Sum of sources minus wood combustion; Primary Mass= sum of all sources.

Table 12-7 summarizes the results for mortality risks associated with UFP mass, species and sources. For all-cause mortality, associations were observed with mass, EC, OC and other metals. Cardiovascular mortality was associated with Cu, EC and SOAa and SOAb. IHD mortality was not associated with UFP mass, but it was associated with Cu, Fe, EC and SOAa and SOAb. No associations were found for either pulmonary or stroke mortality with any of the species or sources (results not presented).

Table 12-7. Hazard ratios (HR) for UFP mass, constituents and sources

		All-cause mortality # deaths=10,830		**CV mortality # deaths=4,069**		**IHD mortality # deaths=1,741**	
	IQR ($\mu g/m^3$)	**HR (95% CI)**	**p value**	**HR (95% CI)**	**p value**	**HR (95% CI)**	**p value**
Pollutant							
Mass	0.42	1.03 (1.01, 1.06)	**.0065**	1.03 (0.99, 1.07)	.2015	1.05 (0.99, 1.11)	.1298
Cu	0.00002	1.00 (0.99, 1.01)	.3550	1.02 (1.00, 1.03)	**.0452**	1.03 (1.02, 1.05)	**.0001**
Fe	0.0007	1.01 (0.99, 1.03)	.1639	1.03 (1.00, 1.05)	.0483	1.04 (1.01, 1.07)	**.0154**
Mn	0.00002	1.00 (1.00, 1.00)	.7789	1.00 (1.00, 1.01)	.2372	1.00 (0.99, 1.01)	.5747
EC	0.03	1.04 (1.01, 1.07)	**.0024**	1.05 (1.00, 1.09)	**.0417**	1.08 (1.01, 1.15)	**.0171**
OC	0.29	1.03 (1.01, 1.06)	**.0159**	1.02 (0.98, 1.06)	.4190	1.04 (0.98, 1.10)	.2169
Other	0.03	1.01 (1.00, 1.01)	.0867	1.01 (1.00, 1.02)	.1421	1.01 (0.99, 1.03)	.2365

		All-cause mortality # deaths=10,830		**CV mortality # deaths=4,069**		**IHD mortality # deaths=1,741**	
	IQR ($\mu g/m^3$)	**HR (95% CI)**	**p value**	**HR (95% CI)**	**p value**	**HR (95% CI)**	**p value**
Metals	0.01	1.02 (1.00, 1.04)	**.0192**	1.02 (0.99, 1.06)	.1319	1.05 (1.01, 1.10)	**.0214**
SOA bio	0.04	1.01 (0.98, 1.04)	.5182	1.09 (1.03, 1.15)	**.0012**	1.26 (1.16, 1.36)	**.0000**
SOA anthro	0.02	1.02 (0.98, 1.06)	.2659	1.07 (1.01, 1.13)	**.0312**	1.21 (1.11, 1.32)	**.0000**
Sources							
On road gas	0.04	1.01 (0.98, 1.03)	.6170	1.02 (0.98, 1.06)	.4010	1.08 (1.02, 1.15)	**.0078**
Off road gas	0.01	1.02 (0.99, 1.05)	.2038	1.02 (0.98, 1.07)	.3138	1.09 (1.02, 1.16)	**.0118**
On road diesel	0.03	1.03 (1.00, 1.06)	**.0294**	1.03 (0.99, 1.08)	.1564	1.07 (1.00, 1.14)	.0506
Off road diesel	0.02	1.02 (1.00, 1.03)	.0908	1.03 (1.00, 1.06)	.0961	1.06 (1.02, 1.10)	**.0062**
Wood smoke	0.17	1.01 (1.00, 1.03)	.1298	0.99 (0.96, 1.01)	.3509	0.94 (0.90, 0.98)	**.0046**
Meat cooking	0.08	1.02 (0.99, 1.04)	.2205	1.03 (0.99, 1.07)	.1821	1.07 (1.01, 1.14)	**.0273**
Aircraft	0.03	1.00 (1.00, 1.01)	.2299	1.00 (1.00, 1.01)	.3840	1.00 (0.99, 1.01)	.9117
Natural gas	0.15	1.02 (1.00, 1.04)	.0590	1.02 (0.99, 1.06)	.1787	1.07 (1.03, 1.12)	**.0013**
Other anthro	0.05	1.01 (1.00, 1.02)	.1077	1.02 (1.00, 1.04)	**.0300**	1.04 (1.02, 1.06)	**.0000**
Netprime	0.39	1.03 (1.01, 1.06)	**.0152**	1.04 (1.00, 1.09)	**.0300**	1.10 (1.05, 1.17)	**.0003**
Primary Mass	0.45	**1.03 (1.01, 1.06)**	**.0050**	1.02 (0.99, 1.06)	.2054	1.04 (0.98, 1.10)	.1599

Netprime = Sum of sources minus wood combustion; Primary Mass= sum of all sources.

Among the sources of UFP, for all-cause mortality, an association was only observed with on-road diesel (with a more modest association for off-road diesel). For CV mortality, only “other” anthropogenic sources showed an association. For IHD mortality, positive associations were observed for many of the sources including all four mobile sources, meat cooking, natural gas combustion and “other” anthropogenic sources. Again, no sources of UFP were associated with pulmonary or stroke mortality.

As a sensitivity analysis, we examined the sum of the primary sources with and without wood smoke (called Netprime”). Exposure to wood smoke was particularly difficult to calculate (possibly due to its intermittent emissions, uncertainty in the primary data source, and possibility of person mitigation) and this source never had a positive association with any of the endpoints. In addition, the greatest exposures were in Marin and Santa Clara Counties, which rank #1 and #4 among women's longevity in California. For $PM_{2.5}$, Netprime was associated with both all-cause and IHD mortality and moderately associated with CV mortality, while the sum of all sources ("Primary mass") was associated only with all-cause mortality. Likewise, for UFP, Netprime was associated with all three mortality outcomes and particularly for IHD mortality, while Primary mass was associated with only all-cause mortality.

In the next sensitivity analysis, we aimed to determine the relative importance of $PM_{2.5}$ versus UFP by considering them together in a model. We examined $PM_{2.5}$ versus UFP mass and Cu, pollutants for which the correlation between the particle sizes was high (0.81 for mass and 0.74 for Cu), but lower than that of many of the other constituent pairs. As summarized in Table 12-8, the results are quite mixed and difficult to interpret given the high correlation.

Table 12-8. Sensitivity Analysis of two pollutant models of $PM_{2.5}$ and UFP

		All-cause mortality		**CV mortality**		**IHD mortality**	
	IQR	**HR (95% CI)**	**p value**	**HR (95% CI)**	**p value**	**HR (95% CI)**	**p value**
Pollutant							
UFP-Mass	0.42	1.05 (1.01, 1.09)	.0243	1.00 (0.94, 1.07)	.9776	0.98 (0.89, 1.08)	.0655
$PM_{2.5}$-Mass	4.20	0.98 (0.94, 1.03)	.5341	1.04 (0.96, 1.12)	.3418	1.11 (0.99, 1.24)	.0800
UFP-Cu	0.00002	1.00 (0.99, 1.01)	.4474	1.01 (1.00, 1.03)	.0927	1.02 (1.01, 1.04)	.0083
$PM_{2.5}$-Cu	0.002	1.00 (0.98, 1.03)	.8014	1.01 (0.97, 1.06)	.6442	1.08 (1.01, 1.15)	.0195

In another two-pollutant analysis focusing on IHD mortality, we reran the constituent models and included UFP mass in each model (Table 12-9). Theoretically, the PM mass term controls for potential confounding from the other constituents by holding them constant and allows one to determine the independent effect of the singled out constituent. The results showed that Cu, EC and SOAa and SOAb were still associated with IHD even with UFP mass in the model (Table 12-9). Fe and Metals show a more modest association with mortality.

Table 12-9. Two pollutant models for IHD mortality with UFP constituents plus mass

Pollutant	IQR	HR (95% CI)	p value
Cu	0.00002	1.03 (1.01, 1.05)	0.0009
Mass	0.42	1.01 (0.95, 1.08)	0.6458
Fe	0.0007	1.04 (1.00 , 1.08)	0.0695
Mass	0.42	1.02 (0.95, 1.09)	0.573
Mn	0.00002	1.00 (0.99, 1.01)	0.6831
Mass	0.42	1.04 (0.99, 1.11)	0.1403
EC	0.03	1.12 (1.00, 1.25)	0.0490
Mass	0.42	0.96 (0.87, 1.07)	0.4773
OC	0.29	0.91 (0.73, 1.13)	0.3714
Mass	0.42	1.15 (0.93, 1.42)	0.1992
Other	0.03	1.01 (0.99, 1.02)	0.5820
Mass	0.42	1.04 (0.97, 1.11)	0.2543
Metals	0.01	1.07 (0.99, 1.15)	0.0745
Mass	0.42	0.98 (0.89, 1.08)	0.6398
SOA bio	0.04	1.24 (1.15, 1.34)	<.0001
Mass	0.42	1.01 (0.95, 1.07)	0.8317
SOA anthro	0.02	1.22 (1.11, 1.34)	<.0001
Mass	0.42	1.01 (0.95, 1.08)	0.7415

In our final sensitivity analysis summarized in Table 12-10, we attempted to further determine the specific effects of UFP. We compared the impacts of EC in the UFP size range, in the UFP range solely due to mobile sources and in fine particles larger than the UFP size range. Associations were observed for all-cause, CV and IHD mortality with EC both in UFP and in $PM_{2.5}$ larger than UFP. We also found associations of UFP EC from mobile sources with both all-cause and IHD mortality.

Table 12-10. Mortality risk estimates for ultrafine elemental carbon, ultrafine elemental carbon from mobiles sources, and elemental carbon in fine particles larger than UFP.

		All-cause mortality		CV mortality		IHD mortality	
	IQR	**HR (95% CI)**	**p value**	**HR (95% CI)**	**p value**	**HR (95% CI)**	**p value**
UFP EC	0.03	1.04 (1.01, 1.07)	.0024	1.05 (1.00, 1.09)	.0417	1.08 (1.01, 1.15)	.0171
UFP EC mobile	0.01	1.03 (1.00, 1.06)	.0426	1.03 (0.99, 1.08)	.1661	1.07 (1.00, 1.15)	.0359
Non-UFP EC*	0.21	1.03 (1.00, 1.06)	.0362	1.05 (1.00, 1.10)	.0344	1.13 (1.05, 1.20)	.0007

*($PM_{2.5}$(EC) - $PM_{0.1}$(EC)

12.1 Comparison to Previous Studies

Table 12-11 provides a summary of sample size, mortality counts and HR for our previous and current studies of the Teachers Cohort. The results for $PM_{2.5}$ mass provide a general proof of concept in that the results are within the range of previous studies including those of the California Teachers Cohort. As indicated by the table, in terms of risks per 10 µg/m^3, the current study generated results that are similar to those in our previous studies. In comparison to previous cohort studies, our mortality risk estimates are similar to those generated from analyses of other U.S. cohorts. Converting our risk estimates to a per 10 µg/m^3 basis, our all-cause mortality estimate is 1.07 (95% CI = 1.00, 1.14). This compares to risk estimates from the largest U.S. studies of Pope et al. [343] using the American Cancer Society (ACS) cohort (486,000 subjects) of 1.06 (1.02, 1.11), Zeger et al. [390] using the Medicare cohort (13.2 million subjects) of 1.06 (1.04, 1.07), and the recent study of the Medicare cohort (61 million subjects) by Di et al. [391] of 1.073 (1.071, 1.075). The meta-analysis of 12 studies by Hoek et al. [392] generated a risk of 1.06 (1.04, 1.08). Study results for $PM_{2.5}$ have been found to vary by region and exposure methodology. For example, a recent study of the Medicare cohort in the southeast U.S. generated an estimate of 1.19 (1.19, 122) [393]. A previous study of the Medicare cohort [390] showed no evidence of an association in the western region, with risk estimates of 1.15 (1.13, 1.18) and 1.18 (1.13, 1.22) in the eastern and central U.S., respectively.

Our risk estimate for IHD mortality per 10 µg/m^3 is 1.20 (1.02, 1.37) is fairly close to the national ACS cohort risk of 1.29 (1.18, 1.41), with a lower estimate for the combined ACS southern and western regions of 1.23 (1.12, 1.34). More recent estimates for ACS [394] generate a central estimate for IHD of 1.10 to 1.16 depending on the statistical model used.

Taken together, the evidence summarized in Table 12-11 strongly supports the approach, data and methodology used in the current study. These findings support the extension of the methods to the UFP size range summarized above.

Table 12-11. Previous Studies $PM_{2.5}$ Results for the California Teachers Cohort.

	Lipsett (2011) ***[388]***	***Ostro (2010)*** ***[249]***	***Ostro (2015)*** ***[7]***	***Current Study***
Exposure Assessment	Monitor plus IDW	Monitor (cohort within 30 km of 8 metro areas monitors)	CTM	CTM Updated
Cohort years	1999-2005	2001-2007	2001-2007	2001-2011
Sample size	73,489	43,220	101,884	88,159
All-cause Mortality (cases; HR per 10 μg/m^3; CI)	4,417 1.01 (0.95,1.09)	2,519 1.06 (0.96, 1.16)	6,285 1.01 (0.98, 1.05)	10,830 1.07 (0.99, 1.06)
Cardiovascular (cases; HR per 10 μg/m^3; CI)	1,630 1.17 (0.95, 1.19)	1,357 1.19 (1.05, 1.36)	2400 1.05 (0.99, 1.12)	4069 1.09 (0.99, 1.22)
Ischemic Heart Disease (cases; HR per 10 μg/m^3; CI)	773 1.20 (1.02, 1.41)	460 1.55 (1.24, 1.93)	1085 1.18 (1.18, 1.30)	1,741 1.20 (1.02, 1.45)

HR = Hazard ratio; NS= Not significant; IDW = Inverse distance weighted estimates for the entire state; CTM = Chemical transport model

12.2 Conclusions

This analysis adds to the limited literature on the effects of long-term exposure to UFP and added four years and improved exposure data over our previous analysis using the CTS [7]. To date, our results demonstrate strong associations between mortality and both primary $PM_{2.5}$ mass (HR=1.12, p-value=0.0021) and primary UFP mass (HR=1.10, p-value=0.0003), particularly for IHD. With a few exceptions, the findings are very similar to our earlier effort. When results are adjusted to a per $\mu g/m^3$ basis, the magnitude of the risks are very similar to the earlier study. Among the constituents, $PM_{2.5}$ EC (HR=1.12, p-value=0.001) and UFP EC (HR=1.08, p-value=0.017) stood out as most robust and consistently associated with all three outcomes. We also observed effects from both EC UFP and EC particles larger than UFP 100nm, as well as EC specifically from mobile sources. SOAa and SOAb generated the greatest risks for IHD mortality. Associations with IHD mortality were also demonstrated with $PM_{2.5}$ nitrate, and for both $PM_{2.5}$ and UFP, with the metal constituents. Taken together, these results provide strong support for the importance of mobile sources as a significant risk to public health. Also, with the four additional years of cohort follow-up, $PM_{2.5}$ mass was now associated with all-cause mortality.

The main results plus those of the two-pollutant models provide support for the importance of EC, Cu and SOA in the ultrafine domain. In many cases, the association of the UFP measure of a given constituent is less uncertainty than the corresponding $PM_{2.5}$ measure. However, given the high correlations and potential differences in exposure error, this observation should be viewed with caution. Overall, it is difficult to provide clear evidence of the relative effects of UFP versus $PM_{2.5}$. It is noteworthy, however, that we observed associations between EC and mortality in both the UFP and larger particles. The findings for EC and Cu are supported by previous studies and meta-analysis examining the relative impacts of $PM_{2.5}$ constituents, which have implications for the ultrafine concentrations as well. For example, Achilleos et al. [395] et al. conducted a meta-analysis of short-term exposure studies using 41 studies covering 142 cities. The studies used both time-series analysis and case-crossover to determine the risks from single- or multi-day exposures on mortality. EC was associated with all-cause and cardiovascular mortality (but not respiratory) and exhibited the highest risk per IQR for the former. Ammonium ion and nitrates were also associated with cardiovascular mortality. In models that added a control for $PM_{2.5}$ mass, associations with all-cause mortality were observed for EC, Cu and K. The latter is a marker for wood smoke. The study also indicates significant differences by region with certain factors explaining the variation in city-specific results including: $PM_{2.5}$ concentration, winter temperature, population density, size of elderly population, city elevation and vegetation. This suggests that the risks associated with a specific constituent or with overall mass can vary by location. Another factor not explored in their analysis would be the number of monitors used in the study and the size of the city. Both of these factors likely impact the accuracy of measurement of these constituents and the subsequent risk estimates. This is especially important for pollutant with high spatial variation.

The meta-analysis by Yang et al. [396] included 30 short-term exposure studies and 11 long-term exposure cohort studies. Their review indicated that black carbon and OC were most consistently associated with all-cause and cardiovascular mortality. In addition, several metals including Fe, Vanadium (a product of combustion of oil) and Zn were considered to have serious health consequences. Cu was only measured in two of their studies demonstrating the bias of both meta-results, since many other constituents were often not measured. Our findings for Cu support the importance of motor vehicle non-combustion sources since it is a marker of brake wear. The importance of Cu has been highlighted in several other reviews and experimental studies [397-399].

The chemical transport model predicted that the highest levels of SOAa in both $PM_{2.5}$ and UFP occurs in southern Los Angeles County, Orange County, Northern San Diego County and the western parts of Riverside and San Bernardino Counties. Approximately 60% or more of the SOAa is generated by gasoline-powered motor vehicles but other sources also contribute including diesel vehicles, meat cooking, wood smoke, natural gas combustion and volatile consumer products (which include many products from paints to perfumes). These highest concentrations of these sources are also found in the Los Angeles air basin. In contrast, in our exposure model, the highest concentrations of SOAb are found mostly in the San Joaquin Valley. It should be noted that the models predicting SOA are extremely complicated and have significant uncertainty, as described earlier.

Among the sources, on-road diesel in both size fractions was associated with all-cause mortality and many of the sources (all four mobile, meat cooking, natural gas combustion and "other" anthropogenic sources) were associated with IHD mortality. The findings for natural gas combustion, primarily from industrial and commercial facilities, are particularly interesting and deserve further study. In the exposure model, residential natural gas combustion is assumed to partially evaporate by 70% leaving 30% that would contribute to ambient UFP concentrations, while industrial and commercial natural gas combustion sources were not scaled down.

The null and negative findings for wood smoke should be particularly viewed with caution. Wood smoke has a different chemical composition than many of the other combustion sources, and there is very limited evidence concerning their effects on mortality. In addition, the estimated concentrations occur sporadically and primarily during the nighttime so exposures may be different than many other sources. Finally, the highest concentrations of particles from wood smoke occur in two high-income counties with low prevalence of IHD mortality, Marin and Santa Clara. Thus, there might be residual confounding that was not controlled for in the regression model.

There are, of course, several caveats to our findings. First, as indicated above, there is some misclassification of the exposures used in this analysis due to the errors in the wind fields and uncertainty in the true spatial distribution of mobile source emissions. In addition, as in all epidemiological studies of air pollution, there is likely to be other errors in the exposure fields. Most analyses suggests that if there is Berkson error (true exposure varies randomly around measured exposure) it is not likely to bias the estimate (in general) but is likely to increase the confidence intervals leading to greater likelihood of finding no association. Classical measurement error, where there is noise in estimating exposure, would likely lead to a lower risk estimate and greater variance. Second, there is fairly high correlation among many of the constituents of both particle size fractions. As discussed in our earlier paper, this is not just a result of the exposure estimates but rather a fact observed in actual measurements. Thus, a single constituent is likely to represents several other highly correlated co-pollutants. This highlights the importance of examining the impact of specific sources which, by definition, aggregate several of the individual constituents. Third, many of the constituents have significant spatial heterogeneity which may not be fully captured in the 4k grids. Fourth, our model did not include the potential impacts of gases such as NO_2 which is often correlated with UFP. Thus, results described above need to viewed with some caution. Nevertheless, the study results add to the existing evidence of effects of long-term exposure to UFP mass and several of its constituents and sources.

12.3 Appendix I - Descriptive statistics for health and covariate variables among study participants and those women excluded from the study

	Among study participants	**Among women excluded**
Covariate	**Percentage or mean ± SD**	**Percentage or mean ± SD**
Age at January 2001 (yr)	57.2 ± 14.0	61.6 ± 15.9
Race (% non-Hispanic white)	86.0	88.4
Smoking status:		
Never smoker	68.3	60.3
Former smoker	27.0	31.9
Current smoker	4.7	5.8
Total pack-years	14.8 ± 17.3	17.1 ± 19.3
Adult second-hand smoke exposure	48.4	51.5
BMI (kg/m^2)	24.9 ± 5.1	24.8 ± 5.0
Married/living with partner	45.5	41.0
Non-drinker	32.2	32.8
Menopausal status and HT use:		
Premenopausal	40.2	31.7
Peri/postmenopausal and no hormone therapy use	12.4	15.9
Peri/postmenopausal and current/past hormone therapy use	34.2	37.8
Unknown menopausal status/hormone therapy use	13.2	14.6
Dietary fat (g/d)	56.0 ± 26.7	56.5 ± 27.2
Dietary fiber (g/d)	15.1 ± 6.4	15.4 ± 6.7
Dietary calories (kcal/d)	1,589.4 ± 555.2	1,592.7 ± 562.9
Physical activity (h/wk)	4.4 ± 4.0	4.4 ± 4.1
Family history of heart disease	45.5	46.1
Taking hypertension medication/aspirin	33.1	34.6

All characteristics were reported on baseline questionnaire, except marital status which was reported on the 2000 questionnaire.

12.4 Appendix II – Spearman correlations between $PM_{2.5}$ and $PM_{0.1}$ species

Species		**PM0.1**									
		Mass	**Cu**	**Fe**	**Mn**	**EC**	**OC**	**Other**	**Metals**	**SOA bio**	**SOA anthro**
PM2.5	**Mass**	0.82									
	Cu		0.74								
	Fe			0.85							
	Mn				0.81						
	EC					0.97					
	OC						0.97				
	Other							0.59			
	Metals								0.72		
	SOA bio									0.95	
	SOA anthro										0.99

13 OVERALL PROJECT CONCLUSIONS

13.1 Review and Analysis of Measured Ultrafine Particle Concentrations

Ambient ultrafine particles ($Dp<0.1$ µm; UFP) can be characterized by number concentration ($Dp>7$ nm; N_7), surface area concentration, or mass concentration ($PM_{0.1}$). None of these metrics was routinely measured prior to the year 2012, and so the historical record of long-term UFP concentrations in California must be constructed from a review and analysis of past fields studies that each cover a short time period within the overall analysis window. Data obtained from eight different studies from 1996 to 2016 in various locations throughout California show that both N_7 and $PM_{0.1}$ concentrations have decreased over the past two decades. Declining UFP concentrations are generally correlated with declining $PM_{2.5}$ concentrations and likely stem from common emissions control measures. The ratio of ultrafine EC/OC has increased over time suggesting the sources of $PM_{0.1}$ OC are declining faster than sources of $PM_{0.1}$ EC. This occurs despite the adoption of diesel particle filters (DPFs) in California that virtually eliminate $PM_{0.1}$ emissions from diesel engines. N_7 concentrations are also declining more slowly than corresponding $PM_{0.1}$ and $PM_{2.5}$ concentrations. These trends may suggest a currently unidentified source of $PM_{0.1}$ EC and N_7 that is not declining at the same rate as other sources of UFPs. Future studies should work to better understand the factors behind these trends.

13.2 Day-of-Week Patterns in Ultrafine Particle Concentrations

Ultrafine particulate matter ($PM_{0.1}$) samples were collected during three-day averaging periods over an annual cycle at four sites across California: Los Angeles, East Oakland, San Pablo, and Fresno. $PM_{0.1}$ samples were analyzed for thermal carbon fractions using a thermal-optical carbon analyzer and trace elements using ICP-MS. A statistical analysis of the day-of-week trends for sixteen $PM_{0.1}$ components reveals location-specific patterns along with important general trends for UFP concentrations. $PM_{0.1}$ elemental carbon (EC) concentrations are elevated in the middle of the week consistent with increased activity for diesel engines during this time period. Just as significantly, $PM_{0.1}$ organic carbon (OC) concentrations do not exhibit a day-of-week pattern. Since OC accounts for the majority of the $PM_{0.1}$ total mass, the lack of a day-of-week pattern for $PM_{0.1}$ OC suggests that diesel engines do not dominate total $PM_{0.1}$ mass in California. A paired t-test constructed using measurements on weekends compared to measurements immediately preceding or immediately following the weekend showed that $PM_{0.1}$ potassium (K) and rubidium (Rb) concentrations were elevated on weekends. This pattern is consistent with increased biomass combustion on weekends (a previously unknown exposure pattern for UFPs). The two closest sampling locations (East Oakland and San Pablo) had the great number of UFP components with identical weekly trends, but even at these locations only 4 out of 16 components displayed the exact same day-of-week profiles. Less similarity was observed in measured day-of-week profiles for UFP components at other sites. The heterogeneity between sites suggests that the details of UFP concentrations at each location reflect the mixture of sources immediately adjacent to that site. By extension, individual neighborhoods across California will each experience unique day-of-week concentration profiles for UFP components that reflect the surrounding sources.

13.3 Source Apportionment of Ultrafine Particulate Using Positive Matrix Factorization

Three-day average samples of $PM_{0.1}$ collected over a full year at Los Angeles, East Oakland, and San Pablo were analyzed using Positive Matrix Factorization to identify source-factor contributions at each location. Seven $PM_{0.1}$ source-factors were identified: Factor1-Gasoline+Motor Oil+Meat Cooking, Factor 2- Diesel, Factor 3-Wood Burning, Factor 4-Shipping, Factor 5-Sea Spray, Factor 6-Sb and Factor 7-Sn. The majority of the $PM_{0.1}$ OC and $PM_{0.1}$ total mass was associated with the blended source Factor 1- Gasoline+Motor Oil+Food Cooking. The majority of the $PM_{0.1}$ EC as associated with source Factor 2 – Diesel Engines. Source Factor 3 – Wood Burning contributions to $PM_{0.1}$ were highest in the winter season when residential wood combustion was active. The monthly-averaged $PM_{0.1}$ source apportionment results calculated by PMF in the current study are consistent with the $PM_{0.1}$ source apportionment results calculated using CMB. Agreement between these results increases confidence in the receptor-oriented source apporitonment calculations for $PM_{0.1}$.

13.4 Source Apportionment of Ultrafine Particles Using Chemical Mass Balance

Samples of ultrafine particle matter mass ($PM_{0.1}$) were collected over twelve months at three cities in California: Los Angeles, East Oakland, San Pablo, and over six months at Fresno. Molecular markers adjusted for volatility and reactivity were used to calculate $PM_{0.1}$ source contributions. Wood burning was a significant source of $PM_{0.1}$ organic carbon (OC) during the winter months in northern California (17-47%) but made smaller contributions in other months (0-8%) and was minor in all seasons in Los Angeles (0-5%), expect December (17%) during holiday celebrations. Meat cooking was the largest source of $PM_{0.1}$ OC across all sites (13-29%), followed by gasoline combustion (7-21%). Motor oil and diesel fuel combustion made smaller contributions to $PM_{0.1}$ OC (3-10% and 3-7%, respectively). Unresolved sources accounted for 22-56% of the $PM_{0.1}$ OC. The lack of a clear seasonal profile for this unresolved OC suggests that it may be a primary source rather than secondary organic aerosol (SOA). $PM_{0.1}$ elemental carbon (EC) was dominated by diesel fuel combustion with less than 15% contribution from other sources. All sources besides wood smoke exhibited relatively constant seasonal source contributions to $PM_{0.1}$ OC reflecting approximately constant emissions over the annual cycle. Annual-average source contributions to $PM_{0.1}$ OC calculated with traditional molecular markers were similar to the source contributions calculated with the modified molecular markers that account for volatility and reactivity.

13.5 Potential For Adoption of New Photochemical Mechanisms In Regional Chemical Transport Models for Ultrafine Particle Predictions

SAPRC16 is an interim update to the SAPRC series of chemical mechanisms that includes updated rate constants, a revised representation of radical chemistry, and a new speciation lumping scheme to better develop predictions of SOA precursors. The ability of the SAPRC16 chemical mechanism to simulate regional ozone episodes was tested in seven (7) major cities across the United States with the hope that the mechanism could be used for long-term UFP simulations in California. The UCD-CIT 3-dimensional (3D) airshed model was configured with both SAPRC11 (base mechanism) and SAPRC16 (updated mechanism). Concentrations of ozone, hydroxyl radical (OH) and hydroperoxyl (HO_2) radical predicted with both mechanisms were compared to measured values. It was generally observed that SAPRC16 predicts slightly lower ozone concentrations than SAPRC11 in NOx rich urban centers. A box model analysis shows that the SAPRC16 mechanism quenches ozone production earlier than SAPRC11 as NOx concentrations increase (yielding decreasing VOC/NOx ratios). This could be caused by more detailed HO_2+RO_2 reactions and RO_2 isomerization reactions in SAPRC16 that compete with the HO_2+NO reaction. Predictions from SAPRC11 are in better agreement with the measurements in the western United States. In general, the SAPRC11 mechanisms slightly over-predicts OH concentration while under-predicting HO_2 radical concentration and the SAPRC16 mechanism slightly under predicts OH and largely under predicts HO_2, sometimes by large amounts. The reasons for this are unknown at this time. These features will influence the secondary organic aerosol (SOA) predictions from each mechanism since the branching between high NOx and low NOx regimes depends on calculated HO_2 concentrations. Further analysis of the HO_2+RO_2 reactions and RO_2 isomerization reactions and the reasons for the lower HO_2 predictions in the updated SAPRC16 chemical mechanism should be carried out before widespread adoption of the new mechanism.

13.6 Predicting Ultrafine Particle Number Concentrations Using a Regional Chemical Transport Model

The UCD/CIT air quality model was used to predict regional concentrations and source contributions for airborne particle number concentration (N_{10}) and ultrafine particle mass concentration ($PM_{0.1}$) in the San Francisco Bay Area (SFBA) and the South Coast Air Basin (SoCAB) surrounding Los Angeles with 4 km spatial resolution and daily time resolution for the year 2012. Performance statistics for daily predictions of N_{10} concentrations meet the threshold normally required for regulatory modeling of $PM_{2.5}$ (MFB< ± 0.5 and MFE < 0.75). Predicted source contributions to $PM_{0.1}$ are in good agreement with results from receptor-based studies that use molecular markers for source apportionment at four locations in California. Different sources dominated concentrations of N_{10} and $PM_{0.1}$ in different regions of California because of the different emitted particle size distributions and different choices for heating fuels. Non-residential natural gas combustion (38-74%) made the largest single contribution to PNC concentrations at the ten regional monitoring locations, followed by nucleation (6-14%), wood smoke (1-8%), food cooking (1-9%), and mobile sources (4-8%). In contrast, wood smoke (25-49%) was the largest source of $PM_{0.1}$ in the SFBA followed by mobile sources (15-33%), non-residential natural gas combustion (13-28%), and food cooking (4%-14%). Non-residential natural gas combustion (42-57%) was the largest $PM_{0.1}$ source at the SoCAB sites, followed by traffic sources (16-35%) and food cooking (6-14%). The study region encompassed in this project is home to more than 25M residents, which should provide sufficient power for future epidemiological studies on the health effects of airborne ultrafine particles. Correlations between $PM_{2.5}$ and PNC are low (R^2=0.35) suggesting that the health effects of these metrics may be assessed independently.

13.7 Predicting Ultrafine Particle Mass Concentrations Using a Regional Chemical Transport Model

Regional concentrations and source contributions were calculated for airborne ultrafine particle (UFP) mass concentrations ($PM_{0.1}$) across California with 4km spatial resolution for the years 2015 – 2016 using the UCD/CIT air quality model. Predicted $PM_{0.1}$ concentrations are in good agreement with measurements at four sites spanning the diverse range of polluted California cities: Los Angeles, East Oakland, San Pablo, and Fresno. Source contributions to $PM_{0.1}$ mass predicted by the regional UCD/CIT calculations are also in good agreement with source contributions calculated using the Chemical Mass Balance (CMB) model for gasoline engines, diesel engines, food cooking, and wood smoke. The UCD/CIT model tracked additional $PM_{0.1}$ source contributions from aircraft and natural gas combustion. The predicted concentrations associated with these sources are consistent with the residual "unidentified" $PM_{0.1}$ mass in the CMB calculations. The UCD/CIT model correctly predicts seasonal trends in source contributions to $PM_{0.1}$ OC, but evidence suggests that the UCD/CIT model does not capture all of the source contributions to $PM_{0.1}$ EC during the winter season. This pattern may stem from an over-prediction of wind speeds during winter stagnation events or it may be caused by an unknown source of $PM_{0.1}$ EC that has increased activity during the winter season. Despite this shortcoming, the otherwise general agreement between the UCD/CIT and CMB model calculations across three major urban areas builds confidence that the $PM_{0.1}$ exposure fields predicted by the UCD/CIT model will provide reasonably accurate exposure assessments for future epidemiological studies.

13.8 Predicting Long-Term Trends in Ultrafine Particle Concentrations Using a Regional Chemical Transport Model

Concentration fields of $PM_{0.1}$ and N_{10} were predicted over a 17 year period (from 2000 to 2016) in California at 4 km horizontal resolution and hourly time resolution using the UCD/CIT air quality model. Simultaneously predictions of ozone, NO, NO_2, CO, $PM_{2.5}$ mass, $PM_{2.5}$ nitrate, and $PM_{2.5}$ ammonium ion meet standard modeling performance criteria (MFB $< \pm 0.5$) when compared to daily, monthly and yearly averaged measurements. Predicted N_{10}, $PM_{0.1}$ EC and $PM_{0.1}$ OC meet the performance criteria for the periods when measurements are available. Long-term source appointment results predict that mobile source contributions to N_{10} and $PM_{0.1}$ mass have significantly decreased from 2000-2016 due to the adoption of cleaner vehicles into the on-road fleet. Wood smoke contributions to N_{10} and $PM_{0.1}$ mass have also decreased significantly due to curtailment efforts on residential wood combustion for home heating after the year 2003. In contrast, food cooking source contributions to N_{10} and $PM_{0.1}$ have remained constant or even increased with increasing population over the 17 year study period. Natural gas combustion makes significant contributions to N_{10} and $PM_{0.1}$ mass at all urban locations across California over the entire 17 year study period. The dataset generated by this study will be provide useful exposure estimates for fine and ultrafine particle concentrations in California.

13.1 High Spatial-Resolution (1km) Predictions for Ultrafine Particle Concentrations in California

Emissions inventories with 1km spatial resolution were created for the South Coast Air Basin, San Francisco Bay Area, and Sacramento for the years 2000 through 2002. Statistical analysis indicates that increasing the model resolution from 4km to 1km increases the accuracy of $PM_{2.5}$ predictions related to mobile sources. The spatial distribution of mobile source pollutant concentrations at 1km resolution follows the location of major highways but these concentrations have a uniform distribution lacking finer spatial detail when simulated with 4km resolution. Likewise, $PM_{0.1}$ predictions at 1km resolution can resolve major freeways in all domains while predictions at 4km resolution produce more uniform regional concentrations. The concentration field around point sources is more focused in simulations that use 1km spatial resolution compared to 4km resolution due to the effects of numerical diffusion. The net effect of this numerical diffusion on population exposure may be minimal because only a small fraction of the total population lives within 4km of a major point source. $PM_{2.5}$ predictions related to area sources are not strongly affected by increasing the model resolution from 4km to 1km. Spatial surrogates used to allocate many area emissions are relatively uniform over urban areas in California leading to uniform emissions and uniform concentration fields irrespective of the increased resolution of the calculations.

Concentration fields for secondary pollutants including particulate nitrate and secondary organic aerosol do not exhibit finer spatial details when simulations are performed at 1km resolution compared to 4km resolution. Slightly higher mobile source emissions rates in the fuel-based inventory at 1km resolution produce higher concentrations of secondary $PM_{2.5}$ and $PM_{0.1}$ components including nitrate and anthropogenic secondary organic aerosol. This finding suggests that some of the model under-predictions noted in Sections 7, 8, and 9 may be related to uncertainty in mobile source emissions estimates.

13.2 Predicting Source Contributions to Ultrafine Particle Mass and Number Concentrations across the United States Using a Regional Chemical Transport Model

The regional concentrations of airborne ultrafine particulate matter mass ($D_p < 0.1$ µm; $PM_{0.1}$) was predicted in 39 cities across the United States (U.S.) during summer time air pollution episodes. Calculations were performed using a regional source-oriented chemical transport model with 4 kilometer (km) spatial resolution operating on the National Emissions Inventory created by the U.S. EPA. Measured source profiles for particle size and composition between 0.01 – 10 µm were used to translate PM total mass to $PM_{0.1}$. Predicted $PM_{0.1}$ concentrations exceeded 2 $\mu g\ m^{-3}$ during summer pollution episodes in major urban regions across the U.S. including Los Angeles, the San Francisco Bay Area, Houston, Miami, and New York. $PM_{0.1}$ spatial gradients were sharper than $PM_{2.5}$ spatial gradients due to the dominance of primary aerosol in $PM_{0.1}$. Artificial source tags were used to track contributions to primary $PM_{0.1}$ and $PM_{2.5}$ from fifteen source categories. On-road gasoline and diesel vehicles made significant contributions to regional $PM_{0.1}$ in all 39 cities even though peak contributions within 0.3 km of the roadway were not resolved by the 4 km grid cells. Food cooking also made significant contributions to $PM_{0.1}$ in all cities but biomass combustion was only important in locations impacted by summer wildfires. Aviation was a significant source of $PM_{0.1}$ in cities that had airports within their urban footprints. Industrial sources including cement manufacturing, process heating, steel foundries, and paper & pulp processing impacted their immediate vicinity but did not significantly contribute to $PM_{0.1}$ concentrations in any of the target 39 cities. Natural gas combustion made significant contributions to $PM_{0.1}$ concentrations due to the widespread use of this fuel for electricity generation, industrial applications, residential and commercial use. The major sources of primary $PM_{0.1}$ and $PM_{2.5}$ were notably different in many cities. Future epidemiological studies may be able to differentiate $PM_{0.1}$ and $PM_{2.5}$ health effects by contrasting cities with different ratios of $PM_{0.1}$ / $PM_{2.5}$. In the current study, cities with higher $PM_{0.1}$ / $PM_{2.5}$ ratios (ratio greater than 0.15) include Houston TX, Los Angeles CA, Birmingham AL, Charlotte NC, and Bakersfield CA. Cities with lower $PM_{0.1}$ to $PM_{2.5}$ ratios (ratio lower than 0.05) include Lake Charles LA, Baton Rouge LA, St. Louis MO, Baltimore MD, and Washington DC.

13.3 Associations between Exposure to Ultrafine Particles and Mortality in the California Teachers Study (CTS) Cohort

Exposures to $PM_{0.1}$ species, sources, and total mass predicted using the UCD/CIT air quality model were combined with the health data from the California Teachers Study (CTS) cohort to analyze the potential health effects of ultrafine particles (UFP). Individualized monthly-averaged exposures between the years 2000 – 2009 were calculated for +90,000 women in the cohort based on their residential address using the 4km resolution of the predicted exposure fields. A Cox proportional hazard model was used to estimate the associations between predicted pollutant concentrations and all-cause, cardiovascular, and ischemic heart disease (IHD) mortality while controlling for covariates (age, race, marital status, smoking, BMI, physical activity, alcohol consumption, diet, menopausal status, family history of heart attacks or stroke, blood pressure medication, and several ecologic variables). Association were examined between the mortality endpoints and both $PM_{2.5}$ and UFP mass and each of their individual constituents and sources. Several sensitivity analyses were conducted. To examine the strength of association for $PM_{2.5}$ versus UFP, we examined two pollutant models that include both $PM_{2.5}$ and UFP terms for mass and a subset of constituents. The calculated risk estimate on all-cause mortality per 10 $\mu g/m^3$ of $PM_{2.5}$ is 1.07 (95% CI = 1.00, 1.14) which compares favorably with estimates developed using central site monitor exposures combined with the ACS cohort (1.06; 95% CI = 1.02, 1.11) and the Medicare cohort (1.06; 95% CI =1.04, 1.07). Likewise, the risk estimate for IHD mortality per 10 $\mu g/m^3$ of predicted $PM_{2.5}$ concentration in the current study is 1.20 (95% CI =1.02, 1.37) which compares favorably with the ACS cohort risk for the southern and western regions of 1.23 (95% CI = 1.12, 1.34). Extending the analysis to the UFP size range, multiple UFP metrics were associated with all-cause mortality at the 95% confidence level including mass, EC, OC, metals, and on-road diesel sources. UFP metrics associated with CV mortality at the 95% confidence level included Cu, EC, and SOA. UFP metrics associated with IHD mortality at the 95% confidence level included Cu, Fe, EC, metals, SOA, gasoline, off-road diesel, food cooking, and natural gas combustion. The most consistent association across all the health endpoints is the sum of primary $PM_{0.1}$ from all sources except wood smoke which is associated with all-cause, CV, and IHD mortality at the 95% confidence level. There is a suggestion from our results that UFP may correlate with the mortality outcomes as well or better than $PM_{2.5}$. However, given the high correlations between the $PM_{2.5}$ and UFP mass and species and the likely differential in measurement error, it is difficult to reach a firm conclusion on this issue. In addition, several constituents of UFP were associated with mortality even in models that included UFP mass. With a few exceptions, the findings are very similar to our earlier results.

13.4 Future research

Natural gas combustion makes a major contribution to predicted $PM_{0.1}$ and N_{10} concentrations across California. These predictions are consistent with measurement-based CMB calculations that leave a major fraction of the $PM_{0.1}$ as “other sources”, but further studies should be carried out to identify a chemical signature for natural gas combustion particles that can be included in CMB calculations to more definitely quantify natural gas combustion source contributions.

The consistent increase in $PM_{0.1}$ EC concentrations during the winter season across the years 2000-2016 merits more investigation. The adoption of diesel particle filters (DPFs) during this time period should have significantly reduced peak $PM_{0.1}$ EC concentrations if diesel engines were a dominant winter-time source. The lack of a significant downward trend in winter EC concentrations suggests that other sources of $PM_{0.1}$ EC may make strong contributions to ambient concentrations. These other $PM_{0.1}$ EC sources should be identified and properly represented in the predicted $PM_{0.1}$ exposure fields so that future epidemiological studies can analyze their potential health effects.

Secondary organic aerosol (SOA) formation mechanisms continue to be a critical issue given the apparent toxicity of this $PM_{0.1}$ component. Numerous projects are reviewing new sources and formation mechanisms for SOA that should improve the accuracy of the predicted ambient SOA concentrations. The $PM_{0.1}$ exposure fields developed in this study should be updated to reflect these new findings when they become available so that future epidemiological studies can analyze the potential health effects of UFP SOA.

Future epidemiological studies should be carried out using additional large cohorts combined with exposure estimates from regional chemical transport models to investigate the health effects of UFPs.

14 REFERENCES

1. Donaldson, K., et al., *The pulmonary toxicology of ultrafine particles.* Journal of Aerosol Medicine-Deposition Clearance and Effects in the Lung, 2002. **15**(2): p. 213-220.
2. U.S. National Research Council, *Research Prioritties for Airorne Particulate Matter: I Immdiate Priorities and a long-range Research Porfolio.* National Academy Press, 1998. **Washington, D.C.**
3. HEI, *Understanding the health effects of ambient ultrafine particles.* HEI review panel on ultrafine particles, 2013.
4. EPA, *Workshop on Ultrafine particles.* Available at: https://drive.google.com/file/d/0B966KhahxN_XekZBanFzQUoydWc/view, 2015.
5. EPA, *Integrated Science Assessment for Particulate Matter: Final Report U.S. EPA National Center for Environmental Assessment-RTP Division, Office of Research and Development.* EPA/600/6-08/139F, 2009. **Available at: https://cfpub.epa.gov/ncea/risk/recordisplay.cfm?deid=216546**.
6. Hu, J., et al., *Predicting Primary PM2.5 and PM0.1 Trace Composition for Epidemiological Studies in California* Environmental Science and Technology, 2014. **48**(9): p. 4971-4979.
7. Ostro, B., et al., *Associations of mortality with long-term exposures to fine and ultrafine particles, species and sources: results from the California Teachers Study Cohort.* Environ Health Persp., 2015. **123**(6): p. 549-56.
8. Laurent, O., et al., *A Statewide Nested Case-Control Study of Preterm Birth and Air Pollution by Source and Composition: California, 2001-2008.* Environmental Health Perspectives, 2016.
9. Krewski, D., et al., *Extended follow-up and spatial analysis of the American Cancer Society study linking particulate air pollution and mortality.* Research report (Health Effects Institute), 2009(140): p. 5-114; discussion 115-36.
10. Elder, A. and G. Oberdorster, *Translocation and effects of ultrafine particles outside of the lung.* Clinics in occupational and environmental medicine, 2006. **5**(4): p. 785-96.
11. Elder, A., et al., *Translocation of inhaled ultrafine manganese oxide particles to the central nervous system.* Environmental Health Perspectives, 2006. **114**(8): p. 1172-1178.
12. Donaldson, K., et al., *Ultrafine particles.* Occupational and Environmental Medicine, 2001. **58**(3): p. 211-+.
13. Oberdorster, G., *Toxicology of ultrafine particles: in vivo studies.* Philosophical Transactions of the Royal Society of London Series a-Mathematical Physical and Engineering Sciences, 2000. **358**(1775): p. 2719-2739.
14. Kreyling, W.G., M. Semmler, and W. Moller, *Dosimetry and toxicology of ultrafine particles.* Journal of Aerosol Medicine-Deposition Clearance and Effects in the Lung, 2004. **17**(2): p. 140-152.
15. Chung, A., J.D. Herner, and M.J. Kleeman, *Detection of alkaline ultrafine atmospheric particles at Bakersfield, California.* Environmental Science & Technology, 2001. **35**(11): p. 2184-2190.
16. Herner, J.D., et al., *Size and composition distribution of airborne particulate matter in northern California: I-particulate mass, carbon, and water-soluble ions.* Journal of the Air & Waste Management Association, 2005. **55**(1): p. 30-51.

17. Kleeman, M.J., S.G. Riddle, and C.A. Jakober, *Size distribution of particle-phase molecular markers during a severe winter pollution episode.* Environmental Science & Technology, 2008. **42**(17): p. 6469-6475.
18. Kleeman, M.J., et al., *Source apportionment of fine (PM1.8) and ultrafine (PM0.1) airborne particulate matter during a severe winter pollution episode.* Environmental science & technology, 2009. **43**(2): p. 272-279.
19. Kuwayama, T., C.R. Ruehl, and M.J. Kleeman, *Daily Trends and Source Apportionment of Ultrafine Particulate Mass (PM0.1) over an Annual Cycle in a Typical California City.* Environmental Science & Technology, 2013. **47**(24): p. 13957-13966.
20. Riddle, S.G., et al., *Size-resolved source apportionment of airborne particle mass in a roadside environment.* Environmental Science & Technology, 2008. **42**(17): p. 6580-6586.
21. Riddle, S.G., et al., *Size distribution of trace organic species emitted from heavy-duty diesel vehicles (vol 41, pg 1962, 2007).* Environmental Science & Technology, 2008. **42**(3): p. 974-976.
22. Riddle, S.G., et al., *Size distribution of trace organic species emitted from light-duty gasoline vehicles.* Environmental Science & Technology, 2007. **41**(21): p. 7464-7471.
23. Robert, M.A., M.J. Kleeman, and C.A. Jakober, *Size and composition distributions of particulate matter emissions: Part 2- Heavy-duty diesel vehicles.* Journal of the Air & Waste Management Association, 2007. **57**(12): p. 1429-1438.
24. Robert, M.A., et al., *Size and composition distributions of particulate matter emissions: Part 1 - Light-duty gasoline vehicles.* Journal of the Air & Waste Management Association, 2007. **57**(12): p. 1414-1428.
25. Ham, W.A. and M.J. Kleeman, *Size-resolved source apportionment of carbonaceous particulate matter in urban and rural sites in central California.* Atmospheric Environment, 2011. **45**(24): p. 3988-3995.
26. Seaton, A., et al., *Particulate Air-Pollution and Acute Health-Effects.* Lancet, 1995. **345**(8943): p. 176-178.
27. Oberdorster, G., et al., *INCREASED PULMONARY TOXICITY OF ULTRAFINE PARTICLES .2. LUNG LAVAGE STUDIES.* Journal of Aerosol Science, 1990. **21**(3): p. 384-387.
28. Brown, D.M., et al., *Increased inflammation and intracellular calcium caused by ultrafine carbon black is independent of transition metals or other soluble components.* Occupational and Environmental Medicine, 2000. **57**(10): p. 685-691.
29. Tran, C.L., et al., *Inhalation of poorly soluble particles. II. Influence of particle surface area on inflammation and clearance.* Inhalation Toxicology, 2000. **12**(12): p. 1113-1126.
30. Renwick, L.C., et al., *Increased inflammation and altered macrophage chemotactic responses caused by two ultrafine particle types.* Occupational and Environmental Medicine, 2004. **61**(5): p. 442-447.
31. Karner, A.A., D.S. Eisinger, and D.A. Niemeier, *Near-Roadway Air Quality: Synthesizing the Findings from Real-World Data.* Environmental Science & Technology, 2010. **44**(14): p. 5334-5344.
32. Kleeman, M.J., et al., *Size distribution of trace organic species emitted from biomass combustion and meat charbroiling.* Atmospheric Environment, 2008. **42**(13): p. 3059-3075.

33. Stanier, C.O., A.Y. Khlystov, and S.N. Pandis, *Nucleation events during the Pittsburgh air quality study: Description and relation to key meteorological, gas phase, and aerosol parameters.* Aerosol Science and Technology, 2004. **38**: p. 253-264.
34. Cheung, H.C., et al., *Influence of medium range transport of particles from nucleation burst on particle number concentration within the urban airshed.* Atmospheric Chemistry and Physics, 2012. **12**(11): p. 4951-4962.
35. Zhu, Y.F., et al., *Study of ultrafine particles near a major highway with heavy-duty diesel traffic.* Atmospheric Environment, 2002. **36**(27): p. 4323-4335.
36. Zhang, K.M., et al., *Evolution of particle number distribution near roadways. Part II: the 'road-to-ambient' process.* Atmospheric Environment, 2004. **38**(38): p. 6655-6665.
37. Peters, A., et al., *Respiratory effects are associated with the number of ultrafine particles.* American Journal of Respiratory and Critical Care Medicine, 1997. **155**(4): p. 1376-1383.
38. Forastiere, F., et al., *A case-crossover analysis of out-of-hospital coronary deaths and air pollution in Rome, Italy.* American Journal of Respiratory and Critical Care Medicine, 2005. **172**(12): p. 1549-1555.
39. Hu, J., et al., *Predicting primary PM2.5 and PM0.1 trace composition for epidemiological studies in California.* Environ Sci Technol, 2014. **48**(9): p. 4971-9.
40. Hu, J., et al., *Identifying PM2.5 and PM0.1 sources for epidemiological studies in California.* Environmental Science and Technology, 2014. **48**(9): p. 4980-4990.
41. Hu, J., et al., *Long-term particulate matter modeling for health effect studies in California – Part 1: Model performance on temporal and spatial variations.* Atmospheric Chemistry and Physics, 2015. **15**(6): p. 3445-3461.
42. Laurent, O., et al., *Low birth weight and air pollution in California: Which sources and components drive the risk?* Environment International, 2016. **92-93**: p. 471-477.
43. Ham, W.A., et al., *Size Distribution of Health-Relevant Trace Elements in Airborne Particulate Matter During a Severe Winter Stagnation Event: Implications for Epidemiology and Inhalation Exposure Studies.* Aerosol Science and Technology, 2010. **44**(9): p. 753-765.
44. Saffari, A., et al., *Seasonal and spatial variation of trace elements and metals in quasi-ultrafine (PM0. 25) particles in the Los Angeles metropolitan area and characterization of their sources.* Environmental pollution, 2013. **181**: p. 14-23.
45. Saffari, A., et al., *Seasonal and spatial variation in reactive oxygen species activity of quasi-ultrafine particles (PM0.25) in the Los Angeles metropolitan area and its association with chemical composition.* Atmospheric Environment, 2013. **79**: p. 566-575.
46. Saffari, A., et al., *Impact of primary and secondary organic sources on the oxidative potential of quasi-ultrafine particles (PM0.25) at three contrasting locations in the Los Angeles Basin.* Atmospheric Environment, 2015. **120**: p. 286-296.
47. Shirmohammadi, F., et al., *Oxidative potential of coarse particulate matter (PM10-2.5) and its relation to water solubility and sources of trace elements and metals in the Los Angeles Basin.* Environmental Science-Processes & Impacts, 2015. **17**(12): p. 2110-2121.
48. Shirmohammadi, F., et al., *Chemical composition and redox activity of PM0.25 near Los Angeles International Airport and comparisons to an urban traffic site.* Science of the Total Environment, 2018. **610**: p. 1336-1346.

49. Viana, M., et al., *Partitioning of trace elements and metals between quasi-ultrafine, accumulation and coarse aerosols in indoor and outdoor air in schools.* Atmospheric Environment, 2015. **106**: p. 392-401.
50. HEI, *Understanding the Health Effects of Ambient Ultrafine Particles HEI Review Panel on Ultrafine Particles*, in *HEI Perspective 3*. 2013, Health Effects Institute Boston, MA.
51. Sioutas, C., R.J. Delfino, and M. Singh, *Exposure assessment for atmospheric Ultrafine Particles (UFPs) and implications in epidemiologic research.* Environmental Health Perspectives, 2005. **113**(8): p. 947-955.
52. Peters, A., et al., *Translocation and potential neurological effects of fine and ultrafine particles a critical update.* Part Fibre Toxicol, 2006. **3**: p. 13.
53. Kulmala, M., et al., *Formation and growth rates of ultrafine atmospheric particles: a review of observations.* Journal of Aerosol Science, 2004. **35**(2): p. 143-176.
54. Ham, W.A. and K. Pinkerton, *Size, Composition, and Sources of Health Relevant Particulate Matter in the San Joaquin Valley.* 2004.
55. Joe, D.K., et al., *Implementation of a high-resolution Source-Oriented WRF/Chem model at the Port of Oakland.* Atmospheric Environment, 2014. **82**: p. 351-363.
56. SCAQMD, *MATES-IV: Multiple Air Toxics Exposure Study in the South Coast Air Basin*. 2015, South Coast Air Quality Management District.
57. Alcorn, S.H., Lurmann, Frederick W. , *Southern California Children's Health Study Exposure Database*. 2004, Sonoma Technology, Inc. .
58. Stanier, C.O., A.Y. Khlystov, and S.N. Pandis, *Nucleation Events During the Pittsburgh Air Quality Study: Description and Relation to Key Meteorological, Gas Phase, and Aerosol Parameters Special Issue ofAerosol Science and Technologyon Findings from the Fine Particulate Matter Supersites Program.* Aerosol Science and Technology, 2004. **38**(sup1): p. 253-264.
59. C.A.R.B, *Evaluation of Particulate Matter Filters in On-Road Heavy-Duty Diesel Vehicle Applications*. 2015.
60. Birch, M.E. and R.A. Cary, *Elemental carbon-based method for monitoring occupational exposures to particulate diesel exhaust.* Aerosol Science and Technology, 1996. **25**(3): p. 221-241.
61. Kuwayama, T., et al., *Particulate Matter Emissions Reductions due to Adoption of Clean Diesel Technology at a Major Shipping Port.* Aerosol Science and Technology, 2013. **47**(March 2015): p. 29-36.
62. CARB. *Title 13, California Code of Regulations. Division 3: Air Resources Board. Chapter 1: Motor Vehicle Pollution Control Devices*. 2014 [cited 2017 Oct. 19]; Available from: https://www.arb.ca.gov/msprog/onrdiesel/documents/tbfinalreg.pdf.
63. Saliba, G., et al., *Comparison of Gasoline Direct-Injection (GDI) and Port Fuel Injection (PFI) Vehicle Emissions: Emission Certification Standards, Cold-Start, Secondary Organic Aerosol Formation Potential, and Potential Climate Impacts.* Environmental Science & Technology, 2017. **51**(11): p. 6542-6552.
64. EPA, C., *Overview of the Statewide Drayage Truck Regulation* 2013.
65. POLA. *About the Port of Los Angeles Clean Truck Program*. 2017 [cited 2017 Oct. 17]; Available from: https://www.portoflosangeles.org/ctp/idx_ctp.asp.
66. Chris Lindhjem, T.S., John Grant, Lit Chan, James King, Rajashi Parikh. *Port of Oakland Seaport 2015 Emission Inventory* 2016; Available from:

http://www.portofoakland.com/files/PDF/Port%20of%20Oakland%202015%20Seaport%20Emissions%20Inventory%20Final-11Oct2016.pdf.

67. CARB. *Wood Burning Handbook* 2005 [cited 2017 Oct. 26]; Available from: https://www.arb.ca.gov/research/indoor/wood_burning_handbook.pdf.
68. EPA, *Strategies for Reducing Residential Woodsmoke*. 2013.
69. Lighthall, D., Nunes, D., Tyner, T., *Environmental Health Effects of Rule 4901: Domestic Wood Burning*. 2008, Central Valley Health Policy Institute, Central California Center for Health and Human Services, College of Health and Human Services, California State University Fresno.
70. Agrawal, H., et al., *In-use gaseous and particulate matter emissions from a modern ocean going container vessel.* Atmospheric Environment, 2008. **42**(21): p. 5504-5510.
71. Tao, L., et al., *Effects of Switching to Lower Sulfur Marine Fuel Oil on Air Quality in the San Francisco Bay Area.* Environmental Science & Technology, 2013. **47**(18): p. 10171-10178.
72. CARB. *Ocean-Going Vessels - Fuel Rule* 2017 [cited 2017 Oct. 17]; Available from: https://www.arb.ca.gov/ports/marinevess/ogv.htm.
73. IMO, *IMO regulations to reduce air pollution from ships and the review of fuel oil availability* 2016.
74. Westerdahl, D., et al., *The Los Angeles International Airport as a source of ultrafine particles and other pollutants to nearby communities.* Atmospheric Environment, 2008. **42**(13): p. 3143-3155.
75. Arnold, F., et al., *Jet engine exhaust chemiion measurements: Implications for gaseous SO3 and H2SO4.* Atmospheric Environment, 1998. **32**(18): p. 3073-3077.
76. Brown, R.C., et al., *Effect of aircraft exhaust sulfur emissions on near field plume aerosols.* Geophysical Research Letters, 1996. **23**(24): p. 3607-3610.
77. Herndon, S.C., et al., *Particulate emissions from in-use commercial aircraft.* Aerosol Science and Technology, 2005. **39**(8): p. 799-809.
78. Hudda, N. and S.A. Fruin, *International Airport Impacts to Air Quality: Size and Related Properties of Large Increases in Ultrafine Particle Number Concentrations.* Environmental Science & Technology, 2016. **50**(7): p. 3362-3370.
79. Hudda, N., et al., *Emissions from an International Airport Increase Particle Number Concentrations 4-fold at 10 km Downwind.* Environmental Science & Technology, 2014. **48**(12): p. 6628-6635.
80. Magill, B. *Countries Embrace New Rules to Limit Airline Emissions*. 2016 [cited 2017 Nov. 7]; Available from: http://www.climatecentral.org/news/countries-embrace-new-rules-airline-emissions-20007.
81. FAA, *Aviation Emissions, Impacts & Mitigation: A Primer*. 2015, FAA Office of Environment and Energy
82. Hymel, K.H., *Factors Influencing Vehicle Miles Traveled in California: Measurement and Analysis* 2014, California State University, Northridge
83. Circella, G., Tiedeman, K., Handy, S., Mokhtarian, P., *Factors Affecting Passenger Travel Demand in the United States*, in *A White Paper from the National Center for Sustainable Transportation*. 2015, National Center for Sustainable Transportation
84. CARB, *Evaluation of Particulate Matter Filters in On-Road Heavy-Duty Diesel Vehicle Applications*. 2015.

85. Hughes, L.S., et al., *Evolution of atmospheric particles along trajectories crossing the Los Angeles basin.* Environmental Science and Technology, 2000. **34**(15): p. 3058-3068.
86. Chow, J.C., et al., *PM2.5 chemical composition and spatiotemporal variability during the Californian Regional PM10/PM2.5 Air Quality Study (CRPAQS).* Journal of Geophysical Research: Atmospheres, 2006. **111**(10).
87. Herner, J.D., et al., *Dominant Mechanisms that Shape the Airborne Particle Size and Composition Distribution in Central California.* Aerosol Science and Technology, 2006. **40**(10): p. 827-844.
88. Hering, S.V., et al., *Comparison of Particle Size Distributions at Urban and Agricultural Sites in California's San Joaquin Valley.* Aerosol Science and Technology, 2007. **41**(September 2010): p. 86-96.
89. Misra, C., et al., *Development and evaluation of a personal cascade impactor sampler (PCIS).* Journal of Aerosol Science, 2002. **33**(7): p. 1027-1047.
90. Venecek, M.A., et al., *Characterization of the 8-stage Rotating Drum Impactor under low concentration conditions.* Journal of Aerosol Science, 2016. **100**: p. 140-154.
91. Kumar, P., et al., *Pseudo-simultaneous measurements for the vertical variation of coarse, fine and ultrafine particles in an urban street canyon.* Atmospheric Environment, 2008. **42**(18): p. 4304-4319.
92. Hughes, L.S., et al., *Size and composition distribution of atmospheric particles in southern California.* Environmental Science & Technology, 1999. **33**(20): p. 3506-3515.
93. Hughes, L.S., et al., *Evolution of atmospheric particles along trajectories crossing the Los Angeles basin.* Environmental Science & Technology, 2000. **34**(15): p. 3058-3068.
94. Kleeman, M.J., et al., *Source contributions to the size and composition distribution of atmospheric particles: Southern California in September 1996.* Environmental Science & Technology, 1999. **33**(23): p. 4331-4341.
95. Johnson, R.L., et al., *A Thermal-Optical Method for the Analysis of Carbonaceous Aerosol.* Abstracts of Papers of the American Chemical Society, 1980. **180**(Aug): p. 119-Nucl.
96. NIOSH, *NIOSH Manual of Analytical Methods, 4th Ed.* 1996.
97. Wu, C., et al., *Determination of Elemental and Organic Carbon in PM2.5 in the Pearl River Delta Region: Inter-Instrument (Sunset vs. DRI Model 2001 Thermal/Optical Carbon Analyzer) and Inter-Protocol Comparisons (IMPROVE vs. ACE-Asia Protocol).* Aerosol Science and Technology, 2012. **46**(6): p. 610-621.
98. EPA, *Pre-Generated Data Files*, in *Annual Summary Data*, EPA, Editor. 2017: AQS Data Mart.
99. URGcorp. *Manual Sampling Systems: URG- 3000N Carbon Sampler*. 2017 [cited 2017 Nov. 9]; Available from: http://www.urgcorp.com/index.php/systems/manual-sampling-systems/urg-3000n-carbon-sampler.
100. EPA, *Parameter and Method Codes for Loading PM2.5 Chemical Speciation Network (CSN) URG 3000N Carbon Data in AQS* 2007, U.S. Environmental Protection Agency
101. USC. *USC Children's Health Study* 2017 [cited 2017 Nov. 9]; Available from: https://healthstudy.usc.edu/.
102. Incorporated, T., *Product Information: Model 3022A Condensation Particle Counter*. 1999.
103. Singh, M., K. Bowers, and C. Sioutas, *Seasonal and spatial trends in particle number concentrations and size distributions at the children's health study sites in Southern*

California. Journal of Exposure Science and Environmental Epidemiology, 2006. **16**(1): p. 3-18.

104. Trinh, N.M., Pakbin, P., Polidori A, *Appendix VII: MATES-IV Final Report*, in *Ultrafine Particle Measurements at Fixed Sites*. 2015, South Coast Air Quality Management District

105. Zetterqvist, L., *Applied problems and use of technology in an aligned way in basic courses in probability and statistics for engineering students-a way to enhance understanding and increase motivation.* Teaching Mathematics and Its Applications, 2017. **36**(2): p. 108-122.

106. Minguillón, M.C., et al., *Seasonal and spatial variations of sources of fine and quasi-ultrafine particulate matter in neighborhoods near the Los Angeles-Long Beach harbor.* Atmospheric Environment, 2008. **42**(32): p. 7317-7328.

107. Kathleen, K., W. Arthur, and F. Scott, *Ultrafine particle size distributions near freeways: Effects of differing wind directions on exposure.* Atmos. Environ., 2012. **63**: p. 250-260.

108. Schwarze, P., et al., *Particulate matter properties and health effects: consistency of epidemiological and toxicological studies.* Human & experimental toxicology, 2006. **25**(10): p. 559-579.

109. Pope III, C.A. and D.W. Dockery, *Health effects of fine particulate air pollution: lines that connect.* Journal of the air & waste management association, 2006. **56**(6): p. 709-742.

110. Kim, S., et al., *Size distribution and diurnal and seasonal trends of ultrafine particles in source and receptor sites of the Los Angeles basin.* Journal of the Air & Waste Management Association, 2002. **52**(3): p. 297-307.

111. Zhu, Y., et al., *Concentration and size distribution of ultrafine particles near a major highway.* Journal of the air & waste management association, 2002. **52**(9): p. 1032-1042.

112. Geiser, M., et al., *Ultrafine particles cross cellular membranes by nonphagocytic mechanisms in lungs and in cultured cells.* Environmental health perspectives, 2005. **113**(11): p. 1555.

113. Cass, G.R., et al., *The chemical composition of atmospheric ultrafine particles.* Philosophical Transactions of the Royal Society of London A: Mathematical, Physical and Engineering Sciences, 2000. **358**(1775): p. 2581-2592.

114. Shirmohammadi, F., et al., *Fine and ultrafine particulate organic carbon in the Los Angeles basin: Trends in sources and composition.* Sci Total Environ, 2016. **541**: p. 1083-1096.

115. Hasheminassab, S., et al., *Source apportionment and organic compound characterization of ambient ultrafine particulate matter (PM) in the Los Angeles Basin.* Atmospheric environment, 2013. **79**: p. 529-539.

116. Daher, N., et al., *Seasonal and spatial variability in chemical composition and mass closure of ambient ultrafine particles in the megacity of Los Angeles.* Environmental Science: Processes & Impacts, 2013. **15**(1): p. 283-295.

117. Ntziachristos, L., et al., *Fine, ultrafine and nanoparticle trace element compositions near a major freeway with a high heavy-duty diesel fraction.* Atmospheric Environment, 2007. **41**(27): p. 5684-5696.

118. Hughes, L.S., et al., *Physical and chemical characterization of atmospheric ultrafine particles in the Los Angeles area.* Environmental Science & Technology, 1998. **32**(9): p. 1153-1161.

119. Hughes, L.S., et al., *Size and composition distribution of atmospheric particles in southern California.* Environmental science & technology, 1999. **33**(20): p. 3506-3515.

120. Austin, J. and H. Tran, *A Characterization of the Weekend-Weekday Behavior of Ambient Ozone Concentrations in California.* Technical Support and Planning Division, California Air Resources Board, Sacramento, CA, 1999.
121. Fujita, E.M., et al., *Evolution of the magnitude and spatial extent of the weekend ozone effect in California's South Coast Air Basin, 1981–2000.* Journal of the Air & Waste Management Association, 2003. **53**(7): p. 802-815.
122. Harley, R.A., et al., *Changes in motor vehicle emissions on diurnal to decadal time scales and effects on atmospheric composition.* Environmental Science & Technology, 2005. **39**(14): p. 5356-5362.
123. Chinkin, L.R., et al., *Weekday versus weekend activity patterns for ozone precursor emissions in California's South Coast Air Basin.* Journal of the Air & Waste Management Association, 2003. **53**(7): p. 829-843.
124. Motallebi, N., et al., *Day-of-week patterns of particulate matter and its chemical components at selected sites in California.* Journal of the Air & Waste Management Association, 2003. **53**(7): p. 876-888.
125. Whynes, D.K., J. Falk-Whynes, and M. Pringle, *Trends in acute admissions: a study of one English district general hospital.* Journal of Public Health, 1999. **21**(4): p. 459-463.
126. Garty, B.Z., et al., *Emergency room visits of asthmatic children, relation to air pollution, weather, and airborne allergens.* Annals of Allergy, Asthma & Immunology, 1998. **81**(6): p. 563-570.
127. Eller, P.M., *NIOSH manual of analytical methods*. Vol. 94. 1994: Diane Publishing.
128. Herner, J.D., P.G. Green, and M.J. Kleeman, *Measuring the trace elemental composition of size-resolved airborne particles.* Environmental science & technology, 2006. **40**(6): p. 1925-1933.
129. USE, P., *Method 6020a: inductively coupled plasma—mass spectrometry.* United States Environmental Protection Agency, Washington, DC USA, 1998.
130. Naeher, L.P., et al., *Woodsmoke health effects: a review.* Inhalation toxicology, 2007. **19**(1): p. 67-106.
131. Ostro, B., et al., *The effects of components of fine particulate air pollution on mortality in California: results from CALFINE.* Environmental health perspectives, 2007. **115**(1): p. 13.
132. Bridgwater, A., D. Meier, and D. Radlein, *An overview of fast pyrolysis of biomass.* Organic geochemistry, 1999. **30**(12): p. 1479-1493.
133. Querol, X., et al., *Source origin of trace elements in PM from regional background, urban and industrial sites of Spain.* Atmospheric Environment, 2007. **41**(34): p. 7219-7231.
134. Greenspan, B.J., et al., *Inhalation toxicity of lithium combustion aerosols in rats.* Journal of Toxicology and Environmental Health, Part A Current Issues, 1986. **18**(4): p. 627-637.
135. Kuschner, W.G., et al., *Human pulmonary responses to experimental inhalation of high concentration fine and ultrafine magnesium oxide particles.* Environmental health perspectives, 1997. **105**(11): p. 1234.
136. Kiviluoto, M., et al., *Effects of vanadium on the upper respiratory tract of workers in a vanadium factory: A macroscopic and microscopic study.* Scandinavian journal of work, environment & health, 1979: p. 50-58.
137. Kiviluoto, M., *Observations on the lungs of vanadium workers.* Occupational and Environmental Medicine, 1980. **37**(4): p. 363-366.

138. Knecht, E.A., et al., *Pulmonary effects of acute vanadium pentoxide inhalation in monkeys.* American Review of Respiratory Disease, 1985. **132**(6): p. 1181-1185.
139. Lagerkvist, B., H. Linderholm, and G.F. Nordberg, *Vasospastic tendency and Raynaud's phenomenon in smelter workers exposed to arsenic.* Environmental research, 1986. **39**(2): p. 465-474.
140. Liu, G., et al., *Health effects of arsenic, fluorine, and selenium from indoor burning of Chinese coal*, in *Reviews of environmental contamination and toxicology*. 2007, Springer. p. 89-106.
141. Manö, S. and M.O. Andreae, *Emission of methyl bromide from biomass burning.* Science, 1994. **263**(5151): p. 1255-1257.
142. Barceloux, D.G. and D. Barceloux, *Molybdenum.* Journal of Toxicology: Clinical Toxicology, 1999. **37**(2): p. 231-237.
143. Nriagu, J.O., *Global metal pollution: poisoning the biosphere?* Environment: Science and Policy for Sustainable Development, 1990. **32**(7): p. 7-33.
144. Bomhard, E.M., *The toxicology of indium tin oxide.* Environmental toxicology and pharmacology, 2016. **45**: p. 282-294.
145. Registry., U.S.A.f.T.S.a.D., *Toxicological Profile for Antimony. Final Report. Atlanta, GA, U.S. Dept. of Health and Human Services Public Health Service Agency for Toxic Substances and Disease Registry.* 1992.
146. Moreno, T., et al., *Recreational atmospheric pollution episodes: inhalable metalliferous particles from firework displays.* Atmospheric Environment, 2007. **41**(5): p. 913-922.
147. Seinfeld, J.H. and S.N. Pandis, *Atmospheric chemistry and physics: from air pollution to climate change*. 2012: John Wiley & Sons.
148. Kleeman, M.J., J.J. Schauer, and G.R. Cass, *Size and composition distribution of fine particulate matter emitted from wood burning, meat charbroiling, and cigarettes.* Environmental Science & Technology, 1999. **33**(20): p. 3516-3523.
149. McDonald, J.D., et al., *Fine particle and gaseous emission rates from residential wood combustion.* Environmental Science & Technology, 2000. **34**(11): p. 2080-2091.
150. Bay Area Air Quality Mangement District, *Winter Spare the Air Study, 2014-2015 Winter Wood Smoke Season.* 2015.
151. May, A.A., et al., *Gas-Particle Partitioning of Primary Organic Aerosol Emissions: (2) Diesel Vehicles.* Environmental Science & Technology, 2013. **47**(15): p. 8288-8296.
152. Li, N., et al., *Ultrafine particulate pollutants induce oxidative stress and mitochondrial damage.* Environmental Health Perspectives, 2003. **111**(4): p. 455-460.
153. Nel, A., et al., *Toxic potential of materials at the nanolevel* Science, 2006. **311**(5761): p. 622-627.
154. Oberdorster, G., et al., *Extrapulmonary translocation of ultrafine carbon particles following whole-body inhalation exposure of rats.* Journal of Toxicology and Environmental Health-Part A, 2002. **65**(20): p. 1531-1543.
155. Kuwayama, T., C. Ruehl, and M.J. Kleeman, *Daily trends and source apportionment of ultrafine particulate mass (PM0.1) over an annual cycle in a typical California City.* Environ Sci. Technology, 2013. **47**: p. 13957-13966.
156. Norris, G., et al., *EPA Positive Matrix Factorization (PMF) 5.0 fundamentals and User Guide Prepared for the US Environmental Protection Agency Office of Research and Development, Washington, DC.* Inc., Petaluma, 2014.

157. Reff, A., S.I. Eberly, and P.V. Bhave, *Receptor modeling of ambient particulate matter data using positive matrix factorization: review of existing methods.* Journal of the Air & Waste Management Association, 2007. **57**(2): p. 146-154.
158. Pereira, E., et al., *Airborne measurements of aerosols from burning biomass in Brazil related to the TRACE A experiment.* Journal of Geophysical Research: Atmospheres, 1996. **101**(D19): p. 23983-23992.
159. BAAQMD, *Ultrafine particulate matter in the San Francisco Bay Area.* Available at: http://www.baaqmd.gov/~/media/files/planning-and-research/research-and-modeling/estimating-public-health-and-monetary-impacts-of-ufpm-in-the-bay-area-final_12182014.pdf, 2014.
160. MATES, *Multiple air toxics exposure study in the south coast air basin, MATES IV.* South coast air quality management district, 2015. **Available at: http://www.aqmd.gov/docs/default-source/air-quality/air-toxic-studies/mates-iv/mates-iv-final-draft-report-4-1-15.pdf**.
161. Ozgen, S., et al., *Analysis of the chemical composition of ultrafine particles from two domestic solid biomass fired room heaters under simulated real-world use.* Atmospheric Environment, 2017. **150**: p. 87-97.
162. Brines, M., et al., *Traffic and nucleation events as main sources of ultrafine particles in high-insolation developed world cities.* Atmospheric Chemistry and Physics, 2015. **15**(10): p. 5929-5945.
163. Ostro, B.H., J.; Goldber, D.; Reynolds, P.; Hertz, A.; Bernstein, L.; Kleeman, M. J. , *Associations of mortality with long-term exposures to fine and ultrafine particles, species and sources: results from the California Teachers Study Cohort.* Environ Health Persp., 2015. **123**(6): p. 549-56.
164. Laurent, O., et al., *A Statewide Nested Case-Control Study of Preterm Birth and Air Pollution by Source and Composition: California, 2001-2008.* Environmental Health Perspectives, 2016. **124**(9): p. 1479-1486.
165. John, W. and G. Reischl, *A Cyclone for Size-Selective Sampling of Ambient Air.* Journal of the Air Pollution Control Association, 1980. **30**(8): p. 872-876.
166. McDow, S.R. and J.J. Huntzicker, *VAPOR ADSORPTION ARTIFACT IN THE SAMPLING OF ORGANIC AEROSOL - FACE VELOCITY EFFECTS.* Atmospheric Environment Part a-General Topics, 1990. **24**(10): p. 2563-2571.
167. Fitz, D.R., *Evaluation and Minimization of Organic Aerosol Sampling Artifacts Using Impactors and Quartz Fiber Filter Denuders*. 2007, U.S. EPA Grant Number R831087: University of California, Riverside.
168. Cheung, H.C., L. Morawska, and Z.D. Ristovski, *Observation of new particle formation in subtropical urban environment.* Atmospheric Chemistry and Physics, 2011. **11**(8): p. 3823-3833.
169. Sunset, *Lab OC-EC aerosol analyzer.* Available at: http://www.sunlab.com/products-services/, 2017.
170. Wu, C. and J.Z. Yu, *Determination of primary combustion source organic carbon-to-elemental carbon (OCaEuro-/aEuro-EC) ratio using ambient OC and EC measurements: secondary OC-EC correlation minimization method.* Atmospheric Chemistry and Physics, 2016. **16**(8): p. 5453-5465.

171. Zheng, M., et al., *Source apportionment of PM2.5 in the southeastern United States using solvent-extractable organic compounds as tracers.* Environmental Science & Technology, 2002. **36**(11): p. 2361-2371.
172. Stone, E.A., et al., *Characterization of emissions from South Asian biofuels and application to source apportionment of carbonaceous aerosol in the Himalayas.* Journal of Geophysical Research-Atmospheres, 2010. **115**.
173. EPA, *EPA-CMB8.2 Users Manual.* Available at: https://www3.epa.gov/scram001/receptor_cmb.htm, 2004.
174. Schauer, J.J. and G.R. Cass, *Source apportionment of wintertime gas-phase and particle-phase air pollutants using organic compounds as tracers.* Environmental Science & Technology, 2000. **34**(9): p. 1821-1832.
175. US-EPA, *EPA-CMB8.2 Users manual.* Available at:https://www3.epa.gov/scram001/models/receptor/EPA-CMB82Manual.pdf, 2004.
176. Zheng, M., et al., *Sources of primary and secondary organic aerosol and their diurnal variations.* Journal of Hazardous Materials, 2014. **264**: p. 536-544.
177. Kuwayama, T., et al., *Volatility of Primary Organic Aerosol Emitted from Light Duty Gasoline Vehicles.* Environmental Science & Technology, 2015. **49**(3): p. 1569-1577.
178. May, A.A., et al., *Gas-particle partitioning of primary organic aerosol emissions: (1) Gasoline vehicle exhaust.* Atmospheric Environment, 2013. **77**: p. 128-139.
179. May, A.A., et al., *Volatility of Organic Molecular Markers Used for Source Apportionment Analysis: Measurements and Implications for Atmospheric Lifetime.* Environmental Science & Technology, 2012. **46**(22): p. 12435-12444.
180. Xie, M.J., M.P. Hannigan, and K.C. Barsanti, *Gas/Particle Partitioning of 2-Methyltetrols and Levoglucosan at an Urban Site in Denver.* Environmental Science & Technology, 2014. **48**(5): p. 2835-2842.
181. Ruehl, C.R., W.A. Ham, and M.J. Kleeman, *Temperature-induced volatility of molecular markers in ambient airborne particulate matter.* Atmospheric Chemistry and Physics, 2011. **11**(1): p. 67-76.
182. Behymer, T.D. and R.A. Hites, *Photolysis of Polycyclic Aromatic-Hydrocarbons Adsorbed on Simulated Atmospheric Particulates.* Environmental Science & Technology, 1985. **19**(10): p. 1004-1006.
183. Pubchem, *compound summary for Benzo[Ghi]Perylene.* Available at: https://pubchem.ncbi.nlm.nih.gov/compound/9117#section=Top, 2017.
184. Keyte, I.J., R.M. Harrison, and G. Lammel, *Chemical reactivity and long-range transport potential of polycyclic aromatic hydrocarbons - a review.* Chemical Society Reviews, 2013. **42**(24): p. 9333-9391.
185. Skiles, M.J., et al., *Source apportionment of PM2.5 organic carbon in the San Joaquin Valley using monthly and daily observations and meteorological clustering.* Environmental Pollution, 2018. **237**: p. 366-376.
186. Nichols, P.D. and Q.I. Espey, *Characterization of Organic-Matter at the Air Sea Interface, in Subsurface Water, and in Bottom Sediments near the Malabar Sewage Outfall in Sydney Coastal Region.* Australian Journal of Marine and Freshwater Research, 1991. **42**(4): p. 327-348.
187. Nolte, C.G., et al., *Highly polar organic compounds present in meat smoke.* Environmental Science & Technology, 1999. **33**(19): p. 3313-3316.

188. Rogge, W.F., et al., *Sources of Fine Organic Aerosol .6. Cigarette-Smoke in the Urban Atmosphere.* Environmental Science & Technology, 1994. **28**(7): p. 1375-1388.
189. Sheesley, R.J., et al., *Trends in secondary organic aerosol at a remote site in Michigan's upper peninsula.* Environmental Science & Technology, 2004. **38**(24): p. 6491-6500.
190. SJV-APCD, *San Joaquin Valley, Air Pollution Control District, FAQs about residential wood burning, Rule 4901 and check before you burn.* Avaiable at: http://valleyair.org/rule4901/documents/FAQ-Rule4901.pdf, 2017.
191. Watson, J.G. and J.C. Chow, *A wintertime PM2.5 episode at the fresno, CA, supersite.* Atmospheric Environment, 2002. **36**(3): p. 465-475.
192. Yu, X., et al., *Sources of Airborne Ultrafine Particle Number and Mass Concentrations in California.* Atmospheric Chemistry and Physics Discussions, 2018.
193. Xue, J., et al., *Ultrafine particle emissions from natural gas, biogas and biomethane combustion.* Environmental Science & Technology, 2018. **in press**.
194. Xiao, S., et al., *Strong atmospheric new particle formation in winter in urban Shanghai, China.* Atmospheric Chemistry and Physics, 2015. **15**(4): p. 1769-1781.
195. Anttila, T. and V.M. Kerminen, *Condensational growth of atmospheric nuclei by organic vapours.* Journal of Aerosol Science, 2003. **34**(1): p. 41-61.
196. Troestl, J., et al., *The role of low-volatility organic compounds in initial particle growth in the atmosphere.* Nature, 2016. **533**(7604): p. 527-+.
197. NBC news, *Flaring at Chevron's Richmond Refinery Alarms Residents.* Available at: https://www.nbcbayarea.com/news/local/Flaring-at-Chevrons-Richmond-Refinery-Alarms-Residents-383586531.html, 2016.
198. CalOEHS, California Governor's Office of Emergency Services,. *Spill Release Reporting.* 2018 [cited 2018; Available from: http://www.caloes.ca.gov/FireRescueSite/pages/spill-release-reporting.aspx.
199. Takegawa, N., et al., *Seasonal and diurnal variations of submicron organic aerosol in Tokyo observed using the Aerodyne aerosol mass spectrometer.* Journal of Geophysical Research-Atmospheres, 2006. **111**(D11).
200. Yuan, Q., et al., *Seasonal cycles of secondary organic aerosol tracers in rural Guangzhou, Southern China: The importance of atmospheric oxidants.* Environmental Pollution, 2018. **240**: p. 884-893.
201. Saha, P.K., S.M. Reece, and A.P. Grieshop, *Seasonally Varying Secondary Organic Aerosol Formation From In-Situ Oxidation of Near-Highway Air.* Environmental Science & Technology, 2018. **52**(13): p. 7192-7202.
202. Galarneau, E., *Source specificity and atmospheric processing of airborne PAHs: Implications for source apportionment.* Atmospheric Environment, 2008. **42**(35): p. 8139-8149.
203. Freijer, J.I., J.C.H. van Eijkeren, and L. van Bree, *A model for the effect on health of repeated exposure to ozone.* Environmental Modelling and Software, 2002. **17**(6): p. 553-562.
204. *8-Hour Ozone (2008) Designated Area/State Information*. U.S. E.P.A. December 31, 2017 [cited 2018 Jan. 7].
205. Hakami, A., et al., *Adjoint Sensitivity Analysis of Ozone Nonattainment of the Continental United States.* Evironmental Science & Technology 2006. **40**: p. 3855-3864.

206. Heo, W.P.L.C.a.G., *Development of revised SAPRC aromatics mechansim* 2012, Report to the California Air Resources Board.

207. Bergin, M.S., A.G. Russel, and J.B. Milford, *Effects of Chemical MEchanism Uncertainties on the Reactivity Quantification of Volatile Organic Compounds Using a Three-Dimensional Air Quality Model.* Environmental Science and Technology, 1998. **32**: p. 694-703.

208. Griffith, S.M., R.F. Hansen , S. Dusanter, V. Michoud, J.B. Gilman ,W. C. Kuster, P. R. Veres, M. Graus, J. A. de Gouw, J. Roberts, C. Young, R. Washenfelder, S. S. Brown, R. Thalman, E. Waxman, R. Volkamer, C. Tsai, J. Stutz, J.H. Flynn, N. Grossberg, B. Lefer, S. L. Alvarez, B. Rappenglueck, L.H. Mielke, H. D. Osthoff, P. S. Stevens, *Measurements of hydroxyl and hydroperoxy radicals during CalNex-LA: Model comparisions and radical budgets.* Journal of Geophysical Research: Atmospheres, 2016. **121**: p. 4211-4232.

209. Gery, M.W., G.Z. Whitten, and J.P. Killus, *Development and Testing of the CBM-IV for urban and regional modeling*. 1988.

210. Stockwell, W.R., et al., *The second generation regional acid deposition model chemical mechanism for regional air quality modeling.* Journal of Geophysical Research, 1990. **95**(D10): p. 16343-16367.

211. Stockwell, W.R., et al., *A new mechanism for regional atmospheric chemistry modeling.* Journal of Geophysical Research, 1997. **102**: p. 25847-25880.

212. Jenkin, M.E., S.M. Saunders, and M.J. Pilling, *The troposheric degradation of volatile organic compounds: a protocol for mechanism development.* Atmospheric Enviornment, 1997. **31**(1): p. 81-104.

213. Yarwood, G., et al., *Updates to the carbon bond chemical mechanism: CB05*. 2005, Final Report to the U.S. E.P.A. RT-0500675.

214. S. M. Griffith, et al., *Measurements of hydroxyl and hydroperoxy radicals during CalNex-LA: Model comparisions and radical budgets.* Journal of Geophysical Research: Atmospheres, 2016. **121**: p. 4211-4232.

215. Emmerson, K.M., et al., *Urban atmospheric chemistry durning the PUMA campaign 1: Comparison of modelled OH and HO2 concentrations with measurements.* J. Atmos. Chem, 2005. **52**: p. 143-164.

216. Ren, X.R., et al., *HOx concentrations and OH reactivity observations in New York City during PMTACS-NY2001.* Atmos. Environ., 2003a. **37**: p. 3627-3637.

217. Ren, X.R.e.a., *OH and HO2 chemistry in the urban atmosphere of New York City.* Atmos. Environ., 2003b. **37**: p. 3639-3651.

218. Sheehy, P.M., et al., *Oxidative capacity of the Mexico City atmosphere - Part 2: A ROx radical cycling perspective.* Atmos. Chem. Phys, 2010. **10**: p. 6993-7008.

219. Shirley, T.R.e.a., *Atmospheric oxidation in the Mexico City Metropolitan Area (MCMA) during April 2003.* Atmos. Chem. Phys., 2006. **6**: p. 2753-2765.

220. George, L.A., T.M. Hard, and R.J. O'Brien, *Measurement of free radicals OH and HO2 in Los Angeles smog.* J. Geophys. Res., 1999. **104**(11): p. 643-655.

221. Emmerson, K.M.e.a., *Free radical modelling studies during the UK TORCH Campaign in Summer 2003.* Atmos. Chem. Phys, 2007. **7**: p. 167-181.

222. Konrad, S.e.a., *Hydrocarbon measurements at Pabstthum during the Berlioz campaign and modeling of free radicals.* J. Geophys. Res., 2003. **108**(D4): p. 8251.

223. Kanaya, Y., et al., *Urban photochemistry in central Tokyo: 1. Observed and modeled PH and HO2 radical concentrations during the winter and summer of 2004.* J. Geophys. Res., 2007. **112**(D21312).
224. Lu, K.D.e.a., *Observation and modeling of OH and HO2 concentrations in the Pearl River Delta 2006: A missing OH source in a VOC rich atmospher.* Atmos. Chem. Phys, 2012. **12**: p. 1541-1569.
225. Carter, W.P.L., *A Detailed Mechanism for the Gas-Phase Atmospheric Reactions of Organic Compounds.* Atmospheric Environment, 1990. **24**(A): p. 481-518.
226. Carter, W.P.L., *Documentation of the SAPRC-99 Chemical MEchanism for VOC Reactivity Assessment*. 2000, Available at http://www.cert.ucr.edu/~carter/absts.htm#saprc99.
227. Carter, W.P.L., *Development of the SAPRC-07 Chemical Mechanism and Updated Ozone*. 2010, Available at www.cert.ucr.edu/~carter/SAPRC. . p. Contract No. 03-318.
228. Carter, W.P.L., *Development of the SAPRC-07 Chemical Mechanism.* Atmospheric Environment, 2010. **44**: p. 5324-5335.
229. Hutzell, W.T., et al., *Interpreting predictions from the SAPRC07 mechanism based on regional and continental simulations.* Atmospheric Environment, 2012. **46**: p. 417-429.
230. Carter, W.P.L. and G. Heo, *Development of Revised SAPRC Aromatics Mechanisms.* Atmospheric Environment, 2013. **77**: p. 404-414.
231. Carter, W.P.L., *Preliminary Deocumentation of the SAPRC16 Mechanism*. 2016, Available at : http://www.cert.ucr.edu/~carter/SAPRC/16/S16doc.pdf.
232. Carter, W.P.L. *Gateway to the SAPRC-16 Mechanism Generation System*. 2018; Available from: http://mechgen.cert.ucr.edu/.
233. Yarwood, G., et al., *Environmental Chamber experiments to evaluate NOx sinks and recycling in atmospheric chemical mechanisms*. 2012, Available at http://aqrp.ceer.utexas.edu/projectinfo/10-042/10-042%20Final%20Report.pdf.
234. Heo, G., W.P.L. Carter, and Q. Ying, *Environmental chamber experiments and CMAQ modeling to improve mechanisms to model ozone formation from HRVOCs*. 2014, Available at http://aqrp.ceer.utexas.edu/projectinfoFY12_13/12-006/12-006%20Final%20Report.pdf.
235. Held, T., et al., *A comparison of the UCD/CIT air quality model and the CMB source-receptor model for primary airborne particulate matter.* Atmospheric Environment, 2005. **39**(12): p. 2281-2297.
236. Hu, J., et al., *Particulate air quality model predictions using prognositc vs diagnostic meteorology in central California.* Atmospheric Enviornment, 2010. **44**(2): p. 215-226.
237. Giglio, L., J.T. Randerson, and G.R. van der Werf, *Analysis of daily, monthly and annual burned area using the fourth-generation global fire emissions database (GFED4).* Journal of Geophysical Research, 2013. **118**(1): p. 317-328.
238. Carter, W.P.L., *Development of a database for chemical mechanism assignments for volatile organic emissions.* Journal of the Air & Waste Management Association, 2015. **65**(10): p. 1171-1184.
239. Ryerson, T.B.e.a., *The 2010 California Research at the Nexus of Air Quality and Climate Change (CalNex) field study* J. Geophys. Res. Atmos., 2013. **118**: p. 5830-5866.

240. Dusanter, S., et al., *Measurements of OH and HO2 concentrations during the MCMA-2006 field campaign - Part 1: Deployment of the Indiana University laser-induced fluorescence instrument.* Atmos. Chem. Phys, 2009. **9**: p. 1665-1685.
241. Carlton, A.G.B., P.V.; Napelenok, S. L.; Edney, E.D.; Sarwa, G.; Pinder, R. W.; Pouliot, G. A.; Houyoux, M.; , *Model representation of secondary organic aerosol in CMAQv4.7.* Environmental Science and Technology, 2010. **44**: p. 8553-8560.
242. Cappa, C.D., et al., *Simulating secondary organic aerosol in a regional air quality model using the statistical oxidation model - Part 2: assessing the influence of vapor wall losses.* Atmos. Chem. Phys, 2016. **16**: p. 3041-3059.
243. Pope, C.A., et al., *Lung cancer, cardiopulmonary mortality, and long-term exposure to fine particulate air pollution.* Jama-Journal of the American Medical Association, 2002. **287**(9): p. 1132-1141.
244. Pope, C.A., et al., *Cardiovascular mortality and long-term exposure to particulate air pollution - Epidemiological evidence of general pathophysiological pathways of disease.* Circulation, 2004. **109**(1): p. 71-77.
245. Pope, C.A., M. Ezzati, and D.W. Dockery, *Fine-Particulate Air Pollution and Life Expectancy in the United States.* New England Journal of Medicine, 2009. **360**(4): p. 376-386.
246. Dockery, D.W. and P.H. Stone, *Cardiovascular risks from fine particulate air pollution.* New England Journal of Medicine, 2007. **356**(5): p. 511-513.
247. Ostro, B., et al., *Associations of mortality with long-term exposures to fine and ultrafine particles, species and sources: results from the California Teachers Study Cohort.* Environ Health Perspect, 2015. **123**(6): p. 549-56.
248. Ostro, B., et al., *Fine particulate air pollution and mortality in nine California counties: Results from CALFINE.* Environ Health Persp., 2006. **114**(1): p. 29-33.
249. Ostro, B., et al., *Long-Term Exposure to Constituents of Fine Particulate Air Pollution and Mortality: Results from the California Teachers Study.* Environmental Health Perspectives, 2010. **118**(3): p. 363-369.
250. Brunekreef, B. and B. Forsberg, *Epidemiological evidence of effects of coarse airborne particles on health.* European Respiratory Journal, 2005. **26**(2): p. 309-318.
251. Fann, N., et al., *Estimating the National Public Health Burden Associated with Exposure to Ambient PM2.5 and Ozone.* Risk Analysis, 2012. **32**(1): p. 81-95.
252. Gauderman, W.J., et al., *Association of Improved Air Quality with Lung Development in Children.* New England Journal of Medicine, 2015. **372**(10): p. 905-913.
253. Miller, K.A., et al., *Long-term exposure to air pollution and incidence of cardiovascular events in women.* New England Journal of Medicine, 2007. **356**(5): p. 447-458.
254. Ogulei, D., et al., *Modeling source contributions to submicron particle number concentrations measured in Rochester, New York.* Aerosol Science and Technology, 2007. **41**(2): p. 179-201.
255. Hu, J., et al., *Identifying PM2.5 and PM0.1 sources for epidemiological studies in California.* Environ Sci Technol, 2014. **48**(9): p. 4980-90.
256. Montagne, D.R., et al., *Land Use Regression Models for Ultrafine Particles and Black Carbon Based on Short-Term Monitoring Predict Past Spatial Variation.* Environmental Science & Technology, 2015. **49**(14): p. 8712-8720.

257. Elleman, R.A. and D.S. Covert, *Aerosol size distribution modeling with the Community Multiscale Air Quality modeling system in the Pacific Northwest: 1. Model comparison to observations.* Journal of Geophysical Research-Atmospheres, 2009. **114**.
258. Zhang, Y., et al., *A comparative study of nucleation parameterizations: 2. Three-dimensional model application and evaluation.* Journal of Geophysical Research-Atmospheres, 2010. **115**.
259. Elleman, R.A. and D.S. Covert, *Aerosol size distribution modeling with the Community Multiscale Air Quality modeling system in the Pacific Northwest: 2. Parameterizations for ternary nucleation and nucleation mode processes.* Journal of Geophysical Research-Atmospheres, 2009. **114**.
260. Ying, Q., et al., *Modeling air quality during the California Regional PM10/PM2.5 Air Quality Study (CPRAQS) using the UCD/CIT Source Oriented Air Quality Model - Part II. Regional source apportionment of primary airborne particulate matter.* Atmospheric Environment, 2008. **42**(39): p. 8967-8978.
261. Ying, Q., et al., *Modeling air quality during the California Regional PM10/PM2.5 Air Quality Study (CRPAQS) using the UCD/CIT source-oriented air quality model - Part I. Base case model results.* Atmospheric Environment, 2008. **42**(39): p. 8954-8966.
262. Hu, J.L., et al., *Long-term particulate matter modeling for health effect studies in California - Part 2: Concentrations and sources of ultrafine organic aerosols.* Atmospheric Chemistry and Physics, 2017. **17**(8): p. 5379-5391.
263. Chen, J.J., Q. Ying, and M.J. Kleeman, *Source apportionment of wintertime secondary organic aerosol during the California regional PM10/PM2.5 air quality study.* Atmospheric Environment, 2010. **44**(10): p. 1331-1340.
264. Held, T., et al., *Modeling particulate matter in the San Joaquin Valley with a source-oriented externally mixed three-dimensional photochemical grid model.* Atmospheric Environment, 2004. **38**(22): p. 3689-3711.
265. Hixson, M., et al., *Influence of regional development policies and clean technology adoption on future air pollution exposure.* Atmospheric Environment, 2010. **44**(4): p. 552-562.
266. Hixson, M., et al., *Resolving the interactions between population density and air pollution emissions controls in the San Joaquin Valley, USA.* Journal of the Air & Waste Management Association, 2012. **62**(5): p. 566-575.
267. Hu, J., et al., *Mobile source and livestock feed contributions to regional ozone formation in Central California.* Environ Sci Technol, 2012. **46**(5): p. 2781-9.
268. Kleeman, M.J. and G.R. Cass, *A 3D Eulerian source-oriented model for an externally mixed aerosol.* Environmental Science & Technology, 2001. **35**(24): p. 4834-4848.
269. Kleeman, M.J., et al., *Source apportionment of secondary organic aerosol during a severe photochemical smog episode.* Atmospheric Environment, 2007. **41**(3): p. 576-591.
270. Kleeman, M.J., G.R. Cass, and A. Eldering, *Modeling the airborne particle complex as a source-oriented external mixture.* Journal of Geophysical Research-Atmospheres, 1997. **102**(D17): p. 21355-21372.
271. Mahmud, A., Hixson, M., Hu, J., Zhao, Z., Chen, S. H., Kleeman, M. J., *Climate impact on airborne particulate matter concentrations in California using seven year analysis periods.* Atmospheric Chemistry and Physics, 2010. **10**(22): p. 11097-11114.

272. Mysliwiec, M.J. and M.J. Kleeman, *Source apportionment of secondary airborne particulate matter in a polluted atmospbere.* Environmental Science & Technology, 2002. **36**(24): p. 5376-5384.

273. Rasmussen, D.J., et al., *The Ozone-Climate Penalty: Past, Present, and Future.* Environmental Science & Technology, 2013. **47**(24): p. 14258-14266.

274. Ying, Q. and M.J. Kleeman, *Source contributions to the regional distribution of secondary particulate matter in California.* Atmospheric Environment, 2006. **40**(4): p. 736-752.

275. Zhang, H.L. and Q. Ying, *Source apportionment of airborne particulate matter in Southeast Texas using a source-oriented 3D air quality model.* Atmospheric Environment, 2010. **44**(29): p. 3547-3557.

276. Hu, X.-M., et al., *Coupling and evaluating gas/particle mass transfer treatements for aerosol simulation and forecast.* J. Geophys. Res., 2008. **113**(D11208).

277. Nenes, A., C. Pilinis, and S.N. Pandis, *ISORROPIA: A new thermodynamic equilibrium model for multiphase multicomponent marine aerosols* Aquat. Geochem, 1998. **4**: p. 123-152.

278. Carlton, A.G., et al., *Model representation of secondary organic aerosol in CMAQv4.7.* Environmental Science and Technology, 2010. **44**: p. 8553-8560.

279. Napari, I., et al., *Parametrization of ternary nucleation rates for H(2)SO(4)-NH(3)-H(2)O vapors* J Geophys Res-Atmos, 2002. **107**.

280. Jung, J.G., et al., *Simulation of in situ ultrafine particle formation in the eastern United States using PMCAMx-UF.* Journal of Geophysical Research-Atmospheres, 2010. **115**.

281. Kerminen, V.M. and M. Kulmala, *Analytical formulae connecting the "real" and the "apparent" nucleation rate and the nuclei number concentration for atmospheric nucleation events.* Journal of Aerosol Science, 2002. **33**(4): p. 609-622.

282. Otte, T.L., *The impact of nudging in the meteorological model for retrospective air quality simulations. Part I: Evaluation against national observation networks.* Journal of Applied Meteorology and Climatology, 2008. **47**(7): p. 1853-1867.

283. Otte, T.L., *The impact of nudging in the meteorological model for retrospective air quality simulations. Part II: Evaluating collocated meteorological and air quality observations.* Journal of Applied Meteorology and Climatology, 2008. **47**(7): p. 1868-1887.

284. Zhao, Z., et al., *The Impact of Climate Change on Air Quality-Related Meteorological Conditions in California. Part I: Present Time Simulation Analysis.* Journal of Climate, 2011. **24**(13): p. 3344-3361.

285. Xue, J., et al., *Ultrafine particle emissions from natural gas, biogas and biomethane combustion.* Environmental Science and Technology, 2018. **in review**.

286. Kleeman, M.J. and G.R. Cass, *Source contributions to the size and composition distribution of urban particulate air pollution.* Atmospheric Environment, 1998. **32**(16): p. 2803-2816.

287. Shet, C.S., M.R. Cholemari, and S.V. Veeravalli, *Eulerian spatial and temporal autocorrelations: assessment of Taylor's hypothesis and a model.* Journal of Turbulence, 2017: p. 1-15.

288. Boylan, J.W. and A.G. Russell, *PM and light extinction model performance metrics, goals, and criteria for three-dimensional air quality models.* Atmospheric Environment, 2006. **40**(26): p. 4946-4959.

289. Watson, J.G., et al., *Comparison of four scanning mobility particle sizers at the Fresno Supersite.* Particuology, 2011. **9**(3): p. 204-209.

290. Lupascu, A., et al., *Modeling particle nucleation and growth over northern California during the 2010 CARES campaign.* Atmospheric Chemistry and Physics, 2015. **15**(21): p. 12283-12313.

291. Kleeman, M.J., et al., *Size distribution of trace organic species emitted from biomass combustion and meat charbroiling.* Atmos. Environ., 2008. **42**(24): p. 3059.

292. Hildemann, L.M., G.R. Markowski, and G.R. Cass, *Chemical composition of emissions from urban sources of fine organic aerosol.* Environmental Science and Technology, 1991. **25**(4): p. 744-759.

293. Li, W. and P.K. Hopke, *Initial Size Distributions and Hygroscopicity of Indoor Combustion Aerosol Particles.* Aerosol Science and Technology, 1993. **19**(3): p. 305-316.

294. Sowlat, M.H., S. Hasheminassab, and C. Sioutas, *Source apportionment of ambient particle number concentrations in central Los Angeles using positive matrix factorization (PMF).* Atmospheric Chemistry and Physics, 2016. **16**(8): p. 4849-4866.

295. Morawska, L., et al., *Ambient nano and ultrafine particles from motor vehicle emissions: Characteristics, ambient processing and implications on human exposure.* Atmospheric Environment, 2008. **42**(35): p. 8113-8138.

296. Gu, J.W., et al., *Source apportionment of ambient particles: Comparison of positive matrix factorization analysis applied to particle size distribution and chemical composition data.* Atmospheric Environment, 2011. **45**(10): p. 1849-1857.

297. Kasumba, J., et al., *Comparison of sources of submicron particle number concentrations measured at two sites in Rochester, NY.* Science of the Total Environment, 2009. **407**(18): p. 5071-5084.

298. Wang, Z.B., et al., *Long-term measurements of particle number size distributions and the relationships with air mass history and source apportionment in the summer of Beijing.* Atmospheric Chemistry and Physics, 2013. **13**(20): p. 10159-10170.

299. Yue, W., et al., *Source apportionment of ambient fine particle size distribution using positive matrix factorization in Erfurt, Germany.* Science of the Total Environment, 2008. **398**(1-3): p. 133-144.

300. Friend, A.J., et al., *Sources of ultrafine particles and chemical species along a traffic corridor: comparison of the results from two receptor models.* Environmental Chemistry, 2013. **10**(1): p. 54-63.

301. Cooper, J.A.E.A., *Dinal AppendixV-G,PM10 source composition library for the South Coast Air Basin*. 1989, South Coast Air Quality Management District, Diamond Bar, California.

302. Harley, R.A., M.P. Hannigan, and G.R. Cass, *Respeciation of Organic Gas Emissions and the Detection of Excess Unburned Gasoline in the Atmosphere.* Environmental Science & Technology, 1992. **26**(12): p. 2395-2408.

303. Hildemann, L.M., G.R. Markowski, and G.R. Cass, *Chemical-Composition of Emissions from Urban Sources of Fine Organic Aerosol.* Environmental Science & Technology, 1991. **25**(4): p. 744-759.

304. Hildemann, L.M., et al., *Submicrometer Aerosol Mass Distributions of Emissions from Boilers, Fireplaces, Automobiles, Diesel Trucks, and Meat-Cooking Operations.* Aerosol Science and Technology, 1991. **14**(1): p. 138-152.

305. Houck, J.E., Chow, J. C., Watson, J. G., Simons, C. A., Prichett, and G. L. C., J. M., Frazier, C. A., *Determination of particle size distribution and chemical composition of particulate matter from selected sources in California*. 1989, California Air Resources Board, OMNI Environment Service Incorporate, Desert Research Institute, Beaverton, Oregon.
306. Kleeman, M.J., J.J. Schauer, and G.R. Cass, *Size and composition distribution of fine particulate matter emitted from motor vehicles.* Environmental Science & Technology, 2000. **34**(7): p. 1132-1142.
307. Schauer, J.J., et al., *Measurement of emissions from air pollution sources. 1. C-1 through C-29 organic compounds from meat charbroiling.* Environmental Science & Technology, 1999. **33**(10): p. 1566-1577.
308. Schauer, J.J., et al., *Measurement of emissions from air pollution sources. 2. C-1 through C-30 organic compounds from medium duty diesel trucks.* Environmental Science & Technology, 1999. **33**(10): p. 1578-1587.
309. Schauer, J.J., et al., *Measurement of emissions from air pollution sources. 3. C-1-C-29 organic compounds from fireplace combustion of wood.* Environmental Science & Technology, 2001. **35**(9): p. 1716-1728.
310. Schauer, J.J., et al., *Measurement of emissions from air pollution sources. 4. C-1-C-27 organic compounds from cooking with seed oils.* Environmental Science & Technology, 2002. **36**(4): p. 567-575.
311. Schauer, J.J., et al., *Measurement of emissions from air pollution sources. 5. C-1-C-32 organic compounds from gasoline-powered motor vehicles.* Environmental Science & Technology, 2002. **36**(6): p. 1169-1180.
312. Taback, H.J., Brienza, A. R., Macko, J., and Brunetz, N., *Fine particle emissions from stationary and miscellaneous sources in the South Coast Air Basin. KVB Report 5806-783.* 1979, KVB Incorporated, Tustin, California.
313. Venecek, M., X. Yu, and M. Kleeman, *Ultrafine Particulate Matter Source Contributions across the Continental United States.* Atmospheric Chemistry and Physics, 2018. **submitted for review**.
314. Wallace, L. and W. Ott, *Personal exposure to ultrafine particles.* J Expo Sci Environ Epidemiol, 2011. **21**(1): p. 20-30.
315. Rim, D.H., L. Wallace, and A. Persily, *Infiltration of Outdoor Ultrafine Panicles into a Test House.* Environmental Science & Technology, 2010. **44**(15): p. 5908-5913.
316. Bhangar, S., et al., *Ultrafine particle concentrations and exposures in seven residences in northern California.* Indoor Air, 2011. **21**(2): p. 132-44.
317. Weichenthal, S., et al., *In-vehicle exposures to particulate air pollution in Canadian metropolitan areas: the urban transportation exposure study.* Environ Sci Technol, 2015. **49**(1): p. 597-605.
318. Fruin, S., et al., *Measurements and predictors of on-road ultrafine particle concentrations and associated pollutants in Los Angeles.* Atmospheric Environment, 2008. **42**(2): p. 207-219.
319. Xue, J., et al., *Seasonal and Annual Source Appointment of Carbonaceous Ultrafine Particulate Matter (PM0.1) in Polluted California Cities.* Environmental Science & Technology, 2019. **53**(1): p. 39-49.

320. Held, T., et al., *A comparision of the UCD/CIT air quality model and the CMB source-receptor model for primary airborne particulate matter.* Atmospheric Enviornment, 2005. **39**: p. 2281-2297.
321. Venecek, M.A., X. Yu, and M.J. Kleeman, *Ultrafine Particulate Matter Source Contributions across the Continental United States.* Atmospheric Chemistry and Physics Discussions, 2018: p. 1-26.
322. Yu, X., et al., *Sources of Airborne Ultrafine Particle Number and Mass Concentrations in California.* Atmos. Chem. Phys. Discuss., 2018. **2018**: p. 1-37.
323. Ying, Q., et al., *Verification of a source-oriented externally mixed air quality model during a severe photochemical smog episode.* Atmospheric Environment, 2007. **41**(7): p. 1521-1538.
324. Guenther, A., et al., *Estimates of global terrestrial isoprene emissions using MEGAN (Model of Emissions of Gases and Aerosols from Nature).* Atmospheric Chemistry and Physics, 2006. **6**: p. 3181-3210.
325. Guenther, A.B., et al., *The Model of Emissions of Gases and Aerosols from Nature version 2.1 (MEGAN2.1): an extended and updated framework modeling biogenic emissions.* Geoscientific Model Development, 2012. **5**: p. 1471-1492.
326. Xue, J., et al., *Seasonal and annual source appointment of carbonaceous ultrafine particulate matter (PM0.1) in polluted California cities.* Environmental Science & Technology, 2018. **in review**.
327. Su, L. and J.C.H. Fung, *Sensitivities of WRF-Chem to dust emission schemes and land surface properties in simulating dust cycles during springtime over East Asia.* Journal of Geophysical Research-Atmospheres, 2015. **120**(21): p. 11215-11230.
328. United States Department of Health and Human Services (US DHHS), Centers for Disease Control and Prevention (CDC), and National Center for Health Statistics (NCHS), *Compressed Mortality File (CMF) 1999-2013 with ICD-10 Codes on on CDC WONDER Online Database.*, in *The current release for years 1999 - 2013 is compiled from: CMF 1999-2013, Series 20, No. 2S, 2014.* 2014.
329. Emmons, L., et al., *Description and evaluation of the Model for Ozone and Related chemical Tracers, version 4 (MOZART-4).* Geoscientific Model Development, 2010. **3**(1): p. 43-67.
330. Herner, J.D., et al., *Effect of Advanced Aftertreatment for PM and NOx Control on Heavy-Duty Diesel Truck Emissions.* Environmental Science & Technology, 2009. **43**(15): p. 5928-5933.
331. Paugam, R., et al., *A review of approaches to estimate wildfire plume injection height within large-scale atmospheric chemical transport models.* Atmospheric Chemistry and Physics, 2016. **16**(2): p. 907-925.
332. Almaraz, M., et al., *Agriculture is a major source of NOx pollution in California.* Science Advances, 2018. **4**(1).
333. Kleeman, M., A. Kumar, and A. Dhiman, *Investigative Modeling of PM2.5 Episodes in the San Joaquin Valley Air Basin during Recent Years*. 2018, California Air Resources Board Research Division Report # 15-301.
334. Hong, S.Y., Y. Noh, and J. Dudhia, *A new vertical diffusion package with an explicit treatment of entrainment processes.* Monthly Weather Review, 2006. **134**(9): p. 2318-2341.

335. Xiu, A.J. and J.E. Pleim, *Development of a land surface model. Part I: Application in a mesoscale meteorological model.* Journal of Applied Meteorology, 2001. **40**(2): p. 192-209.
336. McDonald, B.C., et al., *High-resolution mapping of motor vehicle carbon dioxide emissions.* Journal of Geophysical Research-Atmospheres, 2014. **119**(9): p. 5283-5298.
337. McDonald, B.C., et al., *Long-Term Trends in Motor Vehicle Emissions in US Urban Areas.* Environmental Science & Technology, 2013. **47**(17): p. 10022-10031.
338. Gentner, D.R., et al., *Elucidating secondary organic aerosol from diesel and gasoline vehicles through detailed characterization of organic carbon emissions.* Proceedings of the National Academy of Sciences of the United States of America, 2012. **109**(45): p. 18318-18323.
339. Dallmann, T.R., et al., *Quantifying On-Road Emissions from Gasoline-Powered Motor Vehicles: Accounting for the Presence of Medium- and Heavy-Duty Diesel Trucks.* Environmental Science & Technology, 2013. **47**(23): p. 13873-13881.
340. Dallmann, T.R., et al., *On-Road Measurement of Gas and Particle Phase Pollutant Emission Factors for Individual Heavy-Duty Diesel Trucks.* Environmental Science & Technology, 2012. **46**(15): p. 8511-8518.
341. Dominici, F., et al., *Fine Particulate Air Pollution and Hospital Admission for Cardiovascular and Respiratory Diseases.* JAMA, 2006. **295**(10): p. 1127-1134.
342. Franklin, M., A. Zeka, and J. Schawrtz, *Association between PM2.5 and all-cause and specific-cause moratlity in 27 US communities.* Journal of EXposure Science and Environmental Epidemiology, 2007. **17**: p. 279-287.
343. Pope, C.A., et al., *Lung Cancer, Cardiopulmonary Mortality and Long Term Exposer to Fine Particulate Air Pollution.* JAMA-J AM Med Assoc. , 2002. **287**(8): p. 1132-1141.
344. Pope, C.A., M. Ezzati, and D.W. Dockery, *Fine-Particulate Air Pollution and US County Life Expectancies.* New Engl J Med., 2009. **360**(4): p. 376-386.
345. Laden, F., et al., *Association of fine particulate matter from different sources with daily mortality in six U.S. Cities.* Environ Health Persp., 2000. **108**(10): p. 941-947.
346. Kheirbek, I., et al., *PM2.5 and Ozone health impacts and disparities in New York City: sensitivity to spatial and temporal resolution.* Air Qual Atmos Health, 2013. **6**: p. 473-486.
347. Aneja, A.P., et al., *Particulate matter pollution in the coal-producing regions of the Appalachian Mountains: Integrated ground-based measurements and satellite analysis.* Journal of Air and Waste Management Association, 2017. **67**(4): p. 421-430.
348. EPA, U. *Air Quality Designations for Particle Pollution*. 2017b; Available from: https://www.epa.gov/pm-pollution/forms/contact-us-about-particulate-matter-pm-pollution.
349. Baxter, L.K., R.M. Duvall, and J. Sacks, *Examining the effects of air pollution composition on within region differences in PM2.5 mortality risk estimates.* J Expo Sci Environ Epidemiol, 2013. **23**(5): p. 457-465.
350. Li, N., et al., *Ultrafine particulate pollutants induce oxidative stress and mitochondrial damage.* Environ Health Persp., 2003. **111**(4): p. 455-460.
351. Oberdurster, G., *Toxicology of ultrafine particles: in vivo studies.* The Royal Society, 2000. **358**(1175).
352. Oberdorseter, G., et al., *Association of Particulate Air Pollution and ACute Mortality: Involvement of Ultrafine Particles.* Inhal. Toxicol., 1995. **7**: p. 111-124.

353. Pekkanen, J., et al., *Effects of Ultra-Fine and fine PArticles in Uran Air on Peak Expiratory Flow Among Children with Asthmatic Symptoms.* Environ. Res., 1997. **74**: p. 24-33.

354. Bergin, M.S., et al., *Effects of uncertainty in SAPRC90 rate constants and selected product yields on reactivity adjustment facorts for alternamtive fuel vehicle emissions. Final Report.* 1996.

355. Reff, A., et al., *Emissions Inventory of PM2.5 TRace Elements across the United States.* Environmental Science and Technology, 2009. **43**(15): p. 5790-5796.

356. Zhang, H., et al., *Source apportionment of sulfate and nitrate partiulate matter int he Eastern United States and Effectiveness of emission control programs* Science of the Total Environment, 2014. **490**: p. 171-181.

357. Zheng, M., et al., *Source Apportionment of PM2.5 in the Southeastern United States Using Solvent-Extractable Organic Compounds as Tracers.* Environmental Science and Technology, 2002. **36**(11): p. 2361-2371.

358. Lane, T.E., et al., *Source contributions to primary organic aerosol: Comparison of the results of a source-resolved model and the chemical mass balance approach.* Atmospheric Environment, 2007. **41**: p. 3758-3776.

359. Posner, L.A. and S.N. Pandis, *Sources of ultrafine particles in the Eastern United States.* Atmospheric Environment, 2015. **111**: p. 103-112.

360. Wang, Y., et al., *Long-term study of urban ultrafile particles and other pollutants.* Atmospheric Environment, 2011. **45**: p. 7672-7680.

361. Cattani, G., et al., *Development of land-use regression models for exposure assessment to ultrafine particles in Rome, Italy.* Atmospheric Environment, 2017. **156**: p. 52-60.

362. Wolf, K., et al., *Land use regression modeling of ultrafine particles, ozone, nitrogen oxides and markers of particulate matter pollution in Augsburg, Germany.* Science of the Total Environment, 2017. **579**: p. 1531-1540.

363. Simon, M.C., et al., *Combining Measurements from Mobile Monitoring and a Reference Site to Develop Models of Ambient Ultrafine Particle Number Concentrations at Residences.* Environ. Sci. Technol, 2018. **52**(12): p. 6985-6995.

364. Gaydos, T.M., C.O. Stanier, and S.N. Pandis, *Modeling of in situ ultrafine atmospheric particle formation in the eastern United States.* Journal of Geophysical Research, 2005. **110**.

365. Zhong, J., et al., *Modelling traffic-induced multicomponent ultrafine particles in urban street canyon compartments: Factors that inhibit mixing.* Environmental Pollution, 2018. **238**: p. 186-195.

366. Carter, W.P.L., *Calculation of Reactivity Scales Using an Updated Carbon Bond IV Mechanism*. 1994a, Report Prepared fo Systems Applications Internation for the Auto/Oil Air Quality Improvement Program.

367. Venecek, M.A., W.P.L. Carter, and M.J. Kleeman, *Updating the SAPRC Maximum Incremental Reactivity (MIR) Scale for the United States from 1988 to 2010.* Journal of Air and Waste Management Association, 2018a. **68**(12): p. 1301-1316.

368. Venecek, M.A., et al., *Analysis of the SAPRC16 Chemical Mechanism for Ambient Simulations.* Atmospheric Enviornment, 2018b. **192**: p. 136-150.

369. United States Census Bureau. *Geographic Terms and Concepts - Core Based Statistical Areas and Related Statistical Areas*. 2018; Available from: https://www.census.gov/geo/reference/gtc/gtc_cbsa.html.

370. Yu, X., et al., *Regional Ultrafine Particle Number and Mass Concentrations in California.* Atmos. Chem. Phys, 2018. **submitted for publication**.

371. Robert, M.A., et al., *Size and Composition distributions of particulate matter emissions: Part 1 - Light duty gasoline vehciles.* J. Air Waste Management, 2007a. **57**(12): p. 1414-1428.

372. Robert, M.A., M.J. Kleeman, and C.A. Jakober, *Size and composition distrubtions of particulate matter emissions: Part 2 - Heavy - duty diesel vehicles.* J. Air Waste Management, 2007b. **57**(12): p. 1429-1438.

373. EPA, U. *AQS API / Query AirData*. Available from: aqs.epa.gov/api.

374. Solomon, P.A., et al., *U.S. National PM2.5 Chemical Speciation Monitoring Networs - CSN and IMPROVE: Description of networks.* Journal of Air and Waste Management Association, 2014. **64**(12): p. 1410-1438.

375. Xue, J., et al., *Annual trends in ultrafine particulate matter (PM0.1) source contributions in polluted California cities.* Environmental Science and Technology, 2018. **in review**.

376. Chang, M.-C., et al., *Measurement of Ultrafine Particle Size Distributions from Coal-, Oil-, and Gas-Fired Stationary Combustion Sources.* Journal of Air and Waste Management Association, 2004. **54**(12): p. 1494-1505.

377. U.S. Department of Energy. *Natural Gas Explained, Use of Natural Gas*. 2017; Available from: https://www.eia.gov/energyexplained/index.php?page=natural_gas_use.

378. Li, N., et al., *A work group report on ultrafine particles (American Academy of Allergy, Asthma & Immunology): Why ambient ultrafine and engineered nanoparticles should receive special attention for possible adverse health outcomes in human subjects.* Journal of Allergy and Clinical Immunology, 2016. **138**(2): p. 386-396.

379. Brook, R.D., et al., *Particulate Matter Air Pollution and Cardiovascular Disease An Update to the Scientific Statement From the American Heart Association.* Circulation, 2010. **121**(21): p. 2331-2378.

380. Delfino, R.J., et al., *Air Pollution Exposures and Circulating Biomarkers of Effect in a Susceptible Population: Clues to Potential Causal Component Mixtures and Mechanisms.* Environmental Health Perspectives, 2009. **117**(8): p. 1232-1238.

381. Delfino, R.J., et al., *Circulating biomarkers of inflammation, antioxidant activity, and platelet activation are associated with primary combustion aerosols in subjects with coronary artery disease.* Environmental Health Perspectives, 2008. **116**(7): p. 898-906.

382. Liu, J.Y., et al., *Association of ultrafine particles with cardiopulmonary health among adult subjects in the urban areas of northern Taiwan.* Science of the Total Environment, 2018. **627**: p. 211-215.

383. Stafoggia, M., et al., *Association Between Short-term Exposure to Ultrafine Particles and Mortality in Eight European Urban Areas.* Epidemiology, 2017. **28**(2): p. 172-180.

384. Lanzinger, S., et al., *Ultrafine and Fine Particles and Hospital Admissions in Central Europe Results from the UFIREG Study.* American Journal of Respiratory and Critical Care Medicine, 2016. **194**(10): p. 1233-1241.

385. Lanzinger, S., et al., *Associations between ultrafine and fine particles and mortality in five central European cities - Results from the UFIREG study.* Environment International, 2016. **88**: p. 44-52.

386. Corlin, L., et al., *Longitudinal associations of long-term exposure to ultrafine particles with blood pressure and systemic inflammation in Puerto Rican adults.* Environmental Health, 2018. **17**.

387. Downward, G.S., et al., *Long-Term Exposure to Ultrafine Particles and Incidence of Cardiovascular and Cerebrovascular Disease in a Prospective Study of a Dutch Cohort.* Environmental Health Perspectives, 2018. **126**(12).

388. Lipsett, M.J., et al., *Long-Term Exposure to Air Pollution and Cardiorespiratory Disease in the California Teachers Study Cohort.* American Journal of Respiratory and Critical Care Medicine, 2011. **184**(7): p. 828-835.

389. Mostofsky, E., et al., *Modeling the Association Between Particle Constituents of Air Pollution and Health Outcomes.* American Journal of Epidemiology, 2012. **176**(4): p. 317-326.

390. Zeger, S.L., et al., *Mortality in the Medicare Population and Chronic Exposure to Fine Particulate Air Pollution in Urban Centers (2000-2005).* Environmental Health Perspectives, 2008. **116**(12): p. 1614-1619.

391. Di, Q., et al., *Air Pollution and Mortality in the Medicare Population.* New England Journal of Medicine, 2017. **376**(26): p. 2513-2522.

392. Hoek, G., et al., *Long-term air pollution exposure and cardio- respiratory mortality: a review.* Environmental Health, 2013. **12**.

393. Wang, Y., et al., *Long-term Exposure to PM2.5 and Mortality Among Older Adults in the Southeastern US.* Epidemiology, 2017. **28**(2): p. 207-214.

394. Thurston, G.D., et al., *Ischemic Heart Disease Mortality and Long-Term Exposure to Source-Related Components of US Fine Particle Air Pollution.* Environmental Health Perspectives, 2016. **124**(6): p. 785-794.

395. Achilleos, S., et al., *Acute effects of fine particulate matter constituents on mortality: A systematic review and meta-regression analysis.* Environment International, 2017. **109**: p. 89-100.

396. Yang, Y., *Shortterm and long-term exposures to fine particulate matter constituents and health: A systematic review and meta-analysis.* . Environmental Pollution, 2019. **in press**.

397. Straffelini, G., et al., *Present knowledge and perspectives on the role of copper in brake materials and related environmental issues: A critical assessment.* Environmental Pollution, 2015. **207**: p. 211-219.

398. Gasser, M., et al., *Toxic effects of brake wear particles on epithelial lung cells in vitro.* Particle and Fibre Toxicology, 2009. **6**.

399. Thorpe, A. and R.M. Harrison, *Sources and properties of non-exhaust particulate matter from road traffic: A review.* Science of the Total Environment, 2008. **400**(1-3): p. 270-282.